

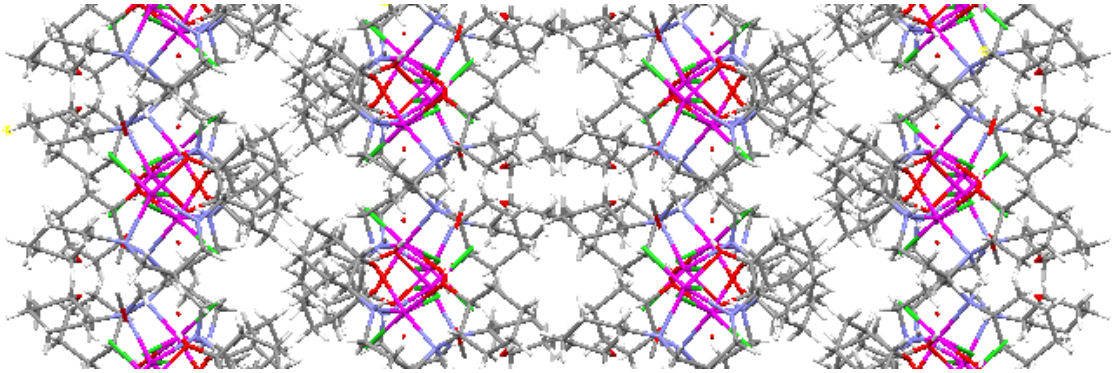
https://dspace.org/

The synthesis and characterisations of metallo-beta-amino alcohol complexes

Birtles, Samantha Lee

2011-07-25
http://hdl.handle.net/10539/10315

Downloaded from a DSpace repository. https://dspace.org/



THE SYNTHESIS AND CHARACTERISATIONS OF METALLO-BETA-AMINO ALCOHOL COMPLEXES

Dissertation submitted to the Faculty of Science, University of the Witwatersrand, South Africa, for the Degree of **Master of Science**

By

Samantha Lee Birtles

Supervised by:

Prof. Helder M. Marques

Dr. Alvaro S. de Sousa

SCHOOL OF CHEMISTRY
UNIVERSITY OF THE WITWATERSRAND
JOHANNESBURG
SOUTH AFRICA

June 2011

Declaration

I hereby declare that this dissertation is my own work. It is submitted for the fulfillment of the degree of Master of Science in the Faculty of Science of the University of the Witwatersrand. This dissertation has never been submitted before for any degree or examination in any other university.



S. L. Birtles

Dedication

I would like to dedicate this dissertation to my mother, Cheryl Birtles.

Abstract

The ligands N,N'-bis(2-hydroxycyclohexyl)-1,3-propanediamine (Cy_2-tn), and 2,2'-[(hydroxypropane-1,3-diyl)diimino]dicyclohexanol, (Cy_2-Otn) and were synthesised and their solid state structures determined by X-ray diffraction experiments. Complexes were formed with the metal ions Pb(II), Cd(II), Ni(II), Cu(II) and Zn(II). The solid state structures of the Ni(II), Zn(II) and Cd(II) complex of Cy_2-tn were determined by X-ray diffraction studies. The solid state structures of both the ligands, and their polymorphs, as well as the Cy_2-tn/metal complexes mentioned, indicated the presence of hydrogen-hydrogen bonds between hydrogens on the cyclohexenyl rings and hydrogens on the propyl bridge. DFT calculations (X3LYP/6-31G(d,p))were performed on the Cy_2-tn free ligand, the Cy_2-tn Ni(II), Cu(II) and Zn(II) complexes, and on the ligand N,N'-bis(2-hydroxycyclohexyl)-trans-cyclohexane-1,2- diamine (TCA) with Cu(II). The wavefunction files generated were used to study topolygical properties of the electron density using Bader's Quantum Theory of Atoms in Molecules (QTAIM). The resulting molecular graphs showed there were bond paths between hydrogen atoms on the cyclohexenyl rings in the TCA/Cu complex, but not in the Cy_2-tn free ligand or the Cy_2-tn/metal complexes. The DFT calculation also indicated that the L-M bonds are ionic with some covalent character, while the M-N bonds are suggested to be stronger, and more covalent in character than the M-O bonds. The slightly shared electron density character in the M-L bonds is seen by the charge on the metal ions being less than the formal 2+ charge. Potentiometric studies were performed on the Cy_2-Otn ligand, and the complexes with Cu(II), Ni(II), Zn(II), Cd(II) and Pb(II). The protonation constant determination of the Cy_2-Otn ligand resulted in pK_{a1} = 8.73 and a pK_{a2} = 7.31, however an impurity was present that was not seen in the characterisations. The Cy_2-Otn/Cd and Pb(II) systems showed precipitation and were not analysed, while the Cy_2-Otn/Zn system gave poor data. The Cy_2-Otn/Cu system showed M(LH), ML and ML(OH) species present, whilst the Cy_2-Otn/Ni system showed the presence of M(LH), ML, ML(OH), and $ML(OH)_2$ species. The stability constants of the Cy_2-Otn/metal ML species were compared to those previously reported for the Cy_2-tn and Cy_2-en ligands and their complexes with the metals studied.

Acknowledgements

I would like to thank my supervisors, Prof Helder Marques and Dr Alvaro de Sousa for their advice and guidance. I would also like to thank Matt Rayner, my friends and family for their support.

A big thanks to Dr. Manuel Fernandes for collecting the XRD data for me, and Mr. Richard Mampa for running NMR samples for me.

I would also like to thank the National Research Foundation (NRF) as well as the University of the Witwatersrand (Wits) for funding my research.

List of Figures

Figure 1.2.1.	Increase in complex stability in going from unidentate, to bidentate, to chelate, to macrocycle, to cryptand ligands	6
Figure 1.2.2.	Ideal geometry for six- and five-membered chelate rings with neutral N-donors	7
Figure 1.2.3.	Ideal geometry for six- and five-membered chelate rings with neutral O-donors	9
Figure 1.3.1.	Example of inner-sphere and outer-sphere complexes	11
Figure 1.5.1.	Ethylenediaminetetraacetic acid, EDTA	14
Figure 1.6.1.	Irving-Williams series	16
Figure 1.6.2.	The ligands Cy_2-Otn and Cy_2-tn, respectively	17
Figure 1.7.1.	Cy_2-Otn	19
Figure 1.7.2.	Cy_2-en	19
Figure 1.7.3.	Cy_2-en/Pb(II)	19
Figure 1.7.4.	Cy_2-en/Cd(II)	19
Figure 1.7.5.	BHEEN/Cd(II)	19
Figure 1.7.6.	BHEEN/Zn(II)	19
Figure 1.7.7a.	N,N'-bis(2-hydroxycylcohexyl)propane-1,3-diamine complexed to copper(II)	20
Figure 1.7.7b.	Cy_2-tn complexed to copper(II) showing H-H interactions	20
Figure 1.7.8.	Fragment of the ligands Cy_2-Otn and Cy_2-tn with any transition metal	22
Figure 1.7.9.	bis[N,N,N',N'-tetrakis-(2-hydroxyehtyl)ehtylenediamine] copper(II) perchlorate (THEEN)	22
Figure 1.7.10.	(5-Hydroxy-3,7-diazanonane-1,9-diamine)-copper(II)diperchlorate	23
Figure 1.7.11.	1,3-bis[(4-methyl-5-imidazol-1-yl)ethylideneamino] propan-2-ol complexed to copper(II)	23
Figure 1.7.12.	1,3-bis(5-methyl-3-formylpyrazolylmethinimino) propane-2-ol chloride complexed to copper(II)	24
Figure 1.7.13.	[Cu(BHEEN)Cl_2] complex	24
Figure 1.7.14.	[Cu(2,2'bpy)(1,2-bis((2-hydroxyethyl)amino)ethane)] complex	25
Figure 1.7.15.	6,10-bis(2-hydroxyethyl)-7,8,9,11,17,18-hexahydro-dibenzo-[e,n]	

[1,4,8,12]-dithiadiaza-cyclopentadecine complexed to Ni(II) and Cu(II) 25

Figure 1.7.16. (Nitrato-O,O')-(8,9,17,18-tetrahydro-5H-dibenzo(e,n)(1,4,8,12) dioxadiazacyclopentadecine-6,10(7H,11H)-diethanol)-nickel(II) nitrate 26
Figure 1.7.17. [Ni(bchtn)(H_2O)$_2$]C1$_2$ (bchtn = N,N'-bis(flcarbamoylethyl)-2-hydroxytrimethylenediamine) 27
Figure 1.7.18. 1,3-bis[(4-methyl-5-imidazol-1-yl)ethylideneamino] propan-2-ol complexed to nickel(II) 27
Figure 1.7.19. Schiff base ligand complexed to nickel(II) 28
Figure 1.9.1. The Bragg scattering angles 32
Figure 1.9.2. Representation of the unit cell and lattice points 32
Figure 1.9.3. The various unit cell types 33
Figure 2.3.1. General setup of the ligand reactions 49
Figure 2.3.2. Cy_2-Otn (Lx) 50
Figure 2.3.3. Cy_2-tn (2Lx) 56
Figure 3.2.1. QTAIM molecular graph of Cy_2-tn 81
Figure 3.2.2. Selected experimental vs. calculated bond lengths for the Cy_2-tn with Ni(II), Cu(II), and Zn(II), and TCA/Cu complexes 84
Figure 3.2.3. Electron density vs. selected calculated bond lengths for the TCA/Cu and the Cy_2-tn with Ni(II), Zn(II), and Cu(II) complexes 84
Figure 3.2.4. Electron density vs. Laplacian values of selected M-L, N-C, NC-CO, and C-O covalent bonds of TCA/Cu and Cy_2-tn with Ni(II), Zn(II), and Cu(II) complexes 85
Figure 3.2.5. Electron density vs. the electron potential energy of M-L bonds of TCA/Cu, and Cy_2-tn with Ni(II), Zn(II), and Cu(II) complexes 86
Figure 3.2.6. Electron density vs. electron kinetic energy of M-L bonds of TCA/Cu, and Cy_2-tn with Ni(II), Zn(II), and Cu(II) complexes 87
Figure 3.2.7. Electron density vs.V/G energy of the M-L and the ligand C-N, NC-CO, andC-O bonds 88
Figure 3.2.8. Electron density vs. total electron density energy of M-L bonds of TCA/Cu, and Cy_2-tn with Ni(II), Zn(II), and Cu(II) complexes 89
Figure 3.2.9. Electron density vs. electron potential energy of M-L bonds of TCA/Cu, and Cy_2-tn with Ni(II), Zn(II), and Cu(II) complexes 89
Figure 3.2.10. Electron density vs. electron kinetic energy of M-L bonds of

TCA/Cu, and Cy_2-tn with Ni(II), Zn(II), and Cu(II) complexes 90

Figure 3.2.11. Electron density vs. total electron density energy of M-L bonds of TCA/Cu, and Cy_2-tn with Ni(II), Zn(II), and Cu(II) complexes 90
Figure 3.2.12. Electron density vs. electron potential energy of ligand TCA and Cy_2-tn C-N, NC-CO, and C-O bonds 91
Figure 3.2.13. Electron density vs. electron kinetic energy of ligand TCA and Cy_2-tn C-N, NC-CO, and C-O bonds 91
Figure. 3.2.14. Electron density vs. total electron density energy of ligand TCA and Cy_2-tn C-N, NC-CO, and C-O bonds 92
Figure 3.2.15. QTAIM molecular graph of Cy_2-tn/Ni complex 93
Figure 3.2.16. QTAIM molecular graph of Cy_2-tn/Zn complex 94
Figure 3.2.17. QTAIM molecular graph of Cy_2-tn/Cu complex 94
Figure 3.2.18. QTAIM molecular graph of TCA/Cu complex 95
Figure 4.1.1. The molecular structure of Cy_2-Otn(a), showing the atom labelling scheme and 50% probability displacement ellipsoids 100
Figure 4.1.2. The molecular structure of Cy_2-Otn(a) without hydrogens showing the atom-labelling scheme and O8 disorder over two positions 101
Figure 4.1.3. Cy_2-Otn(a) with planes through the propyl bridge and cyclohexenyl ring C1-C6 102
Figure 4.1.4. Cy_2-Otn(a) with planes through the propyl bridge and cyclohexenyl ring C10-C15 102
Figure 4.1.5. Cy_2-Otn(a) with planes through both cyclohexenyl rings (C1-C6 and C10-C15) 102
Figure 4.1.6. Cy_2-Otn(a) with planes through the propyl bridge and cyclohexenyl ring C16-C21 103
Figure 4.1.7. Cy_2-Otn(a) with planes through the propyl bridge and cyclohexenyl ring C25-C30 103
Figure 4.1.8. Cy_2-Otn(a) with planes through both cyclohexenyl rings (C1-C6 and C10-C15) 103
Figure 4.1.9. Cy_2-Otn(a) with planes through the propyl bridge and cyclohexenyl ring C31-C36 104
Figure 4.1.10. Cy_2-Otn(a) with planes through the propyl bridge and cyclohexenyl ring $C31^{i}$-$C36^{i}$ 104

Figure 4.1.11. Cy_2-Otn(a) with planes through both cyclohexenyl rings (C31-C36) 104
Figure 4.1.12. Hydrogen bonding between Cy_2-Otn(a) molecules viewed along the *c*-axis, (hydrogens omitted for clarity) 105
Figure 4.1.13. Crystal packing and hydrogen bonding between Cy_2-Otn(a) molecules viewed along the *a*-axis (hydrogens omitted for clarity) 106
Figure 4.1.14. Crystal packing and hydrogen bonding between Cy_2-Otn(a) molecules viewed along the *b*-axis (hydrogens omitted for clarity) 106
Figure 4.1.15. Crystal packing and hydrogen bonding between Cy_2-Otn(a) molecules viewed along the *c*-axis (hydrogens omitted for clarity) 107
Figure 4.1.16. Cy_2-Otn(a) molecules showing H--H close contact distances between HCH--HCH atoms 108
Figure 4.1.17. Cy_2-Otn(a) molecules showing interactions between HO--HN atoms 109
Figure 4.1.18. The molecular structure of Cy_2-Otn(b), showing the atom-labelling scheme and 50% probability displacement ellipsoids 110
Figure 4.1.19. The molecular structure of Cy_2-Otn(b) with its labelling scheme 110
Figure 4.1.20. Cy_2-Otn(b) with planes through the propyl bridge and cyclohexenyl ring C1-C6 111
Figure 4.1.21. Cy_2-Otn(b) with planes through the propyl bridge and cyclohexenyl ring C10-C15 111
Figure 4.1.22. Cy_2-Otn(b) with planes through the cyclohexenyl rings C1-C6 and C10-C15 112
Figure 4.1.23. Cy_2-Otn(b) with planes through the propyl bridge and cyclohexenyl ring C16-C21 112
Figure 4.1.24. Cy_2-Otn(b) with planes through the propyl bridge and cyclohexenyl ring C25-C30 113
Figure 4.1.25. Cy_2-Otn(b) with planes through the cyclohexenyl rings C16-C21 and C25-C30 113
Figure 4.1.26. Hydrogen-bonding network of Cy_2-Otn(b), viewed along the *b*-axis 114
Figure 4.1.27. Crystal packing of Cy_2-Otn(b), viewed along the *b*-axis (hydrogen atoms omitted for clarity) 114
Figure 4.1.28. The H--H close contacts in Cy_2-Otn(b) 115
Figure 4.1.29. Cy_2-Otn(b) close contacts between the amine hydrogens and alcoholic oxygens in the same molecule 116

Figure 4.1.30. The molecular structure of Cy_2-tn(a), showing the atom-labelling scheme and 50% probability displacement ellipsoids 117
Figure 4.1.31. The molecular structure of Cy_2-tn(a) showing the atom-labelling scheme 118
Figure 4.1.32. Cy_2-tn(a) molecule showing planes through the propyl bridge and the cyclohexenyl rings, and the angles between these planes 118
Figure 4.1.33. Cy_2-tn(a) viewed along the *a*-axis 119
Figure 4.1.34. Crystal packing and hydrogen bonding of Cy_2-tn(a) viewed along the *b*-axis 119
Figure 4.1.35. Crystal packing and hydrogen bonding of Cy_2-tn(a) viewed along the *c*-axis 120
Figure 4.1.36. Cy_2-tn(a) H--H close contacts and NH--O interactions 120
Figure 4.1.37. The molecular structure of Cy_2-tn(b), showing the atom-labelling scheme and 50% probability displacement ellipsoids 121
Figure 4.1.38. The molecular structure of Cy_2-tn(b) with its labelling scheme 122
Figure 4.1.39. Cy_2-tn(b) molecule showing planes through the propyl bridge and the cyclohexenyl rings, and the angles between these planes 122
Figure 4.1.40. Cy_2-tn(b) hydrogen bonding network 123
Figure 4.1.41. Cy_2-tn(b) hydrogen bonding viewed along the *a*-axis 123
Figure 4.1.42. Cy_2-tn(b) H--H close contact interactions 124
Figure 4.3.1. The molecular structure of the Cy_2-tn/Ni complex, showing the atom-labelling scheme and 50% probability displacement ellipsoids 127
Figure 4.3.2. The molecular structure of the Cy_2-tn/Ni complex with its labelling scheme 128
Figure 4.3.3. Cy_2-tn/Ni complex with planes through the donor atoms of the ligands 128
Figure 4.3.4. Hydrogen bonding of the Cy_2-tn/Ni complex viewed along the *a*-axis 129
Figure 4.3.5. Hydrogen bonding in the Cy_2-tn/Ni complex viewed along the *b*-axis 129
Figure 4.3.6. H--H close contacts in the Cy_2-tn/Ni complex 130
Figure 4.3.7. The molecular structure of the Cy_2-tn/Zn complex, showing the atom-labelling scheme and 50% probability displacement ellipsoids 131
Figure 4.3.8. The molecular structure of the Cy_2-tn/Zn complex with its labelling scheme (hydrogen atoms omitted for clarity) 132
Figure 4.3.9. Cy_2-tn/Zn complex with a plane through the ligand donor atoms 132
Figure 4.3.10. Hydrogen bonding in the Cy_2-tn/Zn system viewed along the *a*-axis 133

Figure 4.3.11. Hydrogen bonding in the Cy_2-tn/Zn system viewed along the *c*-axis 134
Figure 4.3.12. H--H close contacts in the Cy_2-tn/Zn complex 134
Figure 4.3.13. The molecular structure of the Cy_2-tn/Cu complex, showing the atom-labelling scheme and 50% probability displacement ellipsoids (hydrogens omitted for clarity) 136
Figure 4.3.14. The molecular structure of the Cy_2-tn/Cu complex with its labelling scheme (hydrogen atoms omitted for clarity) 136
Figure 4.3.15. Cy_2-tn/Cu complex with a plane through the ligand donor atoms 137
Figure 4.3.16. Crystal packing and hydrogen bonding in the Cy_2-tn/Cu complex, viewed along the *b*-axis 138
Figure 4.3.17. Hydrogen bonding in the Cy_2-tn/Cu complex viewed along the *a*-axis 138
Figure 4.3.18. H--H close contacts in the Cy_2-tn/Cu complex 139
Figure 4.3.19. The molecular structure of the Cy_2-tn/Cd complex with its labelling scheme (hydrogen atoms omitted for clarity) 141
Figure 4.3.20. Cy_2-tn/Cd dimmer showing planes through the coordinated ligand donor atoms 142
Figure 4.3.21. Cy_2-tn/Cd dimer showing cyclohexenyl ring twisting 142
Figure 4.3.22. Cy_2-tn/Cd dimer hydrogen bonding viewed along the *b*-axis 143
Figure 4.3.23. Cy_2-tn/Cd dimer hydrogen bonding viewed along the *c*-axis 143
Figure 4.3.24. H--H close contacts in the Cy_2-tn/Cd dimmer 144
Figure 5.2.1. The ligand Cy_2-Otn 157
Figure 5.2.2. Experimental (blue) and calculated (pink) protonation curves from the atutotitration of Cy_2-Otn (L7) 158
Figure 5.2.3. Speciation diagram of the autotitration of Cy_2-Otn (L7) 158
Figure 5.2.4. Experimental (blue) and calculated (pink) protonation curves of the autotitration of the starting amine 1,3-diamino-2-poropanol 159
Figure 5.2.5. Experimental (blue) and calculated (pink) protonation curves of the reverse autotitration of Cy_2-Otn (L8) 160
Figure 5.2.6. Speciation diagram of the reverse autotitration of Cy_2-Otn (L8) 161
Figure 5.2.7. Experimental (blue) and calculated (pink) protonation curves of the reverse autotitration of Cy_2-Otn (L7c), with new $NaNO_3$ 161
Figure 5.2.8. Species distribution diagram of Cy_2-Otn (L7c) with new $NaNO_3$ 162
Figure 5.2.9. Experimental (blue) and calculated (pink) potentiometric complex formation curves of Cy_2-Otn/Cu(II) system 165

Figure 5.2.10. Species distribution diagram of Cy_2-Otn/Cu(II) 166

Figure 5.2.11. Experimental (blue) and calculated (pink) potentiometric complex formation curves of Cy_2-Otn/Ni(II) system 167

Figure 5.2.12. Species distribution diagram of Cy_2-Otn/Ni(II) 168

List of Tables

Table 1.1.1. Several common Lewis acids and bases and their classes 3

Table 1.2.1. Selected log *K* values for a five-membered ring system, a six-membered ring system, and the acyclic equivalent in complexations with metal ions 8

Table 1.4.1. Methods available for determining complex equilibrium constants 12

Table 2.1.1. List of chemicals used with suppliers 45

Table 2.3.1. Masses and volumes used to synthesise Cy_2-Otn (L1-4) 50

Table 2.3.2. Masses and volumes used to synthesise Cy_2-Otn (L5-8) 52

Table 2.3.3. Crystal data and structure refinement for Cy_2-Otn 55

Table 2.3.4. Masses and volumes used to synthesise Cy_2-tn 57

Table 2.3.5. Crystal data and structure refinement for Cy_2-tn(a) 58

Table 2.3.6. Crystal data and structure refinement for Cy_2-tn(b) 59

Table 2.5.1. Crystal data and structure refinement for Cy_2-tn/Ni(II) complex 71

Table 2.5.2. Crystal data and structure refinement for Cy_2-tn/Zn(II) complex 74

Table 2.5.3. Crystal data and structure refinement for Cy_2-tn/Zn(II) complex 77

Table 3.2.1. Characterisation of ionic, covalent, and M-L/M-M interactions 82

Table 3.2.2. Selected M-L bond lengths of the crystal structures and DFT calculations of Cy_2-tn/Ni, Cy_2-tn/Zn, TCA/Cu, and Cy_2-tn/Cu complexes 83

Table 3.2.3. Charge on the metal atom (q(A) and the electron transfer from the ligand to the metal (ΔQ) 92

Table 4.1.1. Cy_2-Otn(a) H-H bond distances and torsion angles between HCH--HCH atoms 108

Table 4.1.2. Cy_2-Otn(a) interaction distances and angles between HO--HN atoms 109

Table 4.1.3. H--H close contacts for the Ligand Cy_2-Otn(b) 115

Table 4.1.4. Cy_2-Otn(b) interaction distances and angles between HO-HN atoms 116

Table 4.1.5. Cy_2-tn(a) interaction distances and angles between HO-HN and HCH--HCH atoms 121
Table 4.1.6. Cy_2-tn(b) interaction distances and angles between HCH--HCH atoms 124
Table 4.3.1. H--H close contacts for the Cy_2-tn/Ni complex 130
Table 4.3.2. H--H close contacts for the Cy_2-tn/Zn complex 135
Table 4.3.3. H--H close contacts for the Cy_2-tn/Cu complex 139
Table 4.3.4. H--H close contacts for the Cy_2-tn/Cd complex 144
Table 4.3.5. H--H close contacts distances and angles between HCH--HCH atoms in the Cy_2-tn polymorphs and the metal complexes 147
Table 5.1.1. List of chemicals used and their suppliers 149
Table 5.1.2. Experimental data of the standardisation of 0.05 and 0.01 M NaOH solutions 152
Table 5.1.3. Experimaental data of the standardisation of 0.05 and 0.01 M HNO_3 solutions 153
Table 5.2.1. ESTA data for 1,3-diamino-2-propalnol and Cy_2-Otn 163
Table 5.2.2. Selected log *K* values for a five-membered ring system, a six-membered ring system, and the acyclic equivalent in complexation with metal ions 170

Abbreviations

APCI	Atmospheric Pressure Chemical Ionisation Mass Spectrometry
BCP	Bond critical point
BHEEN	N,N'-bis(2-hydroxyethyl)ethylenediamine
CGE	Combination glass electrode
Cyp_2-en	N,N'-bis(2-hydroxycyclopentyl)ethylenediamine
Cy_2-dien	N,N'-bis(2-hydroxycyclohexyl)diethylenetriamine
Cy_2-en	N,N'-bis(2-hydroxycyclohexyl)ethylenediamine
Cy_2-Otn	2,2'-[(hydroxypropane-1,3-diyl)diimino]dicyclohexanol
Cy_2-tn	N,N'-bis(2-hydroxycyclohexyl)-1,3-propanediamine
DFT	density functional theory
DMF	Dimethylformamide
EDTA	Ethylenediaminetetraacetic acid
en	Ethylenediamine
ESI	Electrospray Ionisation Mass Spectrometry
ESTA	Computer programme *Equilibrium Simulation and Titration Analysis*
GE	Glass electrode
GEP	Glass electrode potentiometry
IR	Infra-Red
KHP	Potassium hydrogen phthalate
NMR	Nuclear Magnetic Resonance
QTAIM	Quantum Theory of Atoms in Molecules
RCP	Ring critical point
r.m.s	root-mean-square
TCA	N,N'-bis(2-hydroxycyclohexyl)-trans-cyclohexane-1,2-diamine
THEEN	Bis[N,N,N',N'-tetrakis-(2-hydroxyehtyl)ehtylenediamine]
XRD	X-Ray Diffraction

Preliminaries

Abstract **i**

Acknowledgements **ii**

List of Figures **iii**

List of Tables **ix**

Abbreviations **xi**

Chapter 1 Introduction **1**

1.1 Complex Formation **1**

1.2 Ligand Design **4**

1.3 Metal Complexes in Solution **10**

1.4 Potentiometry and Stability Constants **11**

1.5 Chelation Therapy **13**

1.6 Transition Metal Chemistry **14**

1.6.1 Copper Chemistry 14

1.6.2 Nickel Chemistry 15

1.6.3 Zinc Chemistry 15

1.6.4 Cadmium Chemistry 15

1.6.5 Lead Chemistry 15

1.7 Literature Survey **17**

1.8 Stability Constant Measurement by Glass Electrode Potentiometry **29**

1.9 X-ray Diffraction **31**

1.10 Density Functional Theory **33**

1.11 Objectives and Scope of the Research Project **40**

1.12 References **41**

Chapter 2 Materials and Methods **45**

2.1 Materials **45**

2.2 Physical Techniques of Characterisation **46**

2.2.1 Nuclear Magnetic Resonance Spectroscopy (NMR) 46

2.2.2 Electrospray Ionization (ESI) or Atmospheric Pressure Chemical Ionization (APCI) – Mass Spectrometry 47
2.2.3 Infra-Red Spectroscopy (IR) 47
2.2.4 Single Crystal X-Ray Diffraction (XRD) 48
2.3 Synthesis of the Free Ligands 49
2.3.1 Synthesis of Cy_2-Otn 50
2.3.2 Synthesis of Cy_2-tn 56
2.4 Synthesis of the Cy_2-Otn/Metal Complexes 60
2.4.1 Synthesis of the Cy_2-Otn/Cu Complex 60
2.4.2 Synthesis of the Cy_2-Otn/Ni Complex 62
2.4.3 Synthesis of the Cy_2-Otn/Zn Complex 63
2.4.5 Synthesis of the Cy_2-Otn/Cd Complex 65
2.4.6 Synthesis of the Cy_2-Otn/Pb Complex 67
2.5 Synthesis of the Cy_2-tn/Metal Complexes 68
2.5.1 Synthesis of the Cy_2-tn/Cu Complex 68
2.5.2 Synthesis of the Cy_2-tn/Ni Complex 70
2.5.3 Synthesis of the Cy_2-tn/Zn Complex 73
2.5.4 Synthesis of the Cy_2-tn/Cd Complex 75
2.5.5 Synthesis of the Cy_2-tn/Pb Complex 78
2.6 References 79

***Chapter 3 Density Functional Theory* 80**
3.1 Computational Methods 80
3.2 Results and Discussion 81
3.2.1 Modelling of the Free Ligand Cy_2-tn 81
3.2.2 Modelling of TCA/Cu and Cy_2-tn with Ni(II), Zn(II), and Cu(II) 82
3.2.3 QTAIM Molecular Graphs 93
3.3 Conclusions 95
3.4 References 97

Chapter 4 Results and Discussion **98**

4.1 Synthesis and Characterisation of the Free Ligands **99**

4.1.1 Synthesis of Cy_2-Otn 99

4.1.2 Synthesis of Cy_2-tn 117

4.1.3 Comparison of the Ligands Cy_2-tn and Cy_2-Otn 124

4.2 Synthesis and Characterisation of the Cy_2-Otn/Metal Complexes **126**

4.3 Synthesis and Characterisation of the Cy_2-tn/Metal Complexes **127**

4.3.1 Synthesis of the Cy_2-tn/Ni Complex 127

4.3.2 Synthesis of the Cy_2-tn/Zn Complex 131

4.3.3 Synthesis of the Cy_2-tn/Cu Complex 135

4.3.4 Synthesis of the Cy_2-tn/Cd Complex 140

4.3.5 Comparison of the Cy_2-tn/Metal Complexes 145

4.4 References **147**

Chapter 5 Potentiometry **148**

5.1 Materials and Method **148**

5.1.1 Solution Preparation 149

5.1.2 Glass Electrode Potentiometry Experimental Set-up 150

5.1.3 Experimental 151

5.1.4 Analysis of Potentiometric Data 154

5.2. Results and Discussion **157**

5.2.1 Protonation Constants of Cy_2-Otn 157

5.2.2 Cy_2-Otn/Metal Stability Constants 164

5.3 Conclusions **171**

5.4 References **172**

Chapter 6 Conclusions and Future Work **173**

Appendices **175**

Appendix A: DFT Data 175

Appendix B: NMR Data 180

Appendix C: MS Data 190
Appendix D: IR Data 206
Appendix E: XRD Data 226

Chapter 1

Introduction

1.1. Complex Formation

The complexation chemistry of metal ions in solution is vitally important, especially in metallurgical, environmental and biological areas. The ligands used in complexation chemistry are of particular importance, especially when dealing with metal ion selective complexes in solution. Selective metal ion complexation is widely used in treating heavy metal poisoning, antibiotic drug design, biological imaging agents, hydrometallurgical selective metal extractants, and the removal of metals from solution in detergents.[1]

The complexation of metals involves a ligand (L) which contains at least one, but may have many, electron donor groups that bind to a central atom or ion that is usually the metal (M) but may be any electron acceptor. The *denticity* of the ligand is used to describe the number of donor groups on the ligand available for metal binding; a unidentate ligand has one donor group available, whereas polydentate ligands have many donors. The ligand donor groups donate some of their electron density to the electron-deficient metal, creating a bond between the metal and ligand which stabilises the metal, making it less reactive; this can remove the metal from the system or solution. Polydentate ligands generally form more stable complexes than unidentate ligands. The choice of the donor atom in the ligand used is based on the hard and soft acid and base (HSAB) principles of Pearson.[2] His principle is based on the concept that a metal acts as a Lewis acid (electron acceptor), and a ligand acts as a Lewis base (electron donor). The general equation that describes the behaviour of Lewis acids and bases, in solution, A and :B, and the resulting complex, A:B, is:

$$A(aq) + B(aq) \rightarrow AB(aq) + nH_2O \qquad \textbf{(1)}$$

Hard acids (metal ions) have a small ionic radius, are highly charged and have fairly stable, unpolarisable valence electrons; these include the alkali metals, alkali earth metals, and

the lighter transition metals in their higher oxidation states. Hard bases contain the smaller electronegative atoms that are not easily polarised or oxidised, and often have inaccessible, empty high energy orbitals, such as O, N, F and Cl. Hard acids form the most stable complexes with hard bases and the bonding between them is predominantly ionic, although they are π donors that back donate electrons to stabilise the positive charge on the metal.[2]

Soft acids have a large ionic radius, lower oxidation states and a readily polarisable electron cloud; these include the heavier transition metals, and the transition metals in their lower oxidation state. Soft bases are the larger, less electronegative, more polarisable and oxidisable atoms that have accessible, empty low energy, orbitals such as S, Se, P, C and As.[3] Soft acids form their most stable complexes with soft bases as they are π acceptors and can accept electrons from the metals which are soft and relatively electron rich; this bonding has significant covalent character.

The classification of acids or bases as hard or soft depends on the energy differences between the highest occupied molecular orbital (HOMO) and the lowest unoccupied molecular orbital (LUMO). In hard species, there is a large gap between the HOMO and LUMO orbitals, which makes them hard to polarise, whereas soft species have much smaller HOMO-LUMO gaps.[4] Some common Lewis acid and bases and their respective classification are given in Table 1.1.1.

Table 1.1.1. Several common Lewis acids and bases and their classes.[5]

Acids	
Class *a* / Hard Acids	Class *b* / Soft Acids
H^+, Li^+, Na^+, K^+	Cu^+, Ag^+, Au^+, Tl^+, Hg^+, Cs^+
Be^{2+}, Mg^{2+}, Ca^{2+}, Sr^{2+}, Sn^{2+}	Pd^{2+}, Cd^{2+}, Pt^{2+}, Hg^{2+}
Al^{3+}, La^{3+}, Cr^{3+}, Co^{3+}, Fe^{3+}, As^{3+}	I^+, Br^+, HO^+, RO^+
$BeMe_2$, BF_3, BCl_3, $B(OR)_3$	I_2, Br_2, INC, etc.
$Al(CH_3)_3$, $Ga(CH_3)_3$, $In(CH_3)_3$	O, Cl, Br, I, R_3C
SO_3, R_3C^+, RCO^+, CO_2, NC^+	M^0 (neutral metals), Bulk metals
Borderline Acids	
Fe^{2+}, Co^{2+}, Ni^{2+}, Cu^{2+}, Zn^{2+}, Pb^{2+}, $B(CH_3)_3$, SO_2, NO^+	
Bases	
Class *a* / Hard Bases	Class *b* / Soft Bases
H_2O, OH^-, F^-	R_2S, RSH, RS^-, H^-, R^-
$CH_3CO_2^-$, PO_4^{3-}, SO_4^{2-}	I^-, SCN^-, $S_2O_3^{2-}$
Cl^-, CO_3^-, ClO_4^-, NO_3^-	R_3P, R_3As, $(RO)_3P$
ROH, RO^-, R_2O, NH_3, RNH_2, N_2H_4	CN^-, RNC, CO, C_2H_4, C_6H_6
Borderline Bases	
$C_6H_5NH_2$, pyridine, N_3^-, Br^-, NO_2^-, SO_3^{2-}, N_2	

The stability of the M–L complexes is a result of σ donation of the ligand donor atoms. It is also possible to have a multiple bond system such as a π-bond in the ligand that acts as the electron-donor. Added stability can arise from back donation of the metal's electrons to empty π orbitals on the ligand donor atom. Complex formation is enthalpically and entropically controlled; soft-soft complex formations are often enthalpically favoured and hard-hard complex formations are often entropically favoured.[6]

1.2. Ligand Design

Ligand design is extremely complicated and it depends on many factors. This includes size-match selectivity for metal ions in macrocycles, which is ensuring that the size of the metal ion selected fits into the cavity in the macrocycle. Another factor is pre-organisation, where ligands which have a conformation closely matching that in the metal complexes tend to have higher complex formation constants and are said to be pre-organised for complex formation.[6] Other factors such as ligand denticity, chelate ring size, displacement of other ligands or solvation spheres in solution complexes, and steric interactions around the metal, must be taken into account.[1]

The 'chelate effect' is of particular importance in ligand design. It involves a ligand with at least two bridged electron-donating groups, and these groups bond to and incorporate the metal ions in a partially or completely closed chelate ring. If the ligand is a cyclic molecule with three or more donor atoms in a ring, it is termed a *macrocyclic ligand*. The complexes formed with this kind of ligand are usually more stable than those with chelating ligands.[7] Chelate ligands need to be able to sterically accommodate the metal to be complexed or complexation will be unfavourable. The chelate ligand can also be designed to selectively bind to a specific metal ion over other metal ions. This chelate ring formation leads to a decrease in the reactivity of the metal ion forming a stable complex that can be safely removed from the system, as in the case of heavy metal poisoning.[8] The chelate effect is mainly entropically driven and may arise from a number of factors. One such factor could be from variations in bonds due to the electron donor abilities of the ligand or the electron acceptor abilities of the metal ion. Other factors could be steric and electrostatic repulsion between ligand and donor groups in the complex, or the comformation of the free ligand. The ligand field effects as well as the coulombic forces involved in chelate ring formation may also contribute to the entropy.[9] The chelate effect can also, to a lesser degree, be enthalpically driven, relating to the number, size and arrangement of chelate rings, as well as the difference in confugurational entropy between free and coordinated ligand.[9]

This can be seen by looking at the stability of chelate complex formation when compared to its acyclic analogue. An example of this is ammonia and ethylenediamine (en). In

the equilibrium, $[Co(NH_3)_6]^{2+}$ + 3en $\rightleftharpoons$ $[Co(en)_3]^{2+}$ + $6NH_3$, entropic effects pushes the equilibrium to the right. Once the chelating agent has bonded to the metal centre, it is less likely to be removed from the metal completely when compared to the acyclic analogue. This is because there is more than one M–L bond and even if one of the chelating bonds is broken, there is a second bond that keeps the ligand connected to the metal. The free arm has limited mobility due to the remaining bonds, and is more likely to reform the bond to the metal ion. The chelating ability of a ligand can be quantified by log *K* values for the reaction **(2)**, in going from the free ligand to the complexed ligand in aqueous solution.[5]

$$M^{n+}(aq) + xL^{m-}(aq) \rightleftharpoons [ML_x]^{(n-xm)+}(aq) + qH_2O \qquad \textbf{(2)}$$

here $q \geq x$, since both the metal and ligand will have to lose water from their solvation sphere.

The chelate effect may be counteracted by adverse energy changes due to necessary conformational variations during complex formation especially when strained rings are formed, showing the advantages of preorganisation.[9] Pre-organisation has entropic advantages as the ligand has fewer degrees of freedom, and enthalpic advantages as complexation may relieve electrostatic repulsion within the ligand.[6]

If there is more than one central atom, the complex formed is said to be *polynuclear*. The polynuclear complexes may be *homo- or heteropolynuclear* depending on whether the metal centres are the same or not.[10] Ligands can also be classified according to their level of pre-organisation. The order of complex stability formed by these ligands generally increases as follows: *unidentate ligands* < *bidentate* < *chelating ligands* < *macrocyclic ligands* < *cryptand ligands* (**Fig. 1.2.1.**).[11]

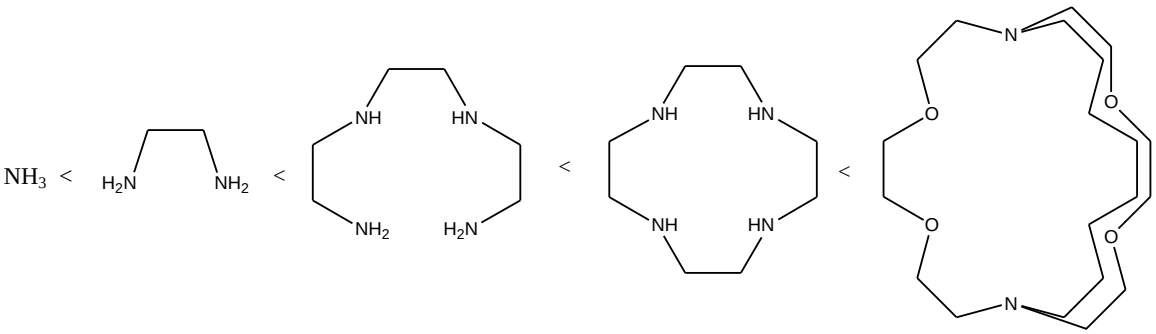


Figure 1.2.1. Increase in complex stability in going from unidentate, to bidentate, to chelate, to macrocycle, to cryptand ligands.

Ligand design is therefore based on making the ligand sterically efficient for a specific metal ion, in order to increase the selectivity of that metal ion over others.[1] The size and coordination number of the metal ion determines the role that steric effects play in complexation. An increase in the number of donor atoms on a ligand favours larger metal ions as they have higher coordination numbers, and can accommodate the extra donor atoms. Addition of alkyl groups can have an inductive effect and donate electron density to the ligand donor atoms which increases the binding ability of the ligand, provided the alkyl groups do not sterically hinder the complex formation.[12] Bridges between the donor atoms on the ligand also play and important role in the steric efficiency of the M–L complex formation. It is found experimentally that the larger metal ions, such as lead and cadmium, favour forming complexes with ligands that contain five-membered rings due to the bite size and angle to minimize steric strain energy on the system, as compared to the formation of a six-membered ring system (**Fig. 1.2.2**.).[13,14] Small metal ions are favoured by ligands that form six-membered chelate rings. This is based on the minimum strain energy chair conformer of cyclohexane. The six-membered chelate ring will have a low strain energy if the metal ion is about the same size and geometry as an sp^3 hybridized carbon. Adjacent five- and six-membered rings produce no steric strain.

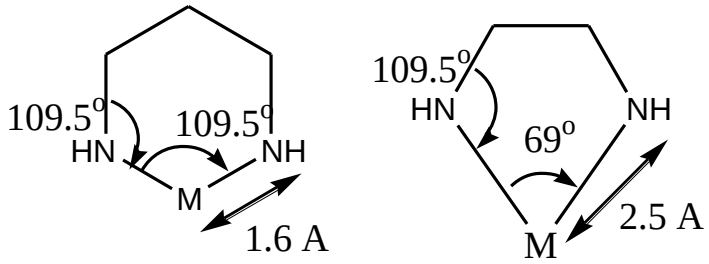
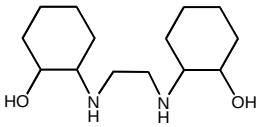
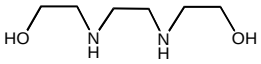
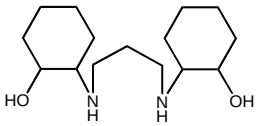
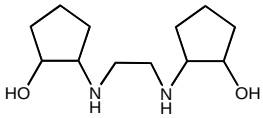
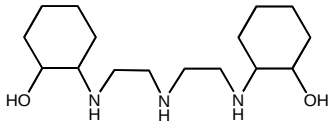


Figure 1.2.2. Ideal geometry for six- and five-membered chelate rings with neutral N-donors.[13,14]

Selected examples of log *K* values for five-membered and six-membered ring systems with metal ions are given in Table 1.2.1. The four metal ions listed are all in the +2 oxidation state and sorted in order of increasing ionic radius. Nickel is the smallest of the metal ions (0.69 Å). The data clearly show that Ni(II) favours complex formation with N,N'-bis(2-hydroxycyclohexyl)ethylenediamine (Cy_2-en) and N,N'-bis(2-hydroxyethyl)ethylenediamine (BHEEN) when compared to N,N'-bis(2-hydroxycyclopentyl)ethylenediamine (Cyp_2-en). The same pattern is observed for the Zn(II) ion (0.74 Å), the Cd(II) ion (0.95 Å), and the Pb(II) ion (1.18 Å).

The addition of a cyclohexenyl ring system to the ligand, as in Cy_2-en when compared to BHEEN, favours the formation of the Cy_2-en complexes. The opposite trend is noted when BHEEN and Cyp_2-en are compared.[5] Both the chelate ring size and the basicity of the ligand are changed and can affect the complex formation.

Table 1.2.1. Selected log *K* values for a five-membered ring system, a six-membered ring system, and the acyclic equivalent in complexations with metal ions.[5,16,17]

Equilibrium	log *K*	Equilibrium	log *K*
L = Cy_2-en = 		L = BHEEN = 	
Cu^{2+} + L ⇌ CuL^{2+}	11.47	Cu^{2+} + L ⇌ CuL^{2+}	9.68
Ni^{2+} + L ⇌ NiL^{2+}	7.75	Ni^{2+} + L ⇌ NiL^{2+}	6.67
Zn^{2+} + L ⇌ ZnL^{2+}	6.27	Zn^{2+} + L ⇌ ZnL^{2+}	4.79
Cd^{2+} + L ⇌ CdL^{2+}	6.15	Cd^{2+} + L ⇌ CdL^{2+}	5.07
Pb^{2+} + L ⇌ PbL^{2+}	6.78	Pb^{2+} + L ⇌ PbL^{2+}	6.12
L = Cy_2-tn = 		L = Cyp_2-en = 	
Cu^{2+} + L ⇌ CuL^{2+}	12.67	Cu^{2+} + L ⇌ CuL^{2+}	6.75
Ni^{2+} + L ⇌ NiL^{2+}	Too slow	Ni^{2+} + L ⇌ NiL^{2+}	3.79
Zn^{2+} + L ⇌ ZnL^{2+}	5.04	Zn^{2+} + L ⇌ ZnL^{2+}	4.52
Cd^{2+} + L ⇌ CdL^{2+}	4.15	Cd^{2+} + L ⇌ CdL^{2+}	3.98
Pb^{2+} + L ⇌ PbL^{2+}	Precipitate	Pb^{2+} + L ⇌ PbL^{2+}	4.85
L = Cy_2-dien = 			
Cu^{2+} + L ⇌ CuL^{2+}	16.74		
Zn^{2+} + L ⇌ ZnL^{2+}	9.57		
Cd^{2+} + L ⇌ CdL^{2+}	9.34		
Pb^{2+} + L ⇌ PbL^{2+}	9.01		

Addition of neutral oxygen donors to a ligand chelate ring increases complex stability of larger metal ions over smaller metal ions, as the oxygen atom prefers a trigonal planar geometry (**Fig. 1.2.3.**).[18] The most stable arrangement of neutral oxygen atoms within the macrocyclic ligands is such that they are *cis* to one another.[16]

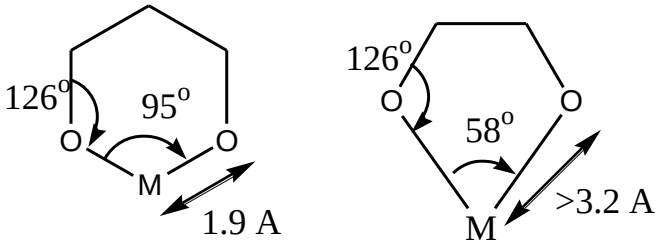


Figure 1.2.3. Ideal geometry for six- and five-membered chelate rings with neutral O-donors.[18]

The negatively charged oxygen donor groups occur in the form of the carboxylate, the phenolate, the hydroxamic acid and the phosphoric acid groups, as well as in ligands such as acetylacetonate, alkoxides and tropolonate to name a few. The effect of the negatively charged oxygen donor on complex stability depends on the acidity (the metal ions affinity for the OH^- ion) of the metal ion considered.[1,19] The selectivity of the ligand for a more acidic metal ion (e.g. Fe(III), Al(III)) over a less acidic metal ion (e.g., Zn(II), Cu(II)) will be increased by an increase in the number and basicity of the charged oxygen groups.[1]

The neutral saturated nitrogen donor show stronger coordinating properties than neutral oxygen donor atoms with many metal ions. The order of basicity toward metal ions is NH_3 < RNH_2 < R_2NH < R_3N in the gas phase.[20] In water, the steric hindrance between the added alkyl groups and waters of solvation leads to a decrease in complex stability along this series.[21] The addition of N-alkyl groups results in increased steric strain, and shows a significant decreases in complex stability and ligand field (LF) strength. The LF strength is a measure of the orbital overlap in the M–L bonds, which decreases with increasing M–L bond lengths, due to the steric crowding caused by N alkyl groups. The N alkyl groups are most stable in a *trans* arrangement.[16,22]

Ligand preference of metal ions is based on HSAB principle as well as the design of the ligand and the electron density on the donor atoms. This plays a role in the ligand field strength, and complex stability. Borderline Lewis acids and bases are strongly affected by the nature of their coordinating ligands; an increase in the electron-donating ability of the nitrogen and oxygen moieties, when fewer carbon groups are present, changes the complexation properties of the acceptor Lewis acids. The way in which the metal binds to the ligand can be seen via single crystal X-ray diffraction. In the absence of crystallographic information, inferences may be made from standard spectroscopic techniques and, increasingly, from computational modelling.

1.3. Metal Complexes in Solution

The properties of the solvent plays an important role in complexation. The pH of the solution can affect the formation of M–L complexes, as the metal has to compete with protons for the donor atoms of the ligand. The ligand also has to displace or compete with the solvation sphere or other ligands the metal is bound to. The complex can either be charged or neutral, and usually retains its identity in solution.[9] Metal ions cannot exist freely in solution due to their charge and size, but they are associated with the counter ion(s), or components of the solution having no-bonding electron pair(s).[10] In aqueous solution, the counter ions are the water molecules. When a ligand bonds covalently to a metal, the complex is known as an *inner-sphere complex*, where ligands replace the water molecules from the inner coordination sphere, forms bonds directly to the metal ion, and occupies a clearly defined space within the coordination shell of the metal. An *outer-sphere complex* is formed when an inner-sphere complex is weakly linked through electrostatic, van der Waals' or hydrogen-bonding to further groups that do not generally occupy specific sites around the metal.[9,19] Outer-sphere complexes are important in the kinetics of complex formation since all complex formations involve the initial formation of an outer-sphere complex, followed by entry of the ligand into the inner-sphere.[23] Figure 1.3.1. shows an example of inner and outer sphere of Ni(II) with water and sulphate.[19]

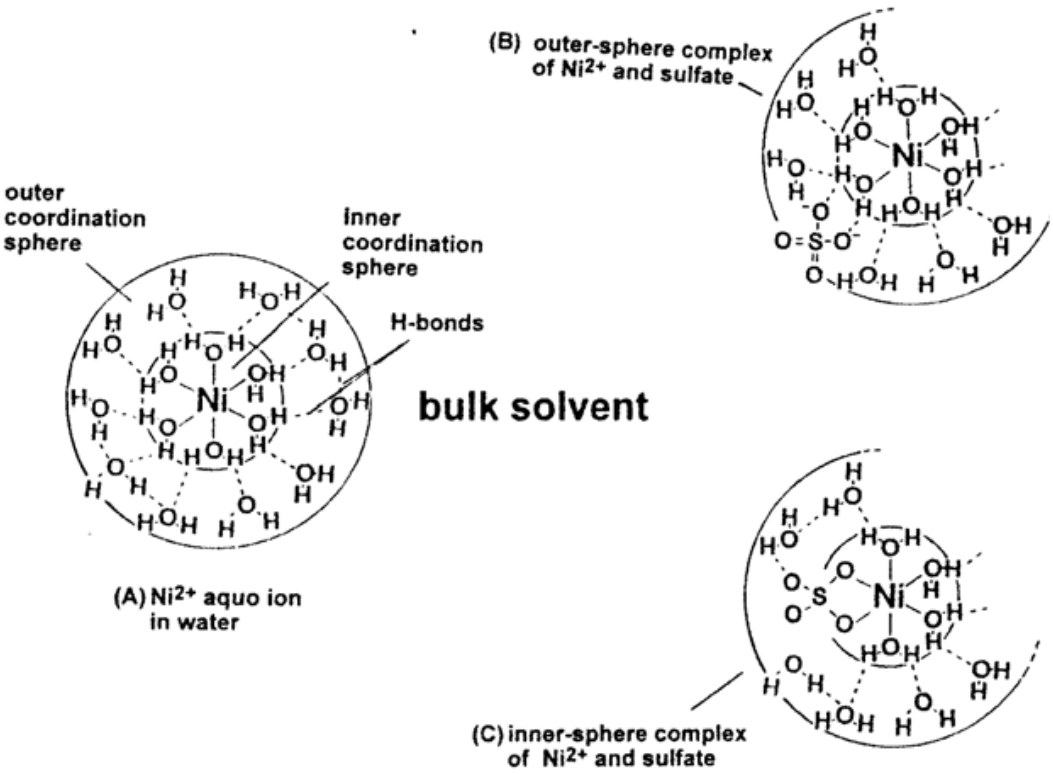


Figure 1.3.1. Example of inner-sphere and outer-sphere complexes.[19]

In the presence of a second ligand, the stepwise substitution of the ligand molecules for the co-ordinated water molecules occurs (**2**). If this second ligand is also a neutral molecule, the charge of the successive complexes is the same as that of the central ion.

1.4. Potentiometry and Stability Constants

There is an equilibrium that exists between metal ions and ligands, and equilibrium constants are important in understanding the behaviour of metal ions in aqueous solutions and the stability of the complexes that may form. The stability constant equation is based on the following reaction:

$$aA + bB \rightleftharpoons cC + dD, \qquad K_{eq} = \frac{a_C^c . a_D^d}{a_A^a . a_B^b} \qquad \textbf{(3)}$$

Because under controlled conditions of temperature and ionic strength, concentrations closely parallel activities in dilute solutions, equilibrium concentration constants can be substituted for activity constants. The equilibrium concentration constant equation is:

$$K'eq = \frac{[C]^c.[D]^d}{[A]^a.[B]^b} \qquad \textbf{(4)}$$

Using the mass balance equations and the concentration of the species involved, the equilibrium constant of formation of the metal ion complexes formed in solution can be calculated.[24] Generally, if the concentration of at least one equilibrium metal complex species can be measured, the equilibrium constants can be calculated using any method. The concentration of that species together with the stoichiometry of the solution allows for the calculation of the concentrations of all species present at the equilibrium.[25] There are many methods used to determine stability constants, but potentiometry is used in this project as approximately 80% of stability constants in literature are measured using this method. Three of the most important reasons for using glass electrode potentiometry as the method of choice, is because most ligands have appreciable basicity and control the hydrogen ion as well as the metal ion concentrations.[19]

Table 1.4.1. Selected methods available for determining complex equilibrium constants.[19]

Standard Methods	
Potentiometry	Spectrophotometry
Ion exchange	Polarography
Ionic conductivity	Colorimetry
Reaction kinetics	Distribution between two phases
Solubility measurements	Partial pressure measurement
Nuclear magnetic resonance spectroscopy	Specific metal ion electrodes
Competition Methods for Strong Complexes	
Ligand-ligand competition measured potentiometrically or spectrophotometrically	
Metal-metal competition measured spectrophotometrically or polarographically	

Stability constants are used in understanding the behaviour of metal ions in solutions, and are important in a wide variety of areas such as biological and biomedical applications, geochemistry and extraction metallurgy, the environment and pollution, analytical and food chemistry.[19] Both plants and animals contain significant quantities of both metal ions and ligands. Some of these metal ions are Na, K, Mg, Ca, Fe, Cu, Zn, etc, which can interact with different ligands found in the human body, such as H_2O, OH^-, Cl^-, HCO^{2-}, SO_4^{2-}, proteins, carbohydrates, carboxylic and nucleic acids, lipids and steroids.[9] During the 1950s it was discovered that a number of metal chelates were active anti-viral agents. Chelating agents have found use as antibiotics due to their ability to form complexes specifically with metal ions.[17] Stability constants of complexes also have an important role in the design of drugs for treatment of metal poisoning.[7]

1.5. Chelation Therapy

Treatment of metal intoxication and clinical diagnosis with imaging agents are two areas where chelating agents are already in use.[26] Ligands designed specifically for selective metal complexation are required in many fields. They are used for the treatment of metal intoxication, as contrast agents in the body, and for the selective extraction of precious metals in hydrometallurgy. Studies are also being done in the field of nuclear medicine and the design of radiopharmaceuticals, where the radionuclides are metals, which have a diagnostic and/or therapeutic application.[27]

Chelation therapy is the use of drugs, known as chelation agents, to bind excess metals in the human body due to illness or poisoning. This excess of metal ions can be due to exposure and uptake of the metals or possibly an inability by the human body to remove excess metal ions from itself. There are several illnesses that lead to heavy metal intoxication and they are easily treated once diagnosed.[5] The chelation agent selectively binds to the metal ion that is to be removed, and transports it from the body. Chelation therapy has been used in the treatment of cancer, heart disease, Alzheimer's disease, and autism.[28]

There are many types of drugs available for chelation therapy today. The most commonly used drug is the chelating agent EDTA or ethylenediaminetetraacetic acid, Figure 1.5.1. The ability of EDTA and its derivatives to form stable complexes with several metal ions allows their use as probes in various areas in chemistry, biology and medicine. Complexation of radioactive metals with EDTA reagents has been used extensivly in medicine.[29] EDTA is the most common chelator that has been used to also reverse the effect of arterial plaque, to preventing further strokes and/or heart attacks.[30] It has also been used in the dental industry for root canal treanment.[31] EDTA has been used in the treatment of Ni(II), Zn(II) and Pb(II) poisoning.[32] Other drugs have recently been developed to be more specific for one metal ion rather than almost all, such as EDTA. This has led to an increase in the research of chelating ligands as potential chelating drugs for human use.

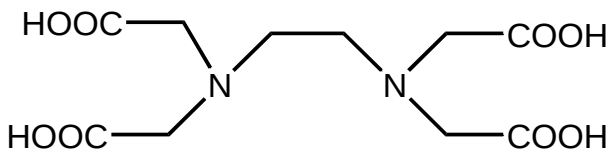


Figure 1.5.1. Ethylenediaminetetraacetic acid, EDTA.

1.6. Transition Metal Chemistry

1.6.1. Copper Chemistry

Copper in its complexes can exist in a +1, +2, +3 and +4 oxidation state but the +1 and +2 oxidation states are most common.[33] Copper can adopt many coordination geometries, but the most common for Cu(II) are distorted octahedral, square planar, square pyramidal, and trigonal bipyramidal.[34] Many Cu(I) complexes are also tetrahedral. Copper is relatively soft, but it does form complexes with hard N and O donors; these complexes are usually blue or green.

1.6.2. Nickel Chemistry

Nickel complexes can have the metal in a -1, 0, +1, +2, +3, and +4 oxidation state, but the most common is the +2 oxidation state.[35] Nickel can adopt many coordination geometries, but the three most common are the six-coordinate octahedral geometry as well as the four-coordinate square planar and tetrahedral geometries. The four-coordinate molecules are generally red or yellow in colour, while the six-coordinate molecules are mostly blue or green.[5] Nickel is a hard metal and would be expected to bind well to the hard O and N donors used in this project.

1.6.3. Zinc Chemistry

Zinc in its complexes only exists in the +2 oxidation state. In its neutral state, zinc has a fully filled d-electron valence shell as well as a filled s electron shell. This makes the metal very stable. The +2 oxidation state is also stable as the d-shell electrons are all paired and the shell is filled. Zinc is a slightly softer metal, although is has been shown to bind equally to hard N and O donors over softer S donors.[36] The expected geometry of zinc is square planar, octahedral and tetrahedral are common, although it can adopt many other coordination geometries, especially in biological systems such as proteins and enzymes.

1.6.4. Cadmium Chemistry

There are only two oxidation states for cadmium, +1 and +2. The +2 oxidation state is the most common. Cadmium is classified as a borderline metal, i.e. it is neither hard nor soft, and as such can bond to both hard and soft ligand donors. Cadmium also has a variety of coordination geometries due to the plasticity of Cd(II).[5]

1.6.5. Lead Chemistry

Lead in its complexes is found in two oxidation states, +2 and +4, with the +2 oxidation state being the more common. In the +2 oxidation state, there is one lone pair of electrons left

and if this lone pair of electrons is stereochemically active, then it will occupy a co-ordination site. Lead is borderline between hard and soft metals, it can therefore bond to both hard and soft donor atoms to form complexes.[37]

Lead can assume many different geometries depending on the nature of the lone pair on Pb(II). These geometries can be classified as either *holodirected* or *hemidirected*. The former are complexes where the ligands are distributed equally around the metal centre, and the latter are complexes where there is a void in the coordination sphere. The most common coordination numbers for Pb(II) are 4 and 6.[38] It is found that *holodirected* Pb(II) complexes usually occur when the coordination number is low (between 2 and 5). The *hemidirected* complexes are more common for the higher coordination numbers (9 and 10), and the intermediate coordination numbers (6 to 8) give a mix of both *holodirected* and *hemidirected* complexes.[38]

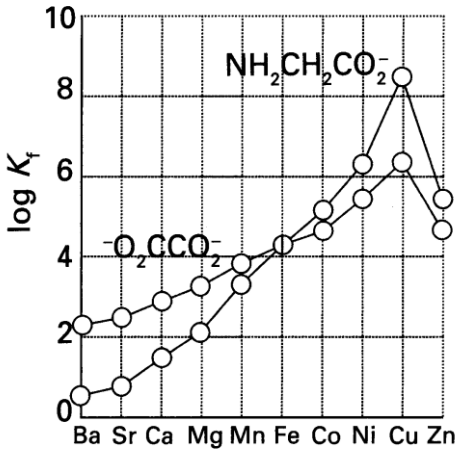


Figure 1.6.1. Irving-Williams series.[2]

If one considers the ionic radii of Ni(II) (69 pm), Cu(II) (73 pm), Zn(II) (74 pm), Cd(II) (95 pm), and Pb(II) (119 pm),[39] Ni(II) only differs from Zn(II) by 5pm. Therefore the steric efficiency of the ligand for nickel should be similar to that of copper and zinc. According to the Irving-Williams series (**Fig. 1.6.1.**), the common trend for divalent metal ions with a given ligand is that as the ionic radius of the metal ion decreases, the stability of the complex increases.[40] Ni(II) is a relatively hard metal ion and therefore forms most stable complexes with the hard bases oxygen and nitrogen in the chosen ligand for this project (**Fig. 1.6.2.**). However copper and zinc are softer metals, and so it would be expected that the complexes formed with

Ni(II) are more stable than those formed with Cu(II) and Zn(II). The ligands used in this project have amine nitrogens connected via a propyl bridge with bulky cyclohexanol substituents on the nitrogens. Based on the design of the Cy_2-Otn and Cy_2-tn ligands, due to the presence of the two 5-membered chelate rings and the two neutral oxygen donor atoms, it is expected that the ligands will favour complex formation of larger metal ions over smaller metal ions.[41] However, the 6-membered chelate ring, adjacent to the two 5-membered rings, is sterically favourable and favours complexes with small metal ions, as does the presence of the two neutral N-donor atoms in the ligands. Studying these ligands aids in identifying the role of the cyclohexyl reinforcenemnts in the ligand backbone, as well as the effects of a propyl bridge compared to that of an ethyl bridge.

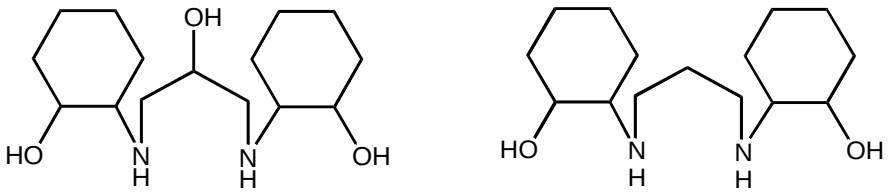


Figure 1.6.2. The ligands Cy_2-Otn and Cy_2-tn, respectively.

1.7. Literature Survey

Amino alcohols are vitally important in synthetic chemistry, due to their synthetic applications and biological properties. They have been used as catalysts in reactions such as the enantioselective alkylation of aldehydes, where an organozinc reagent is added to the aldehyde, and forms a chelate ring with the zinc alkoxide.[42-45] Secondary β-amino alcohols with rigid backbones show high activity and selectivity.[46] Sterically hindered, bicyclic amino alcohols have also been investigated as chiral catalysts in enantioselective alkylation of aldehydes, where the ligand had *trans* disposed aminoalkyl and alcohol groups.[45] Some β-amino alcohols are also used as catalysts in reactions such as asymmetric transfer hydrogenation of ketones. The amino alcohols also react with an achiral metal complex to form the active catalyst.[46] Dilithiated amino alcohols have been used as chiral bases in rearrangement reactions, to form either enantiomer of the product.[47] Structurally rigid *N, N*-disubstituted β-amino alcohols have been used in the

diethylzinc addition to imines, to give high enantioselectivity.[48] *N*-monosubstituted β-amino alcohols, with bulky R groups on the benzene ring, gave high enantioselectivity when used as ligands for the diethyl zinc addition to imines. [48]

Hancock *et al.*[16] investigated the change in selectivity of ligands with ethylene bridges and cyclohexenyl bridges using molecular mechanic (MM) calculations and potentiometric results. The formation constants for Cy_2-tn (Cu(II), Zn(II), Cd(II)), Cy_2-en (Cu(II), Ni(II), Zn(II), Cd(II), Pb(II)), and Cy_2-dien (Cu(II), Zn(II), Cd(II), Pb(II)) complexes were determined using glass-electrode potentiometry (**Table 1.2.1.**). These complexes all showed a higher selectivity for smaller metal ions compared with analogous ligands, where the cyclohexylene bridges of these ligands are replaced by ethylene bridges, as can be seen in Linear Free Energy Relationship diagrams (LFER).[16] The formation constants show the increase in stability of the complexes on adding reinforcing cyclohexcenyl rings to the ethylene bridges. The stability constants also show the ligands preference for smaller metal ions over larger metal ions, due to the presence of the 6-membered chelate ring, compared to the 5-membered chelate ring analog.[16]

In the dissertation *"The Solid State Structure of Metallo-Beta-Amino Alcohol Complexes",*[5] Reisinger synthesized the ligands used in this project, namely (Cy_2-tn) and N,N'-bis(2-hydroxycylcohexyl)2-propanol-1,3-diamine (Cy2-Otn). She reported the crystal structure of the Cy_2-Otn ligand. It crystallized in a monoclinic $P\bar{1}$ space group with two Cy_2-Otn molecules and a water molecule in the asymmetric unit cell. Cy_2-Otn and Cy_2-tn were complexed to Ni(II), Zn(II), Cd(II), and Pb(II), but no crystal structures were obtained. Complexes of these metal ions with Cy_2-en, Cy_2-dien, Cy_2-tn and BHEEN were made. Crystal structures of Cy_2-en, Cy_2-en/Pb(II), Cy_2-en/Cd(II), BHEEN/Cd(II), and BHEEN/Zn(II) were reported.[5]

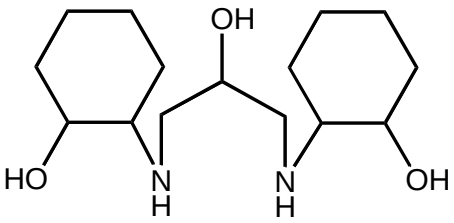


Figure 1.7.1. Cy_2-Otn

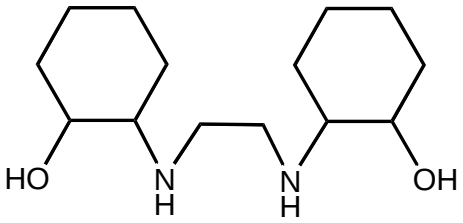


Figure 1.7.2. Cy_2-en

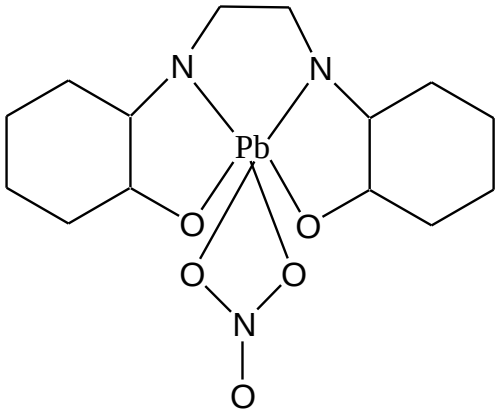


Figure 1.7.3. Cy_2-en/Pb(II)

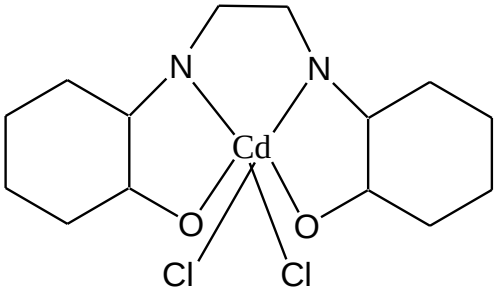


Figure 1.7.4. Cy_2-en/Cd(II)

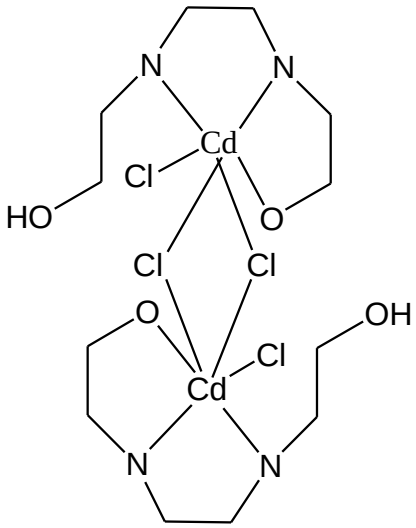


Figure 1.7.5. BHEEN/Cd(II)

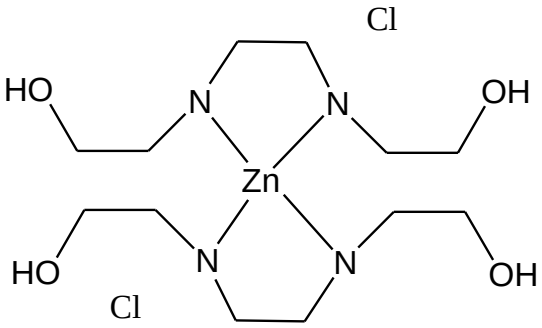


Figure 1.7.6. BHEEN/Zn(II)

Hancock, *et al.*[16] reported the crystal structure of $[Cu(Cy_2\text{-tn})(H_2O)](ClO_4)_2$ complex (**Fig. 1.7.7a.**) where the Cu(II) atom is coordinated in the plane of the ligand to the two N and two O donor atoms, with a long bond to an axially coordinated water molecule and perchlorate ion.[16] An interesting feature of the complex is the short H-H non-bonded interactions between the H atoms on the cyclohexyl bridges and the H atoms on the propyl bridge of the ligand (2.29 and 2.27 Å) as these electrostactic interactions may play a role in metal-ion size-based selectivity (**Fig. 1.7.7b.**).[16] The crystal structure of $[Cu(Cy_2\text{-dien})](ClO_4)_2$ was also reported in this paper.[16]

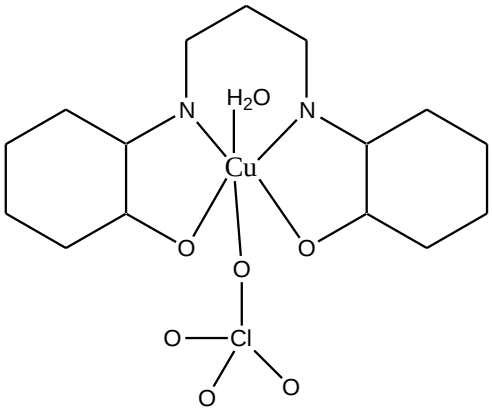


Figure 1.7.7a. N,N'-bis(2-hydroxycylcohexyl)propane-1,3-diamine complexed to copper(II).

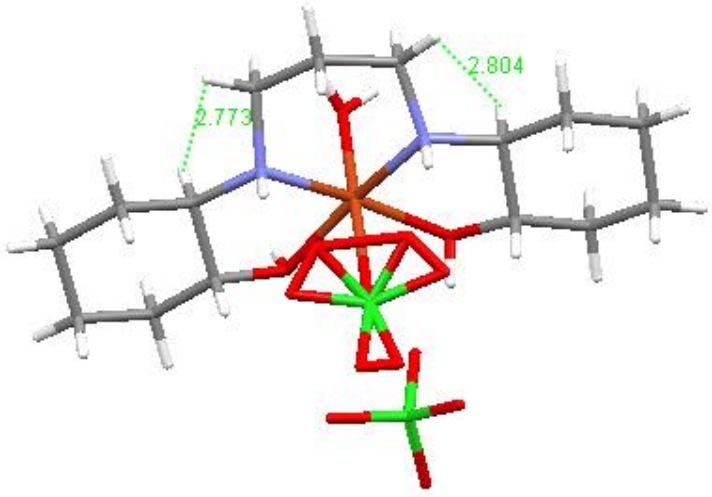


Figure 1.7.7b. Cy_2-tn complexed to copper(II) showing H-H interactions.

There has been considerable research done at the University of the Witwatersrand on the design of chelating agents for potential use in applications such as heavy metal poisoning.[25,50] The dissertation "*Electrochemical Studies of Metal-Ligand Equilibria Involving Chelating Ligands*"[25] looked at determining stability constants of several β-amino alcohol ligands with several metal ions. The ligands consist of those with hydroxycyclohexenyl rings and those with hydroxycyclopentyl rings. The metal ions used in the study were Cu(II), Ni(II), Zn(II), Pb(II) and Cd(II). ML was the dominant species, and ligands with the cyclohexenyl rings form more stable complexes than those with the cyclopentyl rings, due to the greater mobility of the larger rings. ML_2 (minor) complexes were also formed, but only one ML_2 complex is reported for the hydroxycyclopentyl ligands.[49] Ligands with cyclohexyl groups favour smaller metal ions and the cyclopentyl ligands favour larger metal ions (**Table 1.2.1.**).[25]

In another study,[50] the focus was on the chelating ability of several macrocyclic ligands, and molecular mechanics (MM) calculations were performed to find the most suitable chelating ligand as a drug in the treatment of cadmium intoxication. It was found that ligands with amine nitrogen atoms have a marked selectivity for cadmium.

Canepari *et al.*[51] investigated the coordinating power of several β-amino alcohol ligands with Ag(I), Pb(II), Zn(II), and Cd(II) metal ions. It was observed that the hydroxyl groups had an inductive effect predominant for Ag(I), Pb(II), and Zn(II), where as Cd(II) formed weak hydroxo chelates. It was also observed that Ag(I) and Zn(II) systems, on complexation with the β-amino alcohols, had an increased acidity of the bound water molecules with the formation of ternary hydroxyl species, where the stability was dependent of the structure of the ligand.[51]

The behaviour of solutions containing Cu(II) and several β-amino alcohols was also investigated by potentiometric and spectrophotometric techniques. The potentiometric results indicated the ML species coordinate mainly through the primary amino-groups on the ligand as the complex stability correlates with the pK_a values of the ligands. The dependence of complex stability on the ligand structure is seen to increase with the increase in hydroxyl groups present.[51]

A search of the CSD for a fragment of the ligands with any transition metal (**Fig. 1.7.8.**), showed nine structures, but only five with the transition metals that are being looked at in this project. The other structures found were complexes with amino acids, not amino alcohols. A broader search was then conducted.

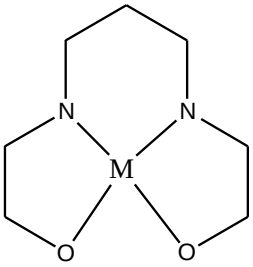


Figure 1.7.8. Fragment of the ligands Cy_2-Otn and Cy_2-tn with any transition metal.

A paper by de Sousa *et al.*[49] continues the investigation of cyclohexenyl bridges in amino-alcohol ligands. The increase in rigidity of the ligand in going from an ethylene bridge to a cyclohexenyl bridge causes the latter ligands to favour complexation of smaller metal ions.[49] Increasing the number of hydroxypropyl groups over hydroxyethyl groups results in an increased stability, as the inductive effects of the additional electron donating methyl groups makes the O-donor a better nucleophile and more attracted to an electron deficient metal ions. de Sousa *et al.*[52] reported the crystal structure of one of these ligands, and the log *K* values for both THEEN and THPED with Co(II), Cu(II), Ni(II), Zn(II) and Cd(II). The complex of Cu(II) with THEEN formed a dimeric species (**Fig. 1.7.9.**). The [Cu(II)THEEN] monomers are bonded by two M-O-M bridges, and the geometry of the coordination sphere around the Cu(II) ion is distorted octahedron.[52]

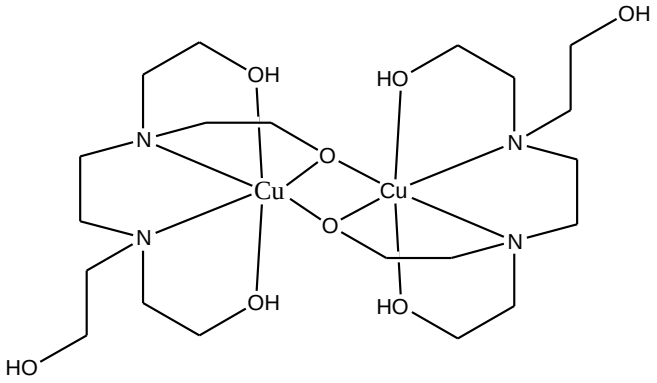


Figure 1.7.9. bis[N,N,N',N'-tetrakis-(2-hydroxyehtyl)ehtylenediamine]copper(II) perchlorate (THEEN).

Bermhardt *et al.*[53] isolated a trinuclear copper(II) complex of a polyamino alcohol ligand that exhibits a structure similar to that found at the active site of ascorbate oxidase. The synthesis of the trinuclear copper complex (5-hydroxy-3,7-diazanonane-1,9-diamine)-copper(II) diperchlorate as a minor product from the reaction is reported, and the major product was crystallised as its perchlorate salt (**Fig. 1.7.10.**). The crystal structure consists of pairs crystallographically independent metal-ligand cations and perchlorate anions. There are no significant differences between the cations, and the uncoordinated hydroxyl group is axially disposed with respect to the six-membered chelate ring. [53]

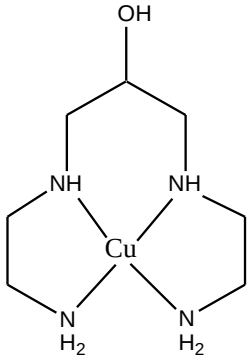


Figure 1.7.10. (5-Hydroxy-3,7-diazanonane-1,9-diamine)-copper(II) diperchlorate.

La-Sheng Long *et al.*[54] found the crystal structure of $[Cu(BIPO)(H_2O)(ClO_4)](ClO_4).H_2O$ showed an elongated octahedral geometry where the axial positions were occupied by an aqua and a perchlorate molecule (**Fig 1.7.11.**).[54]

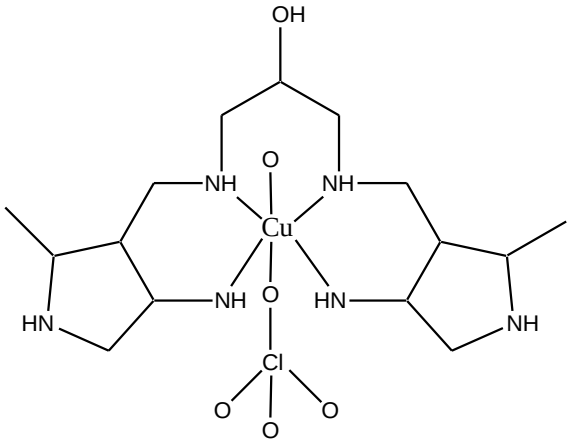


Figure 1.7.11. 1,3-bis[(4-methyl-5-imidazol-1-yl)ethylideneamino]propan-2-ol complexed to copper(II).

Pal *et al.*[55] found that the crystal structure of [Cu(BIPO)Cl] was a distorted square pyramidal geometry, with the four nitrogen atoms of the tetradendate ligand in a plane, and the axial position occupied by a chloride ion (**Fig 1.7.12.**).[55]

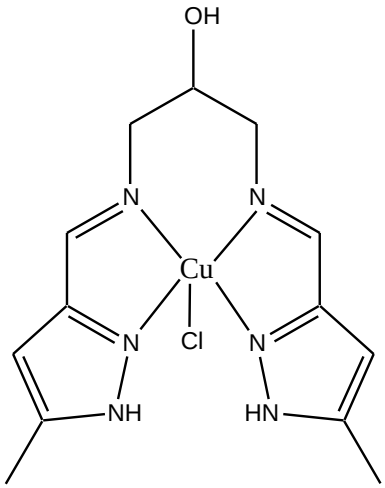


Figure 1.7.12. 1,3-bis(5-methyl-3-formylpyrazolylmethinimino)propane-2-ol chloride complexed to copper(II).

Tanase *et al.*[56] found that the Cu^{2+} complex with BHEEN showed a square pyramidal structure where one chloride ion and three donor atoms on the potentially tetradentate ligand BHEEN (through two nitrogens and one oxygen) were included in the equatorial plane and the other chloride occupies the axial site (**Fig. 1.7.13.**).[56]

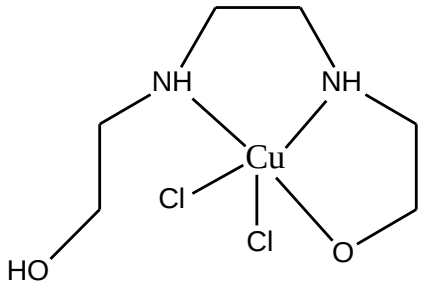


Figure 1.7.13. [Cu(BHEEN)Cl_2] complex.

Xie *et al.*[57] found that the crystal structure of [Cu(2,2'bpy)(1,2-bis((2-hydroxyethyl)amino)ethane)] showed that the mixed ligand complex was a distorted square pyramidal, with ClO_4^- counter anions (**Fig. 1.7.14.**).[57]

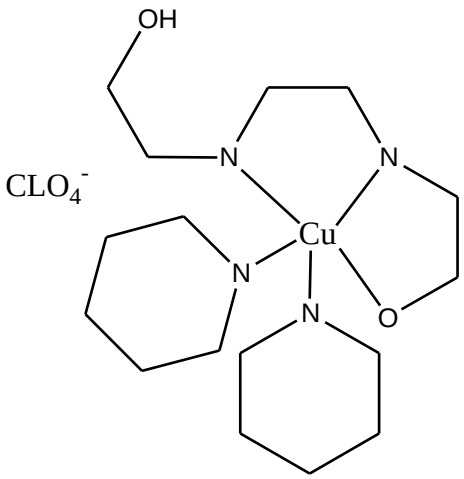
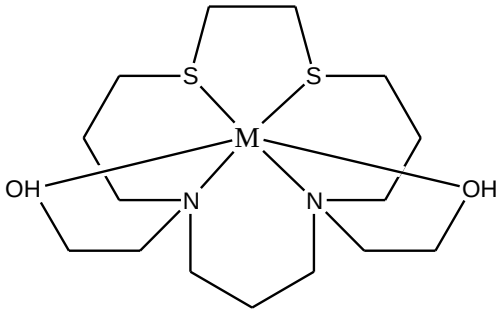


Figure 1.7.14. [Cu(2,2'bpy)(1,2-bis((2-hydroxyethyl)amino)ethane)] complex.

Based on this literature survey, the expected structure of the 2,2'-[(hydroxypropane-1,3-diyl)diimino]dicyclohexanol (Cy_2-Otn) complex with copper would have a octahedron geometry, and likely incorporate a coordinated solvent molecule or anion. Determination of the stability of the complex and crystal structure of Cy_2-Otn complex with copper via single crystal X-ray diffraction will determine the geometry of the complex.

Mattes *et al.*[58] investigated the macrocyclic ligand 6,10-bis(2-hydroxyethyl)-7,8,9,11,17,18-hexahydro-dibenzo-[e,n][1,4,8,12]-dithiadiaza-cyclopentadecine (X) formed the stable complexes $[NiX](ClO_4)_2 \cdot MeOH$, and *rac*-$[CuX](ClO_4)_2 \cdot MeOH$ (**Fig. 1.7.15.).** The characterization of the compounds showed that in the complexes**,** the metal atoms are octahedrally coordinated by the $N_2O_2S_2$ donor set of the ligands. The ligand (X) is folded along the N···M···S axis, this results in the metal atom being in a *all-cis*-configuration.[58]



M = Ni, Cu

Figure 1.7.15. 6,10-bis(2-hydroxyethyl)-7,8,9,11,17,18-hexahydro-dibenzo-[e,n][1,4,8,12]-dithiadiaza-cyclopentadecine complexed to Ni(II) and Cu(II).

Adam *et al.*[59] reported the interaction of O_2N_2-donor macrocycles that incorporated pendant hydroxyethyl or carbamoylethyl arms with Co(II), Ni(II), Cu(II), Zn(II) and Cd(II). The thermodynamic stabilities of the ML complexes of these macrocycles were determined potentiometrically. X-Ray diffraction studies of five Ni(II) complexes show the complexes containing 14-, 15- and 16-membered rings and two pendant alcohol arms, have similar distorted-octahedral structures. All the complexes showed the nickel ion positioned outside the macrocyclic ring, and only coordinated to the ring nitrogen atoms and the pendant alcohol oxygen atoms (**Fig. 1.7.16.**). However, the structure of the related 15-membered, mono-pendant arm derivative has the nickel in the macrocyclic cavity.[59]

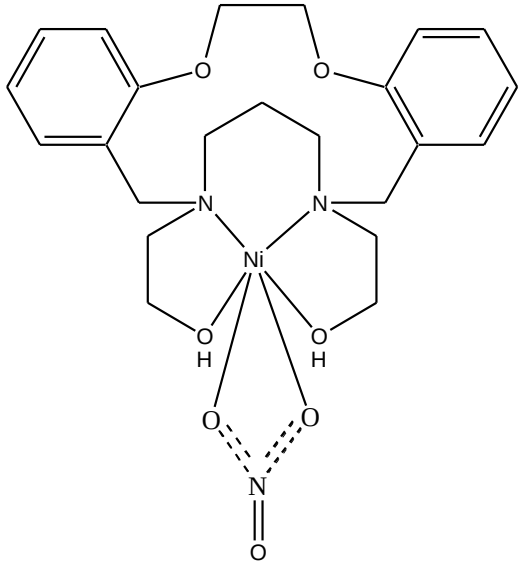


Figure 1.7.16. (Nitrato-O,O')-(8,9,17,18-tetrahydro-5H-dibenzo(e,n)(1,4,8,12) dioxadiazacyclopentadecine-6,10(7H,11H)-diethanol)-nickel(II) nitrate.

Lee *et al.*[60] found the coordination geometry about Ni^{2+} in $[Ni(bchtn)(H_2O)_2]CI_2$ was a pseudo-octahedron comprising of two oxygen atoms from amide groups and two nitrogen atoms from amine groups at the four corners of the equatorial plane and two oxygen atoms of water molecules at the axial positions (**Fig. 1.7.17.**).[60]

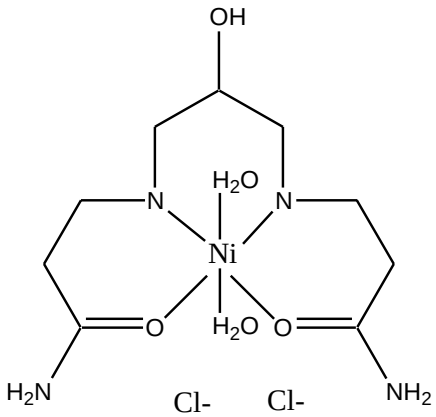


Figure 1.7.17. [Ni(bchtn)(H_2O)$_2$]C1$_2$ (bchtn = N,N'-bis(flcarbamoylethyl)-2-hydroxytrimethylenediamine).

La-Sheng Long *et al.*[54] found that the crystal structure of [Ni(BIPO)(H_2O)$_2$](ClO^4) showed elongated octahedral co-ordination geometries, where the metal atom was ligated by four nitrogen atoms from the tetradentate BIPO ligand at the equatorial positions and two aqua ligands at the axial positions. Ni prefered to adopt a six co-ordinate geometry (**Fig 1.7.18.**).[54]

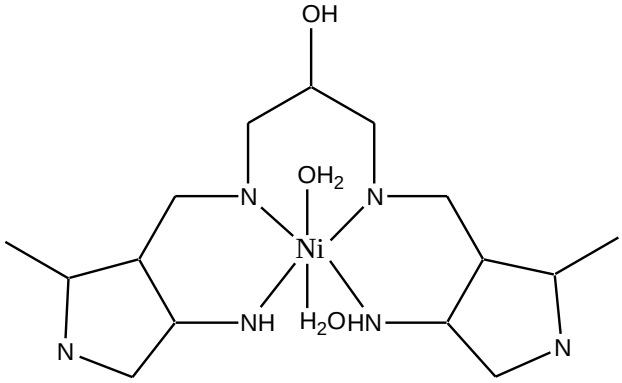


Figure 1.7.18. 1,3-bis[(4-methyl-5-imidazol-1-yl)ethylideneamino]propan-2-ol (BIPO) complexed to nickel(II).

Pal *et al.*[55] found that the potentially tetradentate neutral ligand hydroxylhexahydropyrimidylpyrazole coordinated to the Ni(II) ion through the two iminic and two pyrazole nitrogen atoms. The coordination geometry of the nickel atom in the complex was a distorted octahedral geometry. The four short, in-plane bonds were formed with the four nitrogen atoms of the tetradentate Schiff base ligand. The geometry was completed by the

oxygen atoms of the two coordinated water molecules in axial positions of the octahedron, the metal atom pulled slightly towards one of these axial water molecules (**Fig. 1.7.19.**).[55]

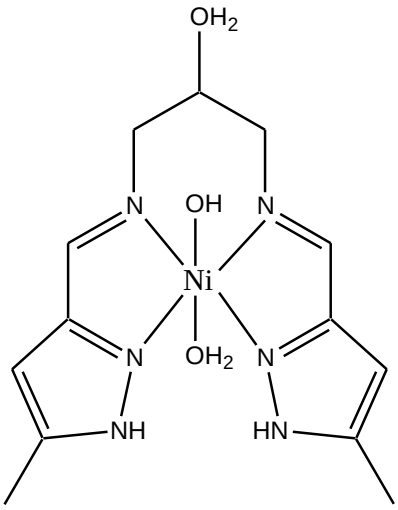


Figure 1.7.19. Schiff base ligand complexed to nickel(II).

Based on this literature survey, the expected structure of *2,2'*-[(hydroxypropane-1,3-diyl)diimino]dicyclohexanol (Cy_2-Otn) and *2,2'*-[(propane-1,3-diyl)diimino]dicyclohexanol (Cy_2-tn) complex with nickel would be octahedral that may be distorted. This is because Ni(II) has a d^8 electron configuration which tends to form a square planar geometry, but the coordination of the two solvent molecules gives it a pseudo-octahedron geometry.[60] Determination of the complex stability and crystal structure of Cy_2-Otn and Cy_2-tn complex with nickel via single crystal X-ray diffraction will either confirm or contradict what is expected.

1.8. Stability Constant Measurement by Glass Electrode Potentiometry

The formation of metal complexes in aqueous solution with a particular ligand occurs via the successive replacement of hydrate molecules.[19] A complexation reaction between a metal ion M, and a ligand, L, where the maximum coordination number *n* is developed, is written as:

$$M(H_2O)_n + nL \rightleftharpoons ML_n + nH_2O \qquad \textbf{(5)}$$

if the ligand is monodentate and no binuclear complex formation occurs. The overall thermodynamic stability constant, β_{MLn} of the species ML_n is defined by:

$$\beta_{MLn} = \frac{[ML_n]}{[M][L]^n} \qquad \textbf{(6)}$$

due to the fact that these complexing processes occurs via a series of stages, it is possible to write a series of n equilibrium expressions for overall bonding stability constants.[17]

$$M + L \rightleftharpoons ML, \qquad \beta_1 = [ML]/[M][L] \qquad \textbf{(7)}$$

$$M + 2L \rightleftharpoons ML_2 \qquad \beta_2 = [ML_2]/[M][L]^2 \qquad \textbf{(8)}$$

$$M + 3L \rightleftharpoons ML_3 \qquad \beta_3 = [ML_4]/[M][L]^2 \qquad \textbf{(9)}$$

$$M + nL \rightleftharpoons ML_n \qquad \beta_n = [ML_n]/[M][L]^n \qquad \textbf{(10)}$$

The above equilibrium each refers to the overall formation reaction in one stage of each complex species. The formation reaction can also be expressed in terms of constants referring to the stepwise addition of ligand:

$$M + L \rightleftharpoons ML, \qquad K_1 = [ML]/[M][L] \qquad \textbf{(11)}$$

$$ML + L \rightleftharpoons ML_2 \qquad K_2 = [ML_2]/[ML][L] \qquad \textbf{(12)}$$

$$ML_2 + L \rightleftharpoons ML_3 \qquad K_3 = [ML_3]/[ML_2][L] \qquad \textbf{(13)}$$

$$ML_{n-1} + L \rightleftharpoons ML_n \qquad K_n = [ML_n]/[ML_{n-1}][L] \qquad \textbf{(14)}$$

the constants K_1 ...K_n are the stepwise stability or formation constants. A relationship exists between the stepwise and overall constants.[9]

$$\beta_n = K_1 \times K_2 \ldots \times K_n \quad \textbf{(15)}$$

Potentiometry is the measurement of the e.m.f. between a sensing and a reference electrode. The reference electrode is usually a calomel or Ag|AgCl electrode. The most used type of pH-electrode is the combination glass electrode (CGE), which has both the glass and the reference electrode in one body. It works on the basis that the potential difference between the surface of a glass membrane and a solution is a linear function of pH.[61] GE measures hydrogen ion activity relative to their reference half-cells; and must be calibrated regularly to ensure accurate, reproducible measurements because its standard potential and the response slope vary with the age and the pre-treatment of the electrode. Electrode calibration can be done in terms of activities by measuring the electrode response using a series of solutions of known ionic composition or buffer solutions,[9] or the electrode can be calibrated in terms of concentration by titrating a strong acid with strong base. The two different types of calibrations, of the same solution, should have the same Nerstian slope but different E° values.

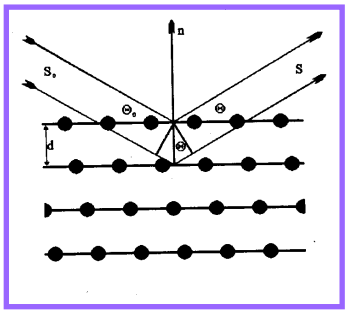
In glass electrode potentiometric speciation studies, the activity of hydrogen ions in the solution are measured, and the proton activity variation is characteristic for a particular metal–ligand model studied at a particular and fixed L_T:M_T ratio.[62] Potentiometry was first used for stability constant measurements by Arrhenius, Ostwald and Nernst.[19] Stability constants are mainly measured in two ways, either by measuring the change of pH as a function of the ligand concentration,[24] or the pH can be measured as a function of the concentration of acid or alkali, added to a constant total metal and total ligand concentration.[24] pH measurement is widely used to determine stability constants, although there are limitations to the method. The main limitation in the use of potentiometry is the requirement for a suitable electrode, as the electrodes develop potentials that are dependent on the activities of the species present, that come from the oxidation-reduction equilibria, and the formation of ionic concentration gradients across membranes. As a result of the occurrence of complex formation processes in solutions, the total (analytical) and free (equilibrium) concentrations of the components involved in the

equilibrium are different.[9] GEP also cannot be used under conditions of extreme pH as it is limited the pH range 2-12, because below pH 2 and above pH 12, the liquid junction potential changes and exerts a notable influence on the measured value.[19] The GEP cannot accurately measure low total metal concentrations, or very stable complexes as the protons are unable to compete effectively with such metal ions for the ligand. These complexes can be studied potentiometrically by replacing the proton with another metal ion that can compete effectively with the metal ion studied. Due to the fact that aqueous solutions always contain hydroxide ions and most metal ions form not only hydroxo-species but also polynuclear species, it is important to either work in sufficiently acidic solutions where hydroxo-complex formation is negligible, or to take it into account during the analysis of the data.[9] As stability constants and measured potential are temperature dependent, it is very important to control the temperature to at least ± 0.1°C.

1.9. X-Ray Diffraction

The study of solid state structures is often performed by X-ray crystallography, where the refractive properties of the crystals are measured when bombarded with X-rays. This bombardment leads to the electrons in the molecule being disrupted and absorbs certain wavelengths, while the rest of the X-ray beam is diffracted. This emission of electrons is detected and the resulting data is analysed to obtain the crystal structure.[2]

The incoming X-ray radiation is scattered by the crystal in a very distinct manner and only at certain wavelengths. The size of each atom affects the degree to which scattering occurs, and the scattering factor helps to determine the identity of each atom when interpreting the diffraction data. This relationship between the incoming radiation and the emitted radiation is given by Bragg's Law (**16**). Figure 1.9.1. shows the relationship between the incoming and outgoing radiation.[2]



Bragg's Law:

$$d = \frac{n \times \lambda}{2 \times \sin\theta} \qquad \textbf{(16)}$$

Figure 1.9.1. The Bragg scattering angles.[2]

The *d*-spacings can be calculated and manipulated from these values to give peaks of distinct intensities and widths, allowing for the determination of the position and nature of that specific atom. The crystal needs to be well-ordered with a definite arrangement in two or three dimensions to give a good diffraction pattern. The crystal is defined as being made up of repeating simple building blocks, called the unit cell. The unit cell contains lattice points, which are points that are uniformly distributed in all three dimensions (**Fig. 1.9.2.**). The combination of the structural motif and the lattice make up the crystal structure, which is determined by its unit cell, symmetry, and its fractional coordinates.[5]

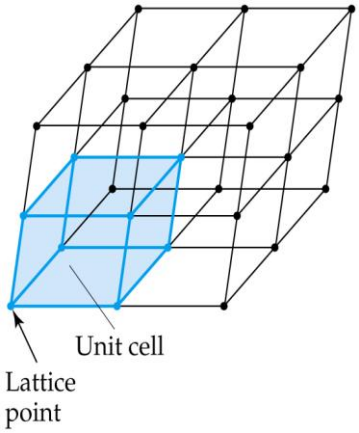


Figure 1.9.2. Representation of the unit cell and lattice points.[2]

The unit cell has six values associated with it: the length, height, and width of the unit cell (a, b, c), and the three angles within the unit cell (α, β, γ). The different arrangements are given different names and summarised in Figure 1.9.3.[2]

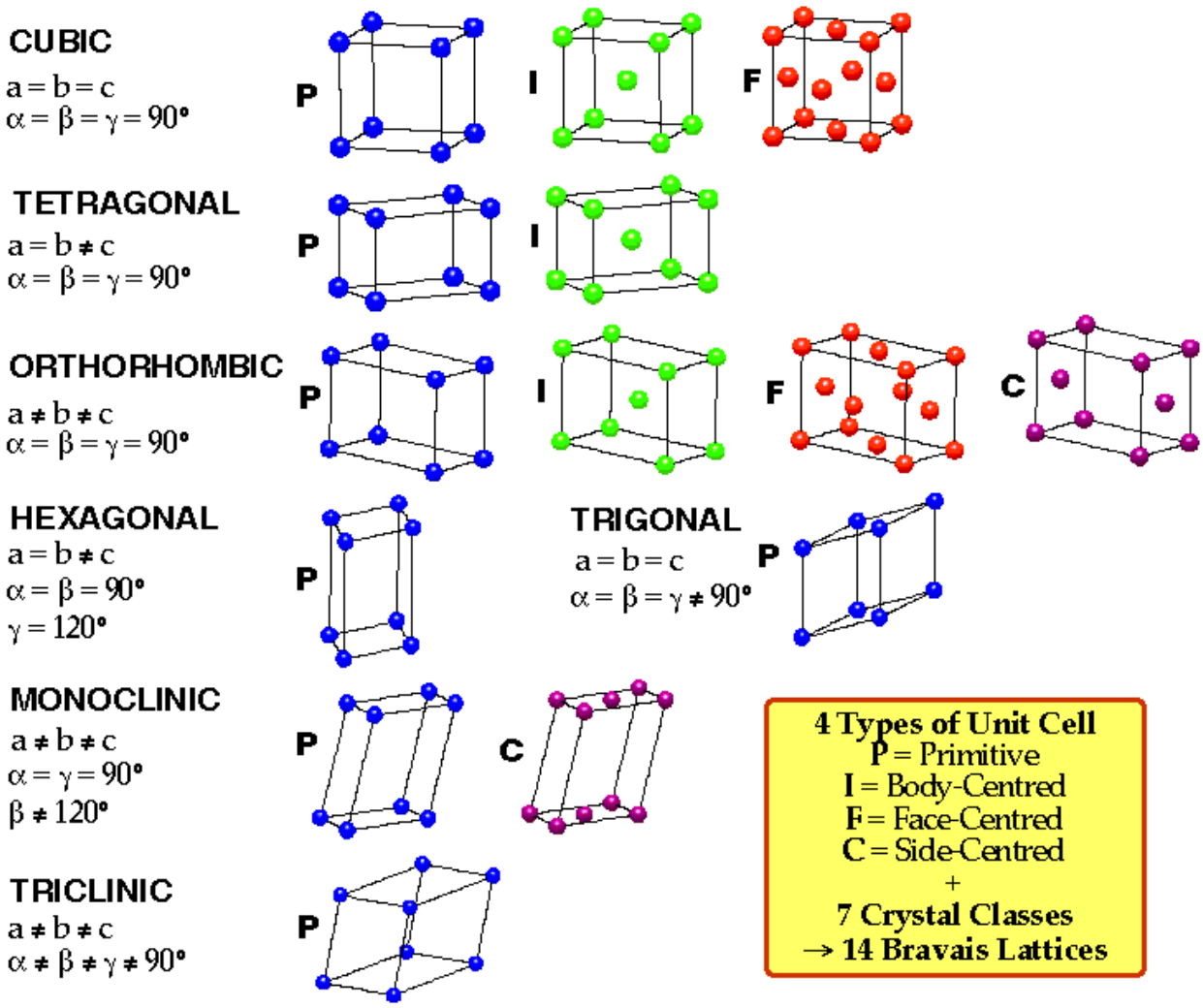


Figure 1.9.3. The various unit cell types.[2]

1.10. Density Functional Theory

Density functional theory (DFT) is a quantum mechanical theory that has been used in physics since the 1970s and in chemistry since the 1990s.[63] It investigates the electronic structure (usually the ground state) of many-electron systems using functionals (a function of a function), such as its electron probability density, ρ. In 1964, Hohenburg and Kohn put forward two theorems that gave DFT a strong theoretical basis.[63]

The first H-K theorem states that there exists a 1-to-1 mapping between the ground state electron density and its wavefunction i.e. the physical properties of a system can be described from a knowledge of its electron density. The electron density depends on only the three spatial coordinates (x, y, z), reducing the many-body problem of N electrons with 3N spatial coordinates, saving computational time.[63-65]

The second H-K theorem states that the ground state electron density corresponds to a minimium in the total electronic energy of a system i.e. finding the electron density of the ground state (ρ_{GS}) enables the determination of the energy of the ground state (E_{GS}).[63-65] Therefore the ground state energy is a function of electron density:

$$E_{GS} = f(\rho) \quad \textbf{(17)}$$

but density is a function of the spatial coordinates:

$$\rho = f(x, y, z) = f(\boldsymbol{r}) \quad \textbf{(18)}$$

therefore:

$$E_{GS} = f(\rho(f(\boldsymbol{r}))) \quad \textbf{(19)}$$

or

$$E_{GS} = E_{GS}[\rho] \quad \textbf{(20)}$$

where $[\rho]$ is a functional of ρ.

The Kohn-Sham method describes the behaviour of non-interacting electrons in an effective local potential. For the exact functional, and therefore the exact local potential, the orbitals yield the exact ground state electron density.[64] This is an approximate method for determining $E_{GS}[\rho]$.[65]

$$E[\rho] = E_K + E_{P,e,N} + E_{P,e,e} + E_{XC}[\rho] \quad \textbf{(21)}$$

where E_K is the total kinetic energy, $E_{P,e,N}$ is the electron-nucleus potential energy, $E_{P,e,e}$ is the electron-electron potential energy, and $E_{XC}[\rho]$ is the exchange correlation energy.[65] The exchange correlation energy is derived from the instantaneous *correlation effects* on the energy

between the motions of the electrons and from the Pauli principle. The wavefunction must be antisymmetric with respect to exchange, resulting in *exchange effects* on the energy.

A basis set is a set of functions (atomic orbitals, AOs) used to create molecular orbitals (MOs) which are expanded as a linear combination of the basis functions. The orbitals used to construct $\rho(\mathbf{r})$ are calculated from the KS equations:[65]

$$\rho(\mathbf{r}) = \sum_{i=1}^{N} \left|\psi_i(r)\right|^2 \qquad \textbf{(22)}$$

The two most common types of orbitals are Slater-type orbitals and Gaussian-type orbitals; the latter are used most frequently as they are more computationally efficient.[65] The choice of basis set is important, and the most common basis sets used are the Pople-type basis sets. The one used in this study is the ***6-31G(d,p)***, where ***6*** is the number of Gaussians comprising each core atomic orbital basis function.[65] The ***31*** indicates that the valence orbitals consist of two basis functions each, the first one is composed of a linear combination of 3 Gaussian functions, the other one is composed of 1 Gaussian function (split-valence triple-zeta basis set), which introduces flexibility to electron density in valence orbitals.[65] The ***G*** indicates that we are dealing with Gaussian basis functions, and the ***(d,p)*** denotes the gas phase model. From the KS equations, it follows:

$$\varepsilon_i\psi_i(r_1) = \psi_i(r_1)\left\{\frac{\hbar}{2m_e}\nabla_1^2 - \sum_{j=1}^{N}\frac{Z_j e^2}{4\pi\varepsilon_0 r_{j1}} + \int\frac{\rho(r_2)e^2}{4\pi\varepsilon_0 r_{12}}dr^2 + V_{XC}(r_1)\right\} \qquad \textbf{(22)}$$

where the first term in the brackets relates to the kinetic energy, the second term to the electron-nucleus attraction, the third term to the electron-electron repulsion, and the fourth term to the exchange-correlation.[63] The first three terms in the brackets are solved in the Hartree-Fock method, whilst:

$$V_{\mathrm{XC}}[\rho] = \frac{\partial E_{\mathrm{XC}}[\rho]}{\partial\rho} \qquad \textbf{(23)}$$

where the initial guess is the superposition of atomic electron densities. Then the *local density approximation* (LDA) is used:

$$E_{XC}[\rho] = \int \rho(r)\varepsilon_{XC}[\rho(r)]dr \qquad \textbf{(24)}$$

where $\varepsilon(r)$ is the exchange-correlation energy per electron in a homogenous gas of a constant or local density. The KS equation is then solved to obtained an initial set of orbitals. These are then used to get a better approximation of $\rho(r)$, which is repeated until a self-consistent solution is arrived at.[64] These KS-LDA-DFT calculations are good for molecular geometry, dipole moments, and vibrational frequencies but poor for atomization energies (ΔU_{at}).[65] In the late 1980s Becke proposed the gradient-corrected functional that gives a generalised-gradient approximation (GGA) DFT method:[63]

$$E_{XC}^{GGA}[\rho] = f([\rho]) + f\left(\frac{\partial\rho}{\partial x} + \frac{\partial\rho}{\partial y} + \frac{\partial\rho}{\partial z}\right) \qquad \textbf{(25)}$$

where the second term is the gradient of the electron density. This greatly improves the ΔU_{at}. The best overall performance is given by a hybrid functional DFT method:

$$E_{XC}^{Hyb}[\rho] = E_{XC}^{GGA}[\rho] + aE_X^{HF} \qquad \textbf{(26)}$$

where, a is an empirical parameter chosen to optimised calculated ΔU_{at}, and E_X^{HF} is the exchange energy, as in a Hartree-Fock calculation, but evaluated using KS orbitals. The most widely used functional in DFT is the hybrid functional ***B3LYP***, where the ***B*** is the Becke term for E_X^{GAA}, ***3*** is for the three empirical parameters chosen to optimise performance against a set of experimental data, and the term ***LYP*** is the term for E_C^{GAA} by Lee, Yang, and Parr.[66] However, an extension of this functional X3LYP[66] was used in this work as it is better able to describe weak inter- and intra-molecular interactions.[65]

The DFT calculations gives data in the form of a wavefunction. This wavefunction data is the input into a program, AIMALL, that performs quantitative and visual QTAIM (Quantum Theory of Atoms In Molecules) analysis of molecular systems.[67]

QTAIM overview

QTAIM put forward by Bader, uses the electron density, ρ, to provide insight into the nature of the bonding in chemical systems.[68,69] QTAIM uses trajectories of the gradient vector field, $\nabla\rho$, of ρ to look at the topology of ρ.[68,69] Points where $\nabla\rho$ vanishes are called *critical points*, and are used to describe the molecular structure. A critical point is characterised by its three eigenvalues of the Hessian matrix, along mutually perpendicular directions, $\lambda_{1\text{-}3}$.[69] Therefore, a (r,ω) critical point is characterised by a rank r (the number of non-zero eigenvalues) and a signature ω (the number of positive less the number of negative eigenvalues). A nucleus position is characterised by a (3,-3) critical point.[69] The nuclei of bonded atoms are linked by a *bond path* line, along which the electron density is a maximum. Along this interaction line is a (3,-1) *bond critical point (BCP).*[69] The presence of a bond path and a BCP indicates that two atoms are bonded to each other. The value of ρ at the BCP gives an indication of the strength of the bond between the atoms.[70] A *ring critical point (RCP)* is a (3,+1) critical point arising from the an annular arrangement of bond paths. A *cage critical point (CCP)* is a (3,+3) critical point and is a minimum in the ρ in a cavity surrounded by three or more rings.[69] The Poincaré-Hopf theorem of topology requires that $n - b + r - c = 1$, where n is the number of nuclei and b, r and c is the number of bond, ring and cage critical points, respectively.[69] The linked network of bond paths defining a system's molecular structure is a *molecular graph.* The presence of a bond path signifies an energetic stabilisation, a *virial path*, along which the potential energy is maximally stabilising.[69] The ρ and the virial field have the same topology.

The characteristics of a closed shell (ionic) interaction:

A low value of electron density at the BCP (ρ_b) (~ 10^{-3} au for a van der Waals' interaction; 10^{-2} au for a hydrogen bond),[72] a relatively small and positive value of the Laplacian of the electron density ($\nabla^2\rho_b$), and a positive value for the total electronic energy density (H_b) that is close to zero,[70] are indicative of ionic interactions. In the case of strong hydrogen bonds H_b becomes negative, and $|V_b|/G_b < 1$ and $G_b/\rho_b > 1$,[73] where V_b is the potential energy of the electrons at the BCP, and G_b is the kinetic energy of the electrons at the BCP.

The characteristics of a shared (i.e., covalent) interaction:

In a covalent interaction, ρ_b is usually > 0.1 au (or > 0.15 au)[72,73] and $\nabla^2\rho_b$, which may be positive or negative (but usually negative),[70] is usually of the same order as ρ_b.[72] Furthermore, $H_b < 0$, $|V_b|/G_b > 2$ and $G_b/\rho_b > 1$.[73,74]

Characteristics of metal-metal or metal-ligand bonding:

In a metal-metal or metal-ligand bond, H_b is usually negative and close to zero and $\nabla^2\rho > 0$ (as found for closed-shell interactions). In O–H···O hydrogen bonds, ρ_b typically has values of 0.03-0.39 e Å^{-3} and $\nabla^2\rho_b$ has values of 0.7-7.0 e Å^{-5}.[70]

Hydrogen bonding, bonding in molecular crystals, and bonding in ionic crystals are examples where bonding occurs between closed shell systems.[71] Espinso *et al.*[71] showed that the energy of a hydrogen bond is related to electron potential energy density $V(\mathbf{r})$:

$$E_{HB} = \tfrac{1}{2}V(\mathbf{r}_b) \qquad \textbf{(27)}$$

Espinosa *et al.*[74] have used the ratio $|V_b|/G_b$ to characterise bonds. Interactions with $|V_b|/G_b < 1$ are characteristic of closed shell interactions; those with $|V_b|/G_b > 2$ are typically shared interactions; and $1 < |V_b|/G_b < 2$ are diagnostic of intermediate interactions. The local statement of the virial theorem gives:

$$\frac{\hbar}{4m}\nabla^2\rho(\mathbf{r}) = 2G(\mathbf{r}) + V(\mathbf{r}) \qquad \textbf{(28)}$$

where the Laplacian is related to the kinetic ($G(\mathbf{r})$), and potential ($V(\mathbf{r})$) energy densities.[69] The first is a positive quantity, while the second is negative for an energy stabilising situation. Therefore, areas where $\nabla^2\rho$ is negative occurs where the potential energy density dominates over the kinetic energy density, as expected at the BCP of a shared (covalent) interactions. Interactions between closed shell systems are characterised by Pauli exclusion of electron

density from the BCP, and the kinetic energy density dominates over the potential energy density so that the Laplacian tends to be positive. The total energy density, $H(\mathbf{r})$, is defined as:[69]

$$H(\mathbf{r}) = G(\mathbf{r}) + V(\mathbf{r}) \qquad \textbf{(29)}$$

where its values at a BCP tends to be negative for a shared interaction but positive for a closed shell interaction.

The DFT and QTAIM modelling are ways to investigate the nature of the bonding in chemical structures using the electron density. The nature of the bonding in the structure gives information as to the types of bonds present in the molecule, and the stability of the molecule or complex.

1.11. Objectives and Scope of the Research Project

The aim of this research was to synthesise and crystallise the two ligands, N,N'-bis(2-hydroxycyclohexyl)-1,3-propanediamine, Cy_2-tn, and 2,2'-[(hydroxypropane-1,3-diyl)diimino]dicyclohexanol, Cy_2-Otn, (**Fig. 1.6.2**.), using the method described by Hancock *et al*.[16] The choice of ligands for this project was to complete the Cy_2-tn/Metal complex series, especially to larger metal ions. The Cy_2-Otn ligand was chosen to determine the role of the alcoholic oxygen group on the propyl bridge, on solubility and complexation stability as a possible extra donor atom.

These ligands were then complexed with Cu(II), Ni(II), Zn(II), Cd(II), and Pb(II). These metals were chosen as they have a broad range between small and large ionic radii. Attempts were made to crystallise Cy_2-tn and Cy_2-Otn/Metal complexes. Because the Cy_2-Otn ligand used in this project is novel, there is no information as to the type of complexes it forms with Ni(II), Cu(II), Cd(II) and Pb(II) or how selective it is for these metals ions over others. The ligands and complexes were characterised by XRD analysis, mass spectrometry, and infra-red spectroscopic methods to confirm their purity and structure. The structures obtained from XRD analysis were used to gain information on the geometry and binding of the metal to the ligand, and to determine non-bonding interactions (hydrogen-hydrogen close contacts[35]) between the hydrogen atoms on the cyclohexenyl rings with the hydrogen atoms on the bridging carbons. This type of interaction is not strictly a bond, but an attractive interaction between the two protons. These interactions were determined by the analysis of the solid state structure and DFT modelling data. DFT calculations were performed in an attempt to determine the stability of the M-L bonds via its electron density.

Potentiometric studies were done on the Cy_2-Otn ligand with the chosen metals to determine the ligand pK_a values and the stability constants of the complexes formed. Variable temperature poentiometric studies were to be performed in order to determine whether the Cy_2-Otn/Metal complex formations were entropically or enthalpically driven. The solution studies aided in determining the effects of the cyclohexenyl rings, the trimethylene bridge between the nitrogen donor atoms, and the propane alcohol group, in metal ion selectivity. A comparison was to be made between the complexes of Cy_2-en, and Cy_2-tn, in order to explain the difference in observed log *K* values as given in Table 1.2.1.

1.12. References

1. R. D. Hancock and A. E. Martell. (1989). *Chem. Rev.,* **89**, 1875.
2. P. Atkins, T. Overton, J. Rourke, M. Weller and F. Armstrong. (2006). *Inorg. Chem.,* 4th Ed., Oxford University Press, United Kingdom.
3. R. G. Pearson and J. Songstad. (1967). *J. Am. Chem. Soc.* **89**, 1827.
4. J. E. Huheey, E. A. Keiter, and R. L. Keiter. (1993). *Inorganic Chemistry: Principles of Structure and Reactivity*; 4th Ed., Harper Collins, New York.
5. S. Reisinger. (2007). *The Solid State Structure of Metallo-beta-amino Alcohol Complexes,* MSc Dissertation, University of the Witwatersrand, Johannessburg.
6. D. J. Cram, T. Kaneda, R. C. Helgeson, S. B. Brown, C. B. Knobler, E. Maverick, and K. N. Trueblood. (1985). *J. Am. Chem. Soc.,* **107**, 3645.
7. E. C. Constable. (1996). *Metal and ligand reactivity*, Weinheim, New York, 135.
8. L. L. Diaddario, L. L. Zimmer, T. E. Jones, L. S. W. L. Sokol, R. B. Cruz, E. L. Yee, L. A. Ochrymowycz, and D. B. Rorabacher. (1979). *J. Am. Chem. Soc.*, **101**, 3511.
9. F. R. Hartley, C. Burgess, and R. Alcock. (1980). *Solution equilibria,*Halsted Press, New York.
10. M. T. Beck, and I. Nagypál. (1990). *Chemistry of complex equilibria,* 7, 192, 220.
11. R. D. Hancock. (1990). *The recognition of metal ions by ligands*, Thesis, University of the Witwatersrand, Johannesburg.
12. R. D. Hancock. (1980). *J. Chem. Soc., Dalton Trans.,* 416.
13. R. D. Hancock. (1990). *Progr. Inorg. Chem.,* **36**, 187.
14. R. D. Hancock. (1990). *Acc. Chem. Res.,* **23**, 253.
15. R. Breslow, S. Belvedere, L. Gershell and D. Leung. (2000). *Pure Appl. Chem*., **72**, 333.
16. R. Hancock, A. de Sousa, G. Walton, and J. Reibenspies. (2007). *Inorg. Chem.,* **46**, 4749.
17. R. B. Lauffer. (1987). *Chem. Rev.,***87**, 901.
18. P. B. Hay, D. Zhang, and J. R. Rustad. (1996). *Inorg. Chem.,* **35**, 2650.
19. A. E Martell, and R.D. Hancock. (1996). *Metal Complexes in aqueous Solutions,* Modern Inorganic Chemistry Series, Plenum Press, New York.
20. R. R. Corderman, and J. L. Beauchamp. (1976). *J. Am. Chem. Soc*., **98**, 3998.

21. B. S. Nakani, J. J. B. Wels, and R. D. Hancock. (1983). *Inorg. Chem.*, **22**, 2956.
22. M. Gerloch. (1973). *Ligands–field parameters*, Cambridge University Press, Cambridge.
23. B. P. Hay, J. R. Rustad, and C. Hostetler. (1993). *J. Am. Chem. Soc.*, **115**, 158.
24. A. E. Martell, and R. J. Motekaitis. (1992). *Determination and use of Stability constants*, 2ND Ed., Wiley-VCH, New York.
25. V. Uwamariya. (2005) "*Electrochemical Studies of Metal-Ligand Equilibria Involving Chelating Ligands*", Dissertation, University of the Witwatersrand, Johannesburg.
26. T. E. Chantson. (1994). *A molecular mechanics study of ligands for selective complexation of metal ions in medical applications*, Thesis, University of the Witwatersrand, Johannesburg.
27. A. S. de Sousa. (1995). *Coordinating properties of more highly preorganised ligands*, Thesis, University of the Witwatersrand Johannesburg.
28. C. F. Bell. (1977). *Principles and applications of metal chelation*; Oxford University Press, Oxford.
29. M. M. Hayward, J. C. Adrian, and A. Schepartz. (1995). *J. Org. Chem.*, **60**, 3924.
30. http://pages.prodigy.net/naturedoctor/chelation.html#One.Last accessed 06/03/09.
31. http://en.wikipedia.org/wiki/Chelation. Last accessed 06/03/09.
32. http://www.benbest.com/nutrceut/EDTA.html.Last accessed 06/03/09.
33. http://en.wikipedia.org/wiki/Copper.Last accessed 10/03/09.
34. C. Ramakrishnan, and Y. S. Geetha. (1990). *Proc. of Indian Academy of Sci., Chem. Sci.*, **102** (4), 481.
35. J. R. Lancaster. (1988). *The Bioinorganic Chemistry of Nickel*, VCH, New York.
36. B. L. Vallee, and D. S. Auld. (1990). *Biochemistry*, **29**, 5647.
37. J. Parr. (1997). *Polyhedron*, **16**, 551.
38. L. Shimoni-Livny, J. P. Glusker, and C. W. Bock. (1998). *Inorg. Chem.*, **37**, 1853.
39. http://en.wikipedia.org/wiki/Ionic_Radius. Last Accessed 28/02/08.
40. H. Irving and R. J. P. Williams. (1948). *Nature*, **162**, 746.
41. A. S. de Sousa and R. D. Hancock. (1985). *J. Chem. Soc., Chem. Comm.*, 415.
42. M. Nevalainen, and V. Nevalainen. (2001). *Tetrahedron: Asymmetry.*, **12**, 1771.
43. W. A. Nugent. (2002). *Org. Lett.*, **4**, 2133.

44. H. Glas, M. Barz, and W. R. Thiel. (2001). *J. Organomet. Chem.*, **621**, 153.
45. S. N. Joshi, and S. V. Malhotra. (2003). *Tetrahedron: Asymmetry*, **14**, 1763.
46. C. C. Watts, P. Thoniyot, F. Cappuccio, J. Verhagen, B. Gallagher, and B. Singaram. (2006). *Tetrahedron: Asymmetry*, **17**, 1031.
47. P. J. Murphy, S. Pinato, D. Thomas, and J. L. Oller-Lopez. (2006). *Chem. Pharm. Bull.*, **54**, 1331.
48. H. Zhang, X. Zhang, L. Gong, A. Mi, X, Cui, Y. Jiang, M. Choi, and A. Chan. (2002). *Organic Lett.*, **4**, 1399.
49. A. S. de Sousa, R. D. Hancock, and J. H. Reibenspies. (1997), *J. Chem. Soc., Dalton Trans.*, 2831.
50. E. M. Casimiro. (20000. Thesis, University of the Witwatersrand, Johannesburg.
51. S. Canepari, V. Carunchio, and R. Schina. (1999). *Polyhedron*, **18**, 3263.
52. A. S. de Sousa, and M. A. Fernandes. (2002). *Polyhedron*, **21**, 1883.
53. P. Bermhardt, and P. Sharpe. (1998). *J. Chem. Soc., Dalton Trans.*, 1087.
54. L. Long, X. Chen, X. Yu, Z. Zhou and L. Nian Ji. (1999). *Polyhedron*, **18**, 1927.
55. S. Pal, A. K. Barik, S. Gupta, A. Hazra, S. K. Kar, S. Peng, G. Lee, R. J. Butcher, M. S. El Fallah, and J. Ribas. (2005). *Inorg. Chem.*, **44**, 3880.
56. T. Tanase, K. Mano, and Y. Yamamoto. (1993). *Inorg. Chem.*, **32**, 3995.
57. Y. Xie, H. Jiang, M. Yu, C. Du, Q. Liu, X. Xu, and Y. Zhu. (2001). *J. Mol. Struct.*, **608**, 169.
58. R. Mattes, C. Muhlenbrock, K. Leeners, C. Pyttel. (2004). *Z Anorg. Allg. Chem.*, **630**, 722.
59. K. R. Adam, C. Clarkson, A. J. Leong, L. F. Lindoy, M. McPartlin, H. R. Powell, and S. V.Smith. (1994). *J. Chem. Soc., Dalton Trans.*, 2791.
60. T. Lee, C. Hong, T. Lee, S. Liu and C. Chung. (1985). *Acta Cryst.*, **C41**, 844.
61. G. Eisenman. (1967). *Glass electrode for hydrogen and other cations*, E. Arnold, London.
62. R. C. Luckay. (1997). *Factors that control selectivity of ligands for metal ions*, Thesis.
63. http://en.wikipedia.org/wiki/Density_functional_theory. Last accessed 08/02/11.
64. N. Harrison. *An introduction to density functional theory,* Imperial college of Science Technology and Medicine, London.

65. H. M. Marques. Private communications, University of the Witwatersrand, Johannesburg.
66. C. Lee, W. Yang, R.G. Parr. (1988). *Phys. Rev.*, **B 37**, 785.
67. http://aim.tkgristmill.com/readme.html. Last accessed 08/02/11.
68. R. Bader. (1990). *Atoms in Molecules: A Quantum Theory*, Oxford University Press, Oxford.
69. H. M. Marques. Private communications.
70. P. Varadwaj, I. Cukrowski, H. M. Marques. (2009). *J. Mol. Struct., Theochem.*
71. E. Espinosa, E. Molins and C. Lecomte. (1998). *Chem. Phys. Lett.*, **285**, 170.
72. R. Bader and H. Essén. (1984). *J. Chem. Phys.*, **80**, 1943.
73. M. Bobrov, G. Popova and V. Tsirelson. (2006). *Russ. J. Phys. Chem.*, **80**, 584.
74. E. Espinosa, I. Alkorta, J. Elguero and E. Molins. (2002). *J. Chem. Phys.*, **117**, 5529.

Chapter 2

Materials, Methods, and Results

2.1. Materials

The ligands in this study were synthesised from commercially readily available materials. The metal salts and solvents were also used as received. The following is a list containing the sources from which all of the starting materials were bought. All chemicals were reagent grade and used without further purification.

Table 2.1.1. List of chemicals used with suppliers

Chemical Name	Formula	Supplier
Sodium hydroxide	NaOH	Merck
Hydrochloric acid	HCl	ACE
Dimethyl formamide	$HCON(CH_3)_2$	SaarChem
1,3-Diaminopropane	$C_3H_{10}N_2$	Merck
Cyclohexene oxide	$C_6H_{10}O$	Aldrich
Absolute ethanol	CH_3CH_2OH	Aldrich
Acetone	CH_3COCH_3	Merck
Lead(II) nitrate	$Pb(NO_3)_2$	Aldrich
Methanol	CH_3OH	ACE
Chloroform	$CHCl_3$	Merck
Cadmium(II) chloride hydrate	$CdCl_2.2.5H_2O$	Riedel-de Haën A.-G. Seelze bei Hannover

Chemical Name	Formula	Supplier
1,3,-Diamino-2-propanol	$C_3H_{10}ON_2$	Fluka (old bottle), Aldrich (new bottle)
Zinc(II) chloride hydrate	$ZnCl_2.xH_2O$	Aldrich
Zinc(II) nitrate hexahydrate	$Zn(NO_3)_2.6H_2O$	Aldrich
Nickel(II) nitrate hexahydrate	$Ni(NO_3)_2.6H_2O$	Aldrich
Nickel(II) chloride hexahydrate	$NiCl_2.6H_2O$	Merck
Potassium hydroxide	KOH	ACE
Cadmium(II) nitrate tetrahydrate	$Cd(NO_3)_2.4H_2O$	Aldrich
Nitric acid	HNO_3	Merck
Copper(II) perchlorate hexahydrate	$Cu(ClO_4)_2.6H_2O$	Aldrich
Copper(II) nitrate hydrate	$Cu(NO_3)_2.xH_2O$	Aldrich
Lead(II) Chloride	$PbCl_2$	Aldrich

2.2. Physical Techniques of Characterisation

2.2.1. Nuclear Magnetic Resonance Spectroscopy (NMR)

Hydrogen (^1H) nuclear magnetic resonance spectra were recorded on Bruker Avance-300 at 300.13 MHz respectively using standard pulse sequences. The probe temperature for all experiments was 300 ± 1 K. All spectra were recorded in either deuterium oxide (D_2O) in 5 mm NMR tubes unless otherwise stated. Chemical shifts are reported in parts per million (ppm) relative to tetramethylsilane as internal standard, in the case of ^1H NMR. The ^1H NMR chemical shifts are reported as: value (splitting pattern, number of hydrogens, assignment). Abbreviations used: s = singlet, d = doublet, t = triplet, q = quartet, m = multiplet.

All NMR data were collected by Richard Mampa and further refined by the author. All NMR data are found in Appendix B on the CD.

2.2.2. Electrospray Ionization (ESI) or Atmospheric Pressure Chemical Ionization (APCI) – Mass Spectrometry

Low-resolution mass spectra were recorded on a VG7-SEQ Double Focussing Mass Spectrometer at 70 eV and 4.5 μA. The polarity was positive, ionisation employed was ESI or APCI, as quoted, with a resolution of 3000, a mass range of 3000 amu (8 kV) and a scan rate of 5 s/decade. The sample was dissolved in water and the mobile phase was a 50:50 methanol:water mixture. Data are quoted as: *m/z* value (relative abundance).

All mass spectrometry data were collected by and analysed by the author. All mass spectrometry data are found in Appendix C on the CD.

2.2.3. Infrared Spectroscopy (IR)

Infrared spectra were recorded on a Bruker Vector 22 spectrometer. The absorptions are reported on the wavenumber (cm^{-1}) scale, in the range 400-4000 cm^{-1}. The signals are reported as: value (assignment if possible).

All IR data were collected and analysed by the author. All IR data are found in Appendix D on the CD.

2.2.4. Single Crystal X-Ray Diffraction (XRD)

Intensity data were collected on a Bruker APEX II CCD area detector diffractometer with graphite monochromated Mo K_α radiation (50kV, 30mA) using the APEX 2 [1] data collection software. The collection method involved ω-scans of width 0.5° and 512x512 bit data frames. Data reduction was carried out using the program *SAINT+* [2] and face indexed absorption corrections were made using the program *XPREP*).[2] The crystal structure was solved by direct methods using *SHELXTL*.[3] Non-hydrogen atoms were first refined isotropically followed by anisotropic refinement by full matrix least-squares calculations based on F^2 using *SHELXTL*. Hydrogen atoms were first located in the difference map then positioned geometrically and allowed to ride on their respective parent atoms. Diagrams as well as publication material were generated using SHELXTL, Mercury, PLATON [4] and ORTEP-3.[5]

All XRD data were collected by Dr. Manuel Fernandes and analysed by the author. All XRD data are found in Appendix E on the CD.

2.3. Synthesis of the Free Ligands

The ligands were synthesised in the manner as shown below in Figure 2.3.1.

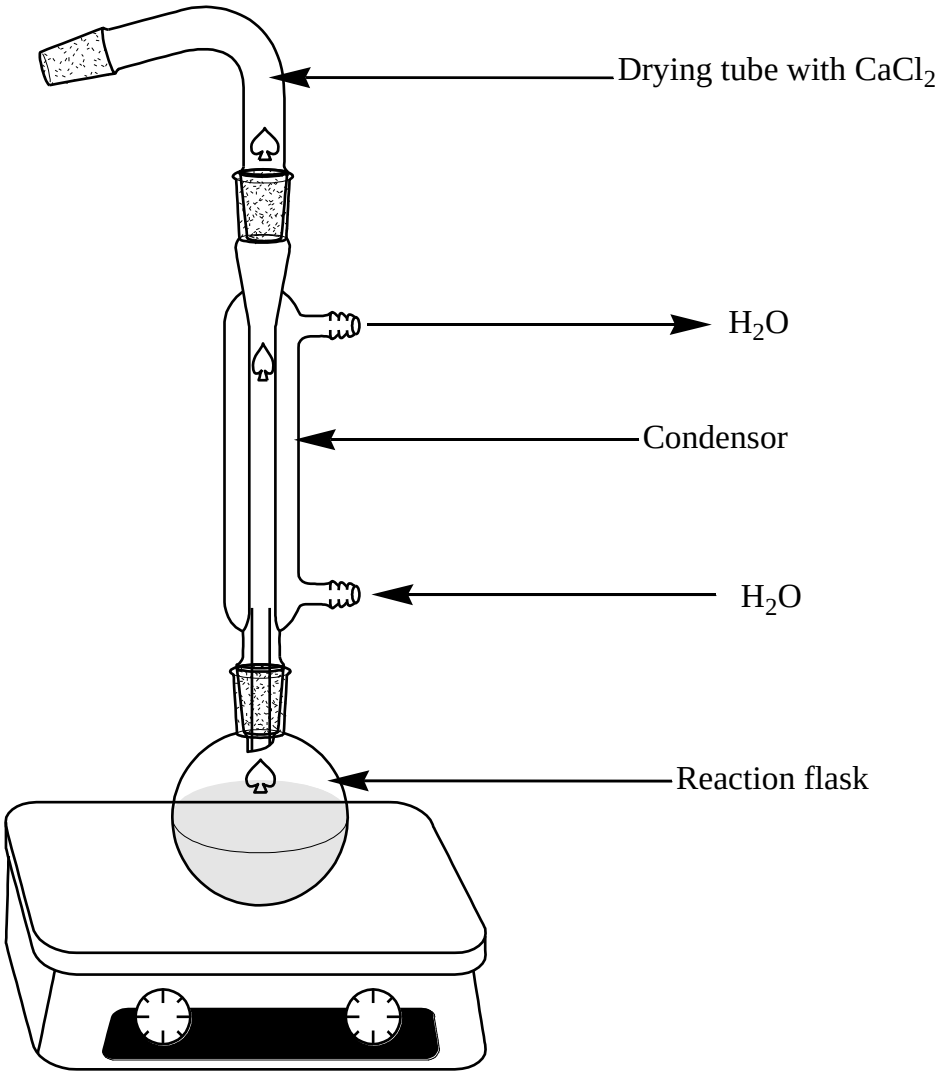


Figure 2.3.1. General setup of the ligand reactions.

The ligands were synthesized in the manner described by Hancock *et al.*[6]

2.3.1. Synthesis of 2,2'-[(hydroxypropane-1,3-diyl)di-imino]dicyclohexanol (Cy_2-Otn)

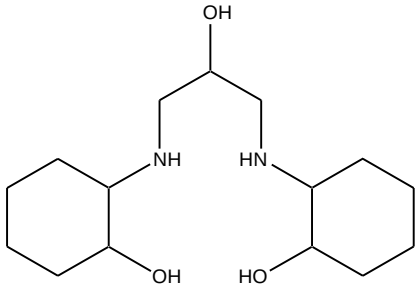


Figure 2.3.2. Cy_2-Otn (Lx).

Using the old bottle of 1,3-diamino-2-propanol, the amino alcohol was dissolved in dry ethanol in a round bottomed flask. Cyclohexene oxide was added to this solution and stirred at room temperature for 24 hours. The solution was slowly evaporated in a fume hood, forming an oil that did not solidify into white crystals.

The reaction was performed four times and the relative masses and volumes of the reagents tabulated below.

Table 2.3.1. Masses and volumes used to synthesise Cy_2-Otn (L1-4).

Sample	**1,3-Diamino-2-propanol**		**Cyclohexene Oxide**		**Ethanol**
	Mass (*g*)	Moles (*mmol*)	Mass (*g*)	Moles (*mmol*)	Volume (*ml*)
L1	0.05561	0.617	1.4505	14.78	30
L2	0.0587	0.1166	1.4500	14.77	30
L3	0.0560	0.6214	1.4516	14.79	30
L4	0.1118	1.241	2.954	30.10	40

Due to the fact that the samples did not solidify as expected, only L3 was characterised by NMR, IR, and mass spectrometry. The H NMR of L3 showed that it was a mixture of the ligand and the zwitter ion of the starting amine. L1, L2, and L4 were characterised by mass spectroscopy only.

Sample L1:

Mixed products were formed.

Mass Spec L1: ITMS+c ESI: m/z 189 (Cy-Otn+1), 287 (Cy_2-Otn+1), 385 (Cy_3-Otn+1).

Sample L2:

Mixed products were formed.

Mass Spec L2: ITMS+c ESI: m/z 116 (blank), 119 (blank), 215 (blank), 189 (Cy-Otn+1), 287 (Cy_2-Otn+1).

Sample L3:

Mixed products were formed.

^{1}H NMR L3: $\delta_H(D_2O)$ 3.75-3.45 (m, 1H, HOC<u>H</u>CH_2), 3.38-3.25 (m, 2H, HOC<u>H</u>CH_2), 2.74-2.45 (m, 2H, C<u>H</u>NHR), 2.35-2.26 (m, 4H, C<u>H_2</u>CHNR), 2.11 (m, 1H, acetone), 1.86 (s, 4H, C<u>H_2</u>CHOH), 1.58 (s, 4H, C<u>H_2</u>NH), 1.19-0.90 (br m, 8H, CH_2C<u>H_2</u>C<u>H_2</u>CH_2), 3.12-2.88 (m, 1H, unknown).

Mass Spec L3: ITMS+c ESI: m/z 287 (Cy_2-Otn+1), 385 (Cy_3-Otn+1), 483 (Cy_4-Otn+1).

IR L3 (cm^{-1}): 3356 (N-H stretch), 3283 (O-H stretch), 2930 (C-H asym. stretch), 2859 (C-H sym. stretch), 1641-1572 (C-H_2 bend), 1450 (C-H bend), 1373 (O-H bend), 1334 (C-N stretch), 1163 (C-O stretch), 1071 and 952 (C-C stretch), 918 (N-H bend), 844-692 (C-H bend).

Sample L4:

Mixed products were formed.

Mass Spec L4: ITMS+c ESI: m/z 189 (Cy-Otn+1), 287 (Cy_2-Otn+1), 385 (Cy_3-Otn+1).

Using the new bottle of 1,3-diamino-2-propanol, and performing the same reaction under Ar. 1,3-diamino-2-propanol was dissolved in the dry ethanol. To this was added the cyclohexene oxide and the resultant mixture left to stir under Ar at room temperature for 24 hours with a $CaCl_2$ drying tube attached. The solution was then left to evaporate slowly when an oil formed that solidified upon standing to form a white powder. This powder was then triturated with ice-cold acetone, filtered and dried.

The reaction was performed several times and the relative masses and volumes of the reagents tabulated below.

Table 2.3.2. Masses and volumes used to synthesise Cy_2-Otn (L5-8).

Sample	1,3-Diamino-2-propanol		Cyclohexene Oxide		Ethanol
	Mass (*g*)	Moles (*mmol*)	Mass (*g*)	Moles (*mol*)	Volume (*ml*)
L5	8.001	88.0	20.002	0.2038	150
L6	8.226	28.7	20.0189	0.204	150
L7	4.1023	45.52	10.0193	0.1021	30
L8	4.0028	44.416	12.7303	0.1297	30

The samples were characterised by NMR, IR, and mass spectrometry.

Sample L5:

The product was obtained in a 5.8% yield (1.4740 g).

^{1}H NMR L5: $\delta_H(D_2O)$ 3.74 (m, 1H, $CH_2C\underline{H}OH$), 3.24 (m, 2H, $C\underline{H}OH$), 2.68-2.57 (m, 4H, $C\underline{H_2}NHR$), 2.28 (m, 2H, $C\underline{H}NHR$), 2.10 (m, 7H, acetone), 1.83 (br d, 4H, $C\underline{H_2}CHOH$), 1.58 (br d, 4H, $C\underline{H_2}CHNHR$), 1.16-0.92 (br m, 8H, $CH_2C\underline{H_2}C\underline{H_2}CH_2$).

Mass Spec L5: ITMS+c ESI: m/z 287 (Cy_2-Otn+1), 288 (Cy_2-Otn+H+1), 309 (Cy_2-Otn+Na), 758 (Blank).

IR L5 (cm^{-1}): 3276 (N-H stretch), 3245 (O-H stretch), 2923 (C-H asym. stretch), 2853 (C-H sym. stretch), 1446 (C-H_2 bend), 1338 (C-H bend), 1221-1199 (O-H bend), 1166 (C-N stretch), 1120 (C-O stretch), 1073 and 963-940 (C-C stretch),907-872 (N-H bend), 841-671 (C-H bend).

Sample L6:

The product was obtained in a 13.7% yield (3.480 g).

^{1}H NMR L6: $\delta_H(D_2O)$ 3.75 (m, 1H, $CH_2C\underline{H}OH$), 3.26 (m, 2H, C$\underline{H}$OH), 2.75-2.58 (m, 4H, C$\underline{H_2}$NHR), 2.33-2.28 (m, 2H, C$\underline{H}$NHR), 2.12 (m, 1H, acetone), 1.83 (br d, 4H, C$\underline{H_2}$CHOH), 1.58 (br d, 4H, C$\underline{H_2}$CHNHR), 1.17-0.93 (br m, 8H, $CH_2C\underline{H_2}C\underline{H_2}CH_2$).

Mass spec L6: ITMS+c ESI: m/z 287 (Cy_2-Otn+1), 288 (Cy_2-Otn+H+1).

IR L6 (cm^{-1}): 3282 (N-H stretch), 3240 (O-H stretch), 2924 (C-H asym. stretch), 2863 (C-H sym. stretch), 1440 (C-H_2 bend), 1338 (C-H bend), 1221-1199 (O-H bend), 1166 (C-N stretch), 1120 (C-O stretch), 1073-1051 and 963 (C-C stretch), 940-907 (N-H bend), 841-671 (C-H bend).

Sample L7:

The product was obtained in a 96.4% yield (12.567 g).

^{1}H NMR L7: 300 Mhz $\delta_H(D_2O)$ 3.75 (m, 1H, $CH_2C\underline{H}OH$), 3.26 (m, 2H, C$\underline{H}$OH), 2.71-2.58 (m, 4H, C$\underline{H_2}$NHR), 2.33-2.28 (m, 2H, C$\underline{H}$NHR), 2.12 (m, 1H, acetone), 1.83 (br d, 4H, C$\underline{H_2}$CHOH), 1.58 (br d, 4H, C$\underline{H_2}$CHNHR), 1.17-0.93 (br m, 8H, $CH_2C\underline{H_2}C\underline{H_2}CH_2$).

Mass Spec L7: ITMS+c ESI: m/z 287 (Cy_2-Otn+1), 288 (Cy_2-Otn+H+1).

IR L7 (cm^{-1}): 3292 (N-H stretch), 3255 (O-H stretch), 2922 (C-H asym. stretch), 2852 (C-H sym. Stretch), 1705 and 917 (N-H bend), 1449 (C-H_2 bend), 1338 (C-H bend), 1217 (O-H bend), 1166 (C-N stretch), 1121 (C-O stretch), 1079 and 963 (C-C stretch), 841-671 (C-H bend).

Recrystallisation of L7 (L7c)

1.0038 g of Cy_2-Otn was ground and dissolved in 10 ml H_2O, the solution was left to evaporate (approx. 1 month), and the solid was filtered.

^{1}H NMR L7c: 300 Mhz $\delta_H(D_2O)$ 3.74 (m, 1H, $CH_2C\underline{H}OH$), 3.27 (m, 2H, C<u>H</u>OH), 2.72-2.59 (m, 4H, C<u>H_2</u>NHR), 2.37-2.34 (m, 2H, C<u>H</u>NHR), 1.84 (br d, 4H, C<u>H_2</u>CHOH), 1.59 (br d, 4H, C<u>H_2</u>CHNHR), 1.17-0.94 (br m, 8H, $CH_2C\underline{H_2}C\underline{H_2}CH_2$).

Mass Spec L7c: ITMS+c APCI: m/z 287 (Cy_2-Otn+1).

IR L7c (cm^{-1}): 3283 (N-H stretch), 3135 (O-H stretch), 2925 (C-H asym. stretch), 2855 (C-H sym. Stretch), 1653 and 909 (N-H bend), 1448 (C-H_2 bend), 1340 (C-H bend), 1223 (O-H bend), 1168 (C-N stretch), 1122 (C-O stretch), 1075 and 965 (C-C stretch), 843-673 (C-H bend).

Sample L8:

The product was obtained in a 55.3% yield (7.0318 g).

^{1}H NMR L8: 300 Mhz $\delta_H(D_2O)$ 3.74 (m, 1H, $CH_2C\underline{H}OH$), 3.25 (m, 2H, C<u>H</u>OH), 2.69-2.56 (m, 4H, C<u>H_2</u>NHR), 2.34-2.27 (m, 2H, C<u>H</u>NHR), 1.82 (br d, 4H, C<u>H_2</u>CHOH), 1.57 (br d, 4H, C<u>H_2</u>CHNHR), 1.16-0.92 (br m, 8H, $CH_2C\underline{H_2}C\underline{H_2}CH_2$).

Mass Spec L8: ITMS+c APCI: m/z 287 (Cy_2-Otn+1), 385 (Cy_3-Otn+1).

IR L8 (cm^{-1}): 3281 (N-H stretch), 3264 (O-H stretch), 2923 (C-H asym. stretch), 2853 (C-H sym. Stretch), 1652 and 907 (N-H bend), 1448 (C-H_2 bend), 1338-1300 (C-H bend), 1220-1200 (O-H bend), 1166 (C-N stretch), 1120 (C-O stretch), 1074-1051 and 963 (C-C stretch), 841-671 (C-H bend).

Recrystallisation of L8 (L8c)

1.0563 g of Cy_2-Otn was ground and dissolved in 10 ml H_2O, the solution was left to evaporate (approx. 1 month), and the solid was filtered.

^{1}H NMR L8c: 300 Mhz $\delta_H(D_2O)$ 3.74 (m, 1H, $CH_2C\underline{H}OH$), 3.27 (m, 2H, $C\underline{H}OH$), 2.72-2.58 (m, 4H, $C\underline{H_2}NHR$), 2.32 (m, 2H, $C\underline{H}NHR$), 2.10 (m, 1H, acetone), 1.82 (br d, 4H, $C\underline{H_2}CHOH$), 1.57 (br d, 4H, $C\underline{H_2}CHNHR$), 1.15-0.92 (br m, 8H, $CH_2C\underline{H_2}C\underline{H_2}CH_2$).

Mass Spec L8c: ITMS+c ESI: m/z 287 (Cy_2-Otn+1), 299 (Cy_2-Otn+1+2H).

IR L8c (cm^{-1}): 3281 (N-H stretch), 3113 (O-H stretch), 2923 (C-H asym. stretch), 2853 (C-H sym. Stretch), 2159-225 and 907 (N-H bend), 1440 (C-H_2 bend), 1387-1300 (C-H bend), 1221-1199 (O-H bend), 1167 (C-N stretch), 1120 (C-O stretch), 1073-1035 and 962 (C-C stretch), 841-671 (C-H bend).

The solid state structure of the free ligand was solved and tabulated in Table 2.8. The full data can be found in Appendix E in tables E.1 to E.6.

Table 2.3.3. Crystal data and structure refinement for Cy_2-Otn.

Temperature	173(2) K	
Crystal system	Monoclinic	
Space group	C 2/c	
Unit cell dimensions	a = 36.145(3) Å	α = 90.00°.
	b = 8.5902(6) Å	β = 104.822(2)°.
	c = 26.4419(18) Å	γ = 90.00°.
Volume	7936.9(9) $Å^3$	
Z	20	

Density (calculated)	1.198 g/cm^3
Absorption coefficient	0.083 mm^{-1}
Goodness-of-fit on F^2	1.049
Final R indices [I>2σ(I)]	R_1 = 0.0786, wR_2 = 0.2015
R indices (all data)	R_1 = 0.1612, wR_2 = 0.2404

2.3.2. Synthesis of N,N'-Bis(2-hydroxycyclohexyl)-1,3-propanediamine (Cy_2-tn)

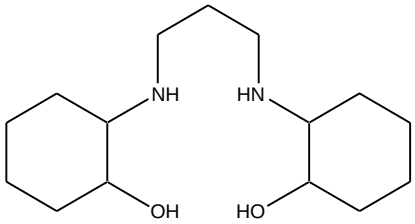


Figure 2.3.3. Cy_2-tn (2Lx).

1,3-Diaminopropane was dissolved in the dry ethanol. The cyclohexene oxide was added to this solution and the resultant mixture refluxed at 80 ^oC for 24 hours with a $CaCl_2$ drying tube attached. The solvent was then removed and the resulting oil placed under reduced pressure to leave behind a white powder. This powder was then triturated with ice-cold acetone, filtered and dried.

Product was not suitable for XRD, some of the ligand was recrystallised in DMF and water and left to evaporate slowly and crystals formed. The reaction was performed twice and the relative masses and volumes of the reagents tabulated below.

Table 2.3.4. Masses and volumes used to synthesise Cy_2-tn.

Sample	1,3-Diaminopropane		Cyclohexene Oxide		Ethanol
	Mass	Moles	Mass	Moles	Volume
2L1	3.008 g	40.469 mmol	15.88 g	0.1619 mol	120 mL
2L2	3.174 g	42.828 mmol	8.714 g	88.792 mmol	30 mL
2L3	2.0089 g	22.296 mmol	5.5748 g	56.805 mmol	30 mL

The samples were characterised by NMR, IR, and mass spectrometry.

Sample 2L1:

The product was obtained in a 97.1% yield (10.631 g).

^{1}H NMR 2L1: 300 Mhz $\delta_H(D_2O)$ 3.20 (m, 2H, C<u>H</u>OH), 2.90 (m, 2H, C<u>H$_2$</u>NHR), 2.58 (m, 2H, C<u>H$_2$</u>HR), 2.21 (m, 2H, C<u>H</u>NHR), 2.01 (br d, 4H, C<u>H$_2$</u>CHOH), 1.69 (br m, 6H, C<u>H$_2$</u>CHNHR and C<u>H$_2$</u>CH$_2$NHR), 1.26-0.96 (br m, 8H, CH$_2$C<u>H$_2$</u>C<u>H$_2$</u>CH$_2$).

Mass Spec 2L1: ITMS+c ESI: m/z 271 (Cy_2-tn+1), 272 (Cy_2-tn+1+H), 147 (*N*'-(3-amino-propyl)-propane-1,3-diamine).

IR 2L1 (cm^{-1}): 3274 (N-H stretch), 3127 (O-H stretch), 2926 (C-H asym. stretch), 2811 (C-H sym. stretch), 2304 and 911 (N-H bend), 1450 (C-H$_2$ bend), 1360 (C-H bend), 1338 (O-H bend), 1209 (C-N stretch), 1111(C-O stretch), 1026-954 (C-C stretch), 840-704 (C-H bend).

Sample 2L2:

The product was obtained in a 99.6% yield (11.5292 g).

^{1}H NMR 2L2: 300 Mhz $\delta_H(D_2O)$ 3.24 (m, 2H, C<u>H</u>OH), 2.66 (m, 2H, C<u>H$_2$</u>NHR), 2.47 (m, 2H, C<u>H$_2$</u>NHR), 2.28 (m, 2H, C<u>H</u>NHR), 1.88 (br d, 4H, C<u>H$_2$</u>CHOH), 1.57 (br m, 6H, C<u>H$_2$</u>CHNHR and C<u>H$_2$</u>CH$_2$NHR), 1.17-0.95 (br m, 8H, CH$_2$C<u>H$_2$</u>C<u>H$_2$</u>CH$_2$).

Mass Spec 2L2: ITMS+c APCI: m/z 271 (Cy_2-tn+1), 369 (Cy_3-tn+1).

IR 2L2 (cm^{-1}): 3277 (N-H stretch), 3123 (O-H stretch), 2925 (C-H asym. stretch), 2817 (C-H sym. stretch), 1450 (C-H_2 bend), 1353-1338 (C-H bend), 1286 (O-H bend), 1232-1203 (C-N stretch), 1111(C-O stretch), 1081-1012 (C-C stretch), 919-689 (N-H bend), 842-741 (C-H bend).

Sample 2L3:

The product was obtained in an 80.9% yield (5.1672 g).

^{1}H NMR 2L3: 300 Mhz $\delta_H(D_2O)$ 3.22 (m, 2H, C<u>H</u>OH), 2.62 (m, 2H, C<u>H</u>$_2$NHR), 2.44 (m, 2H, C<u>H</u>$_2$NHR), 2.26 (m, 2H, C<u>H</u>NHR), 2.07 (m, 1H, acetone), 1.90 (br d, 4H, C<u>H</u>$_2$CHOH), 1.55 (br m, 6H, C<u>H</u>$_2$CHNHR and C<u>H</u>$_2$CH$_2$NHR), 1.15-0.89 (br m, 8H, CH$_2$C<u>H</u>$_2$C<u>H</u>$_2$CH$_2$).

Mass Spec 2L3: ITMS+c APCI: m/z 270 (Cy_2-tn-H+1), 292 (Cy_2-tn-H+Na+1), 368 (Cy_3-tn-H+1).

R 2L3 (cm^{-1}): 3276 (N-H stretch), 3120 (O-H stretch), 2923 (C-H asym. stretch), 2812 (C-H sym. stretch), 2160-1978 and 918-866 (N-H bend), 1450 (C-H_2 bend), 1351-1337 (C-H bend), 1284 (O-H bend), 1230-1202 (C-N stretch), 1117 (C-O stretch), 1082-1009 (C-C stretch), 841-742 (C-H bend).

The solid state structure of the free ligand was solved and tabulated in Tables 2.3.5. and 2.3.6. The full data can be found in Appendix E in tables E.13 to E.18, and E.19 to E.24.

Table 2.3.5. Crystal data and structure refinement for Cy_2-tn(a).

Temperature	173(2) K	
Crystal system	Monoclinic	
Space group	C 2/c	
Unit cell dimensions	a = 24.5923(8) Å	α = 90.00°.

	b = 8.2587(3) Å	β = 90.568(2)°.
	c = 7.6234(3) Å	γ = 90.00°.
Volume	1548.24(10) $Å^3$	
Z	4	
Density (calculated)	1.160 g/cm^3	
Absorption coefficient	0.076 mm^{-1}	
Goodness-of-fit on F^2	1.038	
Final R indices [I>2σ(I)]	R_1 = 0.043, wR_2 = 0.110	
R indices (all data)	R_1 = 0.058, wR_2 = 0.118	

Table 2.3.6. Crystal data and structure refinement for Cy_2-tn(b).

Temperature	293(2) K	
Crystal system	Triclinic	
Space group	$P\bar{1}$	
Unit cell dimensions	a = 8.6048(13) Å	α = 66.971(6)°.
	b = 9.8900(14) Å	β = 77.718(8)°.
	c = 10.8797(17) Å	γ = 72.931(8)°.
Volume	809.5(2) $Å^3$	
Z	2	
Density (calculated)	1.11 g/cm^3	

Absorption coefficient	0.073 mm^{-1}
Goodness-of-fit on F^2	2.709
Final R indices [I>2σ(I)]	R_1 = 0.223, wR_2 = 0.616
R indices (all data)	R_1 = 0.250, wR_2 = 0.625

2.4 Synthesis of the Cy_2-Otn/Metal Complexes

Several methods were employed to obtain the Cy_2-Otn/metal complexes, and the crystal structures. The ligand needed to be heated slightly to dissolve in the solvents, only gels were formed with Cy_2-Otn ligand.

2.4.1. Synthesis of Cy_2-Otn/Cu(II) Complex

Method A1: Cy_2-Otn, 0.2005 g (0.7002 mmol) was dissolved in 10 ml water, to this was added 0.078 g (1.390 mmol) of KOH in 10 ml water (to raise the pH and remove the amine protons to make complexation easier), and stirred in an ice bath for 30 min. Copper perchlorate hexahydrate, $Cu(ClO_4)_2 \cdot 6H_2O$, (0.2633 g, 0.712 mmol) was dissolved in 20 ml water and added to the solution and refluxed at 70 ^{0}C for 20 min. The solution was left to cool and evaporate slowly. Crystals were formed but were of poor quality, and so were recrystallised in water. A film was formed, Mass spec and IR show a complex was formed.

Mass Spec Cy_2-Otn+Cu: ITMS+c ESI: m/z 271 (blank), 287 (Cy_2-Otn+1), 348 (Cy_2-Otn+1+Cu-4H), 350 (Cy_2-Otn+Cu+1-2H), 394 (blank), 408 (Cy_2-Otn+1+Cu+3H_2O+3H), 448 (Cy_2-Otn+Cu+1+ClO_4-4H), 450 (Cy_2-Otn+Cu+1+ClO_4-2H).

IR Cy_2-tn+Cu (cm^{-1}): 3289 (N-H stretch), 3234 (O-H stretch), 2929 (C-H asym. stretch), 2857 (C-H sym. stretch), 1588 and 977 (N-H bend), 1449 (C-H_2 bend), 1342 (C-H bend), 1075-1010 (O-H bend, C-N stretch, and C-O stretch), 985-923 (C-C stretch), 844 (C-H bend), 621 (Cu-N stretch).

Another method was tried.

Method A2: Copper perchlorate hexahydrate, $Cu(ClO_4)_2 \cdot 6H_2O$, (0.2575 g, 0.6950 mmol) was dissolved in 7 ml water. To this was added Cy_2-Otn, 0.2053 g (0.7169 mmol) dissolved in 8 ml water and added to the solution and refluxed at 75 ^{0}C for 3 hrs. The solution was left to evaporate slowly. A gel was formed, mass spec and IR show a complex was formed.

Mass Spec Cy_2-Otn+Cu: ITMS+c ESI: m/z 271 (blank), 287 (Cy_2-Otn+1), 348 (Cy_2-Otn+1+Cu-4H), 350 (Cy_2-Otn+Cu+1-2H), 408 (Cy_2-Otn+1+Cu+3H_2O+3H), 410 (blank), 448 (Cy_2-Otn+Cu+1+ClO_4-4H), 480 (Cy_2-Otn+Cu+1+ClO_4+H_2O-4H).

IR Cy_2-Otn+Cu (cm^{-1}): 3499 (N-H stretch), 3232 (O-H stretch), 2942 (C-H asym. stretch), 2865 (C-H sym. stretch), 1625 and 975 (N-H bend), 1453 (C-H_2 bend), 1360 (C-H bend), 1300-1250 (O-H bend), 1204 (C-N stretch), 1053-1000 (C-O stretch), 926 (C-C stretch), 847 (C-H bend), 620 (Cu-N stretch).

Method A3: Copper perchlorate hexahydrate, $Cu(ClO_4)_2.6H_2O$, (0.6492 g, 1.7521 mmol) was dissolved in 5 ml deionised water, to this Cy_2-Otn (0.5606 g, 1.9573 mmol) dissolved in 10 ml deionised water was added dropwise. The solution was heated to 65 °C for 1 hr. A solution of NaOH (0.6983 M), was added dropwise, checking for precipitation. It was heated to 70 °C for 30 min. The solution was filtered, cooled and left to evaporate slowly. A blue gel was formed. The characterisation shows a complex was formed.

Mass Spec Cy_2-Otn+Cu: ITMS+c ESI: m/z 287 (Cy_2-Otn+1), 348 (Cy_2-Otn+1+Cu-4H), 350 (Cy_2-Otn+Cu+1-2H), 384 (Cy_2-otn+Cu+2H_2O-2H+1), 448 (Cy_2-Otn+Cu+1+ClO_4-4H).

IR Cy_2-Otn+Cu (cm^{-1}): 3507 (N-H stretch), 3232 (O-H stretch), 2944 (C-H asym. stretch), 2867-2673 (C-H sym. stretch), 1629 and 973 (N-H bend), 1456 (C-H_2 bend), 1352 (C-H bend), 1316-1247 (O-H bend), 1206 (C-N stretch), 1055-1024 (C-O stretch), 929-893 (C-C stretch), 850 (C-H bend), 621 (Cu-N stretch).

2.4.2. Synthesis of Cy_2-Otn/Ni(II) Complex

Method B1: Nickel(II) chloride hexahydrate (0.6336 g, 1.956 mmol) was dissolved in 10 ml water. The ligand, Cy_2-Otn (0.5025 g, 1.755 mmol), was dissolved in 10 ml water and added. The solution was stirred at 100^oC in a bomb for 3 days, then at 150 ^oC for 2 days, filtered and left to evaporate slowly. A dark green gel was formed that contained a mixture of products.

Mass Spec Cy_2-Otn+Ni: ITMS+c ESI (m/z) 116 (bank), 169 (blank), 256 ($NiCl_2$.7H_2O+1), 287 (Cy_2-Otn+1), 343 (Cy_2-Otn+Ni+1-2H), 345 (Cy_2-Otn+Ni+1), 379 (Cy_2-Otn-2H+Ni+Cl+1).

IR Cy_2-Otn+Ni (cm^{-1}): 3295 (N-H stretch), 3158 (O-H stretch), 2935 (C-H asy. stretch), 2861 (C-H sym. stretch), 1629 and 923 (N-H bend), 1451 (C-H_2 bend), 1359 (C-H bend), 1263-1242 (O-H bend), 1198 (C-N stretch), 1081 (C-O stretch), 1032-1008 (C-C stretch), 884 (C-H bend), 861 (Ni-N stretch), 637 (Ni-N bend).

Another method was tried.

Method B2: Nickel nitrate hexahydrate, $Ni(NO_3)_2$.6H_2O (0.5077 g, 1.7458 mmol) was dissolved in 5 ml deionised water, to this Cy_2-Otn (0.5001 g, 1.746 mmol) dissolved in 10 ml deionised water was added dropwise. The solution was heated to 65 °C for 24 hrs (pH = 7.6). A

solution of NaOH (0.6983 M), was added dropwise, checking for precipitation (pH = 8.2). It was heated to 70 °C for 30 min. The solution was filtered, cooled and left to evaporate slowly. A light blue gel was formed, showing a mixture of products.

Mass Spec Cy_2-Otn+Ni: ITMS+c ESI (m/z) 214 (blank), 256 (blank), 287 (Cy_2-Otn), 343 (Cy_2-otn+Ni-2H+1), 345 (Cy_2-Otn+Ni+1), 379 (Cy+2+-Otn+Ni+Cl+1), 381 (blank), 388 (blank), 391 (blank), 406 (blank), 462 (Cy_2-Otn+Ni+NO_3+3H_2O+1).

IR Cy_2-Otn+Ni(N) (cm^{-1}): 3295 (N-H stretch), 3153 (O-H stretch), 2935 (C-H asy. stretch), 2861 (C-H sym. stretch), 1633 and 924 (N-H bend), 1452 (C-H_2 bend), 1359-1311 (C-H bend), 1263-1242 (O-H bend), 1198-1142 (C-N stretch), 1063-1031 (C-O stretch), 1008 (C-C stretch), 905-888 (C-H bend), 845-787 (Ni-N stretch), 606 (Ni-N bend).

2.4.3. Synthesis of Cy_2-Otn/Zn(II) Complex

Method C1: Zinc chloride hydrate, $ZnCl_2$, (0.1167 g, 0.856 mmol) was added to a solution of 0.2063 g (0.7203 mmol) Cy_2-Otn in 10 ml water. This solution was heated to 70 ^oC and stirred for 24 hours. The solution was filtered and left to evaporate slowly. A film was formed. Mass spec and IR show a complex was formed.

Mass Spec Cy_2-Otn+Zn: ITMS+c ESI: m/z 270 (blank), 287 (Cy_2-Otn+1), 288 (Cy_2-Otn+H+1), 369 (Cy_2-Otn-2H+Zn+H_2O+1), 385 (Cy_2-Otn-2H+Zn+Cl+1), 408(Cy_2-Otn+Zn+3H_2O+1), 410 (Cy_2-Otn+Zn+3H_2O+2H+1).

IR Cy_2-Otn+Zn (cm^{-1}): 3329 (N-H stretch), 3280 (O-H stretch), 2935 (C-H asym. stretch), 2860 (C-H sym. stretch), 1450 (C-H_2 bend), 1346 (C-H bend), 1281 (O-H bend), 1242 (C-N stretch), 1162 (C-O stretch), 1068-1028 (C-C stretch), 926 (N-H bend), 891 (C-H bend), 847 (Zn-N stretch), 638 (Zn-N bend).

Method C2: Zinc chloride hydrate, $ZnCl_2$, (0.4652 g, 3.4136 mmol) was added to a solution of 0.5013 g (1.7507 mmol) Cy_2-Otn in 12 ml methanol. This solution was heated to 60 ^oC and stirred for 24 hours. The solution was filtered and left to evaporate slowly. A gel was formed. Mass spec and IR show a complex was formed.

Mass Spec Cy_2-Otn+Zn: ITMS+c ESI: m/z 287 (Cy_2-Otn+1), 288 (Cy_2-Otn+H+1), 321 (blank), 385 (Cy_2-Otn-2H+Zn+Cl+1), 483 (Cy_2-Otn+Zn-4H+2Cl+CH_3OH+1).

IR Cy_2-Otn+Zn (cm^{-1}): 3374 (N-H stretch), 3187 (O-H stretch), 2938 (C-H asym. stretch), 2862 (C-H sym. stretch), 2160-2031 and 926 (N-H bend), 1587 (C-H_2 bend), 1450 (C-H bend), 1347 (O-H bend), 1287 (C-N stretch), 1197 (C-O stretch), 1066-1012 (C-C stretch), 892 (C-H bend), 849 (Zn-N stretch), 787 (Zn-N bend).

Method C3: The method was repeated using $ClCH_3$ solvent. Zinc chloride hydrate, $ZnCl_2$, (0.1853 g, 1.360 mmol) was added to a solution of 0.2062 g (0.7212 mmol) Cy_2-Otn in 30 ml $ClCH_3$. This solution was heated to 65 ^oC and stirred for 24 hours. The solution was filtered and left to evaporate slowly. A gel was formed, and mass spec and IR show a complex was formed.

Mass Spec Cy_2-Otn+Zn: ITMS+c ESI: m/z 287 (Cy_2-Otn+1), 288 (Cy_2-Otn+H+1), 316 (blank), 349 (Cy_2-Otn+Zn-3H+1), 385 (Cy_2-Otn-2H+Zn+Cl+1).

IR Cy_2-Otn+Zn (cm^{-1}): 3374 (N-H stretch), 3206 (O-H stretch), 2928 (C-H asym. stretch), 2858 (C-H sym. stretch), 1671 and 927 (N-H bend), 1449 (C-H_2 bend), 1341 (C-H bend), 1287 (O-H bend), 1240 (C-N stretch), 1161 (C-O stretch), 1073-1048 (C-C stretch), 891 (C-H bend), 849 (Zn-N stretch), 664 (Zn-N bend).

Another method was tried.

Method C4: Zinc nitrate hexahydrate, $Zn(NO_3)_2.6H_2O$, (0.5193 g, 1.7457 mmol) was dissolved in 5 ml deionised water, to this Cy_2-Otn (0.500 g, 1.7457 mmol) dissolved in 10 ml deionised water was added dropwise. The solution was heated to 65 °C for 1 hr, check pH (6.4). A solution of NaOH (0.6983 M), was added dropwise, checking for precipitation. A few drops were added before precipitate started, pH = 6.6, and it was heated to 70 °C for 30 min. The solution was filtered, cooled and left to evaporate slowly. A yellow gel was formed, mass spec and IR show a complex was formed.

Mass Spec Cy_2-Otn+Zn: ITMS+c ESI: m/z 287 (Cy_2-Otn+1), 288 (Cy_2-Otn+H+1), 385 (Cy_2-Otn-2H+Zn+Cl+1).

IR Cy_2-Otn+Zn(N) (cm^{-1}): 3336 (N-H stretch), 3195 (O-H stretch), 2935 (C-H asym. stretch), 2860 (C-H sym. stretch), 1589 and 926 (N-H bend), 1450 (C-H_2 bend), 1347 (C-H bend), 1287 (O-H bend), 1239 (C-N stretch), 1198 (C-O stretch), 1067-1016 (C-C stretch), 891 (C-H bend), 848 (Zn-N stretch), 786 (Zn-N bend).

2.4.4. Synthesis of Cy_2-Otn/Cd(II) Complex

Method D1: Cadmium chloride hydrate, $CdCl_2 \cdot 2.5H_2O$, (0.1245 g, 0.5450 mmol) was dissolved in 10 ml water. To this was added 0.1150 g (0.4016 mmol) Cy_2-Otn. This solution was stirred at 80^oC for 24 hours. The solution was then filtered and left to evaporate slowly. A yellow gel was formed. Characterisation show a complex was formed.

Mass Spec Cy_2-Otn+Cd: ITMS+c APCI: m/z 287 (Cy_2-Otn+1), 573 (Cy_2-Otn+1+Cy_2-Otn), 721 (Cy_2-Otn+Cd+Cl+1+Cy_2-Otn).

IR Cy_2-Otn+Cd (cm^{-1}): 3368 (N-H stretch), 3258 (O-H stretch), 2929 (C-H asym. stretch), 2135 (C-H sym. stretch), 1637 and 969-950 (N-H bend), 1454-1301 (C-H_2 bend), 1277-1199

(C-H bend), 1161 (O-H bend), 1065 (C-N stretch), 1053-1040 (C-O stretch), 1009 (C-C stretch), 917 (N-H bend), 893-841 (C-H bend).

Another method was tried.

Method D2: Cadmium Nitrate tetrahydrate, $Cd(NO_3)_2 \cdot 4H_2O$, (0.5928 g, 1.9217 mmol) was dissolved in 3 ml dry Ethanol. To this was added 0.5001 g (1.7461 mmol) Cy_2-Otn dissolved in 7 ml dry Ethanol dropwise. This solution was stirred at 70^oC for 3 hrs. The solution was then filtered and left to evaporate slowly. A yellow oil was formed. Characterisations show no complex was formed.

Mass Spec Cy_2-Otn+Cd(N): ITMS+c APCI: m/z 271 (blank), 287 (Cy_2-Otn+1), 372 (blank).

IR Cy_2-Otn+Cd(N) (cm^{-1}): 3397 (N-H stretch), 3259 (O-H stretch), 2931 (C-H asym. stretch), 2862 (C-H sym. stretch), 1452 and 970 (N-H bend), 1351-1290 (C-H_2 bend), 1213 (C-H bend), 1167 (O-H bend), 1066 (C-N stretch), 1054-1040 (C-O stretch), 1010 (C-C stretch), 918 (N-H bend), 898-844 (C-H bend), 743 (Cd-Nitrate stretch).

Method D3: Cadmium chloride hydrate, $CdCl_2 \cdot 2.5H_2O$, (0.2020 g, 0.8842 mmol) was dissolved in 5 ml water and was added slowly to 0.2045 g (0.7142 mmol) Cy_2-Otn dissolved in 5 ml water. This solution was stirred at 90^oC for 24 hours. The solution was then filtered and left to evaporate slowly. A yellow gel was formed. Mass spec and IR show no complex was formed.

Mass Spec Cy_2-Otn+Cd: ITMS+c ESI: m/z 287 (Cy_2-Otn+1), 299 (blank).

IR Cy_2-Otn+Cd (cm^{-1}): 3397 (N-H stretch), 3259 (O-H stretch), 2932 (C-H asym. stretch), 2861 (C-H sym. stretch), 1580 and 970 (N-H bend), 1451-1416 (C-H_2 bend), 1344-1279 (C-H bend), 11243-1199 (O-H bend), 1066 (C-N stretch), 1040-1011 (C-O stretch), 970 (C-C stretch), 918 (N-H bend), 893-845 (C-H bend).

Another method was tried.

Method D4: Cadmium Nitrate tetrahydrate, $Cd(NO_3)_2.4H_2O$, (0.53851 g, 1.7457 mmol) was dissolved in 5 ml deionised water, to this Cy_2-Otn (0.500 g, 1.7457 mmol) dissolved in 10 ml deionised water was added dropwise, a precipitate formed (pH = 6.6). A solution of HNO_3 (0.1 M), was added dropwise, till precipitate cleared (pH = 1.2). The solution was heated to 65 °C for 24 hrs. The solution was filtered, cooled and left to evaporate slowly. A yellow gel was formed.

Mass Spec Cy_2-Otn+Cd: ITMS+c ESI: m/z 287 (Cy_2-Otn+1), 288 (Cy_2Otn+H+1).

IR Cy_2-Otn+Cd(N) (cm^{-1}): 3315 (N-H stretch), 3256 (O-H stretch), 2937 (C-H asym. stretch), 2861 (C-H sym. stretch), 1597 and 922 (N-H bend), 1367 (C-H_2 bend), 1287 (C-H bend), 1159 (O-H bend), 1067 (C-N stretch), 1031 (C-O stretch), 976 (C-C stretch), 893-848 (C-H bend), 786 (Cd-Nitrate stretch).

2.4.5. Synthesis of Cy_2-Otn/Pb(II) Complex

Method E1: Lead Nitrate, 0.3531 g (1.531 mmol), was dissolved in 10 ml water, and to this solution 0.1926 g (0.8352 mmol) Cy_2-Otn was added. This solution was stirred at 70 ^{0}C for 24 hrs. The solution was then filtered and left to evaporate slowly. A yellow gel was formed, mass spec and IR show a complex was formed.

Mass Spec Cy_2-Otn+Pb: ITMS+c APCI: m/z 271 (blank), 287 (Cy_2-Otn+1), 493 (Cy_2-Otn+1+Pb), 779 (2Cy_2-Otn+Pb+1), 983 (2[Cy_2-Otn+Pb]+1+4H).

IR Cy_2-Otn+Pb (cm^{-1}): 3251 (N-H stretch), 3224 (O-H stretch), 2934 (C-H asym. stretch), 2860 (C-H sym. stretch), 1628 and 920 (N-H bend), 1283 (C-H_2 bend), 1134 (C-H bend), 1068

(O-H bend), 1029 (C-N stretch), 976 (C-O stretch), 893 (C-C stretch), 848-786 (C-H bend) 719-640 (Pb-N stretch).

Method E2: Lead nitrate, $Pb(NO_3)_2$, (0.4030 g, 1.7476 mmol) was dissolved in 5 ml deionised water, to this Cy_2-Otn (0.5004 g, 1.747 mmol) dissolved in 10 ml deionised water was added dropwise. The solution was heated to 65 °C for 24 hrs, no precipitate formed. The solution had a few drops of a NaOH solution (0.6983 M) added, checking for precipitation. It was heated to 70 °C for 30 min, pH = 12.8. This solution was filtered, cooled and left to evaporate slowly. A yellow gel was formed, mass spec and IR show no complex was formed.

Mass Spec Cy_2-Otn+Pb: ITMS+c ESI: m/z 287 (Cy_2-Otn+1), 288 (Cy_2-Otn+1+H), 309 (Cy_2-Otn+Na+1).

IR Cy_2-Otn+Pb(N) (cm^{-1}): 3281 (N-H stretch), 3204 (O-H stretch), 2922 (C-H asym. stretch), 2852 (C-H sym. stretch), 1648 and 906 (N-H bend), 1221 (C-H_2 bend), 1119 (C-H bend), 1077 (O-H bend), 1013 (C-N stretch), 961-941 (C-O stretch), 868 (C-C stretch), 841 (C-H bend) 686 (Pb-Nitrate stretch).

2.5 Synthesis of the Cy_2-tn/Metal Complexes

Several methods were employed to obtain the Cy_2-tn/metal complexes, and the crystal structures. The ligand was heated slightly to dissolve it in the solvents.

2.5.1. Synthesis of Cy_2-tn/Cu(II) Complex

Method F1: Cy_2-tn, 0.4018 g (1.486 mmol) was dissolved in 10 ml water, to this was added 0.18 g (3.208 mmol) of KOH in 10 ml water, and stirred in an ice bath for 30 min. Copper perchlorate hexahydrate, $Cu(ClO_4)_2 \cdot 6H_2O$, (0.5294 g, 1.429 mmol) was dissolved in 20 ml water and added to the solution and refluxed at 70 ^{0}C for 20 min. The solution was left to cool and evaporate slowly. Salt crystals and a film was formed. Mass spec and IR show a complex was formed.

Mass Spec Cy_2-tn+Cu: ITMS+c ESI: m/z 269 (Cy_2-tn+1-2H), 271 (Cy_2-tn+1), 287 (Cy_2-tn+1+H_2O-2H), 288 (Cy_2-tn+1+H_2O-H), 332 (Cy_2-tn+Cu+1-3H), 334 (Cy_2-tn+1+Cu), 391 (Cy_2-Otn+1+Cu+3H_2O+2H), 392 (Cy_2-Otn+1+Cu+3H_2O+3H), 432 (Cy_2-tn+1+Cu+ClO_4-2H).

IR Cy_2-tn+Cu (cm^{-1}): 3476 (N-H stretch), 3234 (O-H stretch), 2930 (C-H asym. stretch), 2857 (C-H sym. stretch), 1638 and 916 (N-H bend), 1448 (C-H_2 bend), 1355 (C-H bend), 1263 (O-H bend), 1210 (C-N stretch), 1067 (C-O stretch), 977-950 (C-C stretch), 916-787 (C-H bend) 620 (Cu-N stretch).

Another method was tried.

Method F2: Copper perchlorate hexahydrate, $Cu(ClO_4)_2 \cdot 6H_2O$, (0.2089 g, 0.5638 mmol) was dissolved in 7 ml water. To this was added Cy_2-tn, 0.2148 g (0.7945 mmol) dissolved in 8 ml water and added to the solution and refluxed at 75 ^{0}C for 3 hrs. The solution was left to evaporate slowly. A dark blue gel was formed. Mass spec and IR show a complex was formed.

Mass Spec Cy_2-tn+Cu: ITMS+c ESI: m/z 269 (Cy_2-tn+1-2H), 271 (Cy_2-tn+1), 287 (Cy_2-tn+1+H_2O-2H), 288 (Cy_2-tn+1+H_2O-H), 332 (Cy_2-tn+Cu+1-3H), 334 (Cy_2-tn+1+Cu), 378 (Blank), 391 (Cy_2-Otn+1+Cu+3H_2O+2H), 392 (Cy_2-Otn+1+Cu+3H_2O+3H), 432 (Cy_2-tn+1+Cu+ClO_4-2H).

IR Cy_2-tn+Cu (cm^{-1}): 3573-3493 (N-H stretch), 3233 (O-H stretch), 2946 (C-H asym. stretch), 2869 (C-H sym. stretch), 1626 and 968 (N-H bend), 1452 (C-H_2 bend), 1344 (C-H bend), 1242 (O-H bend), 1206 (C-N stretch), 1059-1019 (C-O stretch), 950-920 (C-C stretch), 895-794 (C-H bend) 620 (Cu-N stretch).

Method F3: Copper nitrate hydrate, $Cu(ClO_4)_2 \cdot xH_2O$, (0.1422 g, 0.7582 mmol) was dissolved in 5 ml deionised water. To this was added Cy_2-tn, 0.2055 g (0.7175 mmol) dissolved in 10 ml deionised water and added to the solution and refluxed at 75 ^{0}C for 24 hrs. The solution was left to evaporate slowly. A dark blue gel was formed.

Mass Spec Cy_2-tn+Cu(N): ITMS+c APCI: m/z 269 (Cy_2-tn+1-2H), 271 (Cy_2-tn+1).

IR Cy_2-tn+Cu(N) (cm^{-1}): 3422 (N-H stretch), 3207 (O-H stretch), 2934 (C-H asym. stretch), 2858 (C-H sym. stretch), 1628 and 967 (N-H bend), 1395 (C-H_2 bend), 1304 (C-H bend), 1203 (O-H bend), 1079 (C-N stretch), 1029 (C-O stretch), 946-918 (C-C stretch), 897-792 (C-H bend) 721 (Cu-N stretch).

2.5.2. Synthesis of Cy_2-tn/Ni(II) Complex

Method G1: Nickel(II) chloride hexahydrate (0.2262 g, 0.9513 mmol) was dissolved in 10 mL water. The ligand, Cy_2-tn (0.1814 g, 0.6710 mmol), was added. The solution was stirred at 70^{o}C for 4 days, filtered and left to evaporate slowly. Dark blue needle crystals were formed 0.0211 g (% yield = 8.7% - poor due to spillage). Characterisation shows a complex was formed.

Mass Spec Cy_2-tn+Ni: ITMS+c ESI (m/z) 328 (Cy_2-tn+Ni), 363 (Cy_2-tn+Ni+Cl), 597 (2[Cy_2-tn]+Ni), 653 (2[Cy_2tn+Ni-2H]), 689 (2[Cy_2-tn+Ni+OH]), 727 (2[Cy_2-tn+Ni+Cl]), 747 (2[Cy_2-tn+Ni+Cl+H_2O+1]).

IR Cy_2-tn+Ni (cm^{-1}): 3298 (N-H stretch), 3139 (O-H stretch), 2936 (C-H asy. stretch), 2869 (C-H sym. stretch), 1451-1426 (C-H_2 bend), 1350 (C-H bend), 1264-1245 (O-H bend), 1210 (C-N stretch), 1099-1084 (C-O stretch), 1063 (C-C stretch), 974-960 (N-H bend), 910-885 (C-H bend), 840 (Ni-N stretch), 686 (Ni-N bend).

The solid state structure of Cy_2-tn/Ni was solved and tabulated in Table 2.5.1. The full data can be found in Appendix E in tables E.25 to E.30.

Table 2.5.1. Crystal data and structure refinement for Cy_2-tn/Ni(II) complex.

Temperature	173(2) K	
Crystal system	Monoclinic	
Space group	P 2_1/c	
Unit cell dimensions	a = 12.055(5) Å	α = 90.000(5)°.
	b = 11.465(5) Å	β = 107.025(5)°.
	c = 15.139(5) Å	γ = 90.000(5)°.
Volume	2000.7(14) $Å^3$	
Z	4	
Density (calculated)	1.448 g/cm^3	
Absorption coefficient	1.257 mm^{-1}	
Goodness-of-fit on F^2	1.021	
Final R indices [I>2σ(I)]	R_1 = 0.0323, wR_2 = 0.0737	
R indices (all data)	R_1 = 0.0439, wR_2 = 0.0858	

Another method was tried.

Method G2: Nickel(II) Nitrate hexahydrate, $Ni(NO_3)_2.6.H_2O$ (0.2178 g, 0.7489 mmol) was dissolved in 10 ml water. The ligand, Cy_2-tn (0.1998 g, 0.7390 mmol), was added. The solution was stirred at 70^oC for 4 days, filtered and left to evaporate slowly. Dark blue needle crystals were formed, but were poor quality and have been recrystallized. Mass spec and IR show a complex was formed.

Mass Spec Cy_2-tn+Ni(N): ITMS+c ESI (m/z) 271 (Cy_2-tn+1), 272 (Cy_2-tn+h+1), 287 (blank), 327 (Cy_2-tn-2H+Ni+1), 329 (Cy_2-tn+Ni+1), 330 (Cy_2-tn+H+Ni+1), 386 (Cy_2-tn+Ni+), 391 (Cy_2-tn+Ni+NO_3+1), 473 (Cy_2-tn+H+Ni+2NO_3+H_2O+1), 597 (2[Cy_2-tn-H]+Ni), 599 (2[Cy_2-tn]+Ni).

IR Cy_2-tn+Ni(N) (cm^{-1}): 3368 (N-H stretch), 3224 (O-H stretch), 2937 (C-H asy. stretch), 2869 (C-H sym. stretch), 1468-1448 (C-H_2 bend), 1405 (C-H bend), 1307 (O-H bend), 1207-1196 (C-N stretch), 1106-1086 (C-O stretch), 1061-1036 (C-C stretch), 976-949 (N-H bend), 917-889 (C-H bend), 791 (Ni-N stretch), 720 (Ni-N bend).

Method G3: Nickel(II) Nitrate hexahydrate, $Ni(NO_3)_2.6.H_2O$ (0.2218 g, 0.763 mmol) was dissolved in 3 ml water and added to the ligand, Cy_2-tn (0.2012 g, 0.7442 mmol) dissolved in 7 ml water. The solution was stirred at 80 ^oC for 24 hours, filtered and left to evaporate slowly. Dark blue needle crystals were formed, but were twinned, and were recrystallised via acetone diffusion. These crystals were still twinned. Mass spec and IR show a complex was formed.

Mass Spec Cy_2-tn+Ni: ITMS+c ESI (m/z) 327 (Cy_2-tn+Ni-2H+1), 373 (), 390 (Cy_2-tn-2H+Ni+NO_3+1), 471 (Cy_2-tn-2H+Ni+2NO_3+H_2O+1).

IR Cy_2-tn+Ni(N) (cm^{-1}): 3361 (N-H stretch), 3226 (O-H stretch), 2939 (C-H asy. stretch), 2860 (C-H sym. stretch),1662 and 976-949 (N-H bend), 1458-1449 (C-H_2 bend), 1402 (C-H bend), 1308 (O-H bend), 1242-1196 (C-N stretch), 1106-1086 (C-O stretch), 1061-1035 (C-C stretch), 918-889 (C-H bend), 790 (Ni-N stretch), 595 (Ni-N bend).

2.5.3. Synthesis of Cy_2-tn/Zn(II) Complex

Method H1: Zinc Nitrate hexahydrate, $Zn(NO_3)_2.6H_2O$, (0.2255 g, 0.787 mmol) was added to a solution of 0.2052 g (0.71646 mmol) Cy_2-tn in 10 ml water. This solution was heated to 70 ^oC and stirred for 24 hours. The solution was filtered and left to evaporate slowly. A yellow gel was formed. Mass spec and IR show no complex was formed.

Mass Spec Cy_2-tn+Zn(N): ITMS+c APCI: m/z 271 (Cy_2-tn+1), 272 (Cy_2-tn+1+H).

IR Cy_2-tn+Zn(N) (cm^{-1}): 3345 (N-H stretch), 3222 (O-H stretch), 2937 (C-H asym. stretch), 2869 (C-H sym. stretch), 1661 and 975-949 (N-H bend), 1468-1449 (C-H_2 bend), 1402 (C-H bend), 1306 (O-H bend), 1207 (C-N stretch), 1104-1083 (C-O stretch), 1060-1037 (C-C stretch), 917-897 (N-H bend), 859-790 (C-H bend).

Method H2: Zinc Nitrate hexahydrate, $Zn(NO_3)_2.6H_2O$, (0.2425 g, 0.8151 mmol) was added to a solution of 0.2017 g (0.9726. mmol) Cy_2-tn in 10 ml water. This solution was heated to 80 ^oC and stirred for 24 hours. The solution was filtered and left to evaporate slowly. A yellow gel was formed. Mass spec and IR show a complex was formed.

Mass Spec Cy_2-tn+Zn(N): ITMS+c ESI: m/z 271 (Cy_2-tn+1), 272 (Cy_2-tn+1+H), 327 (blank), 369 (Cy_2-tn+Zn+$2H_2O$-3H+1).

IR Cy_2-tn+Zn(N) (cm^{-1}): 3387 (N-H stretch), 3062 (O-H stretch), 2934 (C-H asym. stretch), 2857 (C-H sym. stretch), 1604 and 925 (N-H bend), 1451 (C-H_2 bend), 1350 (C-H bend), 1297

(O-H bend), 1185 (C-N stretch), 1104 (C-O stretch), 1072-1030 (C-C stretch), 925 (N-H bend), 869-761 (C-H bend).

Another method was tried,

Method H3: Zinc chloride hydrate, $ZnCl_2$, (0.1063 g, 0.7800 mmol) was added to a solution of 0.2009 g (0.7431 mmol) Cy_2-tn in 10 ml water. This solution was heated to 70 ^oC and stirred for 24 hours. The solution was filtered and left to evaporate slowly. Clear yellow needle/urchin crystals were formed (0.05025 g, 15.92%). The crystal structure of Cy_2-tn/Zn was obtained.

Mass Spec Cy_2-tn+Zn: ITMS+c ESI: m/z 271 (Cy_2-tn+1), 272 (Cy_2-tn+1+H), 369 (Cy_2-tn+1+Zn+Cl-2H), 373 (Cy_2-tn+1+Zn+Cl), 669 (2[Cy_2-tn-H+Zn]+1), 705 (2[Cy_2-tn+Zn-H]+Cl+1).

IR Cy_2-tn+Zn (cm^{-1}): 3236 (N-H stretch), 3160 (O-H stretch), 2934 (C-H asym. stretch), 2857 (C-H sym. stretch), 1454 (C-H_2 bend), 1352 (C-H bend), 1328 (O-H bend), 1256 (C-N stretch), 1206 (C-O stretch), 1037-944 (C-C stretch), 908-885 (N-H bend), 857 (C-H bend), 787 (Zn-N stretch), 633 (Zn-N bend).

The solid state structure of the Cy_2-tn/Zn complex is described in Table 2.5.2. The full data can be found in Appendix E in tables E.31 to E.36.

Table 2.5.2. Crystal data and structure refinement for Cy_2-tn/Zn(II) complex.

Temperature	173(2) K	
Crystal system	Triclinic	
Space group	$P\bar{1}$	
Unit cell dimensions	a = 7.2982(2) Å	α = 115.3390(10)°.

	b = 12.2314(4) Å	β = 101.5160(10)°.
	c = 12.4397(4) Å	γ = 94.4210(10)°.
Volume	966.71(5) $Å^3$	
Z	2	
Density (calculated)	1.459 g/cm^3	
Absorption coefficient	1.561 mm^{-1}	
Goodness-of-fit on F^2	1.068	
Final R indices [I>2σ(I)]	R_1 = 0.0478, wR_2 = 0.1344	
R indices (all data)	R_1 = 0.0596, wR_2 = 0.1423	

2.5.4. Synthesis of Cy_2-tn/Cd(II) Complex

Mehtod I1: Cadmium chloride hydrate, $CdCl_2 \cdot 2.5H_2O$, (0.1702 g, 0.7450 mmol) was dissolved in 10 ml water. To this was added 0.1833 g (0.6780 mmol) Cy_2-tn. This solution was stirred at 80°C for 24 hours. The solution was then filtered and left to evaporate slowly. Crystals to small for XRD analysis. Synthesis was retried, a yellow gel was formed. Characterisation shows no complex was formed.

Mass Spec Cy_2-tn+Cd: ITMS+c APCI: m/z 271 (Cy_2-tn+1).

IR Cy_2-tn+Cd (cm^{-1}): 3255 (N-H stretch), 3180 (O-H stretch), 2931 (C-H asym. stretch), 2869 (C-H sym. stretch), 1637 and 967-950 (N-H bend), 1451-1420 (C-H_2 bend), 1353 (C-H bend),

1287 (O-H bend), 1241 (C-N stretch), 1210-1125 (C-O stretch), 1097-1000 (C-C stretch), 967-916 (N-H bend), 876-844 (C-H bend), 785 (Cd-N stretch).

Method I2: Cadmium chloride hydrate, $CdCl_2 \cdot 2.5H_2O$, (0.2048 g, 0.8965 mmol) was dissolved in 5 ml water and was added slowly to 0.2090 g (0.7731 mmol) Cy_2-tn dissolved in 5 ml water. This solution was stirred at 90^oC for 24 hours. The solution was then filtered and left to evaporate slowly. A yellow gel was formed, mass spec and IR show no complex was formed.

Mass Spec Cy_2-tn+Cd: ITMS+c ESI: m/z 271 (Cy_2-tn+1).

IR Cy_2-tn+Cd (cm^{-1}): 3306 (N-H stretch), 3254 (O-H stretch), 2922 (C-H asym. stretch), 2875-2859 (C-H sym. stretch), 1636 and 968-949 (N-H bend), 1451-1419 (C-H_2 bend), 1354 (C-H bend), 1286 (O-H bend), 1245 (C-N stretch), 1210-1146 (C-O stretch), 1098-998 (C-C stretch), 968-910 (N-H bend), 877-843 (C-H bend).

Another method was tried.

Method I3: 0.2841 g (1.0509 mmol) Cy_2-tn was dissolved in 9 ml water, the pH was then lowered to 7.1 with 35% HCl, cadmium chloride hydrate, $CdCl_2 \cdot 2.5H_2O$, (0.4668 g, 2.0433 mmol) was dissolved in 3 ml water and was added slowly to this solution. The solution was then stirred at room temperature for 48 hours, and then heated and stirred at 40^oC for 24 hours, and then stirred at room temperature for a further 48 hours. The solution was filtered and left to evaporate slowly. A yellow gel was formed, mass spec and IR show no complex was formed.

Mass Spec Cy_2-tn+Cd: ITMS+c ESI: m/z 271 (Cy_2-tn+1), 287 (blank), 316 (blank).

IR Cy_2-tn+Cd(Cl) (cm^{-1}): 3432 (N-H stretch), 3021 (O-H stretch), 2943 (C-H asym. stretch), 2962 (C-H sym. stretch), 1623 and 986-926 (N-H bend), 1466-1399 (C-H_2 bend), 1360-1333

(C-H bend), 1281 (O-H bend), 1236 (C-N stretch), 1200-1139 (C-O stretch), 1065-1024 (C-C stretch), 873-845 (N-H bend), 753 (C-H bend).

Method I4: Cadmium chloride hydrate, $CdCl_2 \cdot 2.5H_2O$, (0.5923 g, 2.593 mmol) was dissolved in 20 ml water. To this was added 0.5869 g (2.171 mmol) Cy_2-tn. This solution was left to reflux at 90 ^{0}C for 48 hours. The solution was filtered and left to evaporate slowly. The crystal structure was determined, the quality of the crystal is poor due to twinning.

Mass Spec Cy_2-tn+Cd: ITMS+c APCI: m/z 271 (Cy_2-tn+1), 661 (blank), 893 (2[Cy_2-tn+Cd+Cl]+1+3H_2O+4H), 929 (blank).

IR Cy_2-tn+Cd (cm^{-1}): 3306 (N-H stretch), 3245 (O-H stretch), 2928 (C-H asym. stretch), 2856 (C-H sym. stretch), 1450 and 968-949 (N-H bend), 1418 (C-H_2 bend), 1354-1289 (C-H bend), 1245-1210 (O-H bend), 1096-1072 (C-N stretch), 1049-998 (C-O stretch), 968-949 (C-C stretch), 932-910 (N-H bend), 878-855 (C-H bend), 611 (Cd-N stretch).

The solid state structure of the Cy_2-tn/Cd complex is described in Table 2.5.3. The full data can be found in Appendix E in tables E.37 to E.42.

Table 2.5.3. Crystal data and structure refinement for Cy_2-tn/Zn(II) complex.

Temperature	293(2) K	
Crystal system	Monoclinic	
Space group	*C*2/c	
Unit cell dimensions	a = 47.3500(50) Å	α = 90.000(5)°.
	b = 8.0620(50) Å	β = 104.213(5)°.

	c = 22.9460(50) Å γ = 90.000(5)°.
Volume	8491.18(125) $Å^3$
Z	4
Density (calculated)	1.465 g/cm^3
Absorption coefficient	1.294 mm^{-1}
Goodness-of-fit on F^2	1.131
Final R indices [I>2σ(I)]	R_1 = 0.239, wR_2 = 0.557
R indices (all data)	R_1 = 0.229, wR_2 = 0.553

2.5.5. Synthesis of Cy_2-tn/Pb(II) Complex

Method J1: Lead Nitrate, 0.3995 g (1.732 mmol), was dissolved in 10 ml water, and to this solution 0.1978 g (0.7316 mmol) Cy_2-tn was added. This solution was stirred at 70 ^{0}C for 24 hrs. The solution was then filtered and left to evaporate slowly. A gel was formed. Mass Spec and IR show a complex has formed.

Mass Spec Cy_2-tn+Pb: ITMS+c ESI: (m/z) 271 (Cy_2-tn+1), 272 (Cy_2-tn+H+1), 286 (blank), 604 (Cy_2-tn+Pb+2NO_3+2H+1).

IR Cy_2-tn+Pb (cm^{-1}): 3392 (N-H stretch), 3056 (O-H stretch), 2936 (C-H asym. stretch), 2857 (C-H sym. stretch), 1602 (N-H bend), 1450 (CH_2 bend), 1350 (C-H bend), 1294 (O-H bend), 1170 (C-N stretch), 1071 (C-O stretch), 923 (C-C stretch), 869-820 (C-H bend), 760 (Pb-N stretch), 721 (Pb-N bend).

Method J2: Lead chloride, 0.6023 g (2.166 mmol), was dissolved in 5 ml water, and added to 0.4332 g (1.602 mmol) Cy_2-tn dissolved in 10 ml water after the addition of 32% HCl to decrease the pH to 1.4. This solution was stirred at 70 ^{0}C for 24 hrs. The solution was then filtered and left to evaporate slowly. Thin, clear needles of $Pb(Cl)_2$ were formed.

Mass Spec Cy_2-tn+Pb: ITMS+c ESI: (m/z) 270 (Cy_2-tn-H+1), 286 (blank).

IR Cy_2-tn+Pb (cm^{-1}): 3329 (N-H stretch), 2894 (O-H stretch), 2342 (C-H asym. stretch), 2118 (C-H sym. stretch), 1637 (N-H bend), 1480 (CH_2 bend), 1350 (C-H bend), 1294 (O-H bend), 1153 (C-N stretch), 1086 (C-O stretch), 940 (C-C stretch), 870 (C-H bend).

2.6. References

1. Bruker, (2005). *APEX2* (Bruker AXS Inc., Madison, Wisconsin, USA).
2. Bruker, (2005). *SAINT-NT* (Bruker AXS Inc., Madison, Wisconsin, USA).
3. Bruker, (1999). *SHELXTL* (Bruker AXS Inc., Madison, Wisconsin, USA).
4. A. Spek. (2003). *J. Appl. Cryst.* **36**, 7.
5. L. Farrugia. (1997). *J. Appl. Cryst.* **30**, 565.
6. R. Hancock, A. de Sousa, G. Walton, and J. Reibenspies. (2007). *Inorg. Chem.*, **46**, 4749.

Chapter 3

Density Functional Theory

3.1. Computational Methods

Over the last 30 years, there has been a marked interest in both physics and chemistry, in the use of density functional theory (DFT) calculations to investigate the electronic structure (usually the ground state) of many-body systems by means of electron probability density functionals.[1] To rationalize the influence of molecular architecture on metal ion selectivity and affinity, a DFT study of the amino-alcohol ligands N,N'-bis(2-hydroxycyclohexyl)-trans-cyclohexane-1,2- diamine (TCA) with Cu(II) and N,N'-bis(2-hydroxycyclohexyl)-1,3-propanediamine (Cy_2-tn) with Cu(II), Ni(II), and Zn(II), using the X3LYP functionals with a 6-31G(d,p) basis set, performing single point calaculations on the geometry as revealed in the crystal structure, were conducted in combination with Quantum Theory of Atoms in Molecules (QTAIM) analyses.

All calculations were done using Gaussian 03 in a Linux workstation in parallel environment, and images were produced using GaussView 03 suit of programs.[2] A comparison between the calculated and experimental results was done, as well as investigating the bond types via the electron density.

The calculations were performed by Dr. C. B. Perry and Prof. H. M. Marques, but the analyses are those of the author presented below. All data pertaining to the DFT calculations are given in Appendix A on the CD.

3.2. Results and Discussion

3.2.1. Modelling of the Free Ligand Cy_2-tn

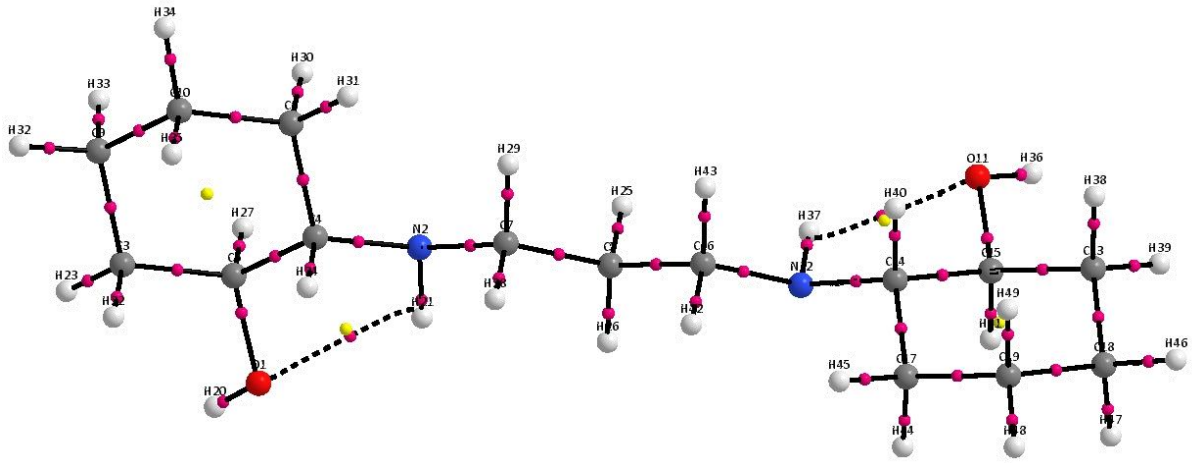


Figure 3.2.1. QTAIM molecular graph of Cy_2-tn.

Figure 3.2.1 shows the molecular graph of Cy_2-tn. The solid black lines are the bond paths where the electron density lies at a maximum. The pink dots in the bond paths are the bond critical points (BCP) at which the value of the density gives an indication of the bond strength and the yellow dots are the ring critical points (RCP). The dotted lines indicate weak intra-molecular interactions, or H-bonds between the hydroxide O on both the cyclohexenyl groups and the hydrogens present on the amine nitrogens (O_1---$H_{21}(N_1)$ and O_2---$H_{37}(N_2)$), as the molecule is centrosymmetric. It can be seen that the BCP in these H-bonds lie slightly more towards the hydrogen than the oxygen atom, and the RCP lies very close to the H-bond bond path, almost coinciding with the BCP, showing the weakness of this interaction.[2] As the O-H interaction weakens, the RCP moves closer to the BCP,and would eventually disappear as the O-H interaction electron density energy tends towards zero.

3.2.2. Modelling of TCA/Cu and Cy_2-tn with Ni(II), Zn(II) and Cu(II)

Tables 3.2.1 summarise, for convenience, the characteristics of ionic, covalent and metal-ligand bonds as obtained from QTAIM analysis (refer to Chapter 1 for a more complete discussion).

Table 3.2.1. Characterisation of ionic, covalent, and M-L/M-M interactions.[3,4,5]

	Closed shell (ionic)	*Shared (covalent)*	*M-M or M-L*
$\boldsymbol{\rho_b}$	Small, > 0 (~ 10^{-3} au)	> 0.1 au (or > 0.15 au)	Small, > 0
$\boldsymbol{\nabla^2\rho_b}$	Small, > 0	< 0, same order as ρ_b	Small, > 0
$\boldsymbol{V_b}$	< 0	< 0	< 0
$\boldsymbol{G_b}$	Large, > 0	Small, > 0	Small, > 0
$\boldsymbol{H_b}$	(+), close to 0	< 0	(-), close to 0
$\boldsymbol{\lvert V_b\rvert/G_b}$	< 1	> 2	$1 < \lvert V_b\rvert/G_b < 2$
$\boldsymbol{G_b/\rho_b}$	> 1	< 1	> 1

Moreover, interactions with $1 < |V_b|/G_b < 2$, are indicative of intermediate interactions.

In Table 3.2.2. are listed selected M-L bond lengths of the crystal structures and DFT calculations of TCA/Cu, Cy_2-tn/Cu, Cy_2-tn/Ni and Cy_2-tn/Zn complexes. **T**he DFT calculations predicted the bond length fairly accurately (average difference of -0.041 Å) as can be seen by the R^2 value of 0.8854 for the comparative graph of the experimental M-L bond lengths vs. the calculated M-L bond lengths (**Fig. 3.2.2.**). However, the calculated M-L bonds lengths are fractionally longer than the observed bond lengths, except for axial Zn-Cl bond in the Cy_2-tn/Zn structure, in which the calculated bond length is slightly shorter than the observed bond length by 0.022 Å.

Table 3.2.2. Selected M-L bond lengths of the crystal structures and DFT calculations of Cy_2-tn/Ni, Cy_2-tn/Zn, TCA/Cu, and Cy_2-tn/Cu complexes.

	CRYSTAL STRUCTURES	**DFT (X3LYP/6-31+G(d,p))**	**Δ(obs-calc)**
	bond lengths (Å)	*bond lengths (Å)*	
Cy_2-tn/Ni			
M-N	2.056	2.076	-0.020
M-N	2.064	2.081	-0.017
M-O	2.054	2.100	-0.046
M-O	2.075	2.103	-0.028
M-Ax1 (H_2O)	2.072	2.173	-0.101
M-Ax2 (H_2O)	2.187	2.206	-0.019
Cy_2-tn/Zn			
M-N	2.073	2.137	-0.064
M-N	2.111	2.137	-0.026
M-O	2.075	2.173	-0.098
M-O	2.127	2.173	-0.046
M-Ax1 (Cl)	2.254	2.232	0.022
TCA/Cu			
M-N	1.986	2.003	-0.017
M-N	1.986	2.003	-0.017
M-O	1.947	1.979	-0.032
M-O	1.947	1.979	-0.032
Cy_2-tn/Cu			
M-N	1.978	2.025	-0.047
M-N	1.998	2.031	-0.033
M-O	1.992	2.017	-0.025
M-O	1.996	2.023	-0.027
M-Ax1 (H_2O)	2.262	2.406	-0.144

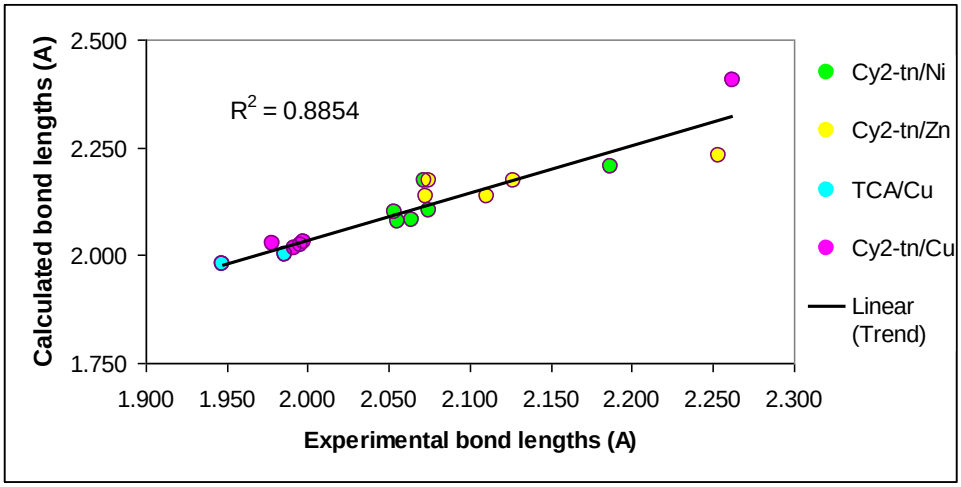


Figure 3.2.2. Selected experimental vs. calculated bond lengths for the Cy_2-tn with Ni(II), Cu(II), and Zn(II), and TCA/Cu complexes.

As the bond lengths increase (**Fig. 3.2.3.**), the electron density decreases. Because the electron density (ρ) correlates with the bond length, the electron density can be used as a measure of bond strength. Another trend that can be seen; is that the longest bonds present in both the calculated and experimental data are the axial bonds to the metal ions in the complexes. The Cy_2-tn/Zn outlier point is the over-estimated Zn-Cl axial bond length, and the longest, weakest bond present is the Cu-H_2O axial bond in the Cy_2-tn/Cu complex. It can also be seen that the TCA/Cu bonds are stronger than the Cy_2-tn/metal bonds. This is attributed to the inductive effect of the extra cyclohexenyl ring in the TCA ligand.

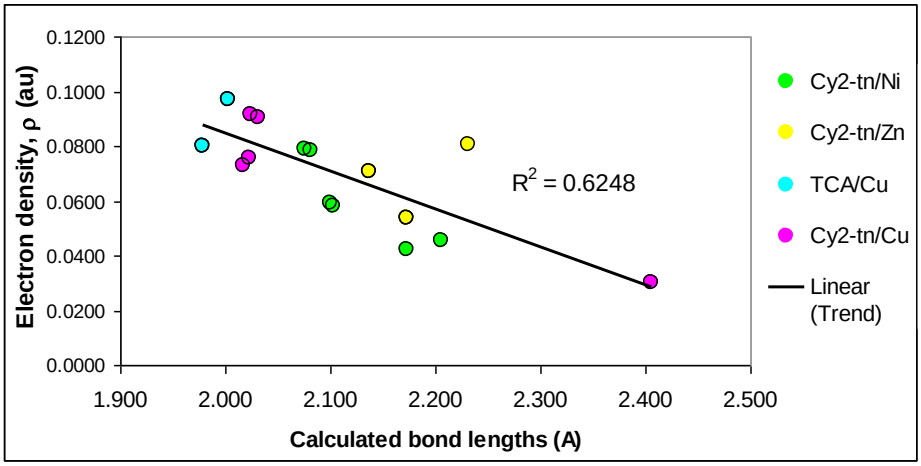


Figure 3.2.3. Electron density vs. selected calculated bond lengths for the TCA/Cu and the Cy_2-tn with Ni(II), Zn(II), and Cu(II) complexes.

From Figure 3.2.4., it is seen that the metal-ligand bonds have a very low electron density and positive Laplacian ($\nabla^2\rho$) values. This suggests that M-L bonds are predominantly ionic whilst the N-C, C-C and C-O bonds, with higher electron density and negative Laplacian values are predominantly covalent. The longer the bond length, the lower the electron density, and the weaker the bond. It follows then that the covalent bonds are stronger than the M-L bonds, as their electron density is greater. The NC-CO bonds have the greatest electron density and are therefore the strongest bonds, followed by the C-N and then the C-O bonds. This is as expected if one looks at typical bond enthalpies of the C-C bond (348 kJ/mol), C-N bond (293 kJ/mol), and the C-O bond (358 kJ/mol).[6] The M-N have a slightly greater electron density than the M-O bonds and are therefore slightly stronger. The hollow circle is the M-Cl bond in the Cy_2-tn/Zn complex and falls in between the M-O, and M-N bond strengths based on the electron density. The M-Cl bond is slightly more covalent in character than the M-O and M-N bonds, this may be unusual and could indicate the involvement of the chlorine lone pair of electrons in the bonding, which may contribute to the covalency of the bond. Additionally, chlorine being a third row element, as opposed to the second row elements N and O, may be more polarisable than expected and therefore lead to more covalent bonding with metals. However, further investigation is needed and is beyond the scope of this project.

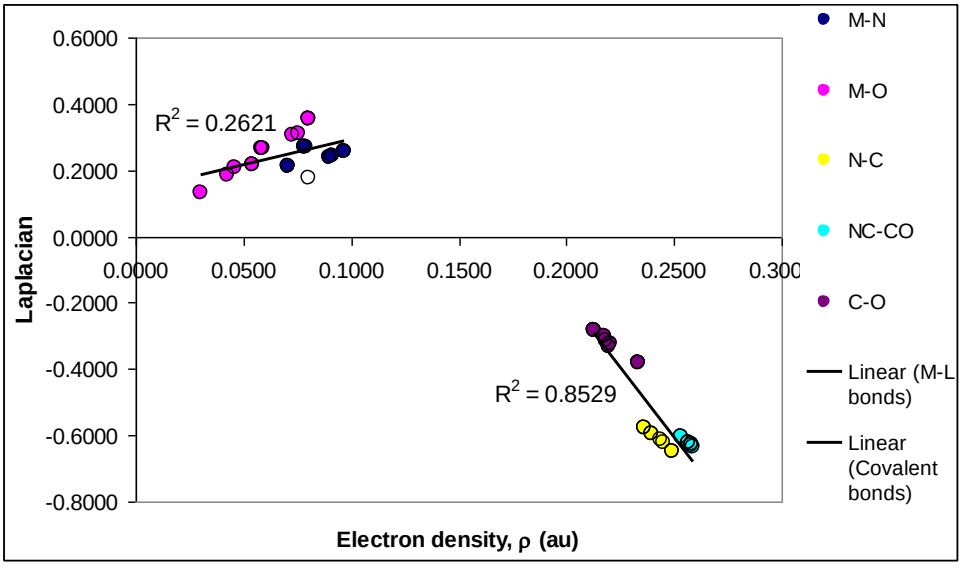


Figure 3.2.4. Electron density vs. Laplacian values of selected M-L, N-C, NC-CO, and C-O covalent bonds of TCA/Cu and Cy_2-tn with Ni(II), Zn(II), and Cu(II) complexes.

Espinosa *et al.*[7] have suggested that for a predominantly covalent interaction one would expect the potential energy density (V(r)), which is a negative quantity, to dominate over the kinetic energy density (G(r)), which is a positive quantity. The total energy density, H(r) = V(r) + G(r), should be negative for a covalent interaction and positive for an ionic interaction. One might, therefore, be tempted to use the values of V(r) and G(r) as an index of bond character.

In Figure 3.2.5., we plot the electron density against the potential energy density. It can be seen that the potential energy density values for M-N bonds tend to be more negative than the potential energy values of M-O bonds. This indicates M-N bonds are more covalent in character than the M-O bonds. As covalency increases, the electron density increases, and as the electron density increases, the electrons spend more time between the atoms increasing the electrons potential energy (which is a negative value).

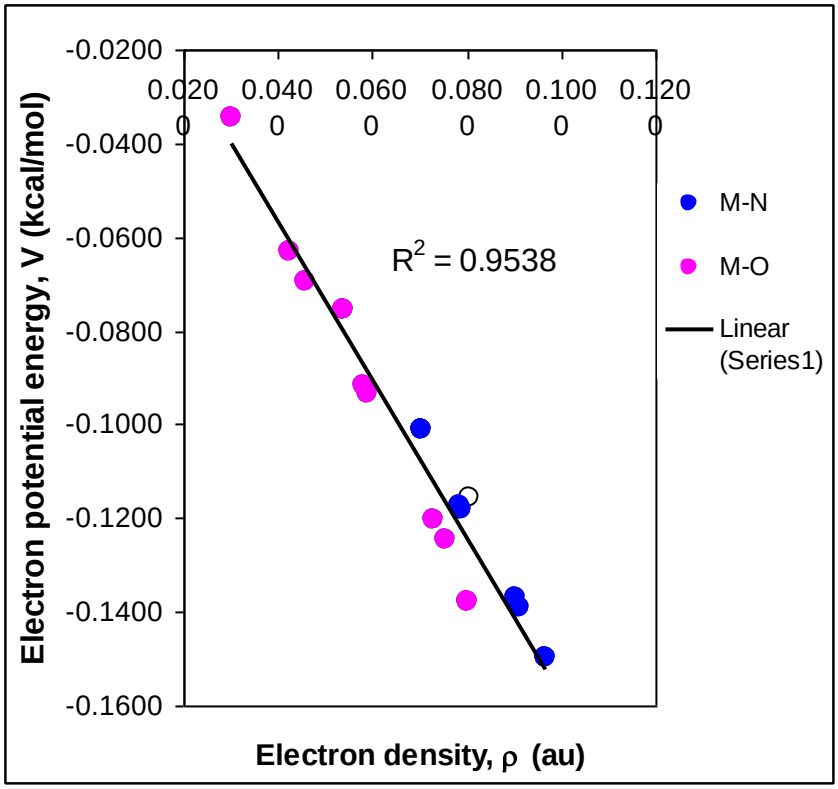


Figure 3.2.5. Electron density vs. the electron potential energy of M-L bonds of TCA/Cu, and Cy_2-tn with Ni(II), Zn(II), and Cu(II) complexes.

In Figure 3.2.6., we plot the electron density against the electron kinetic energy density. It can be seen that the kinetic energy density values for the M-N bonds are more positive than the kinetic energy density values for the M-O bonds. This suggests that the M-N bonds are more ionic in character than the M-O bonds. As covalency increases, the electron density increases, and as the electron density increases the electrons move faster between the atoms increasing the electrons kinetic energy (which is a positive value).

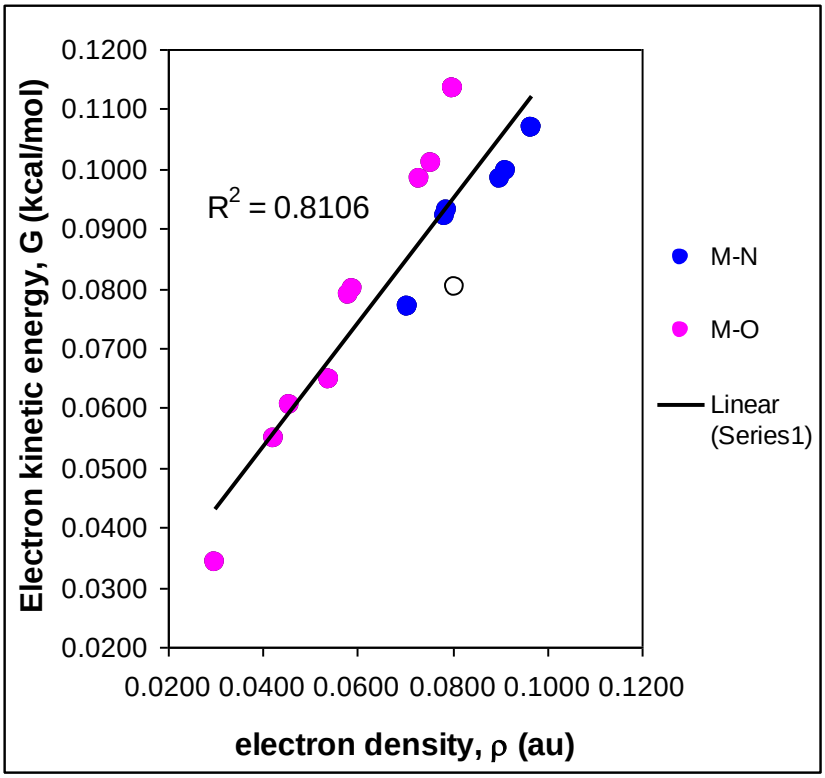


Figure 3.2.6. Electron density vs. electron kinetic energy of M-L bonds of TCA/Cu, and Cy_2-tn with Ni(II), Zn(II), and Cu(II) complexes.

However, these two results are in direct contradiction. Therefore the assumption that these energy density values can be used individually as an indicator of bond type cannot be correct. One should rather use the total energy density (H(r)), or the ratio $|V_b|/G_b$, as these values give a better indication of bond character. Where $|V_b|/G_b < 1$ for ionic bonds, $|V_b|/G_b > 2$ for covalent bonds, and $1 < |V_b|/G_b < 2$ for intermediate bond character.[7]

Looking at the $|V_b|/G_b$ values (**Fig. 3.2.7.**) it can be seen that the M-L bonds lie between 1 and 2, showing that they are intermediate interactions, between close shell and shared interactions. Again, the M-O bonds are somewhat more ionic than the M-N bonds. The ligand bonds N-C, NC-CO, and C-O $|V_b|/G_b$ values lie above 2, showing they are covalent or shared interactions, and again the NC-CO bonds are more covalent that the N-C and C-O bonds, i.e., the last two are clearly polar covalent bonds as might be expected from the difference in electronegativity of the two atoms in question.

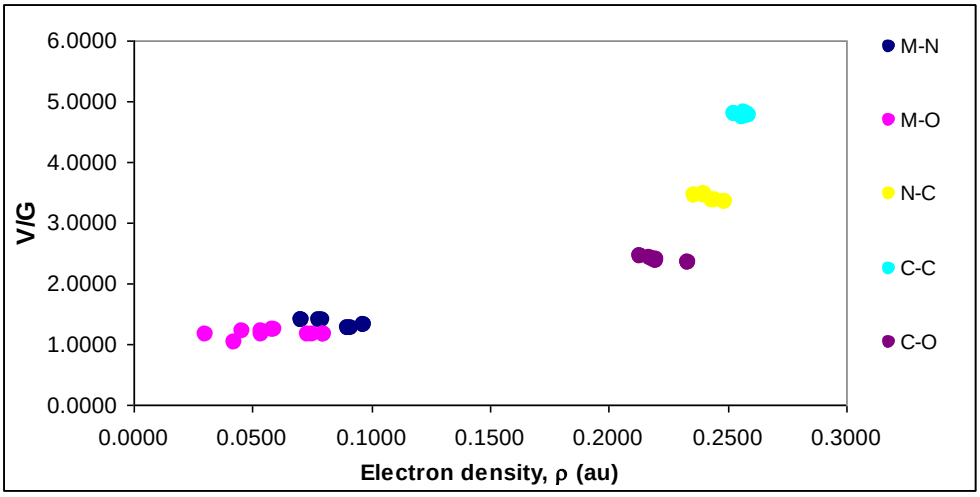


Figure 3.2.7. Electron density vs.V/G energy of the M-L and the ligand C-N, NC-CO, andC-O bonds.

From Figure 3.2.8., the total energy of the electron density for the M-L bonds indicates that the M-L bonds are covalent in nature; however, the values are more positive than those of the C-N, NC-CO, and C-O bonds. The M-L bonds are therefore more ionic in nature than the C-N, NC-CO, and C-O bonds in the ligand.

It can be concluded that the M-N bonds are more covalent in nature than the M-O bonds, as the total energy is more negative, and the electron density is around 0.1 au; this is consistant with the fact that N is less electronegativity than O.

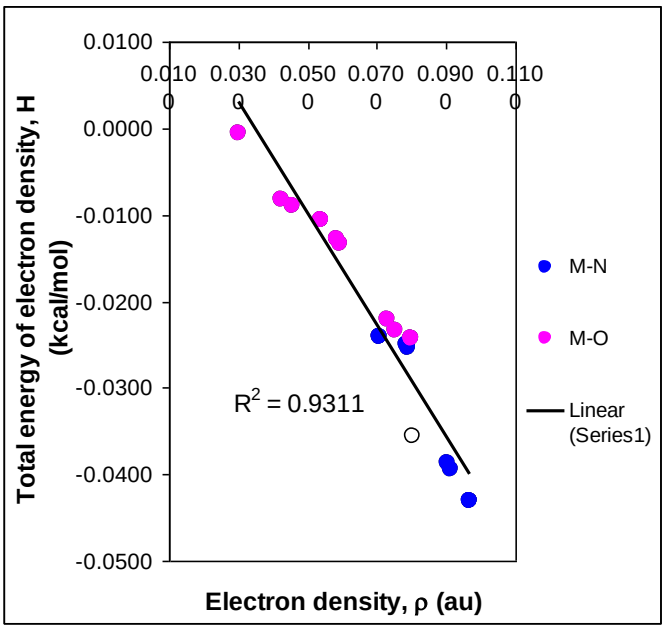


Figure 3.2.8. Electron density vs. total electron density energy of M-L bonds of TCA/Cu, and Cy_2-tn with Ni(II), Zn(II), and Cu(II) complexes.

The data in Figures 3.2.9. and 3.2.10. shows the M-L bonds are indeed ionic in nature, but the TCA/Cu and Cy_2-tn/Cu M-L bonds are more stable and somewhat more ionic in character than the Cy_2-tn/Ni and Cy_2-tn/Zn M-L bonds based on the electron density potential and kinetic energy densities.

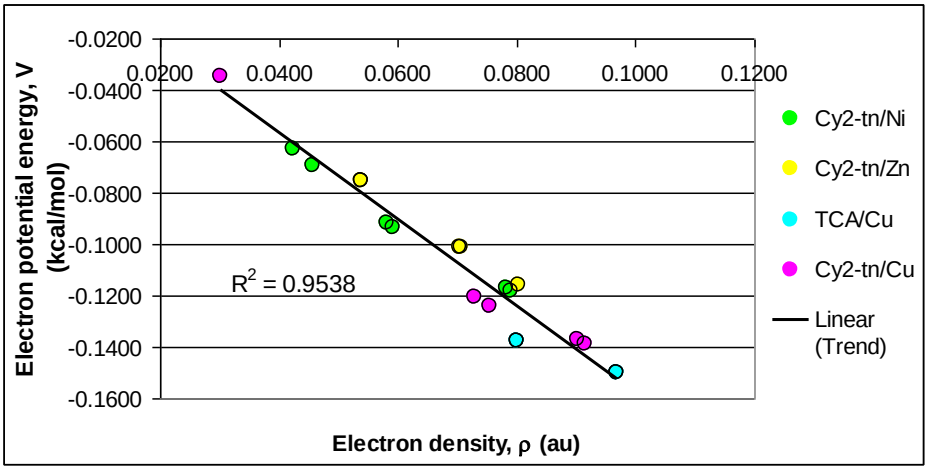


Figure 3.2.9. Electron density vs. electron potential energy of M-L bonds of TCA/Cu, and Cy_2-tn with Ni(II), Zn(II), and Cu(II) complexes.

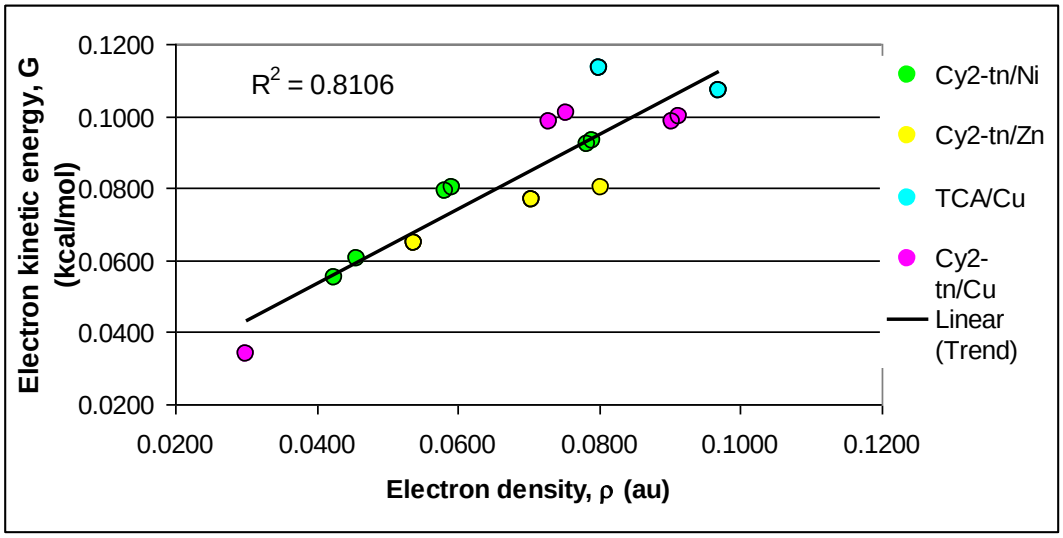


Figure 3.2.10. Electron density vs. electron kinetic energy of M-L bonds of TCA/Cu, and Cy_2-tn with Ni(II), Zn(II), and Cu(II) complexes.

However, based on the total energy of electron density (**Fig. 3.2.11.**), the TCA/Cu and Cy_2-tn/Cu complexes are slightly more covalent in nature than the Cy_2-tn with Zn(II) and Ni(II). This is further supported by the electron density values being around 0.1 au which is expected for covalent interactions.

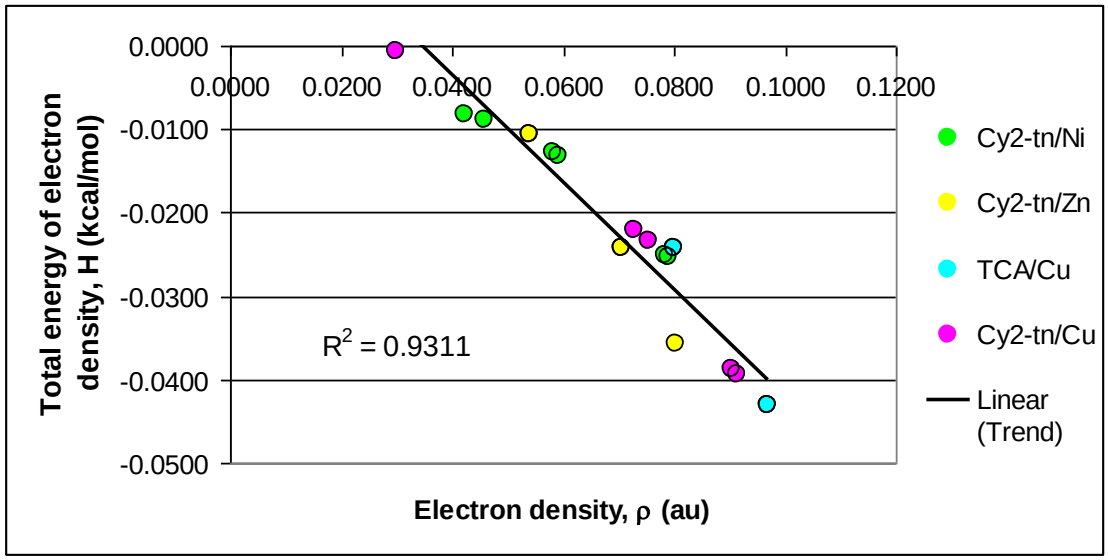


Figure 3.2.11. Electron density vs. total electron density energy of M-L bonds of TCA/Cu, and Cy_2-tn with Ni(II), Zn(II), and Cu(II) complexes.

Figure 3.2.12., shows that potential energy density dominates over the kinetic energy density for these bonds indicating they are covalent in nature, as expected. The NC-CO bonds are stronger, based on the electron density, followed by N-C and then C-O bonds. This trend is also followed when looking at the strength of covalent character of these bonds. Conversely, it can be expected (**Fig. 3.2.13.**) that the C-O bonds have BCPs that are characterised by a higher linetic energy density, and are therefore more ionic in nature, than the N-C bonds, followed by the NC-CO bonds.

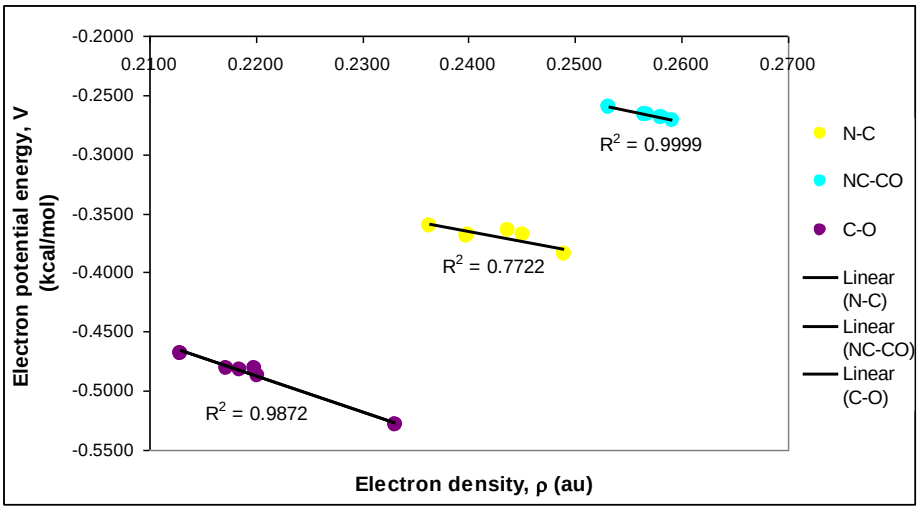


Figure 3.2.12. Electron density vs. electron potential energy of ligand TCA and Cy_2-tn C-N, NC-CO, and C-O bonds.

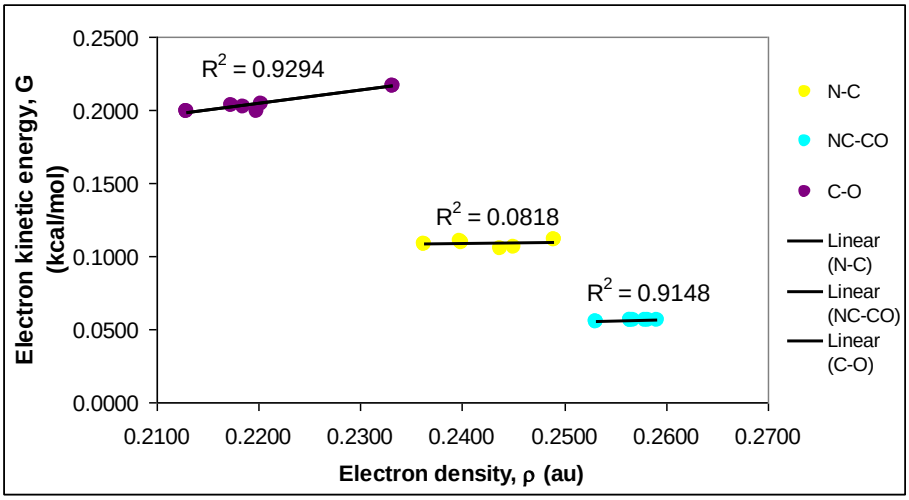


Figure 3.2.13. Electron density vs. electron kinetic energy of ligand TCA and Cy_2-tn C-N, NC-CO, and C-O bonds.

Looking at the total electron density energy of the TCA and Cy_2-tn ligand bonds (**Fig. 3.2.14.**), it can once again be seen that the NC-CO bonds are more stable and are more covalent in nature that the N-C, and then the C-O bonds. The C-O bonds are still covalent bonds, but slightly more ionic in nature than the N-C and NC-CO bonds, consistent with generally accepted polar covalent nature.

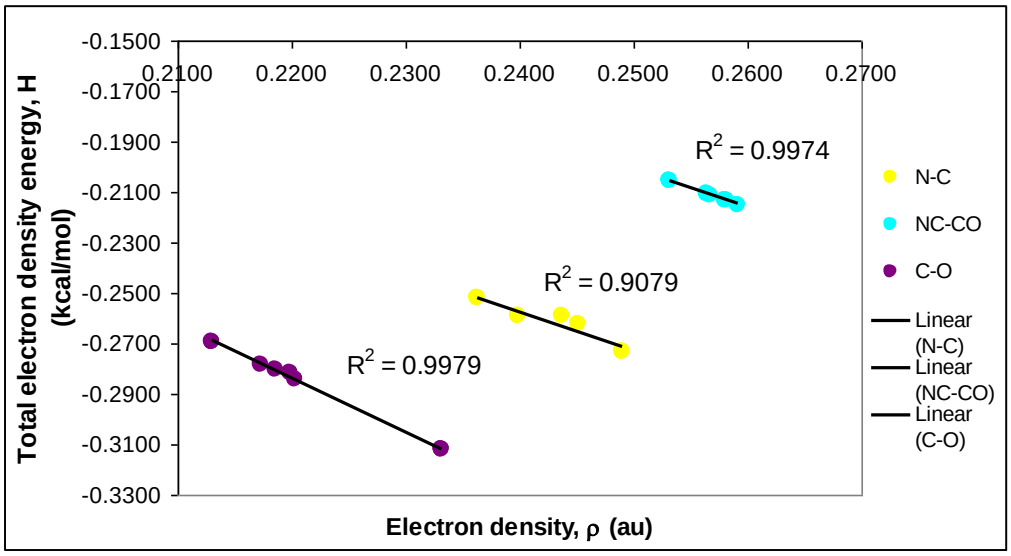


Figure. 3.2.14. Electron density vs. total electron density energy of ligand TCA and Cy_2-tn C-N, NC-CO, and C-O bonds.

In Table 3.2. it can be seen that the charge on the metal ions are not the formal 2+ charge, as the ligand imparts some electron density (ΔQ) onto the metal, decreasing its charge.

Table 3.2.3. Charge on the metal atom (q(A) and the electron transfer from the ligand to the metal (ΔQ).

Complex	q(A)	ΔQ
TCA/Cu (M-L)	1.0439	0.9561
Cy_2-tn/Ni (M-L)	1.2027	0.7973
Cy_2-tn/Zn (M-L)	1.1597	0.8403
Cy_2-tn/Cu (M-L)	1.0605	0.9395

3.2.3. QTAIM Molecular Graphs

The QTAIM molecular graphs of Cy_2-tn with Ni(II), Zn(II) and Cu(II) (**Fig. 3.2.15., 3.2.16, and 3.2.17.**) shows the bond paths and the BCPs where $\nabla\rho$ vanishes. It can be seen that the more polar the bond, the closer the BCP is to the less electronegative atom. In the C-O and C-N bonds, the BCP lies closer to the C atoms than the N and O atoms, and the BCP lies in the middle of the C-C bond. In the M-L bonds, the BCP lies slightly closer to the metal ions than the ligand donor atoms. This confirms the polarity of the bonds, which is in agreement with the conclusion reached earlier, that the M-L bonds are predominantly ionic with some covalent character. The presence of the RCP shows an electron density minimum in the rings present in the ligand.

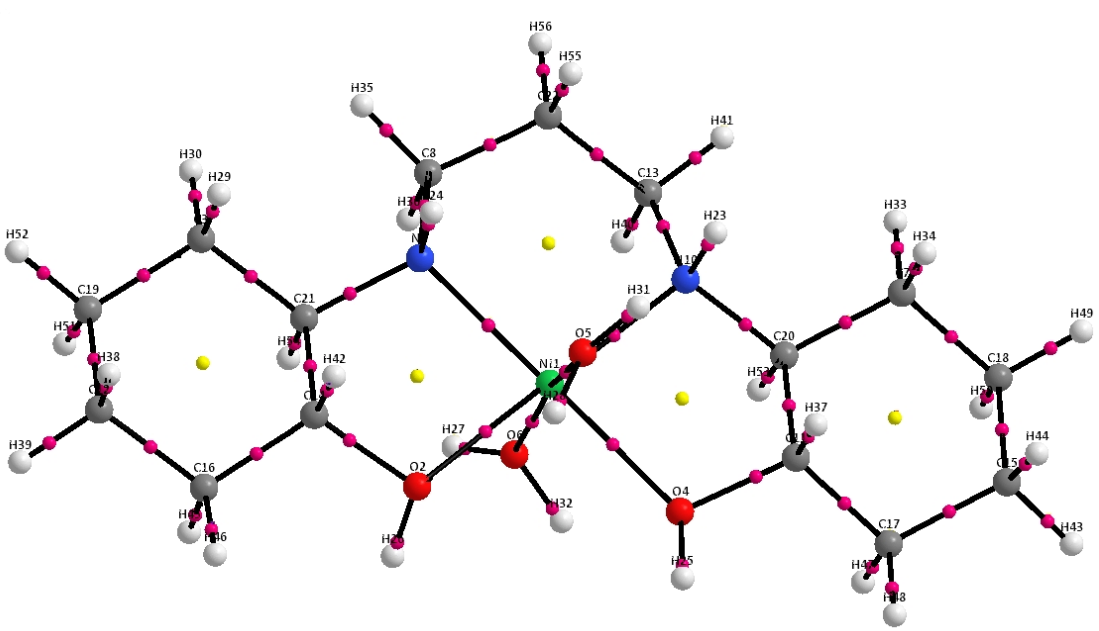


Figure 3.2.15. QTAIM molecular graph of Cy_2-tn/Ni complex.

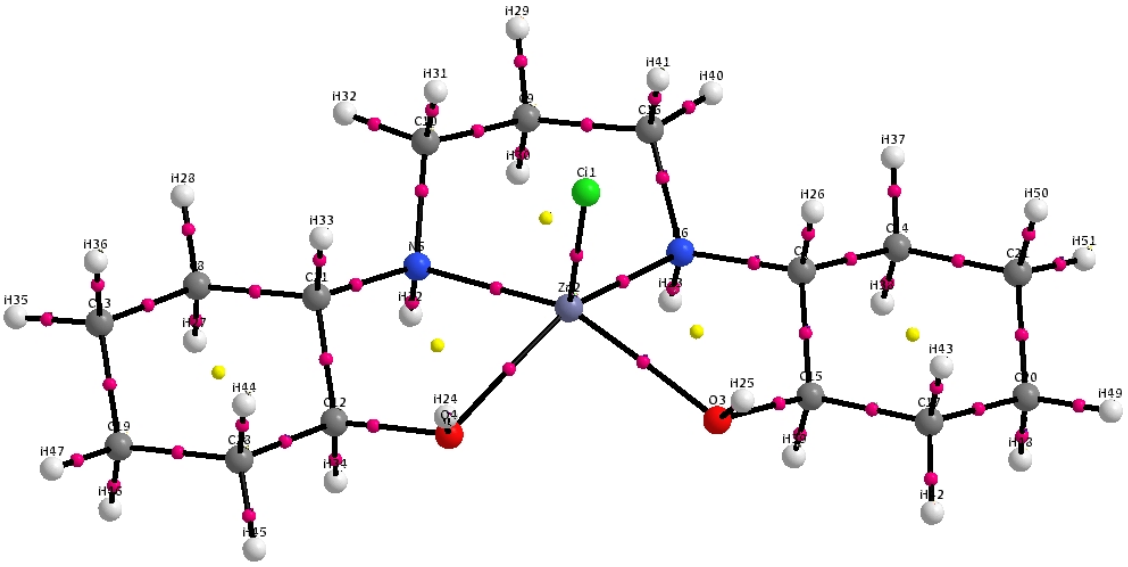


Figure 3.2.16. QTAIM molecular graph of Cy_2-tn/Zn complex.

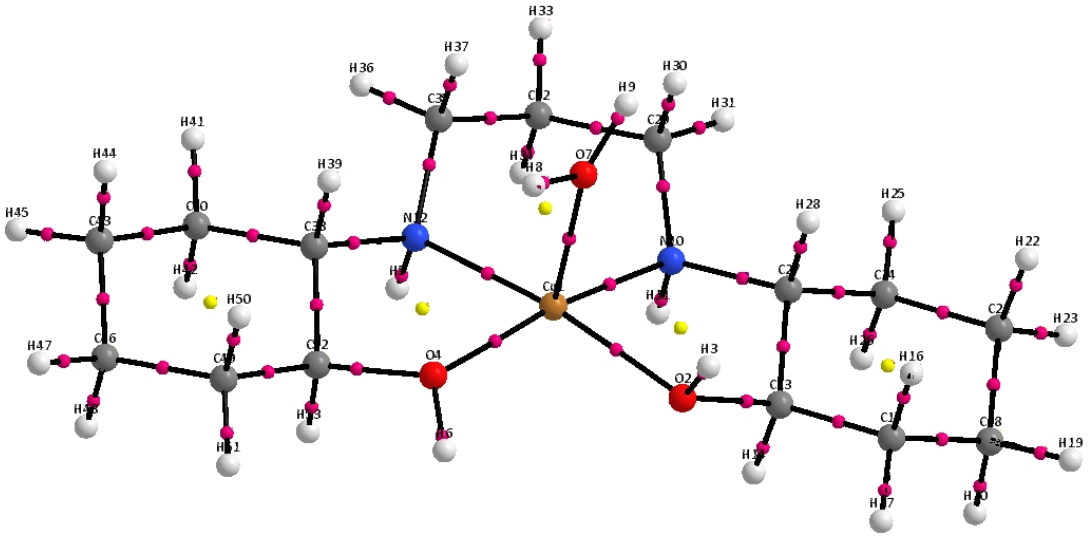


Figure 3.2.17. QTAIM molecular graph of Cy_2-tn/Cu complex.

In the molecular graph of TCA/Cu (**Fig. 3.2.18.**), there are weak intra-molecular interactions between the H atoms on the cyclohexenyl rings (H_{15}---H_{16}, and H_{52}---H_{48}). These H-H interactions have bond paths between them resulting in the addition of two 7-membered rings with the resulting RCPs. These H-H interactions are also present in the crystal structure of TCA/Cu. These H-H interactions are bonds that stabilise the molecule.[2] There are H-H interactions present in the crystal structures of Cy_2-tn with Ni(II), Zn(II), and Cu(II), between

the CH_2 groups on the cyclohexenyl rings and the CH_2 groups on the propyl bridge. These H-H bond distances in the crystal structures are much shorter than the sum of their van der Waals radii (2.40 Å), as discussed in chapter 4, but are not seen in the molecular graphs. The lack of bond paths between these CH_2 groups strongly suggests that these interactions are steric clashes, and not bonds.

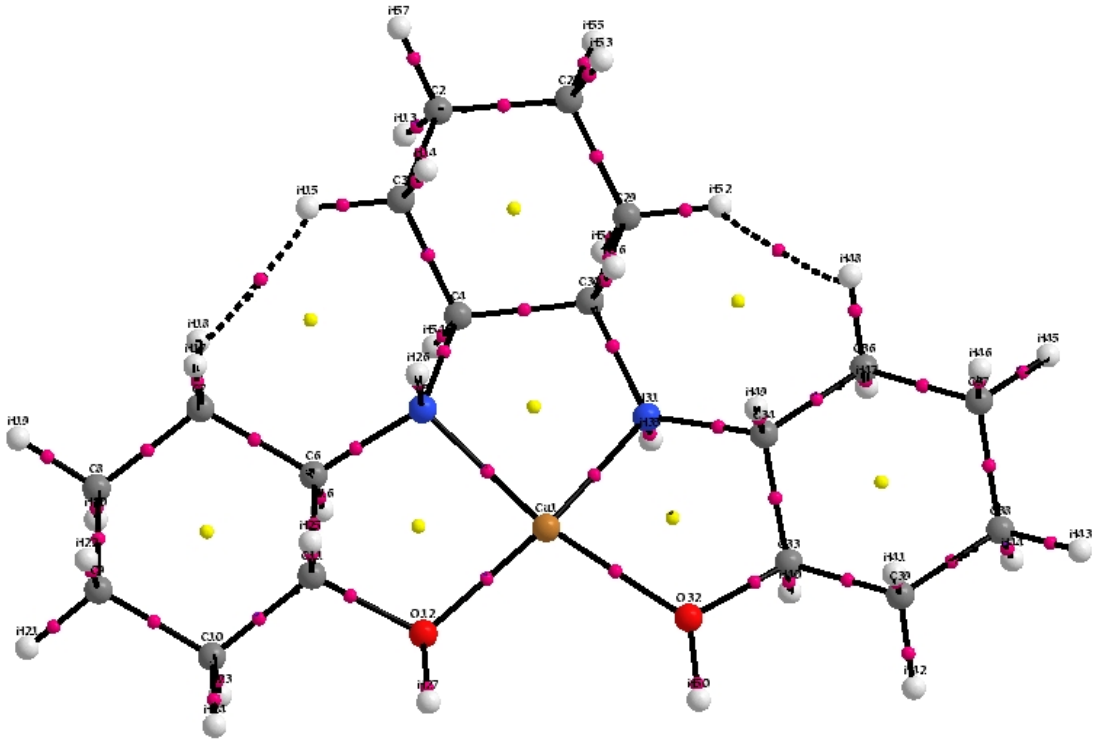


Figure 3.2.18. QTAIM molecular graph of TCA/Cu complex.

3.3. Conclusions

The DFT and QTAIM data allow one to determine the nature of the bonds as well as the stability of the bonds present. The model proved to be fairly accurate based on the small differences between the experimental and calculated bond lengths. In the structure of the free ligand (Cy_2-tn) the H-bonds present were shown to be fairly weak as the RCPs almost coincided with the BCPs. The M-L bonds were shown to be intermediate in nature i.e. ionic with some covalent character. This slightly shared electron density character in the M-L bonds, was seen

by the charge on the metal ions being less than the formal 2+ charge, suggesting that the electronegativity of the metal ions are greater than expected. The M-N bonds were suggested to be stronger than the M-O bonds, based on the electron density, and more covalent in character than the M-O bonds, based on the overall electron density energy, as expected. The axial M-L bonds were shown to be the longest and weakest bonds in the systems. The TCA and Cy_2-tn ligand bonds C-N, NC-CO, and C-O bonds were shown to be covalent in character, and the NC-CN were stronger than the N-C followed by the C-O bonds, based on the electron density. The C-O bonds were also seen to be slightly less covalent in character than the C-N and NC-CO bonds, as expected.

In the QTAIM molecular graphs, it could be seen that in the M-L bonds, the BCPs lie slightly closer to the metal ions than the donor atoms. It could also be seen that the BCPs in the polar bonds lie closer to the less electronegative atom, in the C-O and C-N bonds the BCPs lies closer to the C atoms, and in the C-H, and O-H bonds the BCPs lie closer to the H atoms. The molecular graph of TCA/Cu showed the presence of H-H bonds between hydrogens on the adjacent cyclohexenyl rings, which creates two stabilising 7-membered rings in the system.

Based on electron density, the TCA ligand proved to be the most stable, most likely due to the inductive effect of the extra stabilising cyclohexenyl ring on the amine bridge. Due to the fact that the donor atoms on the ligands TCA and Cy_2-tn were the same, it can be seen that the Cu(II) complexes with both TCA and Cy_2-tn were slightly more stable than the Cy_2-tn complexes with Ni(II) and Zn(II).

This study further demonstrates the use of DFT modelling in bond characterisation as well as determining the stability of M-L complexes via the electron density in the M-L bonds.

3.4. References

1. N. Harrison. *An introduction to density functional theory,* Imperial college of Science Technology and Medicine, London.
2. P. Varadwaj, I. Cukrowski, H. Marques. (2009). *J. Mol. Struct., Theochem.*
3. H. M. Marques. Private communications, University of the Witwatersrand, Johannesburg.
4. R. Bader and H. Essén. (1984). *J. Chem. Phys.*, **80**, 1943.
5. M. Bobrov, G. Popova and V. Tsirelson. (2006). *Russ. J. Phys. Chem.*, **80**, 584.
6. T. L. Brown, H. E. LeMay, B. E. Bursten, J. R. Burdge. (2003). *Chemistry, The Central Science,* **9th Ed.**, Pearson Education Inc., New Jersey.
7. E. Espinosa, I. Alkorta, J. Elguero and E. Molins. (2002). *J. Chem. Phys.*, **117**, 5529.

Chapter 4

Discussion

X-ray diffraction (XRD) is one of the most important and widely used structure determination technique in chemistry.[1] This method allows for the unambiguous determination of the position of the atoms and ions in a compound, resulting in structural data that can aid in predicting other structures and explain trends in many properties.[1] Obtaining the crystal structures of the amino alcohol ligands (Cy_2-tn and Cy_2-Otn) and their complexes to metal ion may aid in investigating features such as the H--H close contact interactions between the hydrogen on the cylohexenyl rings and hydrogens on the propyl bridge, that have been seen in other similar amino alcohol complexes.[2,3] As well as the coordination and bonding of the ligand to the metal ions, and other structural information that may aid in ligand design.

All analytical data are given in detail in Chapter 2, Materials, Methods, and Results.

It should be noted that all discussions referring to hydrogen atoms are based on XRD data, which cannot predict the exact position of a hydrogen atom as it measures the diffraction of the incident X-radiation by electrons. Thus all hydrogen atoms are placed according to a general best-fit formula, meaning all hydrogen positions are calculated from ideal geometries and not placed experimentally. It should also be noted that the solvent of choice was water, so as to possibly determine the structures of complexes that may appear in aqueous solution, and aid in the potentiometric studies. All *cif* files for the crystal structures mentioned in this study can be found on the attached CD.

4.1. Synthesis and Characterisation of the Free Ligands

4.1.1 Synthesis of Cy_2-Otn

The synthesis was performed using a method previously described by de Sousa and Hancock,[2] at room temperature. The first four reactions (L1-L4) were done using an old bottle of 1,3-diamino-2-propanol which had been exposed to air and reacted with the carbon dioxide and formed a carbamate, as reported in the dissertation *The solid state structure of metal-beta-amino alcohol complexes* by Reisinger.[3] The presence of this carbamate prevented the solution from reacting properly forming a brown oil that did not solidify to form the desired pale yellow powder. The mass spectroscopy characterisation of the gels showed a mixture of products, such as the mono-substituted amine, the desired di-substituted amine, and a tri-substituted amine (Appendix C). Increasing the reaction time may have increased the amount of desired product (Cy_2-Otn) but it would have been contaminated with the carbamate, and the cyclohexene oxide may have formed the tri-substitute amine as a major product. Using a new bottle of 1,3-diamino-2-propanol and performing the same reaction under argon (L5-L8), the oil that formed solidified to form a pale yellow powder that was the desired product (Cy_2-Otn). The yields of the first two reactions (L5 & L6) were low as they were not given sufficient time to fully solidify (only two weeks). The third reaction (L7) was left for a month and gave a yield of 96%. L8 was only left for three weeks and so the yield was lower (55%).

All the characterisation data indicate that the reactions (L5-L8) were successful and produced a clean product. The mass spectroscopy values were m/z 287 (Cy_2-Otn+1), as well as the presence of some sodium from the glassware. The NMR spectroscopy data split and integrated as expected for the free ligand, and the IR spectroscopy showed the expected bending and stretching. The characterisation data can be found in Appendices B-E.

The Cy_2-Otn(a) crystallised in a *C*2/c space group and an R-factor of 7.86%, and showed that there are three molecules in the asymmetric unit cell with disorder around the hydroxyl

group on the propyl bridge on one of the molecules. This is a polymorph (Cy_2-Otn(a)) of the structure Reisinger[3] determined (Cy_2-Otn(b)). In Cy_2-Otn(a), all three molecules have the cyclohexenyl rings adopt the chair conformation. The absolute geometry of the molecules are interesting as all the chiral carbon atoms on the cyclohexenyl rings in one molecule adopt the same geometry (C6 and C1, C10 and C15, C16 and C21, C25 and C30, C31 and C36) either *S* or *R* (**Fig. 4.1.1.**). The chiral carbons in the first molecule (C1, C6, C10 and C15) adopt an *S* geometry, while the chiral carbons in the second (C16, C21, C25 and C30) and third molecule (C31 and C36) adopt an *R* geometry.

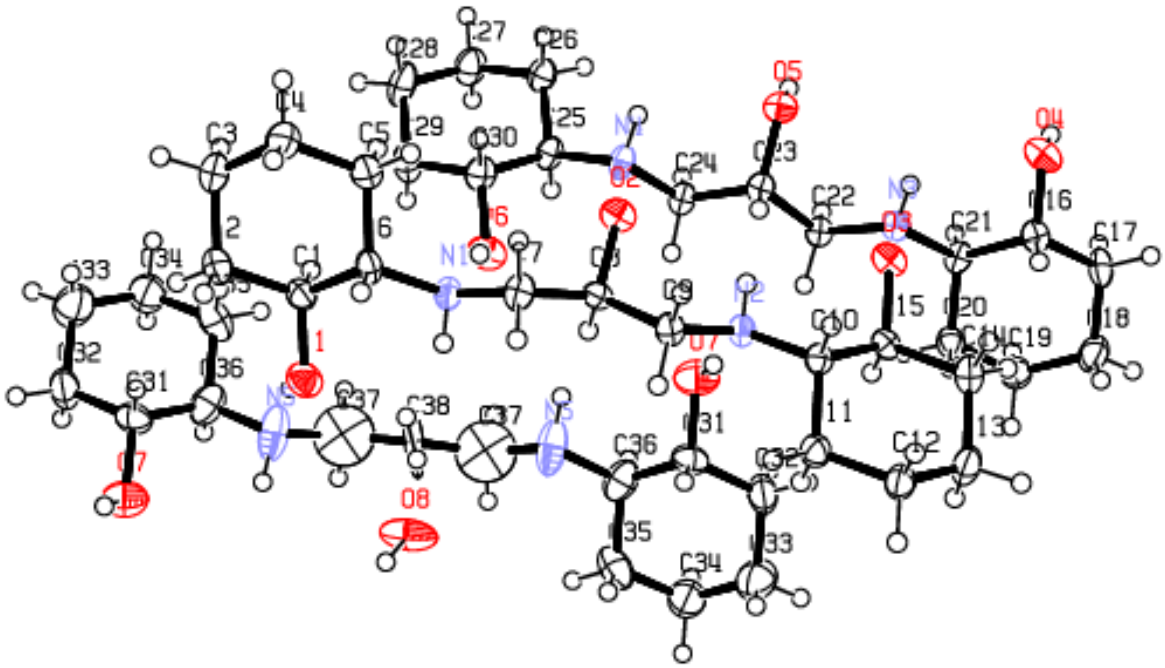


Figure 4.1.1. The molecular structure of Cy_2-Otn(a), showing the atom-labelling scheme and 50% probability displacement ellipsoids.

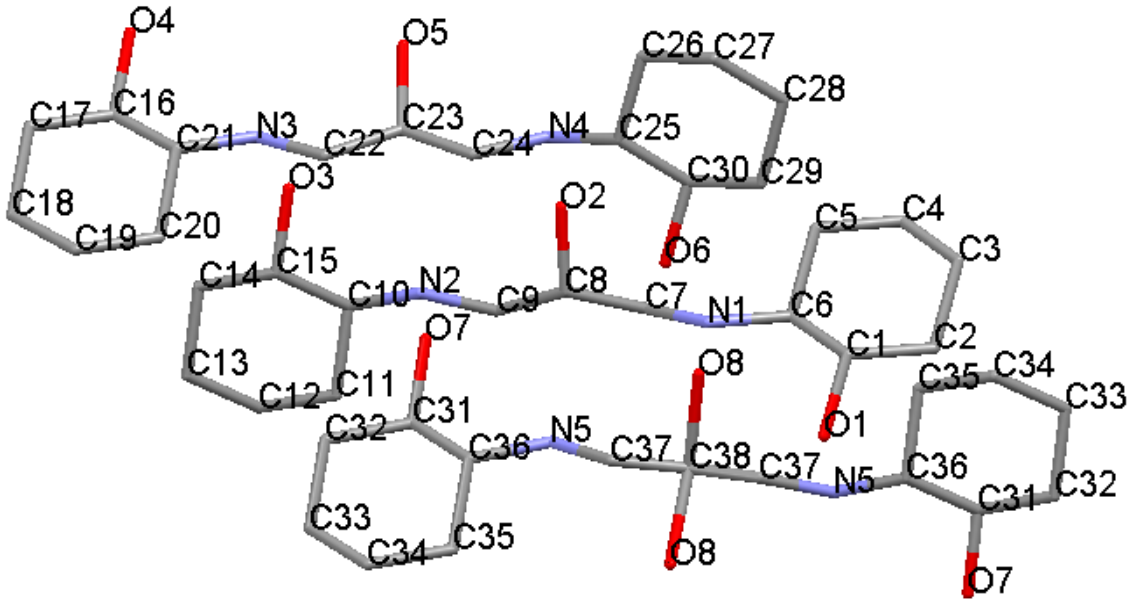


Figure 4.1.2. The molecular structure of Cy_2-Otn(a) without hydrogens showing the atom-labelling scheme and O8 disorder over two positions.

The first molecule (containing C1-C15 and N1 and N2 atoms) has one ring (C1-C6) lying at an angle of 68.59° to the plane of the propyl bridge N1,C7,C8,C9,N2 (**Fig. 4.1.3.**) and the other ring (C10-C15) is twisted at an angle of 51.96° to that plane (**Fig.4.1.4.**). The propyl bridge has an r.m.s fit of 0.1304 Å to the atoms, showing a good deal of planarity between the atoms, and the rings are twisted to almost the same degree with respect to this plane.[4] The cyclohexenyl rings lie at an angle of 59.82° to each other (**Fig. 4.1.5.**), and the hydroxyl groups (O1 and O3) on these rings point in almost opposite directions, while O2 and O3 point in the same direction.

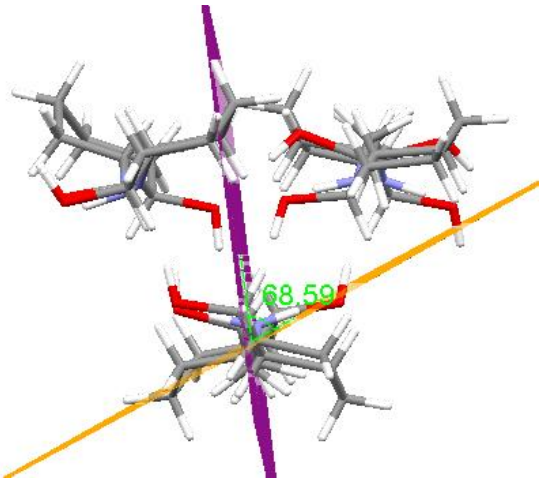


Figure 4.1.3. Cy_2-Otn(a) with planes through the propyl bridge and cyclohexenyl ring C1-C6.

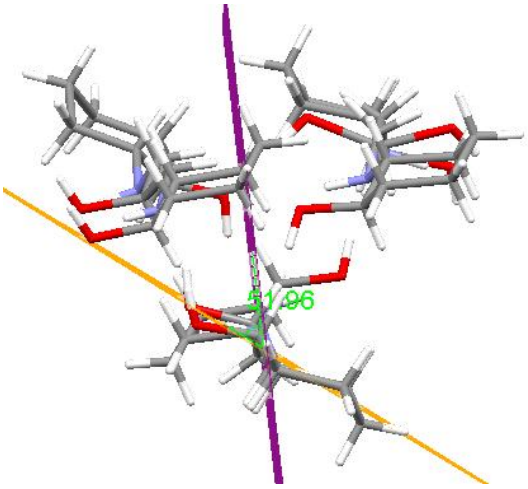


Figure 4.1.4. Cy_2-Otn(a) with planes through the propyl bridge and cyclohexenyl ring C10-C15.

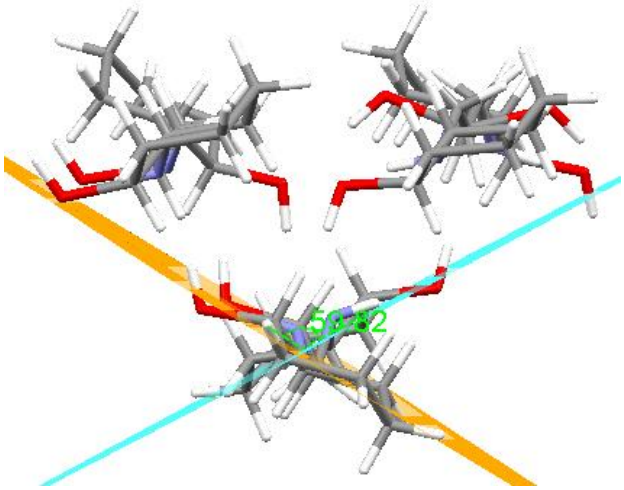


Figure 4.1.5. Cy_2-Otn(a) with planes through both cyclohexenyl rings (C1-C6 and C10-C15).

In the second molecule (containing C16-C30 and N3 and N4 atoms), the bridging atoms N3,C22,C23,C24,N4 have a smaller plane r.m.s. value of 0.0473 Å to the atoms, than the first molecule, showing even greater planarity between the atoms.[4] The one ring (C16-C21) lies at an angle of 36.03° to the plane of the propyl bridge (**Fig. 4.1.6.**) and the second ring (C25-C30) lies at a greater angle of 80.87° to that plane (**Fig.4.1.7.**). The rings lies at an angle of 63.84° to each other (**Fig. 4.1.8.**), the hydroxyl groups (O4 and O6) on these rings point in almost opposite directions, but O4 and O5 point in the same direction.

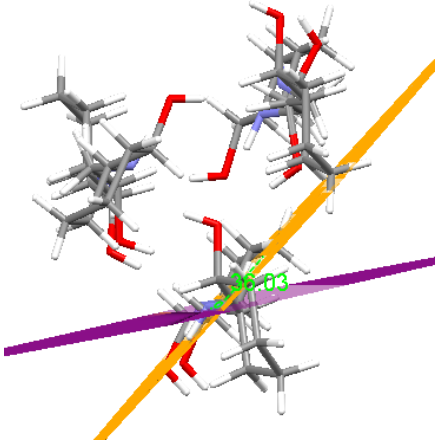


Figure 4.1.6. Cy_2-Otn(a) with planes through the propyl bridge and cyclohexenyl ring C16-C21.

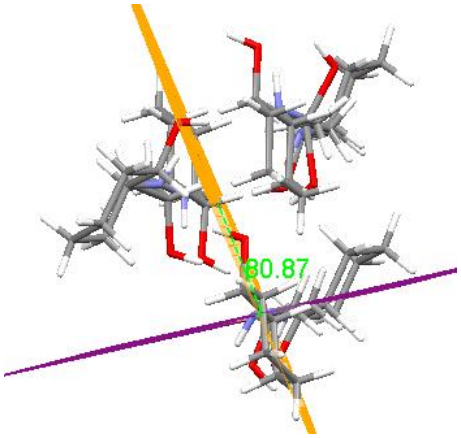


Figure 4.1.7. Cy_2-Otn(a) with planes through the propyl bridge and cyclohexenyl ring C25-C30.

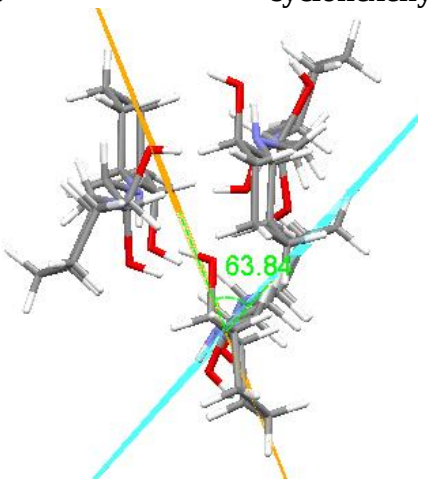


Figure 4.1.8. Cy_2-Otn(a) with planes through both cyclohexenyl rings (C1-C6 and C10-C15).

In the third molecule (containing C31-C38 and N5 atoms), there is disorder around the hydroxyl group on the propyl bridge, where 50% of the molecules have the hydroxyl group in the one position, and the other 50% of the molecules have the hydroxyl group in the other position. The plane through the propyl bridging atoms N5,C37,C38, $C37^{i}$, $N5^{i}$ has an r.m.s. fit of 0.000 Å to the atoms,[4] as there is a symmetry point at C38, where the molecule is inverted, therefore both rings (C31-C36, and $C1^{i}$-$C36^{i}$) are identical and lie at the same angle of 63.17° to the plane of the bridging atoms (**Fig. 4.1.9. and Fig. 4.1.10.**). The rings lie at an angle of 55.04° to each other (**Fig. 4.1.11.**).

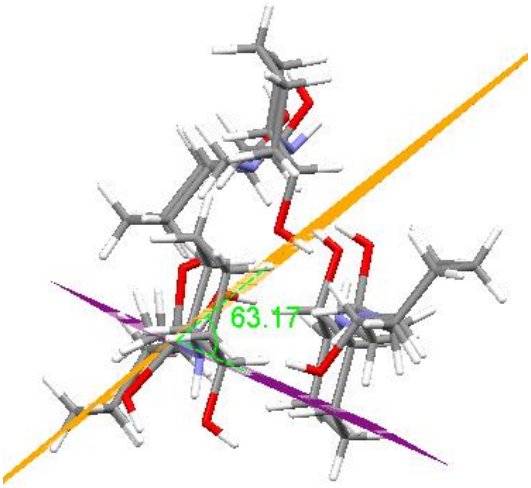


Figure 4.1.9. Cy_2-Otn(a) with planes through the propyl bridge and cyclohexenyl ring C31-C36.

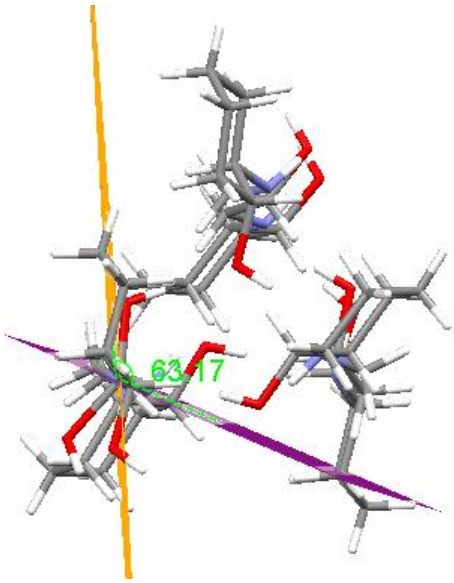


Figure 4.1.10. Cy_2-Otn(a) with planes through the propyl bridge and cyclohexenyl ring $C31^i$-$C36^i$.

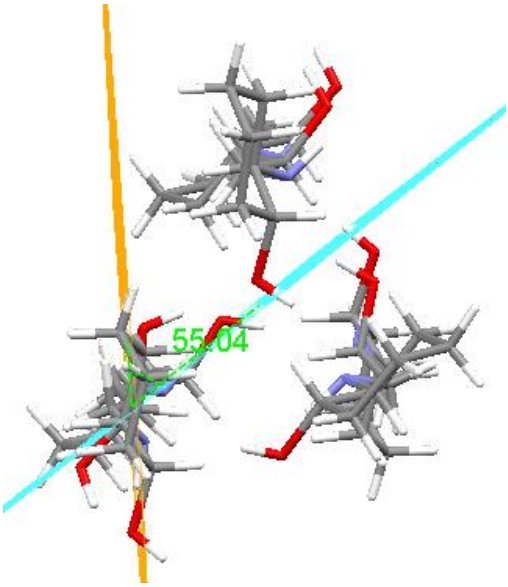


Figure 4.1.11. Cy_2-Otn(a) with planes through both cyclohexenyl rings (C31-C36).

Due to the angles (55°, 59° and 63°) at which the cyclohexenyl rings sit with respect to each other, all three molecules are not planar. There is hydrogen bonding between the molecules. Both amine nitrogens are hydrogen bond donors to the alcohol moieties on a different molecule, and the alcoholic moieties hydrogen bond to both the amine nitrogens and further alcoholic moieties, Figure 4.1.12. This conformation and hydrogen bonding shows that

there is not sufficient pre-organisation of the ligand for complexation in the solid state. However, the observed conformation is only one of many conformations possible in solution, that includes several other conformations with varying predispositions for metal ion complexation. This also allows for several conformations in which dimeric or even polymeric complexes can form. The ideal geometry for complexation would be the formation of a cavity with the two amine nitrogens and the two cyclohexenyl alcoholic oxygen atoms in an equatorial position, where the oxygen moieties on the cyclohexenyl rings pointing the same direction.

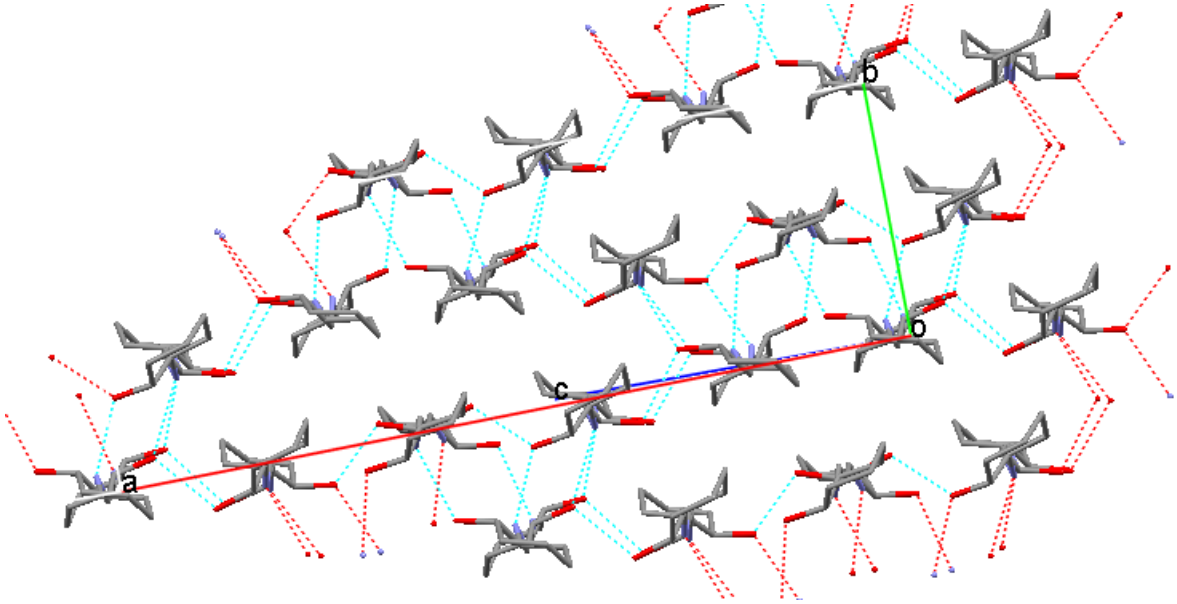


Figure 4.1.12. Hydrogen bonding between Cy_2-Otn(a) molecules viewed along the *c*-axis, (hydrogens omitted for clarity).

Each molecule has five hydrogen bonds to three different molecules. The two cyclohexenyl alcoholic moieties form two hydrogen bonds to one molecule, and the two amine nitrogens and the propyl hydroxyl group hydrogen bond to a different molecule. The hydroxyl group on the porpyl bridge also hydrogen bonds to a third molecule, Figure 4.1.12. These hydrogen bonds extend in all three dimensions. The molecules stack on top of each other (**Fig. 4.1.13 and 4.1.14.**) and form layers (**Fig. 4.1.12. and 4.1.15.**).

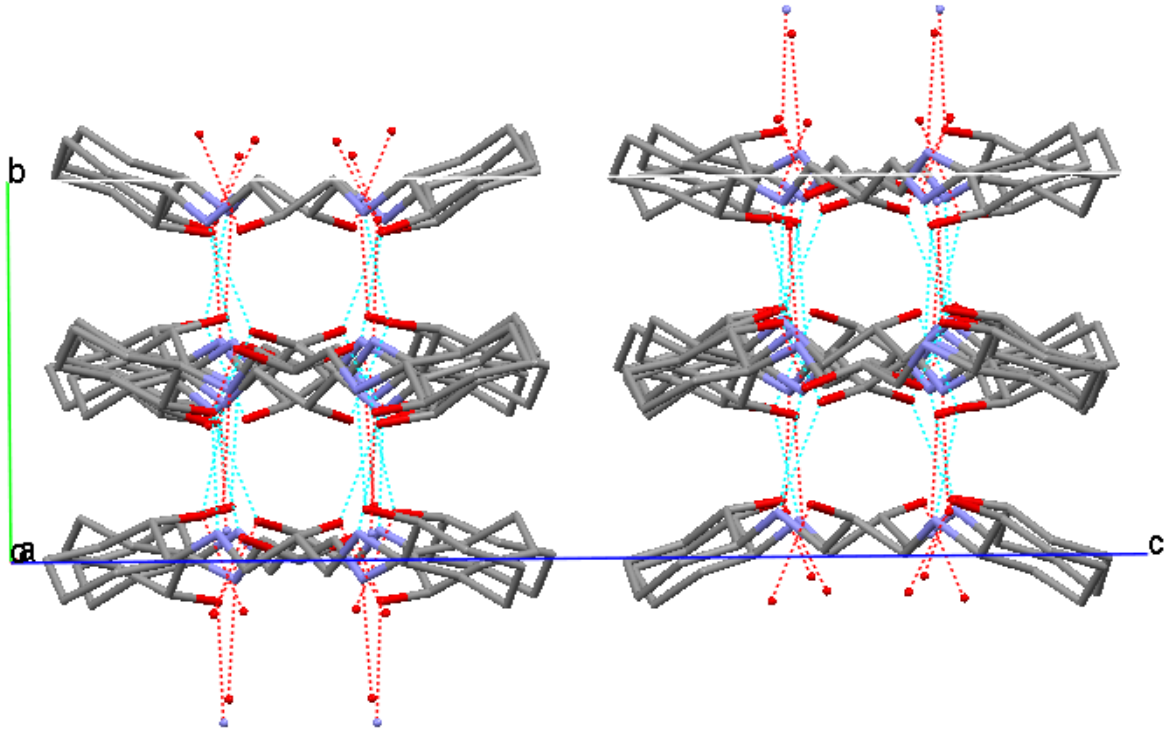


Figure 4.1.13. Crystal packing and hydrogen bonding between Cy_2-Otn(a) molecules viewed along the *a*-axis (hydrogens omitted for clarity).

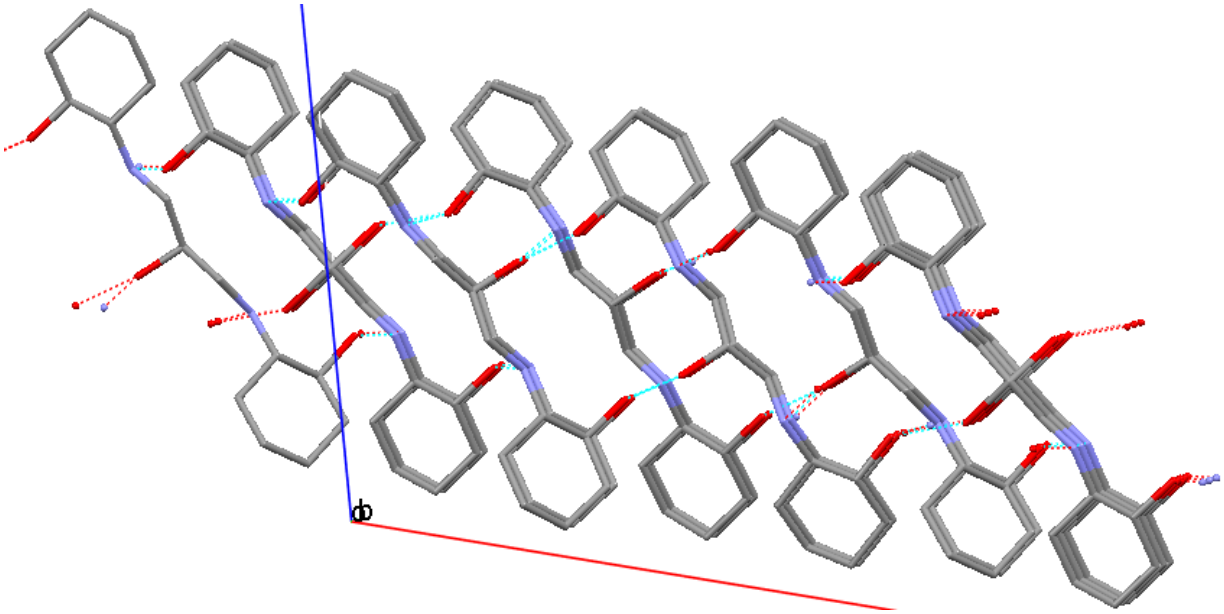


Figure 4.1.14. Crystal packing and hydrogen bonding between Cy_2-Otn(a) molecules viewed along the *b*-axis (hydrogens omitted for clarity).

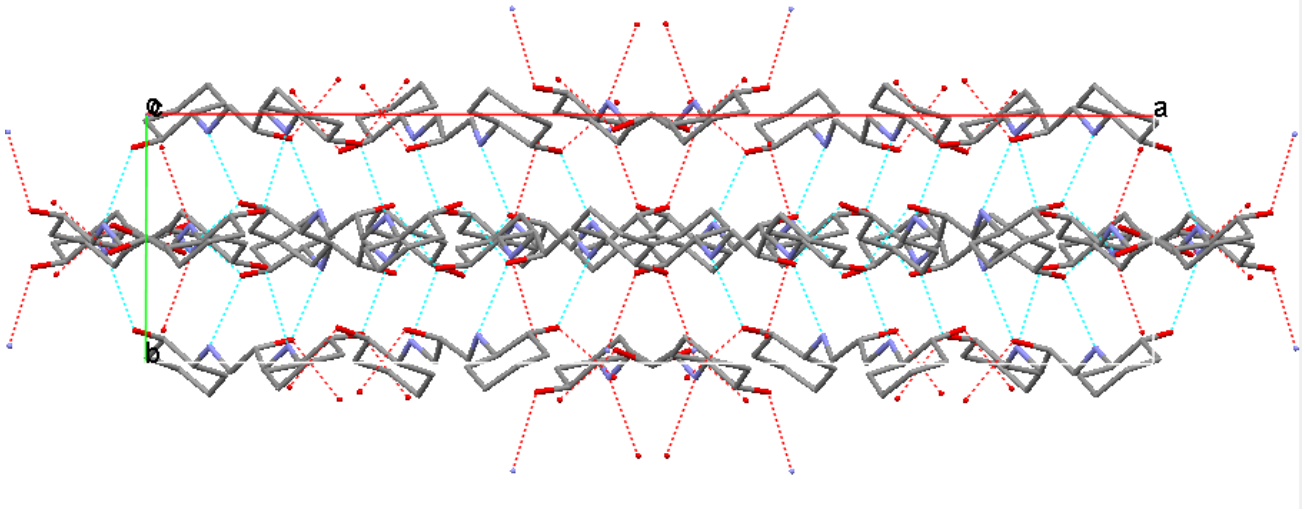


Figure 4.1.15. Crystal packing and hydrogen bonding between Cy_2-Otn(a) molecules viewed along the *c*-axis (hydrogens omitted for clarity).

Hancock *et al.*[2] suggested that hydrogen-hydrogen interactions (H--H close contacts) exist between the hydrogen atoms on the cyclohexenyl rings and the hydrogen atoms on the propyl bridge and may affect complexation reactions. The distance between each of these atoms was then measured, and all of the distances that were less than the sum of the van der Waal radii (2 x 1.20 Å = 2.40 Å) were noted, Figure 4.1.16., Table 4.1.1. These distances range from 2.051 to 2.348. It should be noted that there is no HCH--HCH close contact between H24A and H24B, but there is a CH-H_2C interaction with a distance of 2.348 Å. However, the assignment and values of the hydrogen atoms is an approximation for the XRD data, and so there is some debate as to the exact X-H bond lengths. XRD analysis sets the X-H bonds lengths slightly shorter than neutron diffraction analysis.[5] Therefore, any observations made on hydrogen atoms, is based on this conventional and unnormalised data. These H--H close contacts are likely to be very weak and a consequence of the solid state packing.

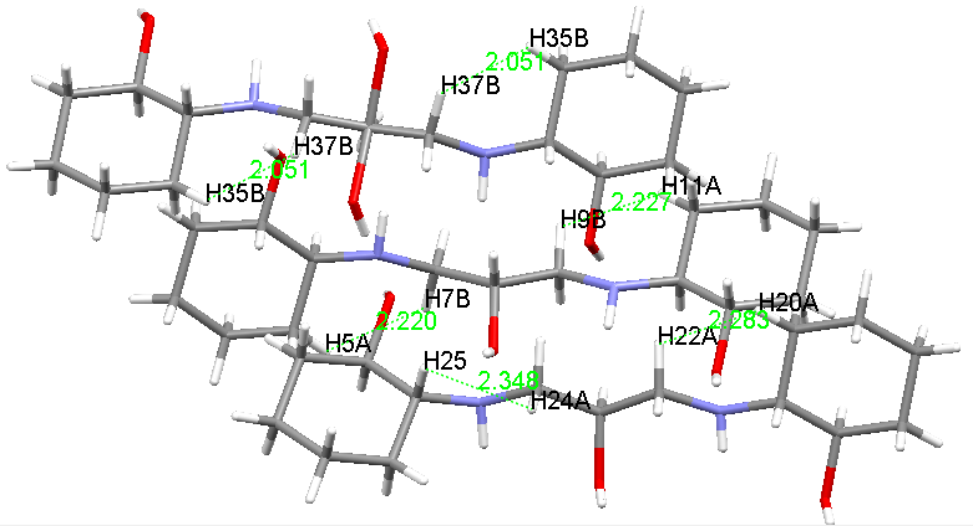


Figure 4.1.16. Cy_2-Otn(a) molecules showing H--H close contact distances between HCH--HCH atoms.

Table 4.1.1. Cy_2-Otn(a) H-H bond distances and torsion angles between HCH--HCH atoms.

Atom 1	Atom 2	H--H Close Contact Distance (Å)	H--H Torsion Angle (˚)
H5A	H7B	2.220	0.92
H9B	H11A	2.227	-31.22
H20A	H22A	2.285	37.37
H35B	H37B	2.051	1.12
H24A	H25	2.348	138.30

There are also close contacts between most of the alcoholic oxygen atoms and the amine hydrogen atoms, Figure 4.1.17. The distance between the two atoms range from 2.342 to 2.615 Å, and are significantly less than the sum of their van der Waals radii (2.72 Å). There are, however, no interactions between H4N and O6, H1N and O2, and between H5N and O8, as the distances between these atoms is larger than the sum of their van der Waals radii (2.72 Å). These interactions are not defined as a hydrogen bond, as the angles between the acceptor and donor atoms are smaller than the average hydrogen bond, which is commonly accepted as having an angle of at least 120˚. This attractive interaction may play a role in the packing behaviour of the molecules.

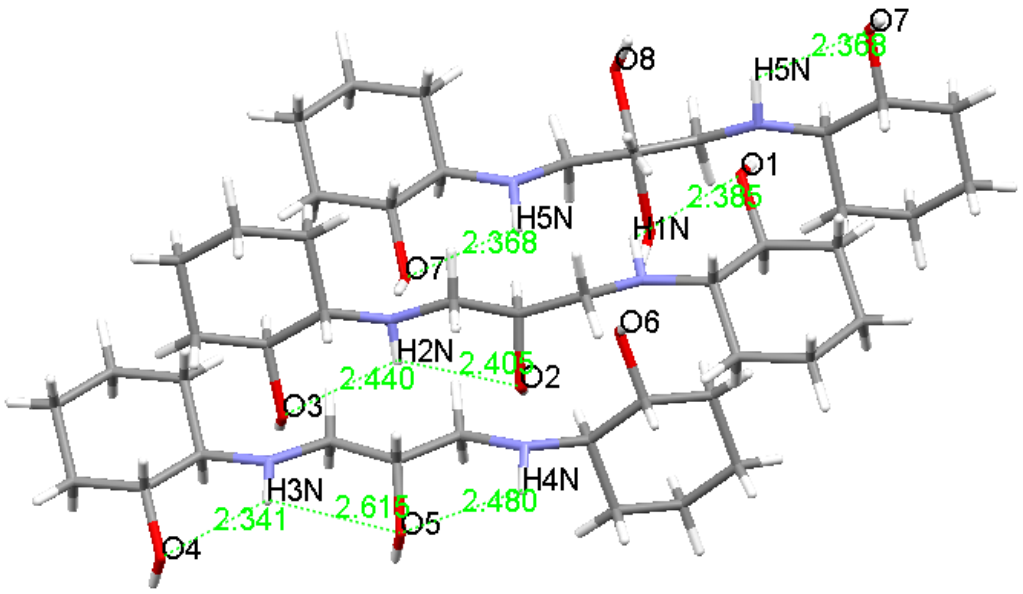


Figure 4.1.17. Cy_2-Otn(a) molecules showing interactions between HO--HN atoms.

Table 4.1.2. Cy_2-Otn(a) interaction distances and angles between HO--HN atoms.

Atom 1	Atom 2	NH--O Bond Distance (Å)	XH-H Bond Angles (˚), where X denotes a donor atom
H1N	O1	2.385	110.89
H2N	O2	2.405	111.88
H2N	O3	2.440	107.31
H3N	O4	2.341	120.94
H3N	O5	2.615	102.17
H4N	O5	2.480	109.60
H5N	O7	2.368	109.38

Reisinger[3] obtained a polymorph of this structure (Cy_2-Otn(b)), that has two ligand molecules and a water molecule in the asymmetric unit cell. It crystallised in *P*ī space group with an R-factor of 5.04%.[3] Both molecules adopt a planar arrangement and the rings are in the chair conformation. The hydroxyl groups on the cyclohexenyl rings point in the same direction, Figure 4.1.18. Both of the molecules adopt the same type of chirality in that the each pair of

chiral carbon atoms in the cyclohexenyl rings are either *R* or *S*, i.e. the each molecule has a an *S,S,R,R* configuration.[3]

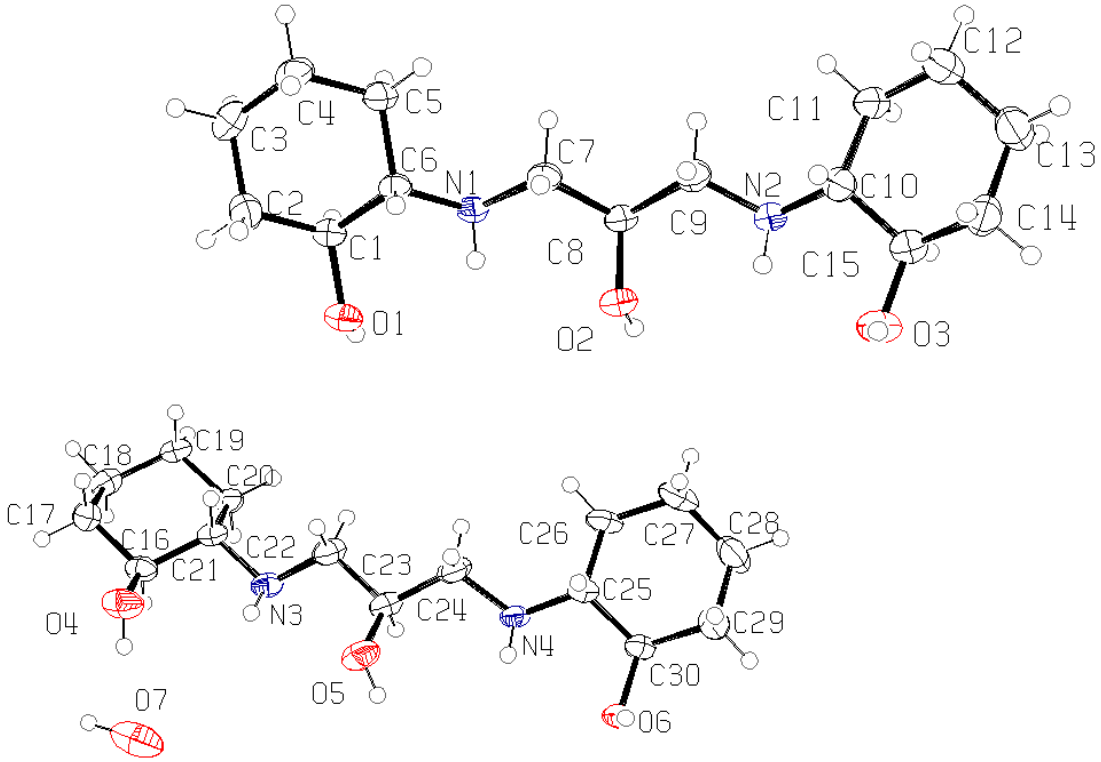


Figure 4.1.18. The molecular structure of Cy_2-Otn(b), showing the atom-labelling scheme and 50% probability displacement ellipsoids.

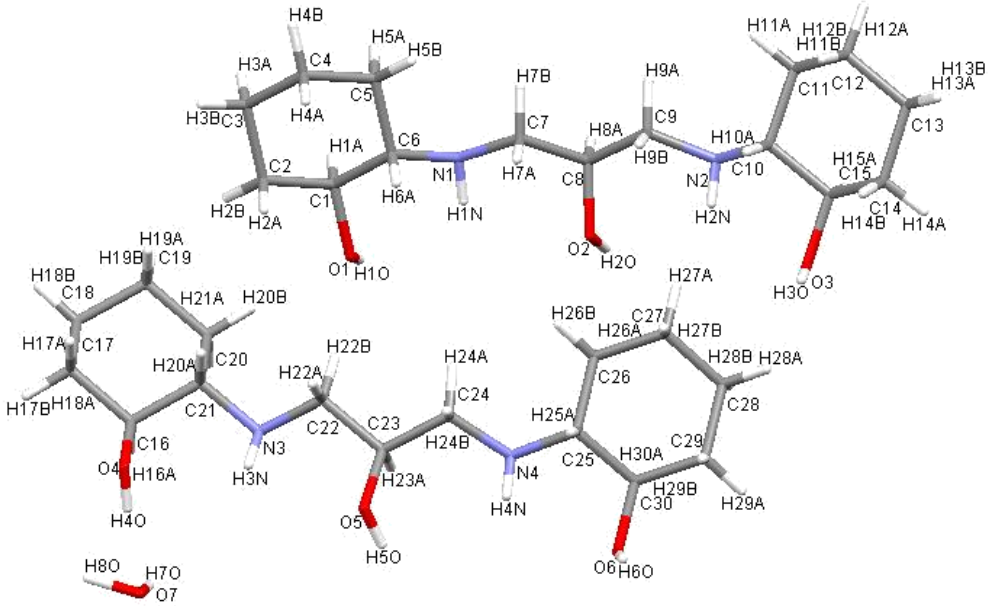


Figure 4.1.19. The molecular structure of Cy_2-Otn(b) with its labelling scheme.

In the first molecule in the asymmetric unit cell (containing C1 to C15 and N1 and N2 atoms), a plane through the bridging group (N1,C7,C8,C9,N2) has an r.m.s. fit of 0.0505 Å,^{3} and the cyclohexenyl ring (C1-C6) lies at an angle of 22.41° (**Fig. 4.1.20.**), and the second ring (C10-C15) lies at an angle of 49.11° to the propyl bridge plane (**Fig. 4.1.21.**). The rings lie at an angle of 37.98° to each other (**Fig. 4.1.22.**). The angle between the cyclohexenyl rings is small and the r.m.s. fit indicates that the atoms on the bridge between the two cyclohexenyl rings are fairly planar.

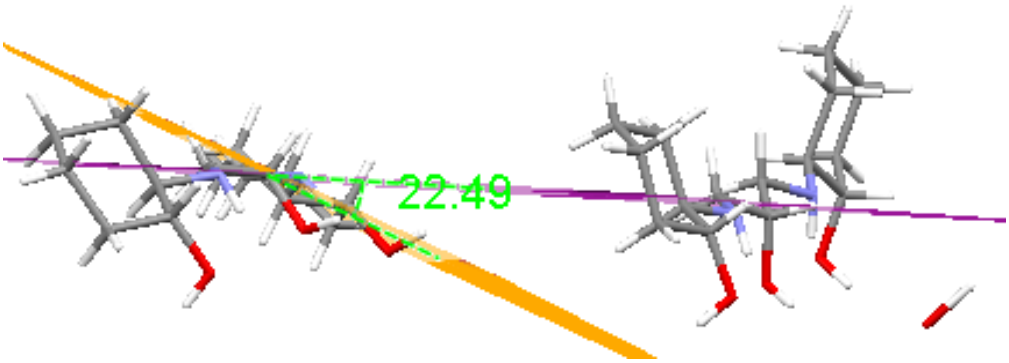


Figure 4.1.20. Cy_2-Otn(b) with planes through the propyl bridge and cyclohexenyl ring C1-C6.

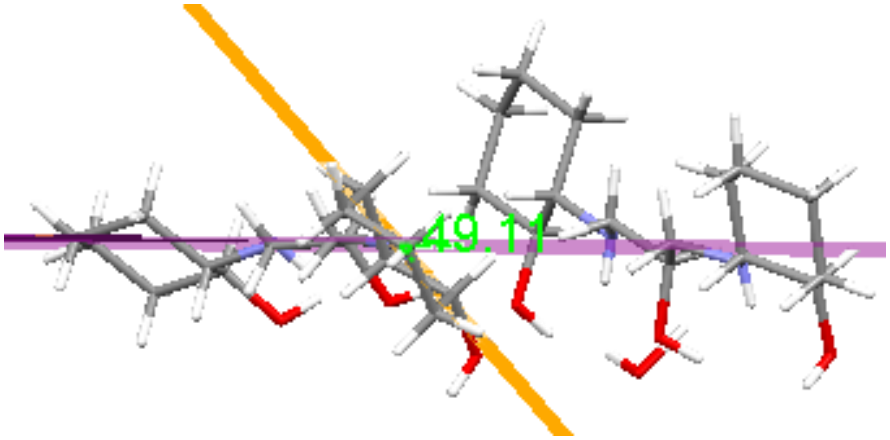


Figure 4.1.21. Cy_2-Otn(b) with planes through the propyl bridge and cyclohexenyl ring C10-C15.

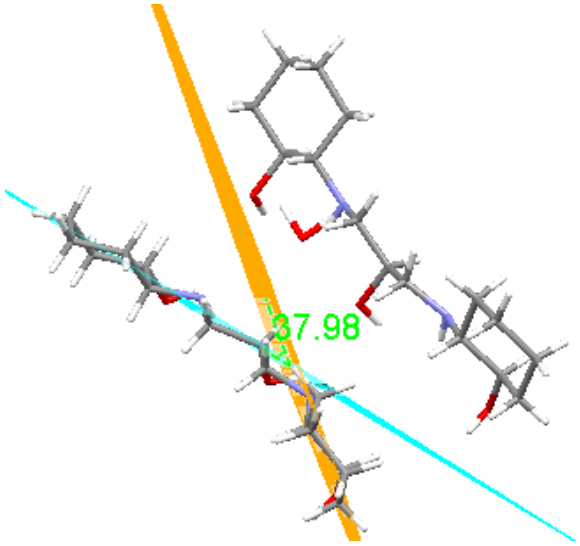


Figure 4.1.22. Cy_2-Otn(b) with planes through the cyclohexenyl rings C1-C6 and C10-C15.

In the second molecule (containing C16 to C30 and N3and N4 atoms), the plane through the bridging atoms (N3,C22,C23,C24,N4) has a larger r.m.s.value of 0.1079 Å to the atoms, there is still some planarity through the atoms.[3] The first cyclohexenyl ring (C16-C21) lies at an angle of 63.45° (**Fig. 4.1.23.**), and the second ring (C25-C30) lies at an angle of 29.45° (**Fig. 4.1.24.**), to this plane. The two rings lie at an angle of 34.15° to each other (**Fig. 4.1.25.**). The rings on the second molecule are twisted at a greater angle than the first molecule, which is most likely due to the proximity of the water molecule.

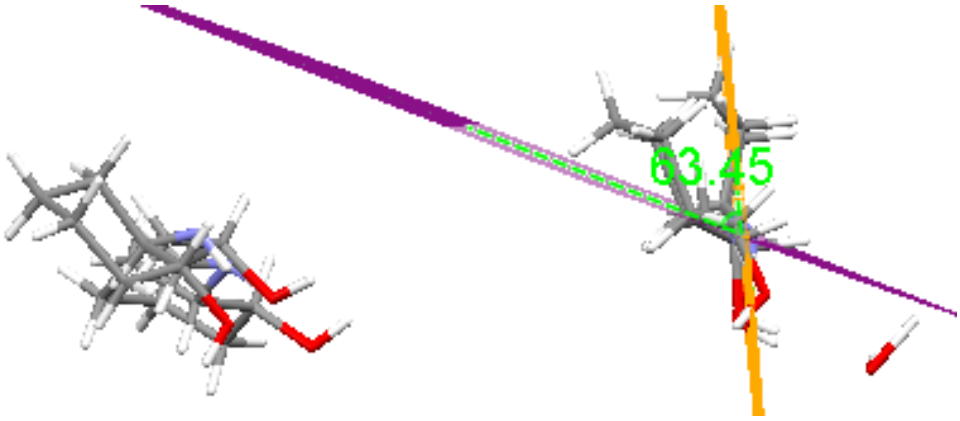


Figure 4.1.23. Cy_2-Otn(b) with planes through the propyl bridge and cyclohexenyl ring C16-C21.

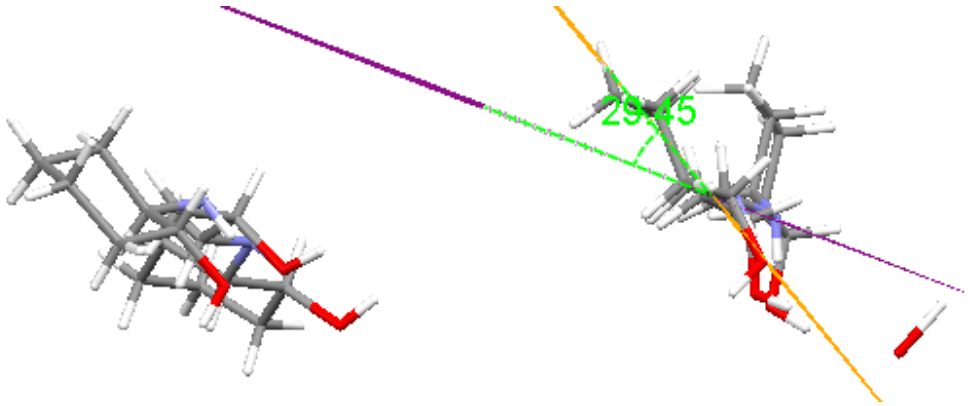


Figure 4.1.24. Cy_2-Otn(b) with planes through the propyl bridge and cyclohexenyl ring C25-C30.

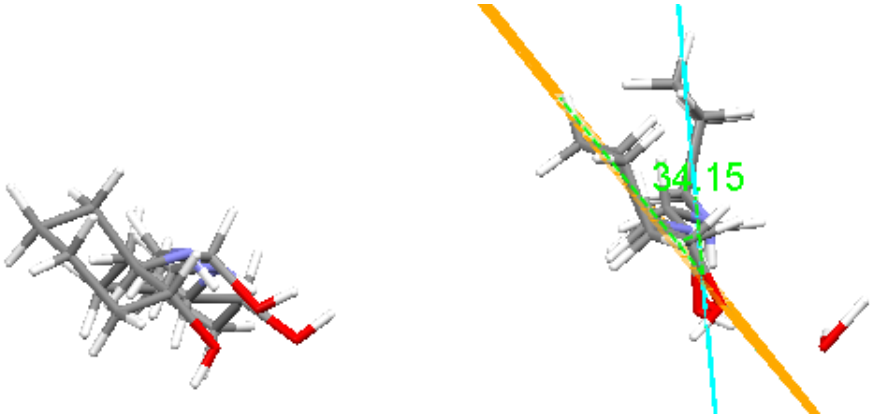


Figure 4.1.25. Cy_2-Otn(b) with planes through the cyclohexenyl rings C16-C21 and C25-C30.

In the Cy_2-Otn(b) polymorph, all three alcoholic oxygen groups in each molecule point in the same direction and form hydrogen bonds to the water molecule, further alcoholic oxygen moieties, and one of the amine nitrogens, Figure 4.1.26. This arrangement shows a higer pre-organisation than Cy_2-Otn(a), as all the donor atoms are on the same side of the molecule which is the preferred orientation for metal ion complexation. This arrangement allows for the maximum number of hydrogen bonds to be formed between the various molecules within the unit cell. The molecules in the unit cell arrange themselves so that the alcoholic moieties in both molecules face each other, i.e. the same direction. Cy_2-Otn(b) forms alternating layers of transposed molecules that have been rotated through 90˚ to one another. The transposition of the molecule by half a molecule length leads to the cyclohexenyl rings not overlapping between the layers but rather interacting via hydrogen bonds with the alcohol group on the propyl bridge.

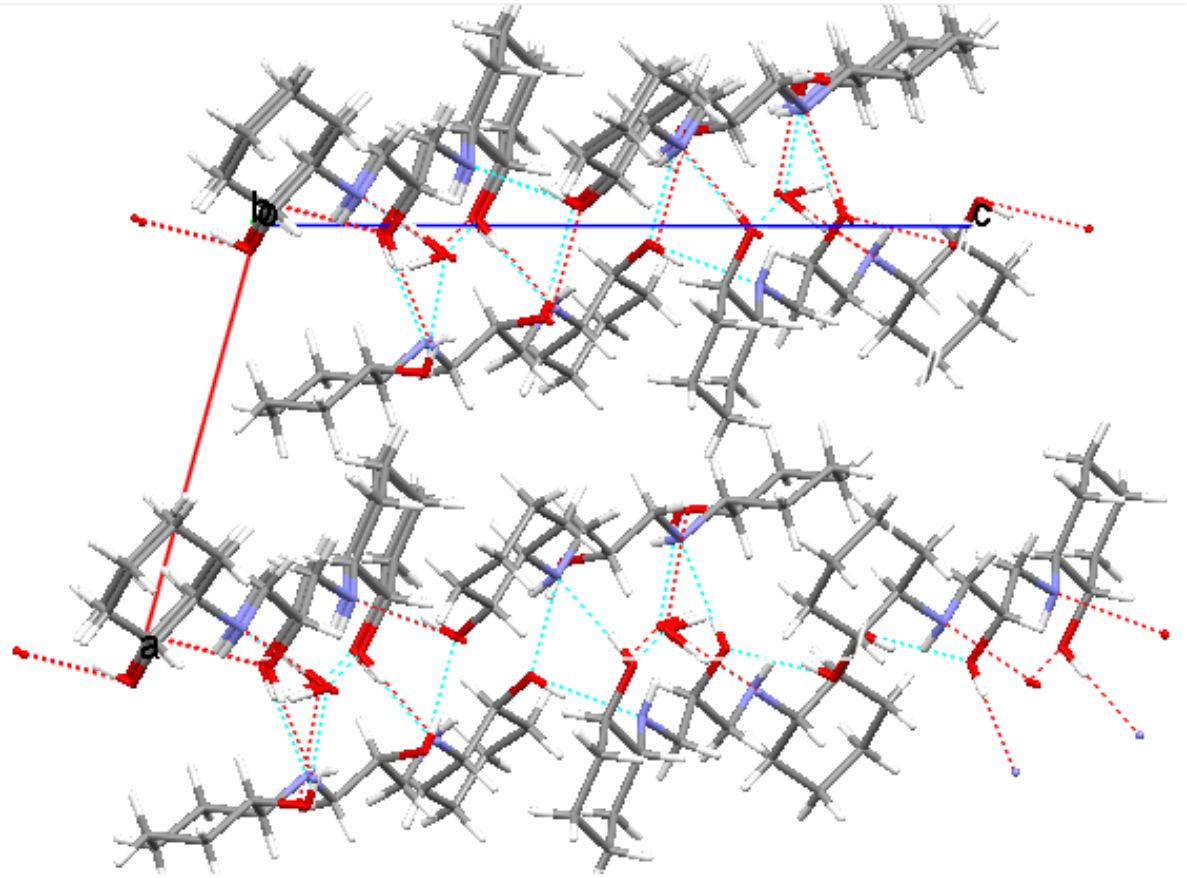


Figure 4.1.26. Hydrogen-bonding network of Cy_2-Otn(b), viewed along the *b*-axis.

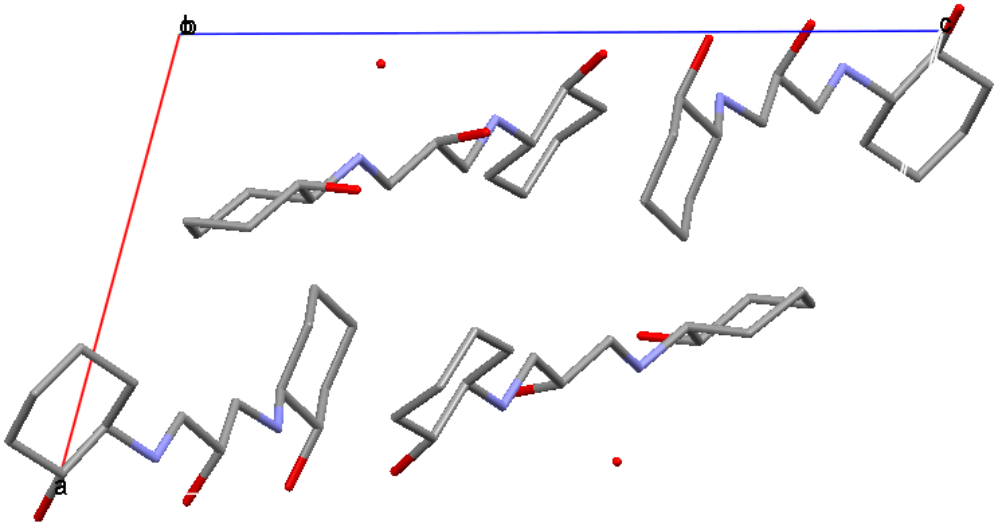


Figure 4.1.27. Crystal packing of Cy_2-Otn(b), viewed along the *b*-axis (hydrogen atoms omitted for clarity).

The H--H close contacts between the hydrogen atoms on the ring with those on the bridge were investigated. The H--H close contacts and their torsion angles are given in Table 4.1.3. and shown in Figure 4.1.28. There are significant contacts between the HCH--HCH hydrogen atoms on the cyclohexenyl rings and the hydrogen atoms in the bridging atoms, as well as interactions between the two CH_2 groups on the propyl bridge, and between the CH on the cyclohexenyl ring and the CH_2 on the propyl bridge. These H--H close contacts are all shorter than the sum of the van der Waals radii (2.40 Å) ranging between 2.136 and 2.362 Å.

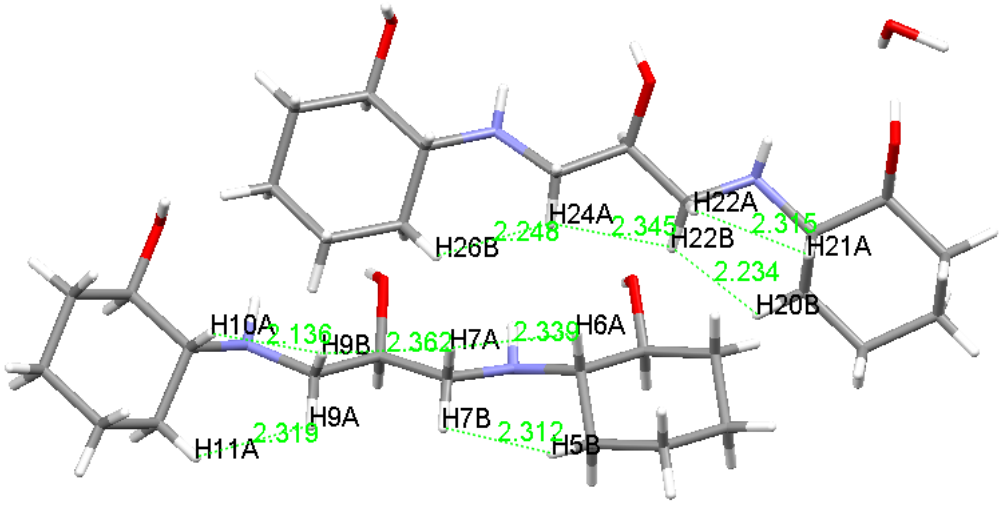


Figure 4.1.28. The H--H close contacts in Cy_2-Otn(b).

Table 4.1.3. H--H close contacts for the Ligand Cy_2-Otn(b).

Atom 1	Atom 2	H--H Close Contact Distance (Å)	H-H Torsion Angles (˚)
H5B	H7B	2.312	-45.02
H9A	H11A	2.319	19.43
H20B	H22B	2.234	6.41
H24A	H26B	2.248	43.94
H6A	H7A	2.339	-10.28
H7A	H9B	2.362	-11.13
H9B	H10A	2.136	-3.61
H21A	H22A	2.315	-18.48
H22B	H24A	2.345	12.61

The molecule has further close contacts that are of interest, Figure 4.1.29. The oxygen atoms on the cyclohexenyl rings have strong attractive interactions with the hydrogen atoms on the amine groups. In addition to these interactions, the alcoholic oxygen on the propyl bridge also interacts very closely with the amine hydrogen, these interactions are not traditional hydrogen bonds as the angles are all less than 120° (**Table 4.1.4.**).

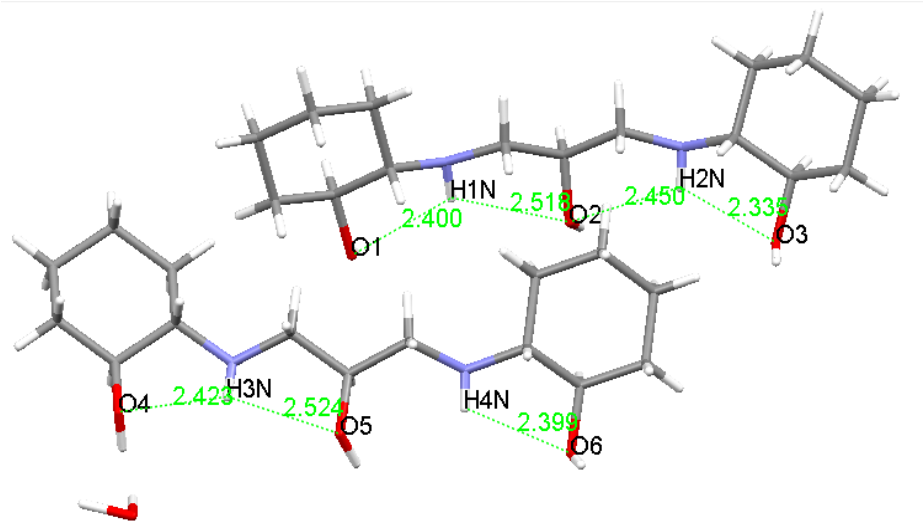


Figure 4.1.29. Cy_2-Otn(b) close contacts between the amine hydrogens and alcoholic oxygens in the same molecule.

Table 4.1.4. Cy_2-Otn(b) interaction distances and angles between HO-HN atoms.

Atom 1	Atom 2	NH--O Bond Distance (Å)	XH-H Bond Angles (°), where X denotes a donor atom
H1N	O1	2.400	110.05
H1N	O2	2.518	109.10
H2N	O2	2.450	110.22
H2N	O3	2.335	114.95
H3N	O4	2.243	112.91
H3N	O5	2.524	104.12
H4N	O6	2.399	111.72

4.1.2. Synthesis of Cy_2-tn

The same method as described for the synthesis of Cy_2-Otn was used to synthesise the ligand Cy_2-tn, although the sysnthesis was conducted at 80 ^oC.[2] The three reactions produced excellent yields above 80%. The mass spectroscopy showed a mixture of products (m/z 270 (Cy_2-tn-H+1), 292 (Cy_2-tn-H+Na+1), 368 (Cy_3-tn-H+1)), the presence of the sodium was from the glassware, and the Cy_3-tn was a minor product, with the bulk of the sample being the desired Cy_2-tn product. The NMR spectroscopy split and integrated as expected, and the IR spectroscopy showed the desired bending and stretching. All characterisation data can be found in Appendices B-E.

No crystals could be obtained of this ligand by slow evaporation of the ligand in water, methanol, or ethanol, and only a fine white powder was produced. However, slow evaporation from DMF produced crystals of XRD quality, with an R-factor of 4.35%. Two polymorphs were isolated, both with one molecule in the asymmetric unit cell, in a *C*2/c space group. In the first polymorph the Cy_2-tn(a) molecule has the cyclohexenyl oxygen moieties pointing in different directions and there is an inversion center at C8, whereas in the second polymorph the Cy_2-tn(b) molecule has the cyclohexenyl oxygen moieties pointing in the same direction.

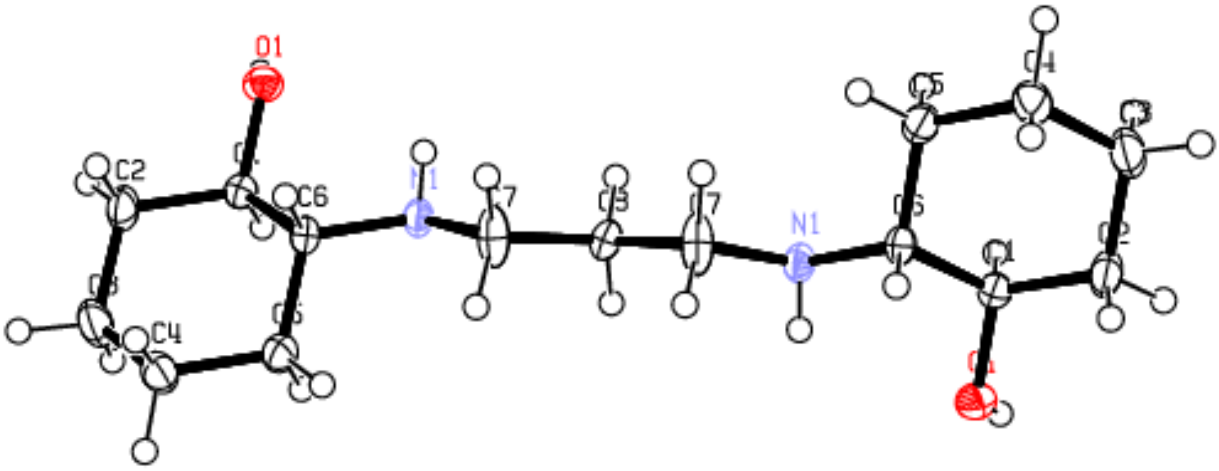


Figure 4.1.30. The molecular structure of Cy_2-tn(a), showing the atom-labelling scheme and 50% probability displacement ellipsoids.

In the Cy_2-tn(a) molecule the cyclohexenyl rings adopt the chair conformation. The geometry of the molecule is similar to that of Cy_2-Otn(a) where all the chiral carbon atoms (C6, and C1) adopt the same arrangement, either *R* or *S* (**Fig. 4.1.30.**).

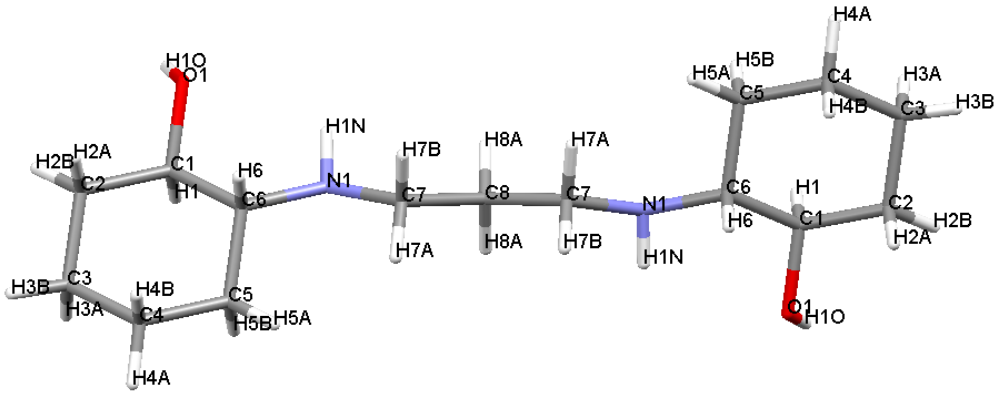


Figure 4.1.31. The molecular structure of Cy_2-tn(a) showing the atom-labelling scheme.

The Cy_2-tn(a) molecule (contains C1-C8, O1, and N1 atoms) has an inversion center around C8, therefore the rings (C1-C6 and $C1^i$-$C6^i$) lie at an angle of 61.20° to the plane of the propyl bridge N1,C7,C8,$C7^i$,$N1^i$ and the rings are twisted at an angle of 58.35° to each other (**Fig. 4.1.31.**). The propyl bridge has an r.m.s fit of 0.000 Å to the atoms, showing the atoms are planar due to the symmetry of the molecule.[4] The angle between the cyclohexenyl rings results in the molecule having a dish shape (**Fig. 4.1.32.**).

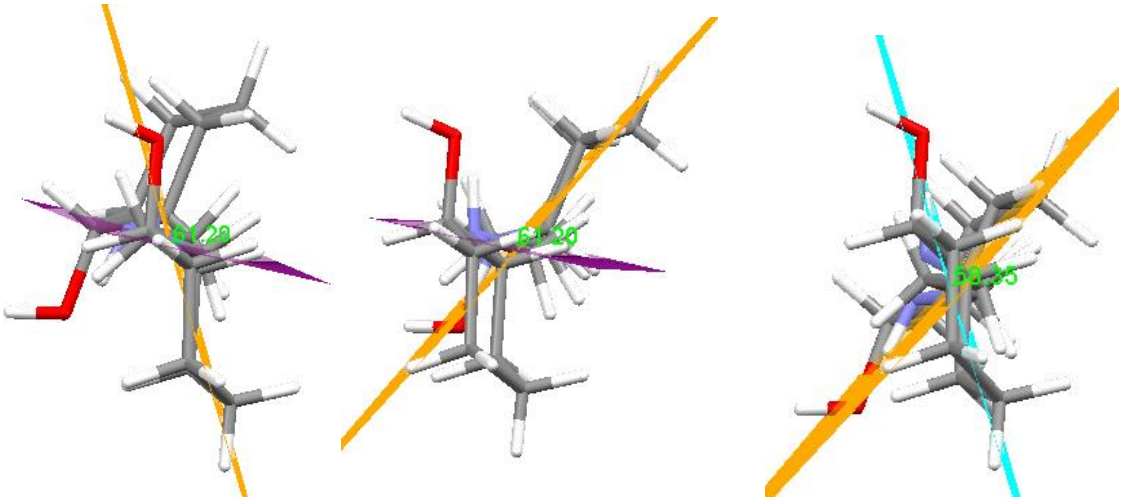


Figure 4.1.32. Cy_2-tn(a) molecule showing planes through the propyl bridge and the cyclohexenyl rings, and the angles between these planes.

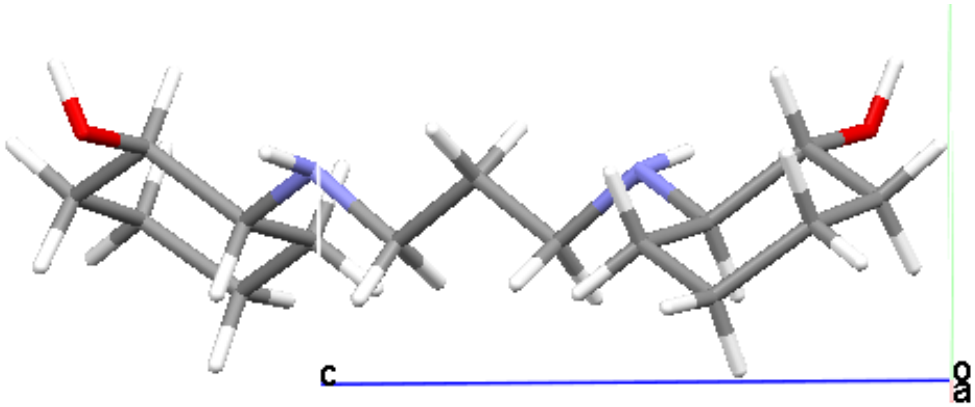


Figure 4.1.33. Cy_2-tn(a) viewed along the *a*-axis.

There is maximum hydrogen bonding between the molecules, both the amine nitrogens are hydrogen donors to the alcohol moieties on two different molecules, Figure 4.1.34. Once again, this conformation allows for little pre-organisation of the ligand for metal ion complexation, as the donor atoms are on different sides of the molecule. The hydrogen bonds form inter-molecular 16-membered rings between the molecules, but there are no hydrogen bonds between the layers of molecules. The layers between the molecules alternate between having the propyl bridges pointing towards each other, or pointing away from each other; the hydrogen bonds that form between the molecules pull the propyl bridges towards each other (**Fig. 4.1.35.**). The layers of molecules alternate between being in the *R* and the *S* conformation.

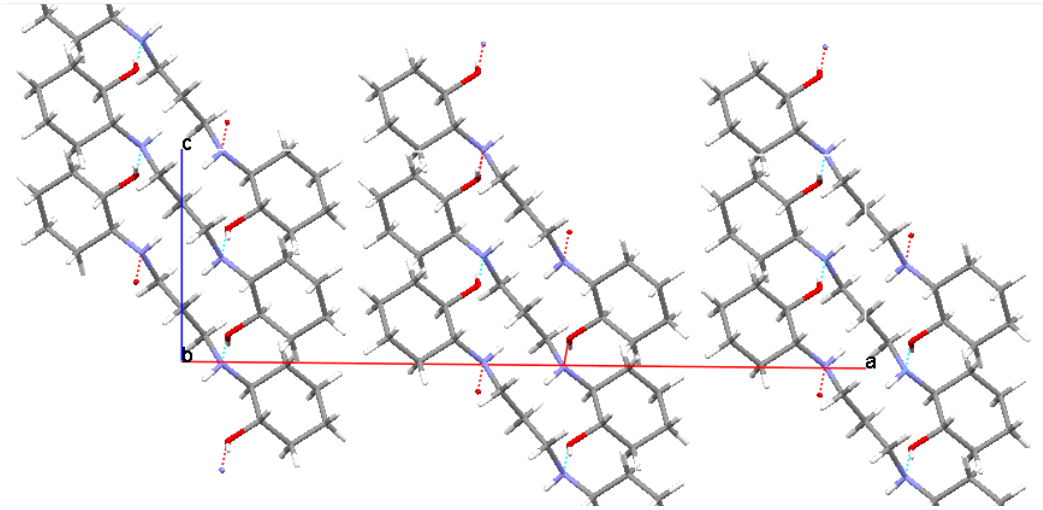


Figure 4.1.34. Crystal packing and hydrogen bonding of Cy_2-tn(a) viewed along the *b*-axis.

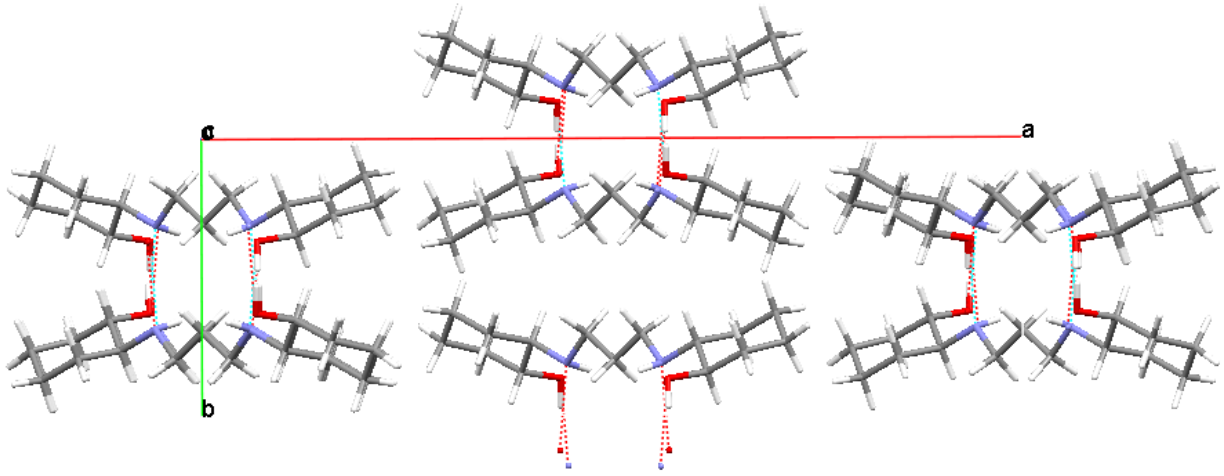


Figure 4.1.35. Crystal packing and hydrogen bonding of Cy_2-tn(a) viewed along the *c*-axis.

Hydrogen-hydrogen interactions (H--H close contacts) between the hydrogen atoms on the cyclohexenyl rings and the hydrogen atoms on the propyl bridge were of interest. The distance between each of these atoms were less than the sum of the van der Waal radii (2.40 Å), Figure 4.1.36., Table 4.1.5. There were only two HCH--HCH interactions, and only two NH--O interactions, but they each have the same values due to the symmetry of the molecule. Bond paths and BCPs between the NH--O atoms can be seen in the QTAIM molecular graphs (Chapter 3), indicating that these bonds exist, even though they are weak.

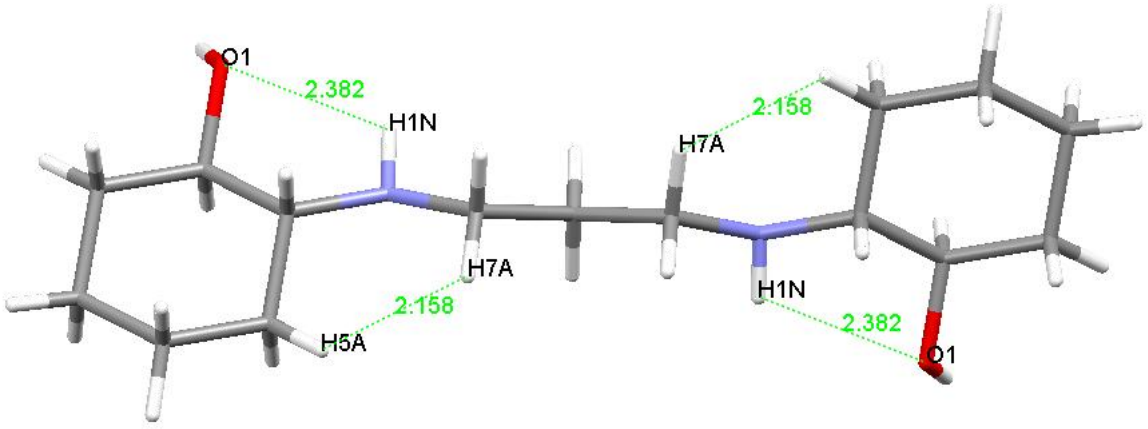


Figure 4.1.36. Cy_2-tn(a) H--H close contacts and NH--O interactions.

Table 4.1.5. Cy_2-tn(a) interaction distances and angles between HO-HN and HCH--HCH atoms.

Atom 1	Atom 2	NH--O Bond Distance (Å)	XH--H Bond Angles (˚), where X denotes a donor atom
H1N	O1	2.382	111.25
Atom 1	**Atom 2**	**H-H Short Contact Distance (Å)**	**H-H Bond Angle (˚)**
H5A	H7A	2.158	7.99

As previously mentioned, the Cy_2-tn(b) polymorph also has one molecule in the unit cell, but the alcoholic molecules on the cyclohexenyl rings point in the same direction (**Fig. 4.1.37.**), similar to the Cy_2-Otn(b) polymorph. The cyclohexenyl rings adopt the chair conformation in Cy_2-tn(b), and the geometry of the molecule is similar to that of Cy_2-Otn(b), where the adjoining chiral carbon atoms (C6 and C1) adopt the same arrangements, either *S* or *R* (**Fig. 4.1.38.**), i.e. the molecule is has a *S,S,R,R* geometry, in a *P*$\bar{1}$ space group. The XRD data has an R-factor of 22.28%, which reflects the poor crystal quality due to twinning. The twinned crystals are not single crystals, but layers of crystals grown together that cannot be easily separated without breaking the crystals. These layers of crystals results in poor diffraction data.

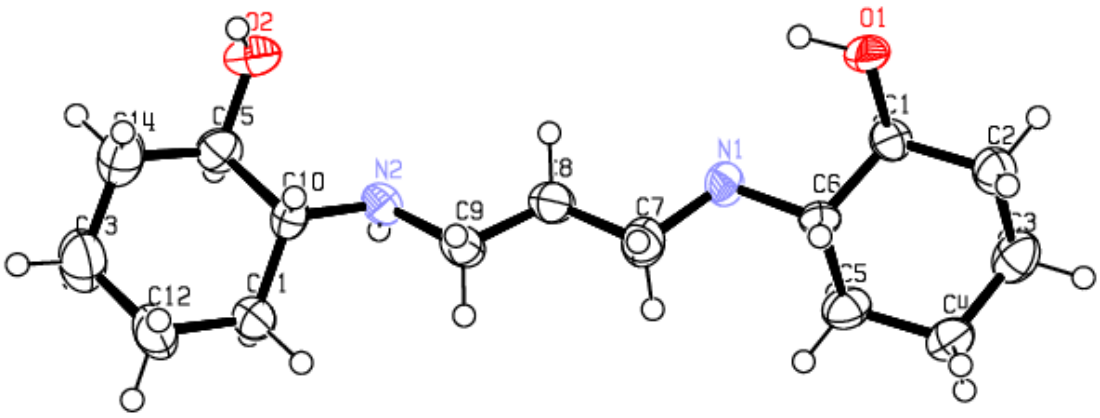


Figure 4.1.37. The molecular structure of Cy_2-tn(b), showing the atom-labelling scheme and 50% probability displacement ellipsoids.

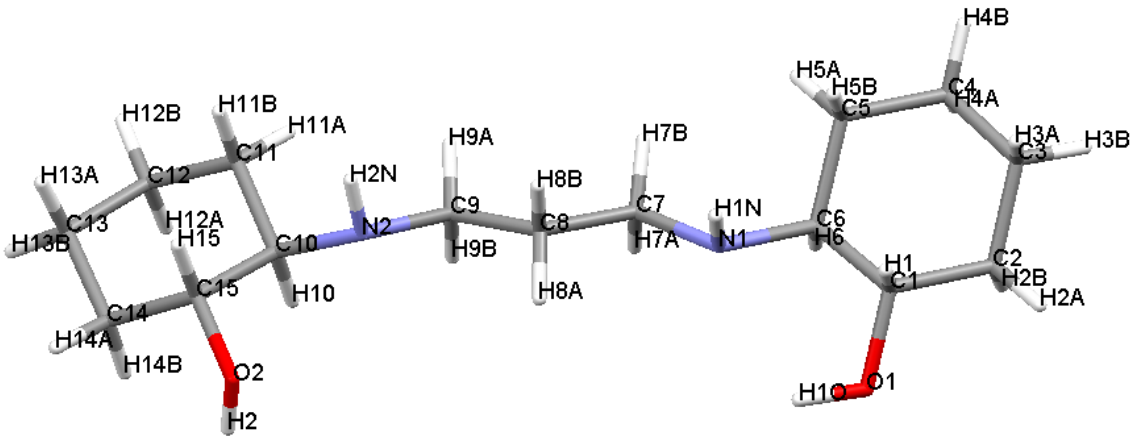


Figure 4.1.38. The molecular structure of Cy_2-tn(b) with its labelling scheme.

The Cy_2-tn(b) molecule (contains C1-C15 and N1 and N2 atoms) has plane r.m.s. value of 0.0533 Å through the propyl bridge N1,C7,C8,C7,N1.[4] The first ring (C1-C6) lies at an angle of 54.08° to the plane of the propyl bridge, and the second ring (C10-C15) lies at an angle of 27.84°. The two cyclohexenyl rings are twisted at an angle of 32.44° to each other (**Fig. 4.1.39.**). The propyl bridge low indicates the atoms have significant planarity. The angle between the cyclohexenyl rings is smaller than the angle in Cy_2-tn(a), therefore the Cy_2-tn(b) molecule is more planar than the Cy_2-tn(a) molecule.

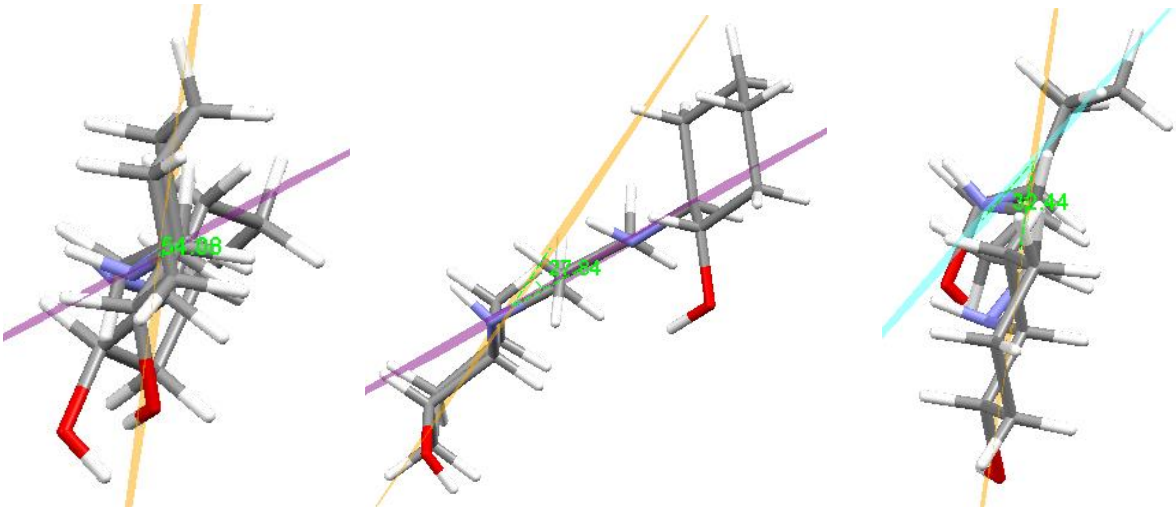


Figure 4.1.39. Cy_2-tn(b) molecule showing planes through the propyl bridge and the cyclohexenyl rings, and the angles between these planes.

There is maximum hydrogen bonding between the molecules, both the amine nitrogens are hydrogen bond acceptors to the alcohol moieties on two different molecules, Figure 4.1.40. This is the opposite of Cy_2-tn(a), where the nitrogens are hydrogen bond donors and the oxygens are the acceptors. The conformation of Cy_2-tn(b) is similar to the conformation needed for complexation, where the N and O atoms adopt an equatorial position on complexation. There are hydrogen bonds between the layers of molecules, and between the molecules in the layer, and the molecules overlap when viewed along the *a*-axis (**Fig. 4.1.41.**).

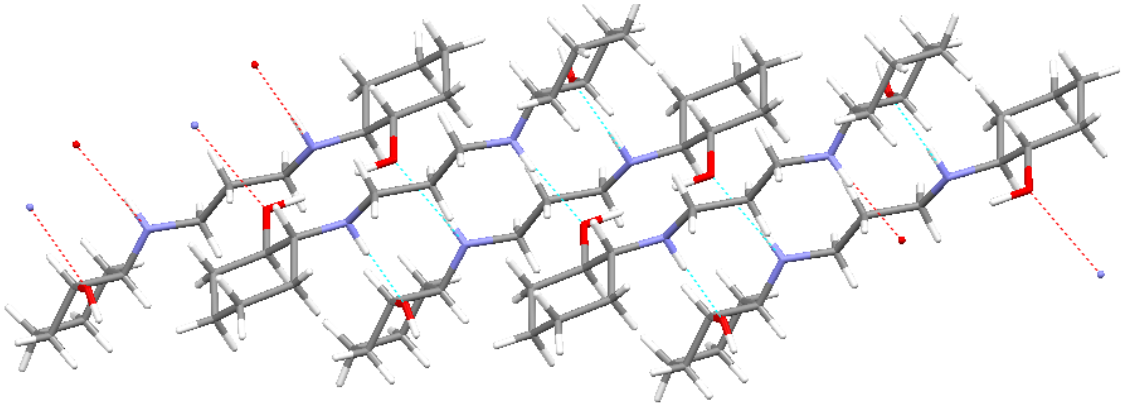


Figure 4.1.40. Cy_2-tn(b) hydrogen bonding network.

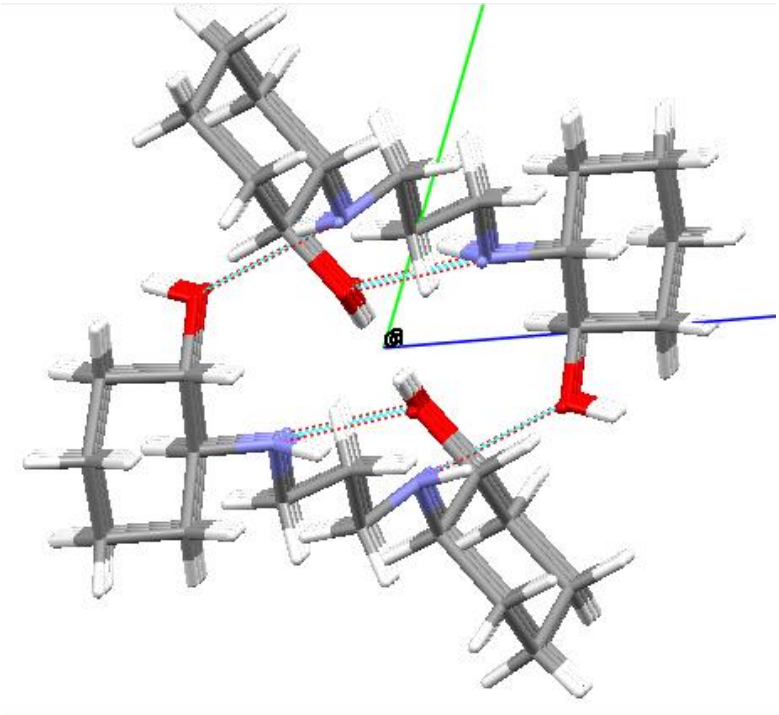


Figure 4.1.41. Cy_2-tn(b) hydrogen bonding viewed along the *a*-axis.

Looking at the H--H close contacts between the hydrogen atoms on the cyclohexenyl rings and the hydrogen atoms on the propyl bridge, Figure 4.1.42., Table 4.1.6., it can be seen that there are only two HCH--HCH interactions. There are no CH--HC or NH-O interactions, as the hydrogen on the amine points in the opposite direction to the oxygen.

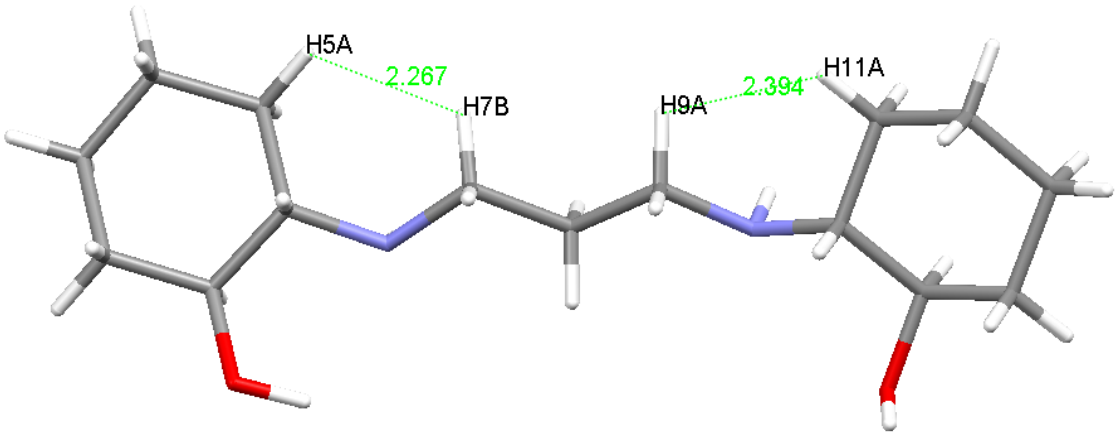


Figure 4.1.42. Cy_2-tn(b) H--H close contact interactions.

Table 4.1.6. Cy_2-tn(b) interaction distances and angles between HCH--HCH atoms.

Atom 1	Atom 2	H--H Close Contact Distance (Å)	H--H Torsion Angles (˚)
H5A	H7B	2.267	-19.24
H9A	H11A	2.394	35.89

4.1.3. Comparison of the Ligands Cy_2-Otn and Cy_2-tn

The synthetic route to obtain the two ligands, Cy_2-Otn, and Cy_2-tn, is the same, only the Cy_2-tn ligand synthesis was performed at 80 °C. However, very different yields were produced. This is most likely due to the nature of the starting amines. The Cy_2-Otn starting amine reacts with the CO_2 in the air, forming a carbamate compound, which results in low yields of Cy_2-Otn.

Looking at both polymorphs of Cy_2-Otn (a and b) it can be seen that the molecules in Cy_2-Otn(b) are more planar than the Cy_2-Otn(a) molecules, based on the angles of the

cyclohexenyl rings between each other, and between the propyl bridge plane. It should also be noted that the geometry of the Cy_2-Otn(a) molecules are either *S,S,S,S*, or *R,R,R,R* as the alcoholic moieties on the cyclohexenyl rings point in opposite directions, while the geometry of the Cy_2-Otn(b) molecules are *S,S,R,R* as the cyclohexenyl alcoholic moieties point in the same direction, i.e. this is the *meso* form.

Looking at both polymorphs of Cy_2-tn (a and b) it can be seen that the molecules in Cy_2-tn(b) are more planar than the Cy_2-tn(a) molecules, based on the angles of the cyclohexenyl rings between each other, and between the propyl bridge plane. It can also be seen that Cy_2-tn(b) has fewer interactions that Cy_2-tn(a). It should also be noted that the geometry of the cyclohexenyl chiral carbon atoms in Cy_2-tn(a) is *S,R,R,S*, which is similar to that of Cy_2-Otn(a), as the alcoholic moieties on the cyclohexenyl rings point in opposite directions, while the geometry of the chiral carbon atoms in the cyclohexenyl rings in Cy_2-tn(b) is *S,S,R,R* which is similar to that of Cy_2-Otn(b), as the alcoholic moieties on the cyclohexenyl rings point in the same direction.

The space groups of Cy_2-Otn(a) is the same as that of Cy_2-tn(a) (*C2/c*), similarly the space group of Cy_2-Otn(b) is the same as that of Cy_2-tn(b) (*P*$\bar{1}$). Both (a) polymorphs also have an inversion centre around the middle carbon in the propyl bridge. The Cy_2-Otn (a and b) and Cy_2-tn(a and b) molecules are arranged to maximise the number of hydrogen bonds that can be formed between the various molecules. Both ligands and their polymorphs have H--H close contacts between atoms on the ring and atoms on the carbon bridge. These interactions are investigated in the ligand-metal complexes. There were other close contacts present in these molecules, involving the amine nitrogens and the alcoholic oxygens. These attractive interactions affect the manner in which the molecules pack in the unit cell.

4.2. Synthesis and Characterisation of the Cy_2-Otn/Metal complexes

Several methods were employed to obtain Cy_2-Otn/metal complexes, and their crystal structures. Only gels were formed by metal complexes with the Cy_2-Otn ligand. This is most likely due to the extra hydroxyl group on the propyl bridge forming hydrogen bonds to the solution molecules, namely water. These hydrogen bonds may be responsible for the water not completely evaporating leading to the formation of gels. The solvent was varied to try remove this possibility but gels were still formed. The characterisations for most of these experiments show that complexes were formed (Appendices B, C, and D).

The mass spectroscopy of Cy_2-tn/Cu showed a complex was formed although a mixture of products was seen, and the IR spectroscopy showed a decrease in the number of peaks also indicating a complex was formed, as the degrees of freedom in the free ligand decrease on complexation. The M-O and M-N bands usually occur below 600 cm^{-1} and often cannot be seen as the equipment does not go below 600 cm^{-1}.

The Cy_2-tn/Ni mass spectroscopy showed a complex was formed but also a mixture of prducts was observed, the IR spectroscopy also showed a complex was formed as there was a decrease in the number of peaks, indicating the free ligand was complexed.

The mass spectroscopy of Cy_2-Otn/Zn indicated a mixture of products was formed as well as a complex, and the IR also shows a complex was formed.

The Cy_2-Otn/Cd characterisations of the first reaction showed a complex was formed (m/z 287 (Cy_2-Otn+1), 573 (Cy_2-Otn+1+Cy_2-Otn), 721 (Cy_2-Otn+Cd+Cl+1+Cy_2-Otn)), but the other reactions were unsuccessful.

The characterisations of the Cy_2-Otn/Pb method 1 showed a complex was formed (m/z 271 (blank), 287 (Cy_2-Otn+1), 493 (Cy_2-Otn+1+Pb), 779 (2Cy_2-Otn+Pb+1), 983 (2[Cy_2-Otn+Pb]+1+4H)) and a mixture of products, but the second reaction was unsuccessful.

4.3. Synthesis and Characterisation of Cy_2-tn/Metal Complexes

Several methods were employed to obtain the Cy_2-tn/metal complexes, and the crystal structures of these complexes. The Cy_2-tn/Pb and Cy_2-tn/Cu complex did not form crystals.

4.3.1. Synthesis of the Cy_2-tn/Ni Complex

The synthesis of Cy_2-tn/Ni was done using both chloride and nitrate nickel salts. Crystals were formed with both metal salts; however, the crystals formed with the nickel nitrate salts were twinned and so no useful XRD data could be collected for those crystals. The crystal structure from the nickel chloride salt was determined and the characterisation can be found in the Appendices C-E.

The XRD structure of the Cy_2-tn/Ni complex has a $P2_1/c$ space group and an R-factor of 2.92% showing the good quality of the crystals. The Ni(II) ion is coordinated to the ligand through the N and O donor atoms in equatorial positions, and has two water molecules in the axial positions, as well as two chloride atoms in the unit cell (**Fig. 4.3.1.**). The chiral carbon atoms have the geometry *S,S,R,R*, which is different to the free ligand Cy_2-tn(a), but the same as the polymorph Cy_2-tn(b), suggesting that Cy_2-tn(b) is more pre-organised.

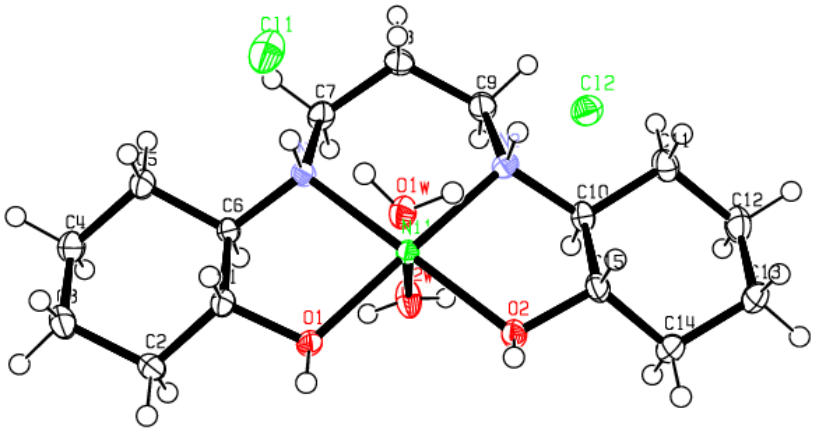


Figure 4.3.1. The molecular structure of the Cy_2-tn/Ni complex, showing the atom-labelling scheme and 50% probability displacement ellipsoids.

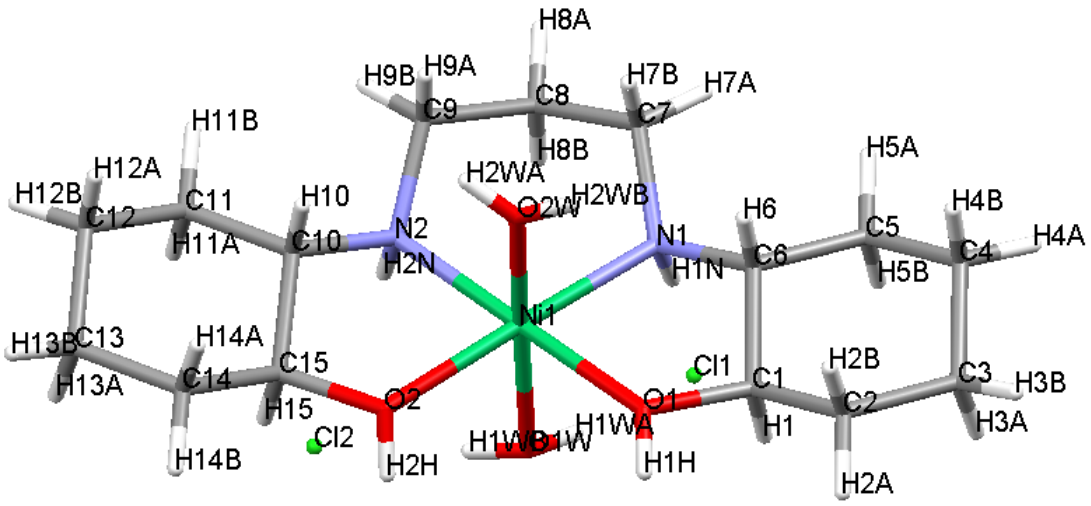


Figure 4.3.2. The molecular structure of the Cy_2-tn/Ni complex with its labelling scheme.

The structure of the complex shows the Ni(II) ions adopts a six-coordinated, octahedral geometry. This one of the most common coordinations for Ni(II) and it accounts for the blue colour of the crystals. The complex formations shows the Ni(II) ion sits in the ligand cavity formed by the four donor atoms, and forms an almost planar molecule with the ligand. A plane through the metal and the ligand donor atoms N1, O1, O2, and N2 has an r.m.s. value of 0.0254 Å to the atoms.[4] The axial water molecules are at right angles to plane through the ligand (89.92°), Figure 4.3.3.

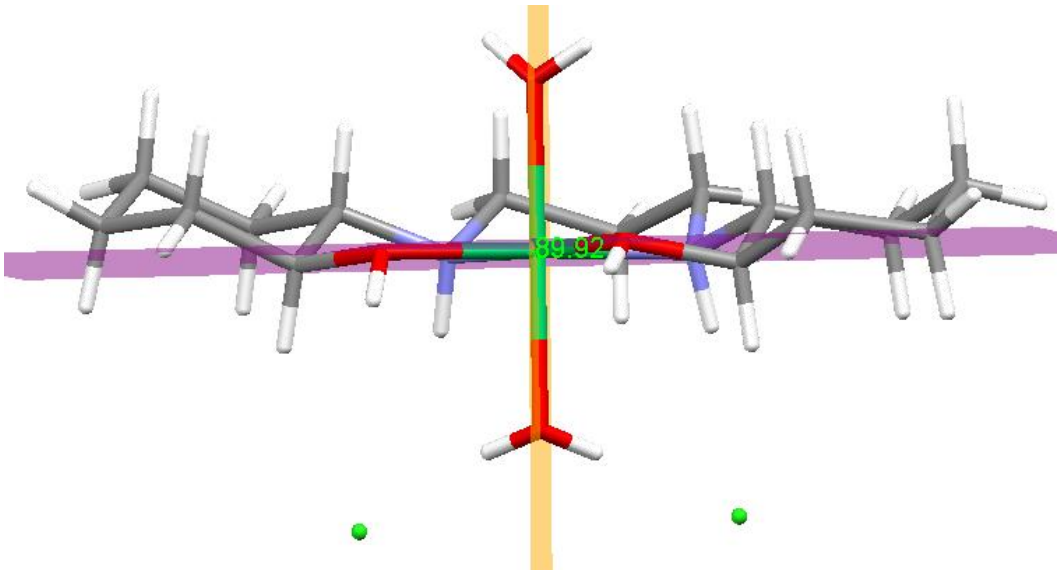


Figure 4.3.3. Cy_2-tn/Ni complex with planes through the donor atoms of the ligands.

The chloride counter ions lie in between the layers formed by the molecules, and layers alternate in the direction the molecules are orientated in, but in each layer the molecules point in the same direction. The layers are also slightly shifted with respect to each other, due to the axial water ligands and the chloride counter ions (**Fig. 4.3.4. and 4.3.5.**).

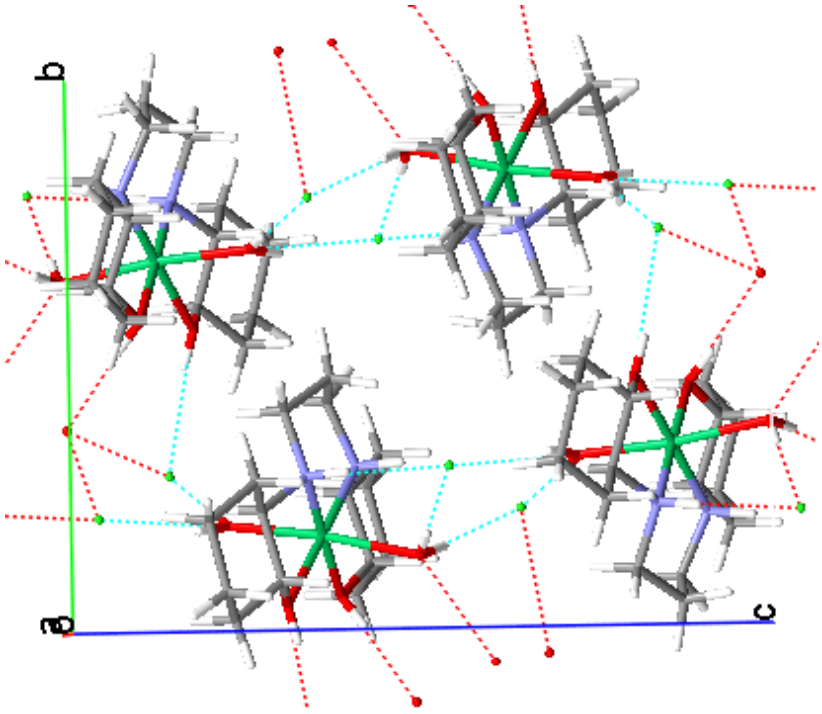


Figure 4.3.4. Hydrogen bonding of the Cy_2-tn/Ni complex viewed along the *a*-axis.

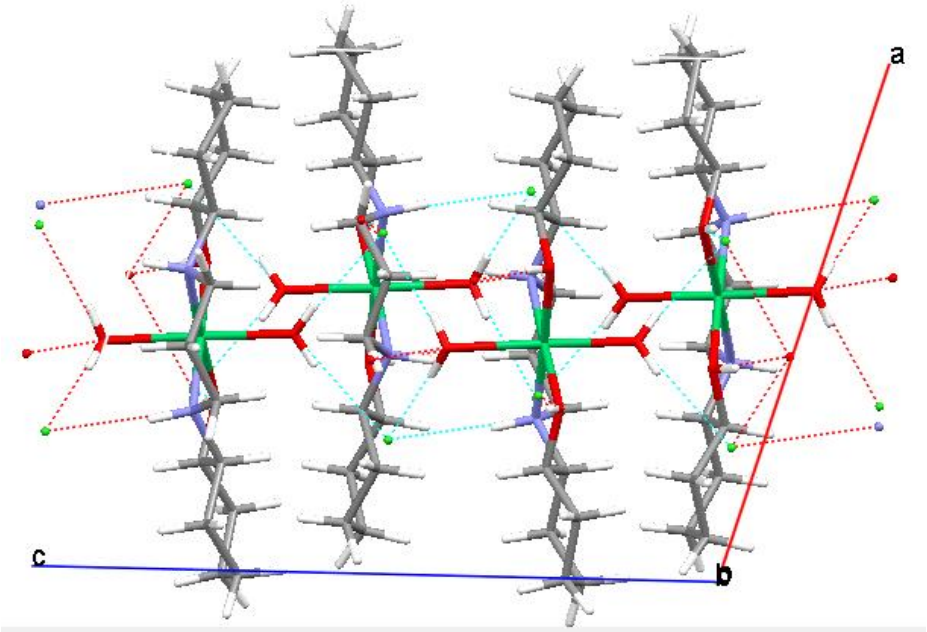


Figure 4.3.5. Hydrogen bonding in the Cy_2-tn/Ni complex viewed along the *b*-axis.

The presence and number of H--H close contacts remain the same when both polymorphs of the free ligand Cy_2-tn and the Ni(II) complex are compared, Table 4.3.1. The distances between the HCH--HCH atoms in the complex are greater than the distances in the Cy_2-tn(a), but less than the Cy_2-tn(b) values (**Fig. 4.3.6.**). It is therefore unclear thus far if these interactions affect complexation behaviour. However, QTAIM analyses show there are no bond paths between the hydrogens on the cyclohexenyl rings and the hydrogens on the propyl bridge. These H--H close contacts are most likely very weak and are a result of the solid state packing arrangements.

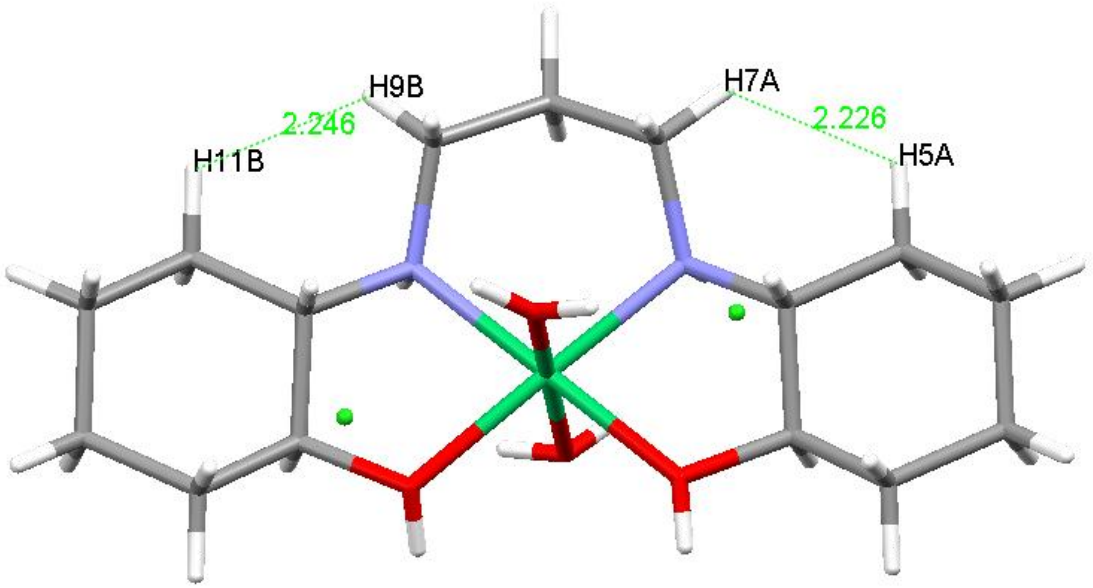


Figure 4.3.6. H--H close contacts in the Cy_2-tn/Ni complex.

Table 4.3.1. H--H close contacts for the Cy_2-tn/Ni complex.

Atom 1	Atom 2	H--H Close Contact Distance (Å)	H--H Torsion Angle (°)
H5A	H7A	2.226	26.88
H9B	H11B	2.246	-34.08

4.3.2. Synthesis of the Cy_2-tn/Zn Complex

The method used to synthesise the Cy_2-tn/Zn complex is similar to the method used to synthesise the Cy_2-tn/Ni complex, but the reaction time was shorter. This is because the kinetics of Zn(II) are faster than Ni(II). The synthesis was done using both zinc chloride and nitrate salts, but only the zinc chloride salt produced crystals. The characterisation data can be found in the Appendices C-E.

The XRD structure of the Cy_2-tn/Zn complex has a *P*ī space group and an R-factor of 3.14% showing the good quality of the crystals. The Zn(II) ion is coordinated to the ligand through the N and O donor atoms in equatorial positions, and has a chloride atom in one of the axial positions, as well as two water molecules and a disordered chloride atom in the unit cell (**Fig. 4.3.7.**). The chiral carbon atoms have the geometry *S*,*S*,*R*,*R* which is, once again, different to the free ligand Cy_2-tn(a), but the same as the polymorph Cy_2-tn(b).

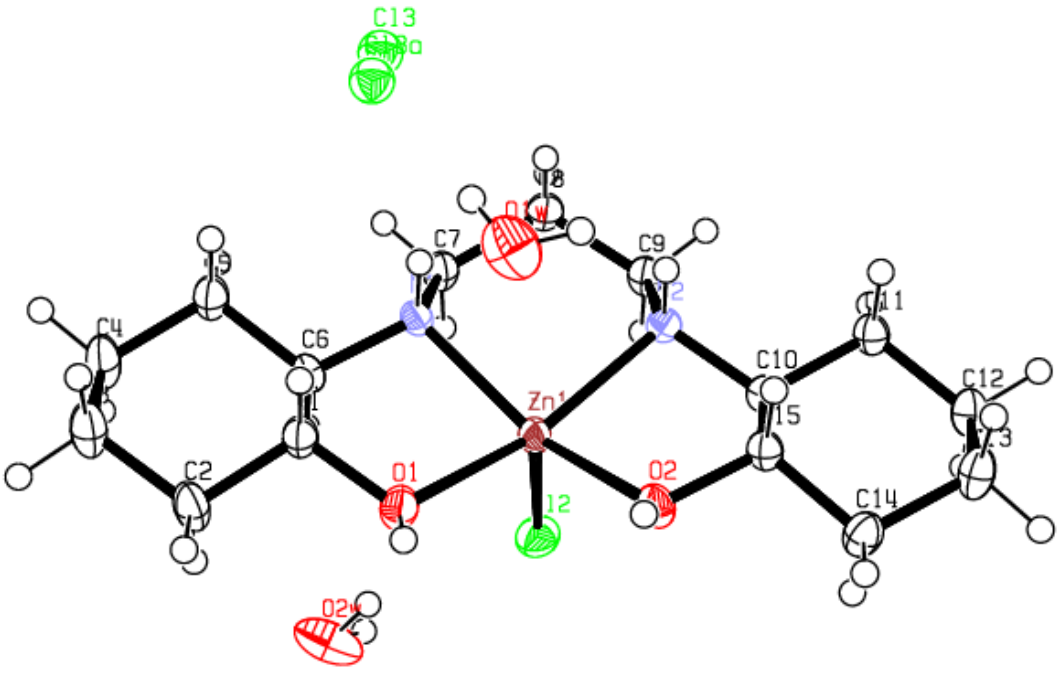


Figure 4.3.7. The molecular structure of the Cy_2-tn/Zn complex, showing the atom-labelling scheme and 50% probability displacement ellipsoids.

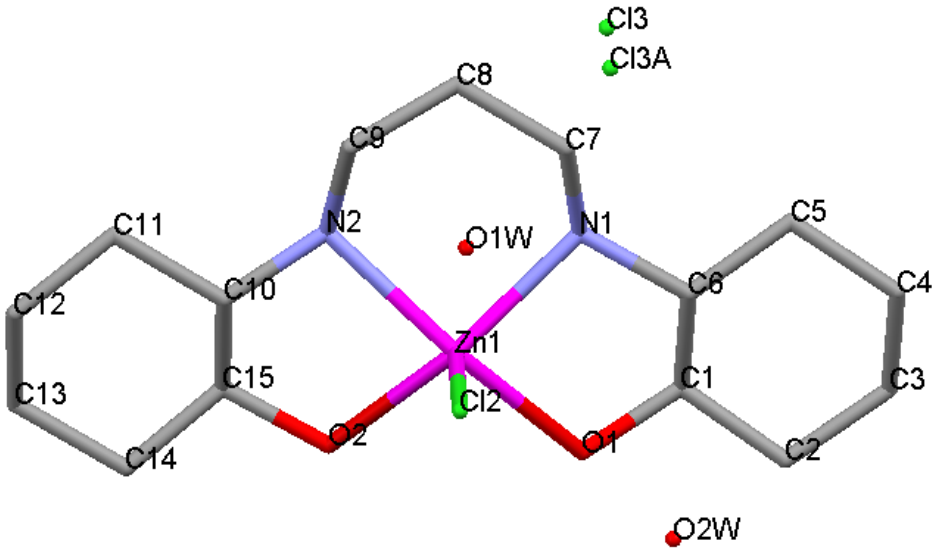


Figure 4.3.8. The molecular structure of the Cy_2-tn/Zn complex with its labelling scheme (hydrogen atoms omitted for clarity).

The structure of the complex shows the Zn(II) ions adopts an uncommon five-coordinated, square pyramidal geometry (**Fig. 4.3.8.**). The Zn(II) ion is pulled out of the ligand plane, made by the donor atoms (N1, O1, O2, and N2), by the axial chloride ion. The r.m.s. value of the ligand plane is 0.0406 Å, and the Zn(II) ion sits 0.506 Å above the plane (**Fig. 4.3.9**).[4]

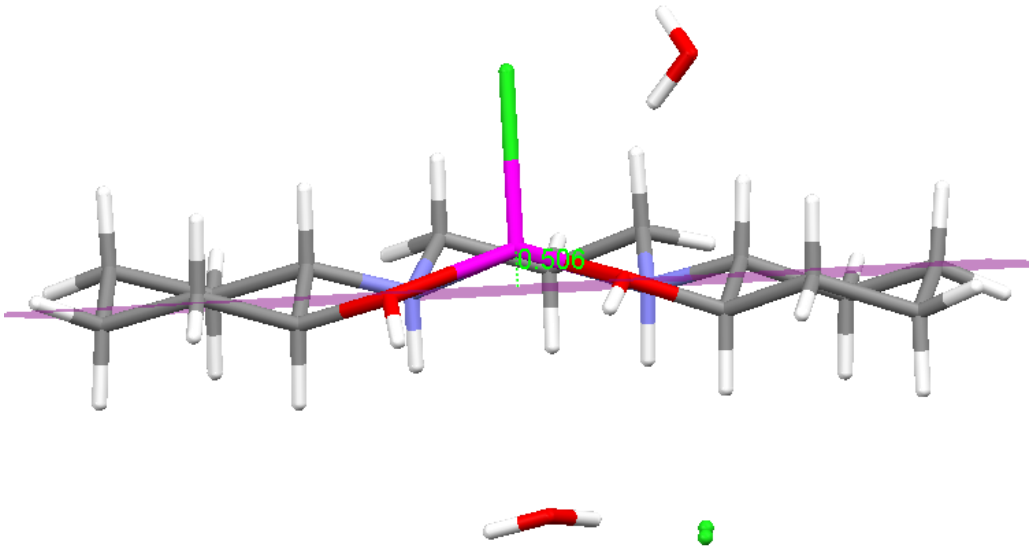


Figure 4.3.9. Cy_2-tn/Zn complex with a plane through the ligand donor atoms.

There are two Cy_2-tn/Zn molecules, four water molecules and two disordered chloride molecules in each unit cell. The Cy_2-tn/Zn molecules arrange themselves in layers where the molecules alternate in the direction the axial chloride molecules face. In these layers, where molecules have the axial chloride ligand away from each other, there is the disordered chloride atom and two water molecules between the complex molecules. For the molecules that have the axial chloride ligand pointing towards each other, there is only one water molecule between the complexes. There are hydrogen bonds between the molecules in these layers, but not between the layers themselves (**Fig. 4.3.10.**). There are also layers formed along the molecules that have the axial ligand pointing in the same direction, these layers overlap and there are hydrogen bonds between these layers but not between the molecules in the layers (**Fig. 4.3.11.**).

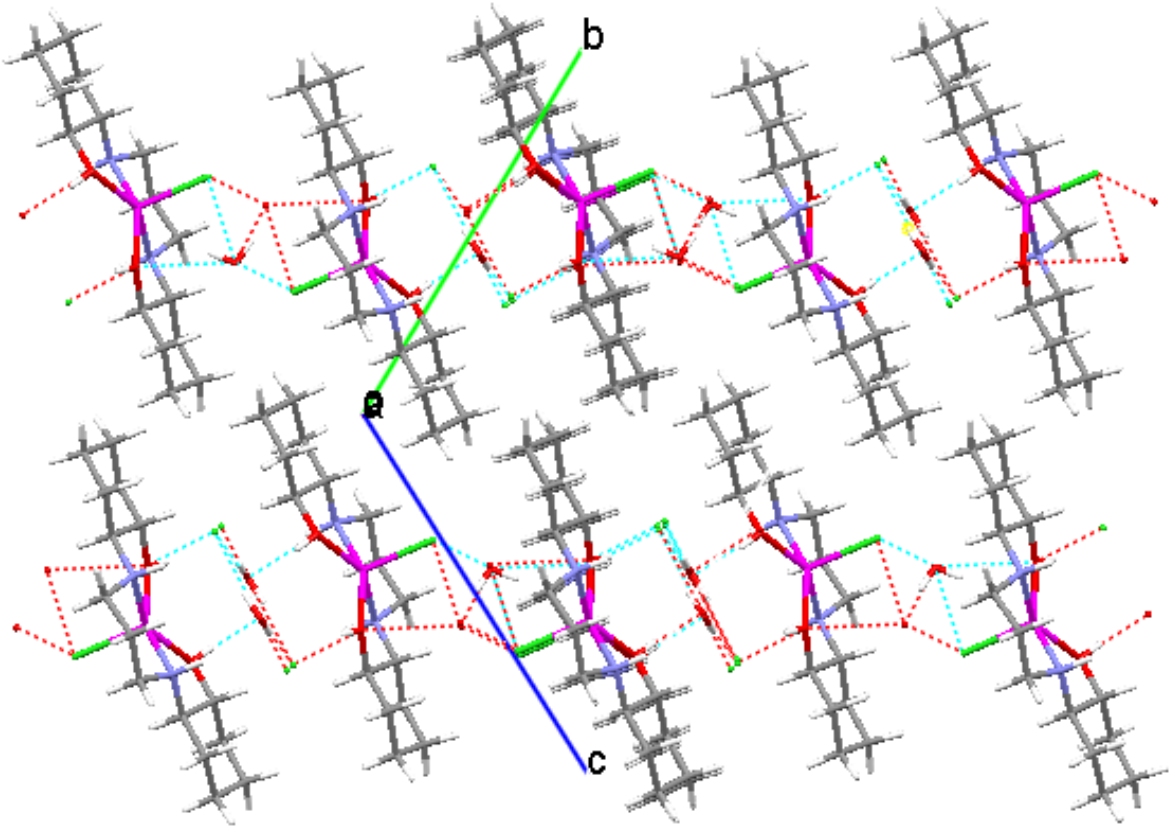


Figure 4.3.10. Hydrogen bonding in the Cy_2-tn/Zn system viewed along the *a*-axis.

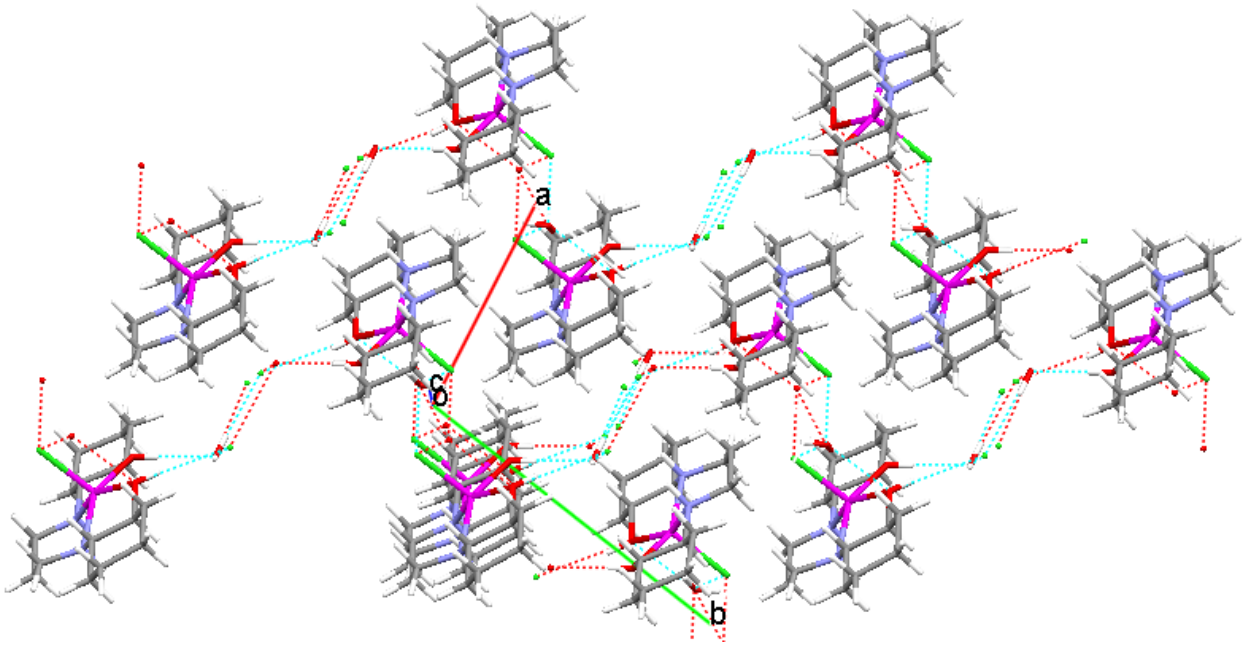


Figure 4.3.11. Hydrogen bonding in the Cy_2-tn/Zn system viewed along the *c*-axis.

The presence and number of H--H close contacts is the same as that seen for both polymorphs of the free ligand Cy_2-tn. The H--H close contact distances in the Cy_2-tn/Zn complex are close to those of the Cy_2-tn(b) ligand, Table 4.3.2. The NH-O interactions are no longer present, as the N and O atoms are now donor atoms to the metal. Once again, the DFT calculations do not show the existence of these H--H close contacts, which are a most likely weak and a result of the crystal packing.

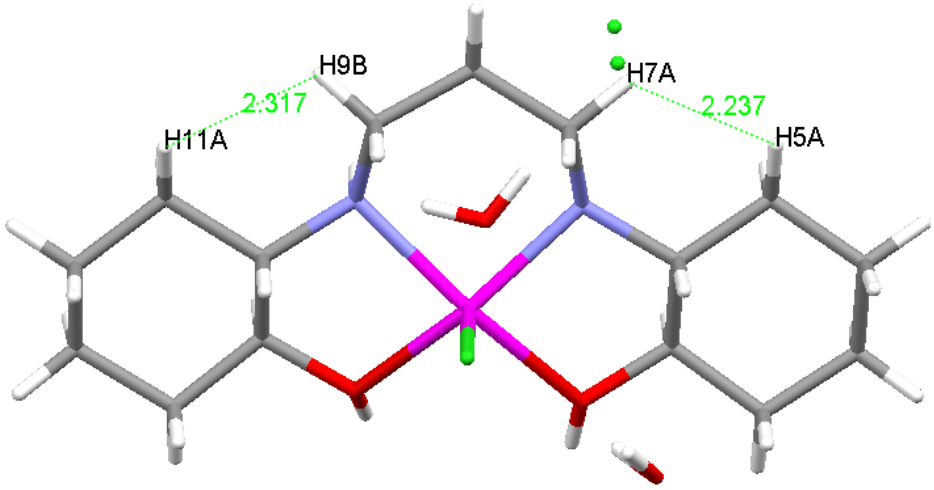


Figure 4.3.12. H--H close contacts in the Cy_2-tn/Zn complex.

Table 4.3.2. H--H close contacts for the Cy_2-tn/Zn complex.

Atom 1	Atom 2	H--H Close Contact Distance (Å)	H--H Torsion Angle (˚)
H5A	H7A	2.237	24.75
H9B	H11A	2.317	-35.69

4.3.3. Synthesis of the Cy_2-tn/Cu Complex

The method used for synthesis of Cy_2-tn/Cu was the same as that used by Hancock *et al.*[2] However, I was unable to replicate the product. A similar method to the ones used for the Cy_2-tn/Ni and Zn(II) complexes, was used as well as trying the perchlorate and nitrate copper salts, but no crystals were formed. The characterisations of the Cy_2-tn/Cu showed a complex was formed as well as a mixture of products, and can be found in the Appendices C-E.

Hancock *et al.*[2] determined the crystal structure of the Cy_2-tn/Cu complex from the perchlorate salt (**Fig. 4.3.13.**), with a *Pn* space group and an R-factor of 5.24%. The Cu(II) ion is bonded to the ligand through the N and O donor atoms in the equatorial positions, a water molecule and a perchlorate molecule are bonded in the axial positions (**Fig. 4.3.14.**). The axial perchlorate molecule has disorder around the chloride oxygen atoms, and both Cu-O axial bonds are fairly long (Cu-OH_2 = 2.262 Å, and Cu-$OClO_3$ = 2.789 Å). There is also a perchlorate ion present in the unit cell. However, the QTAIM molecular graph of Cy_2-tn/Cu does not show a bond path or BCP between the Cu(II) ion and one of the perchlorate ions, indicating that the Cu-$OClO_3$ bond is not a genuine bond.

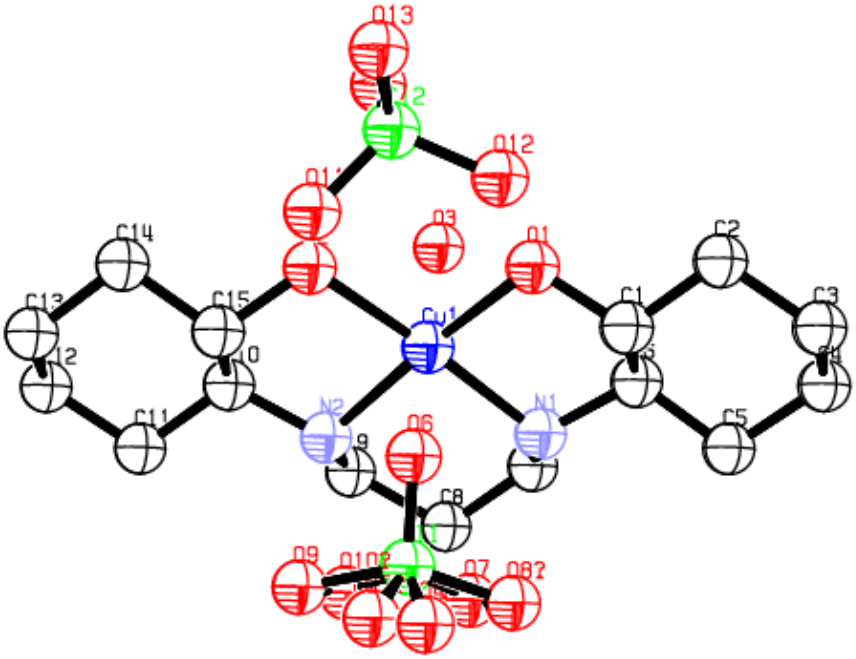


Figure 4.3.13. The molecular structure of the Cy_2-tn/Cu complex, showing the atom-labelling scheme and 50% probability displacement ellipsoids (hydrogens omitted for clarity).

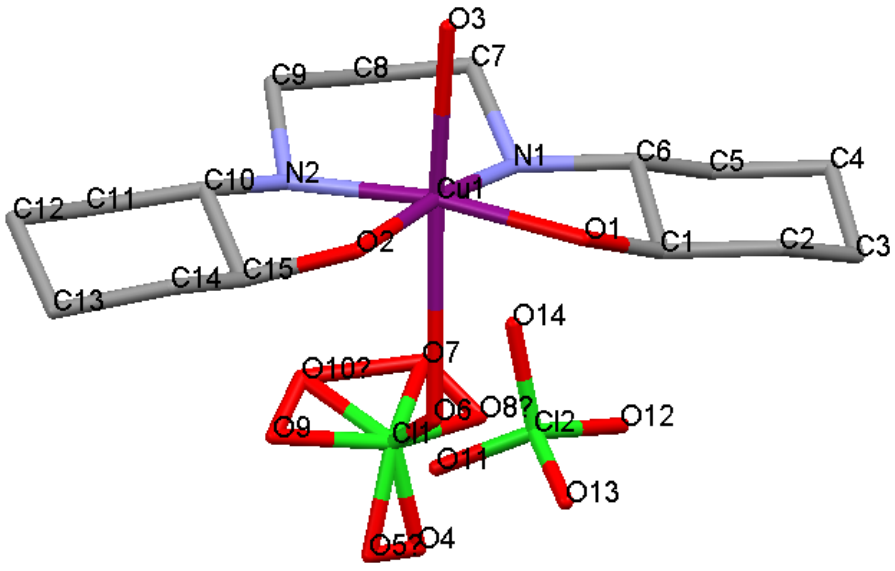


Figure 4.3.14. The molecular structure of the Cy_2-tn/Cu complex with its labelling scheme (hydrogen atoms omitted for clarity).

The ligands around the Cu(II) form a five-coordinate, square pyramidal geometry, and the geometry of the ligand is *S,S,R,R*, which is the same as that of the free ligand Cy_2-tn(b). The Cu(II) ion sits slightly out of the plane (0.141 Å) made by the ligand donor atoms, N1, O1, O2, N2 (**Fig. 4.3.15.**).

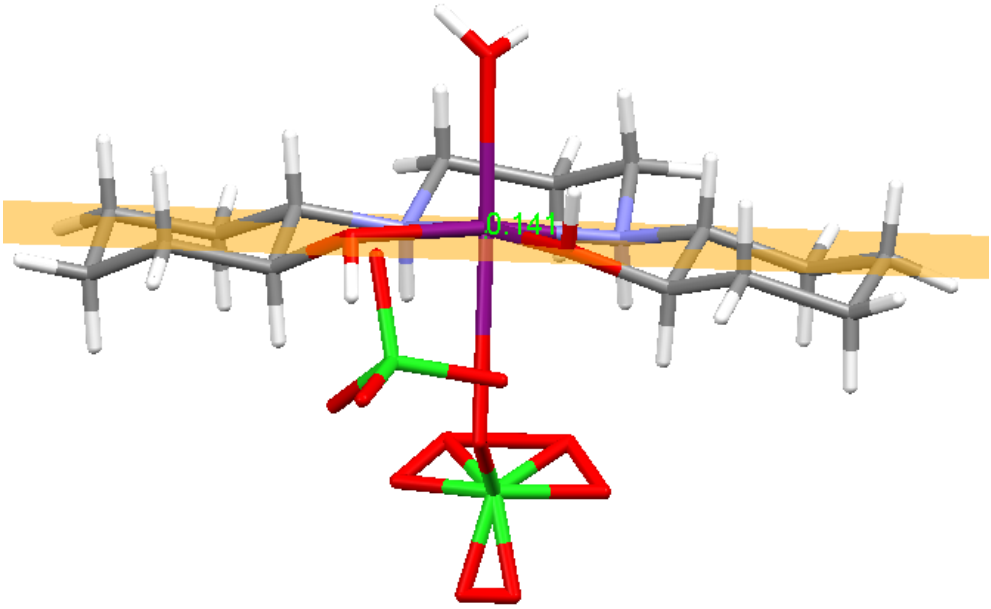


Figure 4.3.15. Cy_2-tn/Cu complex with a plane through the ligand donor atoms.

The molecules arrange themselves so that the axial water molecules are all facing the same direction. The axial perchlorate ion hydrogen bonds to the axial water molecule of the next molecule, linking the layers together via intermolecular bonds (**Fig. 4.3.15.**). The molecules stack on top of each other in the layers, and there are also hydrogen bonds between the layers that occur between the free perchlorate molecule and the alcoholic and water oxygens. The intramolecular hydrogen bonds occur between the anime nitrogen and the axial perchlorate oxygen atoms (**Fig. 4.3.16.**).

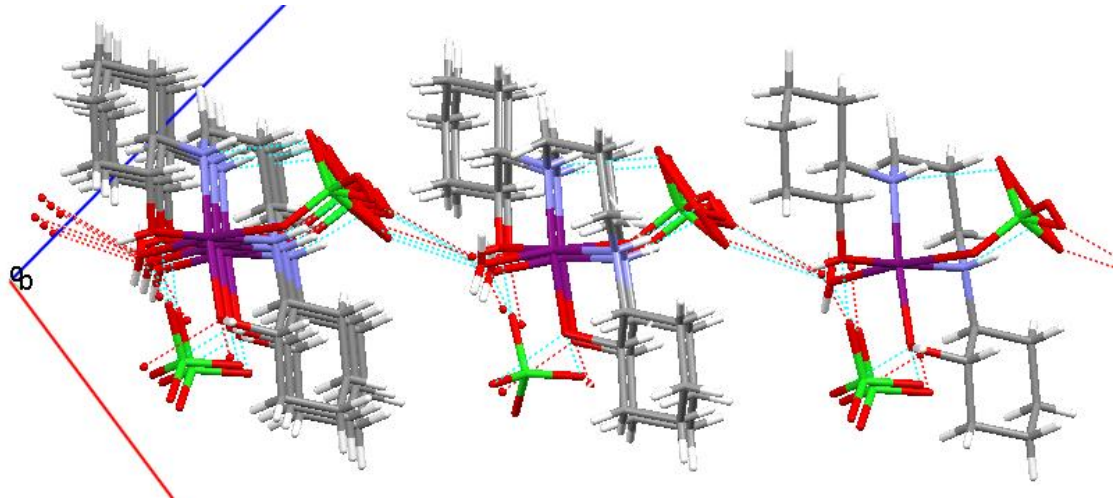


Figure 4.3.16. Crystal packing and hydrogen bonding in the Cy_2-tn/Cu complex, viewed along the *b*-axis.

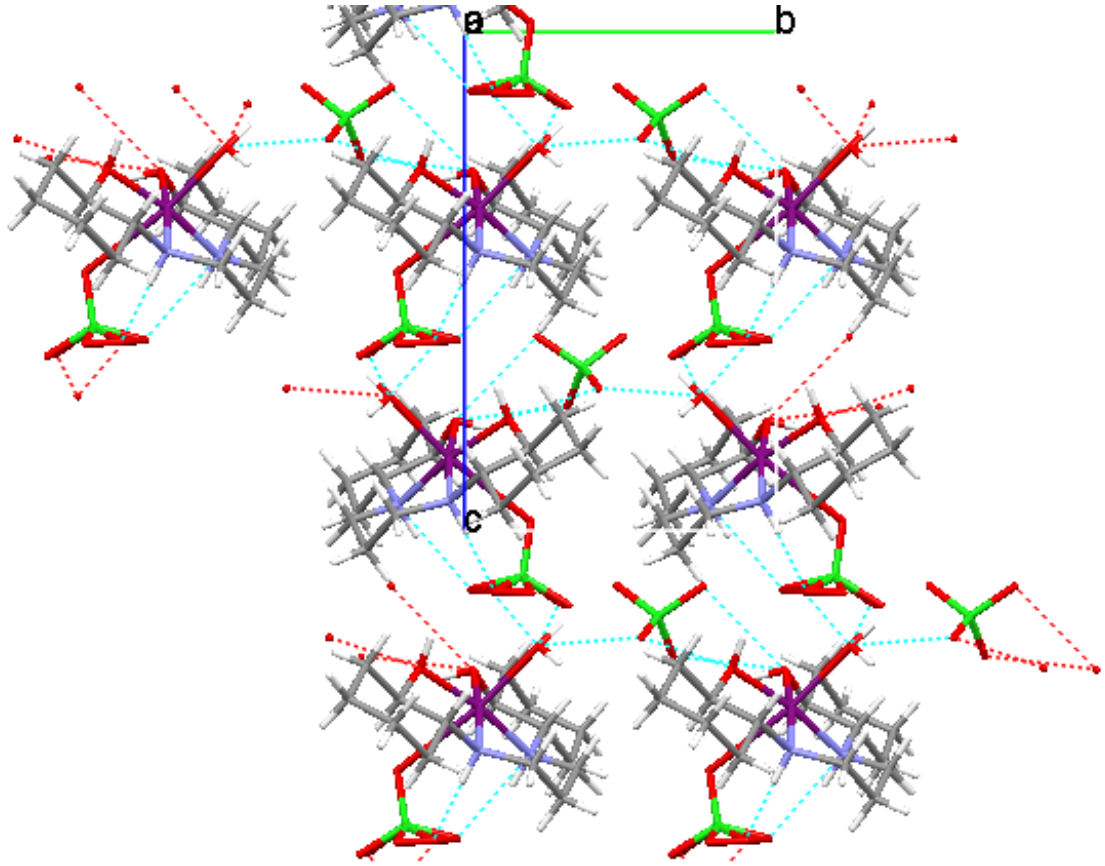


Figure 4.3.17. Hydrogen bonding in the Cy_2-tn/Cu complex viewed along the *a*-axis.

There are H--H close contacts present between the HCH--HCH hydrogens on the cyclohexenyl rings and the propyl bridge. The distances between the HCH--HCH atoms in the complex are, once again, greater than the distances in the Cy_2-tn(a), but less than the Cy_2-tn(b) values (**Fig. 4.3.18.**). DFT calculations also show that no bonds exist where the H--H close contacts are observed.

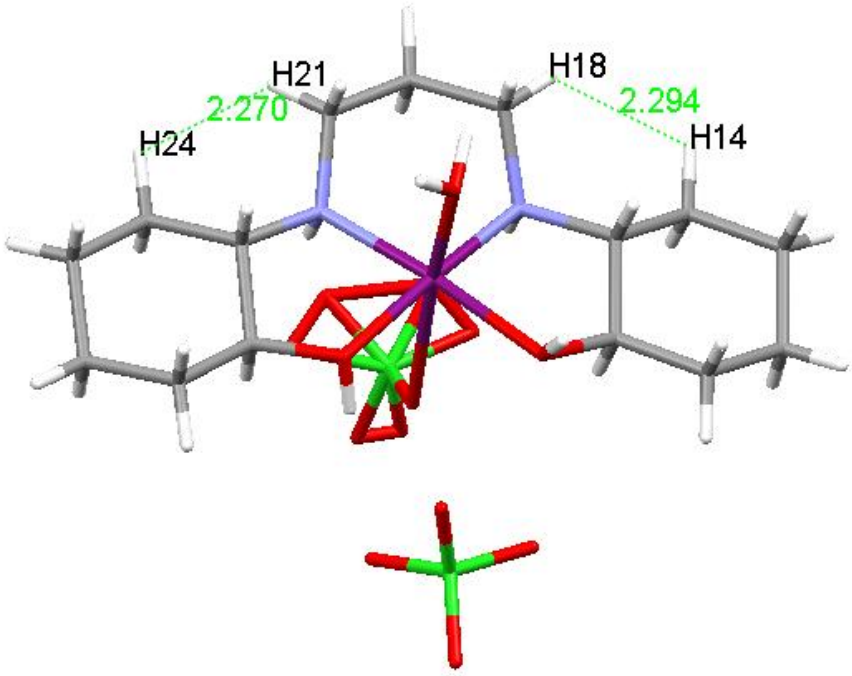


Figure 4.3.18. H--H close contacts in the Cy_2-tn/Cu complex.

Table 4.3.3. H--H close contacts for the Cy_2-tn/Cu complex.

Atom 1	Atom 2	H--H Close Contact Distance (Å)	H-H Torsion Angle (˚)
H14	H18	2.294	16.42
H21	H24	2.270	-25.50

4.3.4. Synthesis of Cy_2-tn/Cd Complex

Various methods were tried to synthesise the Cy_2-tn/Cd complex, as many did not result in complex formation; most likely due to precipitation of the cadmium at elevated pH, since the free ligand in solution was fairly basic (pH 10.35). Attempts were made to decrease the solution pH, to eliminate the cadmium precipitation, but no complex was formed. An increase in the reaction time, as well as the temperature resulted in the formation of crystals of poor quality, recrystalisation attempts did not yield better quality crystals, subject to twinning. The characterisations can be found in Appendices C-E.

The XRD structure of the Cy_2-tn/Cd complex has a *C2/c* space group, and a large R-factor of 22.91% showing the poor quality of the crystals. The crystal structure of the Cy_2-tn/Cd complex shows the formation of a dimer, where the two cadmium molecules are joined by a chloride ion. Both cadmium ions are coordinated through both amine nitrogens from the ligand in equatorial positions. One Cd(II) ion is coordinated through both alcoholic oxygen atoms from the ligand, one being in an equatorial and one in an axial position, and has two chloride donor atoms, also with one in an equatorial and one in an axial position. The second Cd(II) ion is only coordinated to one alcoholic oxygen from the ligand in an equatorial position, and has three chloride ligands, two in axial positions and one in an equatorial position (**Fig. 4.3.19.**). The molecule coordinated to the four ligand donors, has the chiral geometry *S,S,S,S* observed for the Cy_2-tn(a) polymorph. The second molecule coordinated to three chloride ions has the chiral geometry of *S,S,R,R* observed for the free ligand Cy_2-tn(b) polymorph. The dimers have slightly distorted octahedral geometries.

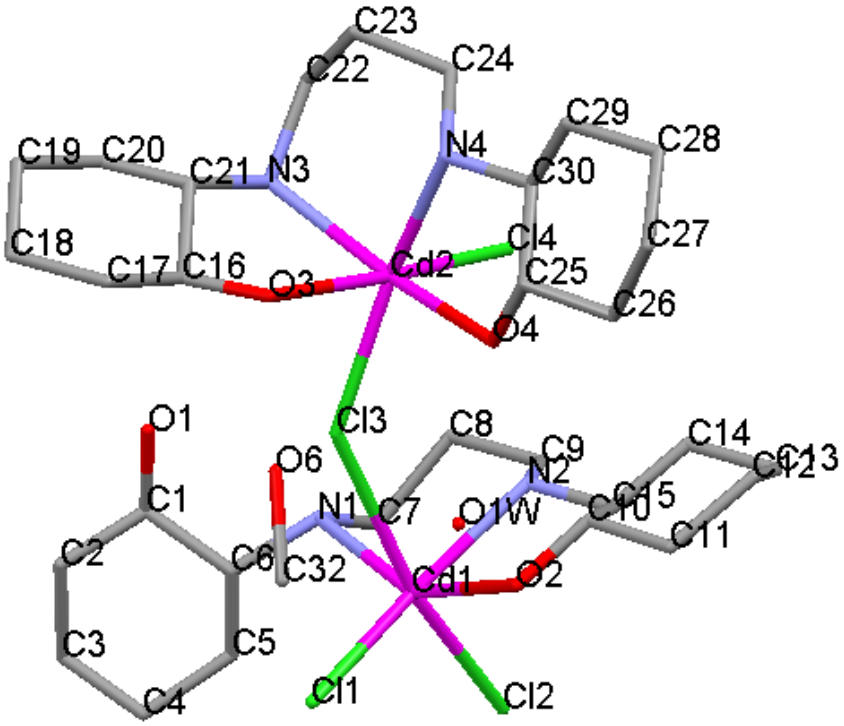


Figure 4.3.19. The molecular structure of the Cy_2-tn/Cd complex with its labelling scheme (hydrogen atoms omitted for clarity).

Both the Cd(II) ions are pulled out of the cavity, and therefore out of the plane made by the ligand donor atoms. The Cd(II) molecule bonded through all four ligand donor atoms, sits 1.092 Å away from the donor atom plane that has an r.m.s. value of 0.6009 Å. This r.m.s. value is fairly high due to the buckling of the ligand to accommodate the larger metal ion that is pulled out of the cavity by the joining chloride ion (**Fig. 4.3.20.**).[4] The Cd(II) molecule bonded to three chloride ions sits 0.501 Å above the plane through the N1, N2, and O2 donor atoms. The cyclohexenyl ring with the unbonded alcoholic moiety is twisted by 84.05° to the coordinated cyclohexenyl ring (**Fig. 4.3.21.**).

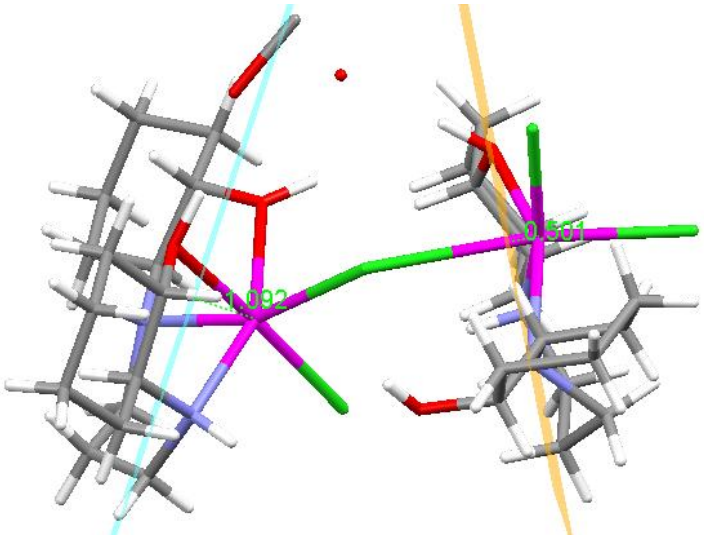


Figure 4.3.20. Cy_2-tn/Cd dimmer showing planes through the coordinated ligand donor atoms.

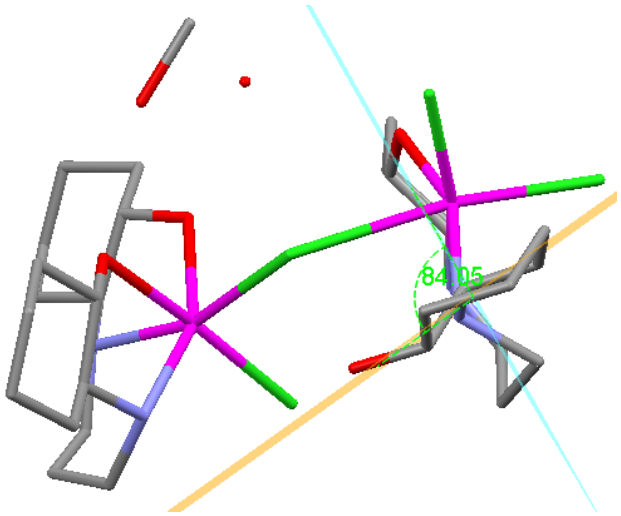


Figure 4.3.21. Cy_2-tn/Cd dimer showing cyclohexenyl ring twisting.

There is hydrogen bonding in the dimers between the uncoordinated alcoholic oxygen and the water molecule. The water molecule is hydrogen bonded to a coordinated alcoholic oxygen atom, and to the axial chloride atom. The molecules form layers that overlap with each other along the *b*-axis, with no hydrogen bonding between the layers, and the dimers facing the same direction (**Fig. 4.3.22.**). The dimers in these layers are hydrogen bonded through the carbon monoxide molecule and the axial chloride molecule. The layers form pairs that alternate directions forming a zig-zag pattern, with cavities in the pair layers that face opposite directions (**Fig. 4.3.23.**).

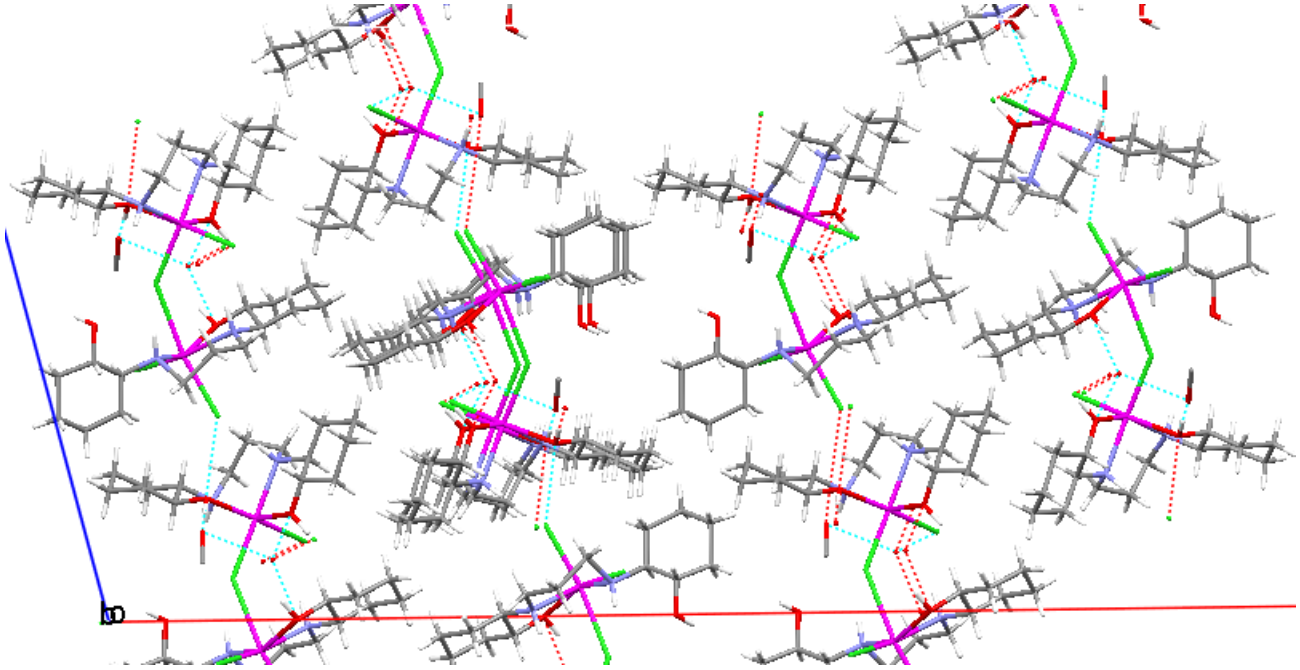


Figure 4.3.22. Cy_2-tn/Cd dimer hydrogen bonding viewed along the *b*-axis.

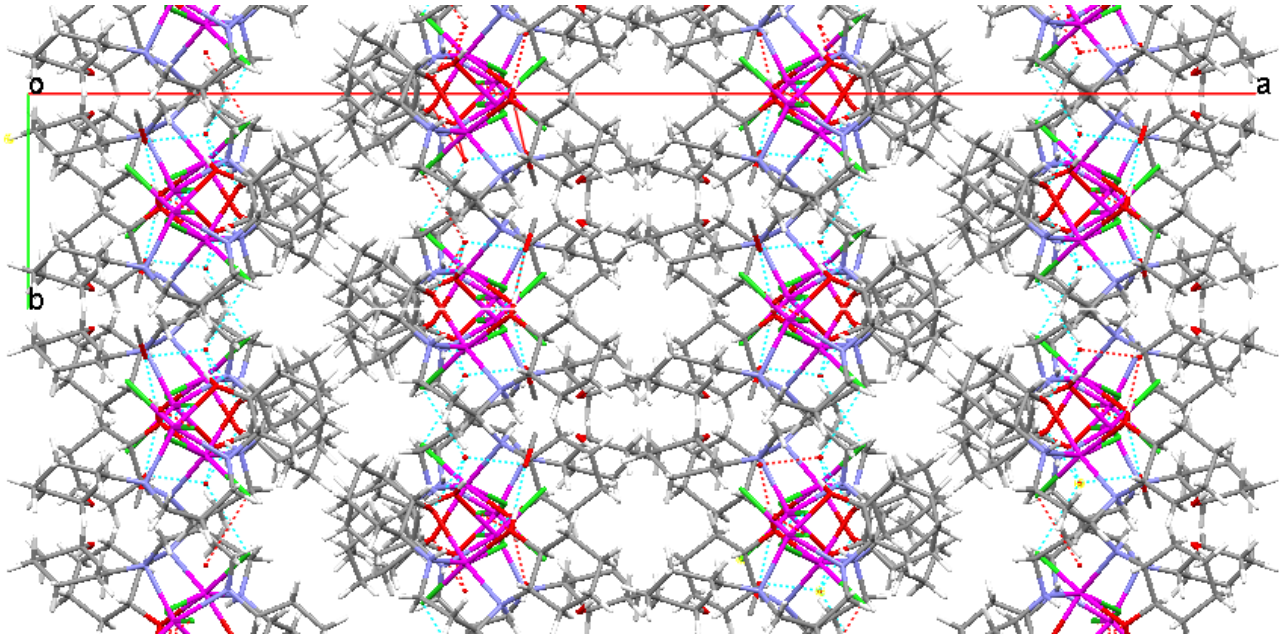


Figure 4.3.23. Cy_2-tn/Cd dimer hydrogen bonding viewed along the *c*-axis.

The H--H close contacts exist between the CH_2 groups on the cyclohexenyl rings and the propyl bridge (**Fig. 4.3.24.**). It can be seen that the H--H close contactd distances vary from 2.071 to 2.340 Å, due to the different conformations of the ligands and the strain in the carbon backbone from complexation and dimer formation.

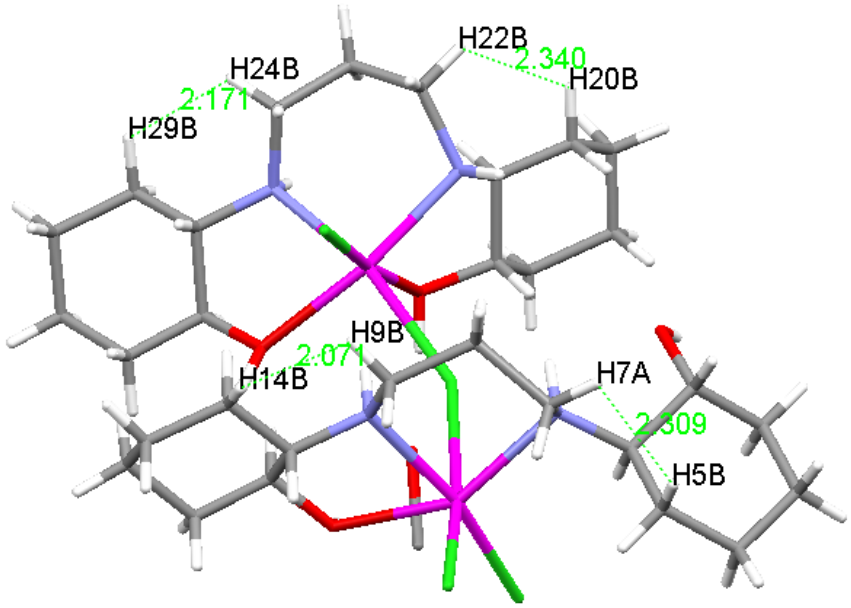


Figure 4.3.24. H--H close contacts in the Cy_2-tn/Cd dimer.

Table 4.3.4. H--H close contacts for the Cy_2-tn/Cd complex.

Atom 1	Atom 2	H--H Close Contact Distance (Å)	H--H Torsion Angle (˚)
H5B	H7A	2.309	28.39
H9B	H14B	2.071	49.79
H20B	H22B	2.340	0.53
H24B	H29B	2.171	-11.15

4.3.5. Comparison of the Cy_2-tn/Metal Complexes

The synthesis of the Cy_2-tn/Metal complexes were similar, varying mostly in the reaction time and temperature. Many different metal salts were tried, but the chloride salts were the most successful. The chiral geometries of the complexed ligands were *S,S,R,R* which are the same as that of the free ligand Cy_2-tn(b), with the exception of the Cy_2-tn/Cd molecule bonded to the four ligand donor atoms which was the same as that of the Cy_2-tn(a) free ligand (*S,S,S,S*). These geometries are dependent on the direction the alcoholic moieties, and it can be seen that the Cy_2-tn(b) polymorph has the preferred orientation for complexation i.e. the most pre-organised polymorph with the alcoholic moieties pointing in the same direction.

Most of the complex geometries are octahedral, or distorted octahedral, except for the Cy_2-tn/Zn and Cy_2-tn/Cu complexes which were square pyramidal. The Cy_2-tn/Cd complex was the only dimer formed. The ligand donor atoms were always in the equatorial positions, except for the Cy_2-tn/Cd molecule with three chloride donor atoms as one of the chloride atom occupied an equatorial site as the one alcoholic oxygen was not bonded. The axial ligands were either the chloride/perchlorate salt or the solvent molecules (water). The planarity of the ligand donor atoms is dependant on many factors, such as the size of the metal ion, the number and type of axial ligands.

The large cadmium ion, in the molecule with all four ligand atoms bonded, sits very far out of the ligand cavity. This could be attributed to a number of factors, such as the metal ion size which leads to buckling of the carbon backbone, as well as the pull of the axial ligands. The second cadmium ion also sits out of the plane through the ligand donor atoms, although it is not as far as the fist cadmium ion. This could be due to the fact that one of the alcoholic oxygen moieties is not bonded to the metal, which allows it to twist and could relieve some strain in the carbon backbone.

The Cy_2-tn/Zn shows the zinc ion sits outside of the plane through the ligand donor atoms, which is due to the axial chloride ligand pulling it out of the plane. There is very little buckling of the ligand backbone.

Both the Cy_2-tn/Ni and Cy_2-tn/Cu complexes have the metal ions almost sitting in the plane through the ligand donor atoms, and the axial ligands in the molecules are almost at right angles to the plane. There is also very little buckling in the ligand backbone in these two complexes, allowing the ligand to be slightly planar.

The presence and number of H--H close contacts is the same as that seen for both polymorphs of the free ligand Cy_2-tn/Metal complexes, but the NH--O interactions present in the free ligand are not present in the complexes. Looking at the H--H close contact distances in Table 4.3.5., it can be seen that the H--H interactions tend to increase as the metal ion size increases. The Cy_2-tn(a) has small H--H close contact distance as the molecule is opened up or as linear as possible, the Cy_2-tn(b) H--H close contact distance is larger as the molecule starts curving around, allowing the two alcoholic moieties to face the same direction. As the metal ion size increases, the metal ion sit further out of the ligand plane, forcing the ligand to curve further around to bond to the metal, increasing the H--H close contact distance. Each of the H--H close contacts occurs when the hydrogen atoms are close to an eclipsed arrangement. However, DTF and QTAIM analyses show no bonds exist between the hydrogen on the cyclohexenyl rings and the hydrogens on the propyl bridge. These H--H close contacts are most likely very weak and a result of the crystal packing. The H--H close contacts are therefore not likely to affect complexation in solution.

Table 4.3.5. H--H close contacts distances and angles between HCH--HCH atoms in the Cy_2-tn polymorphs and the metal complexes.

Molecule	Atom 1	Atom 2	H-H Close Contact Distance (Å)	H-H Torsion Angles (˚)
Cy_2-tn(a)	H5A	H7A	2.158	7.99
Cy_2-tn(b)	H5A	H7B	2.267	-19.24
	H9A	H11A	2.394	35.89
Cy_2-tn/Ni	H5A	H7A	2.226	26.88
	H9B	H11B	2.246	-34.08
Cy_2-tn/Zn	H5A	H7A	2.237	24.75
	H9B	H11A	2.317	-35.69
Cy_2-tn/Cu	H14	H18	2.294	16.42
	H21	H24	2.270	-25.50
Cy_2-tn/Cd	H5B	H7A	2.309	28.39
	H9B	H14B	2.071	49.79
	H20B	H22B	2.340	0.53
	H24B	H29B	2.171	-11.15

4.4. References

1. P. Atkins, T. Overton, J. Rourke, M. Weller and F. Armstrong. (2006). *Inorg. Chem.,* 4th Ed., Oxford University Press, United Kingdom.
2. R. Hancock, A. de Sousa, G. Walton, and J. Reibenspies. (2007). *Inorg. Chem.,* **46**, 4749.
3. S. Reisinger. (2007). *The Solid State Structure of Metallo-beta-amino Alcohol Complexes,* MSc Dissertation, University of the Witwatersrand, Johannesburg.
4. A. Spek. (2003). *J. Appl. Cryst.* **36**, 7.
5. F. H. Allen, O. Kennard, D. G. Watson, L. Brammer, and A. G. Orpen. (1987). *J. Chem. Soc.,Perkin Trans. II,* **S1-S19**.

Chapter 5

Potentiometry

Potentiometry is the most widely used technique in the determination of protonation and stability constants,[1] and recent computing programs has allowed this area of research to expand. As a result of this technology more complex systems, such as biological and environmental ligand systems, are now able to be studied with a fair amount of accuracy.[1] GEP is especially useful, as it accurately measures the hydrogen ion concentration, which provides a measure of the ligand concentration at equilibrium, with and without the metal ion under investigation.[1] This method was used to determine the protonation and stability constants for the Cy_2-Otn ligand system with Cu(II), Ni(II), Zn(II), Cd(II), and Pb(II).

5.1. Materials and Method

The ligand Cy_2-Otn in this study was synthesised from commercially readily available materials as previously stated in chapter 2, and purified via recrystalization for the potentiometric studies. The metal salts and solvents were used as received from suppliers. The following is a list containing the sources from which all of the starting materials were bought. All chemicals were reagent grade and used without further purification.

Table 5.1.1. List of chemicals used and their suppliers

Chemical Name	**Formula**	**Formula Weight** *(g/mol)*	**Purity**	**Supplier**
Sodium nitrate	$NaNO_3$	84.99	99.9%	Merck
Zinc(II) nitrate hexahydrate	$Zn(NO_3)_2.6H_2O$	297.48	98%	Aldrich
Nickel(II) nitrate hexahydrate	$Ni(NO_3)_2.6H_2O$	290.81	99.9%	Aldrich
Cadmium(II) nitrate tetra hydrate	$Cd(NO_3)_2.4H_2O$	308.47	99.9%	Aldrich
Lead(II) nitrate	$Pb(NO_3)_2$	303.44	99%	Aldrich
Copper(II) nitrate hydrate	$Cu(NO_3)_2.xH_2O$	187.56	99.9%	Aldrich
Sodium hydroxide ampule (1 M)	NaOH	40.00	99%	Merck
Potassium hydrogen phthlalate	$C_8H_5KO_4$	204.23	99.5%	Saarchem
Nitric acid Ampule (0.1 M)	HNO_3	63.01	99%	Merck

5.1.1. Solution Preparation

The titrant solution of NaOH with a concentration of approximately 0.01 M was freshly prepared when used, by taking the required amount of 1 M NaOH stock solution and diluting it with deionized water and adding 0.09 M $NaNO_3$ to the solution. The 0.01 M solution of HNO_3 was prepared in the same way from a 0.1 M stock solution and with 0.09 M $NaNO_3$. The NaOH solution was standardised using a potassium hydrogen phthalate solution before further use. The HNO_3 solution was then standardised using the NaOH solution. The metal solutions of Cd(II), Cu(II), Ni(II), Pb(II), and Zn(II) were prepared by weighing the required mass of the appropriate metal salt and dissolving it in deionised water. New metal salts were used and kept in a desiccator so the degree of hydration did not change. The concentration of the metal solutions were 0.0333 M. A 5×10^{-3} M ligand solution was prepared by weighing out the required amount of the ligand and dissolving it in deionized water and adding 0.1 M $NaNO_3$. All experiments were performed at ionic strength 0.1 M using $NaNO_3$ as the background electrolyte.

5.1.2. Glass Electrode Potentiometry Experimental set-up

The potentiometric titrations were performed in a Metrohm jacketed glass vessel equipped with a magnetic stirrer model Metrohm 801, and thermostatted at 25 ± 0.1°C by water circulating from a constant temperature bath. The *e.m.f.* of the cell was measured using a Metrohm combination glass electrode, model 6.0224.100, and the titrations were performed using an autotitrator model Metrohm 809, and a digital burette, Metrohm 800 Dosino.

The standardisation of the acid and base solutions was achieved by dynamic equivalence point titration in which the end point was reached by addition of different volumes of the titrant at each dosing step. The combination glass electrode (CGE) calibration and metal-ligand titrations were performed by monotonic equivalence point titration in which the end point was reached by addition of the same volume of the titrant at each dosing step.

For the electrode calibration, solutions in the flask were stirred for 60 seconds before any measurements were made. The minimum waiting time was 30 seconds between consecutive additions of titrant, which was important for drift-controlled measurements. The measured value was only accepted when the minimum waiting time had passed, even if the measured value drift had already been achieved. The maximum waiting time was 180 seconds; if the measured value drift had not yet been achieved, then the measured value was accepted after the maximum waiting time had passed. The volume increment, which was the volume to be added at each dosing step, was 0.50 ml. The signal drift, i.e., the alteration in the measured value of potential per minute, was set at 0.1 $mV.min^{-1}$ at 25 °C. The electrode calibration was set to stop at 10 ml of titrant added.

The protonation constant determination and the metal-ligand study parameters were set the same. The signal drift was set to be 0.1 $mV.min^{-1}$, a minimum waiting time of 30 seconds and a maximum waiting time of 600 seconds. There was also a 300 second stirring time before any measurements were taken, and the volume increments were 0.02 ml at 25 °C. The titration was set to stop after 15 ml of the titrant was added but may have been stopped earlier if the reaction was completed or if precipitation occurred.

5.1.3. Experimental

A 0.01 M and 0.05 M solutions of NaOH were standardised regularly using a standard solution of KHP, and 0.01 M and 0.05 M solutions of HNO_3 were standardised regularly using the standardised solutions of NaOH. Before running any experiment, the CGE was calibrated using the 0.05 M solutions of NaOH and HNO_3.

i. Standardisation of 0.01 M NaOH using KHP

A standardised solution of 0.05 M KHP was made by weighing out the correct amount of KHP and dissolving it in deionised water in a volumetric flask. A solution of 0.01 M NaOH was placed in a burette, and a fixed volume of 1 ml of the standardised 0.05 M KHP solution was measured and put into a conical flask with a few drops of phenolphthalein indicator. The KHP solution was then manually titrated with a solution of NaOH until the end point was reached. This was repeated at least three times and the average volume of NaOH added was taken to ensure accuracy of the end point. The end point was used to determine the actual concentration of NaOH by the following equation:

$$[\text{NaOH}] = \frac{[KHP]VKHP}{avg.VNaOH} \qquad (\mathbf{30})$$

where [KHP] represents the concentration of KHP used, *V*KHP represent the volume of KHP put in the flask, and avg.*V*NaOH represents the average volume of NaOH added to reach the equivalence point, giving the standard concentration of the standardised 0.01 M NaOH solution.

The 0.05 M NaOH solution was standardised in the same way, using 2 ml of the 0.05 M KHP solution and titrating it with the 0.05 M NaOH. This was also repeated at least three times to get the average volume of NaOH added, and the equivalence point was calculated using the same equation (**30**).

Table 5.1.2. Experimental data of the standardisation of 0.05 and 0.01 M NaOH solutions.

0.05M NaOH Titration	**Reading 1 (ml)**	**Reading 2 (ml)**	**Reading 3 (ml)**	**Reading 4 (ml)**	**Reading 5 (ml)**	**Avg. Vol (ml)**	**[KHP] (M) 2 ml**	**[NaOH] (M)**
1	1.98	1.94	1.92	1.92	1.96	1.9267	0.0500	0.05190
2	2.02	2.00	2.00	2.00	2.00	2.00	0.0500	0.04980
3	1.98	1.98	1.96	1.98	2.00	1.98	0.0500	0.05053
4	1.98	2.01	1.96	1.98	1.97	1.975	0.0500	0.05062
0.01M NaOH Titration	**Reading 1 (ml)**	**Reading 2 (ml)**	**Reading 3 (ml)**	**Reading 4 (ml)**	**Reading 5 (ml)**	**Avg. Vol (ml)**	**[KHP] (M) 1 ml**	**[NaOH] (M)**
1	4.42	4.32	4.50	4.50	4.52	4.5067	0.0500	0.00999
2	4.90	4.80	4.88	4.98	4.84	4.84	0.0500	0.01037
3	5.12	5.16	5.14	5.14	5.14	5.14	0.0500	0.00972

ii. Standardisation of HNO_3 using standardised solution of NaOH

2 ml of 0.01 M HNO_3 solution was placed in conical flask with a few drops of phenolphthalein indicator, and was titrated with a standardised solution of 0.01 M NaOH until the end point was reached. This was repeated at least three times and the average volume of NaOH added was used to determine the concentration of nitric acid solution as follows:

$$[HNO_3] = \frac{avg.VNaOH.[NaOH]}{VHNO_3} \qquad (\mathbf{31})$$

where avg.*V*NaOH represents the average volume of NaOH added to reach the equivalent point; [NaOH] represents the concentration of standardised solution of NaOH, and *V*HNO_3 represents the volume of HNO_3 placed in the flask, giving the standard concentration of the standardised 0.01 M HNO_3 solution.

Table 5.1.3. Experimaental data of the standardisation of 0.05 and 0.01 M HNO_3 solutions.

0.05M HNO_3 Titration	**Reading 1 (ml)**	**Reading 2 (ml)**	**Reading 3 (ml)**	**Reading 4 (ml)**	**Reading 5 (ml)**	**Avg. Vol (ml)**	**[NaOH] (M) x ml**	**[HNO_3] (M) 2 ml**
1	1.62	1.66	1.88	1.90	1.90	1.893	0.05190	0.05483
2	1.94	2.02	1.98	1.99	1.98	1.983	0.04980	0.04917
3	1.98	1.98	2.00	2.00	1.98	1.99	0.05053	0.05027
4	1.96	1.98	1.98	1.98	1.98	1.98	0.05062	0.05012
0.01M HNO_3 Titration	**Reading 1 (ml)**	**Reading 2 (ml)**	**Reading 3 (ml)**	**Reading 4 (ml)**	**Reading 5 (ml)**	**Avg. Vol (ml)**	**[NaOH] (M) x ml**	**[HNO_3] (M) 1 or 5 ml**
1	1.08	1.10	1.12	1.12	1.14	1.113	0.00999	0.01111
2	1.04	1.00	1.02	1.00	1.00	1.012	0.01037	0.01048
3	1.06	1.04	1.04	1.04	1.04	1.04	0.00972	0.01015
4	0.98	1.02	1.00	1.00	1.00	1.00	0.05062	0.01013

iii. Glass electrode calibration

After running each experiment, the glass electrode was calibrated using the standardised 0.05 M solutions. Calibration of the electrode involved titration of 5 ml of standardised 0.05 M HNO_3 solution and 5 ml 0.1 M $NaNO_3$ solution, with a standardised solution of 0.05 M NaOH. A sufficient number of points needed to be taken for the pH range before and after the equivalence point in order to linearly fit the titration data, affording more accurate values of the Nernstian slope and $E°$ for the electrode.

vi. Determination of protonation constants

In order to study the metal complexes of novel ligands, the protonation constants of the ligands were first determined. In the determination of protonation constants, 5 ml of 5×10^{-3} M Cy_2-Otn ligand solution was added to 5 ml of standardised 0.01 M HNO_3 solution, and 5 ml of 0.1 M $NaNO_3$ solution. This was then titrated with a standardised solution of 0.01 M NaOH.

This was repeated a number of times and the data analysed using the program ESTA to obtain the values of the protonation constants.[2] The protonation constants were also determined via a reverse titration, using 10 ml Cy_2-Otn solution and titrating it with 15 ml standardised 0.01 M HNO_3 as the ligand solution has a pH of above 10 and so a base was not needed.

v. Determination of stability constants for different metal complexes formed

Determination of the stability constants for metal complexes was done by adding 5 ml of the standardised 0.01 M HNO_3, 5 ml of the 5×10^{-3} Cy_2-Otn solution and 0.75 ml of the metal solution to the glass vessel and stirred for 60 seconds. The resultant solution in the titration cell was then titrated with a standardised solution of 0.01 M NaOH.

5.1.4. Analysis of Potentiometric Data

i. Description of ESTA program

The computer program ESTA (Equilibrium Simulation and Titration Analysis) is a library that performs calculations dealing with competitive aqueous equilibria, and accounts for variations in ionic strength and the relevant changes in activity coefficients.[2] This program was used in the refinement of potentiometric data, as it aids in investigating chemical interactions in solution and allows for quantitative characterisation.[2] The ESTA library contains different program modules (ESTA0, ESTA1, ESTA2, ESTA3, ESTA4, ESTA5, ESTA6, ESTA7 and ESTA8), but the calculations are mainly performed by the optimisation module ESTA2.[3]

ESTA2 is used when determining the best values based on least squares procedures applied to a whole system of titrations, for one or more parameters. Parameters such as formation constants, vessel and burette concentrations, electrode intercept and slope, and initial vessel volume can be refined. The total number of titrations is dimensioned to 20 and the total number of points to 1000 but these can be varied if necessary. A file of titration data containing the optimized parameter values and with a format identical to ESTA can be generated as an output.[4]

ii. The protonation formation function ($\overline{Z_H}$)

The protonation formation function is defined as:

$$\overline{Z_H} = \frac{(H_T - H + OH)}{L_T} \quad (\mathbf{32})$$

where H_T is the total hydrogen ion concentration and $OH = K_w / H$ (**33**)

where H is the bound proton concentration, and OH is the hydroxide concentration.
The proton formation function $\overline{Z_H}$ is plotted against *pH = - log [H]*. This equation is used to evaluate both the observed and calculated functions. In the absence of the metal, the proton formation function becomes:

$$\overline{Z_H} = \frac{[boundH]}{L_T} \quad (\mathbf{34})$$

where [*boundH*] is given as: $[boundH] = H_T - H + [OH] = H_T - H + K_w H^{-1}$ (**35**)

where OH is the hydroxide ion concentration, and K_w is the dissociation constant of water; then:

$$\overline{Z_H} = \frac{(H_T - H + K_w H^{-1})}{L_T} \quad (\mathbf{36})$$

where H_T and L_T are known from the analytically determined concentrations and K_w is a known literature value. $\overline{Z_H}$ can be calculated at a number of pH values, because H is measure by glass electrode, and the protonation curve can be plotted, i.e., $\overline{Z_H}$ vs. pH. These curves aid in determining information about the state of the ligand in a particular pH range.[5] For this study, $\overline{Z_H}$ was used in the determination of protonation constants of ligands and in the prediction of stability constants for different complexes present in a solution.[5]

iii. The metal formation function $\overline{Z_M}$

The metal formation function is the average number of ligand bound to the metal.

$$\overline{Z_M} = \frac{L_T - A\left(1 + \sum_n \beta_{H_n L} H^n\right)}{M_T} \qquad (\mathbf{37})$$

where n is the number of protons, L_T and M_T are the total ligand and metal concentrations, respectively, and β_{HnL} is the overall protonation constant for the ligand H_nL. A is defined as:

$$A = \frac{\left(H_T - H + OH\right)}{\sum_n n\beta_{H_n L} H^n} \qquad (\mathbf{38})$$

where H_T and H are total and free proton concentrations, respectively. *OH* represents hydroxide concentration. $\overline{Z_M}$ was used in the modelling of M–L systems and in the refinement of computed stability constants. $\overline{Z_M}$ is plotted against pA, which is the negative logarithm of the free ligand concentration. The titrations were performed by starting at low and ending at high pH. Once the model is completed, the calculated β values from Equation (**37**) are used in the calculation of protons. The validity of the model is checked by comparing the resulting calculated and the experimental curves. The functions $\overline{Z_H}$ *a*nd $\overline{Z_M}$ were used here to analyse the data, but should be only be taken as a mathematical transformation of the data.[5]

5.2. Results and Discussion

5.2.1. Protonation Constants of Cy_2-Otn

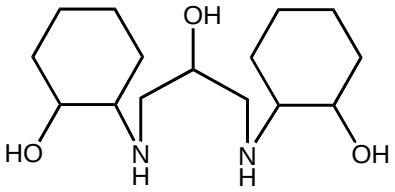


Figure 5.2.1. The ligand Cy_2-Otn.

Before the metal complexes of the ligand Cy_2-Otn can be studied, the protonation constants of the ligand must first be determined. The structure of the ligand shows two protonation constants are expected within the potentiometric window (pH 2-12) of a glass electrode probe. These two protonation constants are expected to arise from the two amine groups present in the ligand (**Fig. 5.2.1***)*.

The first protonation constant determination was done on an autotitrator, 5 ml of standardised 0.01 M HNO_3 was added to 5 ml Cy_2-Otn (L7) solution and 5 ml of 0.1 M $NaNO_3$ solution. This was titrated with standardised 0.01 M NaOH in 0.02 ml increments. The ESTA refined data showed the expected two protonation constants pK_{a1} = 8.585 ± 0.0152 and pK_{a2} = 7.525 ± 0.0140. Around pH 7.7 and again at pH 8.5 there is a poor fit between the calculated data and observed data, most likely due to an unseen impurity present (**Fig. 5.2.2.**).

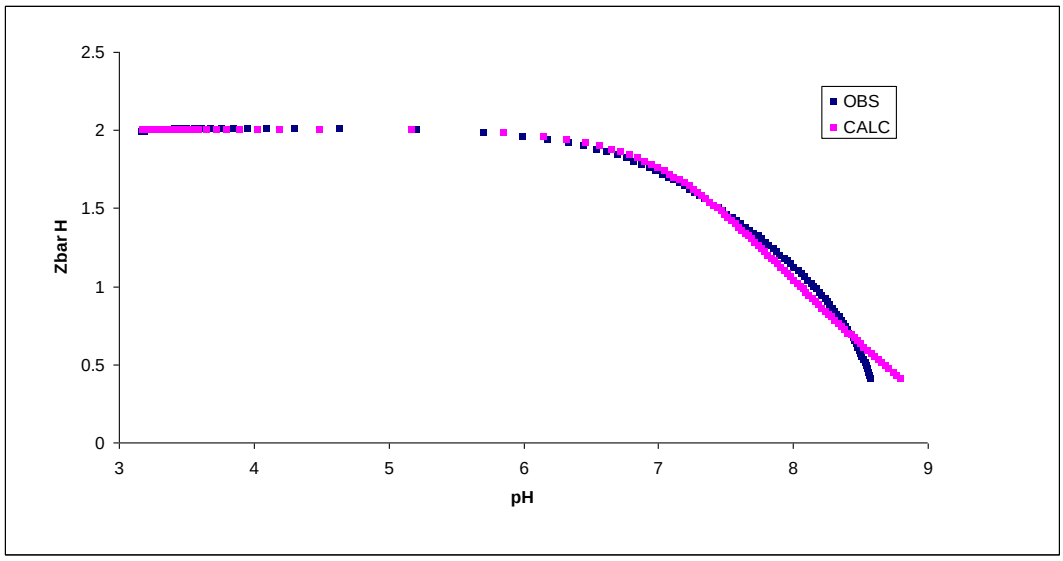


Figure 5.2.2. Experimental (blue) and calculated (pink) protonation curves from the atutotitration of Cy_2-Otn (L7).

The species distribution diagram (**Fig. 5.2.3.**) is as expected, with the conversion of 50 % of the LH_2 to the LH species at pH 7.53 coinciding with pK_{a1}, with the LH species reaching a maximum concentration of 63 % at pH 8. The L species becomes dominant at pH 8.9, coinciding with pK_{a2}.

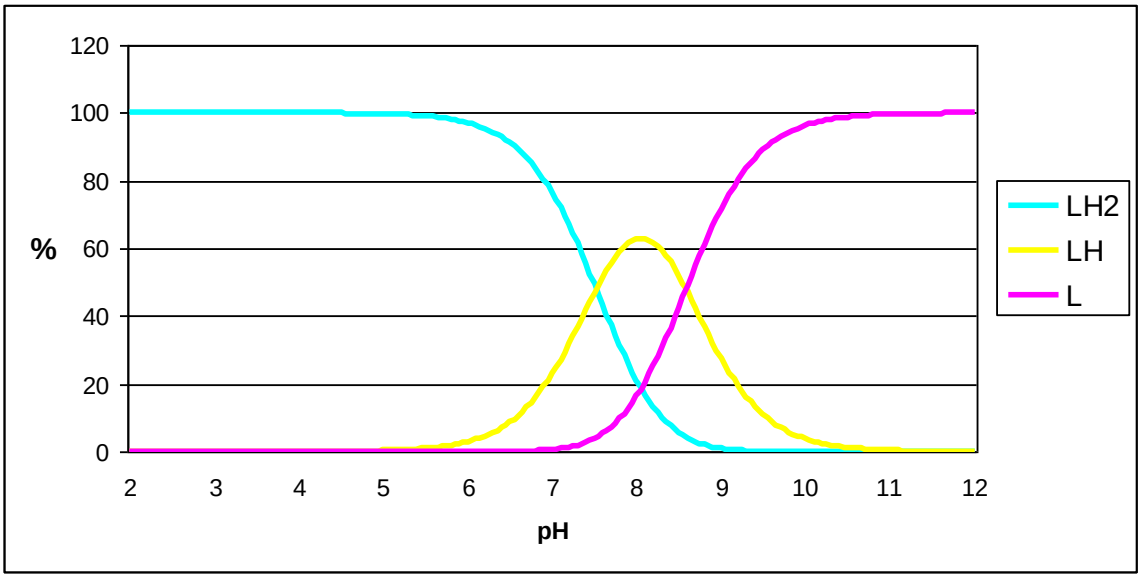


Figure 5.2.3. Speciation diagram of the autotitration of Cy_2-Otn (L7).

To ensure the method of the proton determination was correct, the pK_a's of the starting amine, 1,3-diamino-2-propanol, were determined as they have already been published. New solutions of $NaNO_3$ were also made to try and eliminate impurities.

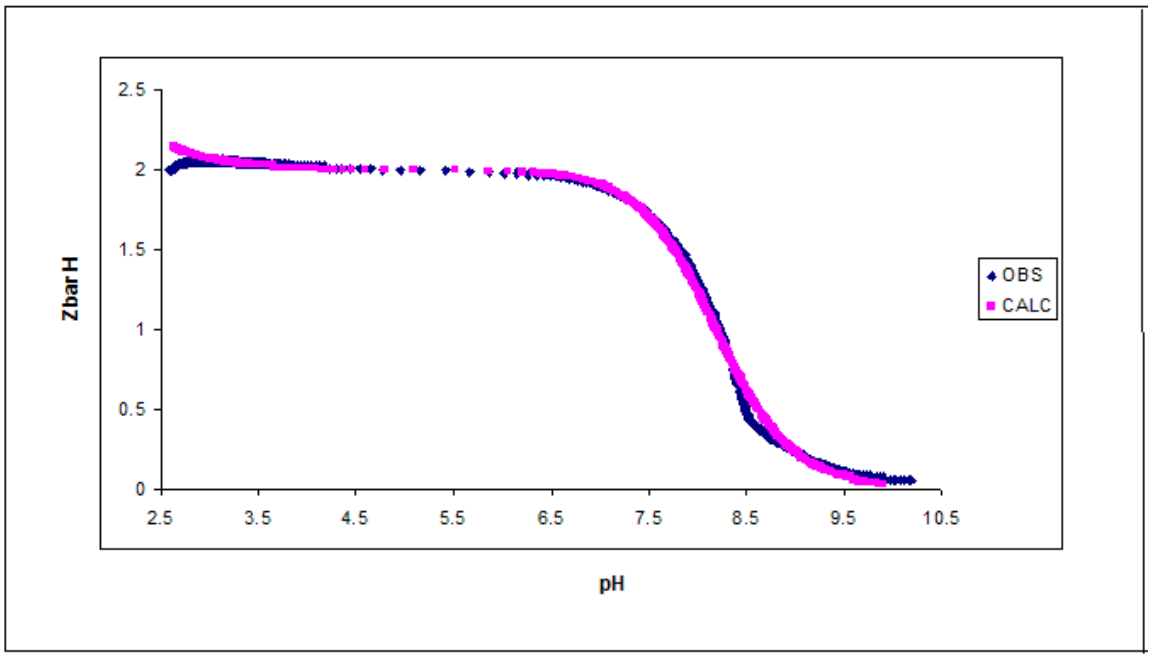


Figure 5.2.4. Experimental (blue) and calculated (pink) protonation curves of the autotitration of the starting amine 1,3-diamino-2-poropanol.

In Figure 5.2.4, it ca be seen that around pH 8.5, the calculated data deviates briefly from the observed data, there were also three pKa's present, the first two were from the amine hydrogens (pK_{a1} = 8.398 ± 0.0054 and pK_{a2} = 7.997 ± 0.0048), but the pK_{a3} = 1.841 ± 0.0258 is most likely from a carbamate that forms when weighing out the starting material as the amine reacts with the CO_2 in the air. S. Reisinger reported the crystal structure of this carbamate (3-ammonio-2-hydroxypropyl)carbamate monohydrate which was seen as a zwitterion.[6] This carbamate impurity could not be avoided or removed. The amine pKa's, are slightly different from the published values (pK_{a1} = 8.02 and pK_{a2} = 9.56) due to the trace presence of the carbamate impurity, but the method used for the proton determination was adequate.

The method was then retried with a new batch of ligand (L8) and new solutions of $NaNO_3$. It was thought that the acid and base reaction could have been masking the protonation constant data, and so a reverse titration was done as the pH of the ligand in solution was around 10, and so the NaOH was not needed.

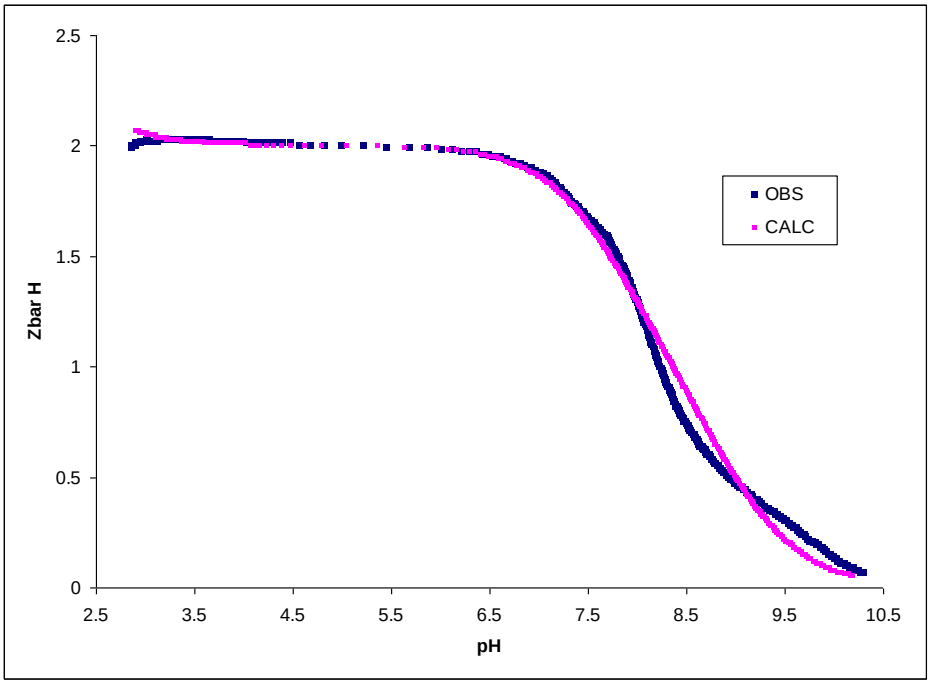


Figure 5.2.5. Experimental (blue) and calculated (pink) protonation curves of the reverse autotitration of Cy_2-Otn (L8).

This titration showed three protonation constants (pK_{a1} = 8.926 ± 0.0065, pK_{a2} = 7.800 ± 0.0072, and pK_{a3} = 1.785 ± 0.0540), and the calculated data deviates significantly from the observed data, showing there is still an impurity present (**Fig. 5.2.5.**). The third pK_a is similar to that of the suspected carbamate that was present in the starting amine solution, and it is possible that there a carbamate present in the Cy_2-Otn L8 solution, although the ligand characterisations are clean (Appendix B and C).

The species distribution diagram (**Fig. 5.2.6.**) shows the LH_3 species decreasing as the LH_2 species increases, the LH species has a concentration of 64 % at pH 8.4.

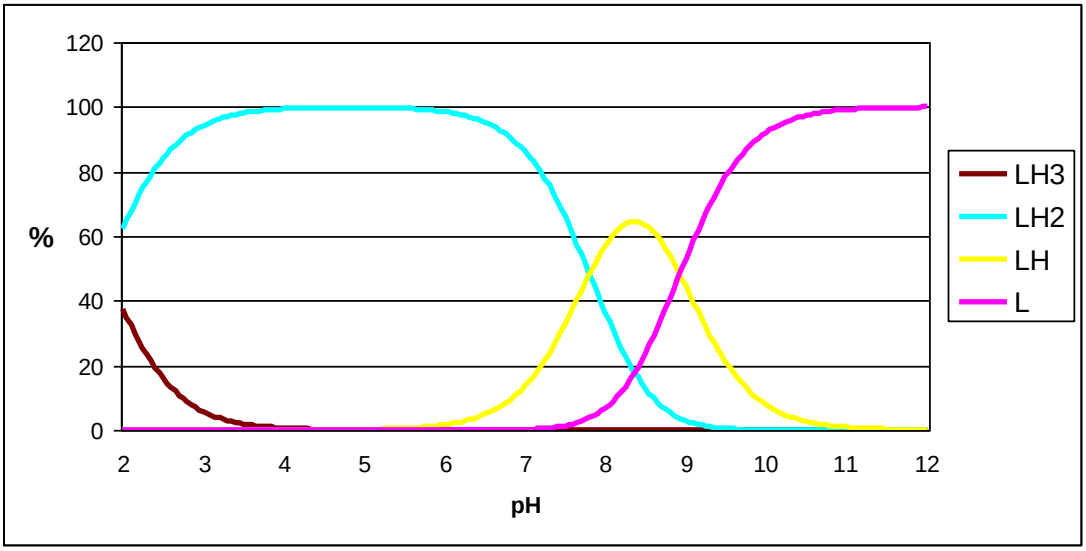


Figure 5.2.6. Speciation diagram of the reverse autotitration of Cy_2-Otn (L8).

Using a new bottle of $NaNO_3$, as well as a recrystallised ligand (L7c), to try remove the impurities from the solution for the proton determination to get a better data fit, and more accurate pK_a's, the reverse titration was repeated.

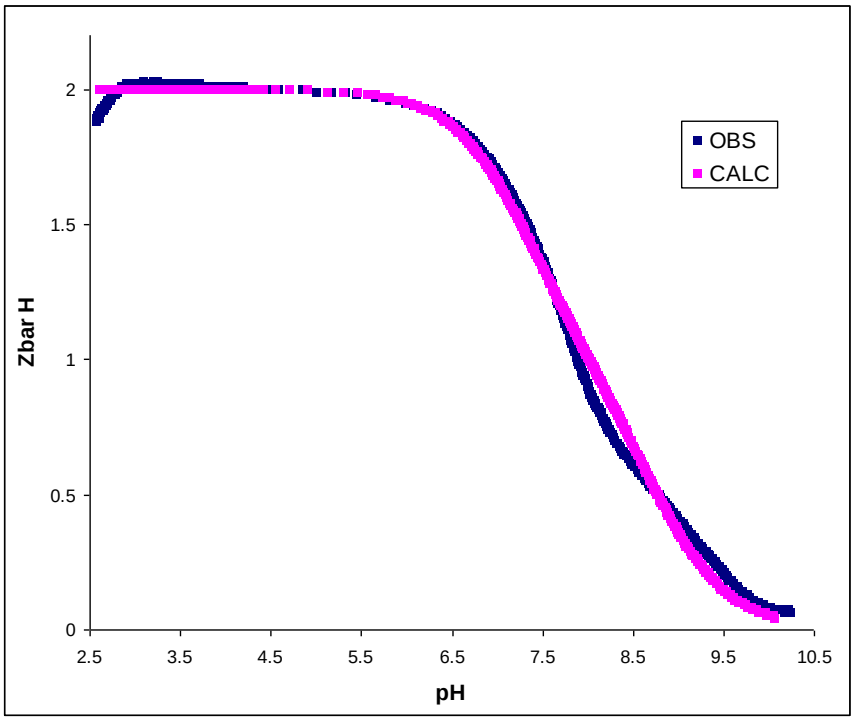


Figure 5.2.7. Experimental (blue) and calculated (pink) protonation curves of the reverse autotitration of Cy_2-Otn (L7c), with new $NaNO_3$.

This titration (**Fig. 5.2.7.**) showed the two amine pK_a's in the expected region (pK_{a1} = 8.732 ± 0.0051 and pK_{a2} = 7.312 ± 0.0060), however, the calculated and observed data still deviate from each other around pH 7.8 and again around pH 9, showing the impurity is still present although it is not seen in the mass spec or NMR of the recrystallised ligand (L7c) or in the solution titrated (Appendix B and C). Although the observed data deviates slightly from the calculated data, these pK_a's were used to determine the stability constants of the metal complexes, because this titration was done using uncontaminated $NaNO_3$, a recrystallised ligand batch (L7c), and the titration went to completion.

The species distribution diagram (**Fig. 5.2.8.**) is as expected, where the LH species becomes dominant at pH 7.3 and the L species becomes dominant at pH 8.7, coinciding with the two pK_a's. The LH species has a maximum concentration of 72 % at pH 8.

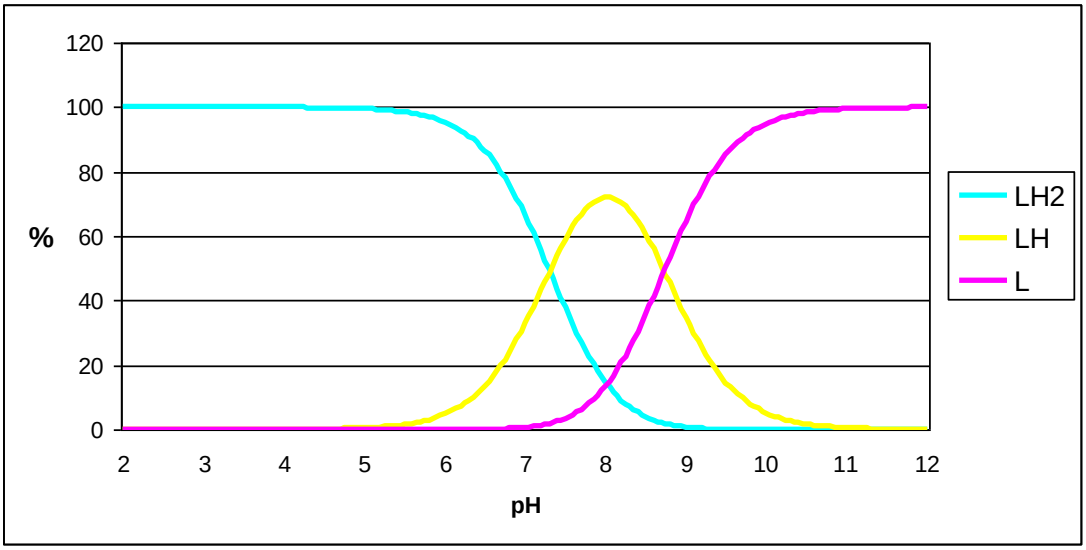


Figure 5.2.8. Species distribution diagram of Cy_2-Otn (L7c) with new $NaNO_3$.

The protonation formation function $\overline{Z_H}$, and the species distribution diagrams show in which pH range different forms of the ligand are predominant. Generally, for the ligand Cy_2-Otn, the form LH_2 of the ligand is predominant below pH 7, the predominant form between pH 7 and 9 is LH, and the ligand is fully deprotonated above pH 10.

Table 5.2.1. ESTA data for 1,3-diamino-2-propalnol and Cy_2-Otn.

Titration	$logB_1$	Std. Dev.	$logB_2$	Std. Dev.	$logB_3$	Std. Dev.	No. of titrations	No. of points	R-factor
Cy_2-Otn (L7)	8.59	0.0152	16.11	0.0140	-	-	1	101	0.04505
1,3-diamino-2-propanol	8.40	0.0054	16.40	0.0048	18.24	0.0258	1	751	0.02408
Cy_2-Otn (L8)	8.93	0.0065	16.73	0.0072	18.51	0.0540	1	645	0.04740
Cy_2-Otn (L7c)	8.73	0.0051	16.04	0.0060	-	-	1	751	0.03083

If one compares the pKa's of ligands similar to Cy_2-Otn with the same donor atoms (**Table 5.2.1.**),[5,7] it can be seen that Cy_2-en has slightly lower pKa's (pKa_1 = 9.66 and pKa_2 = 6.62) than Cy_2-tn (pKa_1 = 10.12 and pKa_2 = 8.21). This is because Cy_2-tn has an extra carbon atom in the amine bridge which has an inductive effect that increases the pKa's slightly. Cy_2-Otn has lower pKa's than Cy_2-tn due to the electronegative hydroxyl group on the propane bridge, which decreases the inductive effect of the propyl bridge, making the N atoms less basic, and requiring a higher concentration of acid to protonate them. The first pKa of Cy_2-Otn is lower than that of Cy_2-en because the hydroxyl group on the propyl bridge removes electron density from the donor atom allowing for the proton to be easily removed at a lower pH. However, pKa_2 of Cy_2-Otn is larger than pKa_2 of Cy_2-en, because adding a second proton to the positively charged species LH^+ incurs and electrostatic repulsion that lowers the affinity of the ligand for the second proton.

5.2.2. Cy_2-Otn/Metal Stability Constants

The protonation constants used for Cy_2-Otn recrystallised ligand (L7c) were pKa_1 = 8.73 and pKa_2 = 7.31, pK_w was 13.78 for these conditions.[7] The concentrations of HNO_3 and NaOH solutions were 0.0101 M and 0.0103 M, respectively. The titrations were done at an ionic strength of 0.1 M, at 25 °C, with the concentrations of the metal solutions being 0.003 M, and the ligand solution concentration being 0.005 M. The acid and/or base concentrations were also optimised separately during the refinement operations using ESTA. The changes in the concentration values were monitored during refinement, if the concentrations changed significantly, they were kept as the original value, so as not to generate fictitious data.[2] Complex formation was generally evident starting from pH 3, and no precipitation was observed for the Cy_2-Otn and Cu(II), Ni(II) or Zn(II) systems, but there was precipitation in the Cd(II) and Pb(II) systems and so these two systems were omitted. The complex formation curves were plotted after the refinement of the titration data. The Cy_2-Otn/Zn data was very poor and was omitted from this project.

i. Cy_2-Otn/Cu(II) Complex

The model from the GEP for Cy_2-Otn/Cu system is ML(H), ML, and ML(OH). The complex formation curve of Cy_2-Otn/Cu (**Fig. 5.2.9.**) shows the back-fanning feature due to the hydroxo species LM(OH) present in solution. A change of $\overline{Z_M}$ observed between pA 10.5 and 12 can suggest the formation of M(LH) complex and a change of $\overline{Z_M}$ between pA 9 and 10.5 might confirm the presence of ML complex. The observed and calculated data only deviated slightly from each other, at pA 12 and in the back-fanning region around pA 8.6. The poor fit is due to the combined errors in the pK_a determinations and the ligand impurity.

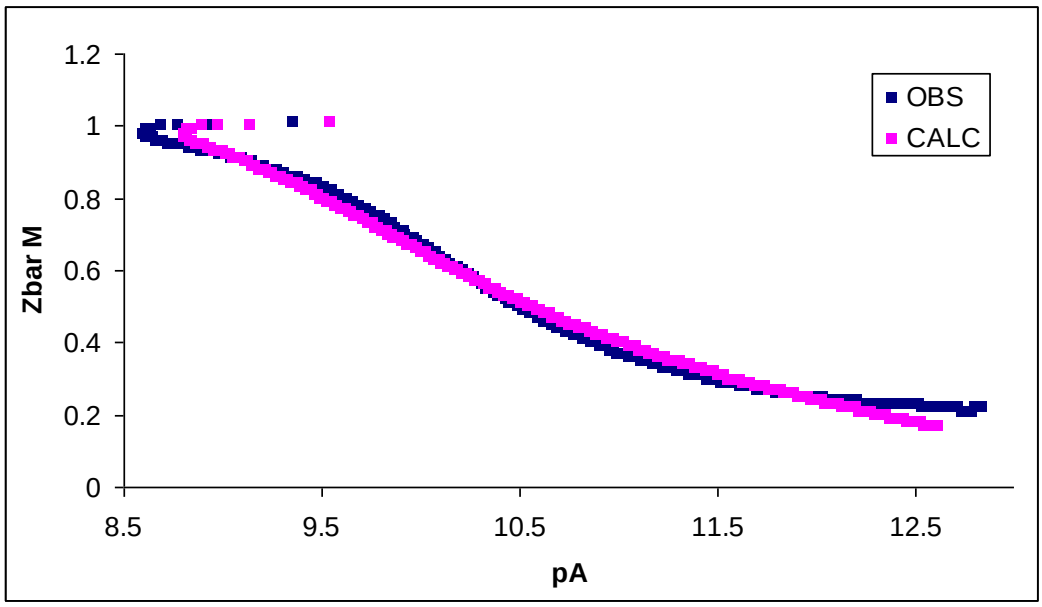


Figure 5.2.9. Experimental (blue) and calculated (pink) potentiometric complex formation curves of Cy_2-Otn/Cu(II) system.

The species distribution diagram (**Fig. 5.2.10.**) was calculated for the model M(LH), ML, and ML(OH). The complexes start to form above pH 4, and the M(LH) is a minor species that forms under the LM species, the concentration of the M(LH) species is low (maximum of 5 %) between pH 4 and 6. The ML species forms between pH 4.5 and 9 has a maximum concentration of almost 60 % around pH 6. The ML(OH) species becomes dominant around pH 7 and has a maximum concentration of 66 %. The dip in the curve of the LH_2 species is due to the competitive formation of the MLH and ML species over the same pH range of around 4.5 to 6.

The stability constants for the Cy_2-Otn/Cu system species are: ML(H) (log K = 15.45), and ML (log K = 10.86). These stability constants are inaccurate, as can be seen by the poor data fits, due to the errors in the pK_a determination, and the Cy_2-Otn ligand impurities.

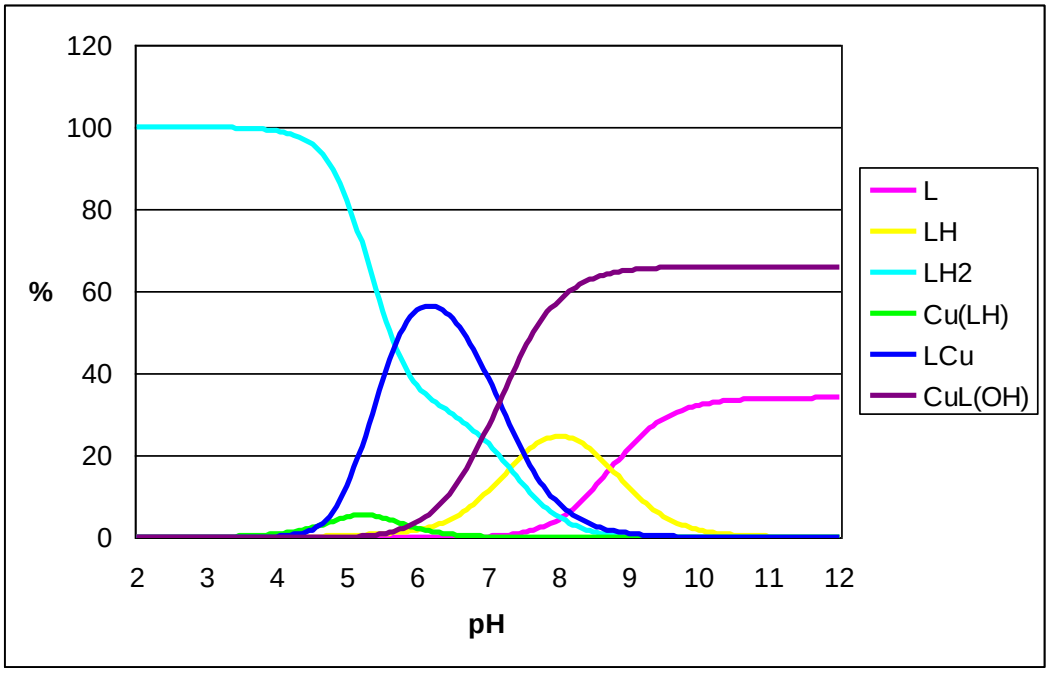


Figure 5.2.10. Species distribution diagram of Cy_2-Otn/Cu(II).

In the dissertation "*Electrochemical studis of metal-ligand equilibria involving chelating ligands"* Uwamariya[5] studied the Cyp_2-en, and Cy_2-en ligand with Cu(II), Ni(II), Zn(II), Cd(II) and Pb(II) using GEP between pH 2 and 12.[5] The Cy_2-en/Cu system showed no M(LH) species, and the dominant ML (log K = 11.47) species was present over a large pH range. The ML(OH) (log K = 6.64) species was present, the main difference is the presence of the $ML(OH)_2$ (log K = 4.59) species from pH 7, that is not present in the Cy_2-Otn/Cu system.[5]

Hancock *et al.*[7] reported the stability constants of the Cy_2-tn ligand with Cu(II), Zn(II), and Cd(II), the equilibria with Ni(II) were very slow and hindered the formation constant measurement. In the Cy_2-tn/Cu system, no M(LH), or ML(OH) complexes were reported, and the log K of the ML complex was 12.67.[7]

Comparing all three formation constants, it can be seen that by adding an extra carbon in the amine bridge when going from Cy_2-en to Cy_2-tn increases the stability constant for the small Cu(II) metal ion, as smaller metal ions prefer six-membered rings over five-membered rings due to the bite size angle and the steric strain in the carbon backbone around the metal ion on

complexation.[7] When adding an extra OH group on the propyl bridge in going from Cy_2-tn to Cy_2-Otn, the stability constant for the Cy_2-Otn/Cu system ML species is less than that for the Cy_2-tn/Cu ML species. This means that the Cy_2-Otn/Cu ML species is less stable than that of the Cy_2-tn/Cu ML species most likely because the electronegative hydroxyl group on the propyl bridge may remove some electron density from the donor atoms resulting in weaker M-L bonds, and thus a less stable complex. This can be seen by the decrease in pK_a values when going from Cy_2-tn (pK_{a1} = 10.12 and pK_{a2} = 8.21) to Cy_2-Otn (pK_{a1} = 8.73 and pK_{a2} = 7.31).

ii. Cy_2-Otn/Ni(II) Complex

The model from GEP for Cy_2-Otn/Ni is ML(H), ML, ML(OH), and $ML(OH)_2$. The complex formation curve of Cy_2-Otn/Ni (**Fig. 5.2.11.**) again show the back-fanning feature due to the hydroxo species present in solution; however, in this region it is difficult to separate the ML(OH) and the $ML(OH)_2$ species. The observed and calculated data follow the same pattern, but the fit is very poor, showing the inaccuracy of the data.

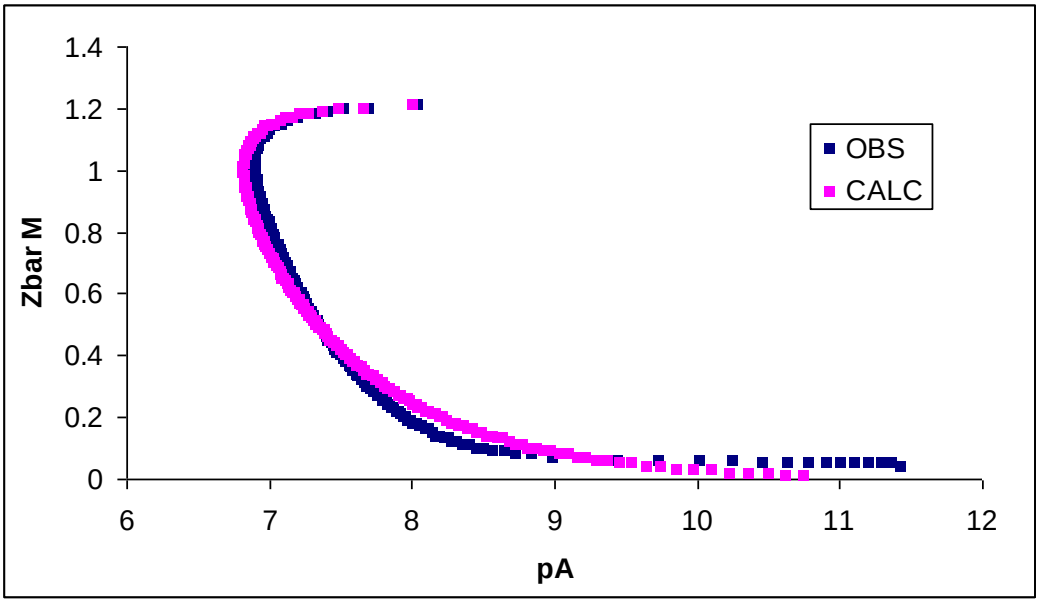


Figure 5.2.11. Experimental (blue) and calculated (pink) potentiometric complex formation curves of Cy_2-Otn/Ni(II) system.

The species distribution diagram of Cy_2-Otn/Ni (**Fig. 5.2.12.**) shows that the all the metal-ligand complexes only start to form after pH 6. The M(LH) complex is present in an extremely low concentration (0.9 %) around pH 6.7 and forms under the ML species which has a maximum concentration of 9.6 % at pH 7. The major species present are the ML(OH) and the $ML(OH)_2$. The ML(OH) species has a maximum concentration of 63% at pH 8.2, and the $ML(OH)_2$ species starts forming around pH 8.5 and has a maximum concentration of around 65 %. The stability constants for the Cy_2-Otn/Ni system species are: ML(H) (log K = 13.12), and ML (log K = 7.276).

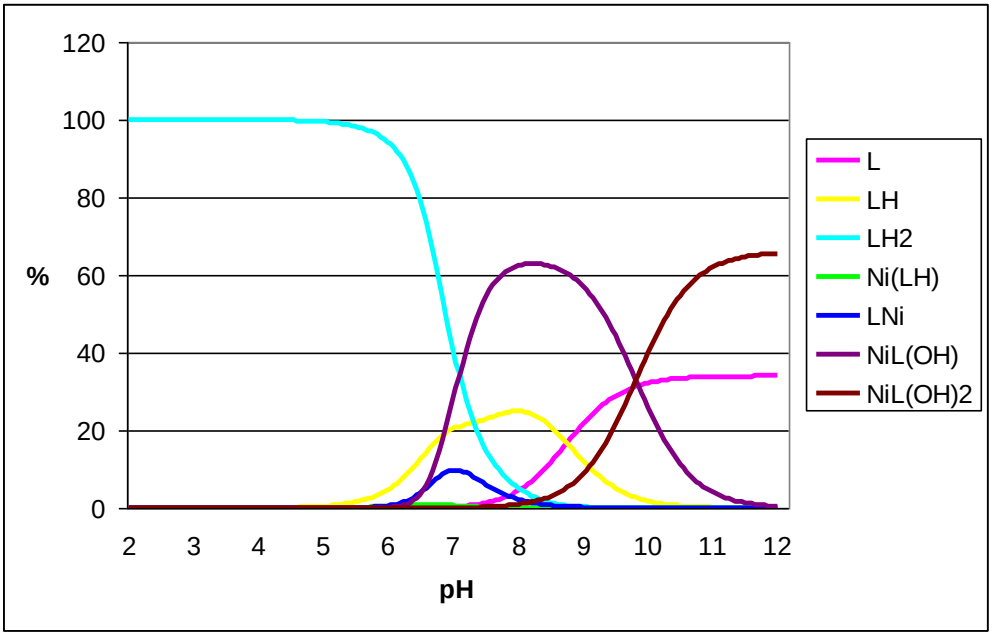


Figure 5.2.12. Species distribution diagram of Cy_2-Otn/Ni(II).

In the Cy_2-en/Ni system, Uwamariya observed a larger concentration of the M(LH) species, which forms under the dominant ML species, as it did in the Cy_2-Otn/Ni system.[5] The ML species in the Cy_2-en/Ni system was present in a large concentration.[5] There was also the presence of the ML_2 species that formed before the hydroxide species. The ML(OH) species in the Cy_2-en/Ni system was present at a fairly high pH, with a low concentration, and the $ML(OH)_2$ species was also present.[5] In the Cy_2-Otn/Ni system, the ML(OH) is the major species present, and $ML(OH)_2$ species can be seen over the same pH range as in the Cy_2-en/Ni system, although not in the same concentrations.

When comparing the stability constants of the ML (log K = 3.8) and M(LH) (log K = 11.3) species of the Cy_2-en/Ni system with the stability constants of the Cy_2-Otn/Ni system, it can be seen that both the ML(H) and ML species of the Cy_2-Otn/Ni system are more stable than the ML(H) and ML species of the Cy_2-en/Ni system. This could be because Ni(II) is a small metal ion (69 pm), and prefers 6-membered chelate rings over 5-membered chelate rings due to the steric strain in the carbon backbone on complexation, similar to that of the Cu(II) metal ion (73 pm), even with the presence of the hydroxyl group on the propyl bridge.[8]

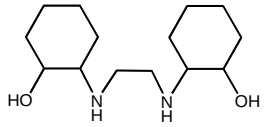
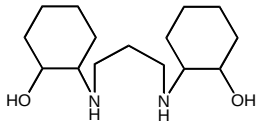
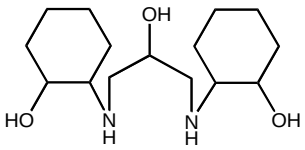
iii. Zn(II) Systems

Looking at the Cy_2-en/Zn system that Uwamariya studied, the ML(H), ML_2 and $ML(OH)_2$ species were seen in the Cy_2-en/Zn system.[5]

Hancock *et al.* also studied the Cy_2-en/Zn system and determined the stability constants of the ML (log K = 6.18), ML(OH) (log K = 5.29) and the $ML(OH)_2$ (log K = 4.17) species.[7] The stability constant for the ML species in the Cy_2-tn/Zn system is log K = 5.04, but no formation constants for ML(H), ML(OH) or $ML(OH)_2$ species were reported.[7]

Comparing the formation constants of the ML species in the Cy_2-en/Zn, and Cy_2-tn/Zn systems (**Table 5.2.2.**), it can be seen that the most stable complex is the Cy_2-en/Zn, followed by the Cy_2-tn/Zn complexes. This is as expected as Zn(II) (74 pm)[8] is slightly larger than both the Cu(II) (73 pm)[8] and Ni(II) (69 pm)[8] metal ions and would therefore form more stable complexes with the 5-membered chelate ring system of Cy_2-en over the 6-membered chelate ring system of Cy_2-tn.[7]

Table 5.2.2. Selected log *K* values for a five-membered ring system, a six-membered ring system, and the acyclic equivalent in complexation with metal ions.[5,7]

Equilibrium	log *K*	Equilibrium	log *K*
L = Cy_2-en = 		L = Cy_2-tn = 	
$L + H^+ \rightleftharpoons LH^+$	9.66	$L + H^+ \rightleftharpoons LH^+$	10.12
$LH^+ + H^+ \rightleftharpoons LH_2^{2+}$	6.62	$LH^+ + H^+ \rightleftharpoons LH_2^{2+}$	8.21
$Cu^{2+} + L \rightleftharpoons CuL^{2+}$	11.47	$Cu^{2+} + L \rightleftharpoons CuL^{2+}$	12.67
$Ni^{2+} + L \rightleftharpoons NiL^{2+}$	7.75	$Ni^{2+} + L \rightleftharpoons NiL^{2+}$	Too slow
$Zn^{2+} + L \rightleftharpoons ZnL^{2+}$	6.27	$Zn^{2+} + L \rightleftharpoons ZnL^{2+}$	5.04
$Cd^{2+} + L \rightleftharpoons CdL^{2+}$	6.15	$Cd^{2+} + L \rightleftharpoons CdL^{2+}$	4.15
$Pb^{2+} + L \rightleftharpoons PbL^{2+}$	6.78	$Pb^{2+} + L \rightleftharpoons PbL^{2+}$	Precipitate
L = Cy_2-Otn = 			
$L + H^+ \rightleftharpoons LH^+$	7.31		
$LH^+ + H^+ \rightleftharpoons LH_2^{2+}$	8.21		
$Cu^{2+} + L \rightleftharpoons CuL^{2+}$	10.86		
$Ni^{2+} + L \rightleftharpoons NiL^{2+}$	7.28		
$Zn^{2+} + L \rightleftharpoons ZnL^{2+}$	Poor data		
$Cd^{2+} + L \rightleftharpoons CdL^{2+}$	Precipitate		
$Pb^{2+} + L \rightleftharpoons PbL^{2+}$	Precipitate		

5.3. Conclusions

The conclusions made here are tentative due to the poor potentiometric data obtained. Looking at the ML species in the Cy_2-Otn systems, it can be seen that the stability constants decrease with an increase in metal ionic radius, similar to the Cy_2-tn systems. This once again shows that smaller metal ions form more stable complexes with six-membered chelate rings. The presence of the hydroxyl group on the propyl bridge in the Cy_2-Otn ligand does not affect this trend. It does, however, decrease the stability constants of the ML complexes with respect to the Cy_2-tn ligand, as previously explained. This study further proves that a ligand designed with a 6-membered chelate ring will favour complexes with smaller metal ions. It also shows that electronegative groups that are not donor atoms to the metal ion can decrease the stability constants of M-L complexes, as it pulls electron density from the donor atoms weakening the M-L bond. To complete the series of Cy_2-Otn ligand, the use of other speciation techniques are highly recommended. These theories would be confirmed by the crystal structure of the ML complexes of Cy_2-Otn with the metals studied. The protonation constants of the Cy_2-Otn ligand are not accurate due to the poor fit of the experimental and calculated data of the protonation curves due to an unknown impurity present. This therefore means that the stability constants of the metal-ligand species of the Cy_2-Otn system are not completely accurate.

Further studies should be done on a ligand with extra carbon atoms between the hydroxyl group and the propyl bridge on the Cy_2-Otn ligand to determine if the hydroxyl group will act as a donor group on the pendant arm. This may lead to increased stability of ML complexes with larger metal ion, as the larger metal ions can accommodate the extra donor group and it is an extra neutral O donor group that favours ML complexes with larger metal ions.

5.4. References

1. A. E Martell, and R.D. Hancock. (1996). *Metal Complexes in aqueous Solutions*, Modern Inorganic Chemistry Series, Plenum Press, New York.
2. K. Murray and P. M. May. (1984). *ESTA Users Manual*, University of Wales Institute of Science and Technology.
3. P. M. May, K. Murray and D. R. Williams. (1988). *Talanta*, 35 No11.
4. P. M. May and K. Murray. (1988). *Talanta*, 35, No 12.
5. V. Uwamariya. (2005) "*Electrochemical Studies of Metal-Ligand Equilibria Involving Chelating Ligands*", Dissertation, University of the Witwatersrand, Johannesburg.
6. S. Reisinger. (2007). *The Solid State Structure of Metallo-beta-amino Alcohol Complexes*, MSc Dissertation, University of the Witwatersrand, Johannesburg.
7. R. Hancock, A. de Sousa, G. Walton, and J. Reibenspies. (2007). *Inorg. Chem.*, **46**, 4749.
8. T. L. Brown, H. E. LeMay, B. E. Bursten, J. R. Burdge. (2003). *Chemistry, The Central Science*, **9th Ed.**, Pearson Education Inc., New Jersey.

Chapter 6

Conclusions and Future Work

The two ligands synthesised produced crystals of suitable quality to determine their structures by XRD methods. Cy_2-Otn yielded a structure of the free ligand, that was a different polymorph to that previously determined. Cy_2-tn was obtained as the free ligand, in two different polymorphs. The two ligands and their polymorphs possess H-H bonds between the hydrogen atoms on the rings and the hydrogen atoms on the propyl bridging carbon atoms. There are also non-bonded interactions between the amine hydrogens and the alcoholic oxygens in the free ligands. The Cy_2-tn(b) polymorph is the more pre-organised form of the ligand, as it is the conformation most Cy_2-tn/Metal adopt.

Most of the Cy_2-tn/Metal complex geometries are octahedral, or distorted octahedral, except for the Cy_2-tn/Zn and Cy_2-tn/Cu complexes which wers square pyramidal. The Cy_2-tn/Cd complex was the only dimer formed. The ligand donor atoms were always in the equatorial positions, except for the Cy_2-tn/Cd molecule with three chloride donor atoms as one of the chloride atom occupied an equatorial site as the one alcoholic oxygen was not bonded. The axial ligands were either the chloride salt or the solvent molecules (water). The planarity of the ligand donor atoms is dependant on many factors, such as the size of the metal ion, the number and type of axial ligands.

The presence and number of H--H close contacts is the same as that seen for both polymorphs of the free ligand Cy_2-tn/Metal complexes, but the NH--O interactions present in the free ligand, and the Cy_2-tn(a) DFT study, are not present in the complexes. The H--H close contact distances tend to increase as the metal ion size increases. As the metal ion size increases, the metal ion sit further out of the ligand plane, forcing the ligand to curve further around to

bond to the metal, increasing the H--H close contact distance, and occur when the hydrogen atoms are close to an eclipsed arrangement. However, DTF and QTAIM analyses show no bonds exist between the hydrogens on the cyclohexenyl rings and the hydrogens on the propyl bridge. These H--H close contacts are most likely very weak and a result of the crystal packing. The H--H close contacts are therefore not likely to affect complexation in solution. However, in order to confirm that these interactions exist and play a role in complex formation, the complexes should be analysed by neutron diffraction experiments so that the exact locations of the hydrogen atoms in the structure can be accurately determined.

The DFT and QTAIM calculations provide a good agreement between the calculated and observed bond lengths as well as a good indication as to the strength and character of bonds present in a system.

The potentiometric studies done provides some insight as to the stability of the Cy_2-Otn/Metal complexes formed. The studies showed that the stability constants decreases with an increase in metal ionic radius, similar to the Cy_2-tn systems. This once again shows that smaller metal ions form more stable complexes with 6-membered chelate rings. The presence of the hydroxyl group on the propyl bridge in the Cy_2-Otn ligand does not affect this trend. It does, however, decrease the stability constants of the ML complexes with respect to the Cy_2-tn ligand systems. The potentiometric data is, however, not very accurate due to an impurity present in the protonation constant determination.

Further studies should be done to complete the series of crystal structures with Cy_2-tn, to determine the effect of the metal ionic radius, as well as the geometry and bonding in these structures. Attempts should also be made to determine Cy_2-Otn/Metal structures. The potentiometric data should be redone, once the impurity has been removed, in order to get more accurate data. This will aid in explaining the trends seen in stability constants of metal ion complexes with ligands that have five- or six-membered chelate rings, as well as the effect the addition of cyclohexenyl rings make on the stability of these complexes.

Appendix A – DFT/AIM Data

All DFT data was generated in the manner described in Chapter 3.

Table A.1. Selected M-L bond lengths, of the crystal structures and DFT calculations, of TCA/Cu and Cy_2-tn with Ni(II), Zn(II), and Cu(II) complexes.

	CRYSTAL STRUCTURES	**DFT (X3LY-6-31+G(d,p))**	**Δ(obs-calc)**
	bond lengths (Å)	*bond lengths (Å)*	
Cy_2-tn/Ni			
M-N	2.056	2.076	-0.020
M-N	2.064	2.081	-0.017
M-O	2.054	2.100	-0.046
M-O	2.075	2.103	-0.028
M-Ax1 (H_2O)	2.072	2.173	-0.101
M-Ax2 (H_2O)	2.187	2.206	-0.019
Cy_2-tn/Zn			
M-N	2.073	2.137	-0.064
M-N	2.111	2.137	-0.026
M-O	2.075	2.173	-0.098
M-O	2.127	2.173	-0.046
M-Ax1 (Cl)	2.254	2.232	0.022
TCA/Cu			
M-N	1.986	2.003	-0.017
M-N	1.986	2.003	-0.017
M-O	1.947	1.979	-0.032
M-O	1.947	1.979	-0.032
Cy_2-tn/Cu			
M-N	1.978	2.025	-0.047
M-N	1.998	2.031	-0.033
M-O	1.992	2.017	-0.025
M-O	1.996	2.023	-0.027
M-Ax1 (H_2O)	2.262	2.406	-0.144

Table A.2. QTAIM analysis data for TCA/Cu, and Cy_2-tn with Cu(II), Ni(II), and Zn(II) complexes.

Bond	Complex	P (au)	$\nabla^2\rho$ (au)	V	G	H	|V|/G	G/ρ	$\varepsilon = \lambda_1/\lambda_2 -1$
	Cy2-tn/Ni								
M-N	Ni1-N9	0.0791	0.2702	-0.1183	0.0929	-0.0254	1.2732	1.1753	0.0445
M-N	Ni1-N10	0.0784	0.2685	-0.1172	0.0922	-0.0250	1.2716	1.1761	0.0401
M-O	Ni1-O2	0.0592	0.2669	-0.0932	0.0800	-0.0133	1.1657	1.3515	0.0732
M-O	Ni1-O4	0.0583	0.2648	-0.0919	0.0790	-0.0129	1.1626	1.3564	0.0684
M-Ax1	Ni1-O5 (H2O)	0.0424	0.1871	-0.0632	0.0550	-0.0082	1.1493	1.2961	0.1915
M-Ax2	Ni1-O6 (H2O)	0.0458	0.2063	-0.0695	0.0605	-0.0089	1.1477	1.3229	0.1586
For Comparison:									
N-C	N9-C21	0.2451	-0.6238	-0.3681	0.1061	-0.2620	3.4703	0.4327	0.0304
	N10-C20	0.2437	-0.6145	-0.3641	0.1053	-0.2589	3.4595	0.4319	0.0289
NC-CO	C21-C14	0.2568	-0.6201	-0.2671	0.0560	-0.2110	4.7672	0.2182	0.0467
	C20-C11	0.2580	-0.6285	-0.2693	0.0561	-0.2132	4.8018	0.2174	0.0429
C-O	C14-O2	0.2199	-0.3297	-0.4811	0.1993	-0.2818	2.4135	0.9065	0.0059
	C11-O4	0.2202	-0.3213	-0.4877	0.2037	-0.2840	2.3944	0.9249	0.0211
	Cy2-tn/Zn								
M-N	Zn2-N5	0.0705	0.2107	-0.1010	0.0769	-0.0242	1.3147	1.0900	0.0184
M-N	Zn2-N6	0.0705	0.2107	-0.1011	0.0769	-0.0242	1.3147	1.0901	0.0184
M-O	Zn2-O4	0.0539	0.2166	-0.0753	0.0647	-0.0106	1.1634	1.2002	0.0397
M-O	Zn2-O3	0.0539	0.2166	-0.0753	0.0647	-0.0106	1.1634	1.2001	0.0397
M-Ax1	Zn2-Cl	0.0804	0.1777	-0.1156	0.0800	-0.0356	1.4450	0.9956	0.0000
For Comparison:									
N-C	N5-C11	0.2490	-0.6488	-0.3847	0.1112	-0.2734	3.4585	0.4467	0.0263
	N6-C7	0.2490	-0.6488	-0.3846	0.1112	-0.2734	3.4584	0.4467	0.0263
NC-CO	C11-C12	0.2532	-0.6022	-0.2608	0.0551	-0.2057	4.7304	0.2178	0.0491
	C7-C15	0.2532	-0.6022	-0.2608	0.0551	-0.2057	4.7304	0.2178	0.0491
C-O	C12-O4	0.2331	-0.3813	-0.5289	0.2168	-0.3121	2.4397	0.9299	0.0113
	C15-O3	0.2331	-0.3813	-0.5289	0.2168	-0.3121	2.4397	0.9298	0.0113
	TCA/Cu								
M-N	Cu1-N5	0.0969	0.2549	-0.1500	0.1068	-0.0431	1.4036	1.1030	0.0049
M-N	Cu1-N31	0.0968	0.2548	-0.1499	0.1068	-0.0431	1.4036	1.1029	0.0049
M-O	Cu1-O12	0.0800	0.3558	-0.1376	0.1133	-0.0243	1.2148	1.4161	1.0049
M-O	Cu1-O32	0.0800	0.3559	-0.1376	0.1133	-0.0243	1.2148	1.4161	2.0049
For Comparison:									
N-C	N5-C6	0.2363	-0.5753	-0.3602	0.1082	-0.2520	3.3298	0.4577	0.0323
	N31-C34	0.2363	-0.5751	-0.3600	0.1081	-0.2519	3.3298	0.4576	0.0322
NC-CO	C6-C11	0.2565	-0.6208	-0.2665	0.0556	-0.2109	4.7895	0.2170	0.0439
	C33-C34	0.2564	-0.6208	-0.2665	0.0556	-0.2108	4.7894	0.2170	0.0439
C-O	C11-O12	0.2129	-0.2813	-0.4679	0.1988	-0.2691	2.3538	0.9336	0.0276
	C33-O32	0.2130	-0.2813	-0.4680	0.1989	-0.2692	2.3536	0.9338	0.0276

Bond	Complex	P (au)	$\nabla^2\rho$ (au)	V	G	H	|V|/G	G/ρ	$\varepsilon = \|\lambda_1\|/\|\lambda_2\|-1$
	Cy2-tn/Cu								
M-N	Cu1-N12	0.0914	0.2412	-0.1390	0.0997	-0.0394	1.3950	1.0903	0.0181
M-N	Cu1-N10	0.0903	0.2380	-0.1369	0.0982	-0.0387	1.3939	1.0877	0.0149
M-O	Cu1-O4	0.0730	0.3041	-0.1203	0.0982	-0.0221	1.2255	1.3448	0.0178
M-O	Cu1-O2	0.0754	0.3099	-0.1244	0.1009	-0.0235	1.2324	1.3384	0.0828
M-Ax1	Cu1-O7 (H2O)	0.0301	0.1338	-0.0346	0.0340	-0.0006	1.0166	1.1306	0.1175
For Comparison:									
N-C	N12-C38	0.2399	-0.5965	-0.3685	0.1097	-0.2588	3.3596	0.4572	0.0290
	N10-C27	0.2398	-0.5971	-0.3691	0.1099	-0.2592	3.3580	0.4584	0.0272
NC-CO	C38-C52	0.2591	-0.6338	-0.2712	0.0564	-0.2148	4.8107	0.2176	0.0445
	C27-C13	0.2582	-0.6264	-0.2695	0.0565	-0.2131	4.7736	0.2187	0.0486
C-O	C52-O4	0.2173	-0.3012	-0.4814	0.2030	-0.2783	2.3708	0.9344	0.0253
	C13-O2	0.2186	-0.3118	-0.4822	0.2021	-0.2801	2.3857	0.9247	0.0096

1 au of q = 6.7483 eÅ^{-3}, and 1 au of $\nabla^2\rho$ = 24.099 eÅ^{-5}. The units for V, G, and H are kcal/mol.

Table A.3. Charge on the metal atom (q(A) and the electron transfer from the ligand to the metal (ΔQ).

Complex		q(A)	ΔQ
TCA/Cu	(M-L)	1.0439	0.9561
Cy_2-tn/Ni	(M-L)	1.2027	0.7973
Cy_2-tn/Zn	(M-L)	1.1597	0.8403
Cy_2-tn/Cu	(M-L)	1.0605	0.9395

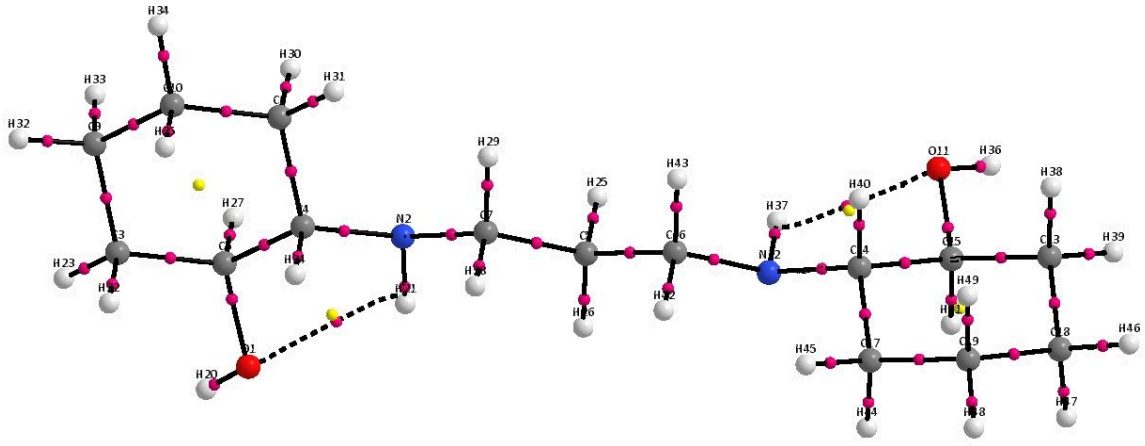


Figure A.1. QTAIM molecular graph of Cy_2-tn.

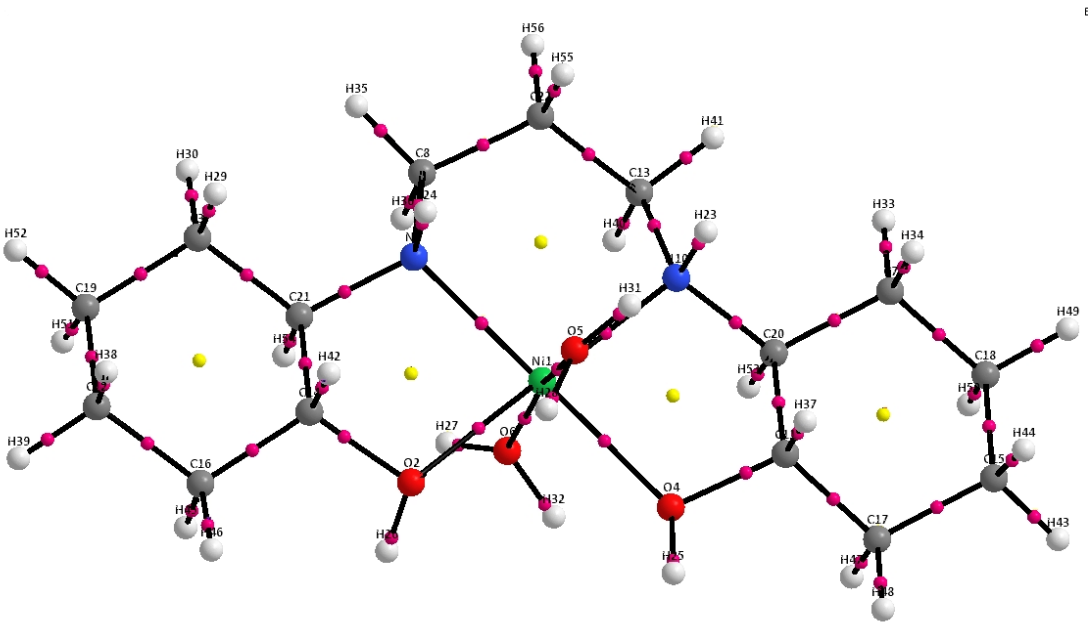


Figure A.2. QTAIM molecular graph of Cy_2-tn/Ni(II) complex.

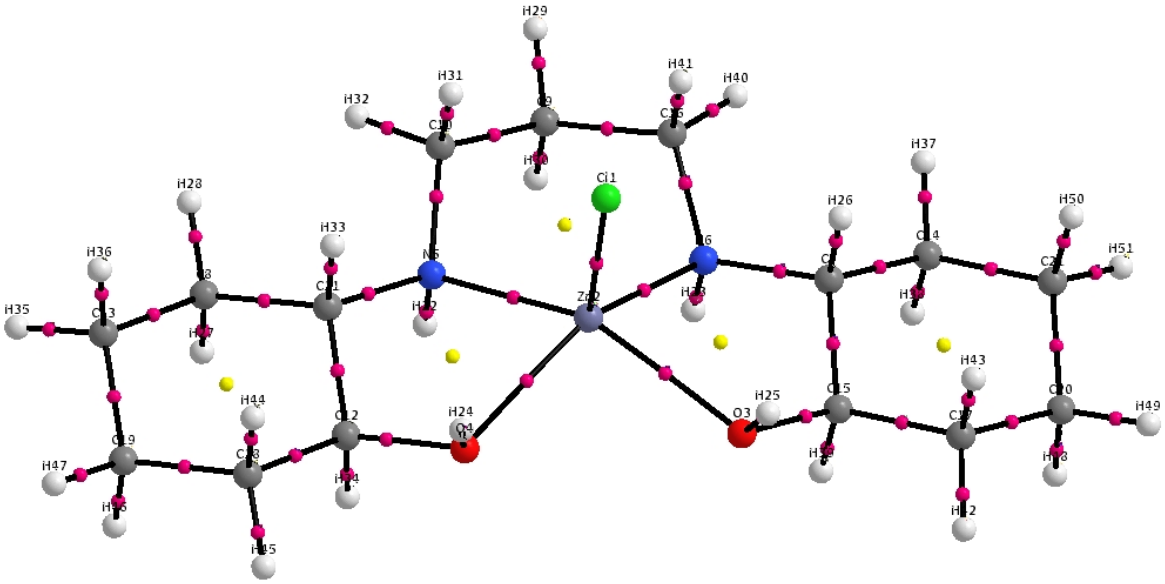


Figure A.3. QTAIM molecular graph of TCA/Cu(II) complex.

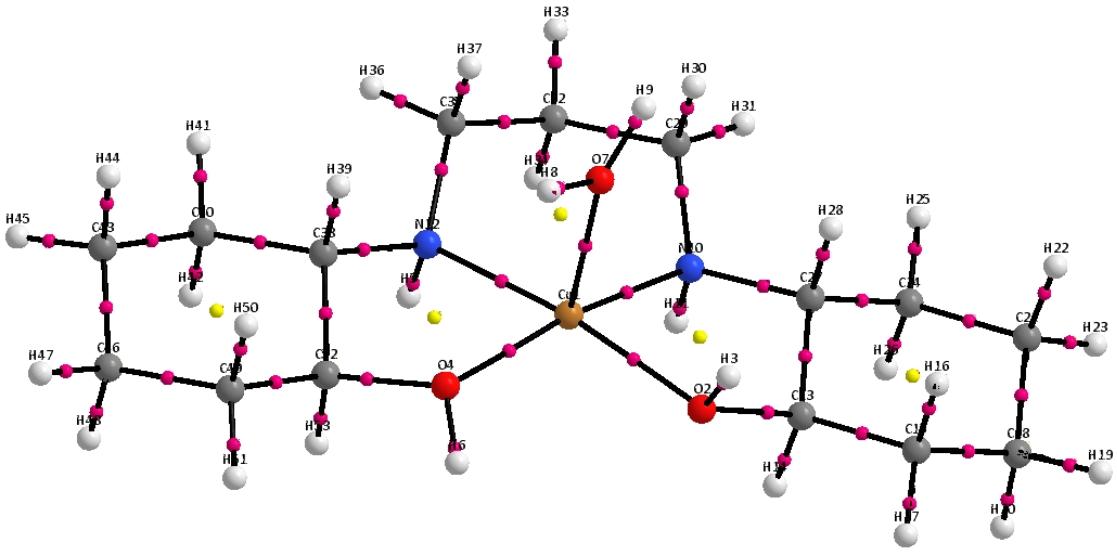


Figure A.4. QTAIM molecular graph of Cy_2-tn/Cu(II) complex.

Appendix B – NMR Data

All NMR data was generated in the manner described in Chapter 2.

Figure B.1. The ^{1}H NMR of Cy_2-Otn (L3)

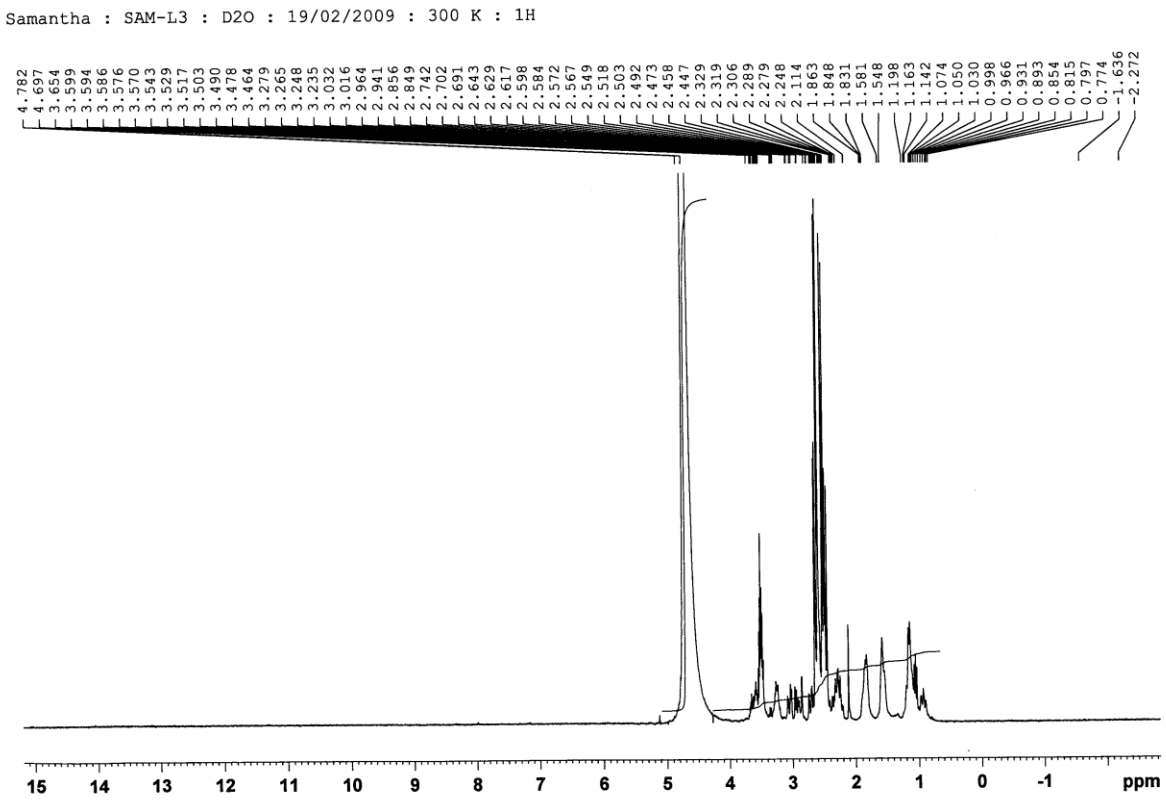


Figure B.2. The ^{1}H NMR of Cy_2-Otn (L5)

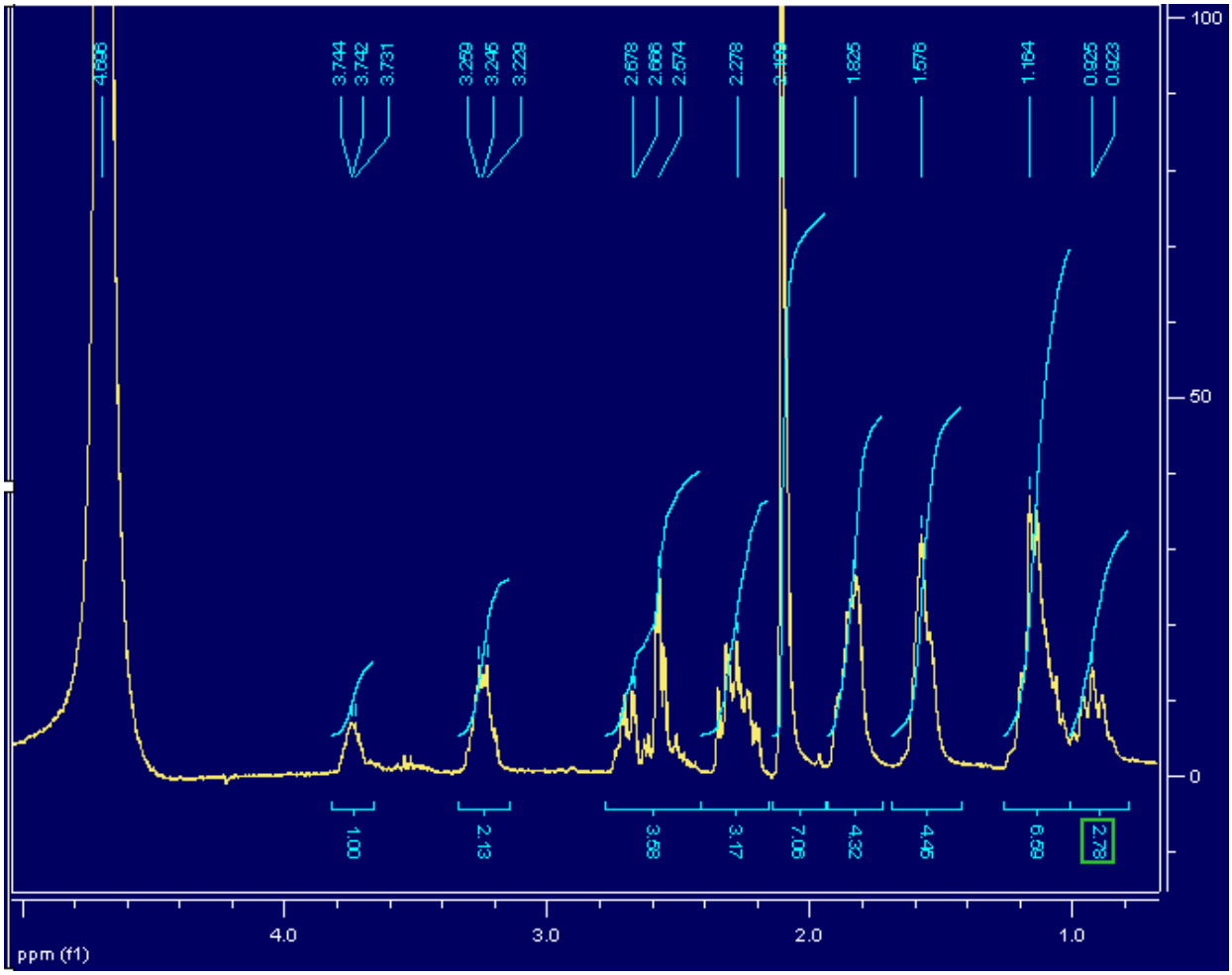


Figure B.3. The ^{1}H NMR of Cy_2-Otn (L6)

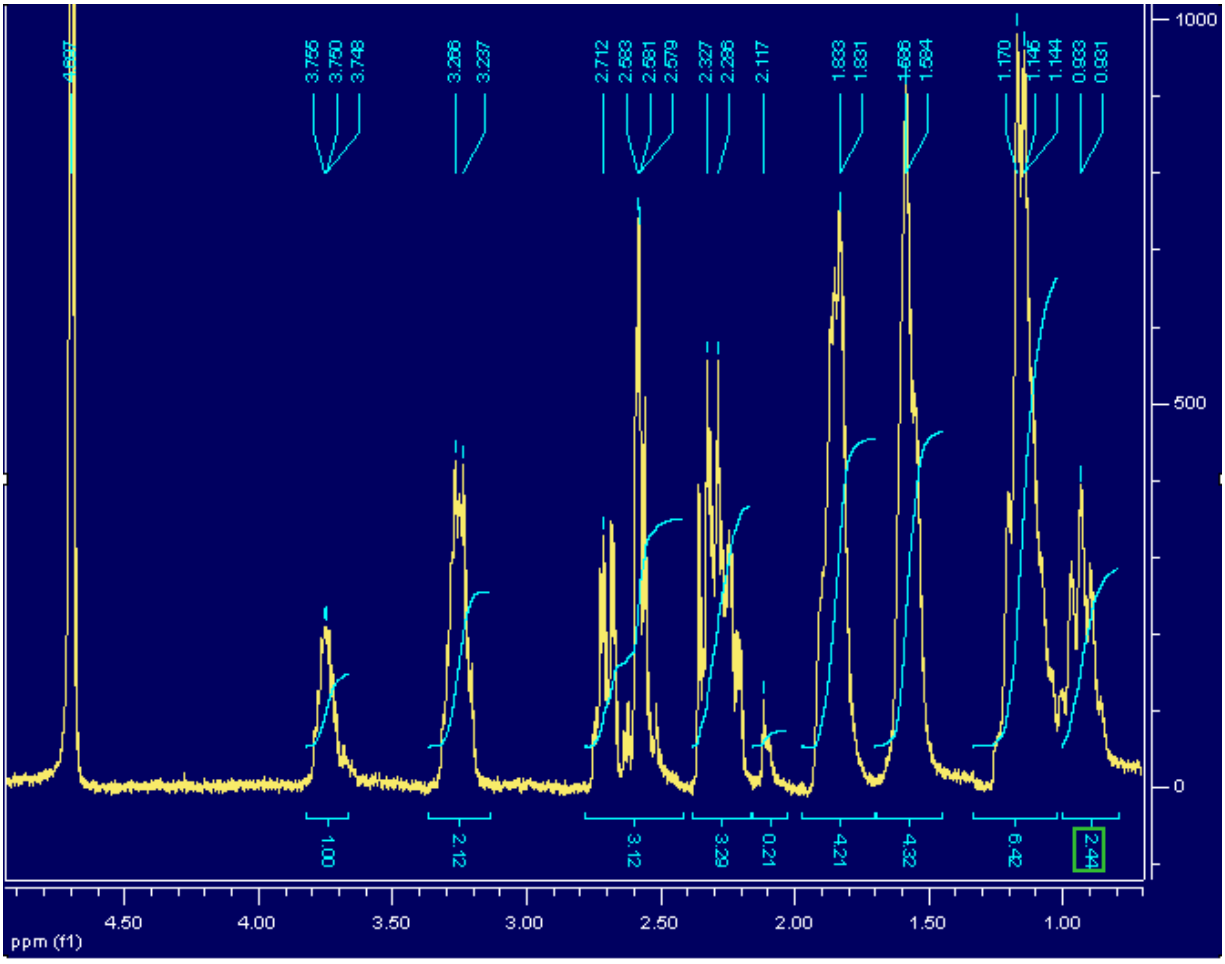


Figure B.4. The ^{1}H NMR of Cy_2-Otn (L7)

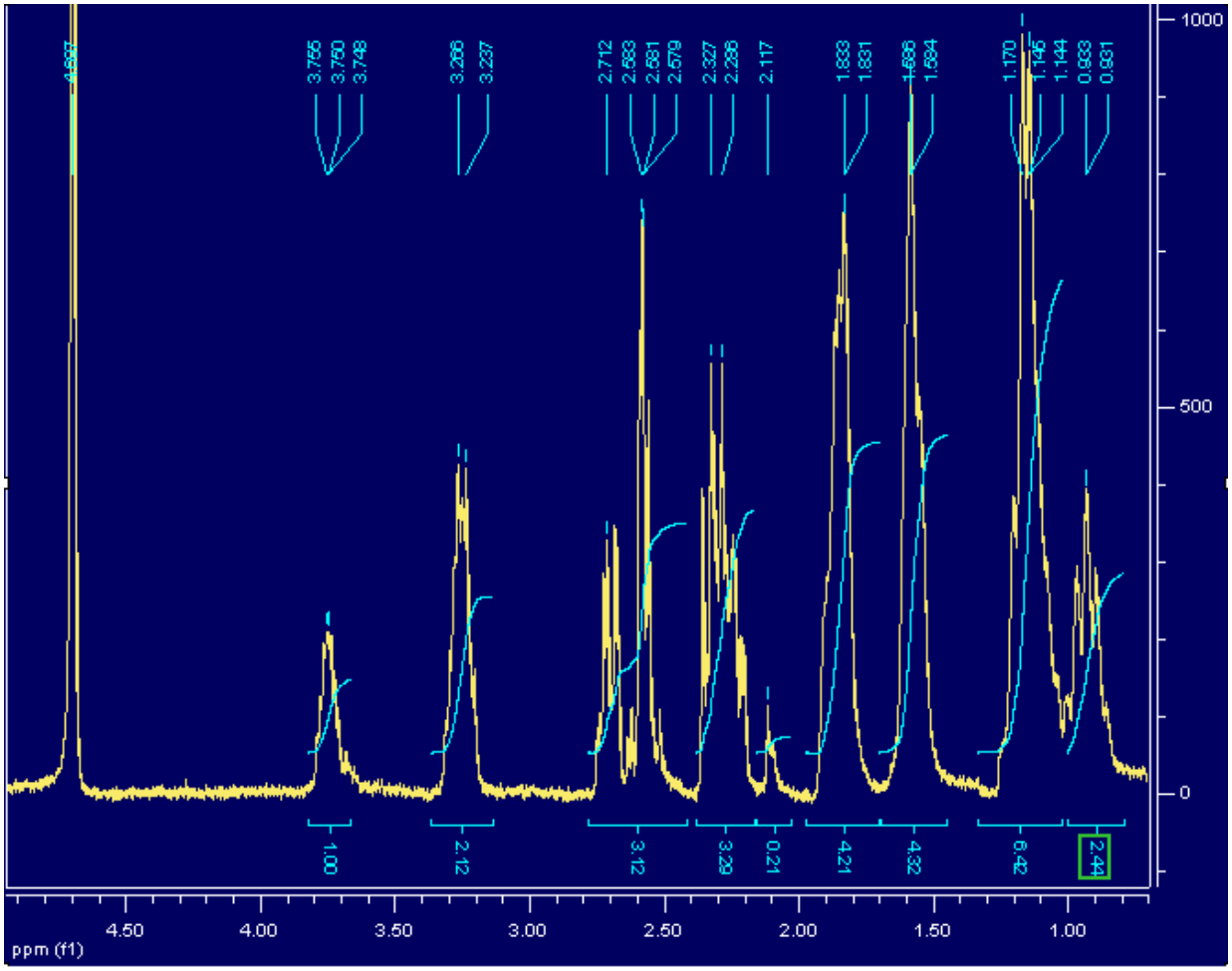


Figure B.5. The ^{1}H NMR of Cy_2-Otn (L7c)

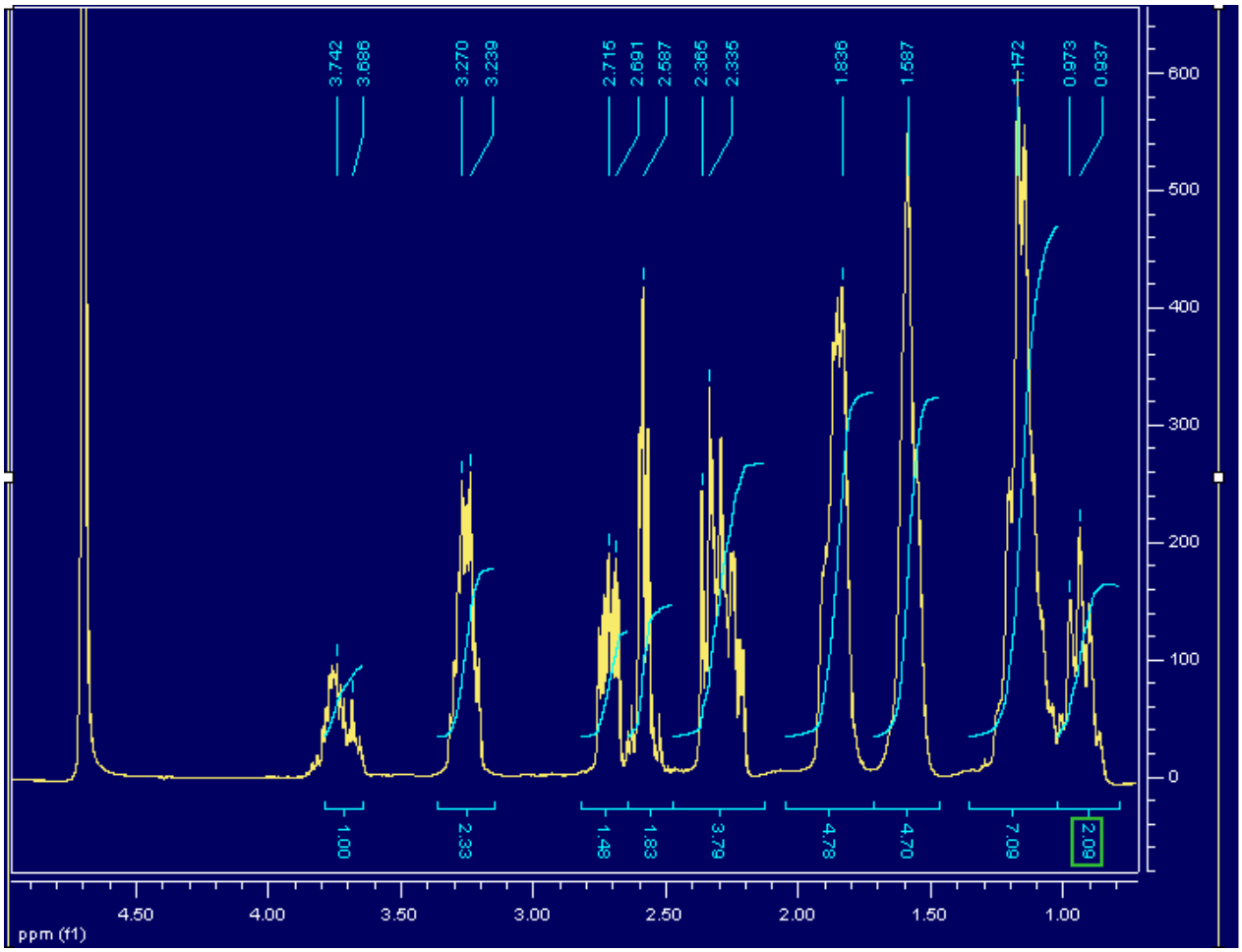


Figure B.6. The ^{1}H NMR of Cy_2-Otn (L8)

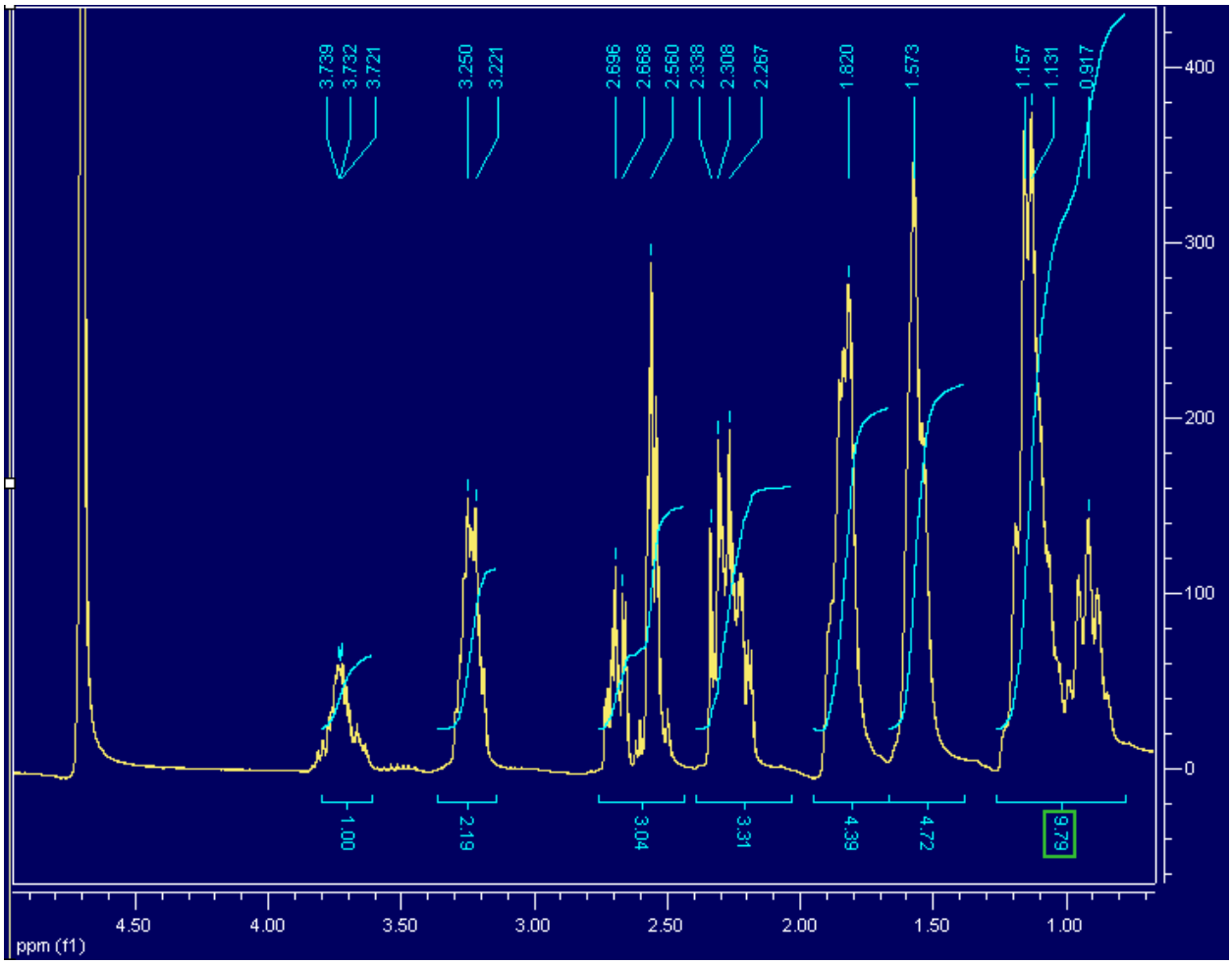


Figure B.7. The ^{1}H NMR of Cy_2-Otn (L8c)

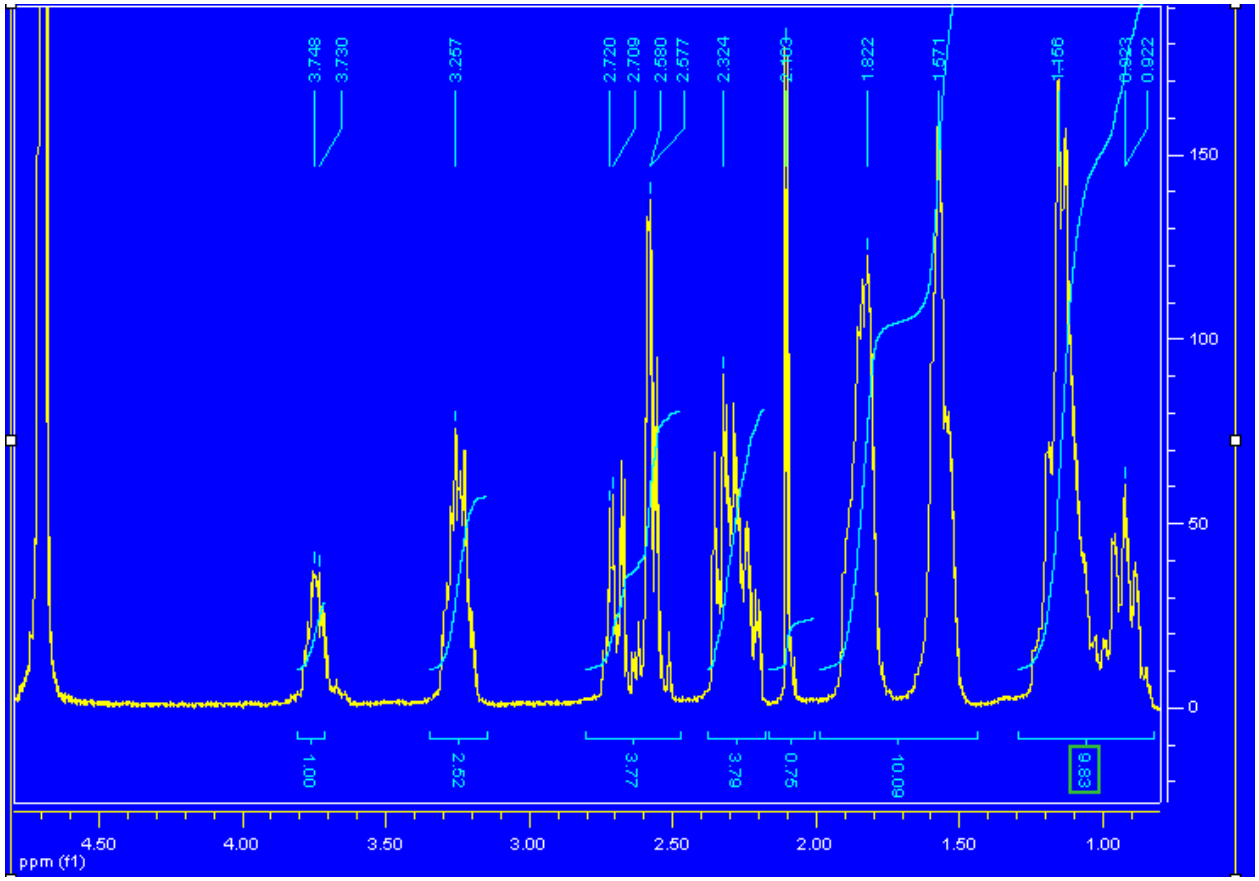


Figure B.8. The ^{1}H NMR of Cy_2-tn (2L1)

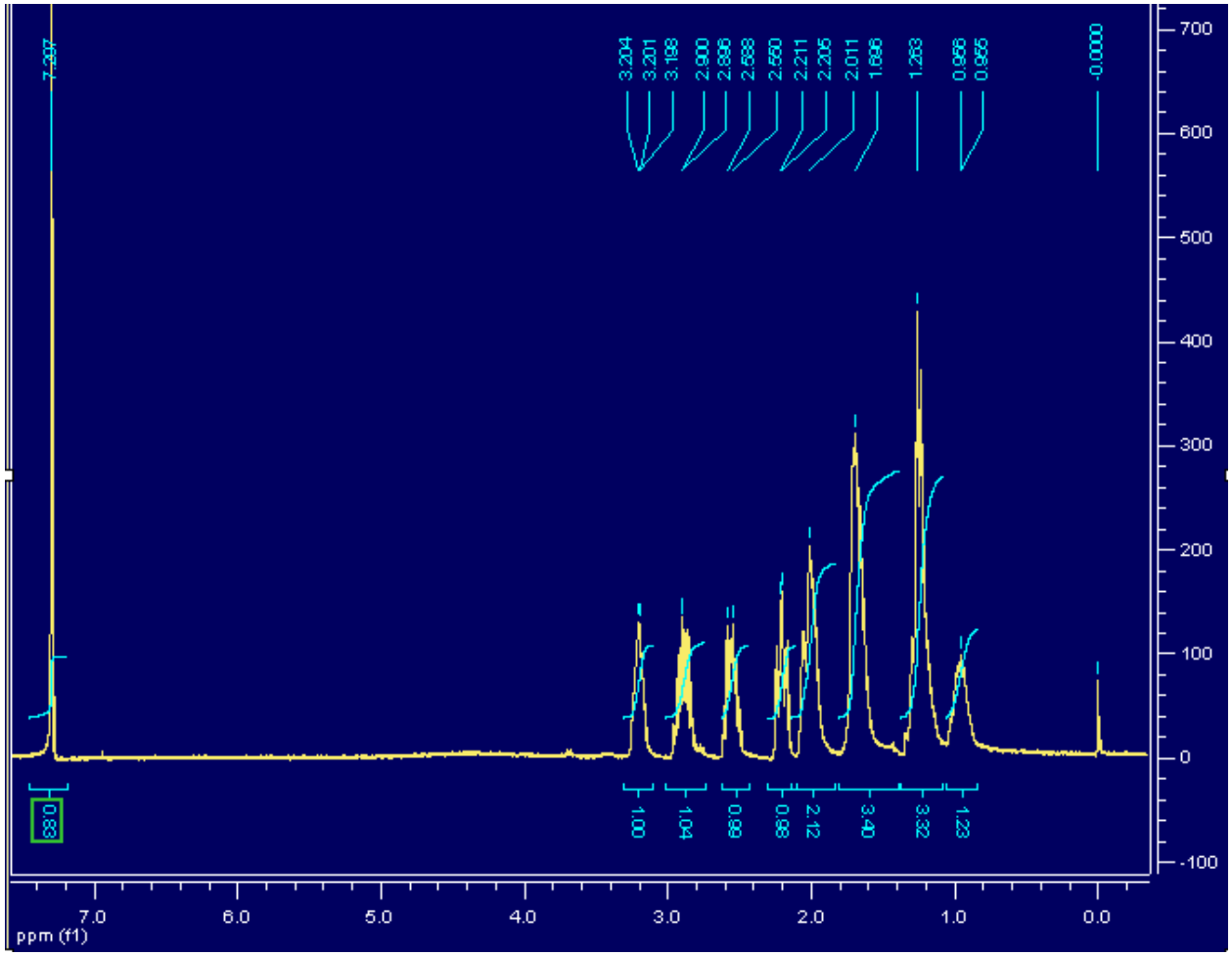


Figure B.9. The ^{1}H NMR of Cy_2-tn (2L2)

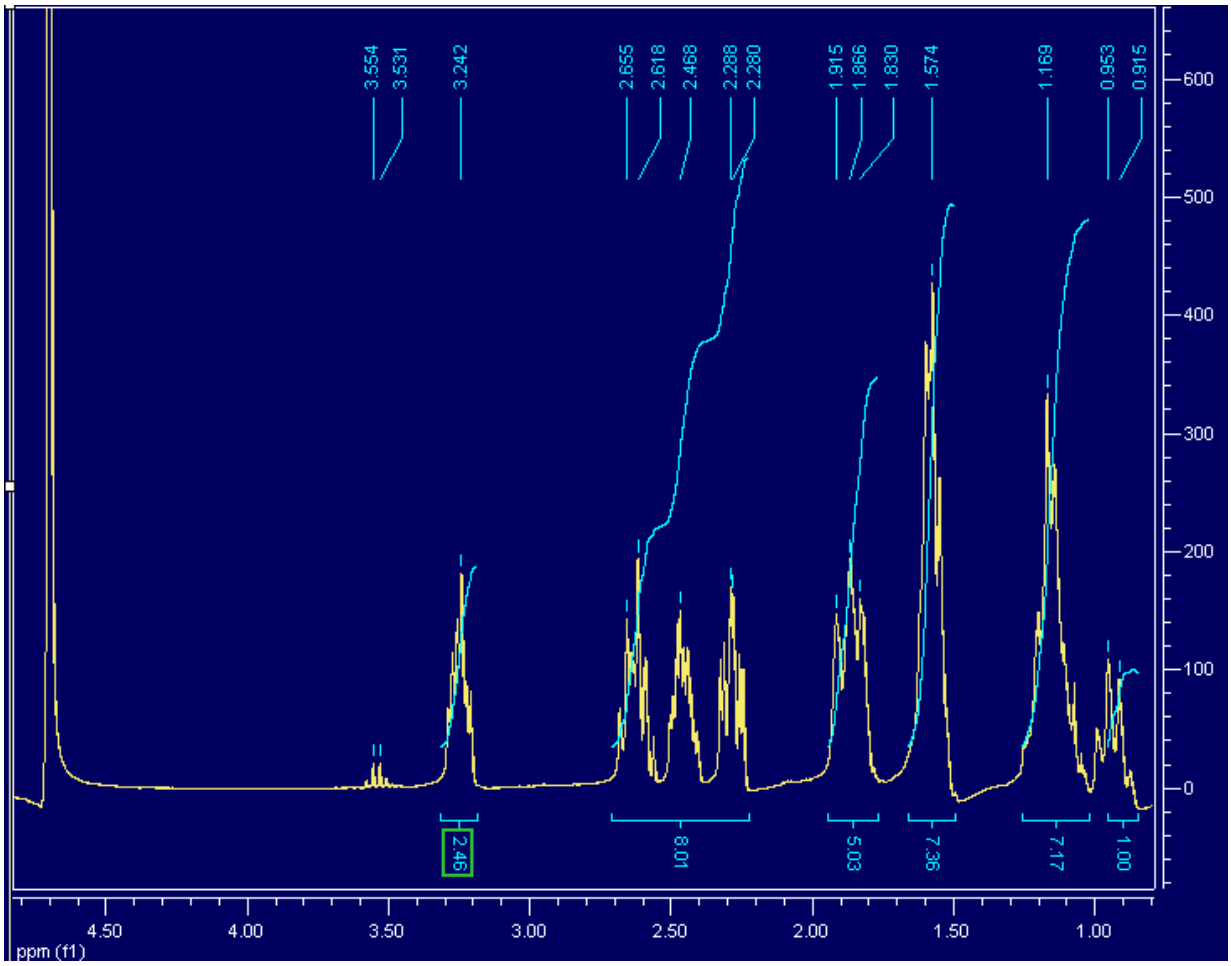
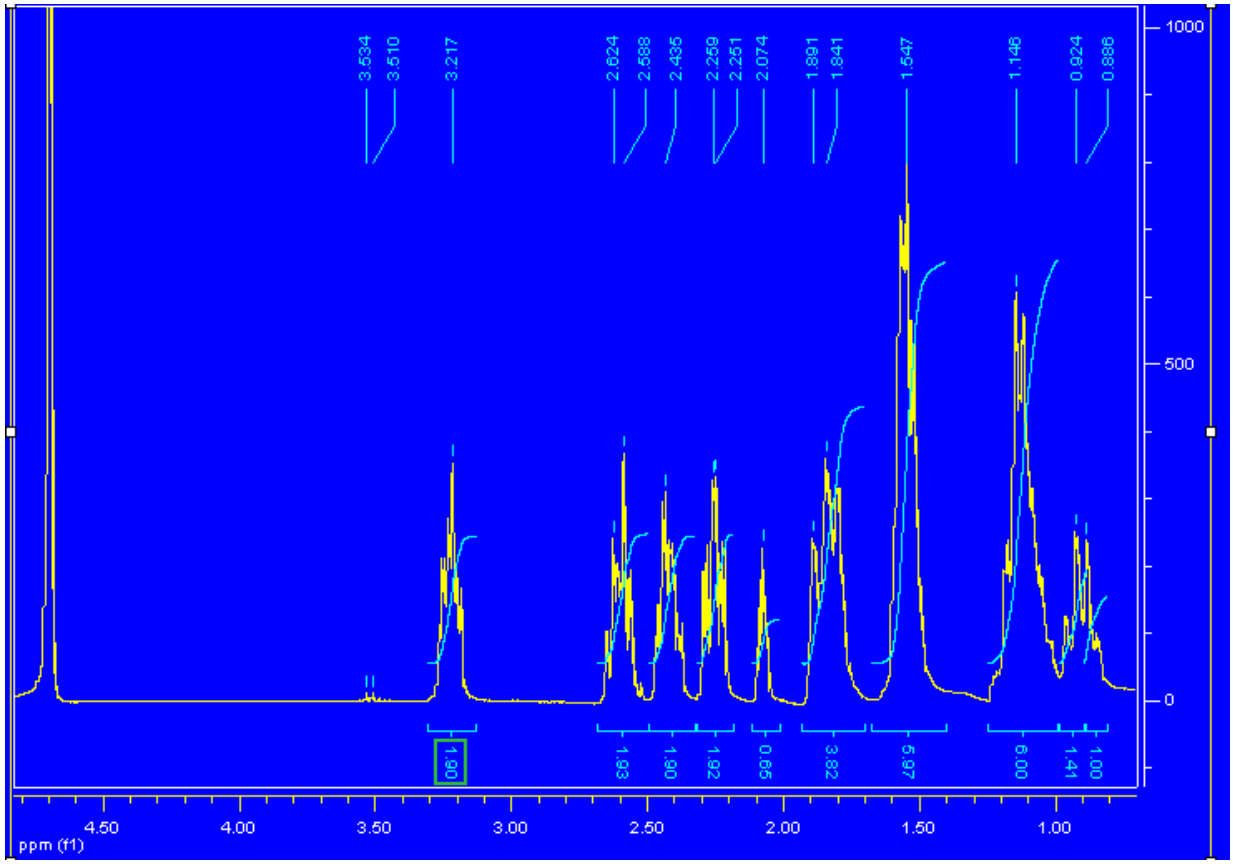


Figure B.10. The ^{1}H NMR of Cy_2-tn (2L3)



Appendix C – MS Data

All MS data was generated in the manner described in Chapter 2.

Figure C.1. The ESI Spectrum of Cy_2-Otn (L1)

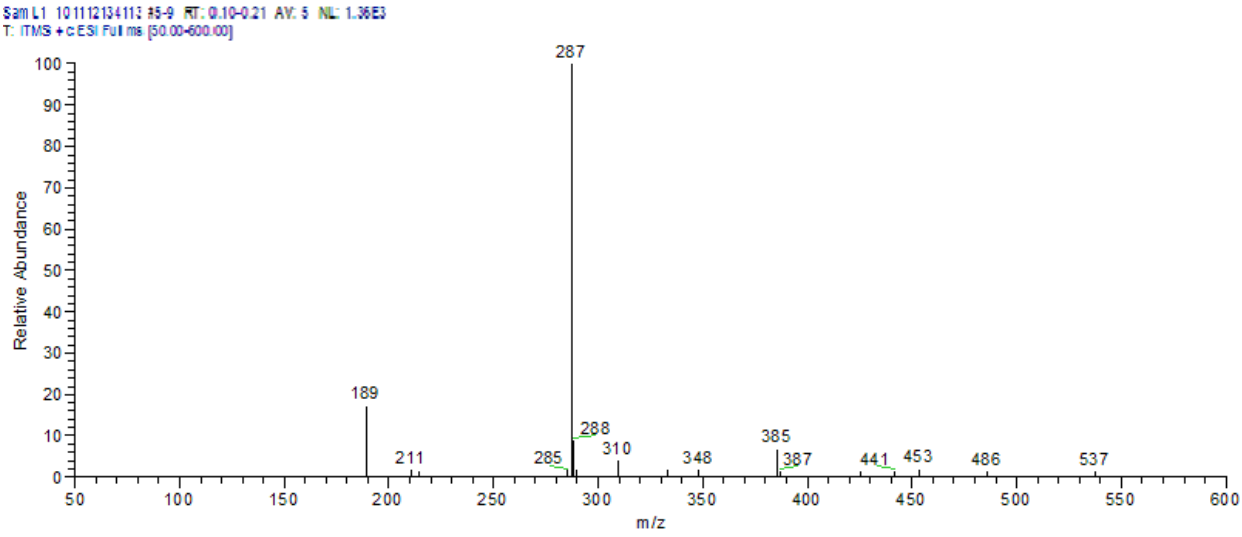


Figure C.2. The ESI Spectrum of Cy_2-Otn (L2)

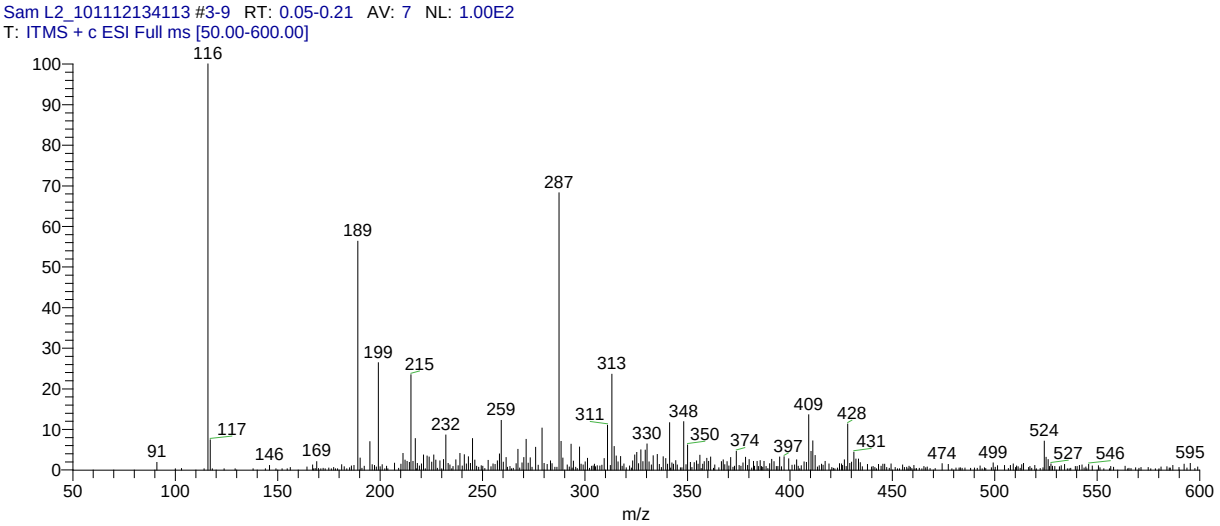


Figure C.3. The ESI Spectrum of Cy_2-Otn (L3)

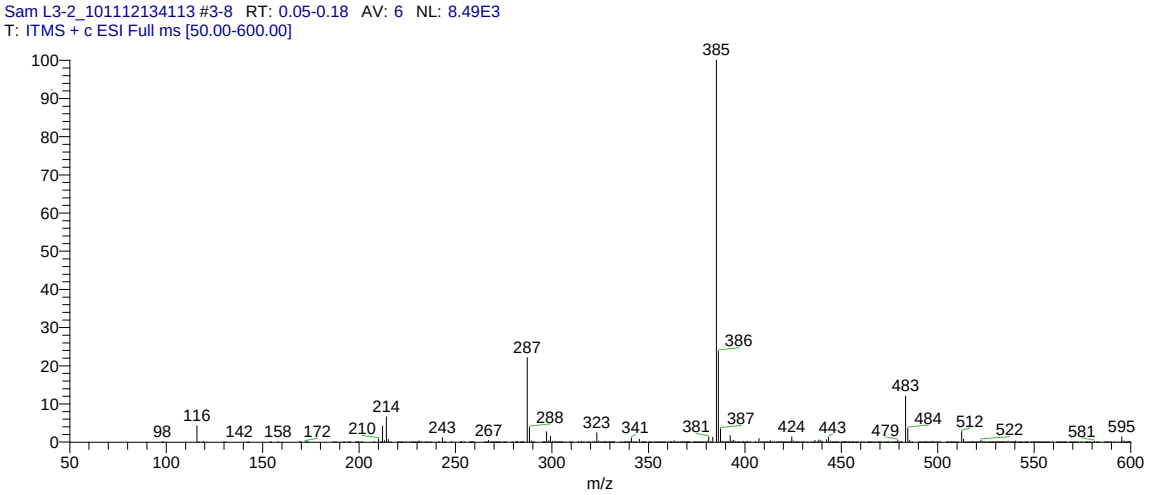


Figure C.4. The ESI Spectrum of Cy_2-Otn (L4)

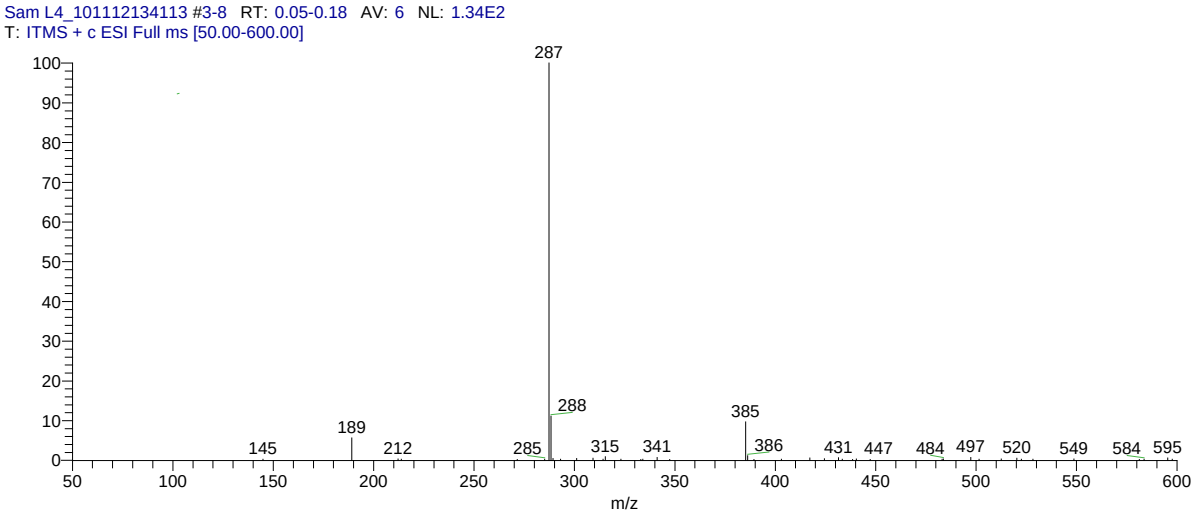


Figure C.5. The ESI Spectrum of Cy_2-Otn (L5)

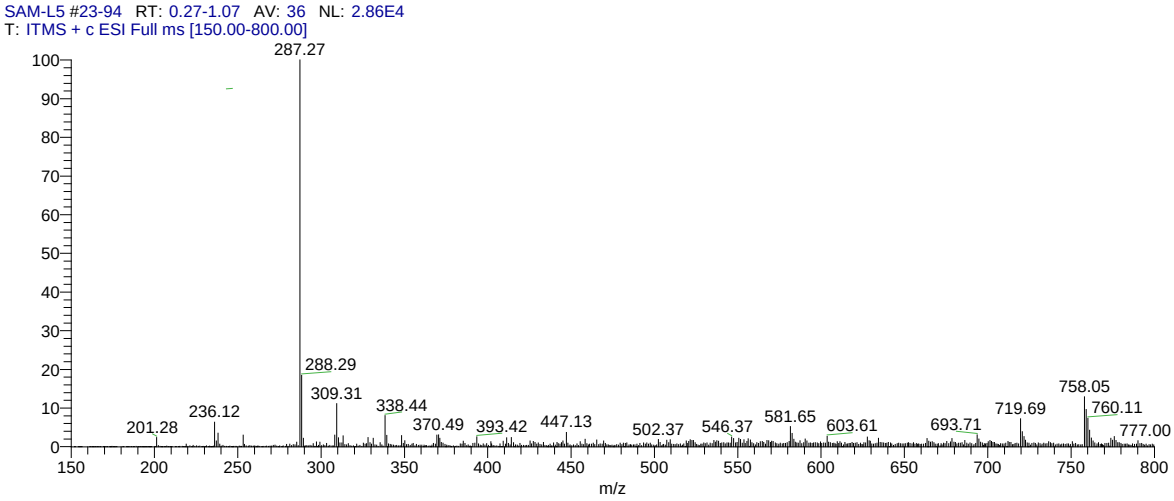


Figure C.6. The ESI Spectrum of Cy_2-Otn (L6)

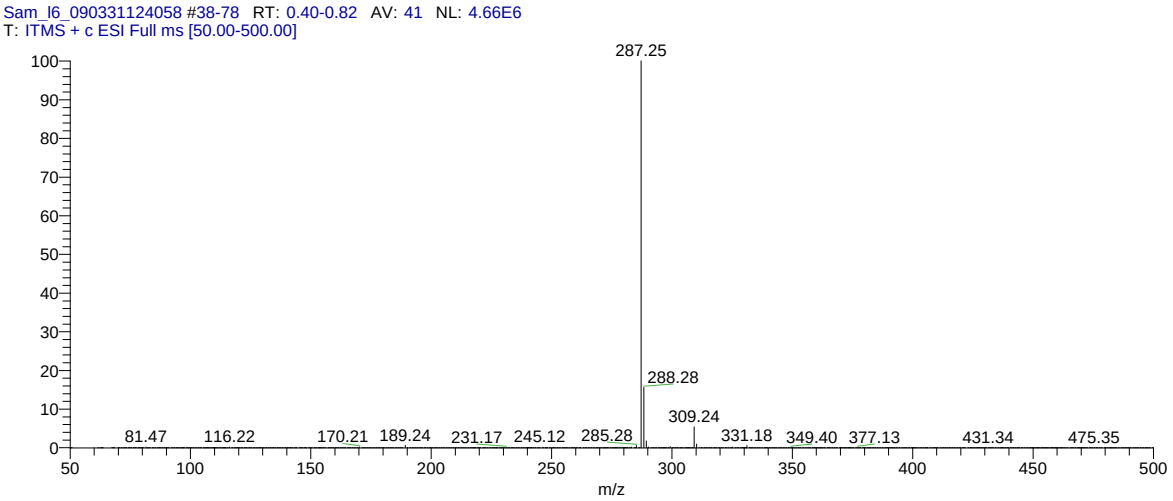


Figure C.7. The ESI Spectrum of Cy_2-Otn (L7)

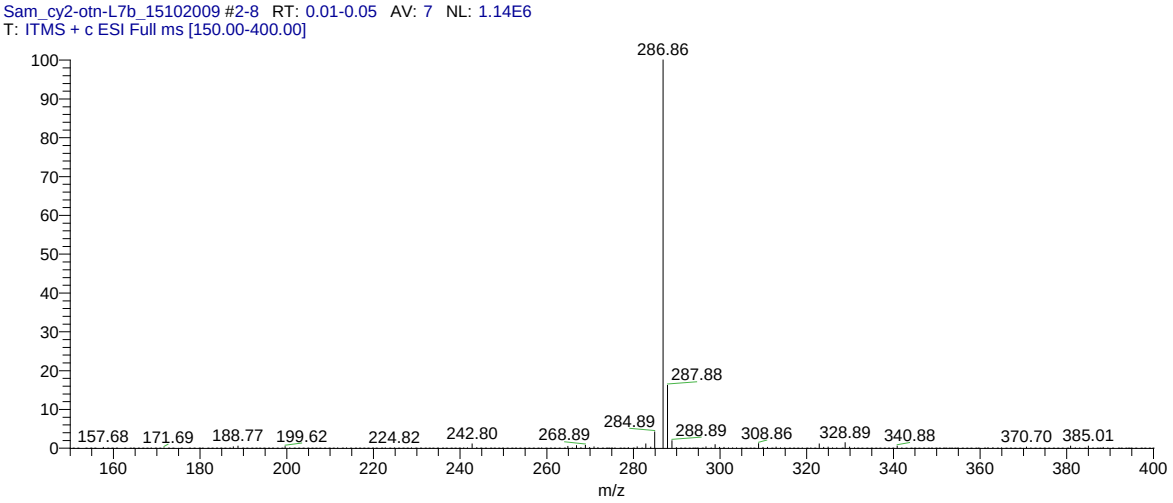


Figure C.8. The APCI Spectrum of Cy_2-Otn (L7c)

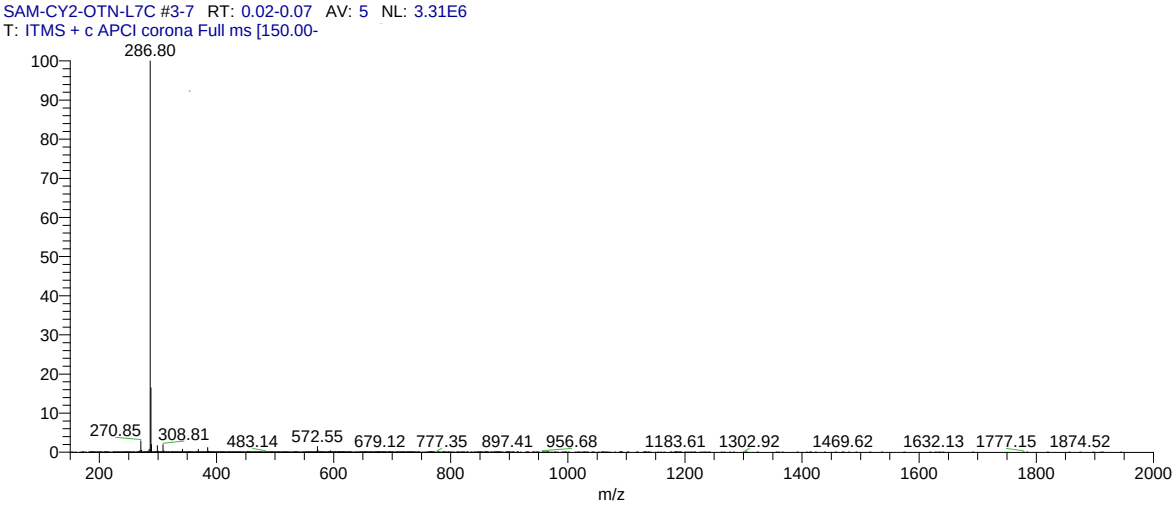


Figure C.9. The APCI Spectrum of Cy_2-Otn (L8)

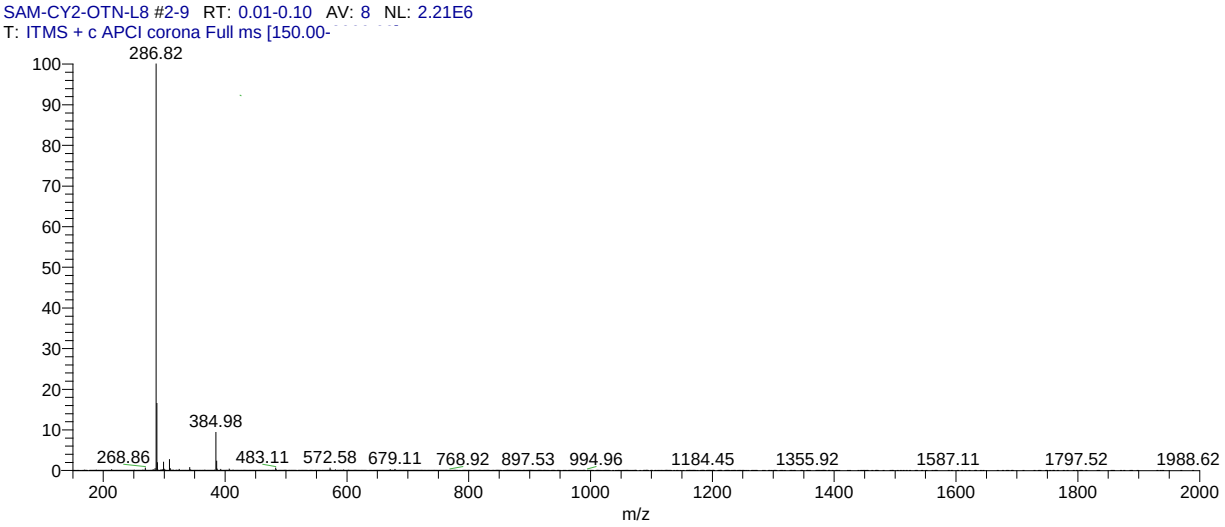


Figure C.10. The ESI Spectrum of Cy_2-Otn (L8c)

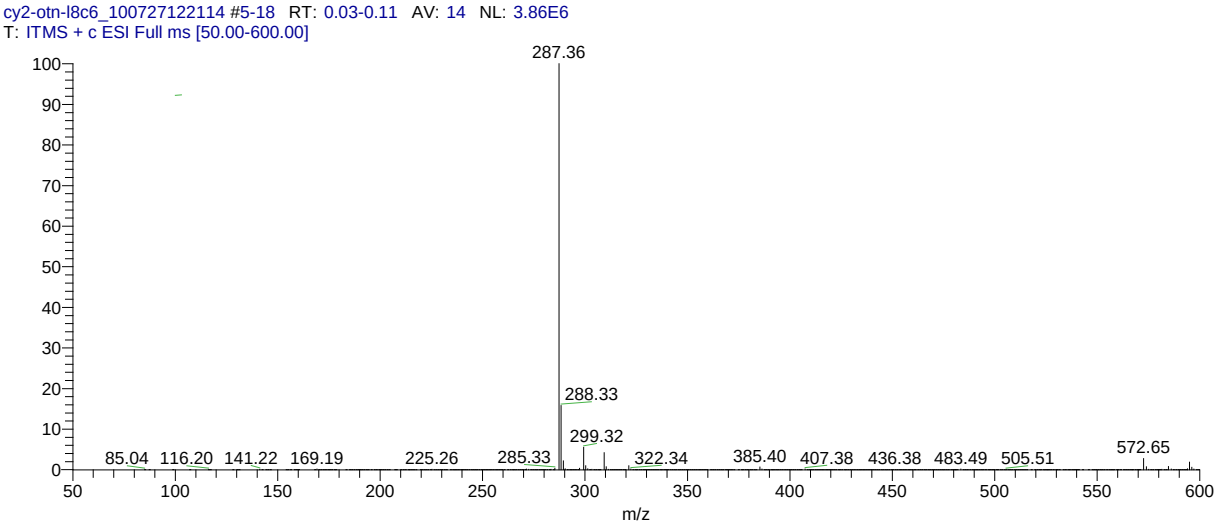


Figure C.11. The ESI Spectrum of Cy_2-tn (2L1)

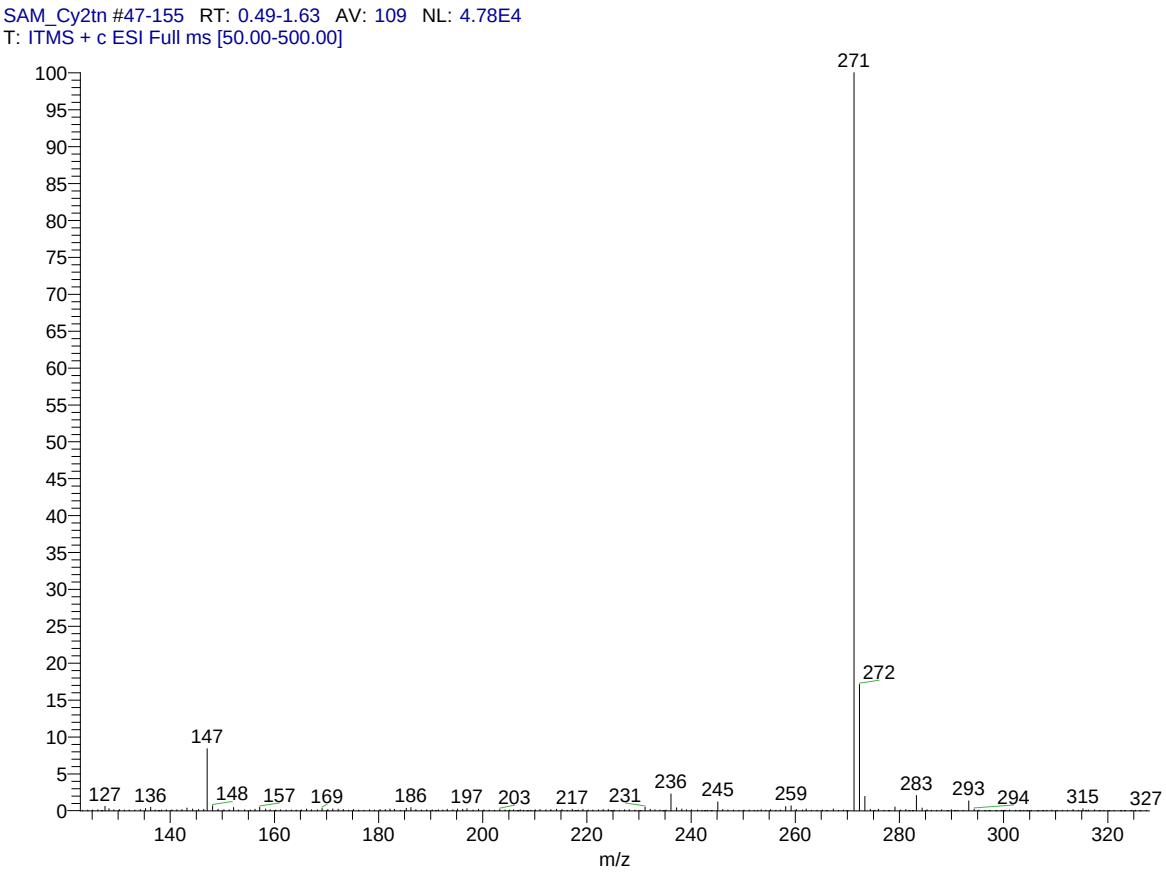


Figure C.12. The APCI Spectrum of Cy_2-tn (2L2)

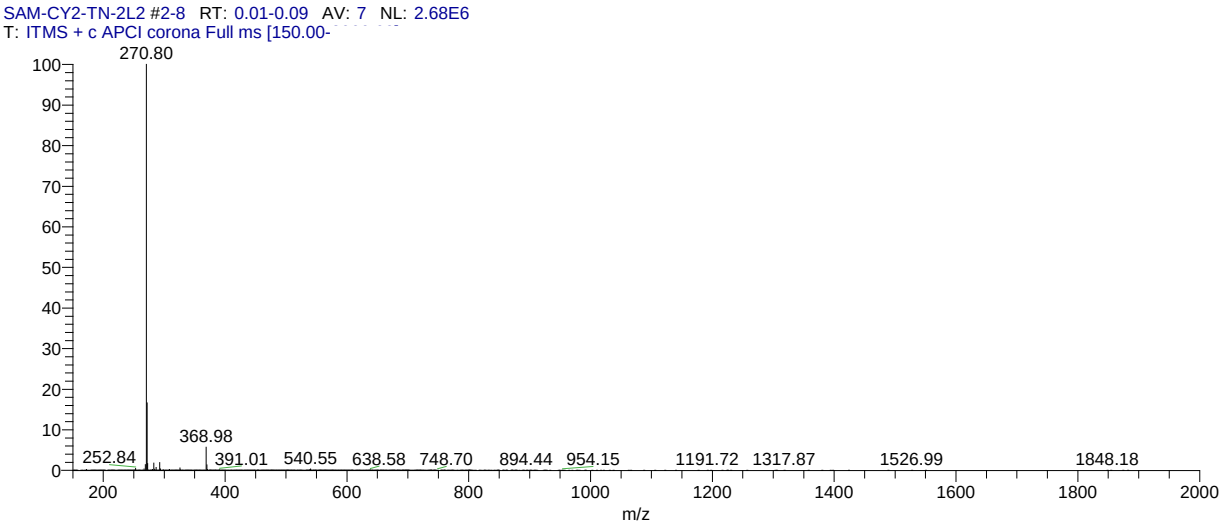


Figure C.13. The ESI Spectrum of Cy_2-tn (2L3)

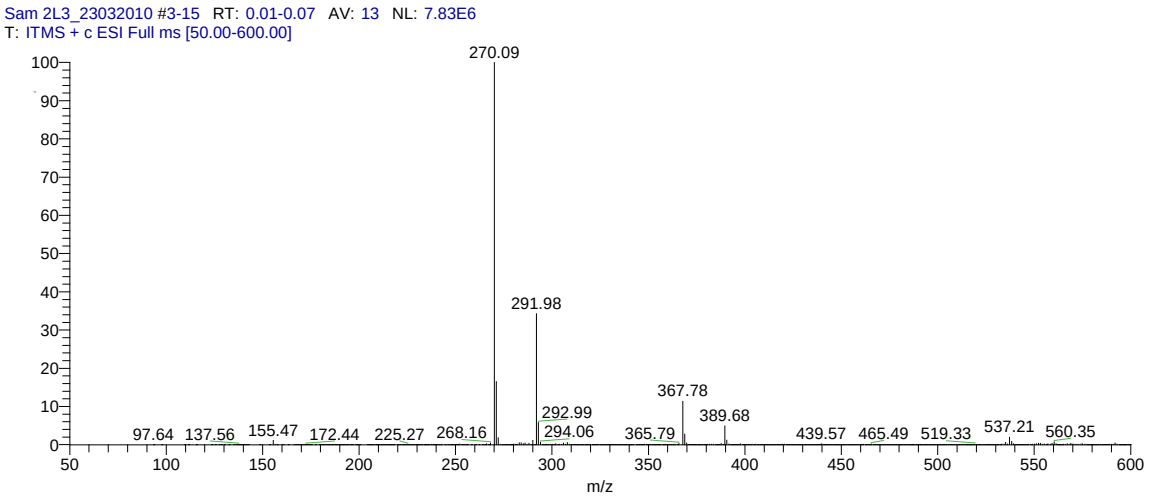


Figure C.14. The ESI Spectrum of Cy_2-Otn/Cu(II) Reaction (Method A1)

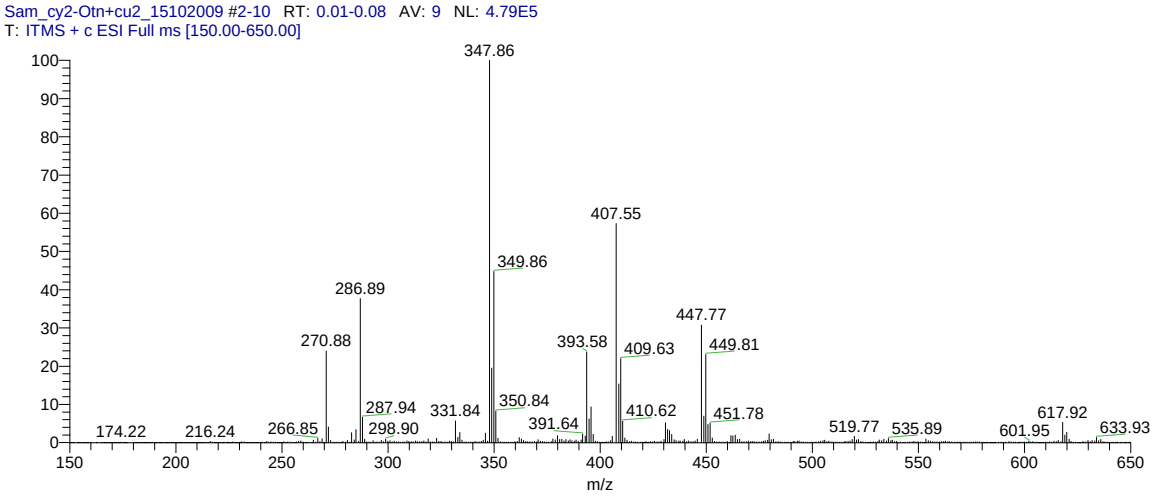


Figure C.15. The ESI Spectrum of Cy_2-Otn/Cu(II) Reaction (Method A2)

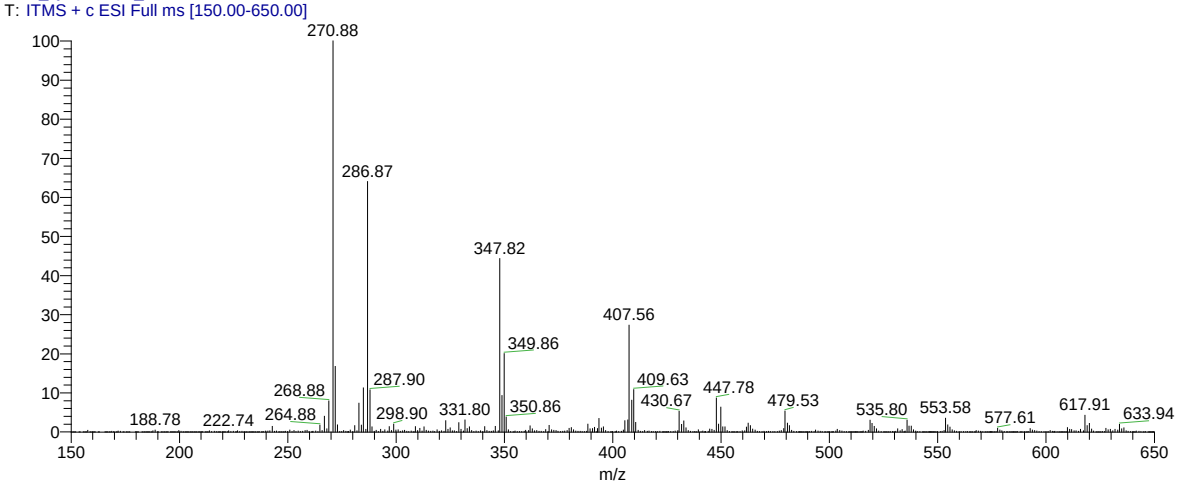


Figure C.16. The ESI Spectrum of Cy_2-Otn/Cu(II) Reaction (Method A3)

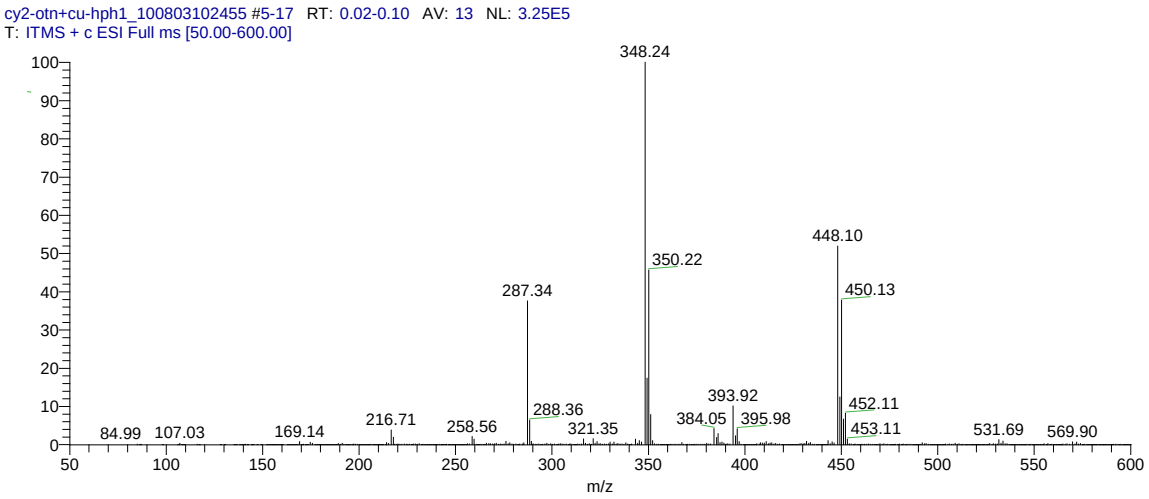


Figure C.17. The ESI Spectrum of Cy_2-Otn/Ni(II) Reaction (Method B1)

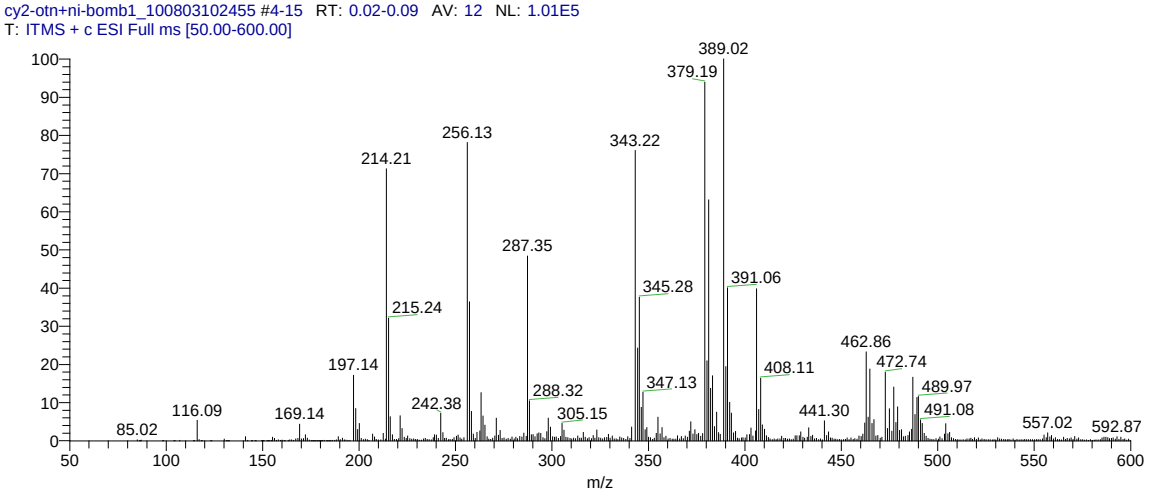


Figure C.18. The ESI Spectrum of Cy_2-Otn/Ni(II) Reaction (Method B2)

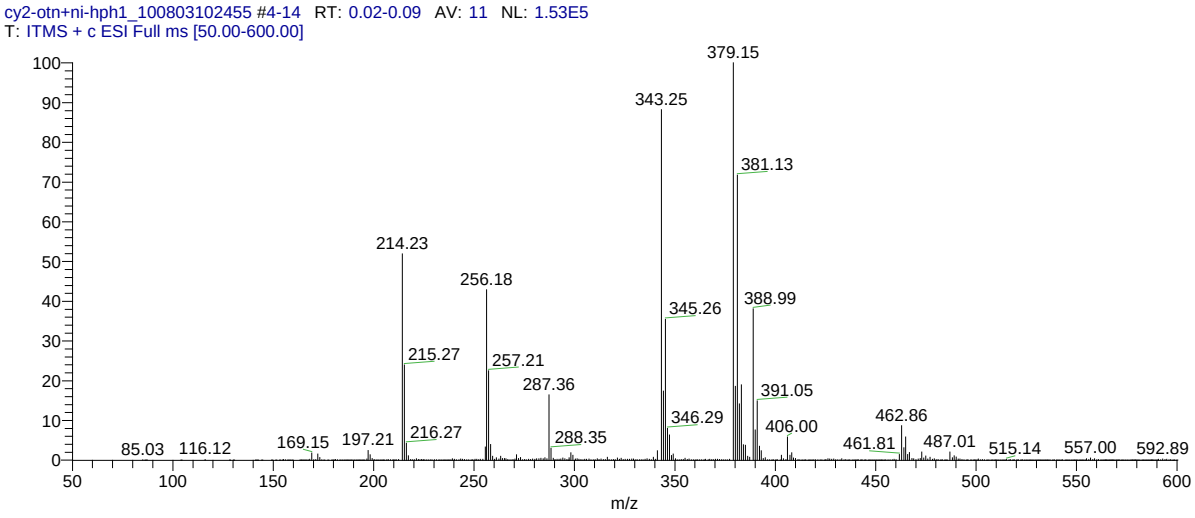


Figure C.19. The ESI Spectrum of Cy_2-Otn/Zn(II) Reaction (Method C1)

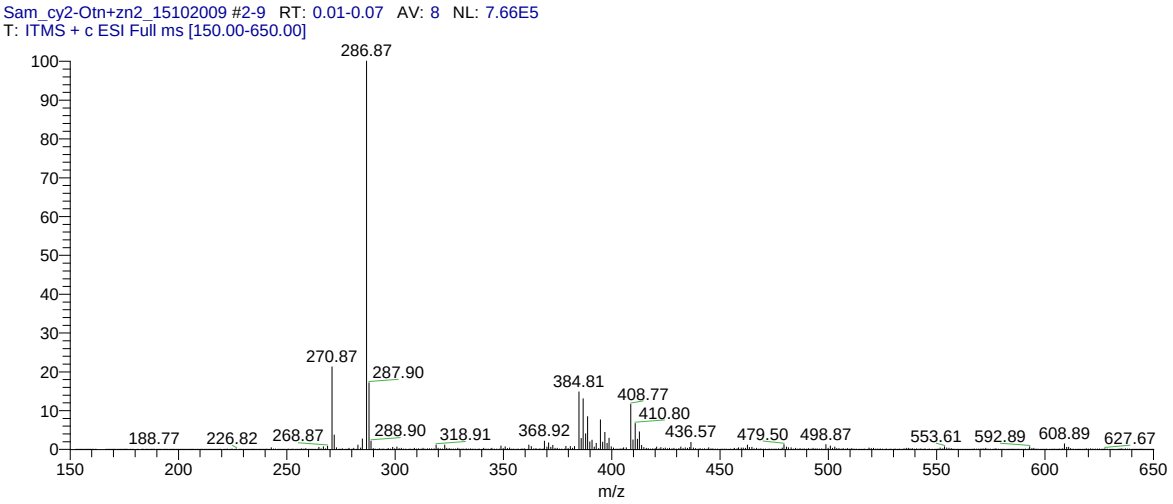


Figure C.20. The ESI Spectrum of Cy_2-Otn/Zn(II) Reaction (Method C2)

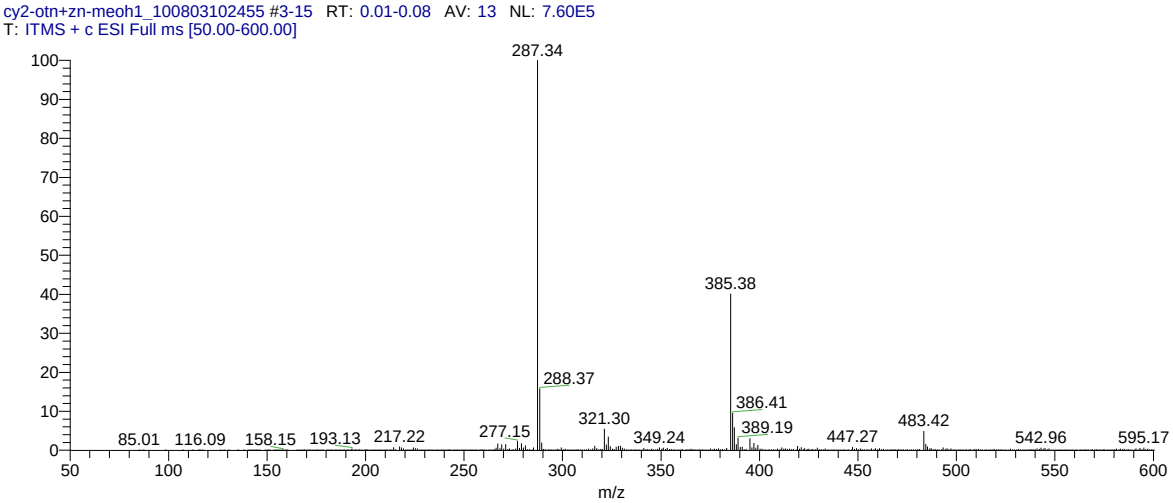


Figure C.21. The ESI Spectrum of Cy_2-Otn/Zn(II) Reaction (Method C3)

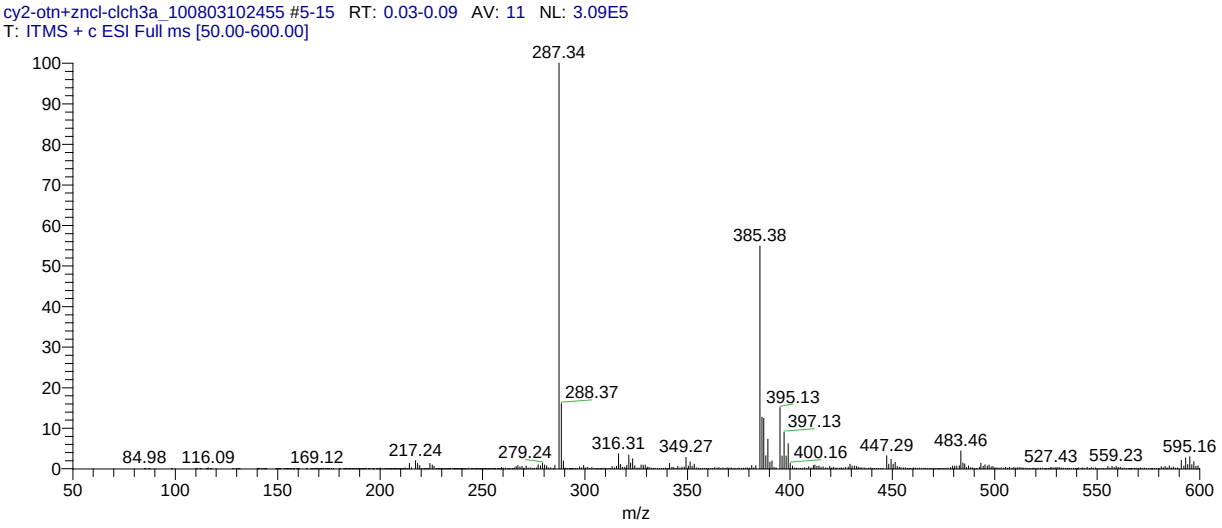


Figure C.22. The ESI Spectrum of Cy_2-Otn/Zn(II) Reaction (Method C4)

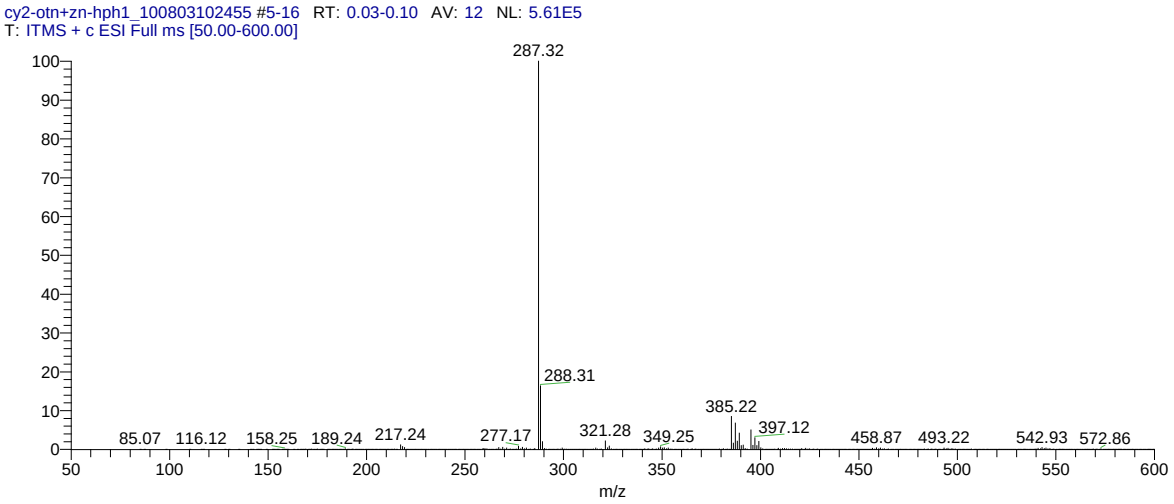


Figure C.23. The APCI Spectrum of Cy_2-Otn/Cd(II) Reaction (Method D1)

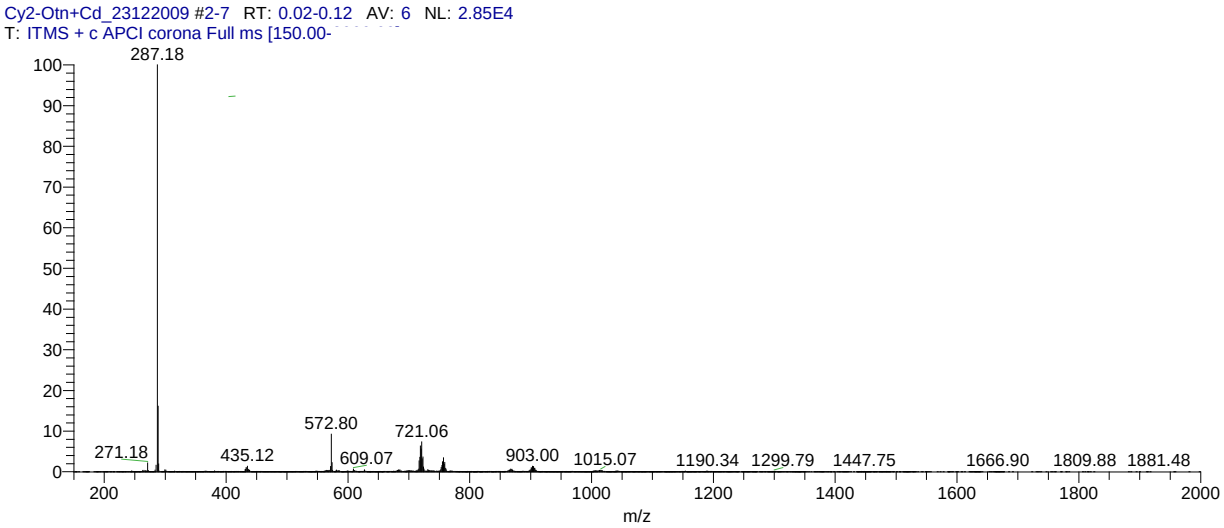


Figure C.24. The APCI Spectrum of Cy_2-Otn/Cd(II) Reaction (Method D2)

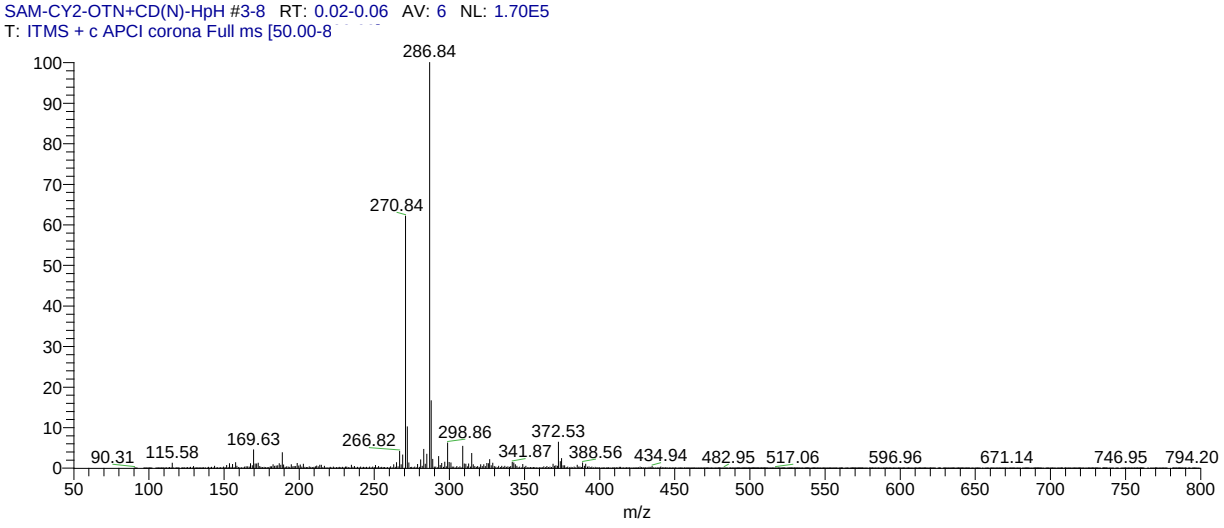


Figure C.25. The ESI Spectrum of Cy_2-Otn/Cd(II) Reaction (Method D3)

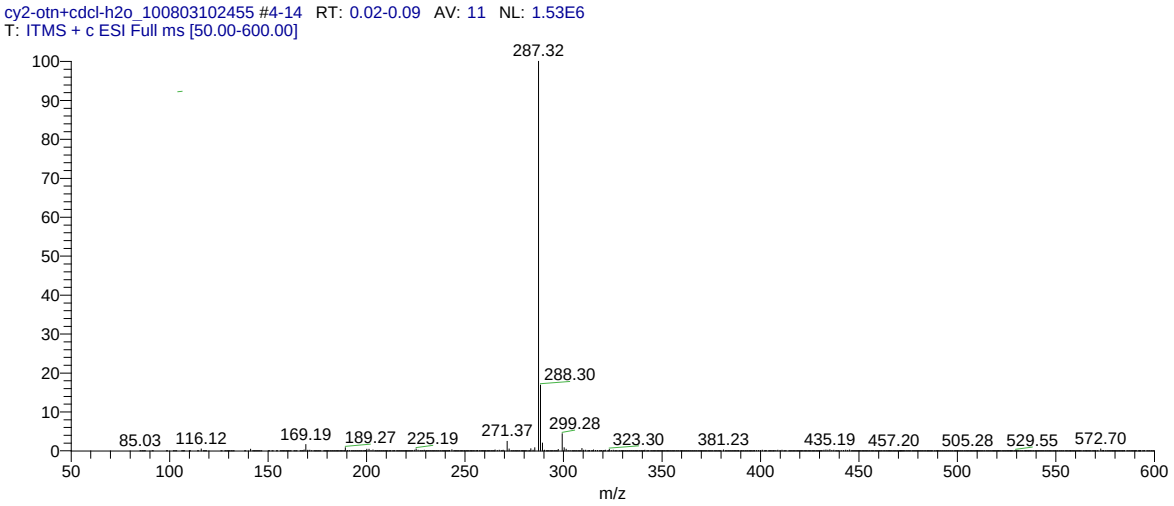


Figure C.26. The ESI Spectrum of Cy_2-Otn/Cd(II) Reaction (Method D4)

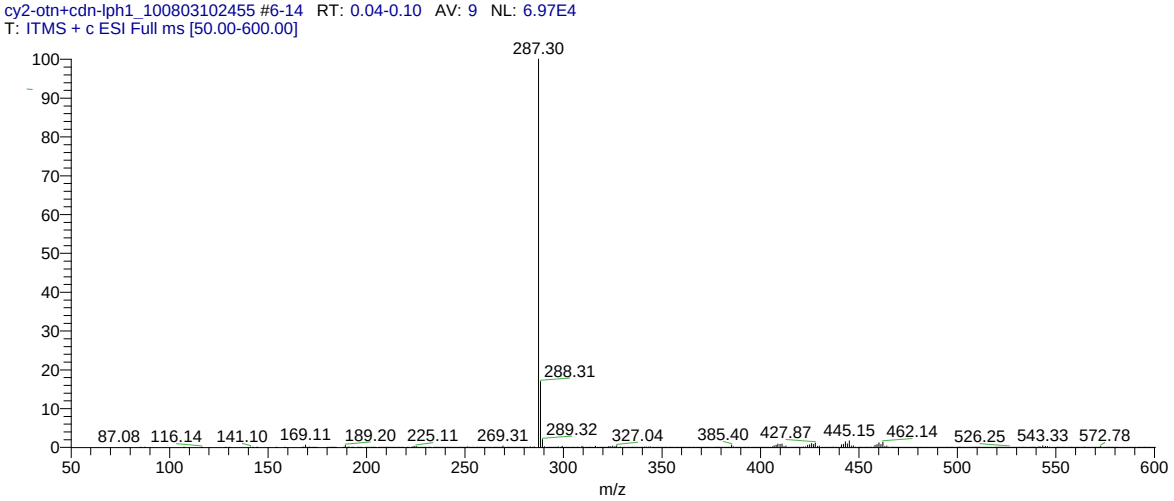


Figure C.27. The APCI Spectrum of Cy_2-Otn/Pb(II) Reaction (Method E1)

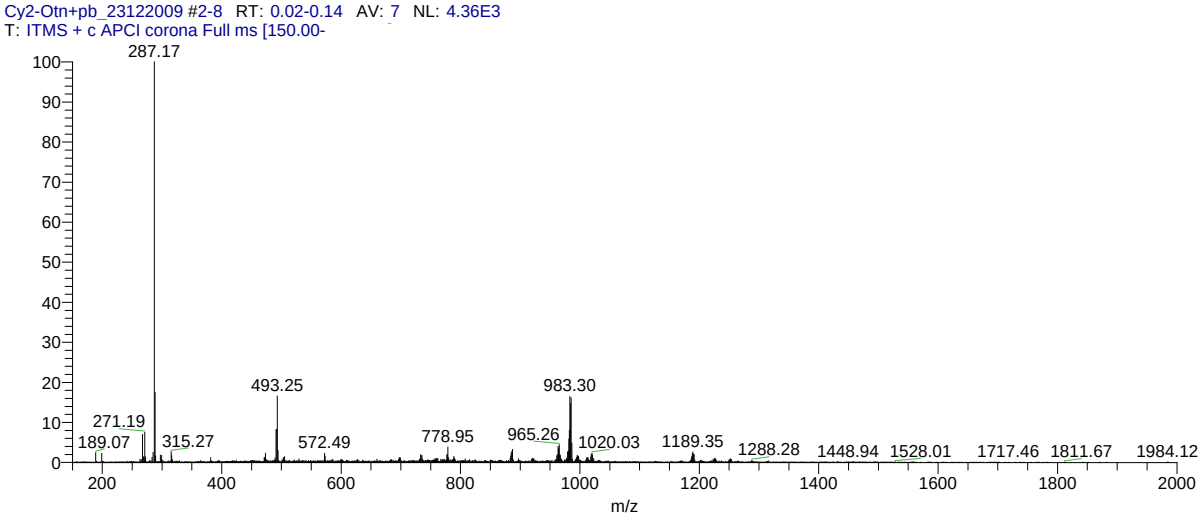


Figure C.28. The ESI Spectrum of Cy_2-Otn/Pb(II) Reaction (Method E2)

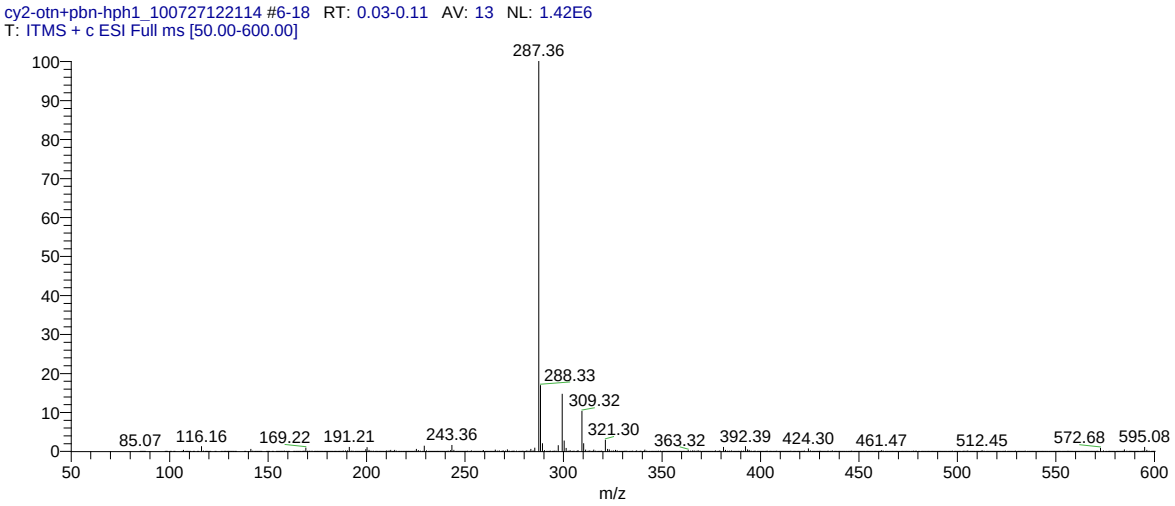


Figure C.29. The ESI Spectrum of Cy_2-tn/Cu(II) Reaction (Method F1)

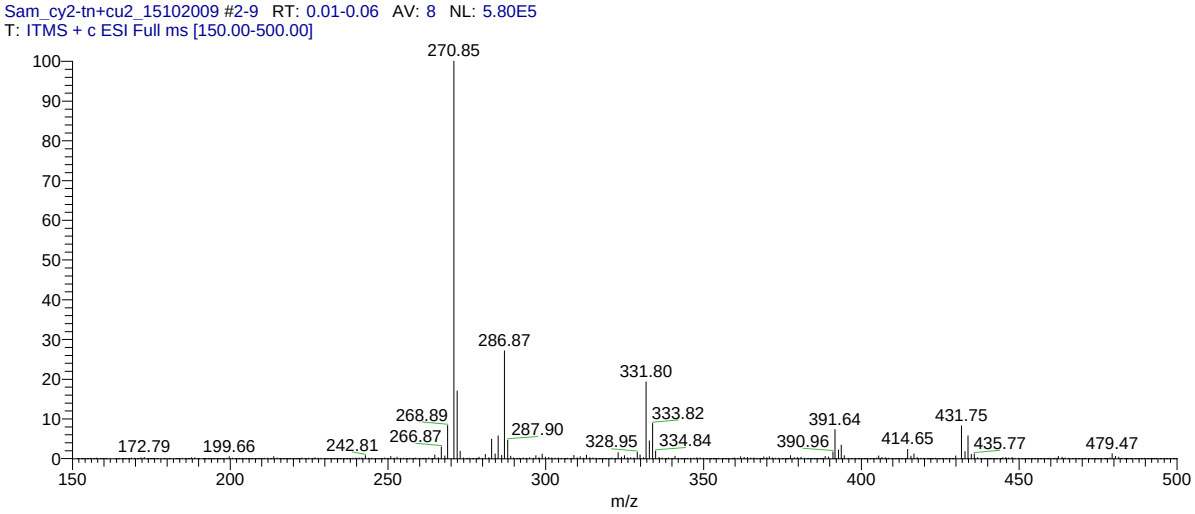


Figure C.30. The ESI Spectrum of Cy_2-tn/Cu(II) Reaction (Method F2)

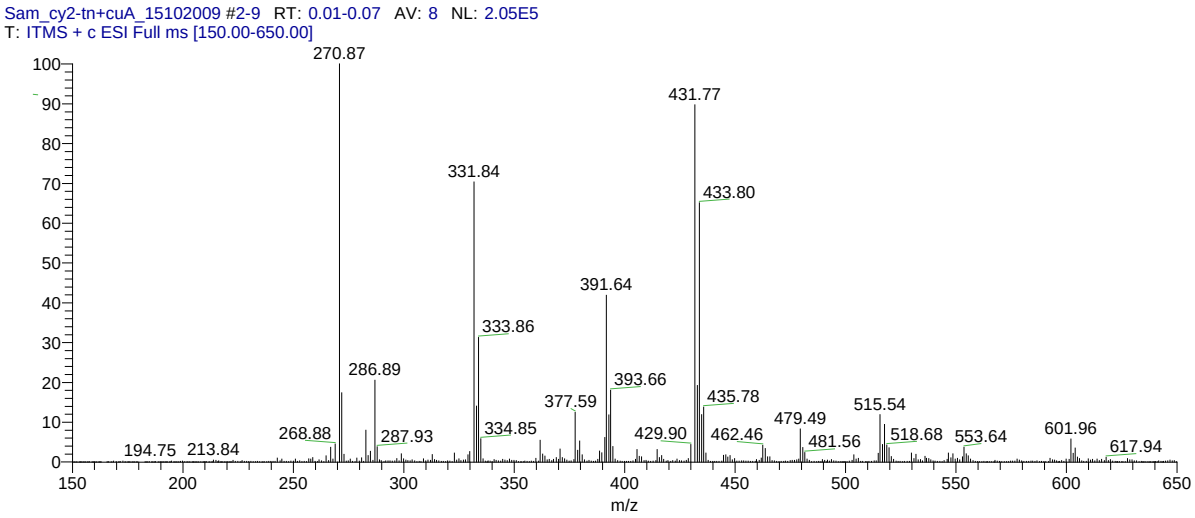


Figure C.31. The APCI Spectrum of Cy_2-tn/Cu Reaction (Method F3)

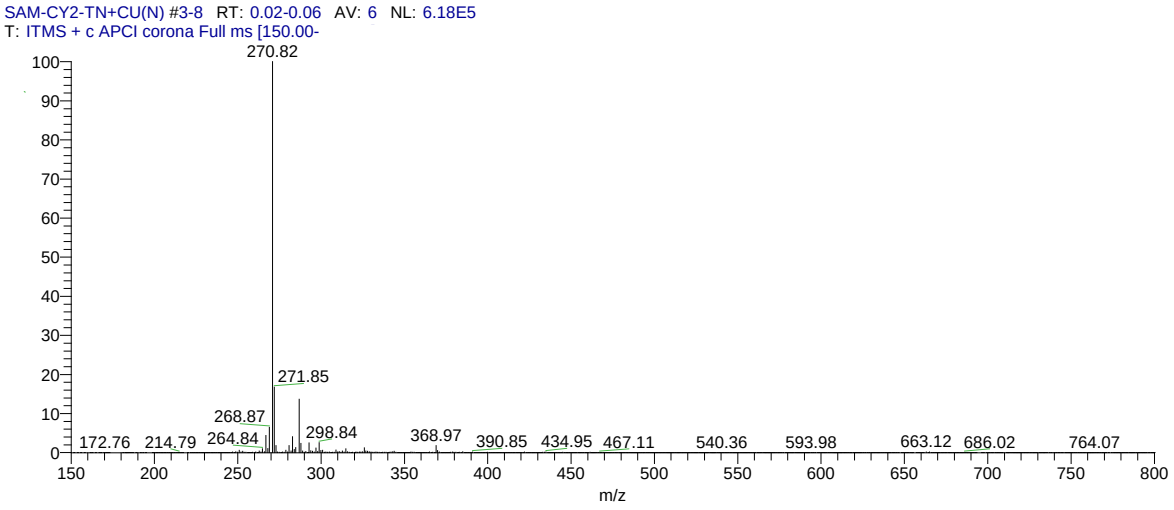


Figure C.32. The ESI Spectrum of Cy_2-tn/Ni(II) Reaction (Method G1)

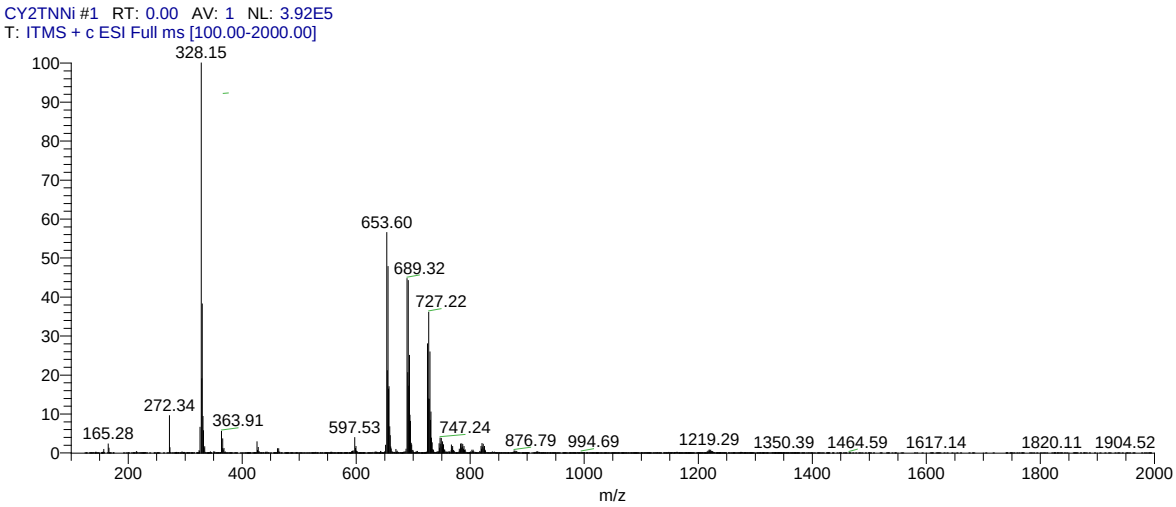


Figure C.33. The ESI Spectrum of Cy_2-tn/Ni(II) Reaction (Method G2)

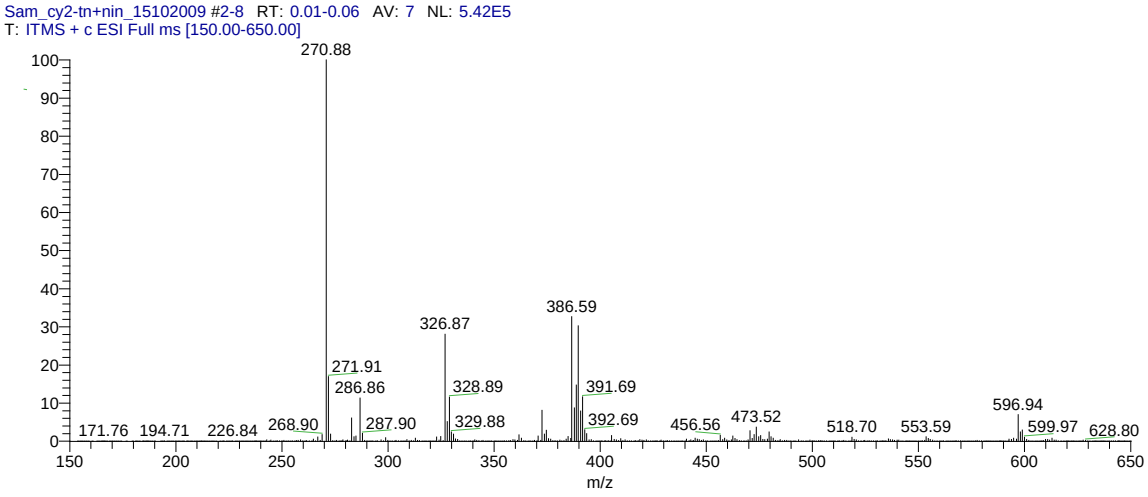


Figure C.34. The ESI Spectrum of Cy_2-tn/Ni(II) Reaction (Method G3)

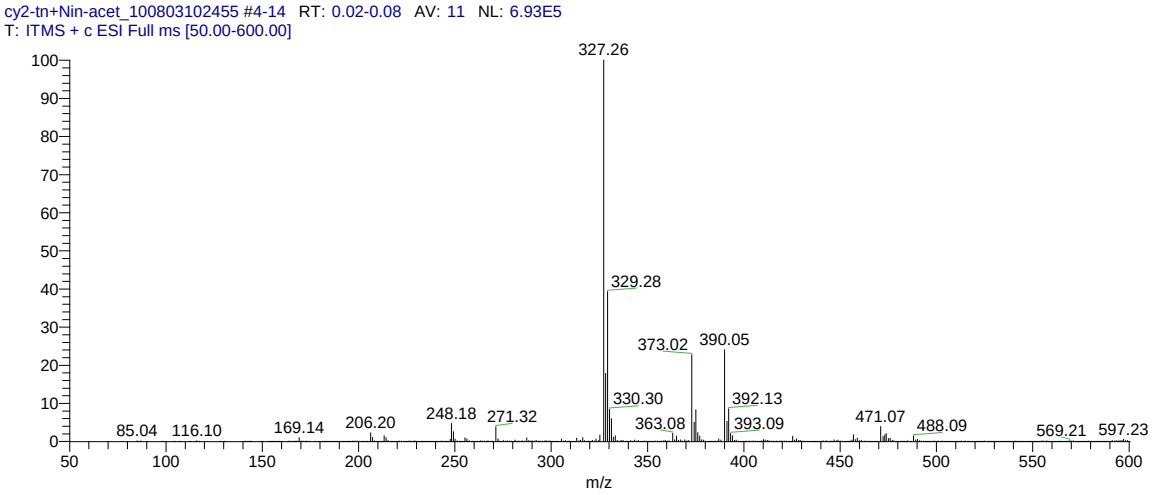


Figure C.35. The APCI Spectrum of Cy_2-tn/Zn(II) Reaction (Method H1)

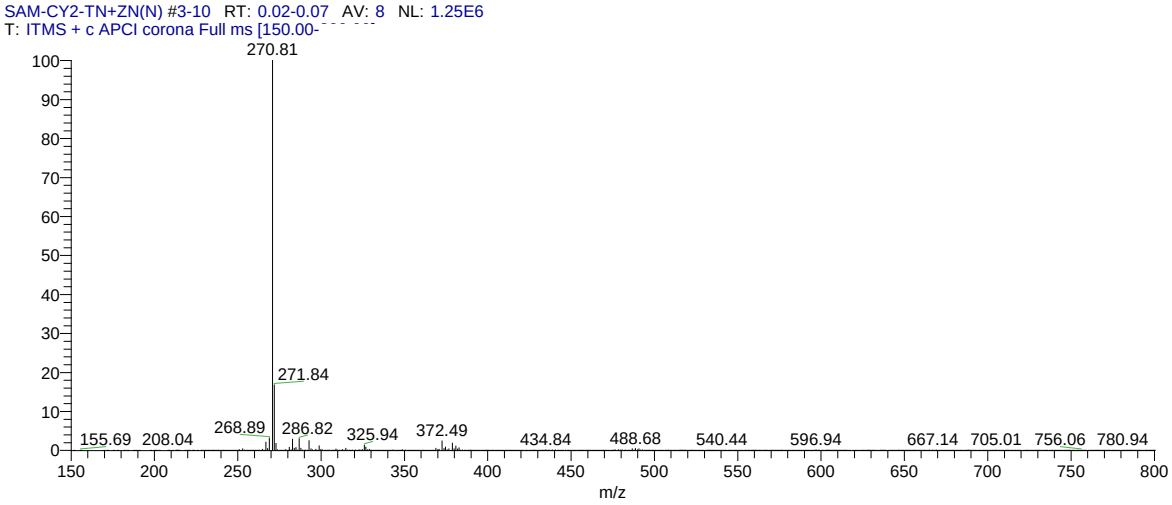


Figure C.36. The ESI Spectrum of Cy_2-tn/Zn(II) Reaction (Method H2)

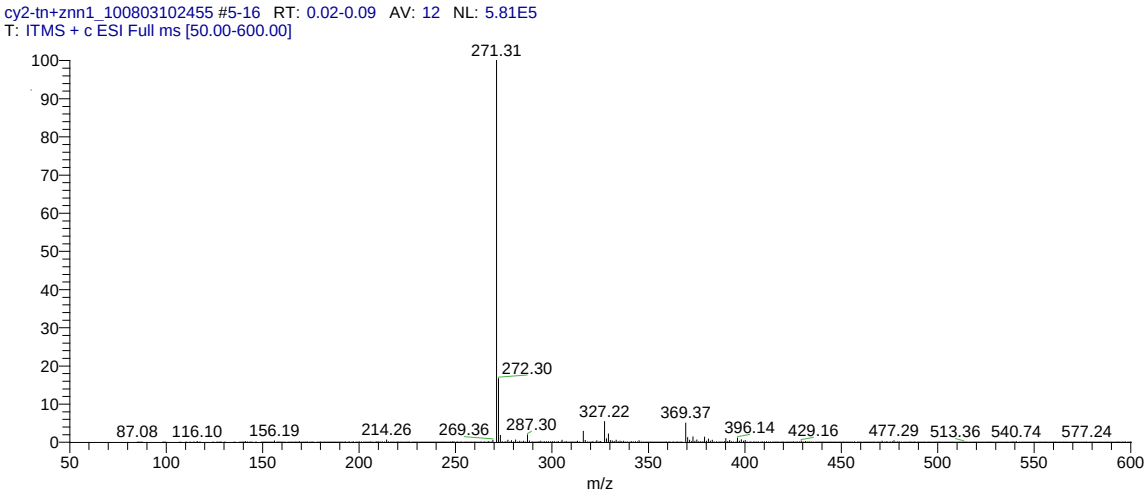


Figure C.37. The ESI Spectrum of Cy_2-tn/Zn(II) Reaction (Method H3)

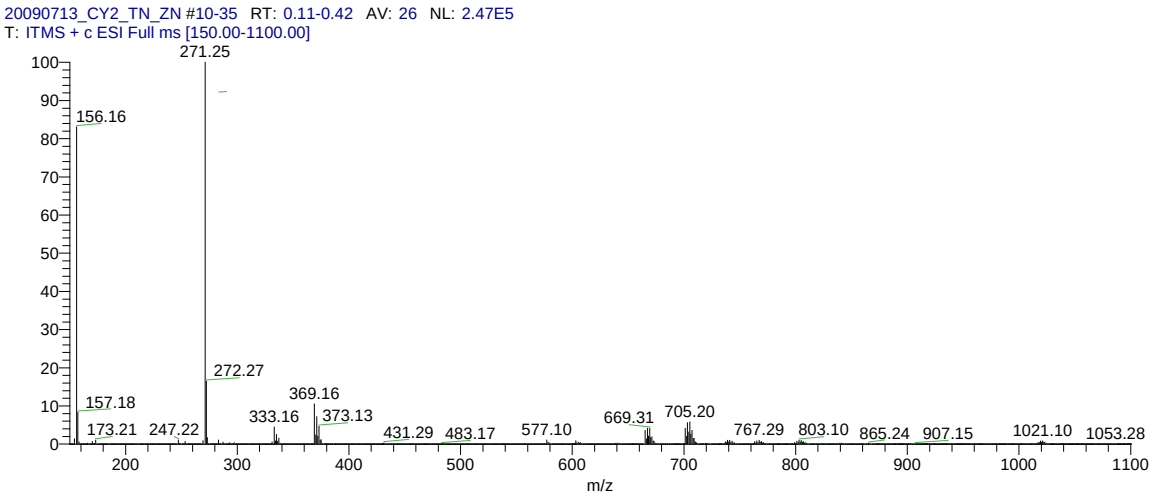


Figure C.38. The APCI Spectrum of Cy_2-tn/Cd(II) Reaction (Method I1)

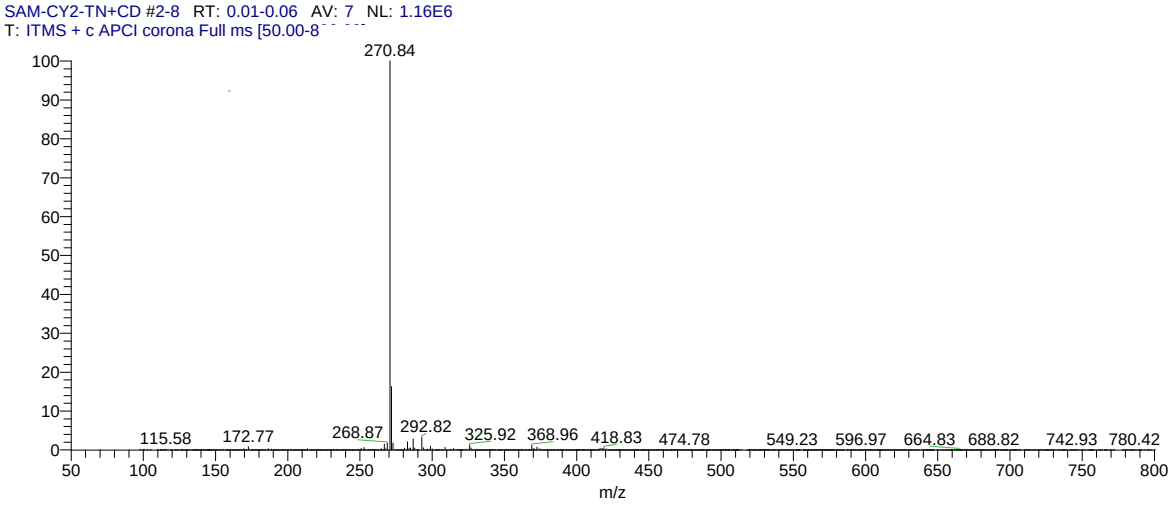


Figure C.39. The ESI Spectrum of Cy_2-tn/Cd(II) Reaction (Method I2)

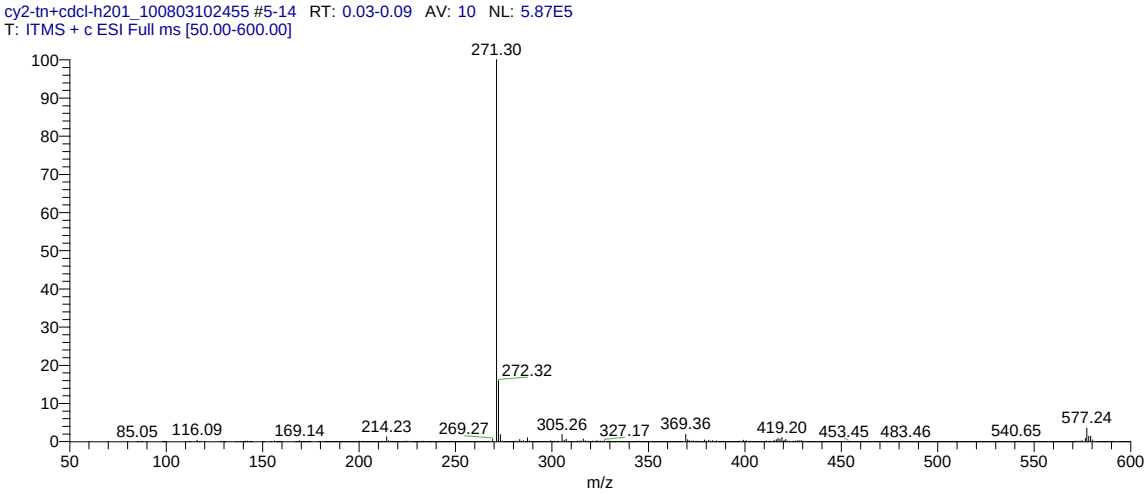


Figure C.40. The ESI Spectrum of Cy_2-tn/Cd(II) Reaction (Method I3)

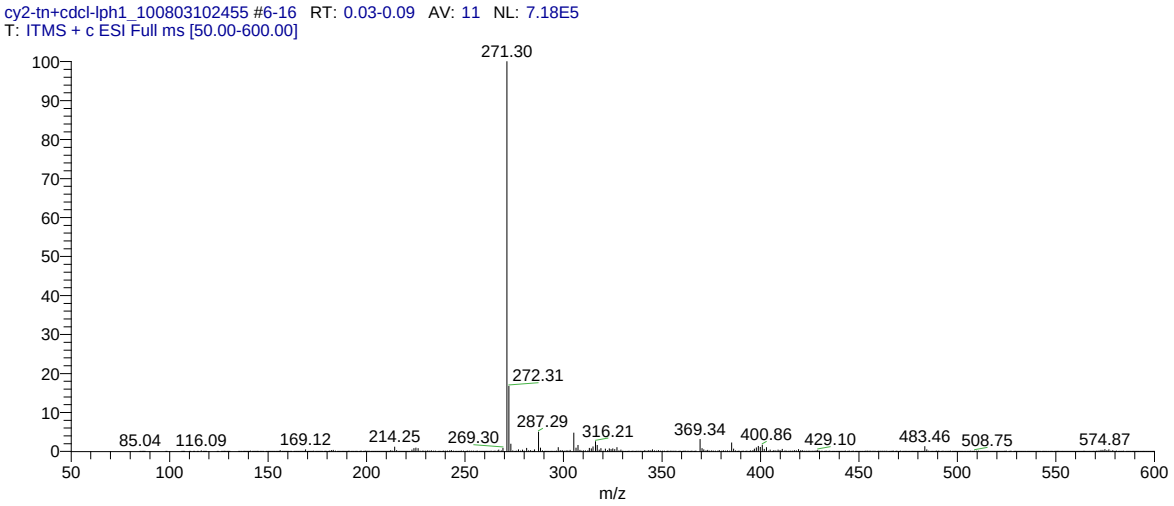


Figure C.41. The APCI Spectrum of Cy_2-tn/Cd(II) Reaction (Method I4)

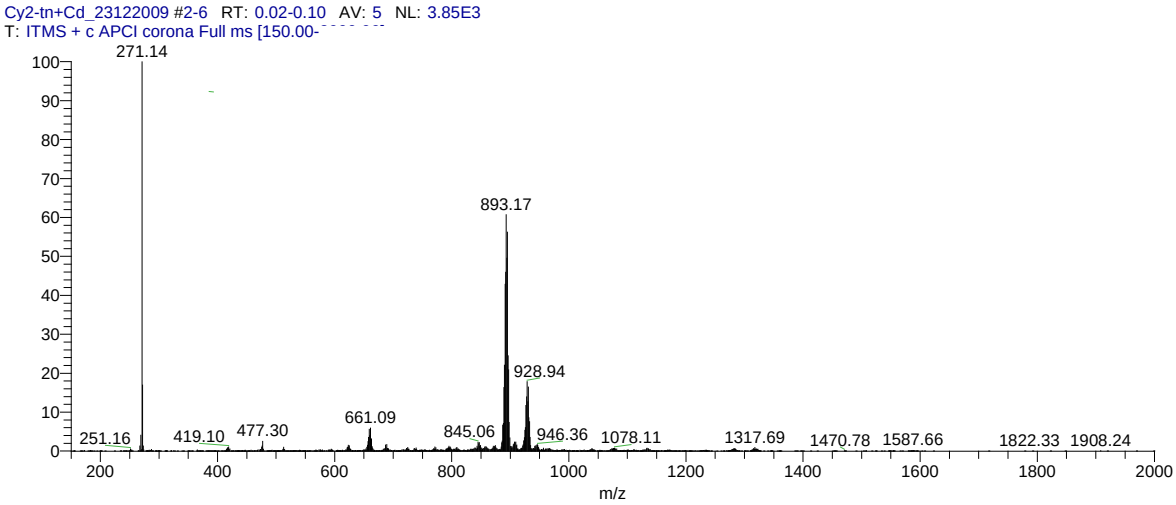


Figure C.42. The ESI Spectrum of Cy_2-tn/Pb(II) Reaction (Method J1)

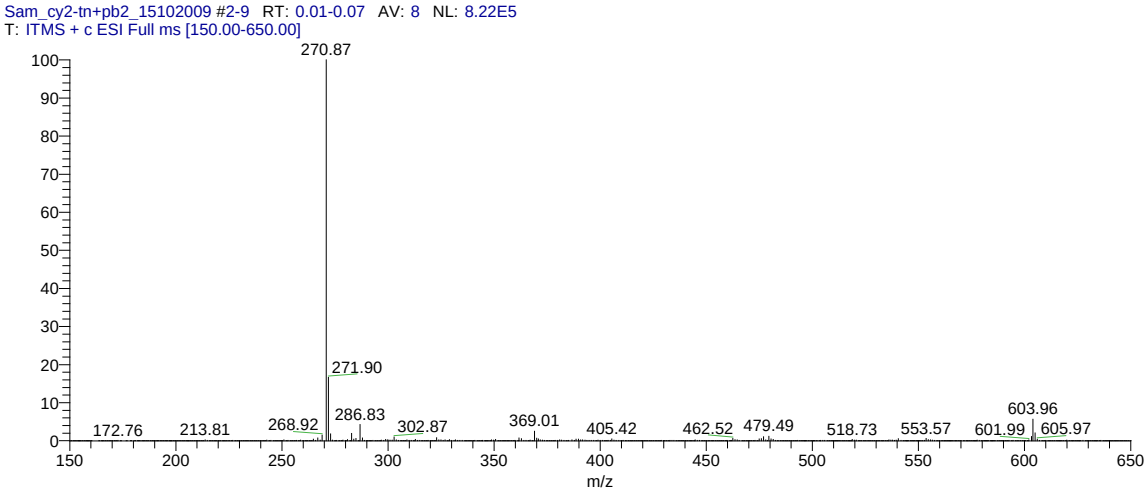
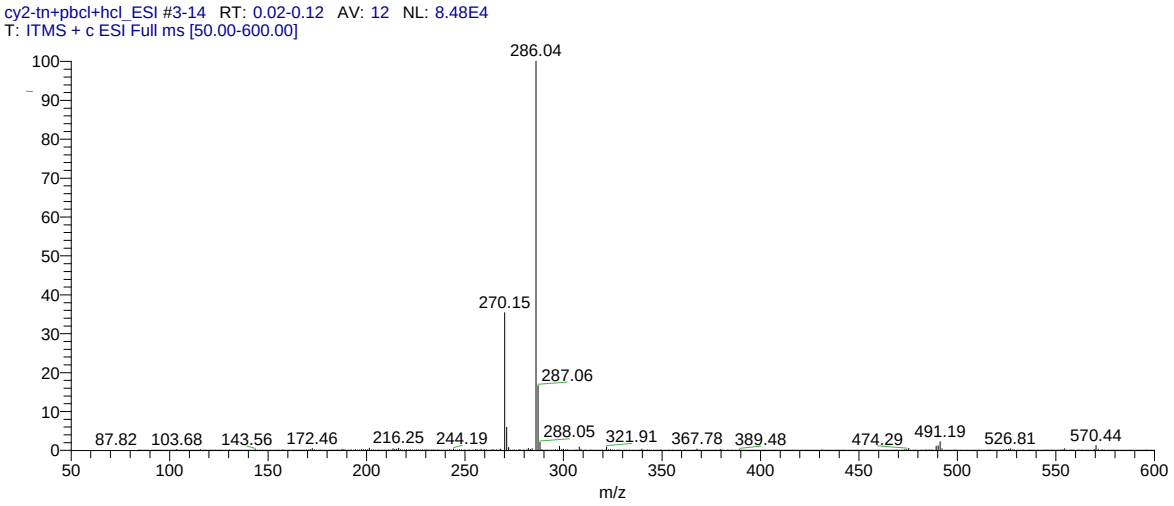


Figure C.43. The ESI Spectrum of Cy_2-tn/Pb(II) Reaction (Method J2)



Appendix D – IR Data

All IR data was generated in the manner described in Chapter 2.

Figure D.1. The IR of Cy_2-Otn (L3)

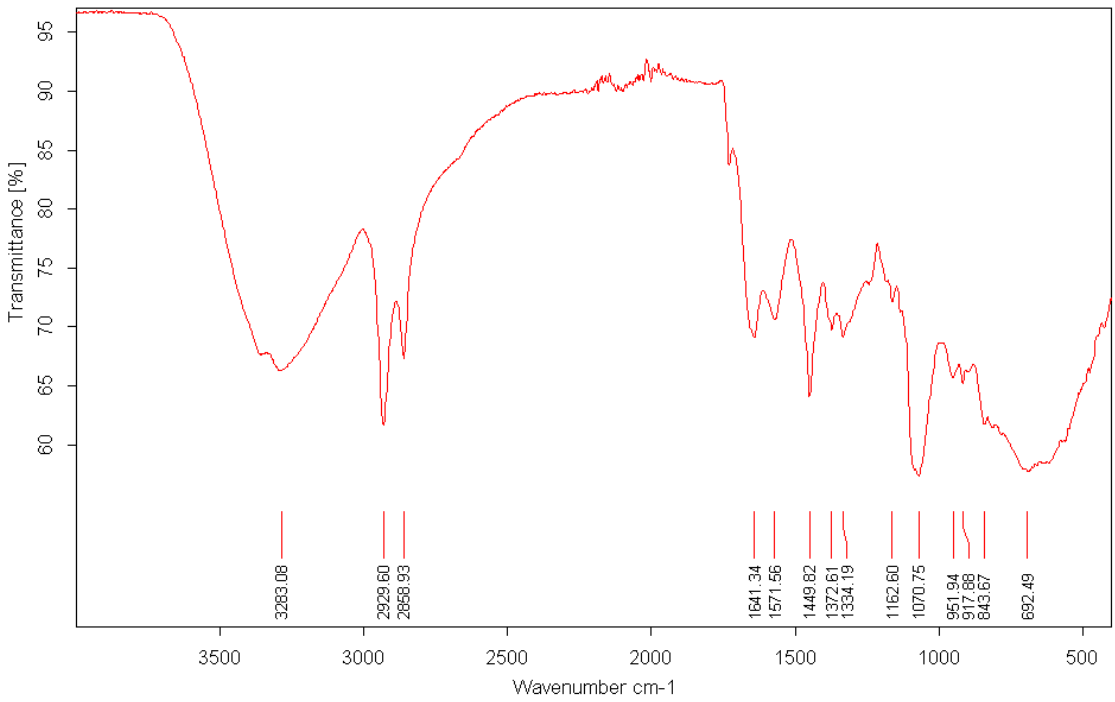


Figure D.2. The IR of Cy_2-Otn (L5)

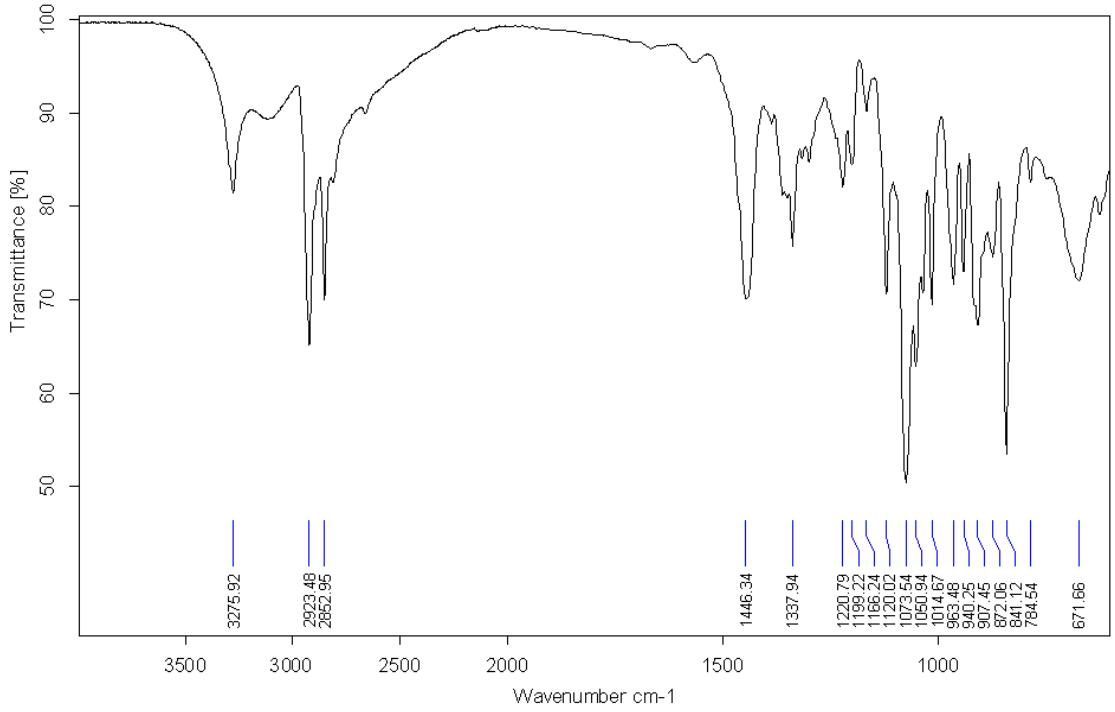


Figure D.3. The IR of Cy_2-Otn (L6)

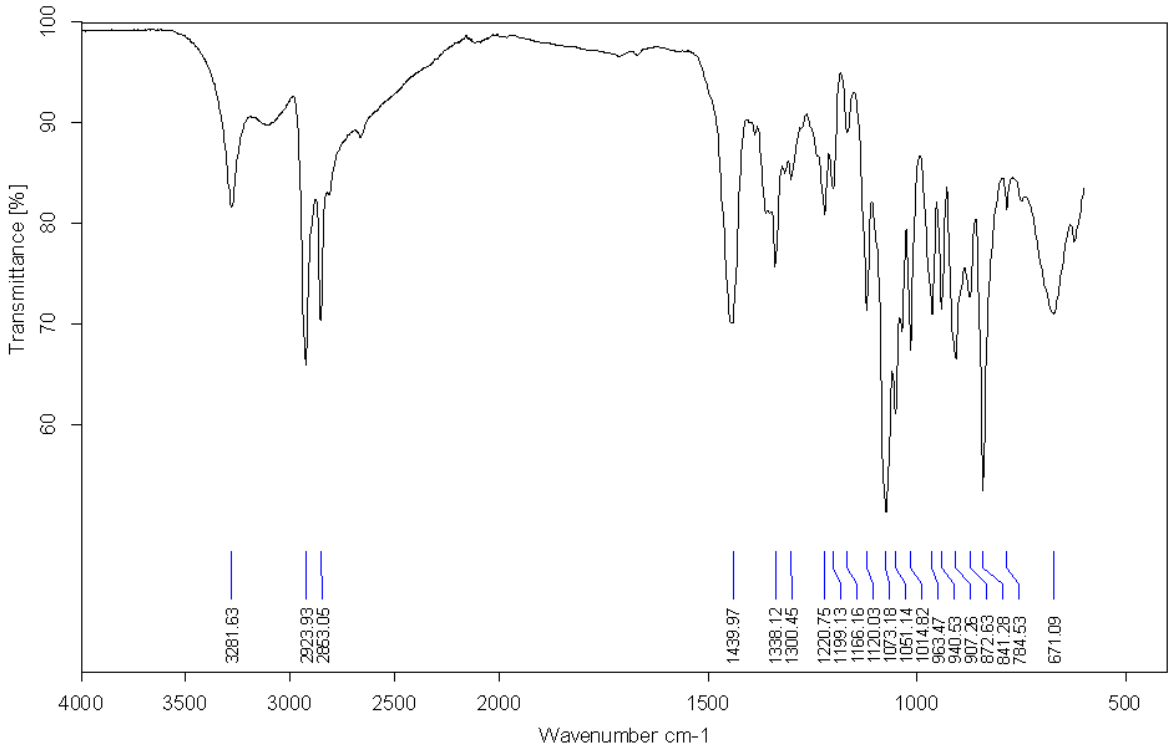


Figure D.4. The IR of Cy_2-Otn (L7)

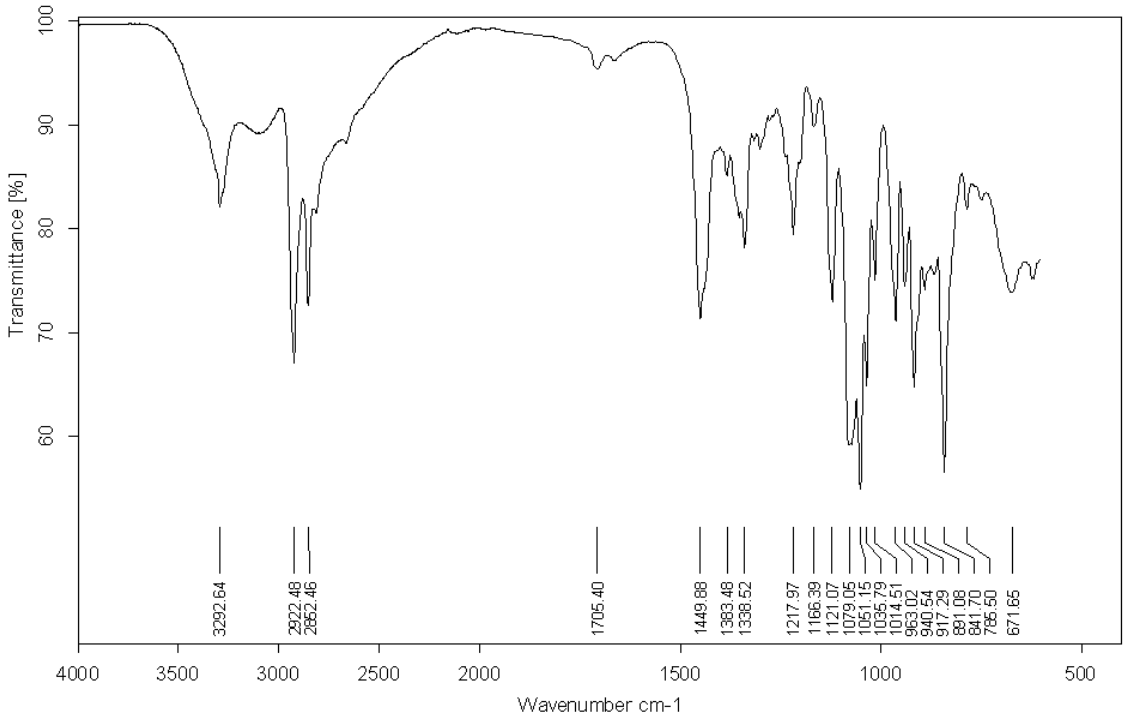


Figure D.5. The IR of Cy_2-Otn (L7c)

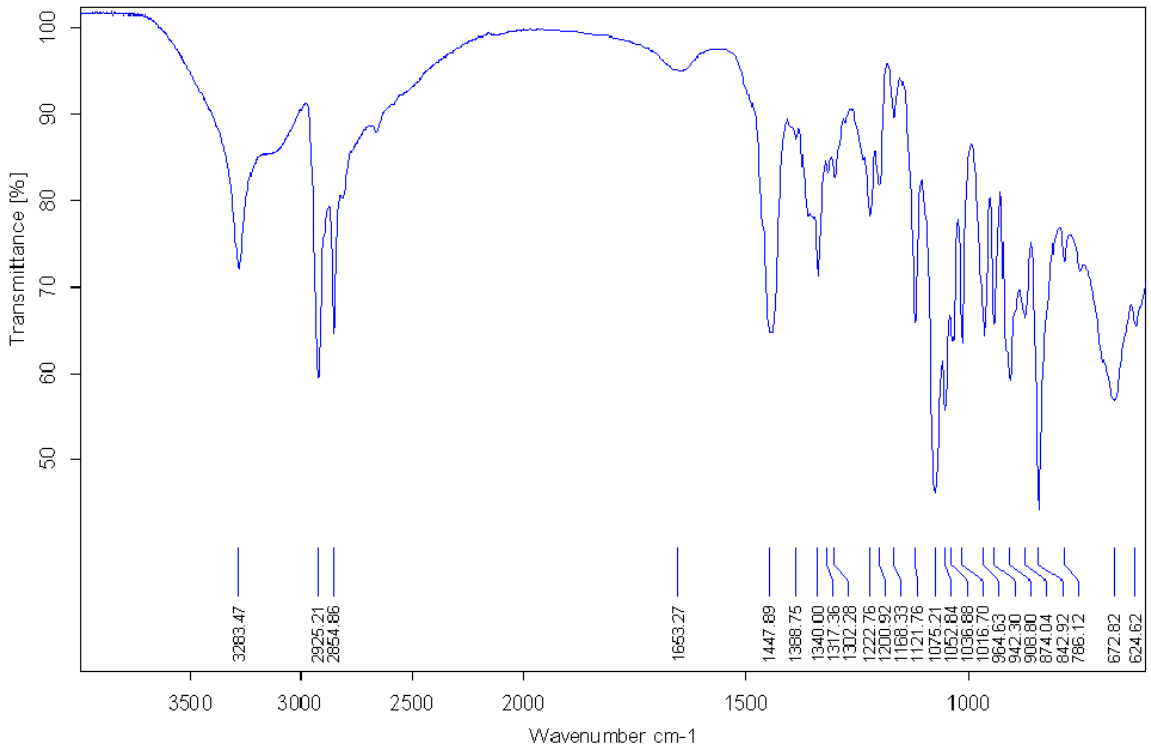


Figure D.6. The IR of Cy_2-Otn (L8)

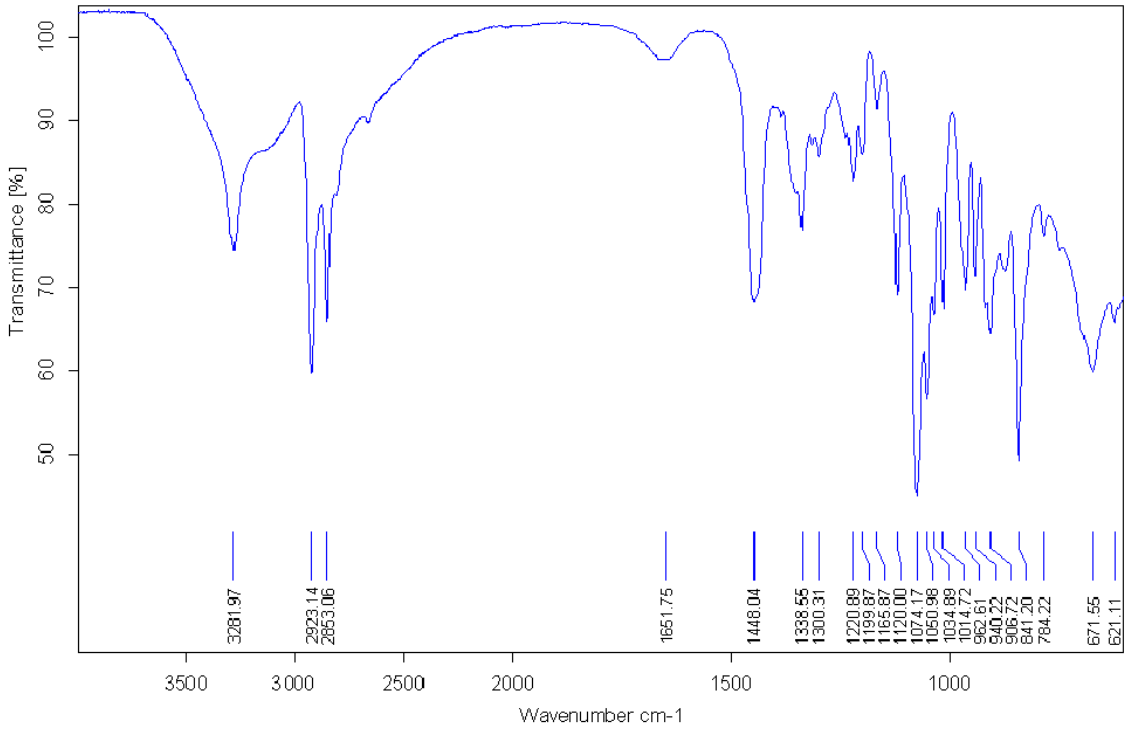


Figure D.7. The IR of Cy_2-Otn (L8c)

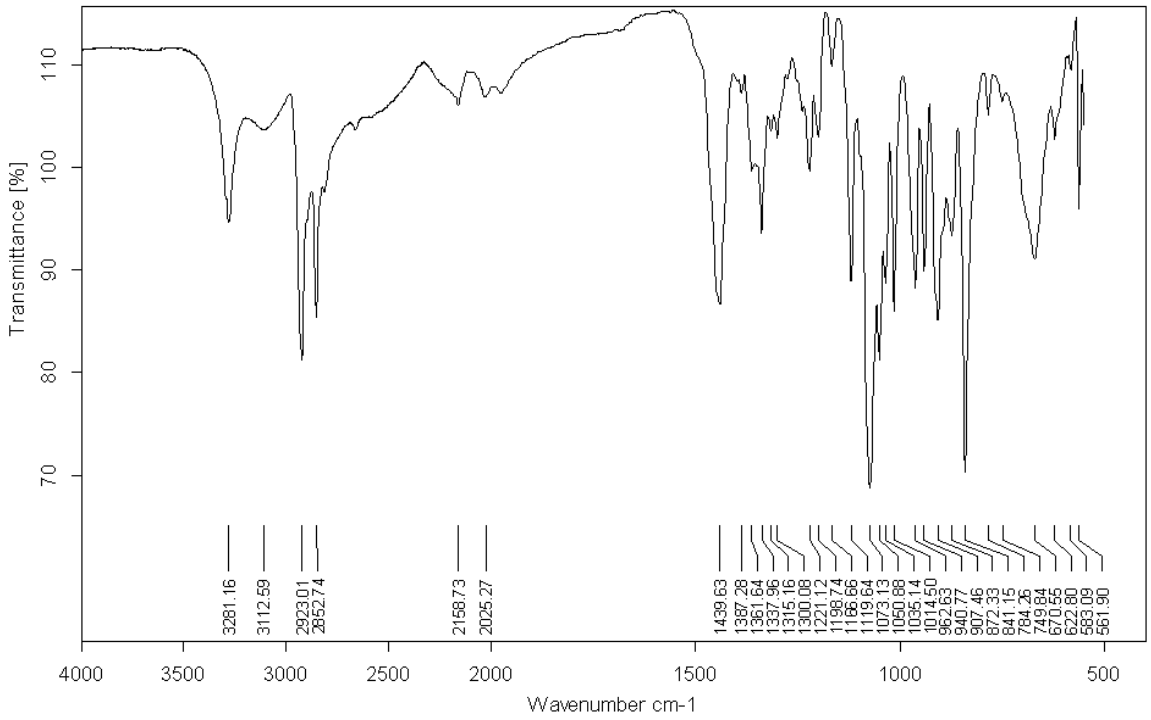


Figure D.8. The IR of Cy_2-tn (2L1)

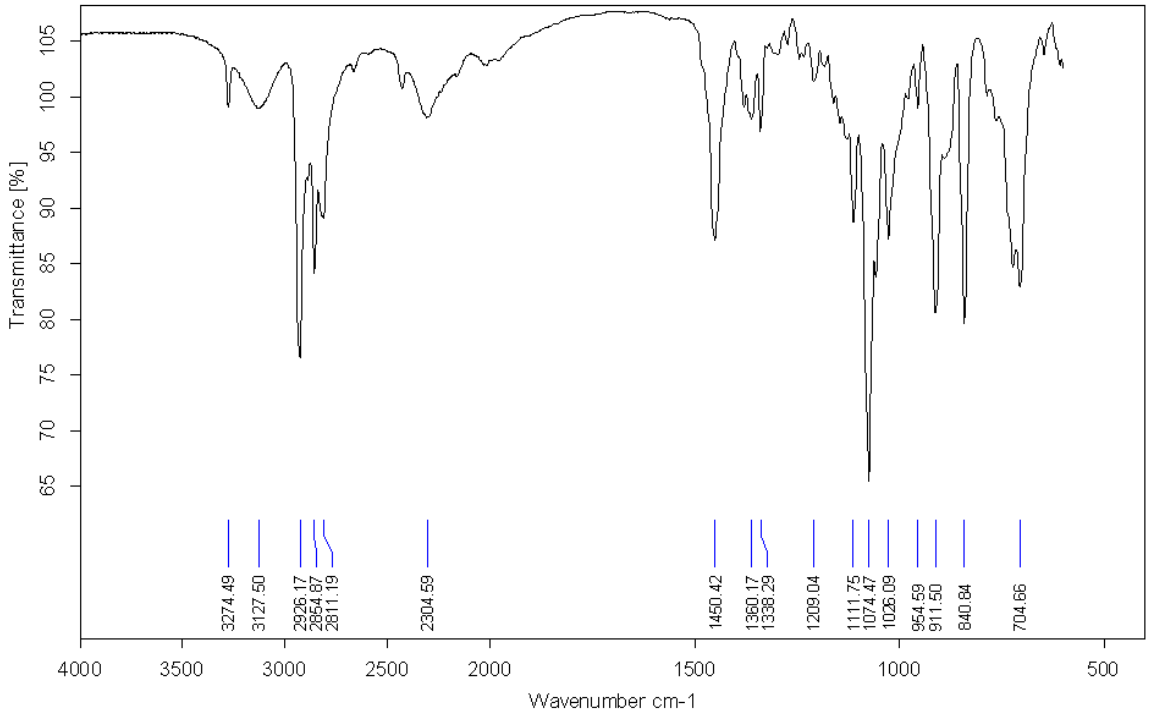


Figure D.9. The IR of Cy_2-tn (2L2)

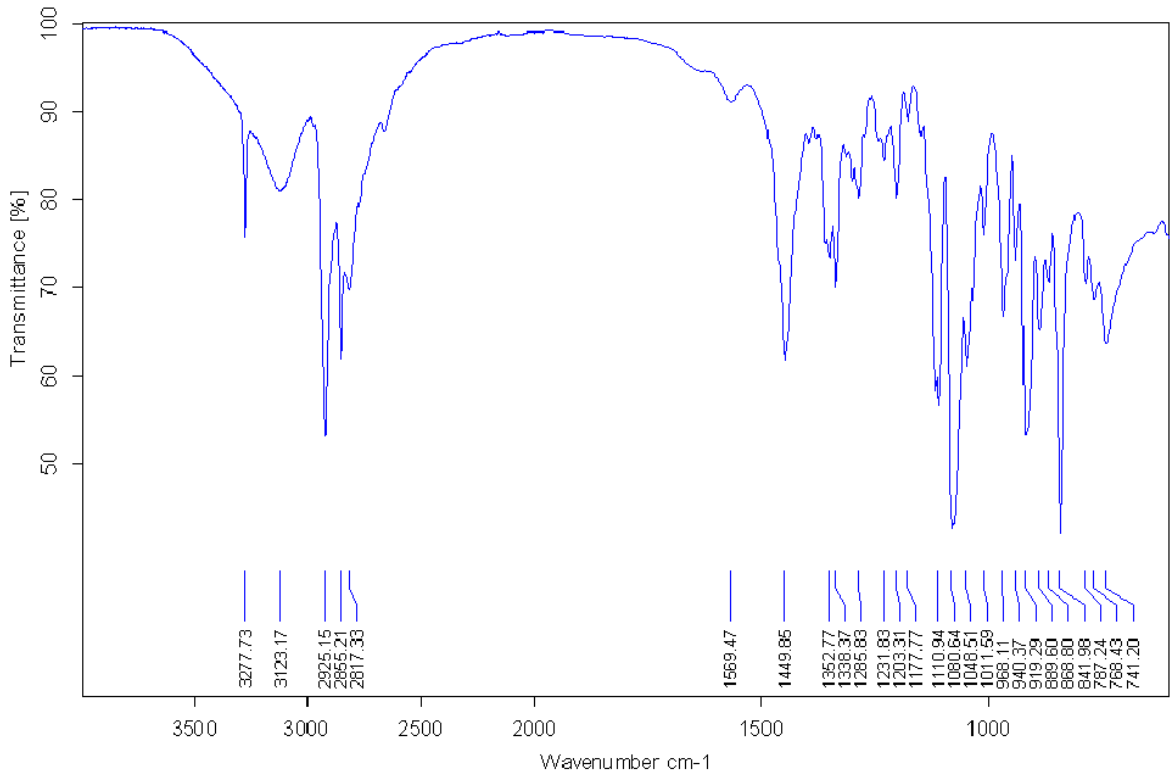


Figure D.10. The IR of Cy_2-tn (2L3)

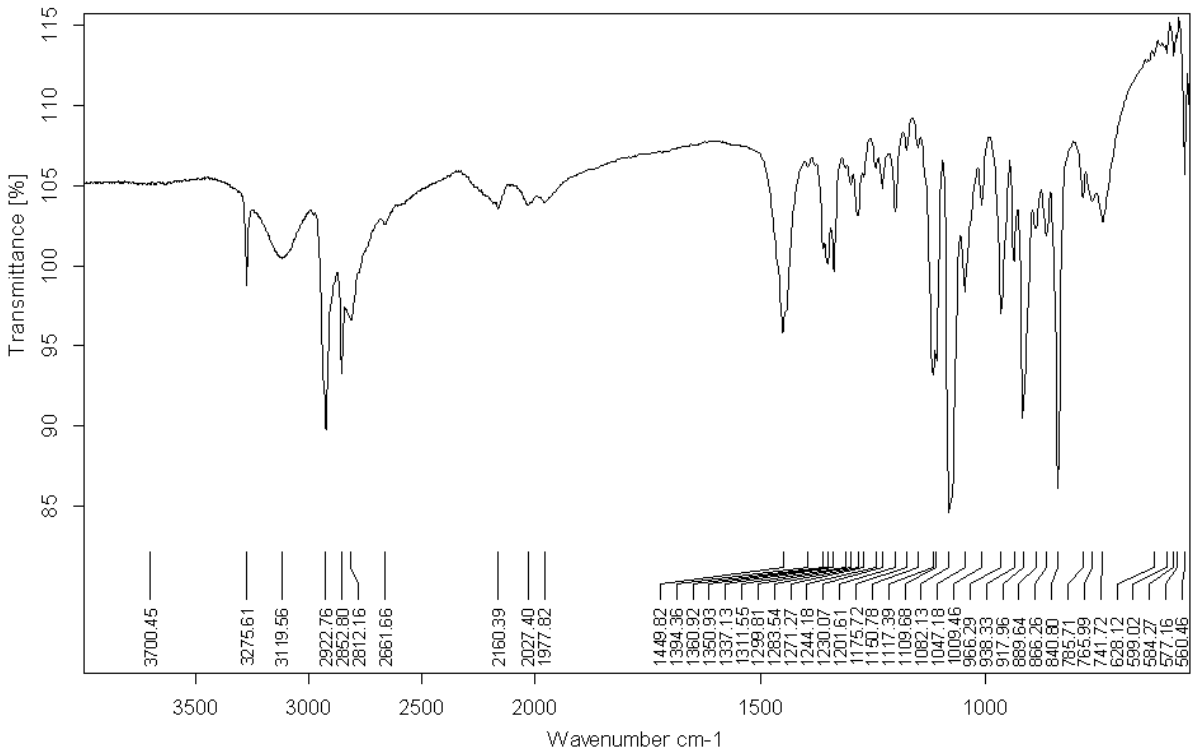


Figure D.11. The IR of Cy_2-Otn/Cu(II) Reaction (Method A1)

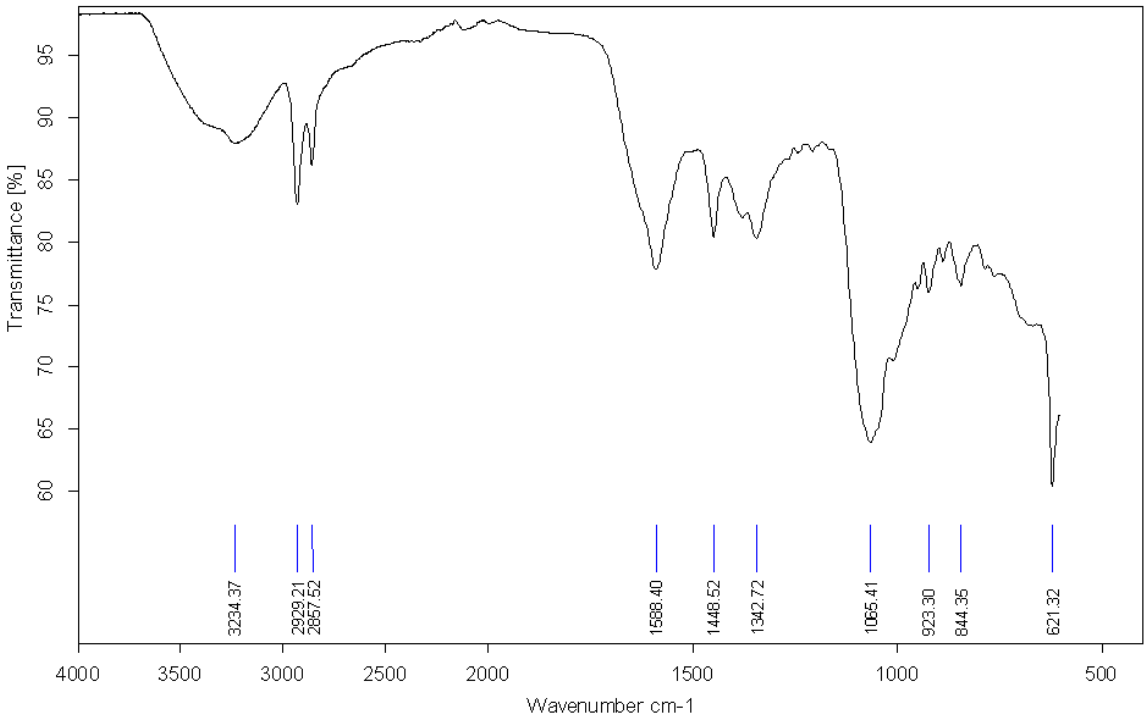


Figure D.12. The IR of Cy_2-Otn/Cu(II) Reaction (Method A2)

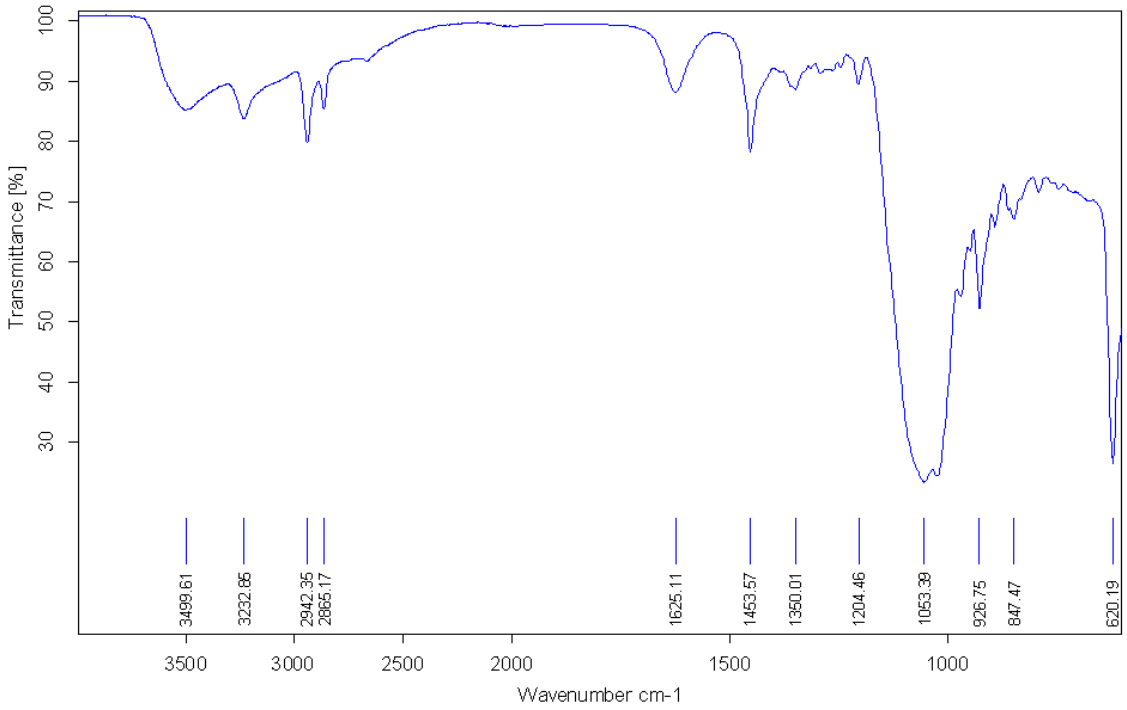


Figure D.13. The IR of Cy_2-Otn/Cu(II) Reaction (Method A3)

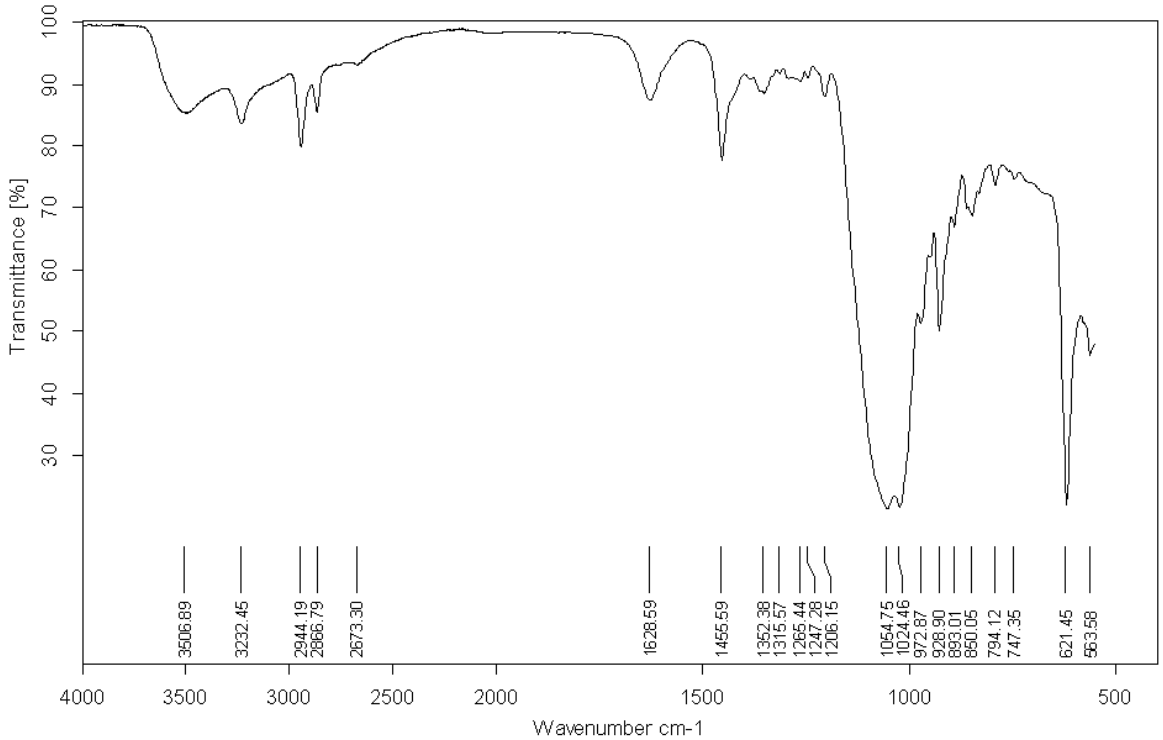


Figure D.14. The IR of Cy_2-Otn/Ni(II) Reaction (Method B1)

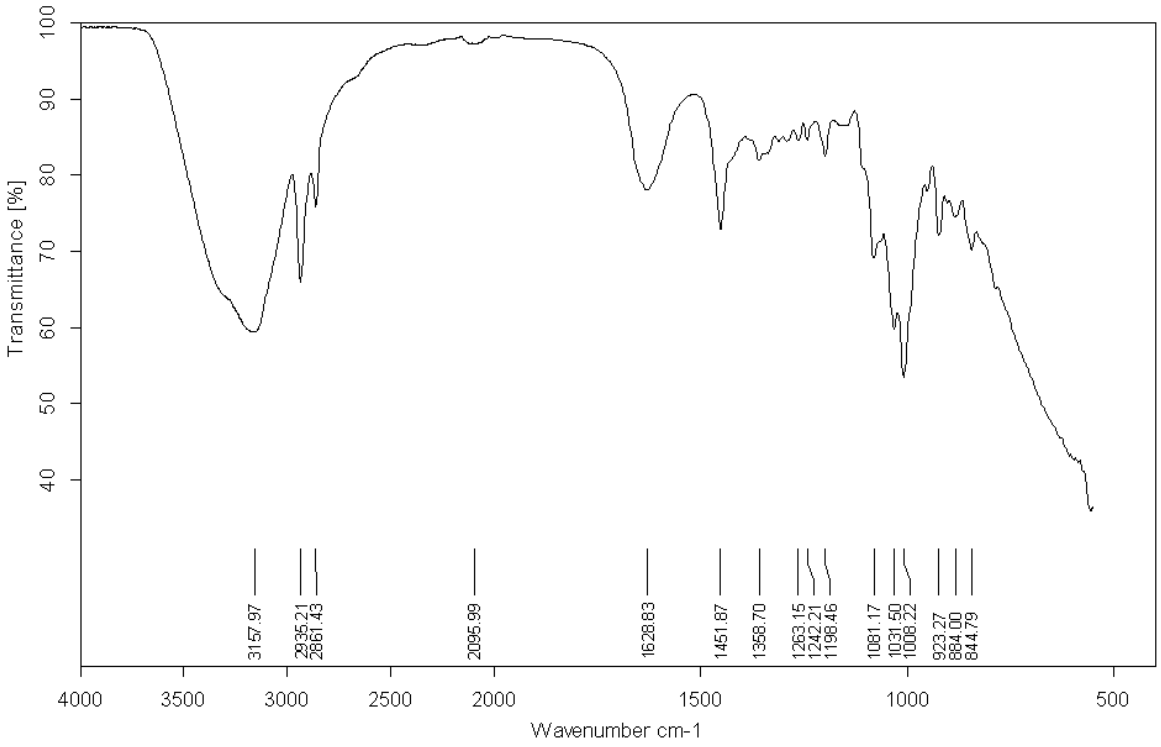


Figure D.15. The IR of Cy_2-Otn/Ni(II) Reaction (Method B2)

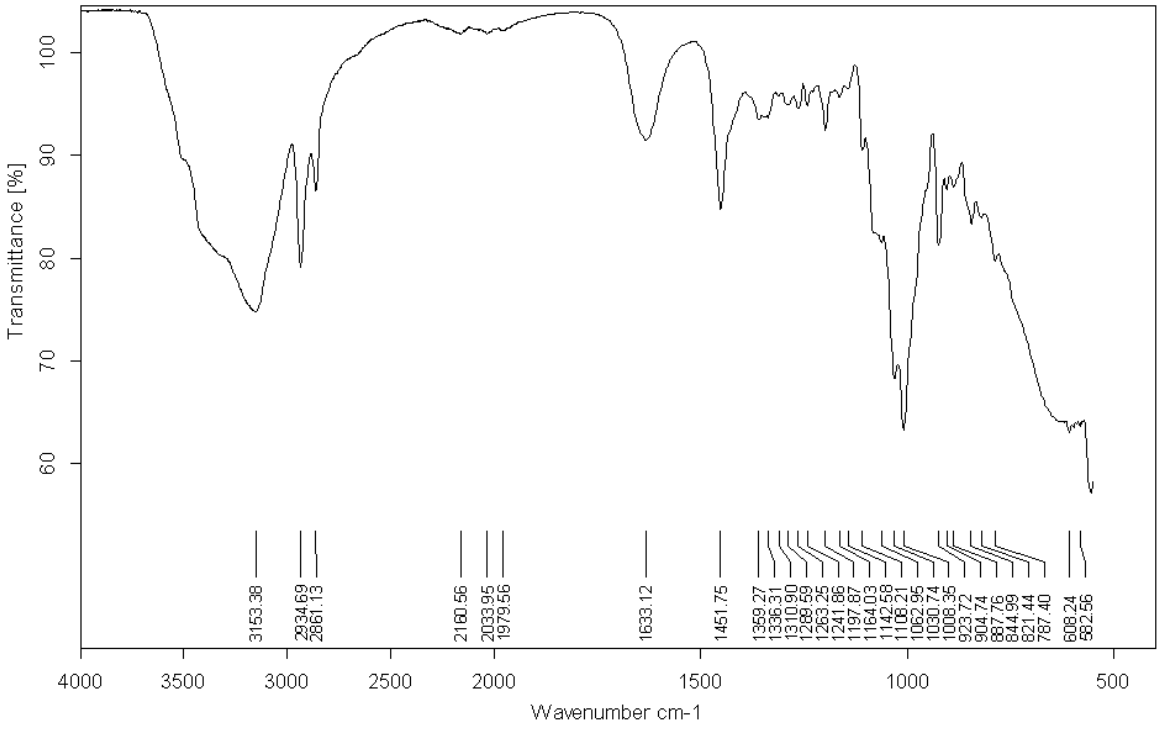


Figure D.16. The IR of Cy_2-Otn/Zn(II) Reaction (Method C1)

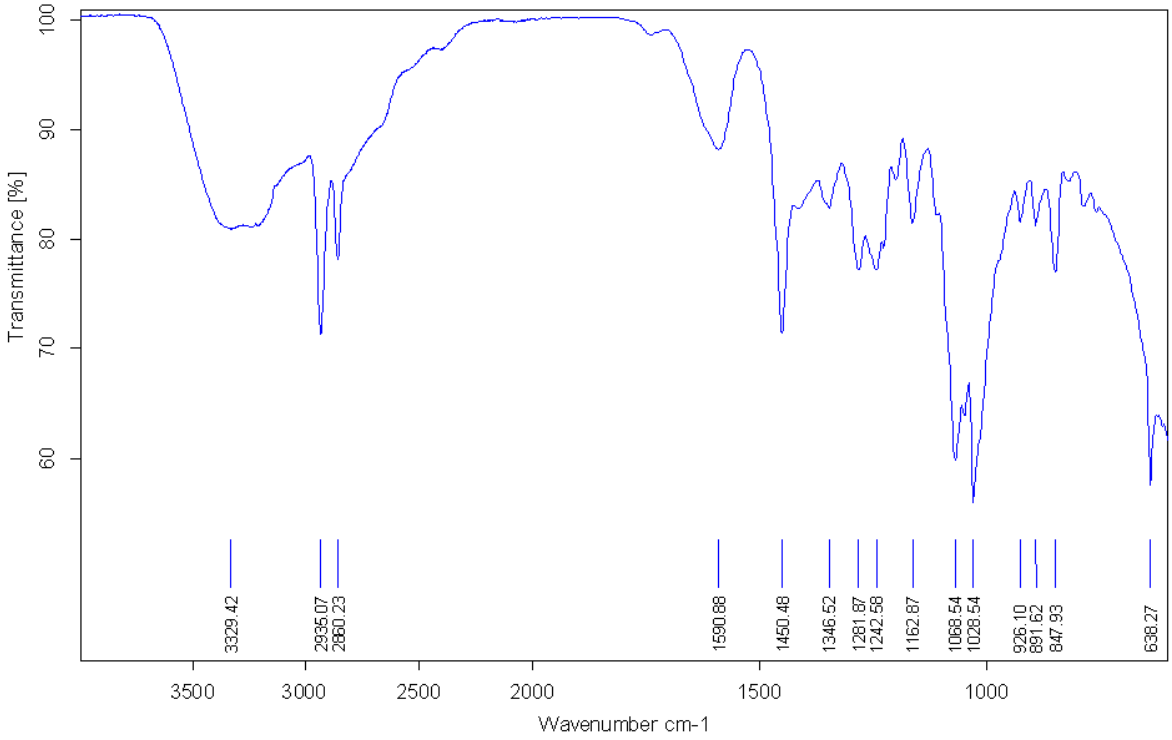


Figure D.17. The IR of Cy_2-Otn/Zn(II) Reaction (Method C2)

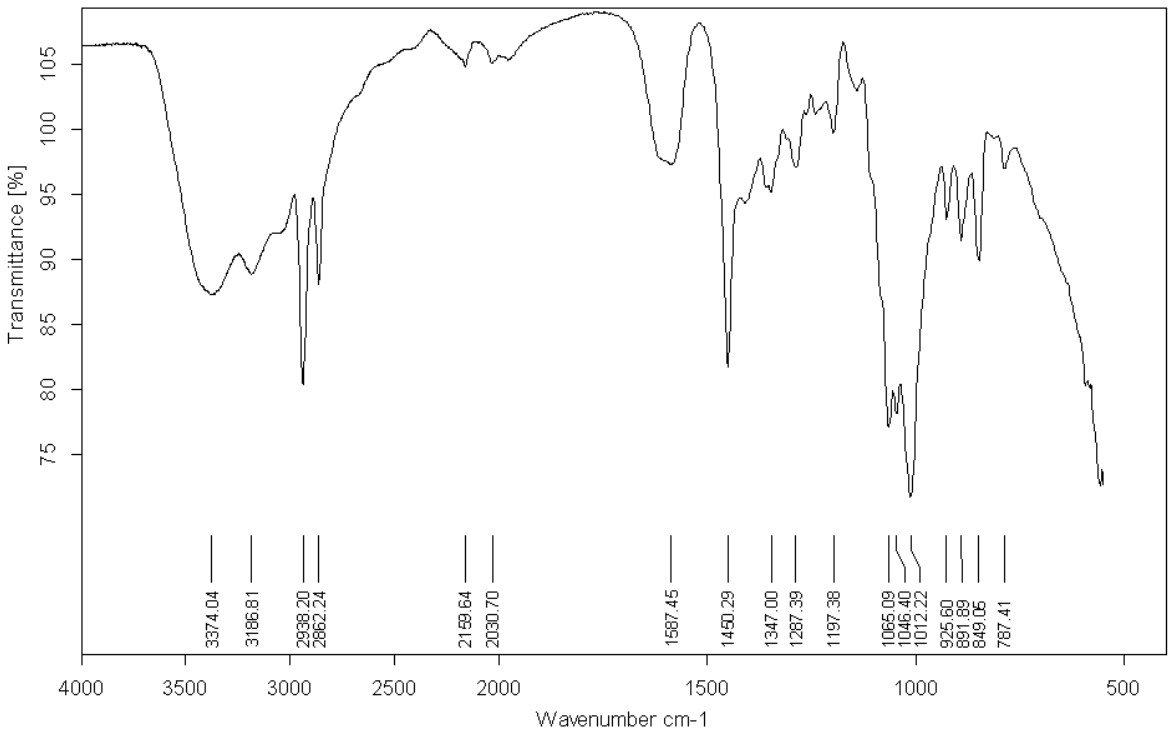


Figure D.18. The IR of Cy_2-Otn/Zn(II) Reaction (Method C3)

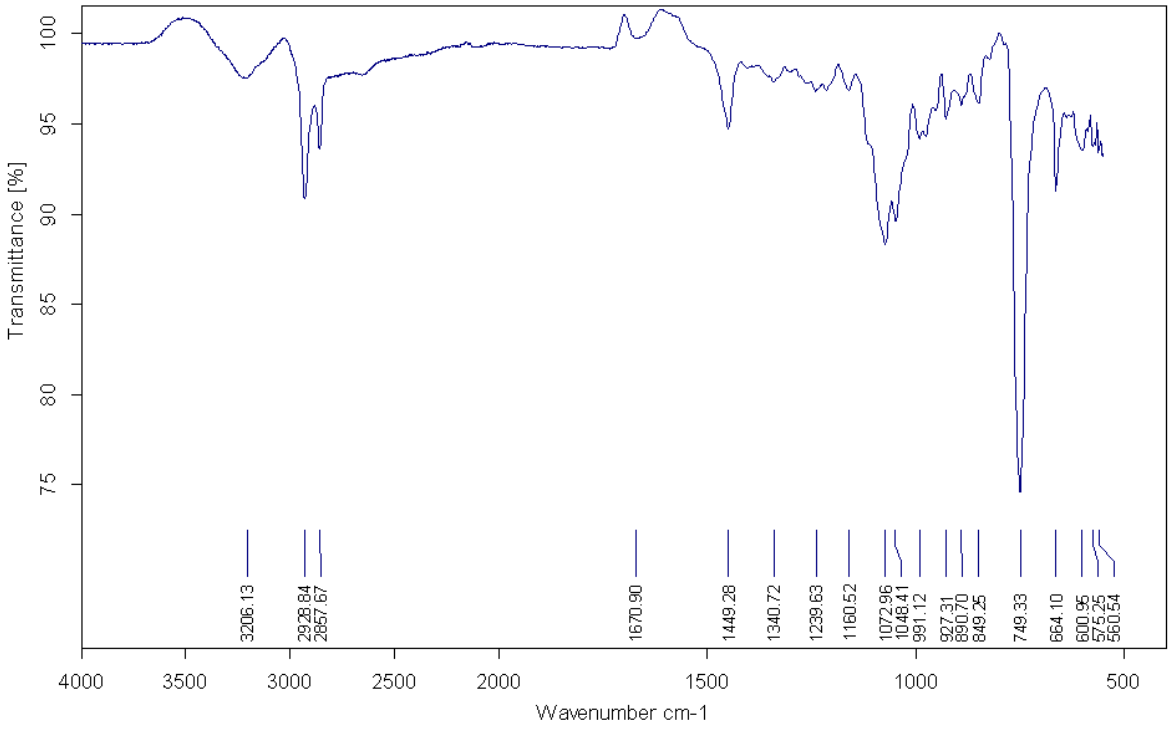


Figure D.19. The IR of Cy_2-Otn/Zn(II) Reaction (Method C4)

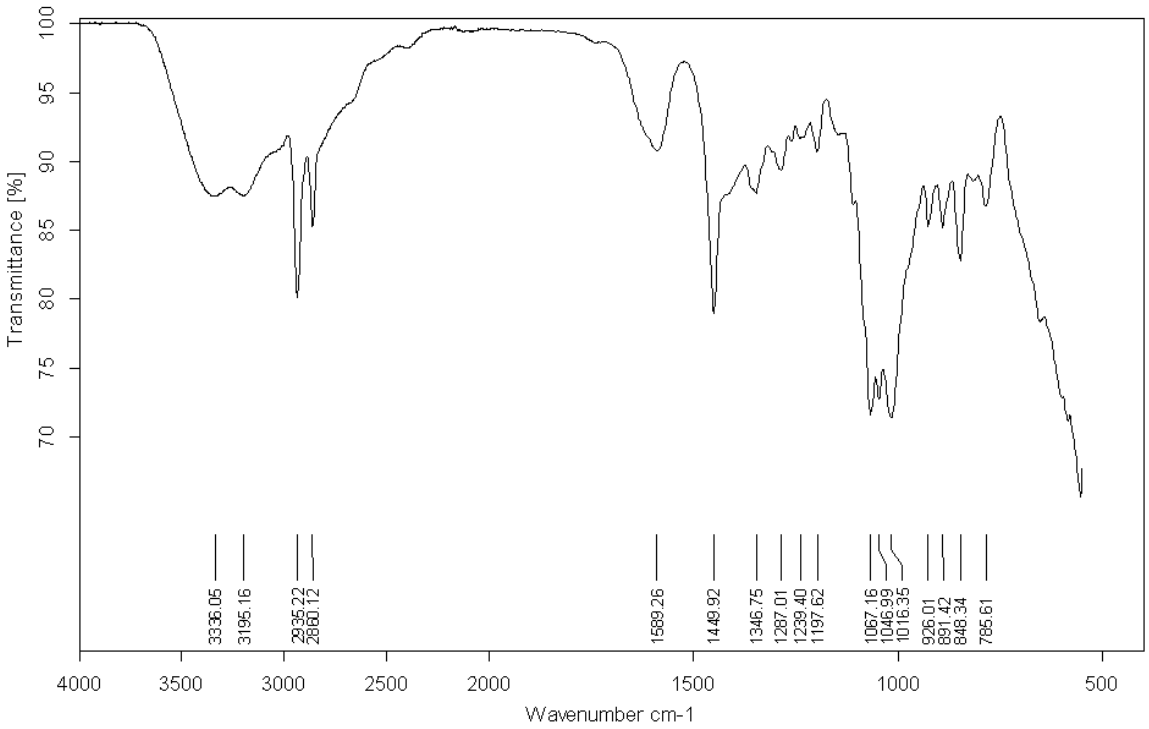


Figure D.20. The IR of Cy_2-Otn/Cd(II) Reaction (Method D1)

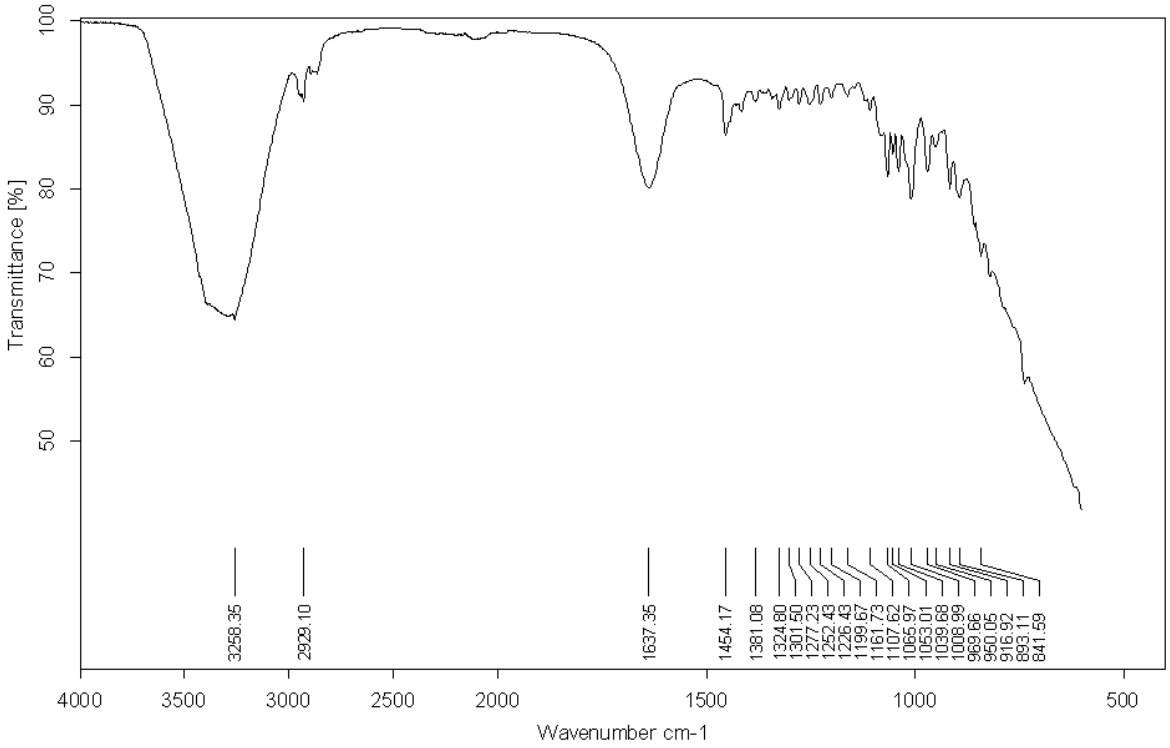


Figure D.21. The IR of the Cy_2-Otn/Cd(II) Reaction (Method D2)

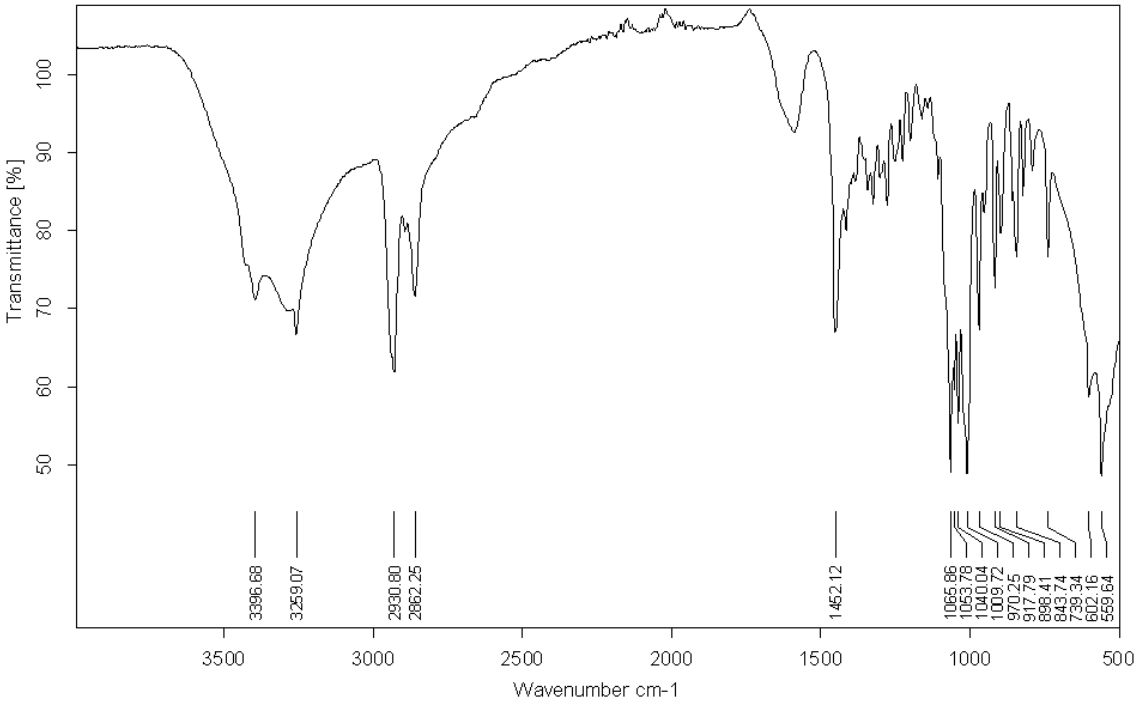


Figure D.22. The IR of Cy_2-Otn/Cd(II) Reaction (Method D3)

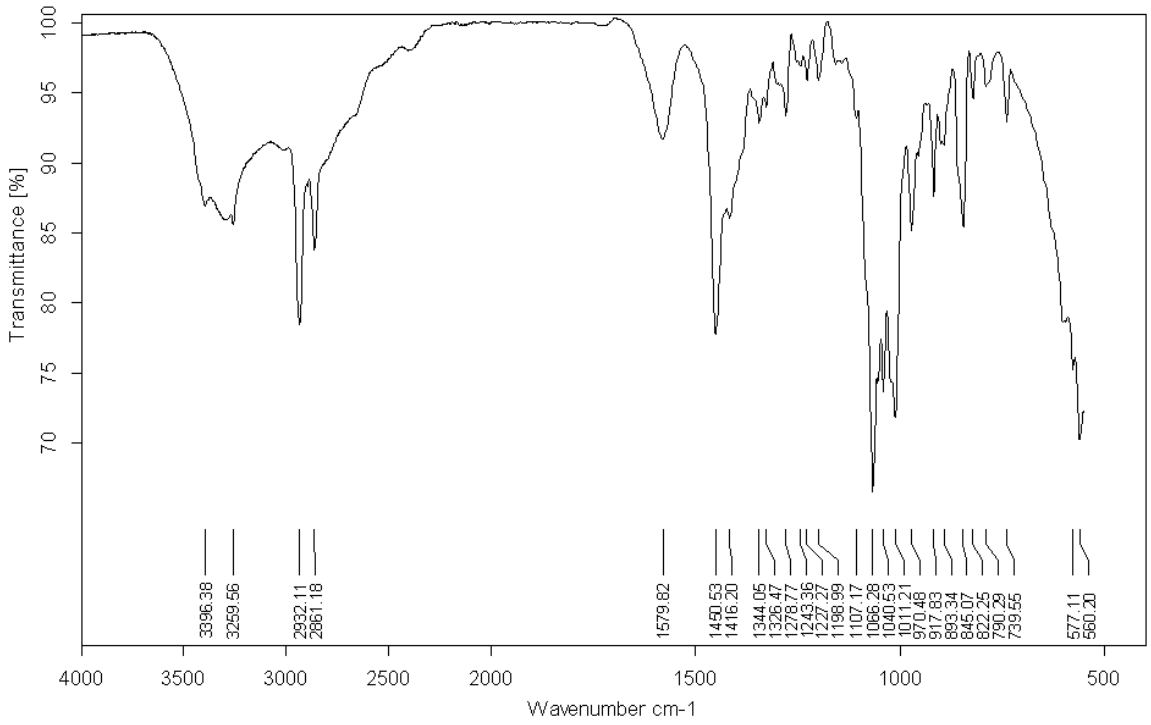


Figure D.23. The IR of Cy_2-Otn/Cd(II) Reaction (Method D4)

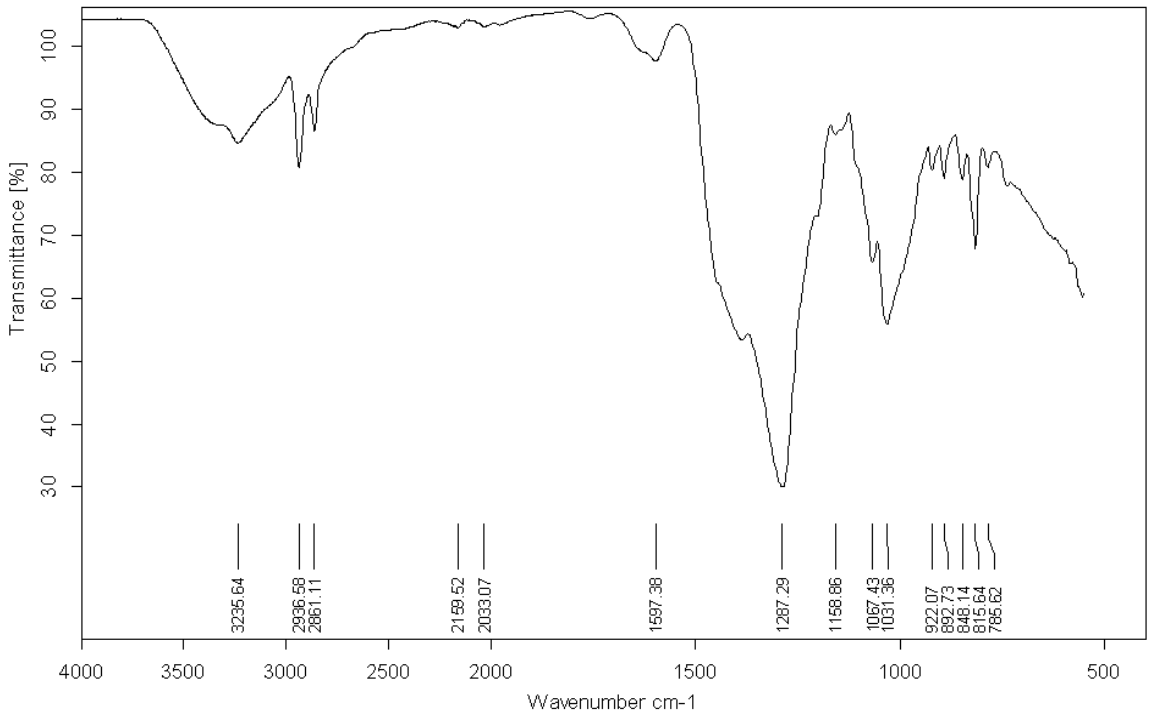


Figure D.24. The IR of Cy_2-Otn/Pb(II) Reaction (Method E1)

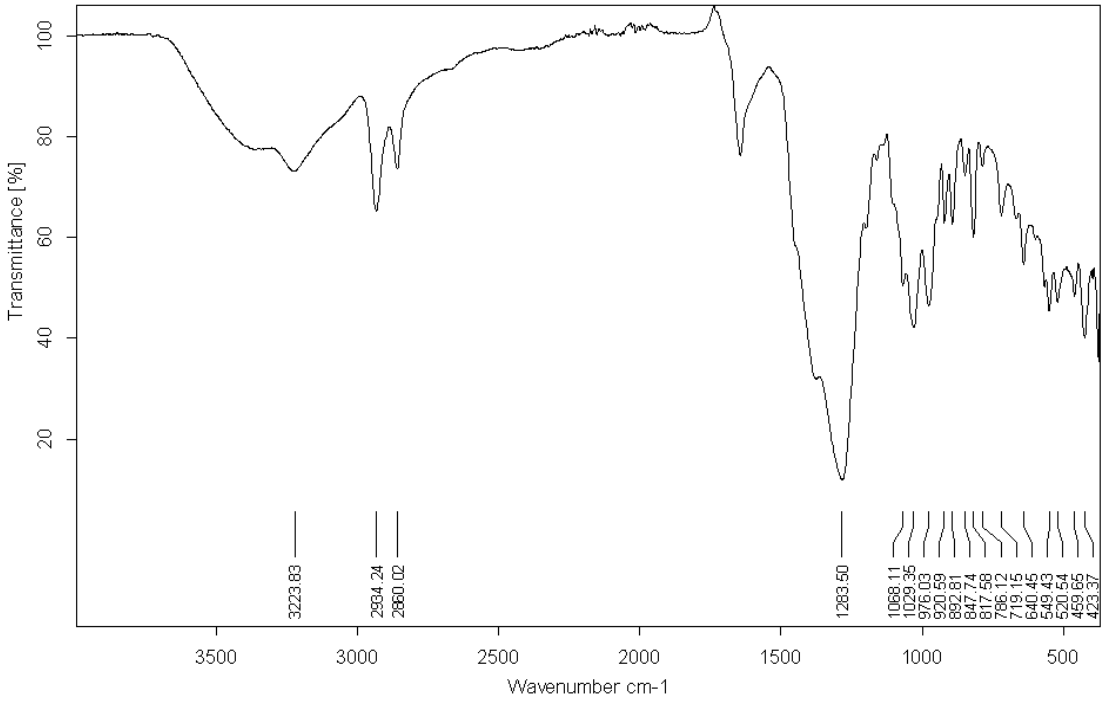


Figure D.25. The IR of Cy_2-Otn/Pb(II) Reaction (Method E2)

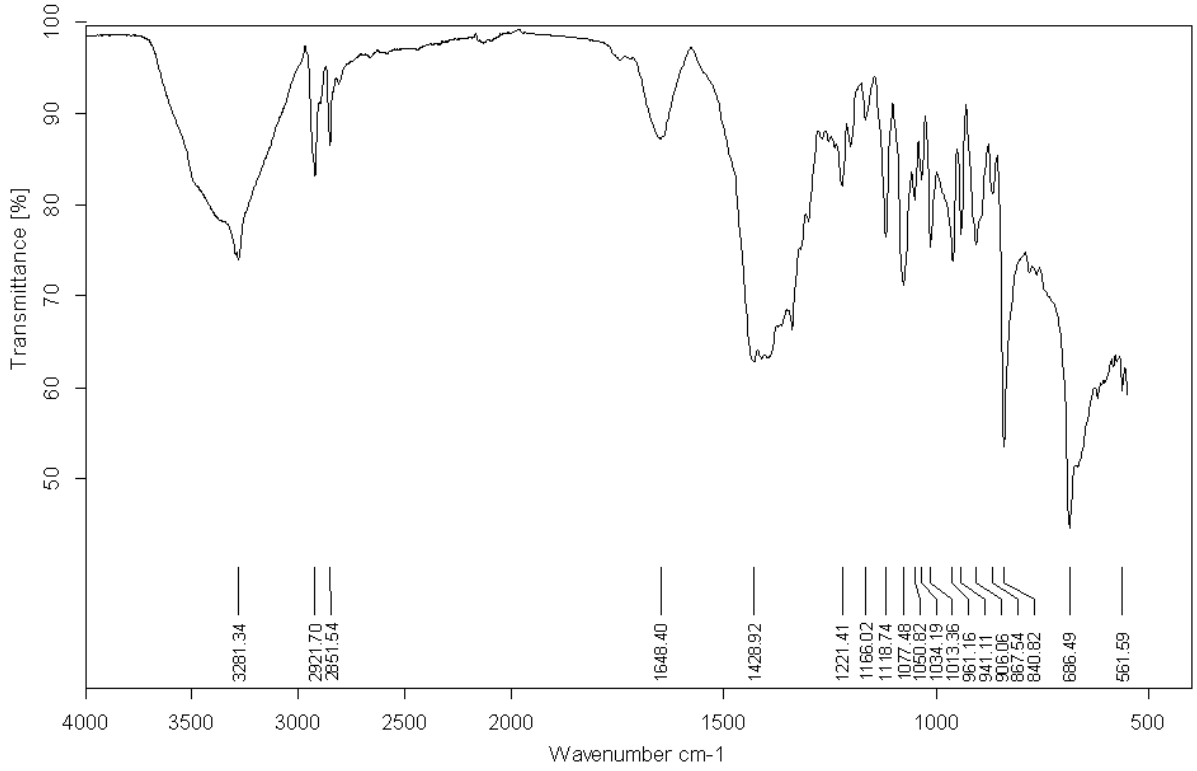


Figure D.26. The IR of Cy_2-tn/Cu(II) Reaction (Method F1)

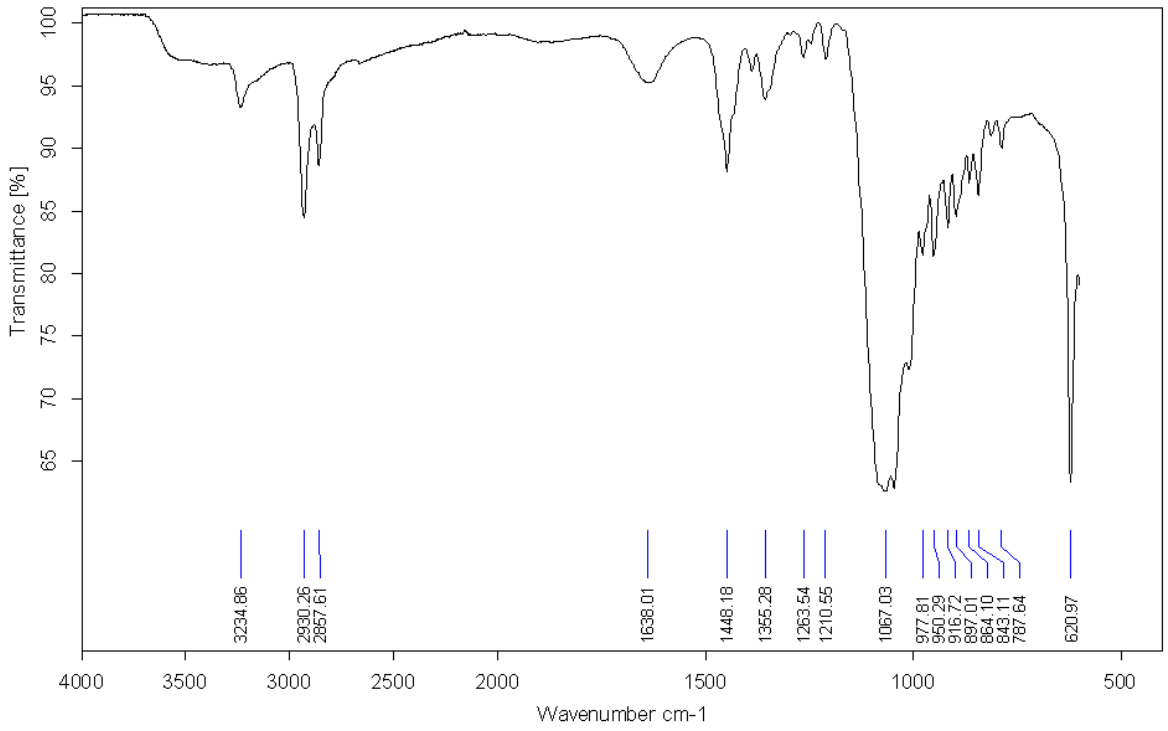


Figure D.27. The IR of Cy_2-tn/Cu(II) Reaction (Method F2)

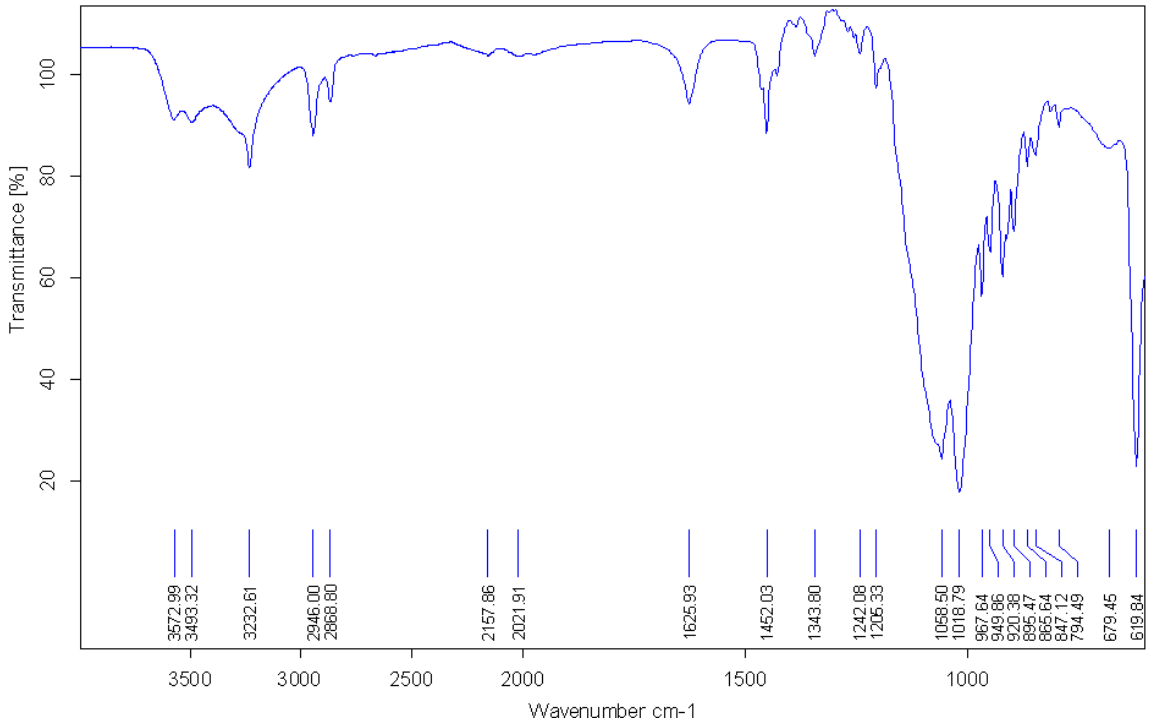


Figure D.28. The IR of Cy_2-tn/Ni(II) Reaction (Method G1)

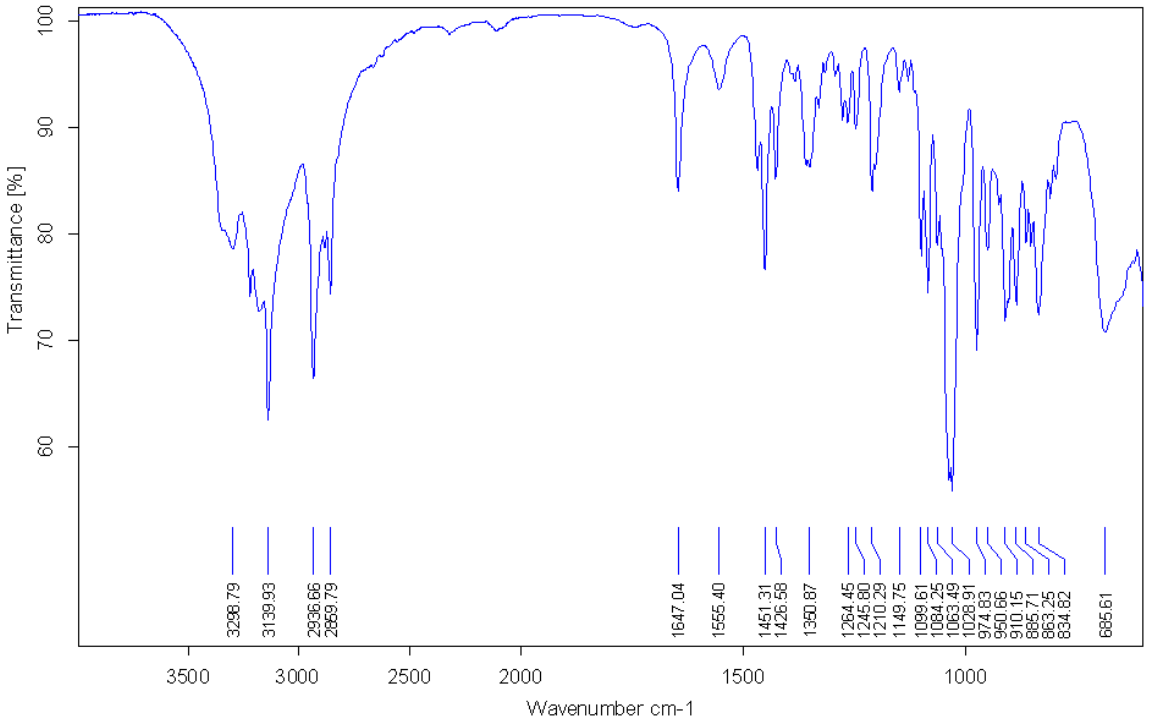


Figure D.29. The IR of Cy_2-tn/Ni(II) Reaction (Method G2)

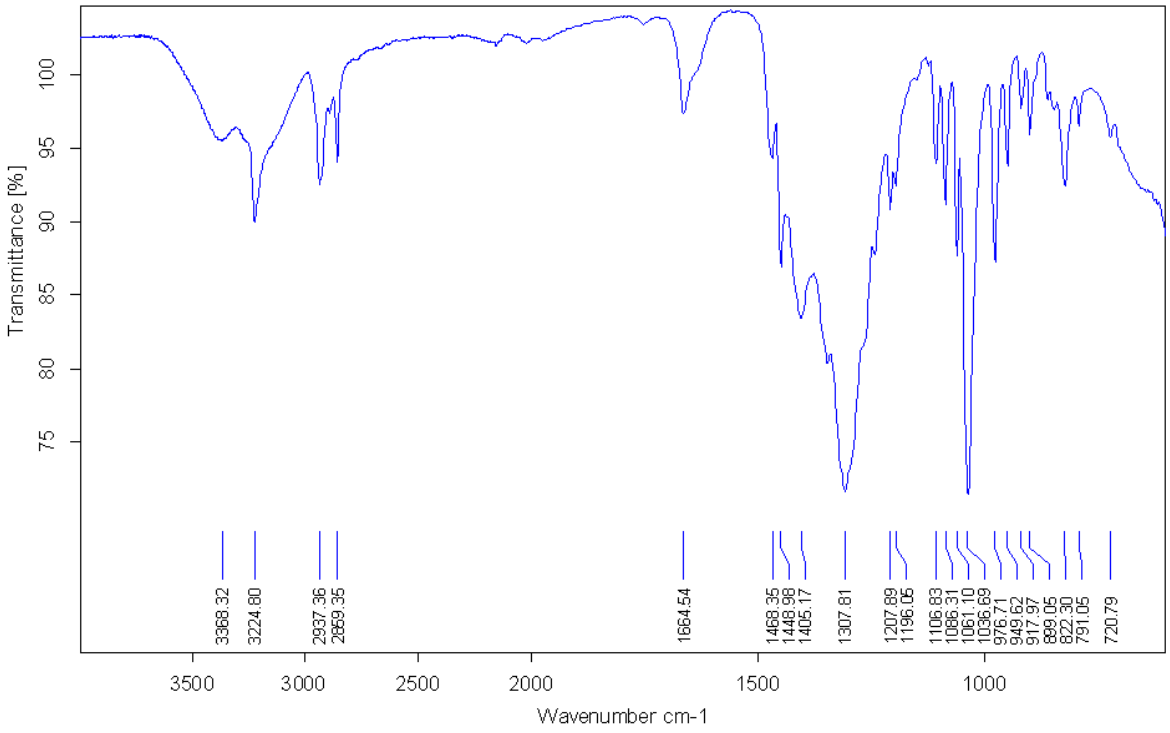


Figure D.30. The IR of Cy_2-tn/Ni(II) Reaction (Method G3)

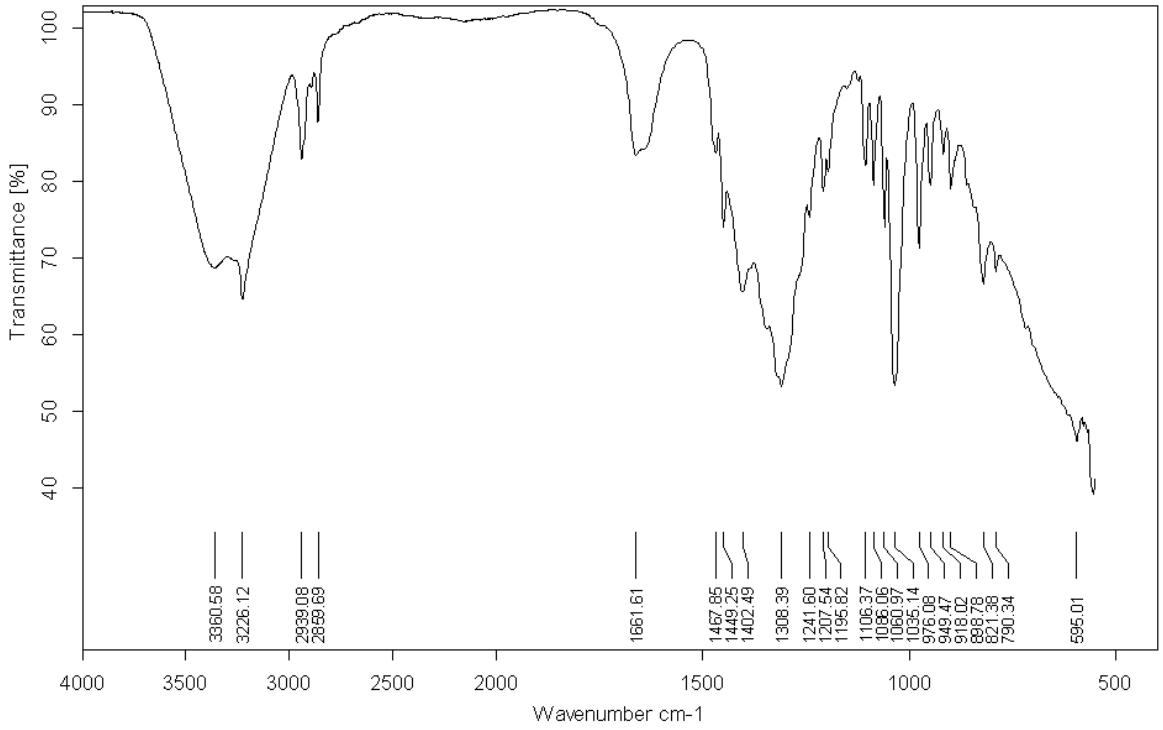


Figure D.31. The IR of Cy_2-tn/Zn(II) Reaction (Method H1)

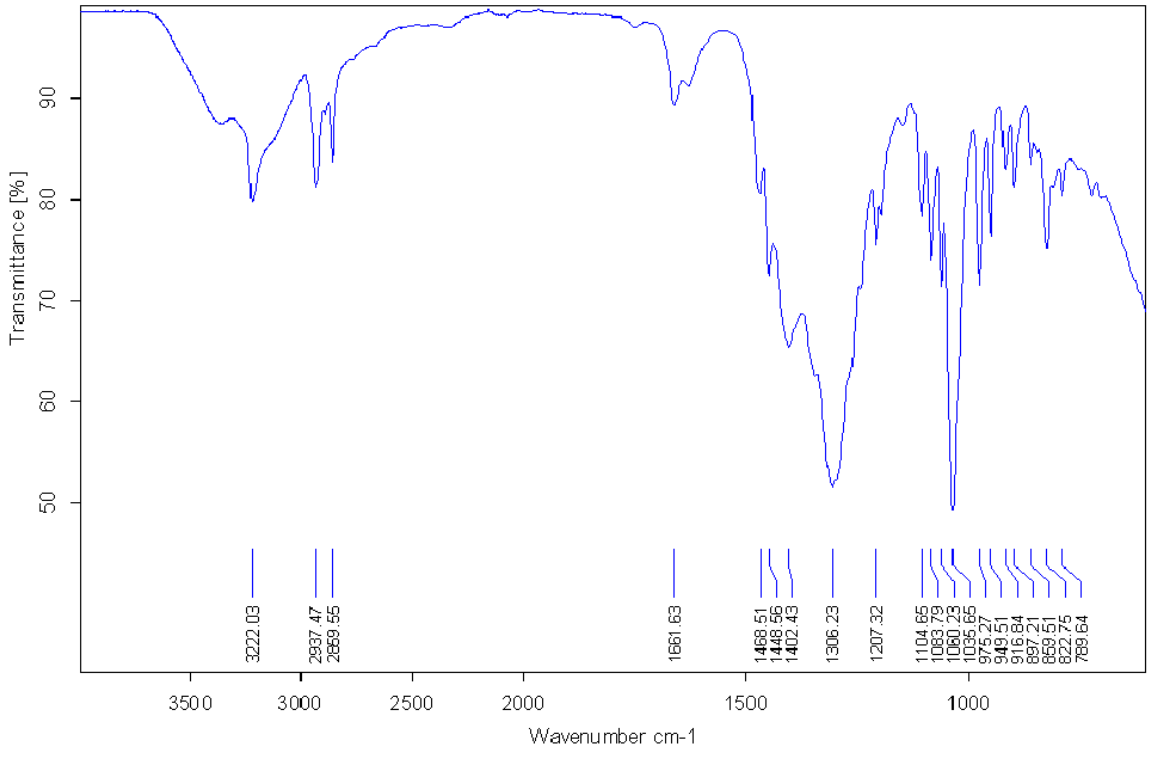


Figure D.32. The IR of Cy_2-tn/Zn(II) Reaction (Method H2)

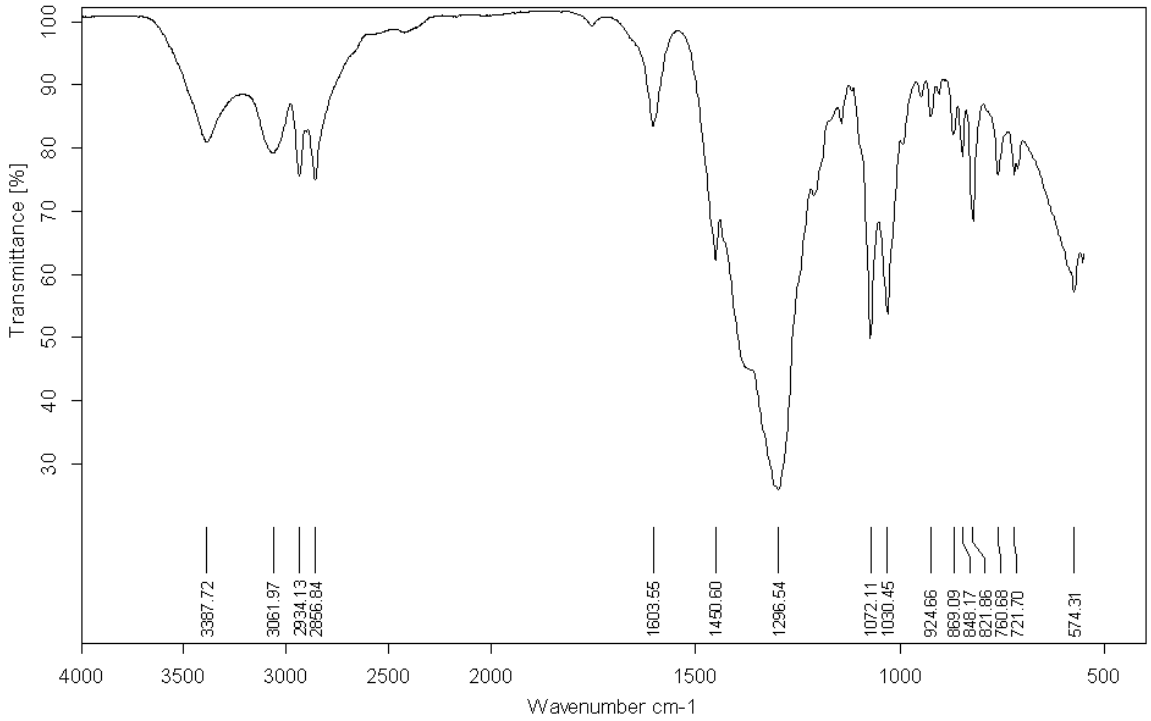


Figure D.33. The IR of Cy_2-tn/Zn(II) Reaction (Method H3)

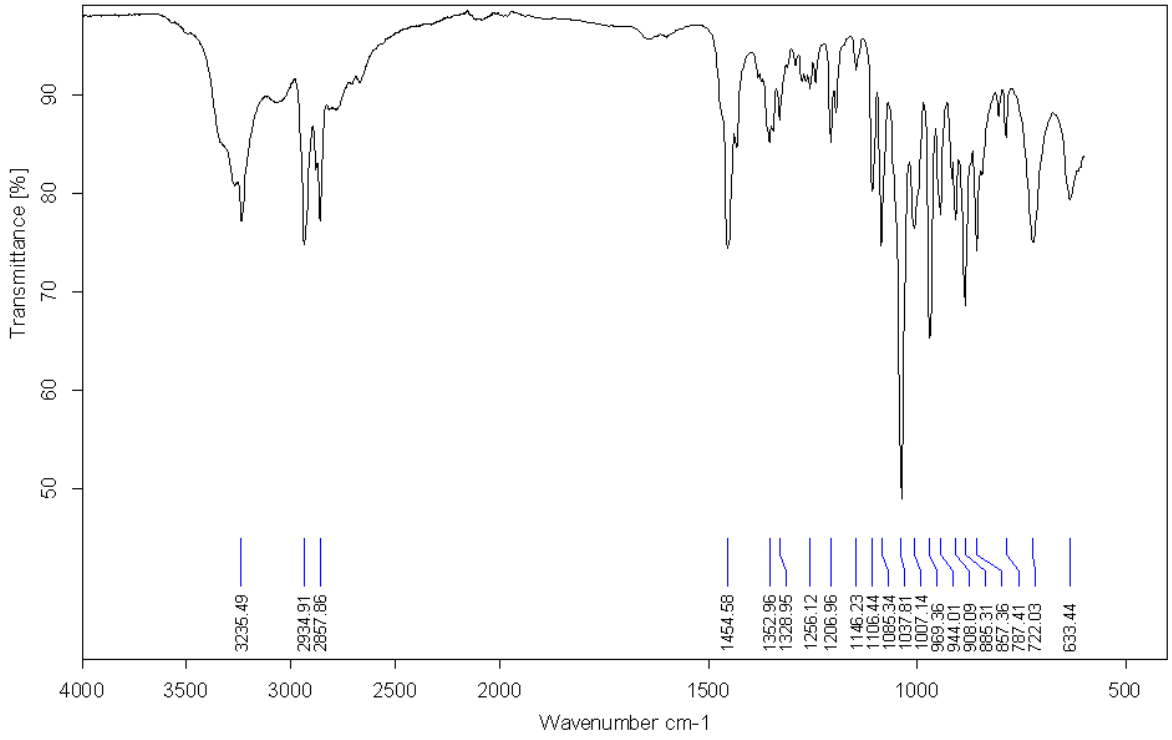


Figure D.34. The IR of Cy_2-tn/Cd(II) Reaction (Method I1)

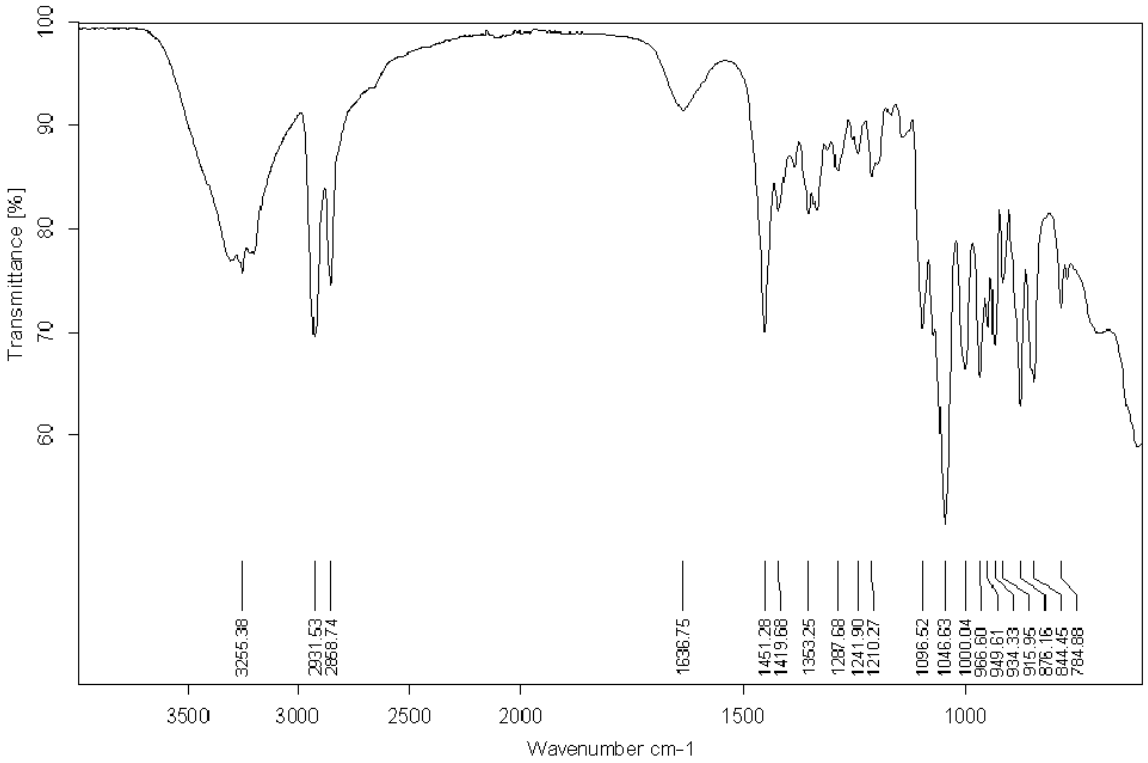


Figure D.35. The IR of Cy_2-tn/Cd(II) Reaction (Method I2)

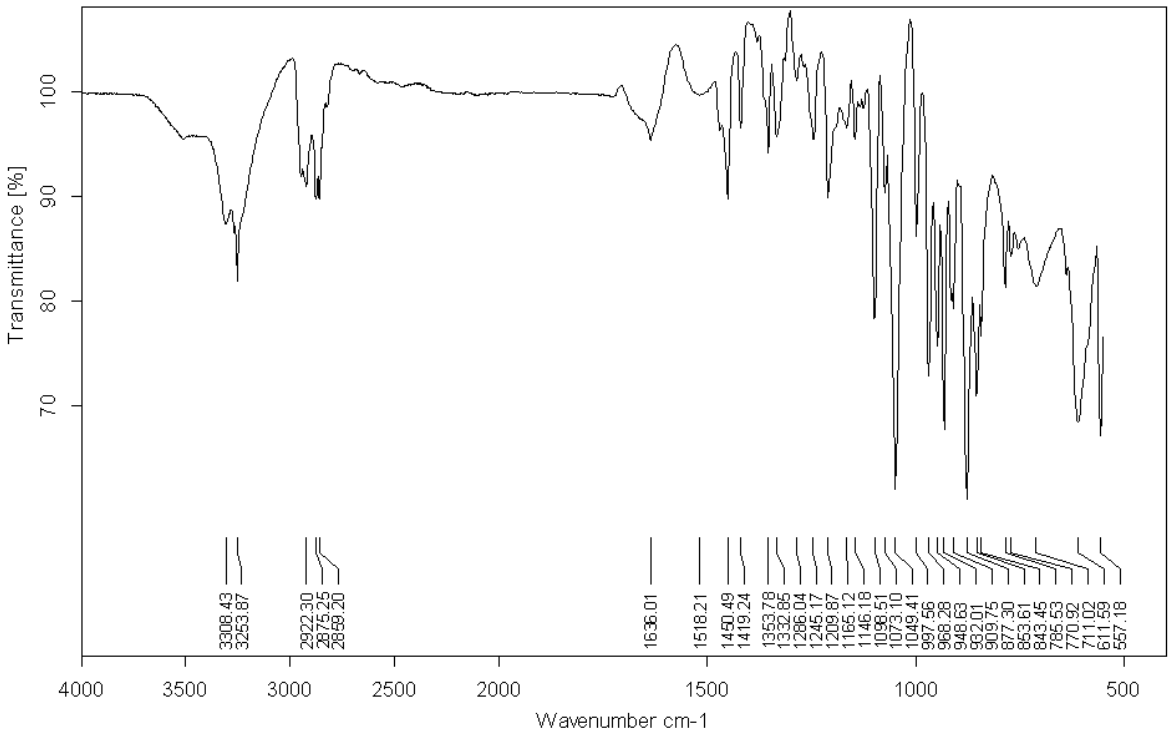


Figure D.36. The IR of Cy_2-tn/Cd(II) Reaction (Method I3)

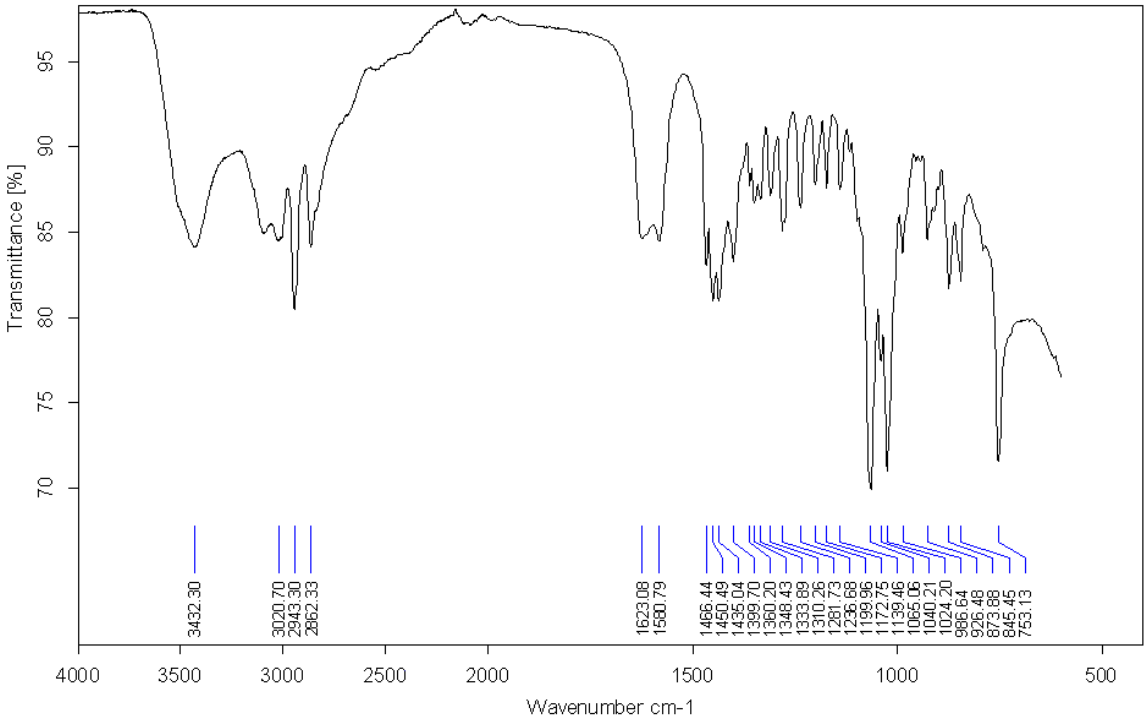


Figure D.37. The IR of Cy_2-tn/Cd(II) Reaction (Method I4)

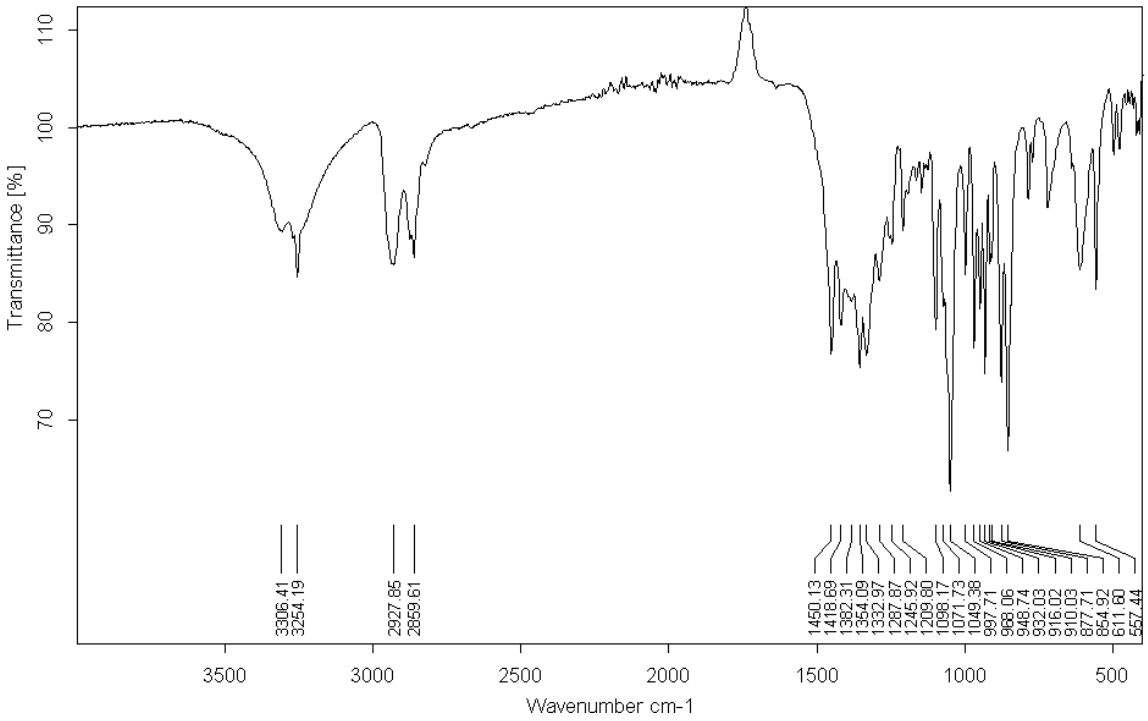


Figure D.38. The IR of Cy_2-tn/Pb(II) Reaction (Method J1)

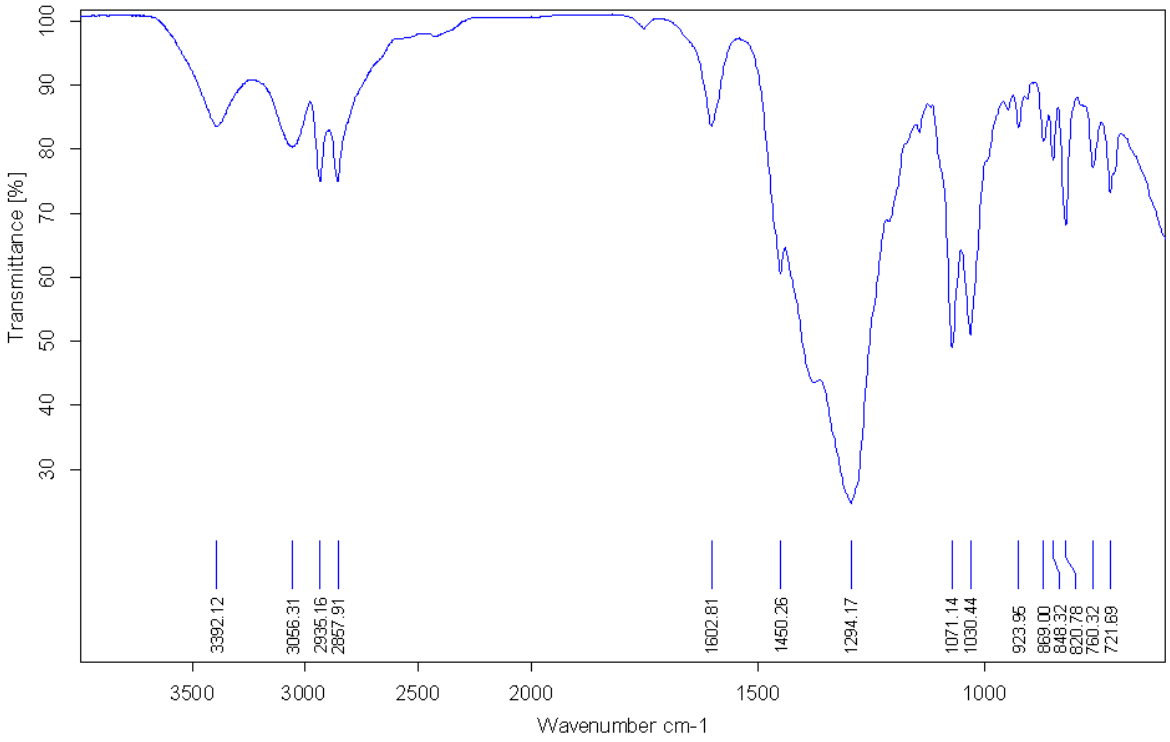
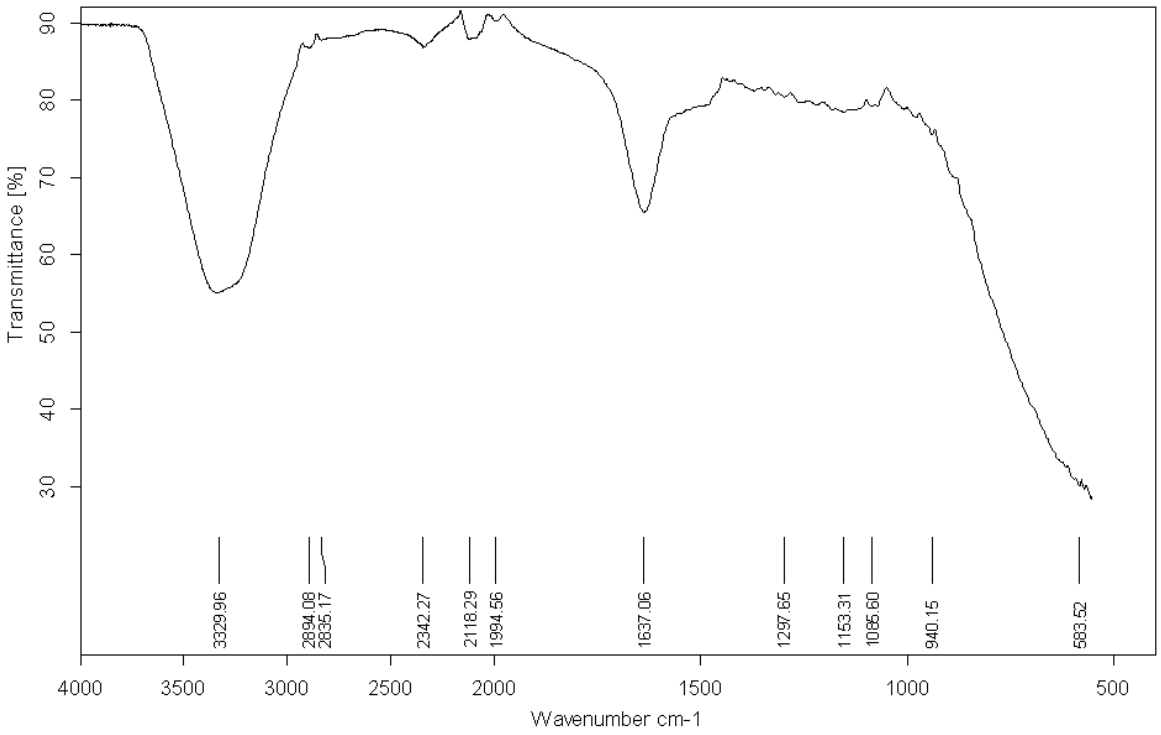


Figure D.39. The IR of Cy_2-tn/Pb(II) Reaction (Method J2)



Appendix E

XRD Data

Cy_2-Otn(a) Data

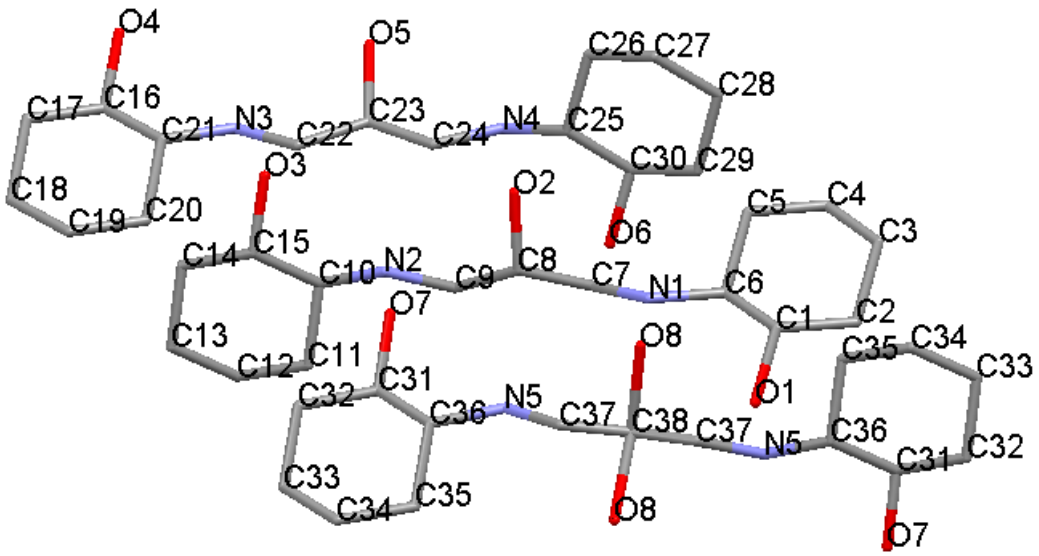


Figure E.1. XRD structure of Cy_2-Otn(a) and the labelling scheme used.

Table E.1. Crystal data and structure refinement for 9m_alvsb2_0f.

Identification code	9m_alvsb2_0f	
Empirical formula	C15 H30 N2 O3	
Formula weight	286.41	
Temperature	293(2) K	
Wavelength	0.71073 Å	
Crystal system	Monoclinic	
Space group	C2/c	
Unit cell dimensions	a = 36.145(3) Å	α= 90°.
	b = 8.5902(6) Å	β= 104.822(2)°.
	c = 26.4419(18) Å	γ = 90°.
Volume	7936.9(9) $Å^3$	

Z	20
Density (calculated)	1.198 Mg/m^3
Absorption coefficient	0.083 mm^{-1}
F(000)	3160
Crystal size	0.31 x 0.25 x 0.09 mm^3
Theta range for data collection	1.59 to 25.00°.
Index ranges	-42<=h<=42, -10<=k<=10, -31<=l<=27
Reflections collected	37765
Independent reflections	6986 [R(int) = 0.1073]
Completeness to theta = 25.00°	100.0 %
Absorption correction	None
Refinement method	Full-matrix least-squares on F^2
Data / restraints / parameters	6986 / 0 / 482
Goodness-of-fit on F^2	1.049
Final R indices [I>2sigma(I)]	R1 = 0.0786, wR2 = 0.2015
R indices (all data)	R1 = 0.1612, wR2 = 0.2404
Largest diff. peak and hole	1.321 and -0.594 $e.Å^{-3}$

Table E.2. Atomic coordinates (x 10^4) and equivalent isotropic displacement parameters ($Å^2$x 10^3) for 9m_alvsb2_0f. U(eq) is defined as one third of the trace of the orthogonalized U^{ij} tensor.

	x	y	z	U(eq)
C(1)	143(1)	992(5)	3591(1)	28(1)
C(2)	-24(1)	240(5)	4002(2)	36(1)
C(3)	287(1)	-195(5)	4490(2)	41(1)
C(4)	593(1)	-1206(5)	4358(2)	38(1)
C(5)	754(1)	-456(5)	3944(1)	34(1)
C(6)	440(1)	-67(5)	3452(1)	27(1)
C(7)	809(1)	-336(4)	2780(1)	28(1)

C(8)	1058(1)	615(4)	2513(1)	23(1)
C(9)	1144(1)	-241(4)	2058(1)	25(1)
C(10)	1504(1)	-25(4)	1382(1)	22(1)
C(11)	1165(1)	-303(5)	912(1)	29(1)
C(12)	1297(1)	-997(5)	458(1)	31(1)
C(13)	1587(1)	50(5)	304(2)	36(1)
C(14)	1925(1)	371(5)	771(1)	31(1)
C(15)	1799(1)	1019(4)	1233(1)	22(1)
C(16)	2801(1)	4044(4)	1299(1)	24(1)
C(17)	2940(1)	4907(5)	878(2)	32(1)
C(18)	2606(1)	5334(5)	418(2)	38(1)
C(19)	2310(1)	6279(5)	605(2)	35(1)
C(20)	2174(1)	5432(4)	1029(1)	29(1)
C(21)	2508(1)	4998(4)	1485(1)	22(1)
C(22)	2140(1)	4960(4)	2159(1)	23(1)
C(23)	2076(1)	4034(4)	2609(1)	23(1)
C(24)	1803(1)	4849(4)	2868(1)	25(1)
C(25)	1529(1)	4718(4)	3628(1)	26(1)
C(26)	1816(1)	5171(4)	4132(1)	29(1)
C(27)	1633(1)	6040(5)	4504(2)	38(1)
C(28)	1310(1)	5119(5)	4611(2)	43(1)
C(29)	1020(1)	4662(5)	4112(2)	39(1)
C(30)	1201(1)	3805(4)	3732(1)	29(1)
C(31)	833(1)	4101(5)	1346(2)	35(1)
C(32)	957(1)	4836(6)	885(2)	44(1)
C(33)	622(1)	5125(6)	426(2)	60(2)
C(34)	331(1)	6095(5)	581(2)	48(1)
C(35)	203(1)	5375(5)	1026(2)	49(1)
C(36)	544(1)	5140(5)	1498(2)	42(1)
C(37)	207(2)	5499(9)	2184(3)	120(3)
C(38)	0	4964(7)	2500	68(3)

N(1)	600(1)	693(4)	3059(1)	26(1)
N(2)	1386(1)	711(3)	1816(1)	23(1)
N(3)	2382(1)	4102(4)	1884(1)	23(1)
N(4)	1710(1)	3864(4)	3269(1)	26(1)
N(5)	431(1)	4468(4)	1938(2)	53(1)
O(1)	-145(1)	1336(4)	3131(1)	36(1)
O(2)	1416(1)	973(3)	2884(1)	28(1)
O(3)	2117(1)	1178(3)	1675(1)	26(1)
O(4)	3110(1)	3578(3)	1722(1)	32(1)
O(5)	2428(1)	3651(3)	2976(1)	27(1)
O(6)	921(1)	3564(3)	3250(1)	36(1)
O(7)	1153(1)	3883(3)	1776(1)	46(1)
O(8)	-362(2)	5566(6)	2005(2)	58(2)

Table E.3. Bond lengths [Å] and angles [°] for 9m_alvsb2_0f.

C(1)-O(1)	1.415(4)
C(1)-C(2)	1.517(5)
C(1)-C(6)	1.521(5)
C(1)-H(1)	0.9800
C(2)-C(3)	1.525(5)
C(2)-H(2A)	0.9700
C(2)-H(2B)	0.9700
C(3)-C(4)	1.516(5)
C(3)-H(3A)	0.9700
C(3)-H(3B)	0.9700
C(4)-C(5)	1.509(5)
C(4)-H(4A)	0.9700
C(4)-H(4B)	0.9700
C(5)-C(6)	1.529(5)

C(5)-H(5A)	0.9700
C(5)-H(5B)	0.9700
C(6)-N(1)	1.466(4)
C(6)-H(6)	0.9800
C(7)-N(1)	1.475(5)
C(7)-C(8)	1.517(5)
C(7)-H(7A)	0.9700
C(7)-H(7B)	0.9700
C(8)-O(2)	1.442(4)
C(8)-C(9)	1.509(5)
C(8)-H(8)	0.9800
C(9)-N(2)	1.460(4)
C(9)-H(9A)	0.9700
C(9)-H(9B)	0.9700
C(10)-N(2)	1.464(4)
C(10)-C(15)	1.521(5)
C(10)-C(11)	1.523(5)
C(10)-H(10)	0.9800
C(11)-C(12)	1.522(5)
C(11)-H(11A)	0.9700
C(11)-H(11B)	0.9700
C(12)-C(13)	1.514(5)
C(12)-H(12A)	0.9700
C(12)-H(12B)	0.9700
C(13)-C(14)	1.524(5)
C(13)-H(13A)	0.9700
C(13)-H(13B)	0.9700
C(14)-C(15)	1.515(5)
C(14)-H(14A)	0.9700
C(14)-H(14B)	0.9700
C(15)-O(3)	1.422(4)

C(15)-H(15)	0.9800
C(16)-O(4)	1.421(4)
C(16)-C(21)	1.519(5)
C(16)-C(17)	1.523(5)
C(16)-H(16)	0.9800
C(17)-C(18)	1.522(5)
C(17)-H(17A)	0.9700
C(17)-H(17B)	0.9700
C(18)-C(19)	1.524(5)
C(18)-H(18A)	0.9700
C(18)-H(18B)	0.9700
C(19)-C(20)	1.519(5)
C(19)-H(19A)	0.9700
C(19)-H(19B)	0.9700
C(20)-C(21)	1.517(5)
C(20)-H(20A)	0.9700
C(20)-H(20B)	0.9700
C(21)-N(3)	1.471(4)
C(21)-H(21)	0.9800
C(22)-N(3)	1.469(4)
C(22)-C(23)	1.497(5)
C(22)-H(22A)	0.9700
C(22)-H(22B)	0.9700
C(23)-O(5)	1.427(4)
C(23)-C(24)	1.509(5)
C(23)-H(23)	0.9800
C(24)-N(4)	1.461(4)
C(24)-H(24A)	0.9700
C(24)-H(24B)	0.9700
C(25)-N(4)	1.480(5)
C(25)-C(30)	1.503(5)

C(25)-C(26)	1.514(5)
C(25)-H(25)	0.9800
C(26)-C(27)	1.514(5)
C(26)-H(26A)	0.9700
C(26)-H(26B)	0.9700
C(27)-C(28)	1.497(5)
C(27)-H(27A)	0.9700
C(27)-H(27B)	0.9700
C(28)-C(29)	1.510(5)
C(28)-H(28A)	0.9700
C(28)-H(28B)	0.9700
C(29)-C(30)	1.523(5)
C(29)-H(29A)	0.9700
C(29)-H(29B)	0.9700
C(30)-O(6)	1.425(4)
C(30)-H(30)	0.9800
C(31)-O(7)	1.413(4)
C(31)-C(36)	1.505(5)
C(31)-C(32)	1.538(5)
C(31)-H(31)	0.9800
C(32)-C(33)	1.499(6)
C(32)-H(32A)	0.9700
C(32)-H(32B)	0.9700
C(33)-C(34)	1.482(6)
C(33)-H(33A)	0.9700
C(33)-H(33B)	0.9700
C(34)-C(35)	1.504(6)
C(34)-H(34A)	0.9700
C(34)-H(34B)	0.9700
C(35)-C(36)	1.528(6)
C(35)-H(35A)	0.9700

C(35)-H(35B)	0.9700
C(36)-N(5)	1.448(5)
C(36)-H(36)	0.9800
C(37)-C(38)	1.337(7)
C(37)-N(5)	1.461(7)
C(37)-H(37A)	0.9700
C(37)-H(37B)	0.9700
C(38)-C(37)#1	1.337(7)
C(38)-O(8)	1.678(6)
C(38)-O(8)#1	1.678(6)
C(38)-H(38)	1.0282
N(1)-H(1N)	0.85(4)
N(2)-H(2N)	0.81(3)
N(3)-H(3N)	0.76(4)
N(4)-H(4N)	0.88(4)
N(5)-H(5N)	0.9000
O(1)-H(1O)	0.80(4)
O(2)-H(2)	0.8200
O(3)-H(3O)	0.77(3)
O(4)-H(4)	0.8200
O(5)-H(5)	0.8191
O(6)-H(6O)	0.83(5)
O(7)-H(7)	0.8200
O(8)-H(8H)	0.8193
O(1)-C(1)-C(2)	111.4(3)
O(1)-C(1)-C(6)	109.1(3)
C(2)-C(1)-C(6)	110.7(3)
O(1)-C(1)-H(1)	108.5
C(2)-C(1)-H(1)	108.5
C(6)-C(1)-H(1)	108.5
C(1)-C(2)-C(3)	111.6(3)

C(1)-C(2)-H(2A)	109.3
C(3)-C(2)-H(2A)	109.3
C(1)-C(2)-H(2B)	109.3
C(3)-C(2)-H(2B)	109.3
H(2A)-C(2)-H(2B)	108.0
C(4)-C(3)-C(2)	111.6(3)
C(4)-C(3)-H(3A)	109.3
C(2)-C(3)-H(3A)	109.3
C(4)-C(3)-H(3B)	109.3
C(2)-C(3)-H(3B)	109.3
H(3A)-C(3)-H(3B)	108.0
C(5)-C(4)-C(3)	111.3(3)
C(5)-C(4)-H(4A)	109.4
C(3)-C(4)-H(4A)	109.4
C(5)-C(4)-H(4B)	109.4
C(3)-C(4)-H(4B)	109.4
H(4A)-C(4)-H(4B)	108.0
C(4)-C(5)-C(6)	111.7(3)
C(4)-C(5)-H(5A)	109.3
C(6)-C(5)-H(5A)	109.3
C(4)-C(5)-H(5B)	109.3
C(6)-C(5)-H(5B)	109.3
H(5A)-C(5)-H(5B)	107.9
N(1)-C(6)-C(1)	109.6(3)
N(1)-C(6)-C(5)	111.1(3)
C(1)-C(6)-C(5)	109.9(3)
N(1)-C(6)-H(6)	108.7
C(1)-C(6)-H(6)	108.7
C(5)-C(6)-H(6)	108.7
N(1)-C(7)-C(8)	110.4(3)
N(1)-C(7)-H(7A)	109.6

C(8)-C(7)-H(7A)	109.6
N(1)-C(7)-H(7B)	109.6
C(8)-C(7)-H(7B)	109.6
H(7A)-C(7)-H(7B)	108.1
O(2)-C(8)-C(9)	108.3(3)
O(2)-C(8)-C(7)	109.6(3)
C(9)-C(8)-C(7)	112.1(3)
O(2)-C(8)-H(8)	108.9
C(9)-C(8)-H(8)	108.9
C(7)-C(8)-H(8)	108.9
N(2)-C(9)-C(8)	110.3(3)
N(2)-C(9)-H(9A)	109.6
C(8)-C(9)-H(9A)	109.6
N(2)-C(9)-H(9B)	109.6
C(8)-C(9)-H(9B)	109.6
H(9A)-C(9)-H(9B)	108.1
N(2)-C(10)-C(15)	108.2(3)
N(2)-C(10)-C(11)	111.9(3)
C(15)-C(10)-C(11)	110.5(3)
N(2)-C(10)-H(10)	108.7
C(15)-C(10)-H(10)	108.7
C(11)-C(10)-H(10)	108.7
C(12)-C(11)-C(10)	110.9(3)
C(12)-C(11)-H(11A)	109.5
C(10)-C(11)-H(11A)	109.5
C(12)-C(11)-H(11B)	109.5
C(10)-C(11)-H(11B)	109.5
H(11A)-C(11)-H(11B)	108.0
C(13)-C(12)-C(11)	110.9(3)
C(13)-C(12)-H(12A)	109.5

C(11)-C(12)-H(12A)	109.5
C(13)-C(12)-H(12B)	109.5
C(11)-C(12)-H(12B)	109.5
H(12A)-C(12)-H(12B)	108.0
C(12)-C(13)-C(14)	110.9(3)
C(12)-C(13)-H(13A)	109.5
C(14)-C(13)-H(13A)	109.5
C(12)-C(13)-H(13B)	109.5
C(14)-C(13)-H(13B)	109.5
H(13A)-C(13)-H(13B)	108.0
C(15)-C(14)-C(13)	111.9(3)
C(15)-C(14)-H(14A)	109.2
C(13)-C(14)-H(14A)	109.2
C(15)-C(14)-H(14B)	109.2
C(13)-C(14)-H(14B)	109.2
H(14A)-C(14)-H(14B)	107.9
O(3)-C(15)-C(14)	110.5(3)
O(3)-C(15)-C(10)	108.4(3)
C(14)-C(15)-C(10)	111.7(3)
O(3)-C(15)-H(15)	108.7
C(14)-C(15)-H(15)	108.7
C(10)-C(15)-H(15)	108.7
O(4)-C(16)-C(21)	111.7(3)
O(4)-C(16)-C(17)	112.0(3)
C(21)-C(16)-C(17)	111.2(3)
O(4)-C(16)-H(16)	107.2
C(21)-C(16)-H(16)	107.2
C(17)-C(16)-H(16)	107.2
C(18)-C(17)-C(16)	111.1(3)
C(18)-C(17)-H(17A)	109.4
C(16)-C(17)-H(17A)	109.4

C(18)-C(17)-H(17B)	109.4
C(16)-C(17)-H(17B)	109.4
H(17A)-C(17)-H(17B)	108.0
C(17)-C(18)-C(19)	110.3(3)
C(17)-C(18)-H(18A)	109.6
C(19)-C(18)-H(18A)	109.6
C(17)-C(18)-H(18B)	109.6
C(19)-C(18)-H(18B)	109.6
H(18A)-C(18)-H(18B)	108.1
C(20)-C(19)-C(18)	111.8(3)
C(20)-C(19)-H(19A)	109.3
C(18)-C(19)-H(19A)	109.3
C(20)-C(19)-H(19B)	109.3
C(18)-C(19)-H(19B)	109.3
H(19A)-C(19)-H(19B)	107.9
C(21)-C(20)-C(19)	111.3(3)
C(21)-C(20)-H(20A)	109.4
C(19)-C(20)-H(20A)	109.4
C(21)-C(20)-H(20B)	109.4
C(19)-C(20)-H(20B)	109.4
H(20A)-C(20)-H(20B)	108.0
N(3)-C(21)-C(20)	111.7(3)
N(3)-C(21)-C(16)	108.7(3)
C(20)-C(21)-C(16)	110.7(3)
N(3)-C(21)-H(21)	108.5
C(20)-C(21)-H(21)	108.5
C(16)-C(21)-H(21)	108.5
N(3)-C(22)-C(23)	111.0(3)
N(3)-C(22)-H(22A)	109.4
C(23)-C(22)-H(22A)	109.4
N(3)-C(22)-H(22B)	109.4

C(23)-C(22)-H(22B)	109.4
H(22A)-C(22)-H(22B)	108.0
O(5)-C(23)-C(22)	111.9(3)
O(5)-C(23)-C(24)	111.8(3)
C(22)-C(23)-C(24)	111.4(3)
O(5)-C(23)-H(23)	107.1
C(22)-C(23)-H(23)	107.1
C(24)-C(23)-H(23)	107.1
N(4)-C(24)-C(23)	111.1(3)
N(4)-C(24)-H(24A)	109.4
C(23)-C(24)-H(24A)	109.4
N(4)-C(24)-H(24B)	109.4
C(23)-C(24)-H(24B)	109.4
H(24A)-C(24)-H(24B)	108.0
N(4)-C(25)-C(30)	111.0(3)
N(4)-C(25)-C(26)	112.1(3)
C(30)-C(25)-C(26)	111.5(3)
N(4)-C(25)-H(25)	107.3
C(30)-C(25)-H(25)	107.3
C(26)-C(25)-H(25)	107.3
C(27)-C(26)-C(25)	112.6(3)
C(27)-C(26)-H(26A)	109.1
C(25)-C(26)-H(26A)	109.1
C(27)-C(26)-H(26B)	109.1
C(25)-C(26)-H(26B)	109.1
H(26A)-C(26)-H(26B)	107.8
C(28)-C(27)-C(26)	110.7(3)
C(28)-C(27)-H(27A)	109.5
C(26)-C(27)-H(27A)	109.5
C(28)-C(27)-H(27B)	109.5
C(26)-C(27)-H(27B)	109.5

H(27A)-C(27)-H(27B)	108.1
C(27)-C(28)-C(29)	111.9(3)
C(27)-C(28)-H(28A)	109.2
C(29)-C(28)-H(28A)	109.2
C(27)-C(28)-H(28B)	109.2
C(29)-C(28)-H(28B)	109.2
H(28A)-C(28)-H(28B)	107.9
C(28)-C(29)-C(30)	112.6(3)
C(28)-C(29)-H(29A)	109.1
C(30)-C(29)-H(29A)	109.1
C(28)-C(29)-H(29B)	109.1
C(30)-C(29)-H(29B)	109.1
H(29A)-C(29)-H(29B)	107.8
O(6)-C(30)-C(25)	109.0(3)
O(6)-C(30)-C(29)	109.5(3)
C(25)-C(30)-C(29)	111.1(3)
O(6)-C(30)-H(30)	109.1
C(25)-C(30)-H(30)	109.1
C(29)-C(30)-H(30)	109.1
O(7)-C(31)-C(36)	110.2(3)
O(7)-C(31)-C(32)	110.3(3)
C(36)-C(31)-C(32)	109.5(3)
O(7)-C(31)-H(31)	109.0
C(36)-C(31)-H(31)	109.0
C(32)-C(31)-H(31)	109.0
C(33)-C(32)-C(31)	111.8(4)
C(33)-C(32)-H(32A)	109.3
C(31)-C(32)-H(32A)	109.3
C(33)-C(32)-H(32B)	109.3
C(31)-C(32)-H(32B)	109.3
H(32A)-C(32)-H(32B)	107.9

C(34)-C(33)-C(32)	110.7(4)
C(34)-C(33)-H(33A)	109.5
C(32)-C(33)-H(33A)	109.5
C(34)-C(33)-H(33B)	109.5
C(32)-C(33)-H(33B)	109.5
H(33A)-C(33)-H(33B)	108.1
C(33)-C(34)-C(35)	111.7(4)
C(33)-C(34)-H(34A)	109.3
C(35)-C(34)-H(34A)	109.3
C(33)-C(34)-H(34B)	109.3
C(35)-C(34)-H(34B)	109.3
H(34A)-C(34)-H(34B)	107.9
C(34)-C(35)-C(36)	110.3(4)
C(34)-C(35)-H(35A)	109.6
C(36)-C(35)-H(35A)	109.6
C(34)-C(35)-H(35B)	109.6
C(36)-C(35)-H(35B)	109.6
H(35A)-C(35)-H(35B)	108.1
N(5)-C(36)-C(31)	109.7(4)
N(5)-C(36)-C(35)	112.0(4)
C(31)-C(36)-C(35)	109.3(3)
N(5)-C(36)-H(36)	108.6
C(31)-C(36)-H(36)	108.6
C(35)-C(36)-H(36)	108.6
C(38)-C(37)-N(5)	122.1(6)
C(38)-C(37)-H(37A)	106.8
N(5)-C(37)-H(37A)	106.8
C(38)-C(37)-H(37B)	106.8
N(5)-C(37)-H(37B)	106.8
H(37A)-C(37)-H(37B)	106.6
C(37)#1-C(38)-C(37)	139.7(9)

C(37)#1-C(38)-O(8)	86.1(4)
C(37)-C(38)-O(8)	81.7(4)
C(37)#1-C(38)-O(8)#1	81.7(4)
C(37)-C(38)-O(8)#1	86.1(4)
O(8)-C(38)-O(8)#1	144.1(6)
C(37)#1-C(38)-H(38)	101.6
C(37)-C(38)-H(38)	116.1
O(8)-C(38)-H(38)	128.0
O(8)#1-C(38)-H(38)	87.7
C(6)-N(1)-C(7)	115.6(3)
C(6)-N(1)-H(1N)	108(3)
C(7)-N(1)-H(1N)	105(3)
C(9)-N(2)-C(10)	115.4(3)
C(9)-N(2)-H(2N)	103(3)
C(10)-N(2)-H(2N)	109(3)
C(22)-N(3)-C(21)	115.2(3)
C(22)-N(3)-H(3N)	114(3)
C(21)-N(3)-H(3N)	100(3)
C(24)-N(4)-C(25)	113.6(3)
C(24)-N(4)-H(4N)	107(3)
C(25)-N(4)-H(4N)	106(3)
C(36)-N(5)-C(37)	114.8(4)
C(36)-N(5)-H(5N)	107.9
C(37)-N(5)-H(5N)	108.0
C(1)-O(1)-H(1O)	106(3)
C(8)-O(2)-H(2)	109.5
C(15)-O(3)-H(3O)	112(3)
C(16)-O(4)-H(4)	109.5
C(23)-O(5)-H(5)	113.6
C(30)-O(6)-H(6O)	106(3)
C(31)-O(7)-H(7)	109.5

C(38)-O(8)-H(8H) 113.3

Symmetry transformations used to generate equivalent atoms: #1 -x,y,-z+1/2

Table E.4. Anisotropic displacement parameters ($Å^2 x\ 10^3$) for 9m_alvsb2_0f. The anisotropic displacement factor exponent takes the form: $-2\pi^2[\ h^2 a^{*2} U^{11} + ... + 2\ h\ k\ a^*\ b^*\ U^{12}\ ]$

	U^{11}	U^{22}	U^{33}	U^{23}	U^{13}	U^{12}	
Table E.5. C(1)		22(2)	34(2)	29(2)	-2(2)	7(2)	-2(2)
C(2)	26(2)	48(3)	37(2)	-2(2)	14(2)	3(2)	
C(3)	39(3)	57(3)	32(2)	4(2)	19(2)	1(2)	
C(4)	38(3)	44(3)	34(2)	5(2)	11(2)	-4(2)	
C(5)	28(2)	42(3)	34(2)	6(2)	10(2)	1(2)	
C(6)	22(2)	30(2)	31(2)	-1(2)	12(2)	-4(2)	
C(7)	36(2)	22(2)	30(2)	1(2)	15(2)	0(2)	
C(8)	20(2)	23(2)	24(2)	-1(2)	3(2)	1(2)	
C(9)	25(2)	23(2)	29(2)	-6(2)	10(2)	-4(2)	
C(10)	24(2)	17(2)	25(2)	-2(2)	8(2)	3(2)	
C(11)	26(2)	33(2)	28(2)	-4(2)	9(2)	-5(2)	
C(12)	30(2)	36(2)	28(2)	-5(2)	12(2)	-2(2)	
C(13)	41(3)	42(3)	28(2)	-5(2)	18(2)	0(2)	
C(14)	33(2)	30(2)	36(2)	-3(2)	18(2)	-2(2)	
C(15)	22(2)	15(2)	29(2)	-1(2)	7(2)	3(2)	
C(16)	26(2)	14(2)	32(2)	-3(2)	11(2)	-2(2)	
C(17)	35(2)	25(2)	43(3)	2(2)	25(2)	6(2)	
C(18)	46(3)	43(3)	30(2)	6(2)	18(2)	4(2)	
C(19)	35(2)	37(2)	33(2)	8(2)	10(2)	6(2)	
C(20)	29(2)	28(2)	31(2)	4(2)	11(2)	5(2)	
C(21)	31(2)	11(2)	26(2)	0(2)	12(2)	-5(2)	

C(22)	26(2)	17(2)	26(2)	-1(2)	9(2)	-1(2)
C(23)	28(2)	16(2)	25(2)	-3(2)	9(2)	-4(2)
C(24)	31(2)	20(2)	27(2)	-3(2)	12(2)	-4(2)
C(25)	34(2)	22(2)	26(2)	-3(2)	13(2)	-3(2)
C(26)	34(2)	25(2)	30(2)	-1(2)	13(2)	-6(2)
C(27)	44(3)	40(3)	34(2)	-10(2)	15(2)	-7(2)
C(28)	59(3)	46(3)	34(3)	-10(2)	28(2)	-8(2)
C(29)	36(3)	44(3)	43(3)	-9(2)	20(2)	-7(2)
C(30)	35(2)	24(2)	30(2)	-8(2)	11(2)	-3(2)
C(31)	29(2)	35(2)	37(2)	5(2)	1(2)	9(2)
C(32)	36(3)	54(3)	46(3)	12(2)	22(2)	10(2)
C(33)	65(4)	72(4)	44(3)	12(3)	14(3)	25(3)
C(34)	48(3)	50(3)	46(3)	5(2)	13(2)	9(2)
C(35)	33(3)	46(3)	69(3)	9(3)	19(2)	9(2)
C(36)	59(3)	34(3)	38(3)	-3(2)	20(2)	-5(2)
C(38)	80(6)	23(3)	139(7)	0	97(6)	0
N(1)	27(2)	27(2)	26(2)	3(2)	13(2)	2(2)
N(2)	24(2)	20(2)	25(2)	-4(2)	10(2)	-4(2)
N(3)	25(2)	18(2)	25(2)	0(2)	8(2)	-2(2)
N(4)	35(2)	21(2)	27(2)	-2(2)	16(2)	-1(2)
N(5)	83(3)	30(2)	66(3)	1(2)	53(3)	4(2)
O(1)	30(2)	39(2)	38(2)	-6(2)	7(1)	6(2)
O(2)	29(2)	20(1)	34(2)	-5(1)	5(1)	-2(1)
O(3)	25(2)	15(2)	37(2)	-6(1)	5(1)	-3(1)
O(4)	26(2)	20(1)	49(2)	7(1)	7(1)	0(1)
O(5)	30(2)	19(1)	31(2)	4(1)	5(1)	-2(1)
O(6)	34(2)	29(2)	41(2)	-9(2)	3(1)	0(1)
O(7)	50(2)	36(2)	46(2)	4(2)	1(2)	2(2)
O(8)	54(4)	32(4)	66(4)	18(3)	-23(3)	-27(3)

Torsion angles [°] for 9m_alvsb2_0f.

O(1)-C(1)-C(2)-C(3)	177.7(3)
C(6)-C(1)-C(2)-C(3)	56.1(4)
C(1)-C(2)-C(3)-C(4)	-54.2(5)
C(2)-C(3)-C(4)-C(5)	53.7(5)
C(3)-C(4)-C(5)-C(6)	-55.7(5)
O(1)-C(1)-C(6)-N(1)	57.7(4)
C(2)-C(1)-C(6)-N(1)	-179.4(3)
O(1)-C(1)-C(6)-C(5)	-179.9(3)
C(2)-C(1)-C(6)-C(5)	-57.0(4)
C(4)-C(5)-C(6)-N(1)	178.7(3)
C(4)-C(5)-C(6)-C(1)	57.2(4)
N(1)-C(7)-C(8)-O(2)	83.4(4)
N(1)-C(7)-C(8)-C(9)	-156.3(3)
O(2)-C(8)-C(9)-N(2)	-58.6(4)
C(7)-C(8)-C(9)-N(2)	-179.7(3)
N(2)-C(10)-C(11)-C(12)	177.3(3)
C(15)-C(10)-C(11)-C(12)	56.7(4)
C(10)-C(11)-C(12)-C(13)	-57.6(4)
C(11)-C(12)-C(13)-C(14)	55.9(4)
C(12)-C(13)-C(14)-C(15)	-54.4(4)
C(13)-C(14)-C(15)-O(3)	175.0(3)
C(13)-C(14)-C(15)-C(10)	54.2(4)
N(2)-C(10)-C(15)-O(3)	60.2(4)
C(11)-C(10)-C(15)-O(3)	-177.0(3)
N(2)-C(10)-C(15)-C(14)	-177.9(3)
C(11)-C(10)-C(15)-C(14)	-55.0(4)
O(4)-C(16)-C(17)-C(18)	177.5(3)
C(21)-C(16)-C(17)-C(18)	-56.8(4)

C(16)-C(17)-C(18)-C(19)	55.8(4)
C(17)-C(18)-C(19)-C(20)	-55.4(5)
C(18)-C(19)-C(20)-C(21)	55.6(4)
C(19)-C(20)-C(21)-N(3)	-176.9(3)
C(19)-C(20)-C(21)-C(16)	-55.5(4)
O(4)-C(16)-C(21)-N(3)	-54.8(4)
C(17)-C(16)-C(21)-N(3)	179.4(3)
O(4)-C(16)-C(21)-C(20)	-177.9(3)
C(17)-C(16)-C(21)-C(20)	56.2(4)
N(3)-C(22)-C(23)-O(5)	58.5(4)
N(3)-C(22)-C(23)-C(24)	-175.6(3)
O(5)-C(23)-C(24)-N(4)	-60.2(4)
C(22)-C(23)-C(24)-N(4)	173.8(3)
N(4)-C(25)-C(26)-C(27)	-179.7(3)
C(30)-C(25)-C(26)-C(27)	-54.6(4)
C(25)-C(26)-C(27)-C(28)	54.8(5)
C(26)-C(27)-C(28)-C(29)	-54.2(5)
C(27)-C(28)-C(29)-C(30)	54.2(5)
N(4)-C(25)-C(30)-O(6)	-60.7(4)
C(26)-C(25)-C(30)-O(6)	173.6(3)
N(4)-C(25)-C(30)-C(29)	178.5(3)
C(26)-C(25)-C(30)-C(29)	52.8(4)
C(28)-C(29)-C(30)-O(6)	-173.6(3)
C(28)-C(29)-C(30)-C(25)	-53.1(5)
O(7)-C(31)-C(32)-C(33)	-178.4(4)
C(36)-C(31)-C(32)-C(33)	-57.0(5)
C(31)-C(32)-C(33)-C(34)	55.5(6)
C(32)-C(33)-C(34)-C(35)	-56.0(6)
C(33)-C(34)-C(35)-C(36)	58.2(5)
O(7)-C(31)-C(36)-N(5)	-57.5(5)
C(32)-C(31)-C(36)-N(5)	-179.0(4)

O(7)-C(31)-C(36)-C(35)	179.3(3)
C(32)-C(31)-C(36)-C(35)	57.9(5)
C(34)-C(35)-C(36)-N(5)	179.2(4)
C(34)-C(35)-C(36)-C(31)	-59.0(5)
N(5)-C(37)-C(38)-C(37)#1	173.2(7)
N(5)-C(37)-C(38)-O(8)	-112.9(7)
N(5)-C(37)-C(38)-O(8)#1	100.9(7)
C(1)-C(6)-N(1)-C(7)	-163.7(3)
C(5)-C(6)-N(1)-C(7)	74.6(4)
C(8)-C(7)-N(1)-C(6)	-162.8(3)
C(8)-C(9)-N(2)-C(10)	177.4(3)
C(15)-C(10)-N(2)-C(9)	-171.7(3)
C(11)-C(10)-N(2)-C(9)	66.4(4)
C(23)-C(22)-N(3)-C(21)	-171.4(3)
C(20)-C(21)-N(3)-C(22)	-66.1(4)
C(16)-C(21)-N(3)-C(22)	171.4(3)
C(23)-C(24)-N(4)-C(25)	165.0(3)
C(30)-C(25)-N(4)-C(24)	137.4(3)
C(26)-C(25)-N(4)-C(24)	-97.2(4)
C(31)-C(36)-N(5)-C(37)	169.1(5)
C(35)-C(36)-N(5)-C(37)	-69.3(6)
C(38)-C(37)-N(5)-C(36)	162.7(5)

Symmetry transformations used to generate equivalent atoms: #1 -x,y,-z+1/2

Table E.6. Hydrogen Bonds for 9m_alvsb2_0f in C2/c [Å and °].

D-H...A	d(D-H)	d(H...A)	d(D...A)	<(DHA)	#
N1 -- H1N .. O1	0.85(4)	2.47(4)	3.202(4)	145(3)	1
O1 -- H1O .. N5	0.81(4)	2.08(4)	2.871(5)	166(5)	1
O4 -- H4 .. O2	0.8200	1.8900	2.710(4)	174.00	2
O5 -- H5 .. O3	0.8200	1.9200	2.736(4)	179.00	2

O8 -- H8H .. O6	0.8200	1.7900	2.609(7)	179.00	1
C21 -- H21 .. O5	0.9800	2.5500	3.429(4)	149.00	2
C24 -- H24A .. O4	0.9700	2.4800	3.371(4)	153.00	2

Symmetry transformations used to generate equ equivalent atoms:

#1 -x,y,1/2-z #2 1/2-x,1/2+y,1/2-z

Cy_2-Otn(b) Data

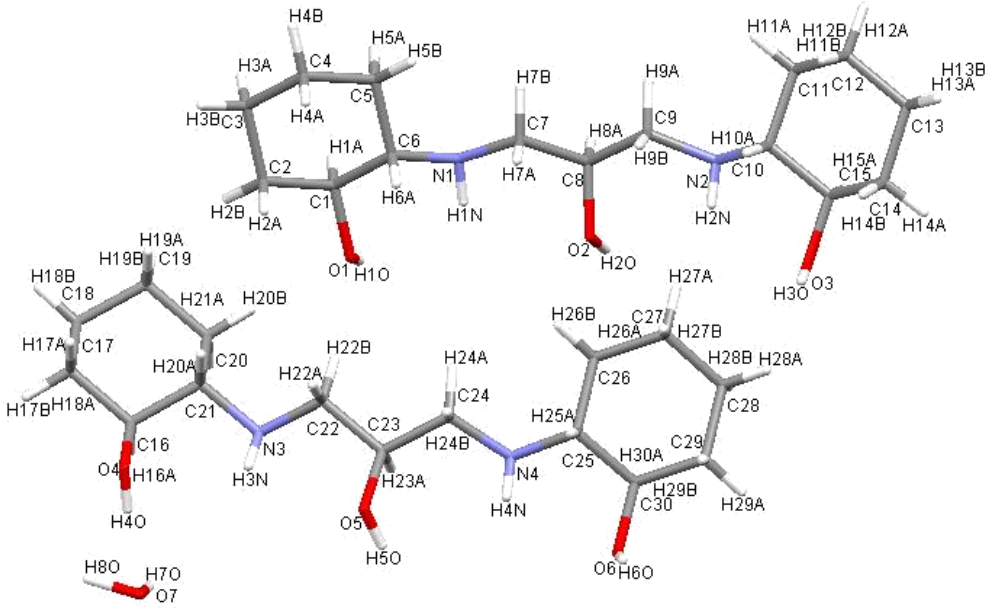


Figure E.2. XRD structure of the protonated Cy_2-Otn(b) and the labelling scheme used.

Table E.7. Crystal data and structure refinement for 7m_al19_0s.

Identification code	7m_al19_0s
Empirical formula	C30 H62 N4 O7
Formula weight	590.84
Temperature	293(2) K
Wavelength	0.71073 Å
Crystal system	Triclinic

Space group	P-1	
Unit cell dimensions	a = 10.0830(2) Å	α = 104.5330(10)°.
	b = 10.6966(3) Å	β = 104.7020(10)°.
	c = 16.6006(4) Å	γ = 90.5310(10)°.
Volume	1671.31(7) $Å^3$	
Z	2	
Density (calculated)	1.174 Mg/m^3	
Absorption coefficient	0.083 mm^{-1}	
F(000)	652	
Crystal size	0.42 x 0.22 x 0.16 mm^3	
Theta range for data collection	1.31 to 28.00°.	
Index ranges	-13<=h<=13, -14<=k<=14, -21<=l<=21	
Reflections collected	29863	
Independent reflections	8075 [R(int) = 0.0548]	
Completeness to theta = 28.00°	100.0 %	
Absorption correction	None	
Max. and min. transmission	0.9869 and 0.9662	
Refinement method	Full-matrix least-squares on F^2	
Data / restraints / parameters	8075 / 0 / 397	
Goodness-of-fit on F^2	1.002	
Final R indices [I>2sigma(I)]	R1 = 0.0504, wR2 = 0.1196	
R indices (all data)	R1 = 0.0868, wR2 = 0.1338	
Largest diff. peak and hole	0.397 and -0.226 e.$Å^{-3}$	

Table E.8. Atomic coordinates (x 10^4) and equivalent isotropic displacement parameters ($Å^2$x 10^3) for 7m_al19_0s. U(eq) is defined as one third of the trace of the orthogonalized U^{ij} tensor.

	x	y	z	U(eq)
C(1)	-1447(2)	5680(2)	3207(1)	28(1)
C(2)	-2250(2)	6857(2)	3151(1)	36(1)

C(3)	-3660(2)	6681(2)	3294(1)	39(1)
C(4)	-4453(2)	5476(2)	2657(1)	38(1)
C(5)	-3657(2)	4283(2)	2714(1)	35(1)
C(6)	-2239(2)	4462(2)	2577(1)	26(1)
C(7)	-1984(2)	2142(2)	2045(1)	31(1)
C(8)	-955(2)	1119(2)	2019(1)	27(1)
C(9)	-1687(2)	-116(2)	1390(1)	35(1)
C(10)	-1480(2)	-2161(2)	432(1)	32(1)
C(11)	-2417(2)	-3078(2)	647(1)	39(1)
C(12)	-3182(2)	-4090(2)	-169(1)	53(1)
C(13)	-2190(2)	-4828(2)	-608(1)	53(1)
C(14)	-1166(2)	-3941(2)	-776(1)	40(1)
C(15)	-452(2)	-2906(2)	29(1)	35(1)
N(1)	-1419(1)	3353(1)	2684(1)	27(1)
N(2)	-774(1)	-1126(1)	1195(1)	30(1)
O(1)	-150(1)	5846(1)	3029(1)	33(1)
O(2)	165(1)	1554(1)	1754(1)	31(1)
O(3)	496(1)	-2064(1)	-126(1)	40(1)
C(16)	6725(2)	10880(2)	7888(1)	32(1)
C(17)	5788(2)	11611(2)	8394(1)	38(1)
C(18)	5927(2)	11229(2)	9231(1)	38(1)
C(19)	5648(2)	9785(2)	9061(1)	32(1)
C(20)	6552(2)	9050(2)	8527(1)	29(1)
C(21)	6396(2)	9438(2)	7691(1)	27(1)
C(22)	6691(2)	7409(2)	6722(1)	37(1)
C(23)	7632(2)	6675(2)	6239(1)	33(1)
C(24)	7059(2)	5297(2)	5791(1)	39(1)
C(25)	7607(2)	3175(2)	5005(1)	27(1)
C(26)	6897(2)	2411(2)	5459(1)	37(1)
C(27)	6490(2)	1022(2)	4942(1)	45(1)
C(28)	7688(2)	354(2)	4687(1)	53(1)

C(29)	8351(2)	1109(2)	4207(1)	43(1)
C(30)	8802(2)	2474(2)	4760(1)	29(1)
N(3)	7290(1)	8712(1)	7198(1)	30(1)
N(4)	8123(1)	4476(1)	5561(1)	28(1)
O(4)	6596(1)	11252(1)	7111(1)	46(1)
O(5)	7833(1)	7341(1)	5631(1)	42(1)
O(6)	9534(1)	3217(1)	4382(1)	31(1)
O(7)	9337(1)	11798(1)	7277(1)	70(1)

Table E.9. Bond lengths [Å] and angles [°] for 7m_al19_0s.

C(1)-O(1)	1.4304(17)
C(1)-C(2)	1.514(2)
C(1)-C(6)	1.517(2)
C(1)-H(1A)	0.9800
C(2)-C(3)	1.517(2)
C(2)-H(2A)	0.9700
C(2)-H(2B)	0.9700
C(3)-C(4)	1.513(2)
C(3)-H(3A)	0.9700
C(3)-H(3B)	0.9700
C(4)-C(5)	1.524(2)
C(4)-H(4A)	0.9700
C(4)-H(4B)	0.9700
C(5)-C(6)	1.521(2)
C(5)-H(5A)	0.9700
C(5)-H(5B)	0.9700
C(6)-N(1)	1.474(2)
C(6)-H(6A)	0.9800
C(7)-N(1)	1.456(2)
C(7)-C(8)	1.515(2)
C(7)-H(7A)	0.9700

C(7)-H(7B)	0.9700
C(8)-O(2)	1.4250(17)
C(8)-C(9)	1.509(2)
C(8)-H(8A)	0.9800
C(9)-N(2)	1.455(2)
C(9)-H(9A)	0.9700
C(9)-H(9B)	0.9700
C(10)-N(2)	1.470(2)
C(10)-C(15)	1.503(2)
C(10)-C(11)	1.520(2)
C(10)-H(10A)	0.9800
C(11)-C(12)	1.523(3)
C(11)-H(11A)	0.9700
C(11)-H(11B)	0.9700
C(12)-C(13)	1.501(3)
C(12)-H(12A)	0.9700
C(12)-H(12B)	0.9700
C(13)-C(14)	1.518(3)
C(13)-H(13A)	0.9700
C(13)-H(13B)	0.9700
C(14)-C(15)	1.512(2)
C(14)-H(14A)	0.9700
C(14)-H(14B)	0.9700
C(15)-O(3)	1.420(2)
C(15)-H(15A)	0.9800
N(1)-H(1N)	0.848(17)
N(2)-H(2N)	0.836(18)
O(1)-H(1O)	0.8200
O(2)-H(2O)	0.8200
O(3)-H(3O)	0.8200
C(16)-O(4)	1.4184(18)

C(16)-C(21)	1.510(2)
C(16)-C(17)	1.516(2)
C(16)-H(16A)	0.9800
C(17)-C(18)	1.518(2)
C(17)-H(17A)	0.9700
C(17)-H(17B)	0.9700
C(18)-C(19)	1.509(2)
C(18)-H(18A)	0.9700
C(18)-H(18B)	0.9700
C(19)-C(20)	1.519(2)
C(19)-H(19A)	0.9700
C(19)-H(19B)	0.9700
C(20)-C(21)	1.518(2)
C(20)-H(20A)	0.9700
C(20)-H(20B)	0.9700
C(21)-N(3)	1.468(2)
C(21)-H(21A)	0.9800
C(22)-N(3)	1.456(2)
C(22)-C(23)	1.498(2)
C(22)-H(22A)	0.9700
C(22)-H(22B)	0.9700
C(23)-O(5)	1.424(2)
C(23)-C(24)	1.508(2)
C(23)-H(23A)	0.9800
C(24)-N(4)	1.458(2)
C(24)-H(24A)	0.9700
C(24)-H(24B)	0.9700
C(25)-N(4)	1.469(2)
C(25)-C(30)	1.515(2)
C(25)-C(26)	1.523(2)
C(25)-H(25A)	0.9800

C(26)-C(27)	1.511(2)
C(26)-H(26A)	0.9700
C(26)-H(26B)	0.9700
C(27)-C(28)	1.508(3)
C(27)-H(27A)	0.9700
C(27)-H(27B)	0.9700
C(28)-C(29)	1.522(3)
C(28)-H(28A)	0.9700
C(28)-H(28B)	0.9700
C(29)-C(30)	1.512(2)
C(29)-H(29A)	0.9700
C(29)-H(29B)	0.9700
C(30)-O(6)	1.4293(17)
C(30)-H(30A)	0.9800
N(3)-H(3N)	0.816(17)
N(4)-H(4N)	0.794(17)
O(4)-H(4O)	0.8200
O(5)-H(5O)	0.8200
O(6)-H(6O)	0.8200
O(7)-H(7O)	1.21(4)
O(7)-H(8O)	1.074(12)

O(1)-C(1)-C(2)	110.36(13)
O(1)-C(1)-C(6)	109.18(12)
C(2)-C(1)-C(6)	111.21(13)
O(1)-C(1)-H(1A)	108.7
C(2)-C(1)-H(1A)	108.7
C(6)-C(1)-H(1A)	108.7
C(1)-C(2)-C(3)	111.50(14)
C(1)-C(2)-H(2A)	109.3
C(3)-C(2)-H(2A)	109.3

C(1)-C(2)-H(2B)	109.3
C(3)-C(2)-H(2B)	109.3
H(2A)-C(2)-H(2B)	108.0
C(4)-C(3)-C(2)	110.52(14)
C(4)-C(3)-H(3A)	109.5
C(2)-C(3)-H(3A)	109.5
C(4)-C(3)-H(3B)	109.5
C(2)-C(3)-H(3B)	109.5
H(3A)-C(3)-H(3B)	108.1
C(3)-C(4)-C(5)	111.07(14)
C(3)-C(4)-H(4A)	109.4
C(5)-C(4)-H(4A)	109.4
C(3)-C(4)-H(4B)	109.4
C(5)-C(4)-H(4B)	109.4
H(4A)-C(4)-H(4B)	108.0
C(6)-C(5)-C(4)	111.00(14)
C(6)-C(5)-H(5A)	109.4
C(4)-C(5)-H(5A)	109.4
C(6)-C(5)-H(5B)	109.4
C(4)-C(5)-H(5B)	109.4
H(5A)-C(5)-H(5B)	108.0
N(1)-C(6)-C(1)	108.28(12)
N(1)-C(6)-C(5)	111.82(13)
C(1)-C(6)-C(5)	110.96(13)
N(1)-C(6)-H(6A)	108.6
C(1)-C(6)-H(6A)	108.6
C(5)-C(6)-H(6A)	108.6
N(1)-C(7)-C(8)	112.57(12)
N(1)-C(7)-H(7A)	109.1
C(8)-C(7)-H(7A)	109.1
N(1)-C(7)-H(7B)	109.1

C(8)-C(7)-H(7B)	109.1
H(7A)-C(7)-H(7B)	107.8
O(2)-C(8)-C(9)	111.27(13)
O(2)-C(8)-C(7)	108.91(13)
C(9)-C(8)-C(7)	107.70(12)
O(2)-C(8)-H(8A)	109.6
C(9)-C(8)-H(8A)	109.6
C(7)-C(8)-H(8A)	109.6
N(2)-C(9)-C(8)	113.71(13)
N(2)-C(9)-H(9A)	108.8
C(8)-C(9)-H(9A)	108.8
N(2)-C(9)-H(9B)	108.8
C(8)-C(9)-H(9B)	108.8
H(9A)-C(9)-H(9B)	107.7
N(2)-C(10)-C(15)	110.39(13)
N(2)-C(10)-C(11)	112.04(14)
C(15)-C(10)-C(11)	109.98(14)
N(2)-C(10)-H(10A)	108.1
C(15)-C(10)-H(10A)	108.1
C(11)-C(10)-H(10A)	108.1
C(10)-C(11)-C(12)	110.22(15)
C(10)-C(11)-H(11A)	109.6
C(12)-C(11)-H(11A)	109.6
C(10)-C(11)-H(11B)	109.6
C(12)-C(11)-H(11B)	109.6
H(11A)-C(11)-H(11B)	108.1
C(13)-C(12)-C(11)	110.74(16)
C(13)-C(12)-H(12A)	109.5
C(11)-C(12)-H(12A)	109.5
C(13)-C(12)-H(12B)	109.5
C(11)-C(12)-H(12B)	109.5

H(12A)-C(12)-H(12B)	108.1
C(12)-C(13)-C(14)	112.32(16)
C(12)-C(13)-H(13A)	109.1
C(14)-C(13)-H(13A)	109.1
C(12)-C(13)-H(13B)	109.1
C(14)-C(13)-H(13B)	109.1
H(13A)-C(13)-H(13B)	107.9
C(15)-C(14)-C(13)	112.13(15)
C(15)-C(14)-H(14A)	109.2
C(13)-C(14)-H(14A)	109.2
C(15)-C(14)-H(14B)	109.2
C(13)-C(14)-H(14B)	109.2
H(14A)-C(14)-H(14B)	107.9
O(3)-C(15)-C(10)	111.23(14)
O(3)-C(15)-C(14)	112.45(14)
C(10)-C(15)-C(14)	110.92(14)
O(3)-C(15)-H(15A)	107.3
C(10)-C(15)-H(15A)	107.3
C(14)-C(15)-H(15A)	107.3
C(7)-N(1)-C(6)	113.95(12)
C(7)-N(1)-H(1N)	107.7(11)
C(6)-N(1)-H(1N)	106.6(12)
C(9)-N(2)-C(10)	110.72(12)
C(9)-N(2)-H(2N)	104.0(12)
C(10)-N(2)-H(2N)	104.8(12)
C(1)-O(1)-H(1O)	109.5
C(8)-O(2)-H(2O)	109.5
C(15)-O(3)-H(3O)	109.5
O(4)-C(16)-C(21)	110.10(14)
O(4)-C(16)-C(17)	110.60(13)
C(21)-C(16)-C(17)	110.38(13)

O(4)-C(16)-H(16A)	108.6
C(21)-C(16)-H(16A)	108.6
C(17)-C(16)-H(16A)	108.6
C(16)-C(17)-C(18)	111.04(14)
C(16)-C(17)-H(17A)	109.4
C(18)-C(17)-H(17A)	109.4
C(16)-C(17)-H(17B)	109.4
C(18)-C(17)-H(17B)	109.4
H(17A)-C(17)-H(17B)	108.0
C(19)-C(18)-C(17)	110.99(14)
C(19)-C(18)-H(18A)	109.4
C(17)-C(18)-H(18A)	109.4
C(19)-C(18)-H(18B)	109.4
C(17)-C(18)-H(18B)	109.4
H(18A)-C(18)-H(18B)	108.0
C(18)-C(19)-C(20)	111.02(13)
C(18)-C(19)-H(19A)	109.4
C(20)-C(19)-H(19A)	109.4
C(18)-C(19)-H(19B)	109.4
C(20)-C(19)-H(19B)	109.4
H(19A)-C(19)-H(19B)	108.0
C(21)-C(20)-C(19)	111.89(13)
C(21)-C(20)-H(20A)	109.2
C(19)-C(20)-H(20A)	109.2
C(21)-C(20)-H(20B)	109.2
C(19)-C(20)-H(20B)	109.2
H(20A)-C(20)-H(20B)	107.9
N(3)-C(21)-C(16)	111.20(13)
N(3)-C(21)-C(20)	110.13(13)
C(16)-C(21)-C(20)	109.60(13)
N(3)-C(21)-H(21A)	108.6

C(16)-C(21)-H(21A)	108.6
C(20)-C(21)-H(21A)	108.6
N(3)-C(22)-C(23)	111.37(13)
N(3)-C(22)-H(22A)	109.4
C(23)-C(22)-H(22A)	109.4
N(3)-C(22)-H(22B)	109.4
C(23)-C(22)-H(22B)	109.4
H(22A)-C(22)-H(22B)	108.0
O(5)-C(23)-C(22)	108.15(14)
O(5)-C(23)-C(24)	110.77(14)
C(22)-C(23)-C(24)	111.62(14)
O(5)-C(23)-H(23A)	108.7
C(22)-C(23)-H(23A)	108.7
C(24)-C(23)-H(23A)	108.7
N(4)-C(24)-C(23)	111.62(13)
N(4)-C(24)-H(24A)	109.3
C(23)-C(24)-H(24A)	109.3
N(4)-C(24)-H(24B)	109.3
C(23)-C(24)-H(24B)	109.3
H(24A)-C(24)-H(24B)	108.0
N(4)-C(25)-C(30)	108.75(12)
N(4)-C(25)-C(26)	111.19(13)
C(30)-C(25)-C(26)	110.26(14)
N(4)-C(25)-H(25A)	108.9
C(30)-C(25)-H(25A)	108.9
C(26)-C(25)-H(25A)	108.9
C(27)-C(26)-C(25)	112.36(14)
C(27)-C(26)-H(26A)	109.1
C(25)-C(26)-H(26A)	109.1
C(27)-C(26)-H(26B)	109.1
C(25)-C(26)-H(26B)	109.1

H(26A)-C(26)-H(26B)	107.9
C(28)-C(27)-C(26)	111.94(15)
C(28)-C(27)-H(27A)	109.2
C(26)-C(27)-H(27A)	109.2
C(28)-C(27)-H(27B)	109.2
C(26)-C(27)-H(27B)	109.2
H(27A)-C(27)-H(27B)	107.9
C(27)-C(28)-C(29)	111.02(17)
C(27)-C(28)-H(28A)	109.4
C(29)-C(28)-H(28A)	109.4
C(27)-C(28)-H(28B)	109.4
C(29)-C(28)-H(28B)	109.4
H(28A)-C(28)-H(28B)	108.0
C(30)-C(29)-C(28)	109.84(15)
C(30)-C(29)-H(29A)	109.7
C(28)-C(29)-H(29A)	109.7
C(30)-C(29)-H(29B)	109.7
C(28)-C(29)-H(29B)	109.7
H(29A)-C(29)-H(29B)	108.2
O(6)-C(30)-C(29)	113.25(13)
O(6)-C(30)-C(25)	111.05(13)
C(29)-C(30)-C(25)	111.67(13)
O(6)-C(30)-H(30A)	106.8
C(29)-C(30)-H(30A)	106.8
C(25)-C(30)-H(30A)	106.8
C(22)-N(3)-C(21)	112.18(13)
C(22)-N(3)-H(3N)	107.9(12)
C(21)-N(3)-H(3N)	108.3(12)
C(24)-N(4)-C(25)	114.56(12)
C(24)-N(4)-H(4N)	110.0(12)
C(25)-N(4)-H(4N)	106.3(12)

C(16)-O(4)-H(4O)	109.5
C(23)-O(5)-H(5O)	109.5
C(30)-O(6)-H(6O)	109.5
H(7O)-O(7)-H(8O)	81.3(16)

Table E.10. Anisotropic displacement parameters ($Å^2 x\ 10^3$)for 7m_al19_0s. The anisotropic displacement factor exponent takes the form: $-2p^2[\ h^2 a^{*2} U^{11} + ... + 2\ h\ k\ a^*\ b^*\ U^{12}\ ]$

	U^{11}	U^{22}	U^{33}	U^{23}	U^{13}	U^{12}
C(1)	24(1)	33(1)	27(1)	10(1)	7(1)	-1(1)
C(2)	36(1)	30(1)	38(1)	9(1)	6(1)	2(1)
C(3)	37(1)	43(1)	38(1)	13(1)	12(1)	17(1)
C(4)	24(1)	46(1)	46(1)	17(1)	10(1)	9(1)
C(5)	23(1)	36(1)	46(1)	12(1)	9(1)	0(1)
C(6)	22(1)	31(1)	27(1)	10(1)	6(1)	2(1)
C(7)	22(1)	34(1)	34(1)	6(1)	4(1)	1(1)
C(8)	21(1)	33(1)	28(1)	8(1)	7(1)	1(1)
C(9)	24(1)	36(1)	40(1)	5(1)	6(1)	3(1)
C(10)	29(1)	31(1)	35(1)	12(1)	6(1)	3(1)
C(11)	32(1)	35(1)	54(1)	13(1)	18(1)	2(1)
C(12)	38(1)	40(1)	77(2)	11(1)	14(1)	-7(1)
C(13)	45(1)	35(1)	69(1)	3(1)	7(1)	-2(1)
C(14)	37(1)	38(1)	40(1)	3(1)	8(1)	6(1)
C(15)	31(1)	39(1)	37(1)	11(1)	10(1)	3(1)
N(1)	19(1)	28(1)	32(1)	7(1)	5(1)	0(1)
N(2)	25(1)	31(1)	34(1)	7(1)	11(1)	1(1)
O(1)	24(1)	40(1)	35(1)	14(1)	5(1)	-4(1)
O(2)	23(1)	42(1)	31(1)	13(1)	8(1)	2(1)
O(3)	33(1)	54(1)	33(1)	11(1)	9(1)	-6(1)

C(16)	25(1)	40(1)	34(1)	19(1)	5(1)	0(1)
C(17)	33(1)	33(1)	50(1)	15(1)	12(1)	6(1)
C(18)	30(1)	44(1)	38(1)	7(1)	13(1)	6(1)
C(19)	23(1)	45(1)	32(1)	13(1)	11(1)	4(1)
C(20)	26(1)	34(1)	30(1)	13(1)	10(1)	4(1)
C(21)	19(1)	37(1)	26(1)	11(1)	6(1)	2(1)
C(22)	26(1)	47(1)	37(1)	3(1)	11(1)	0(1)
C(23)	23(1)	44(1)	32(1)	8(1)	10(1)	3(1)
C(24)	25(1)	47(1)	43(1)	1(1)	15(1)	0(1)
C(25)	22(1)	35(1)	24(1)	8(1)	6(1)	-4(1)
C(26)	33(1)	47(1)	33(1)	12(1)	12(1)	-12(1)
C(27)	46(1)	49(1)	40(1)	12(1)	10(1)	-21(1)
C(28)	70(1)	32(1)	59(1)	10(1)	22(1)	-12(1)
C(29)	48(1)	34(1)	49(1)	4(1)	21(1)	-3(1)
C(30)	29(1)	33(1)	28(1)	11(1)	10(1)	-2(1)
N(3)	28(1)	39(1)	26(1)	10(1)	11(1)	0(1)
N(4)	23(1)	35(1)	28(1)	7(1)	13(1)	-2(1)
O(4)	40(1)	65(1)	48(1)	39(1)	12(1)	4(1)
O(5)	40(1)	57(1)	40(1)	19(1)	21(1)	11(1)
O(6)	28(1)	38(1)	29(1)	8(1)	12(1)	-4(1)
O(7)	49(1)	90(1)	75(1)	49(1)	-1(1)	-18(1)

Table E.11. Torsion angles [°] for 7m_al19_0s.

O(1)-C(1)-C(2)-C(3)	177.27(13)
C(6)-C(1)-C(2)-C(3)	55.95(18)
C(1)-C(2)-C(3)-C(4)	-56.38(19)
C(2)-C(3)-C(4)-C(5)	56.39(19)
C(3)-C(4)-C(5)-C(6)	-56.25(19)
O(1)-C(1)-C(6)-N(1)	59.69(16)
C(2)-C(1)-C(6)-N(1)	-178.30(13)
O(1)-C(1)-C(6)-C(5)	-177.24(12)

C(2)-C(1)-C(6)-C(5)	-55.23(17)
C(4)-C(5)-C(6)-N(1)	176.37(13)
C(4)-C(5)-C(6)-C(1)	55.36(18)
N(1)-C(7)-C(8)-O(2)	-63.77(17)
N(1)-C(7)-C(8)-C(9)	175.45(13)
O(2)-C(8)-C(9)-N(2)	51.38(19)
C(7)-C(8)-C(9)-N(2)	170.67(14)
N(2)-C(10)-C(11)-C(12)	177.08(14)
C(15)-C(10)-C(11)-C(12)	-59.75(18)
C(10)-C(11)-C(12)-C(13)	57.3(2)
C(11)-C(12)-C(13)-C(14)	-53.4(2)
C(12)-C(13)-C(14)-C(15)	52.0(2)
N(2)-C(10)-C(15)-O(3)	-51.94(18)
C(11)-C(10)-C(15)-O(3)	-176.07(14)
N(2)-C(10)-C(15)-C(14)	-177.88(14)
C(11)-C(10)-C(15)-C(14)	57.98(19)
C(13)-C(14)-C(15)-O(3)	-179.34(15)
C(13)-C(14)-C(15)-C(10)	-54.1(2)
C(8)-C(7)-N(1)-C(6)	164.80(13)
C(1)-C(6)-N(1)-C(7)	-172.91(13)
C(5)-C(6)-N(1)-C(7)	64.54(17)
C(8)-C(9)-N(2)-C(10)	-165.84(14)
C(15)-C(10)-N(2)-C(9)	158.02(14)
C(11)-C(10)-N(2)-C(9)	-79.04(17)
O(4)-C(16)-C(17)-C(18)	-179.54(14)
C(21)-C(16)-C(17)-C(18)	58.37(18)
C(16)-C(17)-C(18)-C(19)	-56.08(19)
C(17)-C(18)-C(19)-C(20)	54.06(18)
C(18)-C(19)-C(20)-C(21)	-55.23(18)
O(4)-C(16)-C(21)-N(3)	57.42(16)
C(17)-C(16)-C(21)-N(3)	179.81(13)

O(4)-C(16)-C(21)-C(20)	179.43(12)
C(17)-C(16)-C(21)-C(20)	-58.19(16)
C(19)-C(20)-C(21)-N(3)	179.68(13)
C(19)-C(20)-C(21)-C(16)	57.04(17)
N(3)-C(22)-C(23)-O(5)	-61.64(18)
N(3)-C(22)-C(23)-C(24)	176.27(14)
O(5)-C(23)-C(24)-N(4)	77.77(18)
C(22)-C(23)-C(24)-N(4)	-161.66(14)
N(4)-C(25)-C(26)-C(27)	-173.86(14)
C(30)-C(25)-C(26)-C(27)	-53.16(18)
C(25)-C(26)-C(27)-C(28)	53.2(2)
C(26)-C(27)-C(28)-C(29)	-54.9(2)
C(27)-C(28)-C(29)-C(30)	57.1(2)
C(28)-C(29)-C(30)-O(6)	175.32(15)
C(28)-C(29)-C(30)-C(25)	-58.4(2)
N(4)-C(25)-C(30)-O(6)	-54.17(16)
C(26)-C(25)-C(30)-O(6)	-176.32(12)
N(4)-C(25)-C(30)-C(29)	178.38(13)
C(26)-C(25)-C(30)-C(29)	56.23(17)
C(23)-C(22)-N(3)-C(21)	-178.77(13)
C(16)-C(21)-N(3)-C(22)	-157.87(13)
C(20)-C(21)-N(3)-C(22)	80.44(17)
C(23)-C(24)-N(4)-C(25)	-170.91(14)
C(30)-C(25)-N(4)-C(24)	175.43(13)
C(26)-C(25)-N(4)-C(24)	-62.98(18)

Table E.12. Hydrogen bonds for 7m_al19_0s [Å and °].

D-H...A	d(D-H)	d(H...A)	d(D...A)	<(DHA)
N(1)-H(1N)...O(1)	0.848(17)	2.400(17)	2.8057(17)	110.1(13)
N(2)-H(2N)...O(3)	0.836(18)	2.335(17)	2.7926(18)	114.9(14)
N(2)-H(2N)...O(2)	0.836(18)	2.450(17)	2.8543(18)	110.7(14)

N(3)-H(3N)...O(4)	0.816(17)	2.424(17)	2.842(2)	112.8(14)
N(4)-H(4N)...O(6)	0.794(17)	2.398(16)	2.7912(16)	111.7(14)

Cy_2-tn(a) Data

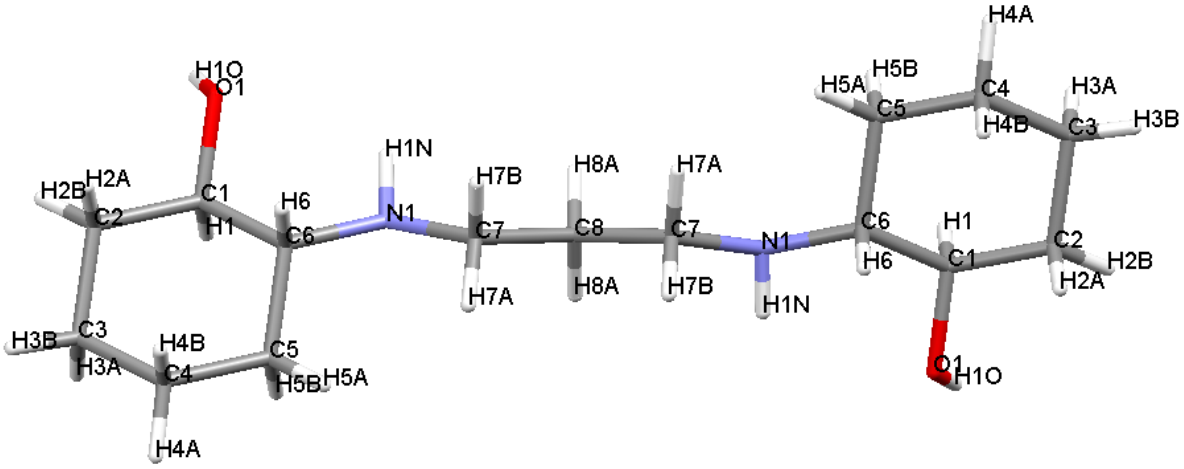


Figure E.2. XRD structure of the protonated Cy_2-tn(a) and the labelling scheme used.

Table E.13. Crystal data and structure refinement for 9m_sb8_0s.

Identification code	9m_sb8_0s
Empirical formula	C15 H30 N2 O2
Formula weight	270.41
Temperature	173(2) K
Wavelength	0.71073 Å
Crystal system	Monoclinic
Space group	C2/c

Unit cell dimensions	a = 24.5923(8) Å	α = 90°.
	b = 8.2587(3) Å	β = 90.568(2)°.
	c = 7.6234(3) Å	γ = 90°.
Volume	1548.24(10) Å3	
Z	4	
Density (calculated)	1.160 Mg/m3	
Absorption coefficient	0.076 mm-1	
F(000)	600	
Crystal size	0.54 x 0.43 x 0.21 mm3	
Theta range for data collection	1.66 to 27.98°.	
Index ranges	-31<=h<=32, -10<=k<=10, -10<=l<=9	
Reflections collected	5998	
Independent reflections	1834 [R(int) = 0.0308]	
Completeness to theta = 25.49°	98.8 %	
Absorption correction	None	
Refinement method	Full-matrix least-squares on F2	
Data / restraints / parameters	1834 / 0 / 95	
Goodness-of-fit on F^2	1.048	
Final R indices [I>2sigma(I)]	R1 = 0.0435, wR2 = 0.1099	
R indices (all data)	R1 = 0.0585, wR2 = 0.1180	
Largest diff. peak and hole	0.288 and -0.176 e.$Å^{-3}$	

Table E.14. Atomic coordinates (x 10^4) and equivalent isotropic displacement parameters ($Å^2$x 10^3) for 9m_sb8_0s. U(eq) is defined as one third of the trace of the orthogonalized Uij tensor.

	x	y	z	U(eq)
C(1)	1147(1)	3462(1)	2276(2)	21(1)
C(2)	1596(1)	2728(2)	1139(2)	28(1)
C(3)	2107(1)	2371(2)	2182(2)	34(1)
C(4)	1975(1)	1312(2)	3768(2)	29(1)

C(5)	1528(1)	2079(2)	4893(2)	25(1)
C(6)	1016(1)	2370(1)	3835(2)	19(1)
C(7)	338(1)	2063(2)	6229(2)	34(1)
C(8)	0	3026(2)	7500	23(1)
N(1)	586(1)	3133(1)	4904(1)	21(1)
O(1)	667(1)	3697(1)	1281(1)	25(1)

Table E.15. Bond lengths [Å] and angles [°] for 9m_sb8_0s .

C(1)-O(1)	1.4100(14)
C(1)-C(6)	1.5292(16)
C(1)-C(2)	1.5354(17)
C(1)-H(1)	1.0000
C(2)-C(3)	1.5082(18)
C(2)-H(2A)	0.9900
C(2)-H(2B)	0.9900
C(3)-C(4)	1.5290(18)
C(3)-H(3A)	0.9900
C(3)-H(3B)	0.9900
C(4)-C(5)	1.5380(17)
C(4)-H(4A)	0.9900
C(4)-H(4B)	0.9900
C(5)-C(6)	1.5090(17)
C(5)-H(5A)	0.9900
C(5)-H(5B)	0.9900
C(6)-N(1)	1.4815(15)
C(6)-H(6)	1.0000
C(7)-N(1)	1.4779(16)
C(7)-C(8)	1.5092(15)

C(7)-H(7A)	0.9900
C(7)-H(7B)	0.9900
C(8)-C(7)#1	1.5092(15)
C(8)-H(8A)	0.9900
C(8)-H(8B)	0.9900
N(1)-H(1N)	0.858(16)
O(1)-H(1O)	0.877(18)

O(1)-C(1)-C(6)	108.45(9)
O(1)-C(1)-C(2)	110.71(10)
C(6)-C(1)-C(2)	111.39(10)
O(1)-C(1)-H(1)	108.7
C(6)-C(1)-H(1)	108.7
C(2)-C(1)-H(1)	108.7
C(3)-C(2)-C(1)	112.25(11)
C(3)-C(2)-H(2A)	109.2
C(1)-C(2)-H(2A)	109.2
C(3)-C(2)-H(2B)	109.2
C(1)-C(2)-H(2B)	109.2
H(2A)-C(2)-H(2B)	107.9
C(2)-C(3)-C(4)	110.36(11)
C(2)-C(3)-H(3A)	109.6
C(4)-C(3)-H(3A)	109.6
C(2)-C(3)-H(3B)	109.6
C(4)-C(3)-H(3B)	109.6
H(3A)-C(3)-H(3B)	108.1
C(3)-C(4)-C(5)	111.29(11)
C(3)-C(4)-H(4A)	109.4
C(5)-C(4)-H(4A)	109.4
C(3)-C(4)-H(4B)	109.4

C(5)-C(4)-H(4B)	109.4
H(4A)-C(4)-H(4B)	108.0
C(6)-C(5)-C(4)	111.42(10)
C(6)-C(5)-H(5A)	109.3
C(4)-C(5)-H(5A)	109.3
C(6)-C(5)-H(5B)	109.3
C(4)-C(5)-H(5B)	109.3
H(5A)-C(5)-H(5B)	108.0
N(1)-C(6)-C(5)	111.69(10)
N(1)-C(6)-C(1)	109.54(9)
C(5)-C(6)-C(1)	109.12(9)
N(1)-C(6)-H(6)	108.8
C(5)-C(6)-H(6)	108.8
C(1)-C(6)-H(6)	108.8
N(1)-C(7)-C(8)	110.97(10)
N(1)-C(7)-H(7A)	109.4
C(8)-C(7)-H(7A)	109.4
N(1)-C(7)-H(7B)	109.4
C(8)-C(7)-H(7B)	109.4
H(7A)-C(7)-H(7B)	108.0
C(7)#1-C(8)-C(7)	116.45(14)
C(7)#1-C(8)-H(8A)	108.2
C(7)-C(8)-H(8A)	108.2
C(7)#1-C(8)-H(8B)	108.2
C(7)-C(8)-H(8B)	108.2
H(8A)-C(8)-H(8B)	107.3
C(7)-N(1)-C(6)	115.06(9)
C(7)-N(1)-H(1N)	106.2(10)
C(6)-N(1)-H(1N)	105.8(10)
C(1)-O(1)-H(1O)	107.1(11)

Symmetry transformations used to generate equivalent atoms: #1 -x,-y+1,-z

Table E.16. Anisotropic displacement parameters ($Å^2 x\ 10^3$) for 9m_sb8_0s. The anisotropic displacement factor exponent takes the form: $-2p^2[\ h^2 a^{*2} U^{11} + ... + 2\ h\ k\ a^*\ b^*\ U^{12}\ ]$

	U11	U22	U33	U23	U13	U12
C(1)	20(1)	23(1)	18(1)	0(1)	1(1)	1(1)
C(2)	30(1)	34(1)	21(1)	4(1)	9(1)	6(1)
C(3)	25(1)	45(1)	33(1)	7(1)	11(1)	8(1)
C(4)	23(1)	35(1)	28(1)	3(1)	3(1)	7(1)
C(5)	26(1)	30(1)	20(1)	2(1)	2(1)	4(1)
C(6)	21(1)	20(1)	18(1)	-2(1)	5(1)	1(1)
C(7)	40(1)	24(1)	37(1)	4(1)	23(1)	3(1)
C(8)	26(1)	28(1)	16(1)	0	5(1)	0
N(1)	21(1)	24(1)	18(1)	0(1)	5(1)	3(1)
O(1)	25(1)	27(1)	23(1)	2(1)	-3(1)	1(1)

Table E.17. Torsion angles [°] for 9m_sb8_0s.

O(1)-C(1)-C(2)-C(3)	-176.76(11)
C(6)-C(1)-C(2)-C(3)	-55.99(14)
C(1)-C(2)-C(3)-C(4)	53.94(15)
C(2)-C(3)-C(4)-C(5)	-54.41(16)
C(3)-C(4)-C(5)-C(6)	57.59(14)
C(4)-C(5)-C(6)-N(1)	-179.09(10)
C(4)-C(5)-C(6)-C(1)	-57.84(13)
O(1)-C(1)-C(6)-N(1)	-58.58(12)
C(2)-C(1)-C(6)-N(1)	179.34(10)
O(1)-C(1)-C(6)-C(5)	178.87(9)
C(2)-C(1)-C(6)-C(5)	56.79(13)
N(1)-C(7)-C(8)-C(7)#1	171.98(14)
C(8)-C(7)-N(1)-C(6)	167.57(9)
C(5)-C(6)-N(1)-C(7)	-71.40(14)

C(1)-C(6)-N(1)-C(7)	167.59(10)

Symmetry transformations used to generate equivalent atoms: #1 -x,y,-z+3/2

Table E.18. Hydrogen bonds for 9m_sb8_0s [Å and °].

D-H...A	d(D-H)	d(H...A)	d(D...A)	<(DHA)	#
N1 -- H1N .. O1	0.860(15)	2.488(15)	3.2375(12)	146.2(13)	1
O1 -- H1O .. N1	0.874(16)	1.960(16)	2.8270(13)	171.4(16)	2
C8 -- H8A .. O1	0.9900	2.5700	3.3489(9)	136.00	3
C8 -- H8B .. O1	0.9900	2.5700	3.3489(9)	136.00	1

Symmetry transformations used to generate equivalent atoms:

#1 -x,y,1/2-z, #2 x,1-y,-1/2+z #3 x,y,1+z

Cy_2-tn(b) Data

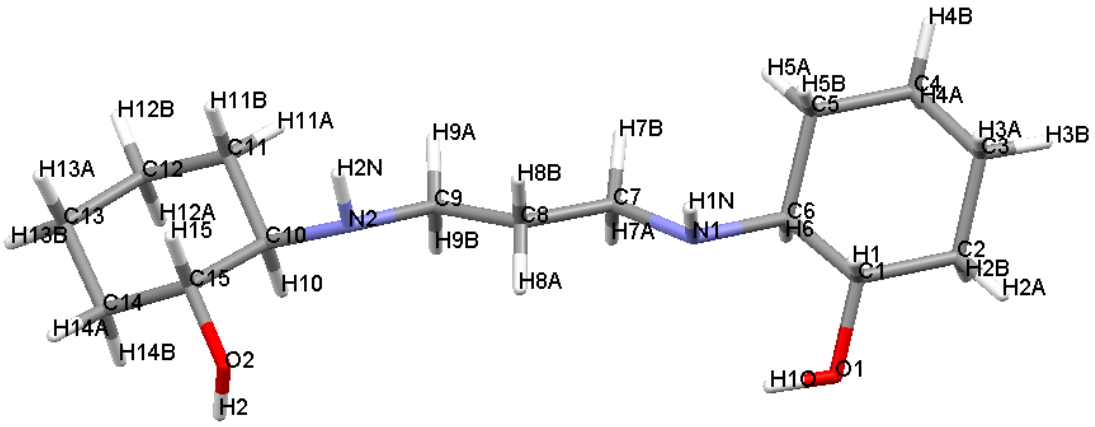


Figure E.4. XRD structure of Cy_2-tn(b) and the labelling scheme used.

Table E.19. Crystal data and structure refinement for 9m_sb6_0b.

Identification code	9m_sb6_0b	
Empirical formula	C15 H30 N2 O2	
Formula weight	270.41	
Temperature	173(2) K	
Wavelength	0.71073 Å	
Crystal system	Triclinic	
Space group	P-1	
Unit cell dimensions	a = 8.6048(13) Å	α= 66.971(6)°.
	b = 9.8900(14) Å	β= 77.718(8)°.
	c = 10.8797(17) Å	γ = 72.931(8)°.
Volume	809.5(2) $Å^3$	
Z	2	
Density (calculated)	1.109 Mg/m^3	
Absorption coefficient	0.073 mm^{-1}	
F(000)	300	
Crystal size	0.59 x 0.38 x 0.10 mm^3	
Theta range for data collection	2.05 to 25.00°.	
Index ranges	-10<=h<=10, -11<=k<=11, -12<=l<=12	
Reflections collected	12281	
Independent reflections	2833 [R(int) = 0.0557]	
Completeness to theta = 25.00°	99.3 %	
Absorption correction	None	

Refinement method	Full-matrix least-squares on F^2
Data / restraints / parameters	2833 / 0 / 174
Goodness-of-fit on F^2	2.709
Final R indices [I>2sigma(I)]	R1 = 0.2228, wR2 = 0.6156
R indices (all data)	R1 = 0.2499, wR2 = 0.6247
Largest diff. peak and hole	0.921 and -0.889 e.Å^{-3}

Table E.20. Atomic coordinates (x 10^4) and equivalent isotropic displacement parameters (Å^2 x 10^3) for 9m_sb6_0b. U(eq) is defined as one third of the trace of the orthogonalized U_{ij} tensor.

	x	y	z	U(eq)
C(1)	-1534(11)	2328(11)	8001(10)	35(2)
C(2)	-3063(12)	3197(12)	7328(10)	41(3)
C(3)	-2740(15)	4486(13)	6078(11)	49(3)
C(4)	-2013(13)	5536(11)	6339(10)	42(3)
C(5)	-458(13)	4672(12)	7022(10)	43(3)
C(6)	-748(10)	3315(10)	8302(9)	28(2)
C(7)	1510(13)	3062(13)	9513(12)	50(3)
C(8)	3181(12)	2046(12)	9933(12)	44(3)
C(9)	3874(12)	2488(12)	10810(12)	45(3)
C(10)	5957(11)	1472(11)	12365(9)	34(2)
C(11)	6461(13)	2893(12)	12129(12)	44(3)
C(12)	6941(15)	2883(14)	13391(14)	60(3)
C(13)	8331(17)	1482(16)	13935(15)	67(4)
C(14)	7859(15)	31(15)	14111(13)	58(3)
C(15)	7374(12)	104(11)	12831(11)	40(3)
N(1)	798(9)	2390(9)	8848(8)	35(2)
N(2)	5449(9)	1462(9)	11180(8)	33(2)
O(1)	-1819(8)	1076(7)	9193(7)	43(2)
O(2)	6929(10)	-1237(8)	13029(8)	52(2)

Table E.21. Bond lengths [Å] and angles [°] for 9m_sb6_0b.

C(1)-O(1)	1.436(12)
C(1)-C(2)	1.503(13)
C(1)-C(6)	1.500(13)
C(1)-H(1)	1.0000
C(2)-C(3)	1.498(16)
C(2)-H(2A)	0.9900
C(2)-H(2B)	0.9900
C(3)-C(4)	1.495(16)
C(3)-H(3A)	0.9900
C(3)-H(3B)	0.9900
C(4)-C(5)	1.526(14)
C(4)-H(4A)	0.9900
C(4)-H(4B)	0.9900
C(5)-C(6)	1.545(13)
C(5)-H(5A)	0.9900
C(5)-H(5B)	0.9900
C(6)-N(1)	1.468(11)
C(6)-H(6)	1.0000
C(7)-N(1)	1.464(14)
C(7)-C(8)	1.535(14)
C(7)-H(7A)	0.9900
C(7)-H(7B)	0.9900
C(8)-C(9)	1.476(14)
C(8)-H(8A)	0.9900
C(8)-H(8B)	0.9900
C(9)-N(2)	1.461(12)
C(9)-H(9A)	0.9900
C(9)-H(9B)	0.9900
C(10)-N(2)	1.452(12)
C(10)-C(11)	1.502(14)
C(10)-C(15)	1.527(13)
C(10)-H(10)	1.0000
C(11)-C(12)	1.511(16)
C(11)-H(11A)	0.9900

C(11)-H(11B)	0.9900
C(12)-C(13)	1.545(17)
C(12)-H(12A)	0.9900
C(12)-H(12B)	0.9900
C(13)-C(14)	1.535(19)
C(13)-H(13A)	0.9900
C(13)-H(13B)	0.9900
C(14)-C(15)	1.506(15)
C(14)-H(14A)	0.9900
C(14)-H(14B)	0.9900
C(15)-O(2)	1.411(13)
C(15)-H(15)	1.0000
N(1)-H(1N)	0.9200
N(2)-H(2N)	0.9200
O(1)-H(1O)	0.9800
O(2)-H(2)	0.8400

O(1)-C(1)-C(2)	112.0(7)
O(1)-C(1)-C(6)	110.6(8)
C(2)-C(1)-C(6)	112.5(8)
O(1)-C(1)-H(1)	107.1
C(2)-C(1)-H(1)	107.1
C(6)-C(1)-H(1)	107.1
C(3)-C(2)-C(1)	111.3(8)
C(3)-C(2)-H(2A)	109.4
C(1)-C(2)-H(2A)	109.4
C(3)-C(2)-H(2B)	109.4
C(1)-C(2)-H(2B)	109.4
H(2A)-C(2)-H(2B)	108.0
C(4)-C(3)-C(2)	112.5(9)
C(4)-C(3)-H(3A)	109.1
C(2)-C(3)-H(3A)	109.1
C(4)-C(3)-H(3B)	109.1
C(2)-C(3)-H(3B)	109.1
H(3A)-C(3)-H(3B)	107.8

C(3)-C(4)-C(5)	110.5(9)
C(3)-C(4)-H(4A)	109.6
C(5)-C(4)-H(4A)	109.6
C(3)-C(4)-H(4B)	109.6
C(5)-C(4)-H(4B)	109.6
H(4A)-C(4)-H(4B)	108.1
C(4)-C(5)-C(6)	112.0(8)
C(4)-C(5)-H(5A)	109.2
C(6)-C(5)-H(5A)	109.2
C(4)-C(5)-H(5B)	109.2
C(6)-C(5)-H(5B)	109.2
H(5A)-C(5)-H(5B)	107.9
N(1)-C(6)-C(1)	108.2(7)
N(1)-C(6)-C(5)	111.2(7)
C(1)-C(6)-C(5)	110.6(8)
N(1)-C(6)-H(6)	108.9
C(1)-C(6)-H(6)	108.9
C(5)-C(6)-H(6)	108.9
N(1)-C(7)-C(8)	109.8(8)
N(1)-C(7)-H(7A)	109.7
C(8)-C(7)-H(7A)	109.7
N(1)-C(7)-H(7B)	109.7
C(8)-C(7)-H(7B)	109.7
H(7A)-C(7)-H(7B)	108.2
C(9)-C(8)-C(7)	113.9(8)
C(9)-C(8)-H(8A)	108.8
C(7)-C(8)-H(8A)	108.8
C(9)-C(8)-H(8B)	108.8
C(7)-C(8)-H(8B)	108.8
H(8A)-C(8)-H(8B)	107.7
N(2)-C(9)-C(8)	110.7(8)
N(2)-C(9)-H(9A)	109.5
C(8)-C(9)-H(9A)	109.5
N(2)-C(9)-H(9B)	109.5
C(8)-C(9)-H(9B)	109.5

H(9A)-C(9)-H(9B)	108.1
N(2)-C(10)-C(11)	113.2(8)
N(2)-C(10)-C(15)	108.5(7)
C(11)-C(10)-C(15)	109.8(8)
N(2)-C(10)-H(10)	108.4
C(11)-C(10)-H(10)	108.4
C(15)-C(10)-H(10)	108.4
C(10)-C(11)-C(12)	111.8(10)
C(10)-C(11)-H(11A)	109.3
C(12)-C(11)-H(11A)	109.3
C(10)-C(11)-H(11B)	109.3
C(12)-C(11)-H(11B)	109.3
H(11A)-C(11)-H(11B)	107.9
C(11)-C(12)-C(13)	110.1(9)
C(11)-C(12)-H(12A)	109.6
C(13)-C(12)-H(12A)	109.6
C(11)-C(12)-H(12B)	109.6
C(13)-C(12)-H(12B)	109.6
H(12A)-C(12)-H(12B)	108.1
C(14)-C(13)-C(12)	110.7(10)
C(14)-C(13)-H(13A)	109.5
C(12)-C(13)-H(13A)	109.5
C(14)-C(13)-H(13B)	109.5
C(12)-C(13)-H(13B)	109.5
H(13A)-C(13)-H(13B)	108.1
C(15)-C(14)-C(13)	111.7(11)
C(15)-C(14)-H(14A)	109.3
C(13)-C(14)-H(14A)	109.3
C(15)-C(14)-H(14B)	109.3
C(13)-C(14)-H(14B)	109.3
H(14A)-C(14)-H(14B)	107.9
O(2)-C(15)-C(14)	110.4(9)
O(2)-C(15)-C(10)	110.4(8)
C(14)-C(15)-C(10)	109.7(8)
O(2)-C(15)-H(15)	108.7

C(14)-C(15)-H(15)	108.7
C(10)-C(15)-H(15)	108.8
C(7)-N(1)-C(6)	115.0(7)
C(7)-N(1)-H(1N)	108.0
C(6)-N(1)-H(1N)	108.1
C(10)-N(2)-C(9)	114.3(7)
C(10)-N(2)-H(2N)	108.4
C(9)-N(2)-H(2N)	108.8
C(1)-O(1)-H(1O)	109.0
C(15)-O(2)-H(2)	109.5

Table E.22. Anisotropic displacement parameters ($Å^2$ x 10^3)for 9m_sb6_0b. The anisotropic displacement factor exponent takes the form: -2p2[h2a*2U11 + ... + 2 h k a* b* U12]

	U11	U22	U33	U23	U13	U12
C(1)	23(4)	37(5)	41(6)	-11(5)	3(4)	-10(4)
C(2)	41(6)	43(6)	43(6)	-18(5)	-8(4)	-8(5)
C(3)	58(7)	49(7)	38(6)	-17(5)	-14(5)	-1(5)
C(4)	52(6)	34(6)	36(6)	-11(5)	-9(5)	-3(5)
C(5)	45(6)	36(6)	39(6)	-4(5)	-1(5)	-12(5)
C(6)	29(5)	24(5)	28(5)	-10(4)	1(4)	-6(4)
C(7)	47(6)	45(7)	62(7)	-23(6)	-21(5)	0(5)
C(8)	40(6)	35(6)	60(7)	-16(5)	-9(5)	-9(5)
C(9)	38(6)	36(6)	69(8)	-24(6)	-14(5)	-5(5)
C(10)	30(5)	37(6)	31(5)	-13(4)	-7(4)	0(4)
C(11)	45(6)	37(6)	55(7)	-18(5)	-16(5)	-7(5)
C(12)	59(7)	57(8)	83(9)	-39(7)	-31(6)	-3(6)
C(13)	66(8)	74(9)	73(9)	-41(8)	-26(7)	-1(7)
C(14)	54(7)	61(8)	56(7)	-25(6)	-19(6)	4(6)
C(15)	34(5)	36(6)	49(6)	-19(5)	-4(4)	-1(4)
N(1)	24(4)	37(5)	44(5)	-17(4)	-5(3)	-2(3)

N(2)	26(4)	39(5)	36(5)	-15(4)	2(3)	-12(3)
O(1)	37(4)	28(4)	54(5)	3(3)	-10(3)	-13(3)
O(2)	65(5)	33(4)	52(5)	-8(4)	-3(4)	-14(4)

Table E.23. Torsion angles [°] for 9m_sb6_0b.

O(1)-C(1)-C(2)-C(3)	-179.3(8)
C(6)-C(1)-C(2)-C(3)	55.3(11)
C(1)-C(2)-C(3)-C(4)	-56.3(12)
C(2)-C(3)-C(4)-C(5)	55.5(12)
C(3)-C(4)-C(5)-C(6)	-53.5(12)
O(1)-C(1)-C(6)-N(1)	58.6(9)
C(2)-C(1)-C(6)-N(1)	-175.2(8)
O(1)-C(1)-C(6)-C(5)	-179.4(7)
C(2)-C(1)-C(6)-C(5)	-53.2(10)
C(4)-C(5)-C(6)-N(1)	172.9(8)
C(4)-C(5)-C(6)-C(1)	52.6(11)
N(1)-C(7)-C(8)-C(9)	-170.3(9)
C(7)-C(8)-C(9)-N(2)	179.3(9)
N(2)-C(10)-C(11)-C(12)	178.6(8)
C(15)-C(10)-C(11)-C(12)	-60.0(11)
C(10)-C(11)-C(12)-C(13)	56.9(14)
C(11)-C(12)-C(13)-C(14)	-53.2(15)
C(12)-C(13)-C(14)-C(15)	54.7(14)
C(13)-C(14)-C(15)-O(2)	-179.3(9)
C(13)-C(14)-C(15)-C(10)	-57.4(12)
N(2)-C(10)-C(15)-O(2)	-54.5(11)
C(11)-C(10)-C(15)-O(2)	-178.7(8)
N(2)-C(10)-C(15)-C(14)	-176.5(9)
C(11)-C(10)-C(15)-C(14)	59.3(12)
C(8)-C(7)-N(1)-C(6)	-175.4(8)
C(1)-C(6)-N(1)-C(7)	-164.9(8)

C(5)-C(6)-N(1)-C(7)	73.4(11)
C(11)-C(10)-N(2)-C(9)	-71.5(10)
C(15)-C(10)-N(2)-C(9)	166.3(8)
C(8)-C(9)-N(2)-C(10)	-160.2(9)

Table E.24. Hydrogen bonds for 9m_sb6_0b [Å and °].

D-H...A	d(D-H)	d(H...A)	d(D...A)	<(DHA)	#
N1 -- H1N .. O2	0.9200	1.9600	2.848(12)	163.00	1
N2 -- H2N .. O1	0.9200	2.0500	2.881(11)	149.00	2
C8 -- H8A .. O1	0.9900	2.4300	3.341(14)	152.00	3

Symmetry transformations used to generate equivalent atoms:

#1 -x,-y,-z #2 1+x,y,z #3 -x,-y,-z

Cy_2-tn/Ni complex

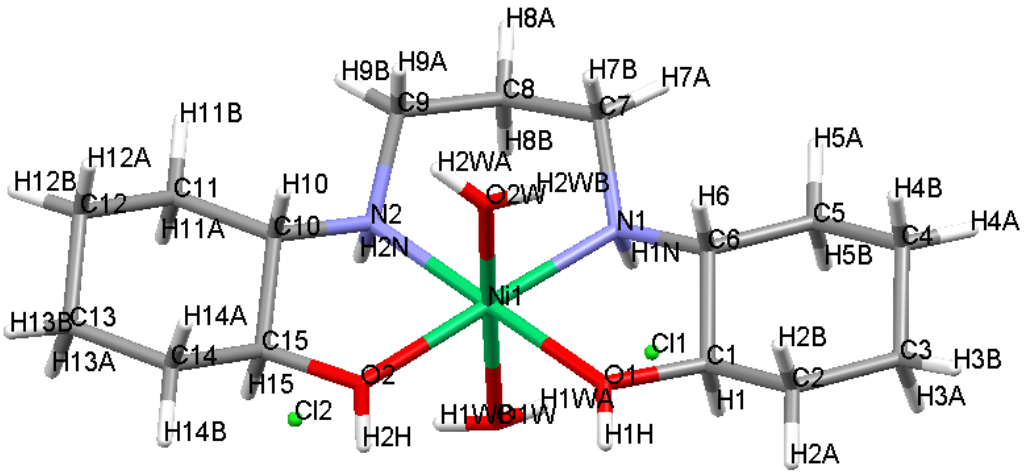


Figure E.5. XRD structure of the Cy_2-tn/Ni Complex and the labelling scheme used.

Table E.25. Crystal data and structure refinement for 9m_sbl1_0a.

Identification code	9m_sb11_0a	
Empirical formula	C15 H34 Cl2 N2 Ni O4	
Formula weight	436.05	
Temperature	173(2) K	
Wavelength	0.71073 Å	
Crystal system	Monoclinic	
Space group	P2(1)/c	
Unit cell dimensions	a = 12.0549(3) Å	α= 90°.
	b = 11.4655(3) Å	β= 107.0250(10)°.
	c = 15.1392(4) Å	γ = 90°.
Volume	2000.77(9) $Å^3$	
Z	4	
Density (calculated)	1.448 Mg/m^3	
Absorption coefficient	1.257 mm^{-1}	
F(000)	928	
Crystal size	0.32 x 0.29 x 0.19 mm^3	
Theta range for data collection	1.77 to 27.00°.	
Index ranges	-15<=h<=12, -13<=k<=14, -16<=l<=19	

Reflections collected	10164
Independent reflections	4362 [R(int) = 0.0399]
Completeness to theta = 27.00°	99.8 %
Absorption correction	Integration
Max. and min. transmission	0.7961 and 0.6891
Refinement method	Full-matrix least-squares on F^2
Data / restraints / parameters	4362 / 15 / 241
Goodness-of-fit on F^2	1.028
Final R indices [I>2sigma(I)]	R1 = 0.0292, wR2 = 0.0605
R indices (all data)	R1 = 0.0409, wR2 = 0.0716
Largest diff. peak and hole	0.392 and -0.380 e.$Å^{-3}$

Table E.26. Atomic coordinates (x 10^4) and equivalent isotropic displacement parameters ($Å^2$x 10^3) for 9m_sbl1_0a. U(eq) is defined as one third of the trace of the orthogonalized U^{ij} tensor.

	x	y	z	U(eq)
C(1)	2089(2)	894(2)	3031(1)	18(1)
C(2)	1173(2)	206(2)	2336(2)	23(1)
C(3)	-27(2)	713(2)	2214(2)	28(1)
C(4)	-59(2)	2002(2)	1964(2)	27(1)
C(5)	888(2)	2687(2)	2662(2)	23(1)
C(6)	2073(2)	2168(2)	2743(1)	15(1)
C(7)	3243(2)	3973(2)	3104(1)	20(1)
C(8)	4285(2)	4556(2)	3783(2)	22(1)
C(9)	5462(2)	4136(2)	3749(2)	22(1)
C(10)	6848(2)	2485(2)	4044(1)	17(1)
C(11)	7939(2)	3170(2)	4536(2)	22(1)
C(12)	9000(2)	2611(2)	4349(2)	27(1)
C(13)	9123(2)	1333(2)	4631(2)	26(1)
C(14)	8016(2)	657(2)	4162(2)	22(1)
C(15)	6992(2)	1224(2)	4374(1)	19(1)
N(1)	3054(1)	2779(1)	3408(1)	15(1)
N(2)	5752(1)	2956(1)	4162(1)	16(1)
O(1)	3242(1)	473(1)	3109(1)	20(1)

O(2)	5915(1)	618(1)	3919(1)	19(1)
O(1W)	4357(1)	1328(1)	5030(1)	20(1)
O(2W)	4569(1)	1907(2)	2312(1)	26(1)
Ni(1)	4485(1)	1715(1)	3651(1)	14(1)
Cl(1)	2584(1)	2938(1)	5440(1)	32(1)
Cl(2)	6531(1)	2173(1)	6513(1)	20(1)

Table E.27. Bond lengths [Å] and angles [°] for 9m_sbl1_0a.

C(1)-O(1)	1.444(2)
C(1)-C(2)	1.506(3)
C(1)-C(6)	1.524(3)
C(1)-H(1)	1.0000
C(2)-C(3)	1.519(3)
C(2)-H(2A)	0.9900
C(2)-H(2B)	0.9900
C(3)-C(4)	1.523(3)
C(3)-H(3A)	0.9900
C(3)-H(3B)	0.9900
C(4)-C(5)	1.526(3)
C(4)-H(4A)	0.9900
C(4)-H(4B)	0.9900
C(5)-C(6)	1.519(3)
C(5)-H(5A)	0.9900
C(5)-H(5B)	0.9900
C(6)-N(1)	1.485(2)
C(6)-H(6)	1.0000
C(7)-N(1)	1.483(2)
C(7)-C(8)	1.525(3)
C(7)-H(7A)	0.9900
C(7)-H(7B)	0.9900
C(8)-C(9)	1.513(3)
C(8)-H(8A)	0.9900
C(8)-H(8B)	0.9900
C(9)-N(2)	1.489(2)

C(9)-H(9A)	0.9900
C(9)-H(9B)	0.9900
C(10)-N(2)	1.485(2)
C(10)-C(15)	1.523(3)
C(10)-C(11)	1.525(3)
C(10)-H(10)	1.0000
C(11)-C(12)	1.529(3)
C(11)-H(11A)	0.9900
C(11)-H(11B)	0.9900
C(12)-C(13)	1.521(3)
C(12)-H(12A)	0.9900
C(12)-H(12B)	0.9900
C(13)-C(14)	1.527(3)
C(13)-H(13A)	0.9900
C(13)-H(13B)	0.9900
C(14)-C(15)	1.511(3)
C(14)-H(14A)	0.9900
C(14)-H(14B)	0.9900
C(15)-O(2)	1.456(2)
C(15)-H(15)	1.0000
N(1)-Ni(1)	2.0566(16)
N(1)-H(1N)	0.9300
N(2)-Ni(1)	2.0646(16)
N(2)-H(2N)	0.9300
O(1)-Ni(1)	2.0558(14)
O(1)-H(1H)	0.785(10)
O(2)-Ni(1)	2.0760(14)
O(2)-H(2H)	0.785(10)
O(1W)-Ni(1)	2.1849(16)
O(1W)-H(1WA)	0.786(10)
O(1W)-H(1WB)	0.787(10)
O(2W)-Ni(1)	2.0697(16)
O(2W)-H(2WA)	0.787(10)
O(2W)-H(2WB)	0.788(10)

O(1)-C(1)-C(2)	111.94(17)
O(1)-C(1)-C(6)	105.93(15)
C(2)-C(1)-C(6)	110.95(16)
O(1)-C(1)-H(1)	109.3
C(2)-C(1)-H(1)	109.3
C(6)-C(1)-H(1)	109.3
C(1)-C(2)-C(3)	111.21(17)
C(1)-C(2)-H(2A)	109.4
C(3)-C(2)-H(2A)	109.4
C(1)-C(2)-H(2B)	109.4
C(3)-C(2)-H(2B)	109.4
H(2A)-C(2)-H(2B)	108.0
C(2)-C(3)-C(4)	110.81(18)
C(2)-C(3)-H(3A)	109.5
C(4)-C(3)-H(3A)	109.5
C(2)-C(3)-H(3B)	109.5
C(4)-C(3)-H(3B)	109.5
H(3A)-C(3)-H(3B)	108.1
C(3)-C(4)-C(5)	111.62(18)
C(3)-C(4)-H(4A)	109.3
C(5)-C(4)-H(4A)	109.3
C(3)-C(4)-H(4B)	109.3
C(5)-C(4)-H(4B)	109.3
H(4A)-C(4)-H(4B)	108.0
C(6)-C(5)-C(4)	110.44(17)
C(6)-C(5)-H(5A)	109.6
C(4)-C(5)-H(5A)	109.6
C(6)-C(5)-H(5B)	109.6
C(4)-C(5)-H(5B)	109.6
H(5A)-C(5)-H(5B)	108.1
N(1)-C(6)-C(5)	114.43(16)
N(1)-C(6)-C(1)	108.55(15)
C(5)-C(6)-C(1)	109.35(16)
N(1)-C(6)-H(6)	108.1
C(5)-C(6)-H(6)	108.1

C(1)-C(6)-H(6)	108.1
N(1)-C(7)-C(8)	111.45(16)
N(1)-C(7)-H(7A)	109.3
C(8)-C(7)-H(7A)	109.3
N(1)-C(7)-H(7B)	109.3
C(8)-C(7)-H(7B)	109.3
H(7A)-C(7)-H(7B)	108.0
C(9)-C(8)-C(7)	115.65(18)
C(9)-C(8)-H(8A)	108.4
C(7)-C(8)-H(8A)	108.4
C(9)-C(8)-H(8B)	108.4
C(7)-C(8)-H(8B)	108.4
H(8A)-C(8)-H(8B)	107.4
N(2)-C(9)-C(8)	112.50(17)
N(2)-C(9)-H(9A)	109.1
C(8)-C(9)-H(9A)	109.1
N(2)-C(9)-H(9B)	109.1
C(8)-C(9)-H(9B)	109.1
H(9A)-C(9)-H(9B)	107.8
N(2)-C(10)-C(15)	108.97(15)
N(2)-C(10)-C(11)	115.12(17)
C(15)-C(10)-C(11)	109.26(16)
N(2)-C(10)-H(10)	107.7
C(15)-C(10)-H(10)	107.7
C(11)-C(10)-H(10)	107.7
C(10)-C(11)-C(12)	109.98(18)
C(10)-C(11)-H(11A)	109.7
C(12)-C(11)-H(11A)	109.7
C(10)-C(11)-H(11B)	109.7
C(12)-C(11)-H(11B)	109.7
H(11A)-C(11)-H(11B)	108.2
C(13)-C(12)-C(11)	111.74(18)
C(13)-C(12)-H(12A)	109.3
C(11)-C(12)-H(12A)	109.3
C(13)-C(12)-H(12B)	109.3

C(11)-C(12)-H(12B)	109.3
H(12A)-C(12)-H(12B)	107.9
C(12)-C(13)-C(14)	110.94(17)
C(12)-C(13)-H(13A)	109.5
C(14)-C(13)-H(13A)	109.5
C(12)-C(13)-H(13B)	109.5
C(14)-C(13)-H(13B)	109.5
H(13A)-C(13)-H(13B)	108.0
C(15)-C(14)-C(13)	109.89(17)
C(15)-C(14)-H(14A)	109.7
C(13)-C(14)-H(14A)	109.7
C(15)-C(14)-H(14B)	109.7
C(13)-C(14)-H(14B)	109.7
H(14A)-C(14)-H(14B)	108.2
O(2)-C(15)-C(14)	111.40(16)
O(2)-C(15)-C(10)	107.36(15)
C(14)-C(15)-C(10)	111.10(17)
O(2)-C(15)-H(15)	109.0
C(14)-C(15)-H(15)	109.0
C(10)-C(15)-H(15)	109.0
C(7)-N(1)-C(6)	112.88(15)
C(7)-N(1)-Ni(1)	113.92(12)
C(6)-N(1)-Ni(1)	107.52(11)
C(7)-N(1)-H(1N)	107.4
C(6)-N(1)-H(1N)	107.4
Ni(1)-N(1)-H(1N)	107.4
C(10)-N(2)-C(9)	112.84(15)
C(10)-N(2)-Ni(1)	106.93(12)
C(9)-N(2)-Ni(1)	114.30(12)
C(10)-N(2)-H(2N)	107.5
C(9)-N(2)-H(2N)	107.5
Ni(1)-N(2)-H(2N)	107.5
C(1)-O(1)-Ni(1)	111.94(11)
C(1)-O(1)-H(1H)	104.2(17)
Ni(1)-O(1)-H(1H)	128.9(17)

C(15)-O(2)-Ni(1)	112.16(12)
C(15)-O(2)-H(2H)	106.4(18)
Ni(1)-O(2)-H(2H)	113.7(19)
Ni(1)-O(1W)-H(1WA)	109(2)
Ni(1)-O(1W)-H(1WB)	106.6(18)
H(1WA)-O(1W)-H(1WB)	111(3)
Ni(1)-O(2W)-H(2WA)	126.8(19)
Ni(1)-O(2W)-H(2WB)	121(2)
H(2WA)-O(2W)-H(2WB)	112(3)
O(1)-Ni(1)-N(1)	82.20(6)
O(1)-Ni(1)-N(2)	178.32(6)
N(1)-Ni(1)-N(2)	98.52(6)
O(1)-Ni(1)-O(2W)	85.50(6)
N(1)-Ni(1)-O(2W)	92.39(7)
N(2)-Ni(1)-O(2W)	92.94(7)
O(1)-Ni(1)-O(2)	97.15(6)
N(1)-Ni(1)-O(2)	178.54(6)
N(2)-Ni(1)-O(2)	82.16(6)
O(2W)-Ni(1)-O(2)	88.86(6)
O(1)-Ni(1)-O(1W)	89.60(6)
N(1)-Ni(1)-O(1W)	90.02(6)
N(2)-Ni(1)-O(1W)	91.92(6)
O(2W)-Ni(1)-O(1W)	174.20(7)
O(2)-Ni(1)-O(1W)	88.67(6)

Table E.28. Anisotropic displacement parameters ($Å^2 x\ 10^3$)for 9m_sbl1_0a. The anisotropic displacement factor exponent takes the form: $-2p^2[\ h^2 a^{*2} U^{11} + ... + 2\ h\ k\ a^*\ b^*\ U^{12}\ ]$

	U^{11}	U^{22}	U^{33}	U^{23}	U^{13}	U^{12}
C(1)	13(1)	18(1)	22(1)	0(1)	3(1)	2(1)
C(2)	18(1)	17(1)	31(1)	-5(1)	1(1)	-2(1)
C(3)	16(1)	26(1)	36(1)	-3(1)	2(1)	-3(1)
C(4)	17(1)	29(1)	31(1)	-5(1)	-1(1)	4(1)
C(5)	16(1)	20(1)	31(1)	-1(1)	4(1)	2(1)

C(6)	13(1)	16(1)	14(1)	-1(1)	2(1)	1(1)
C(7)	19(1)	13(1)	26(1)	7(1)	5(1)	2(1)
C(8)	22(1)	12(1)	32(1)	0(1)	6(1)	-2(1)
C(9)	20(1)	18(1)	26(1)	2(1)	4(1)	-1(1)
C(10)	14(1)	21(1)	15(1)	3(1)	4(1)	-2(1)
C(11)	18(1)	21(1)	26(1)	2(1)	5(1)	-5(1)
C(12)	16(1)	36(1)	28(1)	-1(1)	6(1)	-2(1)
C(13)	16(1)	31(1)	30(1)	-7(1)	7(1)	5(1)
C(14)	19(1)	24(1)	24(1)	-4(1)	7(1)	3(1)
C(15)	15(1)	23(1)	16(1)	-2(1)	1(1)	-2(1)
N(1)	15(1)	14(1)	15(1)	1(1)	2(1)	1(1)
N(2)	17(1)	16(1)	16(1)	1(1)	7(1)	1(1)
O(1)	15(1)	11(1)	31(1)	2(1)	5(1)	2(1)
O(2)	15(1)	16(1)	24(1)	2(1)	2(1)	0(1)
O(1W)	16(1)	24(1)	19(1)	2(1)	3(1)	2(1)
O(2W)	18(1)	43(1)	16(1)	2(1)	6(1)	-5(1)
Ni(1)	12(1)	14(1)	15(1)	1(1)	3(1)	0(1)
Cl(1)	25(1)	53(1)	18(1)	-2(1)	7(1)	8(1)
Cl(2)	21(1)	20(1)	18(1)	-1(1)	5(1)	3(1)

Table E.29. Torsion angles [°] for 9m_sbl1_0a.

O(1)-C(1)-C(2)-C(3)	-175.99(17)
C(6)-C(1)-C(2)-C(3)	-57.9(2)
C(1)-C(2)-C(3)-C(4)	54.7(2)
C(2)-C(3)-C(4)-C(5)	-54.0(3)
C(3)-C(4)-C(5)-C(6)	56.3(3)
C(4)-C(5)-C(6)-N(1)	179.94(17)
C(4)-C(5)-C(6)-C(1)	-58.1(2)
O(1)-C(1)-C(6)-N(1)	-53.5(2)
C(2)-C(1)-C(6)-N(1)	-175.22(17)
O(1)-C(1)-C(6)-C(5)	-179.00(15)
C(2)-C(1)-C(6)-C(5)	59.3(2)
N(1)-C(7)-C(8)-C(9)	75.5(2)

C(7)-C(8)-C(9)-N(2)	-73.6(2)
N(2)-C(10)-C(11)-C(12)	-179.11(17)
C(15)-C(10)-C(11)-C(12)	57.9(2)
C(10)-C(11)-C(12)-C(13)	-56.2(2)
C(11)-C(12)-C(13)-C(14)	55.0(2)
C(12)-C(13)-C(14)-C(15)	-55.7(2)
C(13)-C(14)-C(15)-O(2)	178.65(17)
C(13)-C(14)-C(15)-C(10)	59.0(2)
N(2)-C(10)-C(15)-O(2)	51.0(2)
C(11)-C(10)-C(15)-O(2)	177.58(16)
N(2)-C(10)-C(15)-C(14)	173.05(16)
C(11)-C(10)-C(15)-C(14)	-60.4(2)
C(8)-C(7)-N(1)-C(6)	-177.77(17)
C(8)-C(7)-N(1)-Ni(1)	-54.8(2)
C(5)-C(6)-N(1)-C(7)	-67.5(2)
C(1)-C(6)-N(1)-C(7)	170.05(16)
C(5)-C(6)-N(1)-Ni(1)	166.00(14)
C(1)-C(6)-N(1)-Ni(1)	43.56(17)
C(15)-C(10)-N(2)-C(9)	-172.80(16)
C(11)-C(10)-N(2)-C(9)	64.1(2)
C(15)-C(10)-N(2)-Ni(1)	-46.29(17)
C(11)-C(10)-N(2)-Ni(1)	-169.41(14)
C(8)-C(9)-N(2)-C(10)	173.99(16)
C(8)-C(9)-N(2)-Ni(1)	51.5(2)
C(2)-C(1)-O(1)-Ni(1)	158.69(14)
C(6)-C(1)-O(1)-Ni(1)	37.63(17)
C(14)-C(15)-O(2)-Ni(1)	-152.52(14)
C(10)-C(15)-O(2)-Ni(1)	-30.67(18)
C(1)-O(1)-Ni(1)-N(1)	-11.76(13)
C(1)-O(1)-Ni(1)-O(2W)	-104.80(13)
C(1)-O(1)-Ni(1)-O(2)	166.92(13)
C(1)-O(1)-Ni(1)-O(1W)	78.31(13)
C(7)-N(1)-Ni(1)-O(1)	-143.77(13)
C(6)-N(1)-Ni(1)-O(1)	-17.90(12)
C(7)-N(1)-Ni(1)-N(2)	34.69(14)

C(6)-N(1)-Ni(1)-N(2)	160.56(12)
C(7)-N(1)-Ni(1)-O(2W)	-58.64(13)
C(6)-N(1)-Ni(1)-O(2W)	67.23(13)
C(7)-N(1)-Ni(1)-O(1W)	126.64(13)
C(6)-N(1)-Ni(1)-O(1W)	-107.49(12)
C(10)-N(2)-Ni(1)-N(1)	-158.50(12)
C(9)-N(2)-Ni(1)-N(1)	-32.86(14)
C(10)-N(2)-Ni(1)-O(2W)	-65.64(12)
C(9)-N(2)-Ni(1)-O(2W)	60.00(14)
C(10)-N(2)-Ni(1)-O(2)	22.80(12)
C(9)-N(2)-Ni(1)-O(2)	148.44(14)
C(10)-N(2)-Ni(1)-O(1W)	111.19(12)
C(9)-N(2)-Ni(1)-O(1W)	-123.17(14)
C(15)-O(2)-Ni(1)-O(1)	-176.73(13)
C(15)-O(2)-Ni(1)-N(2)	4.82(13)
C(15)-O(2)-Ni(1)-O(2W)	97.95(13)
C(15)-O(2)-Ni(1)-O(1W)	-87.30(13)

Table E.30. Hydrogen bonds for 9m_sbl1_0a [Å and °].

D-H...A	d(D-H)	d(H...A)	d(D...A)	<(DHA)	#
O(1)-H(1H)...Cl(2)	0.785(10)	2.314(11)	3.0849(15)	168(2)	1
O(2)-H(2H)...O(1W)	0.785(10)	2.032(11)	2.814(2)	175(2)	1
O(2W)-H(2WA)...Cl(2)	0.787(10)	2.356(11)	3.1379(17)	172(2)	2
O(2W)-H(2WB)...Cl(1)	0.788(10)	2.373(13)	3.1343(17)	163(3)	2

Symmetry transformations used to generate equivalent atoms:

#1 -x+1,-y,-z+1 #2 x,-y+1/2,z-1/2

Cy_2-tn/Zn Data

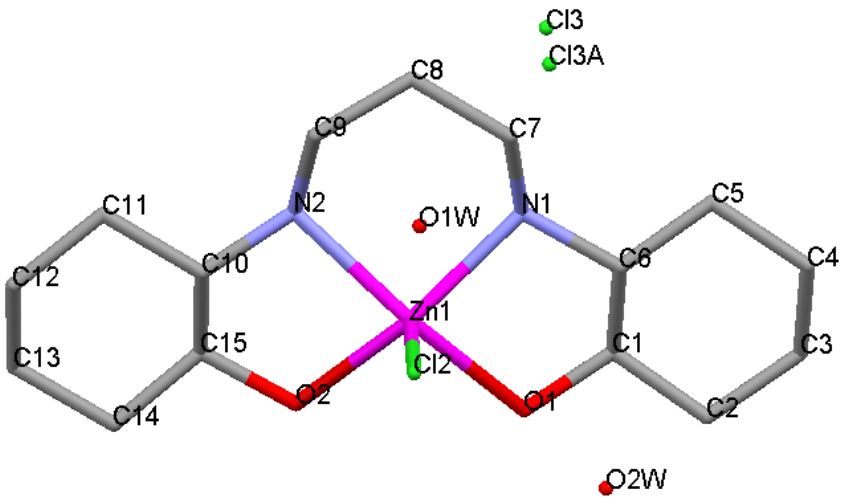


Figure E.6. The XRD structure of the Cy_2-tn/Zn complex and the labelling scheme used.

Table E.31. Crystal data and structure refinement for 9m_sb9_0f.

Identification code	9m_sb9_0f	
Empirical formula	C15 H32.50 Cl2 N2 O3 Zn	
Formula weight	425.20	
Temperature	173(2) K	
Wavelength	0.71073 Å	
Crystal system	Triclinic	
Space group	P-1	
Unit cell dimensions	a = 7.2982(2) Å	α= 115.3390(10)°.
	b = 12.2314(4) Å	β= 101.5160(10)°.
	c = 12.4397(4) Å	γ = 94.4210(10)°.
Volume	966.71(5) $Å^3$	
Z	2	
Density (calculated)	1.461 Mg/m^3	
Absorption coefficient	1.561 mm^{-1}	
F(000)	449	
Crystal size	0.42 x 0.19 x 0.17 mm^3	
Theta range for data collection	1.87 to 28.00°.	
Index ranges	-9<=h<=8, -16<=k<=9, -16<=l<=16	

Reflections collected	10022
Independent reflections	4661 [R(int) = 0.0408]
Completeness to theta = 28.00°	99.7 %
Absorption correction	Integration
Max. and min. transmission	0.7772 and 0.5601
Refinement method	Full-matrix least-squares on F^2
Data / restraints / parameters	4661 / 1 / 227
Goodness-of-fit on F^2	0.979
Final R indices [I>2sigma(I)]	R1 = 0.0314, wR2 = 0.0678
R indices (all data)	R1 = 0.0424, wR2 = 0.0717
Largest diff. peak and hole	0.482 and -0.484 e.Å^{-3}

Table E.32. Atomic coordinates (x 10^4) and equivalent isotropic displacement parameters (Å^2 x 10^3) for 9m_sb9_0f. U(eq) is defined as one third of the trace of the orthogonalized Uij tensor.

	x	y	z	U(eq)
C(1)	1831(3)	6515(2)	3529(2)	23(1)
C(2)	1055(3)	6468(2)	4556(2)	30(1)
C(3)	2426(3)	6021(2)	5303(2)	33(1)
C(4)	4415(3)	6811(2)	5794(2)	33(1)
C(5)	5160(3)	6880(2)	4756(2)	26(1)
C(6)	3774(3)	7344(2)	4034(2)	20(1)
C(7)	6090(3)	8343(2)	3338(2)	23(1)
C(8)	6674(2)	8302(2)	2213(2)	24(1)
C(9)	5401(2)	8752(2)	1422(2)	22(1)
C(10)	2190(2)	8278(2)	-26(2)	18(1)
C(11)	2826(3)	8346(2)	-1096(2)	22(1)
C(12)	1277(3)	8671(2)	-1870(2)	26(1)
C(13)	-603(3)	7775(2)	-2331(2)	29(1)
C(14)	-1221(3)	7705(2)	-1254(2)	26(1)
C(15)	328(2)	7359(2)	-521(2)	20(1)
N(1)	4353(2)	7421(1)	2986(1)	19(1)
N(2)	3546(2)	7913(1)	759(1)	18(1)
O(1)	570(2)	6956(2)	2822(1)	32(1)
O(2)	-201(2)	7307(1)	517(1)	25(1)

O(1W)	2465(3)	4849(1)	426(2)	45(1)
O(2W)	578(10)	9261(7)	5043(7)	48(3)
Cl(2)	2063(1)	9851(1)	3224(1)	32(1)
Cl(3)	6683(2)	4956(1)	1794(1)	29(1)
Cl(3A)	5938(7)	4728(3)	1719(3)	29(1)
Zn(1)	2082(1)	7851(1)	2039(1)	20(1)

Table E.33. Bond lengths [Å] and angles [°] for 9m_sb9_0f.

C(1)-O(1)	1.439(2)
C(1)-C(2)	1.517(2)
C(1)-C(6)	1.520(2)
C(1)-H(1)	1.0000
C(2)-C(3)	1.522(3)
C(2)-H(2A)	0.9900
C(2)-H(2B)	0.9900
C(3)-C(4)	1.529(3)
C(3)-H(3A)	0.9900
C(3)-H(3B)	0.9900
C(4)-C(5)	1.529(2)
C(4)-H(4A)	0.9900
C(4)-H(4B)	0.9900
C(5)-C(6)	1.521(3)
C(5)-H(5A)	0.9900
C(5)-H(5B)	0.9900
C(6)-N(1)	1.485(2)
C(6)-H(6)	1.0000
C(7)-N(1)	1.485(2)
C(7)-C(8)	1.524(2)
C(7)-H(7A)	0.9900
C(7)-H(7B)	0.9900
C(8)-C(9)	1.521(3)
C(8)-H(8A)	0.9900
C(8)-H(8B)	0.9900
C(9)-N(2)	1.477(2)

C(9)-H(9A)	0.9900
C(9)-H(9B)	0.9900
C(10)-N(2)	1.479(2)
C(10)-C(11)	1.525(2)
C(10)-C(15)	1.526(2)
C(10)-H(10)	1.0000
C(11)-C(12)	1.525(3)
C(11)-H(11A)	0.9900
C(11)-H(11B)	0.9900
C(12)-C(13)	1.526(3)
C(12)-H(12A)	0.9900
C(12)-H(12B)	0.9900
C(13)-C(14)	1.530(3)
C(13)-H(13A)	0.9900
C(13)-H(13B)	0.9900
C(14)-C(15)	1.510(3)
C(14)-H(14A)	0.9900
C(14)-H(14B)	0.9900
C(15)-O(2)	1.444(2)
C(15)-H(15)	1.0000
N(1)-Zn(1)	2.0734(16)
N(1)-H(1N)	0.9300
N(2)-Zn(1)	2.1106(14)
N(2)-H(2N)	0.9300
O(1)-Zn(1)	2.1268(14)
O(1)-H(1O)	0.778(17)
O(2)-Zn(1)	2.0716(14)
O(2)-H(2O)	0.76(2)
O(1W)-H(1WA)	0.8020
O(1W)-H(1WB)	0.8073
O(2W)-H(2WA)	0.8053
O(2W)-H(2WB)	0.8057
Cl(2)-Zn(1)	2.2545(5)

O(1)-C(1)-C(2)	111.33(15)

O(1)-C(1)-C(6)	108.55(16)
C(2)-C(1)-C(6)	111.31(15)
O(1)-C(1)-H(1)	108.5
C(2)-C(1)-H(1)	108.5
C(6)-C(1)-H(1)	108.5
C(1)-C(2)-C(3)	110.39(17)
C(1)-C(2)-H(2A)	109.6
C(3)-C(2)-H(2A)	109.6
C(1)-C(2)-H(2B)	109.6
C(3)-C(2)-H(2B)	109.6
H(2A)-C(2)-H(2B)	108.1
C(2)-C(3)-C(4)	111.28(17)
C(2)-C(3)-H(3A)	109.4
C(4)-C(3)-H(3A)	109.4
C(2)-C(3)-H(3B)	109.4
C(4)-C(3)-H(3B)	109.4
H(3A)-C(3)-H(3B)	108.0
C(3)-C(4)-C(5)	111.41(16)
C(3)-C(4)-H(4A)	109.3
C(5)-C(4)-H(4A)	109.3
C(3)-C(4)-H(4B)	109.3
C(5)-C(4)-H(4B)	109.3
H(4A)-C(4)-H(4B)	108.0
C(6)-C(5)-C(4)	110.71(16)
C(6)-C(5)-H(5A)	109.5
C(4)-C(5)-H(5A)	109.5
C(6)-C(5)-H(5B)	109.5
C(4)-C(5)-H(5B)	109.5
H(5A)-C(5)-H(5B)	108.1
N(1)-C(6)-C(1)	107.79(14)
N(1)-C(6)-C(5)	114.86(15)
C(1)-C(6)-C(5)	109.93(16)
N(1)-C(6)-H(6)	108.0
C(1)-C(6)-H(6)	108.0
C(5)-C(6)-H(6)	108.0

N(1)-C(7)-C(8)	111.82(15)
N(1)-C(7)-H(7A)	109.3
C(8)-C(7)-H(7A)	109.3
N(1)-C(7)-H(7B)	109.3
C(8)-C(7)-H(7B)	109.3
H(7A)-C(7)-H(7B)	107.9
C(9)-C(8)-C(7)	117.33(16)
C(9)-C(8)-H(8A)	108.0
C(7)-C(8)-H(8A)	108.0
C(9)-C(8)-H(8B)	108.0
C(7)-C(8)-H(8B)	108.0
H(8A)-C(8)-H(8B)	107.2
N(2)-C(9)-C(8)	111.70(15)
N(2)-C(9)-H(9A)	109.3
C(8)-C(9)-H(9A)	109.3
N(2)-C(9)-H(9B)	109.3
C(8)-C(9)-H(9B)	109.3
H(9A)-C(9)-H(9B)	107.9
N(2)-C(10)-C(11)	115.84(14)
N(2)-C(10)-C(15)	107.14(15)
C(11)-C(10)-C(15)	109.56(14)
N(2)-C(10)-H(10)	108.0
C(11)-C(10)-H(10)	108.0
C(15)-C(10)-H(10)	108.0
C(12)-C(11)-C(10)	110.95(15)
C(12)-C(11)-H(11A)	109.4
C(10)-C(11)-H(11A)	109.4
C(12)-C(11)-H(11B)	109.4
C(10)-C(11)-H(11B)	109.4
H(11A)-C(11)-H(11B)	108.0
C(11)-C(12)-C(13)	111.82(17)
C(11)-C(12)-H(12A)	109.3
C(13)-C(12)-H(12A)	109.3
C(11)-C(12)-H(12B)	109.3
C(13)-C(12)-H(12B)	109.3

H(12A)-C(12)-H(12B)	107.9
C(12)-C(13)-C(14)	110.60(16)
C(12)-C(13)-H(13A)	109.5
C(14)-C(13)-H(13A)	109.5
C(12)-C(13)-H(13B)	109.5
C(14)-C(13)-H(13B)	109.5
H(13A)-C(13)-H(13B)	108.1
C(15)-C(14)-C(13)	110.14(15)
C(15)-C(14)-H(14A)	109.6
C(13)-C(14)-H(14A)	109.6
C(15)-C(14)-H(14B)	109.6
C(13)-C(14)-H(14B)	109.6
H(14A)-C(14)-H(14B)	108.1
O(2)-C(15)-C(14)	111.46(15)
O(2)-C(15)-C(10)	107.69(14)
C(14)-C(15)-C(10)	111.75(16)
O(2)-C(15)-H(15)	108.6
C(14)-C(15)-H(15)	108.6
C(10)-C(15)-H(15)	108.6
C(7)-N(1)-C(6)	114.99(14)
C(7)-N(1)-Zn(1)	109.28(12)
C(6)-N(1)-Zn(1)	106.78(11)
C(7)-N(1)-H(1N)	108.5
C(6)-N(1)-H(1N)	108.5
Zn(1)-N(1)-H(1N)	108.5
C(9)-N(2)-C(10)	115.98(14)
C(9)-N(2)-Zn(1)	109.61(11)
C(10)-N(2)-Zn(1)	103.52(10)
C(9)-N(2)-H(2N)	109.2
C(10)-N(2)-H(2N)	109.2
Zn(1)-N(2)-H(2N)	109.2
C(1)-O(1)-Zn(1)	111.38(10)
C(1)-O(1)-H(1O)	112(3)
Zn(1)-O(1)-H(1O)	125(3)
C(15)-O(2)-Zn(1)	113.38(10)

C(15)-O(2)-H(2O)	107.5(19)
Zn(1)-O(2)-H(2O)	118(2)
H(1WA)-O(1W)-H(1WB)	115.3
H(2WA)-O(2W)-H(2WB)	91.1
O(2)-Zn(1)-N(1)	149.40(6)
O(2)-Zn(1)-N(2)	80.39(5)
N(1)-Zn(1)-N(2)	93.06(6)
O(2)-Zn(1)-O(1)	92.31(6)
N(1)-Zn(1)-O(1)	80.87(5)
N(2)-Zn(1)-O(1)	154.60(6)
O(2)-Zn(1)-Cl(2)	104.83(4)
N(1)-Zn(1)-Cl(2)	105.77(4)
N(2)-Zn(1)-Cl(2)	103.09(4)
O(1)-Zn(1)-Cl(2)	102.30(5)

Table E.34. Anisotropic displacement parameters ($Å^2$ x 10^3)for 9m_sb9_of. The anisotropic displacement factor exponent takes the form: -2p2[h2a*2U11 + ... + 2 h k a* b* U12]

	U11	U22	U33	U23	U13	U12
C(1)	22(1)	28(1)	21(1)	14(1)	4(1)	2(1)
C(2)	26(1)	40(1)	27(1)	21(1)	6(1)	-2(1)
C(3)	34(1)	40(1)	29(1)	23(1)	4(1)	-4(1)
C(4)	33(1)	43(1)	25(1)	22(1)	2(1)	-2(1)
C(5)	24(1)	33(1)	24(1)	18(1)	3(1)	1(1)
C(6)	23(1)	22(1)	16(1)	10(1)	8(1)	3(1)
C(7)	18(1)	29(1)	23(1)	14(1)	1(1)	0(1)
C(8)	15(1)	32(1)	28(1)	17(1)	4(1)	1(1)
C(9)	17(1)	26(1)	24(1)	14(1)	4(1)	-3(1)
C(10)	18(1)	18(1)	19(1)	9(1)	3(1)	2(1)
C(11)	21(1)	23(1)	22(1)	12(1)	4(1)	-1(1)
C(12)	30(1)	27(1)	23(1)	14(1)	3(1)	0(1)
C(13)	29(1)	32(1)	25(1)	16(1)	-3(1)	-2(1)
C(14)	22(1)	30(1)	28(1)	16(1)	2(1)	2(1)
C(15)	18(1)	22(1)	20(1)	11(1)	4(1)	-1(1)
N(1)	19(1)	21(1)	18(1)	10(1)	6(1)	3(1)

N(2)	15(1)	18(1)	20(1)	10(1)	4(1)	1(1)
O(1)	17(1)	51(1)	38(1)	33(1)	5(1)	4(1)
O(2)	20(1)	31(1)	24(1)	16(1)	5(1)	-2(1)
O(1W)	41(1)	44(1)	45(1)	19(1)	11(1)	-7(1)
O(2W)	40(5)	38(5)	49(5)	1(4)	25(4)	-1(3)
Cl(2)	35(1)	29(1)	29(1)	10(1)	7(1)	12(1)
Zn(1)	17(1)	27(1)	21(1)	14(1)	5(1)	3(1)

Table E.35. Torsion angles [°] for 9m_sb9_0f.

O(1)-C(1)-C(2)-C(3)	-179.02(16)
C(6)-C(1)-C(2)-C(3)	-57.8(2)
C(1)-C(2)-C(3)-C(4)	55.2(2)
C(2)-C(3)-C(4)-C(5)	-54.4(2)
C(3)-C(4)-C(5)-C(6)	55.4(2)
O(1)-C(1)-C(6)-N(1)	-52.44(19)
C(2)-C(1)-C(6)-N(1)	-175.31(16)
O(1)-C(1)-C(6)-C(5)	-178.32(14)
C(2)-C(1)-C(6)-C(5)	58.8(2)
C(4)-C(5)-C(6)-N(1)	-178.88(15)
C(4)-C(5)-C(6)-C(1)	-57.1(2)
N(1)-C(7)-C(8)-C(9)	69.8(2)
C(7)-C(8)-C(9)-N(2)	-69.0(2)
N(2)-C(10)-C(11)-C(12)	177.35(15)
C(15)-C(10)-C(11)-C(12)	56.1(2)
C(10)-C(11)-C(12)-C(13)	-55.6(2)
C(11)-C(12)-C(13)-C(14)	55.1(2)
C(12)-C(13)-C(14)-C(15)	-55.9(2)
C(13)-C(14)-C(15)-O(2)	178.95(15)
C(13)-C(14)-C(15)-C(10)	58.4(2)
N(2)-C(10)-C(15)-O(2)	52.51(18)
C(11)-C(10)-C(15)-O(2)	178.92(15)
N(2)-C(10)-C(15)-C(14)	175.24(14)
C(11)-C(10)-C(15)-C(14)	-58.3(2)

C(8)-C(7)-N(1)-C(6)	175.80(16)
C(8)-C(7)-N(1)-Zn(1)	-64.17(17)
C(1)-C(6)-N(1)-C(7)	171.28(16)
C(5)-C(6)-N(1)-C(7)	-65.8(2)
C(1)-C(6)-N(1)-Zn(1)	49.88(16)
C(5)-C(6)-N(1)-Zn(1)	172.79(13)
C(8)-C(9)-N(2)-C(10)	179.23(15)
C(8)-C(9)-N(2)-Zn(1)	62.50(17)
C(11)-C(10)-N(2)-C(9)	62.61(19)
C(15)-C(10)-N(2)-C(9)	-174.80(14)
C(11)-C(10)-N(2)-Zn(1)	-177.31(12)
C(15)-C(10)-N(2)-Zn(1)	-54.73(14)
C(2)-C(1)-O(1)-Zn(1)	151.76(13)
C(6)-C(1)-O(1)-Zn(1)	28.91(17)
C(14)-C(15)-O(2)-Zn(1)	-146.25(13)
C(10)-C(15)-O(2)-Zn(1)	-23.35(18)
C(15)-O(2)-Zn(1)-N(1)	-84.75(15)
C(15)-O(2)-Zn(1)-N(2)	-5.12(12)
C(15)-O(2)-Zn(1)-O(1)	-160.63(12)
C(15)-O(2)-Zn(1)-Cl(2)	96.00(12)
C(7)-N(1)-Zn(1)-O(2)	129.58(12)
C(6)-N(1)-Zn(1)-O(2)	-105.47(13)
C(7)-N(1)-Zn(1)-N(2)	53.35(11)
C(6)-N(1)-Zn(1)-N(2)	178.30(11)
C(7)-N(1)-Zn(1)-O(1)	-151.47(12)
C(6)-N(1)-Zn(1)-O(1)	-26.52(11)
C(7)-N(1)-Zn(1)-Cl(2)	-51.17(11)
C(6)-N(1)-Zn(1)-Cl(2)	73.78(11)
C(9)-N(2)-Zn(1)-O(2)	157.04(13)
C(10)-N(2)-Zn(1)-O(2)	32.71(10)
C(9)-N(2)-Zn(1)-N(1)	-53.06(13)
C(10)-N(2)-Zn(1)-N(1)	-177.39(10)
C(9)-N(2)-Zn(1)-O(1)	-128.10(15)
C(10)-N(2)-Zn(1)-O(1)	107.56(15)
C(9)-N(2)-Zn(1)-Cl(2)	53.91(12)

C(10)-N(2)-Zn(1)-Cl(2)	-70.42(10)
C(1)-O(1)-Zn(1)-O(2)	148.43(13)
C(1)-O(1)-Zn(1)-N(1)	-1.57(12)
C(1)-O(1)-Zn(1)-N(2)	76.16(18)
C(1)-O(1)-Zn(1)-Cl(2)	-105.85(12)

Table E.36. Hydrogen bonds for 9m_sb9_0f [Å and °].

D-H...A	d(D-H)	d(H...A)	d(D...A)	<(DHA)	#
O1W -- H1WA .. Cl3	0.8000	2.2700	3.049(2)	163.00	1
O1 -- H1O .. Cl3	0.78(3)	2.47(3)	3.236(2)	166(4)	2
N2 -- H2N .. Cl3	0.9300	2.6800	3.5479(18)	155.00	1
O2 -- H2O .. O1W	0.76(3)	1.88(3)	2.640(3)	176(2)	3

Symmetry transformations used to generate equivalent atoms:
#1 1-x,1-y,-z #2 -1+x,y,z #3 -x,1-y,-z

Cy_2-tn/Cd Data

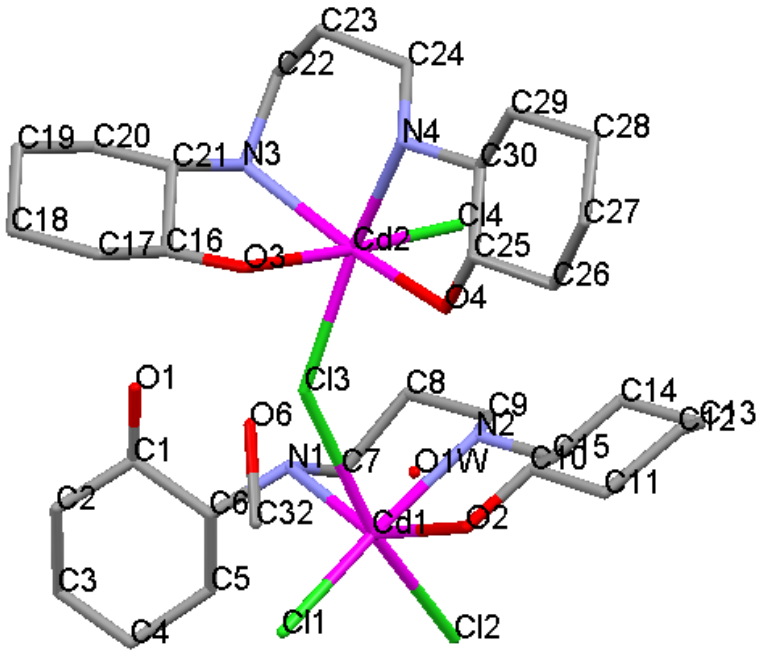


Figure E.7. The XRD structures of Cy_2-tn/Cd Complex and the labelling scheme used.

Table E.37. Crystal data and structure refinement for 9m_alvsb3_0b.

Identification code	9m_alvsb3_0b	
Empirical formula	C80 H80 Cd4 Cl4 N8 O8	
Formula weight	1872.92	
Temperature	293(2) K	
Wavelength	0.71069 Å	
Crystal system	Monoclinic	
Space group	Cc	
Unit cell dimensions	a = 47.350(5) Å	α= 90.000(5)°.
	b = 8.062(5) Å	β= 104.213(5)°.
	c = 22.946(5) Å	γ = 90.000(5)°.
Volume	8491(6) $Å^3$	
Z	4	
Density (calculated)	1.465 Mg/m^3	
Absorption coefficient	1.169 mm^{-1}	
F(000)	3760	
Crystal size	0.40 x 0.36 x 0.28 mm^3	
Theta range for data collection	0.89 to 25.00°.	

Index ranges	-56<=h<=55, -9<=k<=9, -27<=l<=27
Reflections collected	33711
Independent reflections	7481 [R(int) = 0.0795]
Completeness to theta = 25.00°	99.9 %
Absorption correction	None
Max. and min. transmission	0.7355 and 0.6520
Refinement method	Full-matrix least-squares on F^2
Data / restraints / parameters	7481 / 114 / 220
Goodness-of-fit on F^2	1.131
Final R indices [I>2sigma(I)]	R1 = 0.2291, wR2 = 0.5530
R indices (all data)	R1 = 0.2390, wR2 = 0.5569
Largest diff. peak and hole	8.461 and -4.121 e.Å^{-3}

Table E.38. Atomic coordinates (x 10^4) and equivalent isotropic displacement parameters (Å^{2}x 10^3) for 9m_alvsb3_0b. U(eq) is defined as one third of the trace of the orthogonalized U^{ij} tensor.

	x	y	z	U(eq)
C(1)	4565(9)	3970(80)	5600(20)	290(80)
C(2)	4870(9)	3430(120)	5820(30)	290(90)
C(3)	4957(10)	3300(100)	6540(30)	130(30)
C(4)	4762(11)	2160(100)	6750(30)	180(40)
C(5)	4441(9)	2590(70)	6454(17)	73(15)
C(6)	4358(8)	2750(60)	5817(17)	86(18)
O(1)	4478(10)	4070(80)	4974(18)	128(19)
N(1)	4048(6)	3100(40)	5547(14)	48(8)
C(7)	3891(16)	4270(100)	5970(30)	100(20)
C(8)	3592(8)	4780(50)	5456(16)	33(8)
C(9)	3333(8)	3440(50)	5359(16)	33(8)
C(10)	3194(6)	-800(30)	4691(14)	40(9)
C(11)	2963(6)	-2060(40)	4624(17)	42(9)
C(12)	2651(7)	-1290(50)	4329(18)	55(11)
C(13)	2595(7)	140(40)	4687(18)	44(10)
C(14)	2849(7)	1390(40)	4758(19)	56(11)
C(15)	3131(6)	750(40)	5040(15)	42(9)

O(2)	3469(5)	-1420(30)	4994(11)	42(6)
N(2)	3373(5)	1950(30)	5106(14)	38(7)
C(16)	4175(6)	1300(30)	2983(15)	37(8)
C(17)	4394(8)	490(50)	2730(20)	69(14)
C(18)	4668(9)	1680(60)	2770(30)	120(30)
C(19)	4577(11)	3270(60)	2470(30)	120(30)
C(20)	4333(9)	4030(50)	2730(20)	83(17)
C(21)	4082(8)	3030(40)	2700(20)	85(18)
O(3)	3924(5)	310(30)	2923(12)	44(6)
N(3)	3851(6)	3760(30)	2952(14)	39(7)
C(22)	3648(10)	4930(60)	2480(20)	52(11)
C(23)	3449(10)	4310(60)	1950(20)	51(11)
C(24)	3189(8)	3390(50)	2082(16)	34(8)
C(25)	3134(6)	-1120(30)	2623(12)	29(7)
C(26)	2886(7)	-2210(50)	2648(15)	51(10)
C(27)	2706(9)	-2660(50)	1982(16)	56(11)
C(28)	2596(8)	-1120(50)	1650(18)	59(12)
C(29)	2855(8)	80(50)	1681(15)	53(11)
C(30)	3028(6)	490(40)	2263(13)	36(8)
O(4)	3292(5)	-640(30)	3202(9)	40(6)
N(4)	3271(5)	1660(30)	2295(11)	27(6)
C(32)	4124(11)	-4150(70)	4010(20)	64(13)
O(1W)	3555(5)	-3100(30)	3980(11)	36(6)
O(6)	4048(10)	-2750(60)	3500(20)	95(13)
Cl(1)	4196(2)	-1617(13)	5730(6)	61(3)
Cl(2)	3665(2)	521(15)	6528(4)	52(3)
Cl(3)	3878(2)	967(15)	4276(4)	49(3)
Cl(4)	3210(2)	3657(11)	3657(4)	37(2)
Cd(1)	3810(1)	495(3)	5503(1)	31(1)
Cd(2)	3562(1)	1802(3)	3268(1)	24(1)

Table E.39. Bond lengths [Å] and angles [°] for 9m_alvsb3_0b.

C(1)-O(1)	1.41(3)
C(1)-C(2)	1.48(4)
C(1)-C(6)	1.55(4)
C(2)-C(3)	1.60(4)
C(3)-C(4)	1.47(4)
C(4)-C(5)	1.55(4)
C(5)-C(6)	1.42(4)
C(6)-N(1)	1.48(3)
N(1)-C(7)	1.65(8)
N(1)-Cd(1)	2.37(3)
C(7)-C(8)	1.65(8)
C(8)-C(9)	1.61(5)
C(9)-N(2)	1.36(4)
C(10)-O(2)	1.41(3)
C(10)-C(11)	1.47(3)
C(10)-C(15)	1.56(3)
C(11)-C(12)	1.59(4)
C(12)-C(13)	1.48(4)
C(13)-C(14)	1.55(4)
C(14)-C(15)	1.43(3)
C(15)-N(2)	1.48(3)
O(2)-Cd(1)	2.33(2)
N(2)-Cd(1)	2.36(3)
C(16)-O(3)	1.41(3)
C(16)-C(17)	1.47(3)
C(16)-C(21)	1.55(3)
C(17)-C(18)	1.60(4)
C(18)-C(19)	1.47(4)
C(19)-C(20)	1.55(4)
C(20)-C(21)	1.43(4)
C(21)-N(3)	1.48(3)
O(3)-Cd(2)	2.38(2)
N(3)-C(22)	1.58(5)
N(3)-Cd(2)	2.32(3)

C(22)-C(23)	1.42(6)
C(23)-C(24)	1.53(6)
C(24)-N(4)	1.50(4)
C(25)-O(4)	1.41(3)
C(25)-C(26)	1.48(3)
C(25)-C(30)	1.55(3)
C(26)-C(27)	1.60(4)
C(27)-C(28)	1.48(4)
C(28)-C(29)	1.55(4)
C(29)-C(30)	1.43(3)
C(30)-N(4)	1.48(3)
O(4)-Cd(2)	2.33(2)
N(4)-Cd(2)	2.32(2)
C(32)-O(6)	1.59(7)
Cl(1)-Cd(1)	2.459(11)
Cl(2)-Cd(1)	2.605(11)
Cl(3)-Cd(2)	2.516(9)
Cl(3)-Cd(1)	2.937(10)
Cl(4)-Cd(2)	2.558(9)

O(1)-C(1)-C(2)	112(3)
O(1)-C(1)-C(6)	108(3)
C(2)-C(1)-C(6)	110(3)
C(1)-C(2)-C(3)	110(3)
C(4)-C(3)-C(2)	111(3)
C(3)-C(4)-C(5)	110(3)
C(6)-C(5)-C(4)	118(3)
C(5)-C(6)-N(1)	116(3)
C(5)-C(6)-C(1)	110(3)
N(1)-C(6)-C(1)	113(3)
C(6)-N(1)-C(7)	114(4)
C(6)-N(1)-Cd(1)	105(2)
C(7)-N(1)-Cd(1)	105(3)
N(1)-C(7)-C(8)	99(4)
C(9)-C(8)-C(7)	115(4)

N(2)-C(9)-C(8)	118(3)
O(2)-C(10)-C(11)	112(2)
O(2)-C(10)-C(15)	108(2)
C(11)-C(10)-C(15)	112(2)
C(10)-C(11)-C(12)	112(2)
C(13)-C(12)-C(11)	110(3)
C(12)-C(13)-C(14)	109(3)
C(15)-C(14)-C(13)	115(3)
C(14)-C(15)-N(2)	115(2)
C(14)-C(15)-C(10)	109(2)
N(2)-C(15)-C(10)	110(2)
C(10)-O(2)-Cd(1)	117.1(16)
C(9)-N(2)-C(15)	116(3)
C(9)-N(2)-Cd(1)	118(2)
C(15)-N(2)-Cd(1)	107.3(17)
O(3)-C(16)-C(17)	112(2)
O(3)-C(16)-C(21)	109(2)
C(17)-C(16)-C(21)	113(2)
C(16)-C(17)-C(18)	111(3)
C(19)-C(18)-C(17)	111(3)
C(18)-C(19)-C(20)	109(3)
C(21)-C(20)-C(19)	117(3)
C(20)-C(21)-N(3)	116(3)
C(20)-C(21)-C(16)	110(3)
N(3)-C(21)-C(16)	111(2)
C(16)-O(3)-Cd(2)	109.9(16)
C(21)-N(3)-C(22)	111(3)
C(21)-N(3)-Cd(2)	113.6(17)
C(22)-N(3)-Cd(2)	109(2)
C(23)-C(22)-N(3)	122(4)
C(22)-C(23)-C(24)	114(4)
N(4)-C(24)-C(23)	111(3)
O(4)-C(25)-C(26)	112(2)
O(4)-C(25)-C(30)	107(2)
C(26)-C(25)-C(30)	111(2)

C(25)-C(26)-C(27)	110(2)
C(28)-C(27)-C(26)	110(3)
C(27)-C(28)-C(29)	109(3)
C(30)-C(29)-C(28)	117(3)
C(29)-C(30)-N(4)	117(2)
C(29)-C(30)-C(25)	110(2)
N(4)-C(30)-C(25)	111(2)
C(25)-O(4)-Cd(2)	116.6(16)
C(30)-N(4)-C(24)	116(2)
C(30)-N(4)-Cd(2)	110.5(15)
C(24)-N(4)-Cd(2)	108.4(19)
Cd(2)-Cl(3)-Cd(1)	137.4(4)
O(2)-Cd(1)-N(1)	150.6(10)
O(2)-Cd(1)-N(2)	72.7(7)
N(1)-Cd(1)-N(2)	86.5(10)
O(2)-Cd(1)-Cl(1)	92.0(6)
N(1)-Cd(1)-Cl(1)	106.4(8)
N(2)-Cd(1)-Cl(1)	164.3(7)
O(2)-Cd(1)-Cl(2)	98.9(7)
N(1)-Cd(1)-Cl(2)	100.5(8)
N(2)-Cd(1)-Cl(2)	86.8(8)
Cl(1)-Cd(1)-Cl(2)	99.3(4)
O(2)-Cd(1)-Cl(3)	80.2(7)
N(1)-Cd(1)-Cl(3)	76.3(8)
N(2)-Cd(1)-Cl(3)	81.8(8)
Cl(1)-Cd(1)-Cl(3)	92.4(4)
Cl(2)-Cd(1)-Cl(3)	168.3(3)
N(3)-Cd(2)-N(4)	89.3(9)
N(3)-Cd(2)-O(4)	155.6(9)
N(4)-Cd(2)-O(4)	73.2(7)
N(3)-Cd(2)-O(3)	73.2(8)
N(4)-Cd(2)-O(3)	87.8(9)
O(4)-Cd(2)-O(3)	88.9(8)
N(3)-Cd(2)-Cl(3)	102.0(8)
N(4)-Cd(2)-Cl(3)	161.7(7)

O(4)-Cd(2)-Cl(3)	91.5(6)
O(3)-Cd(2)-Cl(3)	81.9(7)
N(3)-Cd(2)-Cl(4)	101.3(6)
N(4)-Cd(2)-Cl(4)	94.6(7)
O(4)-Cd(2)-Cl(4)	97.0(7)
O(3)-Cd(2)-Cl(4)	174.1(6)
Cl(3)-Cd(2)-Cl(4)	97.3(3)

Table E.40. Anisotropic displacement parameters ($Å^2 x\ 10^3$)for 9m_alvsb3_0b. The anisotropic displacement factor exponent takes the form: $-2p^2[\ h^2 a^{*2} U^{11} + ... + 2\ h\ k\ a^*\ b^*\ U^{12}\ ]$

	U^{11}	U^{22}	U^{33}	U^{23}	U^{13}	U^{12}
Cl(1)	47(6)	28(5)	98(9)	5(5)	-2(6)	5(4)
Cl(2)	57(6)	63(7)	34(5)	14(5)	11(4)	-5(5)
Cl(3)	51(6)	69(7)	25(4)	8(5)	8(4)	15(5)
Cl(4)	45(5)	25(4)	47(5)	0(4)	22(4)	6(4)
Cd(1)	29(1)	34(1)	29(1)	3(1)	6(1)	0(1)
Cd(2)	30(1)	18(1)	25(1)	-2(1)	9(1)	0(1)

Table E.41. Torsion angles [°] for 9m_alvsb3_0b.

O(1)-C(1)-C(2)-C(3)	-179(5)
C(6)-C(1)-C(2)-C(3)	-58(5)
C(1)-C(2)-C(3)-C(4)	57(6)
C(2)-C(3)-C(4)-C(5)	-49(6)
C(3)-C(4)-C(5)-C(6)	51(7)
C(4)-C(5)-C(6)-N(1)	178(4)
C(4)-C(5)-C(6)-C(1)	-52(5)
O(1)-C(1)-C(6)-C(5)	179(4)
C(2)-C(1)-C(6)-C(5)	56(5)
O(1)-C(1)-C(6)-N(1)	-49(5)
C(2)-C(1)-C(6)-N(1)	-172(4)
C(5)-C(6)-N(1)-C(7)	34(5)
C(1)-C(6)-N(1)-C(7)	-95(5)
C(5)-C(6)-N(1)-Cd(1)	-80(4)

C(1)-C(6)-N(1)-Cd(1)	151(3)
C(6)-N(1)-C(7)-C(8)	165(3)
Cd(1)-N(1)-C(7)-C(8)	-80(4)
N(1)-C(7)-C(8)-C(9)	84(5)
C(7)-C(8)-C(9)-N(2)	-68(5)
O(2)-C(10)-C(11)-C(12)	175(3)
C(15)-C(10)-C(11)-C(12)	54(4)
C(10)-C(11)-C(12)-C(13)	-56(4)
C(11)-C(12)-C(13)-C(14)	54(4)
C(12)-C(13)-C(14)-C(15)	-59(4)
C(13)-C(14)-C(15)-N(2)	180(3)
C(13)-C(14)-C(15)-C(10)	56(4)
O(2)-C(10)-C(15)-C(14)	-178(3)
C(11)-C(10)-C(15)-C(14)	-54(3)
O(2)-C(10)-C(15)-N(2)	55(3)
C(11)-C(10)-C(15)-N(2)	179(3)
C(11)-C(10)-O(2)-Cd(1)	-154(2)
C(15)-C(10)-O(2)-Cd(1)	-30(3)
C(8)-C(9)-N(2)-C(15)	179(3)
C(8)-C(9)-N(2)-Cd(1)	50(4)
C(14)-C(15)-N(2)-C(9)	51(4)
C(10)-C(15)-N(2)-C(9)	175(3)
C(14)-C(15)-N(2)-Cd(1)	-175(2)
C(10)-C(15)-N(2)-Cd(1)	-51(3)
O(3)-C(16)-C(17)-C(18)	177(3)
C(21)-C(16)-C(17)-C(18)	54(4)
C(16)-C(17)-C(18)-C(19)	-57(5)
C(17)-C(18)-C(19)-C(20)	54(5)
C(18)-C(19)-C(20)-C(21)	-56(5)
C(19)-C(20)-C(21)-N(3)	180(4)
C(19)-C(20)-C(21)-C(16)	53(5)
O(3)-C(16)-C(21)-C(20)	-178(3)
C(17)-C(16)-C(21)-C(20)	-53(4)
O(3)-C(16)-C(21)-N(3)	53(4)
C(17)-C(16)-C(21)-N(3)	177(3)

C(17)-C(16)-O(3)-Cd(2)	-175(2)
C(21)-C(16)-O(3)-Cd(2)	-50(3)
C(20)-C(21)-N(3)-C(22)	83(4)
C(16)-C(21)-N(3)-C(22)	-151(3)
C(20)-C(21)-N(3)-Cd(2)	-154(3)
C(16)-C(21)-N(3)-Cd(2)	-28(4)
C(21)-N(3)-C(22)-C(23)	71(5)
Cd(2)-N(3)-C(22)-C(23)	-54(5)
N(3)-C(22)-C(23)-C(24)	70(5)
C(22)-C(23)-C(24)-N(4)	-79(5)
O(4)-C(25)-C(26)-C(27)	178(3)
C(30)-C(25)-C(26)-C(27)	58(3)
C(25)-C(26)-C(27)-C(28)	-59(4)
C(26)-C(27)-C(28)-C(29)	54(4)
C(27)-C(28)-C(29)-C(30)	-55(5)
C(28)-C(29)-C(30)-N(4)	-179(3)
C(28)-C(29)-C(30)-C(25)	53(4)
O(4)-C(25)-C(30)-C(29)	-177(3)
C(26)-C(25)-C(30)-C(29)	-55(3)
O(4)-C(25)-C(30)-N(4)	51(3)
C(26)-C(25)-C(30)-N(4)	174(3)
C(26)-C(25)-O(4)-Cd(2)	-156(2)
C(30)-C(25)-O(4)-Cd(2)	-34(3)
C(29)-C(30)-N(4)-C(24)	65(4)
C(25)-C(30)-N(4)-C(24)	-167(3)
C(29)-C(30)-N(4)-Cd(2)	-171(3)
C(25)-C(30)-N(4)-Cd(2)	-43(3)
C(23)-C(24)-N(4)-C(30)	-163(3)
C(23)-C(24)-N(4)-Cd(2)	73(3)
C(10)-O(2)-Cd(1)-N(1)	-44(3)
C(10)-O(2)-Cd(1)-N(2)	3(2)
C(10)-O(2)-Cd(1)-Cl(1)	-173(2)
C(10)-O(2)-Cd(1)-Cl(2)	87(2)
C(10)-O(2)-Cd(1)-Cl(3)	-81(2)
C(6)-N(1)-Cd(1)-O(2)	-138(2)

C(7)-N(1)-Cd(1)-O(2)	102(3)
C(6)-N(1)-Cd(1)-N(2)	178(2)
C(7)-N(1)-Cd(1)-N(2)	57(3)
C(6)-N(1)-Cd(1)-Cl(1)	-11(2)
C(7)-N(1)-Cd(1)-Cl(1)	-132(3)
C(6)-N(1)-Cd(1)-Cl(2)	92(2)
C(7)-N(1)-Cd(1)-Cl(2)	-29(3)
C(6)-N(1)-Cd(1)-Cl(3)	-100(2)
C(7)-N(1)-Cd(1)-Cl(3)	140(3)
C(9)-N(2)-Cd(1)-O(2)	159(3)
C(15)-N(2)-Cd(1)-O(2)	25.9(19)
C(9)-N(2)-Cd(1)-N(1)	-42(3)
C(15)-N(2)-Cd(1)-N(1)	-175(2)
C(9)-N(2)-Cd(1)-Cl(1)	172(2)
C(15)-N(2)-Cd(1)-Cl(1)	39(4)
C(9)-N(2)-Cd(1)-Cl(2)	58(2)
C(15)-N(2)-Cd(1)-Cl(2)	-74.5(19)
C(9)-N(2)-Cd(1)-Cl(3)	-119(2)
C(15)-N(2)-Cd(1)-Cl(3)	108.1(19)
Cd(2)-Cl(3)-Cd(1)-O(2)	59.3(9)
Cd(2)-Cl(3)-Cd(1)-N(1)	-102.8(10)
Cd(2)-Cl(3)-Cd(1)-N(2)	-14.4(9)
Cd(2)-Cl(3)-Cd(1)-Cl(1)	150.9(7)
Cd(2)-Cl(3)-Cd(1)-Cl(2)	-27(2)
C(21)-N(3)-Cd(2)-N(4)	-86(3)
C(22)-N(3)-Cd(2)-N(4)	38(2)
C(21)-N(3)-Cd(2)-O(4)	-42(4)
C(22)-N(3)-Cd(2)-O(4)	81(3)
C(21)-N(3)-Cd(2)-O(3)	2(2)
C(22)-N(3)-Cd(2)-O(3)	126(2)
C(21)-N(3)-Cd(2)-Cl(3)	80(2)
C(22)-N(3)-Cd(2)-Cl(3)	-157(2)
C(21)-N(3)-Cd(2)-Cl(4)	180(2)
C(22)-N(3)-Cd(2)-Cl(4)	-57(2)
C(30)-N(4)-Cd(2)-N(3)	-179(2)

C(24)-N(4)-Cd(2)-N(3)	-50.4(19)
C(30)-N(4)-Cd(2)-O(4)	18.5(19)
C(24)-N(4)-Cd(2)-O(4)	147(2)
C(30)-N(4)-Cd(2)-O(3)	108(2)
C(24)-N(4)-Cd(2)-O(3)	-124(2)
C(30)-N(4)-Cd(2)-Cl(3)	53(3)
C(24)-N(4)-Cd(2)-Cl(3)	-179(76)
C(30)-N(4)-Cd(2)-Cl(4)	-77.4(19)
C(24)-N(4)-Cd(2)-Cl(4)	50.9(19)
C(25)-O(4)-Cd(2)-N(3)	-36(3)
C(25)-O(4)-Cd(2)-N(4)	10.0(19)
C(25)-O(4)-Cd(2)-O(3)	-78(2)
C(25)-O(4)-Cd(2)-Cl(3)	-159.8(19)
C(25)-O(4)-Cd(2)-Cl(4)	102.7(19)
C(16)-O(3)-Cd(2)-N(3)	26.8(19)
C(16)-O(3)-Cd(2)-N(4)	117(2)
C(16)-O(3)-Cd(2)-O(4)	-170.1(19)
C(16)-O(3)-Cd(2)-Cl(3)	-78.4(19)
C(16)-O(3)-Cd(2)-Cl(4)	3(8)
Cd(1)-Cl(3)-Cd(2)-N(3)	132.5(9)
Cd(1)-Cl(3)-Cd(2)-N(4)	-101(2)
Cd(1)-Cl(3)-Cd(2)-O(4)	-67.9(9)
Cd(1)-Cl(3)-Cd(2)-O(3)	-156.6(9)
Cd(1)-Cl(3)-Cd(2)-Cl(4)	29.3(7)

Table E.42. Hydrogen bonds for 9m_alvsb3_0b [Å and °].

D-H...A	d(D-H)	d(H...A)	d(D...A)	<(DHA)	#
N3 -- H3 .. O6	0.9100	2.3900	3.13(5)	138.00	1
N4 -- H4 .. Cl2	0.9100	2.4700	3.36(3)	166.00	2
C8 -- H8A .. O2	0.9700	2.5700	3.25(5)	127.00	1

Symmetry transformations used to generate equivalent atoms:
#1 x,1+y,z #2 x,1-y,1/2+z